①

Introduction
(standard model and neutrinos)

- ν oscillation
- ν mass experiments

・νの予言

Pauliにより 1930年に予言された。

β崩壊：$(Z, A) \longrightarrow (Z+1, A) + e^-$

原子核の質量：$M_Z \times Z + M_n \times N - B$

$\uparrow$ 原子番号　$\uparrow$ 中性子数　$\uparrow$ Binding energy

したがって e^-の energyは、

になるはず、

しかし実験では、

broadな分布

したがって β崩壊では 未知の粒子が出ているにちがいない。
それが、ニュートリノ。

・素粒子の種類

$\begin{pmatrix} u_L \\ d_L' \end{pmatrix} \begin{pmatrix} c_L \\ s_L' \end{pmatrix} \begin{pmatrix} t_L \\ b_L' \end{pmatrix}$ $u_R, d_R', c_R, s_R', t_R, b_R'$

'は弱い相互作用の固有状態
'なし 質量の固有状態　$\updownarrow$ Kobayashi-Masukawa matrix

$\begin{pmatrix} \nu_{eL} \\ e^-_L \end{pmatrix} \begin{pmatrix} \nu_{\mu L} \\ \mu^-_L \end{pmatrix} \begin{pmatrix} \nu_{\tau L} \\ \tau_L \end{pmatrix}$ e_R, μ_R, τ_R

ニュートリノ F.Reines により 1953年に発見

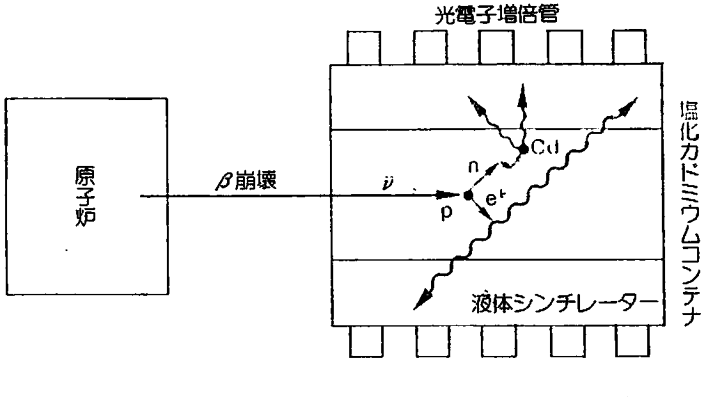

図2.2　電子ニュートリノの発見（$\bar{\nu}_e$ がpに吸収されると n と e^+ が生成される。e^+ は e^- と対消滅を起こし、2個の γ 線が発生する。一方、nはCd原子核に吸収され、X線が発生する。）

た（一九三四）。そして、ベータ崩壊を引き起こす力は弱い相互作用とよばれるようになった。

しかし、理論ができても肝心なニュートリノ自体はすぐには発見されなかった。ようやく、一九五〇年代半ばライネス（F. Reines）とコーワン（C. Cowan）は原子炉から出る強力な反ニュートリノ・ビームを標的にあて

$$\bar{\nu}_e + p \longrightarrow n + e^+$$

という反応によって電子の反粒子である陽電子（e^+）が生成されることを確認し、実際にニュートリノが存在していることを確かめたのである（図2・2）。実にパウリの予言から約四半世紀もの時間がかかってしまったのである。それほどまでに、ニュートリノは捉えるのが難しい粒子なのである。

- 物質に働く力

強い相互作用 ---- QCD　グルーオン　クォーク間　SU(3)　8コのグルーオン

弱い相互作用 ----- weak interaction

電磁相互作用 --- QED　charge を持った物の間。

(重力)

$$i\frac{\partial \psi}{\partial t} = H\psi$$

フェルミ理論

$$\mathcal{L} = G_B(\bar{e}\gamma_\mu \nu)(\bar{p}\gamma^\mu n) + h.c. = G_B j^{-}_{e\mu} J_n^{+\mu}$$

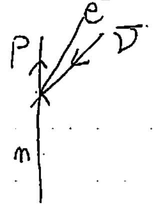

パリティ非保存により。

β崩壊の $\mathcal{L}$ は

$$-\mathcal{L} = \frac{G_B}{\sqrt{2}}\left[\bar{p}\gamma^\mu(1-1.26\gamma^5)n\right]\left[\bar{e}\gamma_\mu(1-\gamma^5)\nu\right]$$

となった。

パリティの破れ

発端：τ−θ パズル　1957 Dalitz　パリティ $(-1)^{\ell}$ × intrisic × intrinsic

$K \to 3\pi \xrightarrow{(\tau)} (-1)^{3+L+\ell}$

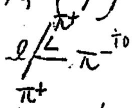

total spin 0　L と ℓ は同じ　$L=\ell$ ⇓ パリティ −1

Kはスピン0　or

$2\pi^{\theta}$ parity $(-1)\times(-1) = 1$

パリティ

$\mathbb{P} \to -\mathbb{P}$

$\mathbb{J} \to \mathbb{J}$

$\boxed{\mathbb{J}\cdot\mathbb{P}}$ がそんざいすれば　パリティをやぶる。

C.S.Wu　1957年

ウーの実験　^{60}Co を 0.01K まで冷却

常磁性体 Co に数百ガウスの弱い磁場で電子を偏極させる。

スピンスピン相互作用で、Co原子核を偏極。

$^{60}Co(5^+) \to {}^{60}Ni(4^+)$

Co の偏極率

$W(\theta) \propto 1 + AP\,v\cos\theta$　電子の速度

パリティは最大限やぶれている。

β崩壊のラグランジアンは、

$$-\mathcal{L} = G_\beta/\sqrt{2}\,[\bar{p}\gamma^\mu(1-1.26\gamma^5)n][\bar{e}\gamma_\mu(1-\gamma_5)\nu]$$

$$\to i\frac{\partial\psi}{\partial t} = (\alpha\cdot P + \beta m)\psi$$

$$\sum_i \alpha_i \frac{1}{i}\frac{\partial}{\partial x_i}$$

ディラック方程式 $(\gamma^\mu i\partial_\mu - m)\psi(x) = 0$

$$\alpha = \begin{pmatrix} 0 & \sigma \\ \sigma & 0 \end{pmatrix}$$

$$\gamma^\mu\gamma^\nu + \gamma^\nu\gamma^\mu = 2g^{\mu\nu}$$

↑ 4x4 matrix

$$\gamma^5 \equiv i\gamma^0\gamma^1\gamma^2\gamma^3 \quad \beta = \left(\begin{matrix}1 \\ 0\end{matrix}\right.$$

$$\gamma^0 = \begin{bmatrix} 1 & 0 \\ 0 & -1 \end{bmatrix},\quad \gamma = \begin{bmatrix} 0 & \sigma \\ -\sigma & 0 \end{bmatrix},\quad \gamma^5 = \begin{pmatrix} 0 & 1 \\ 1 & 0 \end{pmatrix}$$

$$\sigma_1 = \begin{pmatrix} 0 & 1 \\ 1 & 0 \end{pmatrix}\quad \sigma_2 = \begin{pmatrix} 0 & -i \\ i & 0 \end{pmatrix}$$

$$\sigma_3 = \begin{pmatrix} 1 & 0 \\ 0 & -1 \end{pmatrix}$$

γ^5に対する固有値

$$\gamma^5\psi_L = -\psi_L \quad , \gamma^5\psi_R = \psi_R$$

↑負

$$\psi_L = \left(\frac{1-\gamma_5}{2}\right)\psi, \quad \psi_R = \left(\frac{1+\gamma_5}{2}\right)\psi$$

$\boxed{\pi\ 中間子}$

~100% $\pi^+ \to \mu^+ + \nu$ $\tau = 26$ nsec

$BR(\pi^\pm \to e^\pm\nu) = (1.218^{\pm 0.014}) \times 10^{-4}$

↑ lepton side; $\bar{\mu}\gamma_\mu(1-\gamma^5)\nu$

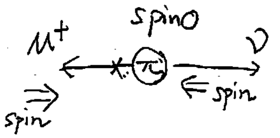

角運動量保存則から μ^+のヘリシティも負でないといけない。

$(1-\gamma^5)$のfactorにより負成分は$\left(\frac{m_e}{p}\right)$になる。

↓

amplitudeは$\left(\frac{m_e}{p}\right)^2$に比例

Phase spaceの比 $\dfrac{(m_\pi - m_e^2)^2}{(m_\pi^2 - m_\mu^2)^2}$

$$\frac{\Gamma(\pi\to e\nu)}{\Gamma(\pi\to\mu\nu)} = \frac{m_e^2}{m_\mu^2}\frac{(m_\pi^2 - m_e^2)^2}{(m_\pi^2 - m_\mu^2)^2} = 1.284\times 10^{-4}$$

- ニュートリノのヘリシティ Goldhaber (1958) Phys. Rev. 109 (1958) 1015.

$$-\mathcal{L} = G_\beta/\sqrt{2}\,[\bar{p}\gamma^\mu(1-1.26\gamma^5)n][\bar{e}\gamma_\mu(1-\gamma^5)\nu]$$

$(1-\gamma^5)\nu$ ：左巻きのみ弱い相互作用をする。

ヘリシティ
e^- : $-v$ e^+ : $+v$
$\bar{\nu}$: $+1$ ν : -1

$$e^- + {}^{152}Eu^{m} \longrightarrow {}^{152}Sm^* + \nu$$

(9.2h)

J $\frac{1}{2}$ 0 1 $\frac{1}{2}$

Electron-capture reaction

K-electron captureなのでスピンのみが初期状態にあり。

$$\hookrightarrow {}^{152}Sm^* \to Sm + \gamma$$

↑963keV

J 1 0 + 1

スピンの向き 電子 ⇑ ${}^{152}Sm^*$ ⇑ ⇓ ν

$E = E_\gamma + E_R$ $E_R = \frac{E_\gamma}{2M}$ M 核の質量，吸収の時にもE_Rが必要。$2E_R$をドップラー効果でおぎなう。

Sm^*の運動方向の前方に放出されるγを共鳴散乱により拾う。

→中間状態の $\tau = 7\times 10^{-14}$sec

$$\gamma + {}^{152}Sm \to {}^{152}Sm^* \to {}^{152}Sm + \gamma$$

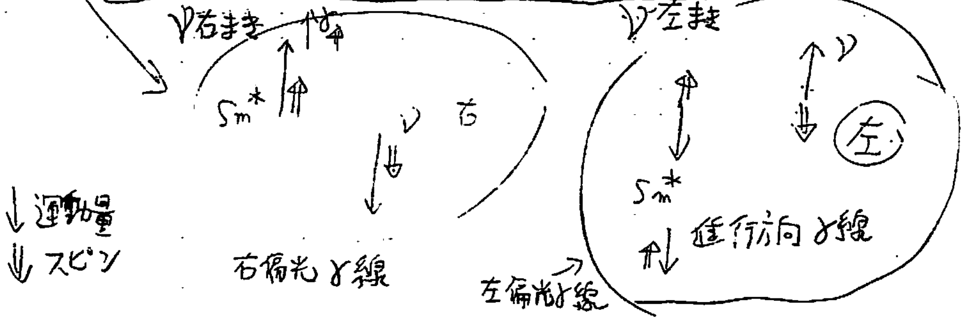

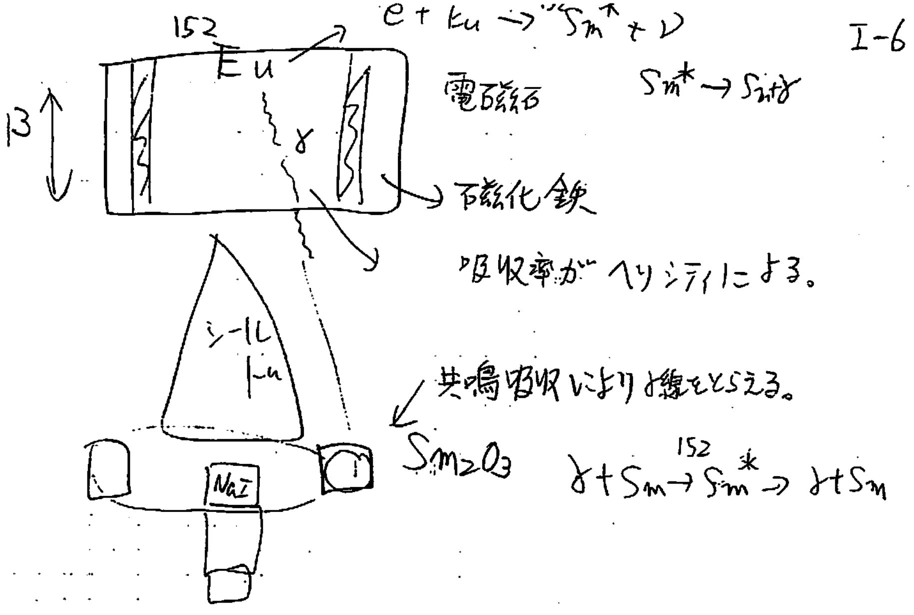

$e + Eu \rightarrow Sm^* + \nu$

$Sm^* \rightarrow Sm + \gamma$

吸収率がヘリシティによる。

共鳴吸収によりγ線をとらえる。

$\gamma + {}^{152}Sm \rightarrow Sm^* \rightarrow \gamma + Sm$

1. 鉄の中の γ

鉄のスピン ⇓ ↓ ⇑ のとき、スピン反転可能

おきやすい。

鉄のスピン ⇓ ↓ γ ⇓ 反転不可能。

反応がおきにくい。

実験結果 γは ⇑↓ となり νは左まきに なった。

Reprinted from the Phys. Rev. 109 (1958) 1015 - 1017
by permission of the American Physical Society and the authors

Helicity of Neutrinos*

M. GOLDHABER, L. GRODZINS, AND A. W. SUNYAR
Brookhaven National Laboratory, Upton, New York

(Received December 11, 1957)

A COMBINED analysis of circular polarization and resonant scattering of γ rays following orbital electron capture measures the helicity of the neutrino. We have carried out such a measurement with Eu^{152m}, which decays by orbital electron capture. If we assume the most plausible spin-parity assignment for this isomer compatible with its decay scheme,[1] 0−, we find that the neutrino is "left-handed," i.e., $\sigma_\nu \cdot \hat{p}_\nu = -1$ (negative helicity).

Our method may be illustrated by the following simple example: take a nucleus A (spin $I=0$) which decays by allowed orbital electron capture, to an excited state of a nucleus $B(I=1)$, from which a γ ray is emitted to the ground state of $B(I=0)$. The conditions necessary for resonant scattering are best fulfilled for those γ rays which are emitted opposite to the neutrino, which have an energy comparable to that of the neutrino, and which are emitted before the recoil energy is lost. Since the orbital electrons captured by a nucleus are almost entirely s electrons (K, L_I, $\cdots$ electrons of spin $S=\frac{1}{2}$), the substates of the daughter nucleus B, formed when a neutrino is emitted in the Z direction, are $m=-1$, 0 if the neutrino has positive helicity, and $m=+1$, 0 if the neutrino has negative helicity. In either case, the helicity of the γ ray emitted in the $(-Z)$ direction is the same as that of the neutrino. Thus, a measurement of the circular polarization of the γ rays which are resonant-scattered by the nucleus B, yields directly the helicity of the neutrino, if one assumes only the well-established conservation laws of momentum and angular momentum.

To carry out this measurement we have used a nucleus which appears to have the properties postulated in the example given: ${}_{63}Eu^{152m}$(9.3 hr). It probably has spin 0 and odd parity.[1] It decays to an excited state of ${}_{62}Sm^{152}(1-)$ with emission of neutrinos which have an energy of 840 kev in the most prominent case of K-electron capture. This is followed by an $E1$ γ-ray transition of 960 kev to the ground state (0+). The excited state has a mean life of $(3\pm1)\times10^{-14}$ sec, as determined by Grodzins.[1] Thus, even in a solid source most of the γ-ray emission takes place before the momentum of the recoil nucleus has changed appreciably.

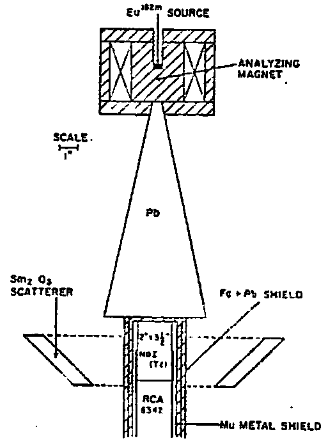

FIG. 1. Experimental arrangement for analyzing circular polarization of resonant scattered γ-rays. Weight of Sm_2O_3 scatterer: 1850 grams.

The experimental arrangement used is shown in Fig. 1. The Eu^{152m} source is inserted inside an electromagnet which is alternately (every three minutes) magnetized in the up or down direction. The γ rays which pass through the magnet are resonant-scattered from a Sm_2O_3 scatterer (26.8% Sm^{152}), and detected in a 2-in.×3½-in. cylindrical NaI(Tl) scintillation counter. The photomultiplier (RCA 6342) is magnetically shielded by an iron cylinder and a mu-metal shield. The effectiveness of this magnetic shield was demonstrated by check experiments with a Cs^{137} γ-ray source

μの崩壊　$\mu^- \to e^- + \bar{\nu}_e + \nu_\mu$

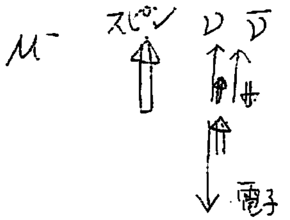

e^-は左巻き　ν_μ左
$\bar{\nu}_e$右

$$-\mathcal{L} = \frac{G_\mu}{\sqrt{2}} \left[\bar{\nu}_\mu \gamma^\mu (1-\gamma^5) \mu \right] \left[\bar{e} \gamma_\mu (1-\gamma^5) \nu_e \right]$$

$$\frac{d\Gamma}{dx} = \frac{G_\mu^2 m_\mu^5}{96\pi^3} x^2 (3-2x)$$

$$x = \frac{E}{\frac{m_\mu}{2}}$$

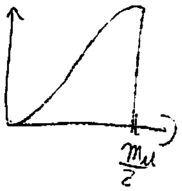

$$\Gamma = \frac{G_\mu^2 m_\mu^5}{192\pi^3}$$

$$\tau = \frac{1}{\Gamma} = 2.197 \times 10^{-6} \sec$$

$$G_\mu = 10^{-5} m_p^{-2}$$

$$\boxed{G_B = G_\mu \cos\theta_C}$$

グラショー・ワインバーグサラム理論　における質量の起源

$\Phi = \begin{pmatrix} \varphi^+ \\ \varphi^0 \end{pmatrix}$ ヒッグス場

$\Psi = \begin{bmatrix} \nu \\ e \end{bmatrix}$

ゲージ変換 $SU(2) \times U(1)$

$\psi \to \psi' = \exp\left(-i W(x) \cdot t - i Y \alpha(x)\right] \psi$ に対して不変。

SU(2) 演算子　U(1) 演算子

$D_\mu = \partial_\mu + i g_W W_\mu \cdot t + i \left(\frac{g_0}{2}\right) B_\mu Y$

共変微分を定義してゲージ不変性を入れる。

$\uparrow$ SU(2)のゲージ場　$\uparrow$ U(1) ゲージ場

$$\mathcal{L}_{mass} = - G_e \left[\bar{e}_R (\Phi^\dagger \Psi) + (\bar{\Psi} \Phi) e_R \right]$$
$$= - G_e \left[\bar{e}_R (\varphi^{+\dagger} \nu_L + \varphi^{0*} e_L) + \bar{\nu}_L \varphi^+ + \bar{e}_L \varphi^0) e_R \right]$$

$\varphi^+ \to 0$, $\varphi^0 \to (v + \varphi) / \sqrt{2}$

$m_e = G_e v / \sqrt{2}$

$G_e = \sqrt{2} m_e / v$

一般的には
$$\phi = \frac{1}{\sqrt{2}} \begin{bmatrix} (W_2 + i W_1)/2 \\ v + \varphi - i W_3/2 \end{bmatrix}$$
だが
$$\phi = \exp(i W \cdot \tau / 2v) \begin{bmatrix} 0 \\ \frac{v+\varphi}{\sqrt{2}} \end{bmatrix}$$

ヒッグス機構

$$\mathcal{L}_G = (\partial_\mu \phi)^\dagger (\partial^\mu \phi) - \underbrace{V(\phi)}$$ ポテンシャル
$$= \mu^2 \phi^2 + \lambda \phi^4$$

$\mu^2 > 0$なら

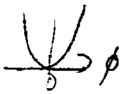

$\mu^2 < 0$なら

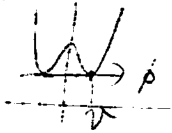

自発的対称性の破れ

$$\mathcal{L}_{mass} = -\frac{G_e v}{\sqrt{2}} (\bar{e}_R e_L + \bar{e}_L e_R) - \frac{G_e}{\sqrt{2}} (\bar{e}_R e_L + \bar{e}_L e_R) \varphi$$

$m_e \bar{e} e$　mass term　higgsとの相互作用

質量項は e_L アイソスピン2 / アイソスピン0だから e_R 0

$m_e = G_e v / \sqrt{2}$

$G_e = \sqrt{2} m_e / v$

単なる mass term は、ゲージ SU(2) 不変ではなかった。

-$\mathcal{L}$ の中の mass term

~~$m\bar{\Psi}\psi$~~ Dirac 場 ψ の方程式を与えるラグランジアン

$$\mathcal{L} = \bar{\Psi}(i\gamma^\mu\partial_\mu - m)\psi$$

質量項 $m\bar{\Psi}\psi = m\times(\bar{\Psi}_R\psi_L + \bar{\psi}_L\psi_R)$

$$\psi_L = \frac{1-\gamma_5}{2}\psi$$

$$\psi_R = \frac{1+\gamma_5}{2}\psi$$

$$(1-\gamma_5)(1+\gamma_5) = 1-\gamma_5^2 = 0$$

$$(1-\gamma_5)(1-\gamma_5) = 1+\gamma_5^2$$

$$\begin{bmatrix}0 & 1\\ 1 & 0\end{bmatrix}\begin{bmatrix}0 & 1\\ 1 & 0\end{bmatrix} = \begin{bmatrix}1 & 0\\ 0 & 1\end{bmatrix}$$

$$\bar{\Psi} = \psi^\dagger\gamma_0 \qquad \gamma_5^\dagger = \gamma_5$$

$$\gamma_5\gamma_0 = -\gamma_0\gamma_5$$

$$\bar{\psi}_R = \left[\left(\frac{1+\gamma_5}{2}\right)\psi\right]^\dagger\gamma_0$$

$$= \psi^\dagger\left(\frac{1+\gamma_5}{2}\right)\gamma_0 = \psi^\dagger\gamma_0\times\left(\frac{1-\gamma_5}{2}\right)$$

電子とニュートリノについて $SU(2)\times U(1)$ 対称性をみたす

ラグランジアン

共変微分 ゲージ変換に対して不変。

$\psi_L = \begin{pmatrix}\nu_L\\ e_L\end{pmatrix}$, $\psi_R = e_R$

$$\mathcal{L} = -\frac{1}{4}\mathbb{F}_{\mu\nu}\cdot\mathbb{F}^{\mu\nu} - \frac{1}{4}B_{\mu\nu}B^{\mu\nu} + \bar{\Psi}i\gamma^\mu D_\mu\psi$$ ← ゲージセクター

$$\boxed{D_\mu = \partial_\mu + ig_w\mathbb{W}_\mu\cdot\text{[illegible]} + i(g_B/2)B_\mu\cdot Y}$$

$$+(D_\mu\Phi)^\dagger(D^\mu\Phi) - V(\Phi) - G_e\left[\bar{e}_R(\Phi^\dagger\psi_L) + (\bar{\psi}_L\Phi)e_R\right]$$

↑ ヒッグス場

$\mathbb{F}_{\mu\nu} = \partial_\mu\mathbb{W}_\nu - \partial_\nu\mathbb{W}_\mu - g_w\mathbb{W}_\mu\times\mathbb{W}_\nu$ $SU(2)$の場

$B_{\mu\nu} = \partial_\mu B_\nu - \partial_\nu B_\mu$ — $U(1)$ field

$V(\Phi) = \lambda\left(|\phi|^2 + \frac{\mu^2}{2\lambda}\right)^2$

中性ベクトル場とフェルミオン場の相互作用

$$\mathcal{L}_{int} = -\bar{\Psi}\gamma^\mu\left(g_w W_\mu^0 I_3 + (g_3/2)B_\mu Y\right)\psi$$

$$= -\bar{\nu}_L\gamma^\mu\left(\frac{g_w}{2}W_\mu^0 - \frac{g_B}{2}B_\mu\right)\nu_L$$

$$+\bar{e}_L\gamma^\mu\left(\frac{g_w}{2}W_\mu^0 + \frac{g_B}{2}B_\mu\right)e_L + \bar{e}_R\gamma^\mu(g_B B_\mu)e_R$$

($Q = I_3 + \frac{Y}{2}$ 西島ゲルマン則が成立すると仮定。

$I_3(\nu_L) = \frac{1}{2}$, $I_3(e_L) = -\frac{1}{2}$; $I_3(e_R) = 0$

$Y(\psi_L) = Y_L = -1$, $Y(e_R) = Y_R = -2$)

ニュートリノは、電磁相互作用に関係しないので

$$Z_\mu^0 = \frac{1}{\sqrt{g_W^2+g_B^2}}(-g_B B_\mu + g_W W_\mu^0) \equiv -\sin\theta_W B_\mu + \cos\theta_W W_\mu^0$$

$$A_\mu = \frac{1}{\sqrt{\ }} \quad (g_W B_\mu + g_B W_\mu^0) \equiv \cos\theta_W B_\mu + \sin\theta_W W_\mu^0$$

電磁場 ↗

$$\sin\theta_W = \frac{g_B}{\sqrt{g_W^2+g_B^2}}$$

$$\mathcal{L}_{Int} = -[e\bar{\psi}\gamma^\mu A_\mu Q\psi + g_Z\bar{\psi}\gamma^\mu Z_\mu^0(I_{3L} - Q\sin^2\theta_W)\psi]$$

$$g_Z = \sqrt{g_W^2+g_B^2}\ ;\ e = g_Z\sin\theta_W\cos\theta_W$$

$$Q_\nu = 0,\ Q_e = -1$$

W, Zの質量

$(D^\mu\Phi)^\dagger(D_\mu\Phi)$ ヒッグス場

$$\Phi \to \begin{pmatrix} 0 \\ \frac{v}{\sqrt{2}} \end{pmatrix}$$

$$\downarrow$$

$$\frac{g_W^2 v^2}{4} W^- W^+ + \frac{g_Z^2 v^2}{8} Z^0 Z^0$$

荷電ボソンと中性ボソンとでは、質量項の因子がちがう。

$$m_W = \frac{g_W v}{2},\ m_Z = \frac{g_Z v}{2}$$

$$m_Z = \frac{g_Z}{g_W} m_W = \frac{m_W}{\cos\theta_W}$$

$W^\pm$を介しての相互作用

$$\mathcal{L} = -\frac{g_W}{\sqrt{2}}\bar{\psi}_L\gamma^\mu[\tau_+ W_\mu^+ + \tau_- W_\mu^-]\psi_L$$

ψ_Rにははたらかない。

$$\tau^- = \begin{pmatrix} 0 & 0 \\ 1 & 0 \end{pmatrix} \quad \tau^+ = \begin{pmatrix} 0 & 1 \\ 0 & 0 \end{pmatrix}$$

$$\Rightarrow \quad \frac{G_F}{\sqrt{2}} = \frac{g_W^2}{8m_W^2} = \frac{1}{2v^2}$$

$$\boxed{v = 246\,\mathrm{GeV}}$$

Z^0:

Wの発見:

CERN SPS $\bar{P}P \to q\bar{q}$ 例

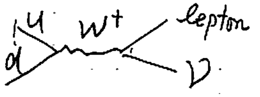

LEP e^+e^-

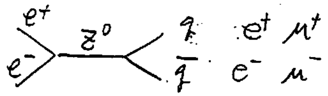

Z^0の mass : 91.19 GeV

W 〃 : 80.4 GeV

$\sin^2\theta_W$ = 0.231

GWSの特徴

- 電弱統一理論
- くり込み可能 ← t. Hooft
- 中性カレントの存在
- $W^\pm, Z^0$の質量を定量的に予言。
- クオークレプトンの分類

$$\begin{pmatrix} \nu_L \\ e_L \end{pmatrix}\begin{pmatrix} \ \\ \ \end{pmatrix}\begin{pmatrix} \ \\ \ \end{pmatrix} \quad e_R, \mu_R, \tau_R$$

$$\begin{pmatrix} u \\ d \end{pmatrix}\begin{pmatrix} c \\ s \end{pmatrix}\begin{pmatrix} t \\ b \end{pmatrix} \quad u_R, d_R, c_R, s_R, t_R, b_R$$

ニュートリノの数

$e^+e^- \to Z^0 \to$

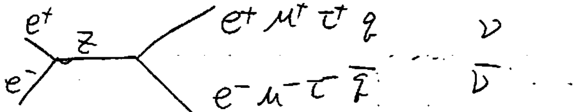

多くあればあるほど
Γは大きくなる。

$e^+e^- \to q\bar{q}$ ハドロンfinal stateが数が多い。

$$\sigma_h^0 = \frac{12\pi}{m_Z^2} \frac{\Gamma_e \Gamma_h}{\Gamma_Z^2} \qquad m_\nu < \frac{1}{2} m_Z$$

$$N_\nu = \frac{\Gamma_{inv.}}{\Gamma_\nu} = \frac{1}{\Gamma_\nu}(\Gamma_Z - \Gamma_h - 3\Gamma_e)$$

$N_\nu =$ 2.994 ± 0.012 (LEPの結果)

Generationの数は 3

$Z \to e^+e^-$ 3.3%
$\mu^+\mu^-$
$\tau^+\tau^-$
10%位

$Z \to \nu\bar{\nu}$ 21.5%

残り70%は
$q\bar{q}$

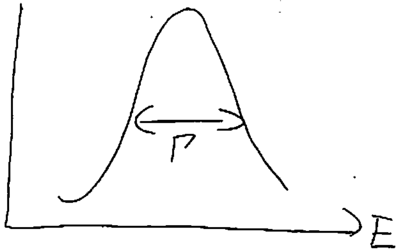

ブライトウィグナーの共鳴公式

$$\propto \frac{1}{(E-E_0)^2 + \left(\frac{\Gamma}{2}\right)^2}$$

Γ：崩壊幅、

$$\frac{1}{\Gamma} = \tau$$

$\Delta E \cdot \Delta t \fallingdotseq \Gamma \times \tau$ に布

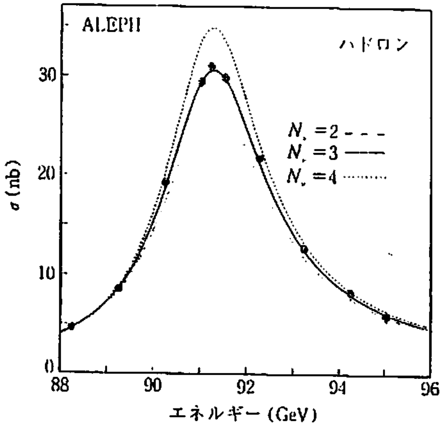

図 7.3 $e^+e^- \to Z \to$ ハドロンの全断面積
実線が $N_\nu=3$ としたときの標準理論値．$N_\nu=2, 4$ の曲線も示してある[8]．

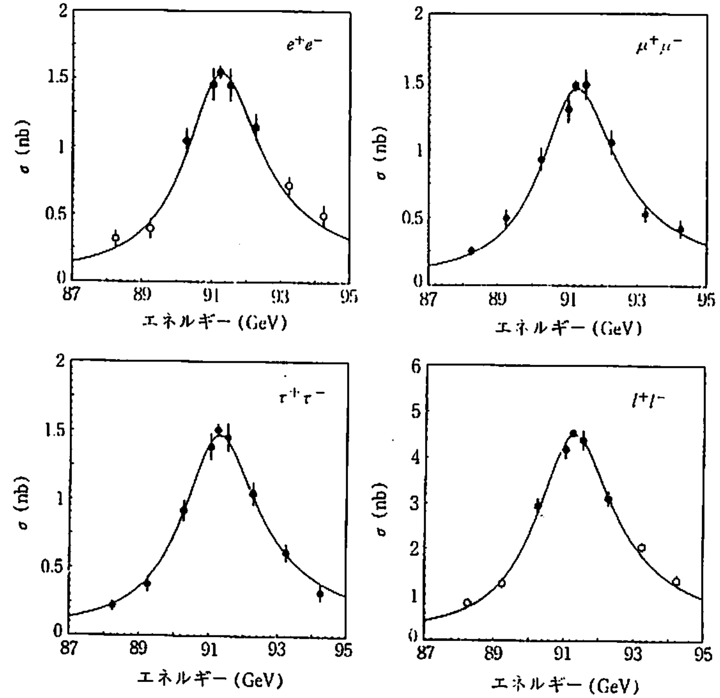

図 7.4 $e^+e^- \to Z \to l\bar{l}$ の全断面積[8]
実線は標準理論値 ($\sin^2\bar{\theta}_W=0.232$)

νe 散乱

$\nu_e e^-$

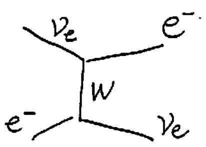

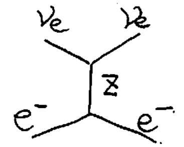

$\bar{\nu}_e e^-$

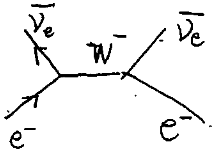

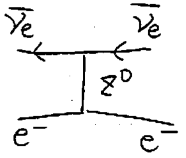

$\nu_\mu e^-$

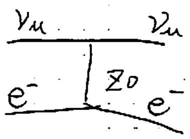

$\bar{\nu}_\mu e^-$

νP 散乱

例

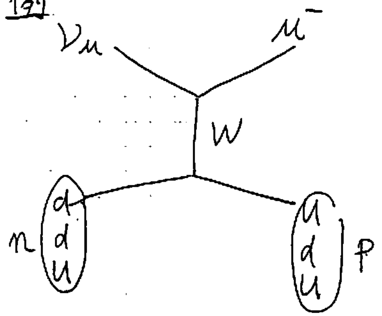

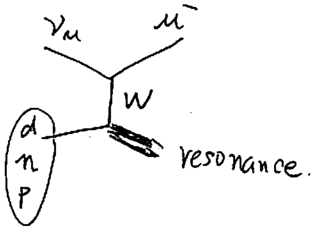

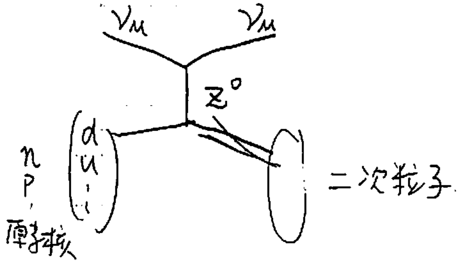

ν の mass

Charged lepton mass : 例 Higgs メカニズム

$$\mathcal{L} = \bigcirc(\overline{e_R}e_L + \overline{e_L}e_R)$$

↑ 係数 mass

これを Dirac massと言う

$$\underline{e_L \times e_R}$$

GWS modelでは、ν_L しか 相互作用をしない。

マヨラナ粒子

1、$(\gamma^\mu i\partial_\mu - m)N(x) = 0$ ディラック方程式

2、$N^c = N$

$$C = i\gamma^2\gamma^0 \quad N^c \equiv C\bar{\varphi}^T$$

$$N_1(x) = D\begin{bmatrix}\eta(x)\\ -i\sigma_2\eta(x)^*\end{bmatrix} \quad N_2(x) = D\begin{bmatrix}i\sigma_2\xi(x)^*\\ \xi(x)\end{bmatrix}$$

は、$N^c = N$をみたす。

ワイル表示で書くと

$$(\partial_0 + \sigma\cdot\nabla)\xi - m\sigma_2\xi^* = 0$$

$$(\partial_0 - \sigma\cdot\nabla)\eta + m\sigma_2\eta^* = 0$$

→ Dirac方程式 $i\frac{\partial\psi}{\partial t} = (\alpha\cdot P + \beta m)\psi$ で

ワイル表示

$$\alpha = \begin{bmatrix}-\sigma & 0\\ 0 & \sigma\end{bmatrix},\ \beta = \gamma^0 = \begin{pmatrix}0 & 1\\ 1 & 0\end{pmatrix}$$

$$\gamma^5 = \begin{pmatrix}-1 & 0\\ 0 & 1\end{pmatrix}$$

$m=0$として 平面波解 $\propto \exp(iP\cdot x - iEt)$

$$E\xi = \sigma\cdot P\xi \qquad \xi = \frac{\sigma\cdot P}{E}\xi \qquad \boxed{\text{右巻き}}$$

$$E\eta = -\sigma\cdot P\eta \qquad \eta = -\frac{\sigma\cdot P}{E}\eta \qquad \boxed{\text{左巻き}}$$

$\bar{\psi} = \psi^+\gamma^0$, $C = i\gamma^2\gamma^0$, $\sigma_1 = \begin{pmatrix}0 & 1\\ 1 & 0\end{pmatrix}$, $\sigma_2 = \begin{pmatrix}0 & -i\\ i & 0\end{pmatrix}$, $\sigma_3 = \begin{pmatrix}1 & 0\\ 0 & -1\end{pmatrix}$

adjoint spinor

ξ, η は右巻き,左巻きの粒子に対応。独立な解。

$\xi \to m_R$
$\eta \to m_L$ } 必ずしも等しくない。

$C\gamma^0\psi^* = C\bar{\psi}^T = \psi_c$
Bjorken-Drell
Relativistic Quantum Mechanics

マヨラナ粒子 N を $1 \pm \gamma^5$ による左右に分離

$$(N_L)^c = C\overline{N_L}^T = i\gamma^2\gamma^0\overline{N_L}^T = i\gamma^2\{(1-\gamma^5)/2\}N^*$$
$$= \{(1+\gamma^5)/2\}i\gamma^2\gamma^0\overline{N}^T = \left\{\frac{1+\gamma^5}{2}\right\}N^c = (N^c)_R$$

$$(N_L)^c = (N^c)_R = N_R$$

マヨラナ粒子には、粒子、反粒子の区別はなく、左巻き、右巻きの区別があるのみ。

C変換
P変換 } どちらも により 左巻き → 右巻きになる。

以上 マヨラナ粒子
~~マヨラナ質量~~

$m\,\overline{\psi^c_L}\,\psi_R$ → R粒子をLの反粒子に変える。

$m\,\overline{\psi^c}_R\,\psi_L$
↓
L粒子→Rの反粒子へ

荷電レプトンやクォークでは 荷電保存則により もたない。
ニュートリノ は可。
でもレプトン数 保存則 は OKか。

$$\nu_\mu + n \to \mu^- + p \qquad \nu_\mu + p \not\to \mu^+ n$$
$$\overline{\nu_\mu} + p \to \mu^+ + n \qquad \overline{\nu_\mu} + n \not\to \mu^- + p$$

弱相互作用の V−A 型という性質から
レプトン → 左巻き, 反レプトン → 右巻き が1対1対応

したがって ヘリシティ保存則をテストしているだけであって
レプトン数保存則というものが ないのかもしれない。
そうすると ニュートリノは $\overline{\psi^c_L}\psi_R$ や $\overline{\psi^c_R}\psi_L$ を持つことが可能となる。

$$-\mathcal{L} = \bar{\psi}i\gamma^\mu\partial_\mu\psi + m_D(\overline{\psi_L}\psi_R + h.c.)$$
$$+ \frac{m_L}{2}(\overline{\psi^c_R}\psi_L + h.c.) + \frac{m_R}{2}(\overline{\psi^c_L}\psi_R + h.c.)$$

2個のマヨラナ場を定義して

$$N_1 = \frac{\psi_L + (\psi_L)^c}{\sqrt{2}}, \quad N_2 = \frac{\psi_R + (\psi_R)^c}{\sqrt{2}}$$

$$-\mathcal{L} = \overline{N_1}i\gamma^\mu\partial_\mu N_1 + \overline{N_2}i\gamma^\mu\partial_\mu N_2$$
$$+ m_D(\overline{N_1}N_2 + \overline{N_2}N_1) + m_L\overline{N_1}N_1 + m_R\overline{N_2}N_2$$
$$= \overline{N_1}i\gamma^\mu\partial_\mu N_1 + i\overline{N_2}i\gamma^\mu\partial_\mu N_2 + (\overline{N_1}, \overline{N_2})\underbrace{\begin{bmatrix} m_L & m_D \\ m_D & m_R \end{bmatrix}}_{M}\begin{bmatrix} N_1 \\ N_2 \end{bmatrix}$$

M. neutrino mass matrix

いちばんおもしろいケース

シーソー メカニズム
質量行列を対角化して得られる2つの場を ν, N とすると
その固有質量をそれぞれ m_ν, m_N とする。

$m_L \simeq 0$, $m_R \gg m_D, m_L$ とすると

$$\nu \fallingdotseq N_1 - \frac{m_D}{m_R}N_2, \quad N \fallingdotseq N_2 + \frac{m_D}{m_R}N_1$$

$$m_\nu \fallingdotseq \ominus\frac{m_D^2}{m_R}, \quad m_N \fallingdotseq m_R$$

$\gamma^5\nu \to \nu$ とすると m の ⊖ は きえる

Neutrino oscillation

$$\begin{pmatrix}\nu_e\\ \nu_\mu\\ \nu_\tau\end{pmatrix} = M_{(3\times3)}\begin{pmatrix}\nu_1\\ \nu_2\\ \nu_3\end{pmatrix}$$

↳ weak interaction ↳ mass eigenstate

$$\begin{pmatrix}\nu_\alpha\\ \nu_\beta\end{pmatrix} = M\begin{pmatrix}\nu_1\\ \nu_2\end{pmatrix}$$

$$= \begin{pmatrix}\cos\theta & \sin\theta\\ -\sin\theta & \cos\theta\end{pmatrix}\begin{pmatrix}\nu_1\\ \nu_2\end{pmatrix} \qquad 0 \leqq \theta \leqq \frac{\pi}{4}$$

$$|\nu(t)\rangle = \nu_\alpha(t)|\nu_\alpha\rangle + \nu_\beta(t)|\nu_\beta\rangle$$

$$\nu_1(t) = e^{iE_1t}|\nu_1(0)\rangle,\quad \nu_2 = e^{iE_2t}|\nu_2(0)\rangle$$

t=0のとき

$$\nu(t=0) = \nu_1\times\cos\theta + \nu_2\times\sin\theta$$

初期状態

$$\nu_1(t) = e^{-iE_1t}|\nu_1(0)\rangle,\quad \nu_2(t) = e^{-iE_2t}|\nu_2(0)\rangle$$

$\begin{pmatrix}\nu_1\\ \nu_2\end{pmatrix} = \begin{pmatrix}\cos\theta & -\sin\theta\\ \sin\theta & \cos\theta\end{pmatrix}\begin{pmatrix}\nu_\alpha\\ \nu_\beta\end{pmatrix}$ を入れて

t秒後

$$|\nu(t)\rangle = e^{-iE_1t}|\nu_1(0)\rangle\cos\theta + e^{-iE_2t}|\nu_2(0)\rangle\sin\theta$$

$$= \left[e^{-iE_1t}\cos^2\theta + e^{-iE_2t}\sin^2\theta\right]|\nu_\alpha\rangle$$

$$+ \cos\theta\sin\theta\left[e^{-iE_2t} - e^{-iE_1t}\right]|\nu_\beta\rangle$$

$\sin2\theta = 2\cos\theta$ ...

$$P(\nu_\alpha\to\nu_\beta) = \langle\nu_\beta|\nu(t)\rangle^2 = \cos^2\theta\sin^2\theta\,\left|e^{-iE_2t} - e^{-iE_1t}\right|^2$$

$$= \frac{1}{4}\sin^2 2\theta\ \times$$

$$\left|e^{iE_2t} - e^{-iE_1t}\right|^2$$

$$= \left|e^{-iE_1t}\right|^2\left|e^{-i(E_2-E_1)t} - 1\right|^2$$

$$= 2\times\{1 - \cos(E_2-E_1)t]$$

$$|e^{ia}-1)^2$$

$$(e^{ia}-1)(e^{-ia}-1)$$

$$1+1-(e^{ia}+e^{-ia})$$

$$P(\nu_\alpha\to\nu_\beta) = \frac{1}{2}\sin^2 2\theta\left[1 - \cos(E_2-E_1)t\right)$$

$$E_i = \sqrt{m_i^2+p^2} \simeq p + \frac{1}{2}\frac{m_i^2}{p}$$

$$= \frac{1}{2}\sin^2 2\theta\left(1 - \cos\underbrace{\frac{m_2^2-m_1^2}{2p}\frac{c^3}{\hbar}t}\right)$$

$$\equiv \frac{2\pi L}{L_\nu}$$ → まより と書く。

$$L = ct$$

$$L_\nu = \frac{4\pi\hbar p}{(m_2^2-m_1^2)\,c^2}$$

$$= \frac{\overset{2.48}{\cancel{2.5}}\,p\,(\mathrm{MeV}/c)}{m_2^2-m_1^2\ (eV/c^2)^2}\ \text{meters}$$

$$= \frac{1}{2}\sin^2 2\theta\left(1 - \cos\frac{2\pi L}{L_\nu}\right)$$

$$= \sin^2 2\theta\,\sin^2\left(\frac{\pi L}{L_\nu}\right)$$

$$= \sin^2 2\theta\,\sin^2\left(1.27\,\underset{eV^2}{\Delta m^2}\,\underset{m}{L}\,/\,\underset{MeV/c}{p}\right]$$

I-26

$$L_\nu = \frac{2.48\ P\ (\mathrm{MeV}/c)}{m_2^2 - m_1^2\ (\mathrm{eV}/c^2)^2}\ \text{meters}$$

例

Δm^2	P	L_ν
$3\times10^{-3}\,\mathrm{eV}^2$	1 GeV	830 km
$1.7\times10^{-11}\,\mathrm{eV}^2$	1 MeV	1.5×10^{11} m

太陽 → 地球

$$P(\nu_\alpha \to \nu_\beta) = \sin^2 2\theta\ \sin^2\left(1.27\,\underset{\mathrm{eV}^2}{\Delta m^2}\,\underset{\mathrm{m}}{L}/\underset{\mathrm{MeV}}{E}\right)$$

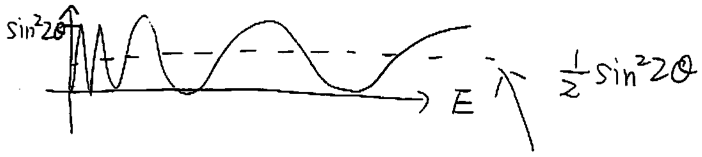

poor E resolution

No. 1

$$i\frac{d}{dt}\begin{pmatrix}\nu_\alpha\\ \nu_\beta\end{pmatrix} = i\frac{d}{dt}\begin{pmatrix}\cos\theta & \sin\theta\\ -\sin\theta & \cos\theta\end{pmatrix}\begin{pmatrix}\nu_1\\ \nu_2\end{pmatrix}$$

$$i\frac{d}{dt}|\nu_\alpha\rangle = i\frac{d}{dt}\left[\cos\theta\,|\nu_1\rangle + \sin\theta\,|\nu_2\rangle\right] \quad -①$$

$$i\frac{d}{dt}|\nu_\beta\rangle = i\frac{d}{dt}\left[-\sin\theta\,|\nu_1\rangle + \cos\theta\,|\nu_2\rangle\right] \quad -②$$

$$|\nu_1\rangle = e^{-iE_1t}\,|\nu_1\rangle$$

$$|\nu_2\rangle = e^{-iE_2t}\,|\nu_2\rangle$$

$$① \rightarrow\ i\frac{d}{dt}|\nu_\alpha\rangle = E_1\cos\theta\,|\nu_1\rangle + E_2\sin\theta\,|\nu_2\rangle$$

$$= E_1\cos\theta\left[\cos\theta\,|\nu_\alpha\rangle - \sin\theta\,|\nu_\beta\rangle\right] + E_2\sin\theta\left[+\sin\theta\,|\nu_\alpha\rangle + \cos\theta\,|\nu_\beta\rangle\right]$$

$$= \left[E_1\cos^2\theta + E_2\sin^2\theta\right]|\nu_\alpha\rangle + \left[E_2\sin\theta\cos\theta - E_1\sin\theta\cos\theta\right]|\nu_\beta\rangle$$

$$i\frac{d}{dt}|\nu_\beta\rangle = -E_1\sin\theta\,|\nu_1\rangle + E_2\cos\theta\,|\nu_2\rangle$$

$$= -E_1\sin\theta\left[\cos\theta\,|\nu_\alpha\rangle - \sin\theta\,|\nu_\beta\rangle\right] + E_2\cos\theta\left[\sin\theta\,|\nu_\alpha\rangle + \sin\theta\,|\nu_\beta\rangle\right]$$

$$= (-E_1+E_2)\sin\theta\cos\theta\,|\nu_\alpha\rangle + \left[E_1\sin^2\theta + E_2\sin^2\theta\right]\nu_\beta$$

No. 2

$$\begin{bmatrix} E_1\cos^2\theta + E_2\sin^2\theta & \sin\theta\cos\theta\left[E_2 - E_1\right] \\ \sin\theta\cos\theta\left[E_2 - E_1\right] & E_1\sin^2\theta + E_2\cos^2\theta \end{bmatrix}$$

$$\underbrace{\sin\theta\cos\theta}_{\frac{1}{2}\sin 2\theta}\ \underbrace{\left[E_2 - E_1\right]}_{\downarrow\ \frac{1}{2}\frac{\Delta m^2}{P}} = \frac{1}{4}\sin 2\theta \times \frac{\Delta m^2}{P}$$

$$\left[E_1\cos^2\theta + E_2\sin^2\theta\right] - \frac{1}{2}\left[E_1 + E_2\right]$$

$$\cos 2\theta = \cos^2\theta - \sin^2\theta$$

$$= 2\cos^2\theta - 1$$

$$= 1 - 2\sin^2\theta$$

$$= \frac{1}{2}E_1\left[2\cos^2\theta - 1\right] + \frac{1}{2}E_2\left[2\sin^2\theta - 1\right]$$

$$= \frac{1}{2}E_1\cos 2\theta - \frac{1}{2}E_2\cos 2\theta$$

$$= \frac{1}{2}\left[E_1 - E_2\right] \times \cos 2\theta$$

$$= -\frac{1}{4}\frac{\Delta m^2}{P}\cos 2\theta$$

Matter oscillationのために別の方法による導出

$$|\nu^\alpha\rangle_t = \sum_i U_{\alpha i} e^{-E_i t} |\nu^i\rangle .$$

α：interaction 固有状態
i：mass 固有状態

transition amplitude は

$$\boxed{\langle \nu^\beta | \nu^\alpha \rangle_t = \sum U_{\alpha i} (U^\dagger)_{i\beta} e^{-iE_i t}}$$

For $p = |\vec{p}| \gg m_i$

$$E_i = \sqrt{p^2 + m_i^2} \simeq p + \frac{m_i^2}{2p} \simeq p + m_i^2/2E$$

$$|\nu^\alpha\rangle_t \simeq e^{-ipt}\, U \begin{bmatrix} e^{-im_1^2 t/2E} & \\ & e^{-im_2^2 t/2E} \\ & & \ddots \end{bmatrix} U^\dagger |\nu^\beta\rangle$$

$$= e^{-ipt}\, U \begin{bmatrix} 1 - i\frac{m_i^2 t}{2E} + \cdots & \\ & \ddots \end{bmatrix} U^\dagger |\nu^\beta\rangle$$

$$\begin{pmatrix} m_1 & & \\ & \ddots & \\ & & m_n \end{pmatrix}$$

$$m = U\, m_{diag}\, U^\dagger$$

$$U^\dagger m^\dagger m U = m_{diag}^2 = \begin{pmatrix} m_1^2 & & \\ & m_2^2 & \\ & & \ddots \end{pmatrix},$$

$[U\, m_{diag}^2\, U^\dagger]^2 = U\, m_{diag}^4\, U^\dagger$
- - - - -
- - - - - のようになるから。

$$|\nu^\alpha\rangle_t = e^{-ipt} \left[e^{-i\frac{m^\dagger m}{2E} t} \right]_{\alpha\beta} |\nu^\beta\rangle \longrightarrow ①$$

i.e. $i\frac{d}{dt}|\nu^\alpha\rangle = \frac{m^\dagger m}{2E}|\nu^\alpha\rangle$ をみたす。

2ν case：$U = \begin{pmatrix} \cos\theta & \sin\theta \\ -\sin\theta & \cos\theta \end{pmatrix}$

$$m^\dagger m = U\, m_{diag}^2\, U^\dagger = \begin{pmatrix} m_1^2\cos^2\theta + m_2^2\sin^2\theta & \frac{1}{2}(m_2^2 - m_1^2)\sin 2\theta \\ \frac{1}{2}(m_2^2 - m_1^2)\sin 2\theta & m_1^2\sin^2\theta + m_2^2\cos^2\theta \end{pmatrix}$$

$$= \frac{m_1^2 + m_2^2}{2} + \frac{\Delta m^2}{2}\begin{pmatrix} -\cos 2\theta & \sin 2\theta \\ \sin 2\theta & \cos 2\theta \end{pmatrix}$$

$$\Delta m^2 = m_2^2 - m_1^2 .$$

$$\boxed{i\frac{d}{dt}\begin{pmatrix} \nu_\alpha \\ \nu_\beta \end{pmatrix} = \begin{pmatrix} -\frac{\Delta m^2}{4E}\cos 2\theta & \frac{\Delta m^2}{4E}\sin 2\theta \\ \frac{\Delta m^2}{4E}\sin 2\theta & \frac{\Delta m^2}{4E}\cos 2\theta \end{pmatrix}\begin{pmatrix} \nu_\alpha \\ \nu_\beta \end{pmatrix}}$$

をみたす。

$$① \rightarrow |\nu^\alpha\rangle_t = e^{-i\left(p + \frac{m_1^2 + m_2^2}{4E}\right)t} \Big[e^{-i\frac{\Delta m^2}{4E}\underset{\uparrow}{\sigma^a} r^a t} \Big]_{\alpha\beta} |\nu^\beta\rangle$$

Pauli matrix

$r^a = (\sin 2\theta, 0, -\cos 2\theta)$

$\sigma^1 = \begin{pmatrix} 0 & 1 \\ 1 & 0 \end{pmatrix}$ $\sigma^3 = \begin{pmatrix} 1 & 0 \\ 0 & -1 \end{pmatrix}$

$\sigma^2 = \begin{pmatrix} 0 & -i \\ i & 0 \end{pmatrix}$

$$\downarrow$$

$$|\nu^\alpha\rangle_t = e^{-i\left(p + \frac{m_1^2 + m_2^2}{4E}\right)t} \begin{pmatrix} \cos\frac{\Delta m^2}{4E}t - i\sin\frac{\Delta m^2}{4E}t\cos 2\theta & -i\sin\frac{\Delta m^2}{4E}t\sin 2\theta \\ -i\sin\frac{\Delta m^2}{4E}t\sin 2\theta & \cos\frac{\Delta m^2}{4E}t + i\sin\frac{\Delta m^2}{4E}t\cos 2\theta \end{pmatrix} |\nu_\beta\rangle$$

$$P_{\nu_\alpha \to \alpha_\beta} = |\langle \nu^\alpha | \nu^\beta \rangle|^2$$

$$= \sin^2 2\theta \times \sin^2\frac{\Delta m^2}{4E}t = \sin^2 2\theta \cdot \sin^2\left(\frac{\pi L}{L_\nu}\right)$$

$$L_\nu = \frac{4\pi E}{\Delta m^2}$$

ν - matter oscillation (Mikheyev, Smirnov, Wolfenstein)

ν_e

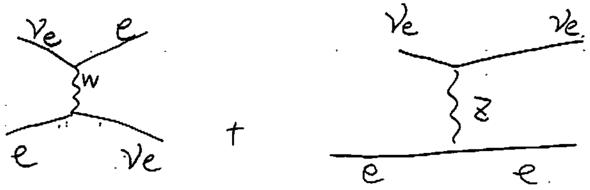

$\nu_\mu(\nu_\tau)$

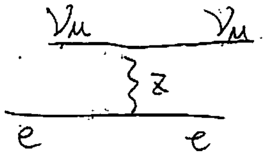

νが感じる potential がちがう。

$$\sqrt{2}\,G_F n_e$$

$$i\frac{d}{dt}\begin{pmatrix}\nu_e\\ \nu_\mu\end{pmatrix} = \begin{pmatrix} -\frac{\Delta m^2}{4E}\cos 2\theta + \sqrt{2}G_F n_e & \frac{\Delta m^2}{4E}\sin 2\theta \\ \frac{\Delta m^2}{4E}\sin 2\theta & \frac{\Delta m^2}{4E}\cos 2\theta \end{pmatrix}\begin{pmatrix}\nu_e\\ \nu_\mu\end{pmatrix}$$

$\begin{pmatrix}1&0\\0&1\end{pmatrix}$ の倍数をひいて traceless にする。

$$\begin{pmatrix} -\frac{\Delta m^2}{4E}\cos 2\theta + \frac{G_F n_e}{\sqrt{2}} & \frac{\Delta m^2}{4E}\sin 2\theta \\ \frac{\Delta m^2}{4E}\sin 2\theta & \frac{\Delta m^2}{4E}\cos 2\theta - \frac{G_F n_e}{\sqrt{2}} \end{pmatrix}\begin{pmatrix}\nu_e\\ \nu_\mu\end{pmatrix}$$

$$\begin{pmatrix}\nu_{1m}\\ \nu_{2m}\end{pmatrix} = \begin{pmatrix}-\cos\theta_m & -\sin\theta_m\\ \sin\theta_m & \cos\theta_m\end{pmatrix}\begin{pmatrix}\nu_e\\ \nu_\mu\end{pmatrix}$$ と考えると

$$\begin{pmatrix} -\frac{\Delta m^2}{4E}\cos 2\theta_m & \frac{\Delta m^2}{4E}\sin 2\theta_m \\ \frac{\Delta m^2}{4E}\sin 2\theta_m & \frac{\Delta m^2}{4E}\cos\theta_m \end{pmatrix}$$

effective mixing angle

$$\tan 2\theta_m = \sin 2\theta \,/ (\cos 2\theta - l_\nu/l_0)$$

$$l_\nu = 4\pi E/\Delta m^2 ,\quad l_0 = 2\pi/\sqrt{2}\,G_F N_e = 1.6\times 10^7 m/\rho$$

$$\rho = N / 6\times 10^{23} \text{ Avogadro's \# } / \text{cm}^3$$

$$\sin^2 2\theta_m = \frac{\sin^2 2\theta}{\sin^2 2\theta + (L_\nu/L_0 - \cos 2\theta)^2}$$

$L_\nu/L_0 = \cos 2\theta$ のとき、$\sin^2 2\theta_m \simeq 1$ になる。

$$L_m = \frac{L_\nu}{\sqrt{1 - 2\left(\frac{L_\nu}{L_0}\right)\cos 2\theta + \left(\frac{L_\nu}{L_0}\right)^2}}$$

$P(\nu_e \to \nu_e) = 1 - \sin^2 2\theta_m \sin^2(\pi L/L_m)$ と書ける。

$\frac{L_\nu}{L_0} \simeq \cos 2\theta$ のとき

$$\frac{L_\nu}{\sqrt{1 - 2\cos^2 2\theta + \cos^2 2\theta}}$$

$$= \frac{L_\nu}{\sqrt{1 - \cos^2 2\theta}}$$

$$L_m = \frac{L_\nu}{\sin 2\theta}$$

$\bar{\nu}$ では、$\sqrt{2}G_F n_e$ の factor の sign がかわるため、

$\sin^2 2\theta_m$ は enhance はされない。

n_e：密度が変化する所における matter oscillation

H. Bethe による analysis

$$i\frac{d}{dt}|\nu^\alpha\rangle_t = \frac{m^+ m}{2E}|\nu^\alpha\rangle + \begin{pmatrix}\sqrt{2}G_F n_e & 0\\ 0 & 0\end{pmatrix}$$

mass eigenstate　　$A = 2\sqrt{2}E\,G_F n_e$

$$m_{\frac{1}{2}}^2 = \frac{1}{2}(m_1^2 + m_2^2 + A) \mp \frac{1}{2}\sqrt{(A - \Delta m^2\cos 2\theta)^2 + (\Delta m^2)^2\sin^2 2\theta}$$

$\Delta m^2 = m_2^2 - m_1^2$

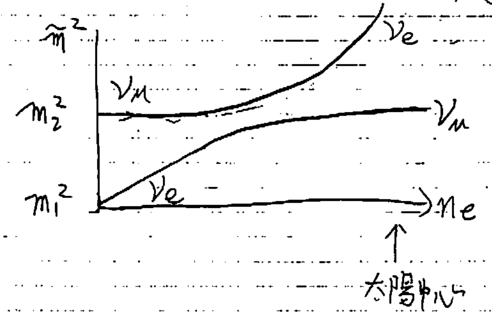

adiabatic case

Smirnov による Graphic representation

$$\vec{\nu}\,(\mathrm{Re}\,\nu_e^+\nu_\mu,\ \mathrm{Im}\,\nu_e^+\nu_\mu,\ \nu_e^+\nu_e - \tfrac{1}{2})$$

$$\vec{B} = \frac{2\pi}{l_m}(\sin 2\theta_m, 0, \cos 2\theta_m)$$

↑ oscillation length in medium

$$i\frac{d\nu}{dt} = \left(\frac{M^2}{2E} + V_f\right)\nu$$ は、

$$\frac{d\vec{\nu}}{dt} = (\vec{B}\times\vec{\nu})$$ となる。

$$P \equiv \nu_e^+\nu_e = \nu_z + \frac{1}{2} = \cos^2\frac{\theta_z}{2}$$

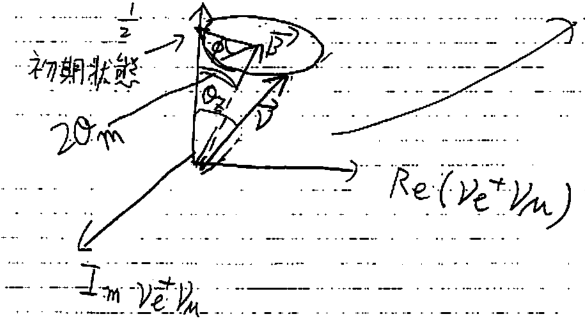

Vacuum oscillation で θ_n が小さい。

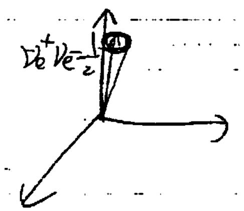

$$1 - \sin^2 2\theta\,\sin^2\left(\frac{\pi L}{L_\nu}\right)$$

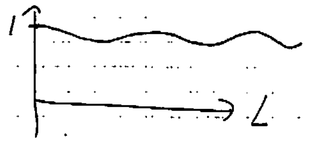

$\theta_m = 45°$

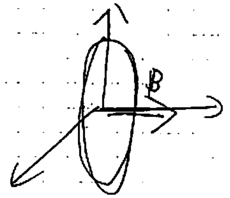

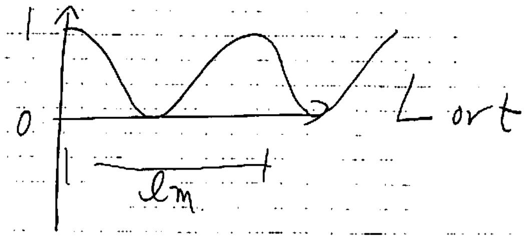

変化する ρ での oscillation.

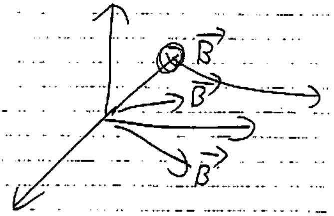

→ φの回転速度

$\phi \equiv (H_2 - H_1)\, t$

↖ ハミルトニアンのちがい。
m^2のちがい.

$\ell_m = 2\pi / \Delta H$

の変化 $\propto \dfrac{1}{\ell_m}$

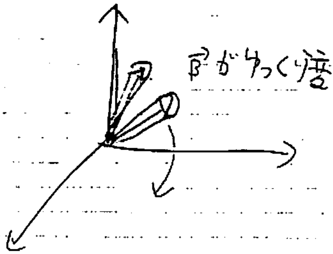

βがゆっくり変化する。

Δm [illegible]

$$\boxed{|\dot{\theta}_m| \ll |H_2 - H_1|}$$

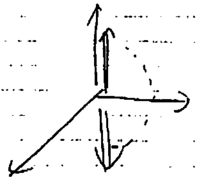

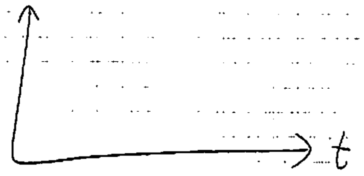

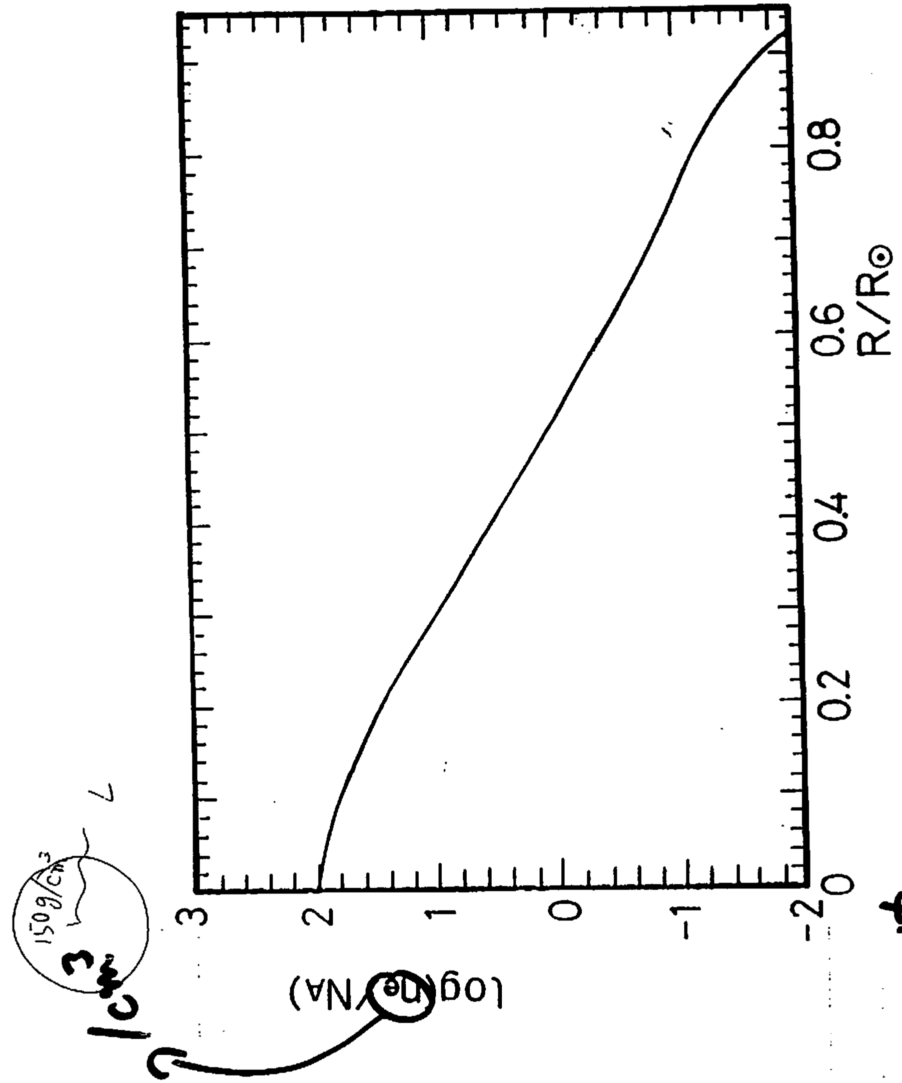

Fig. 1.10

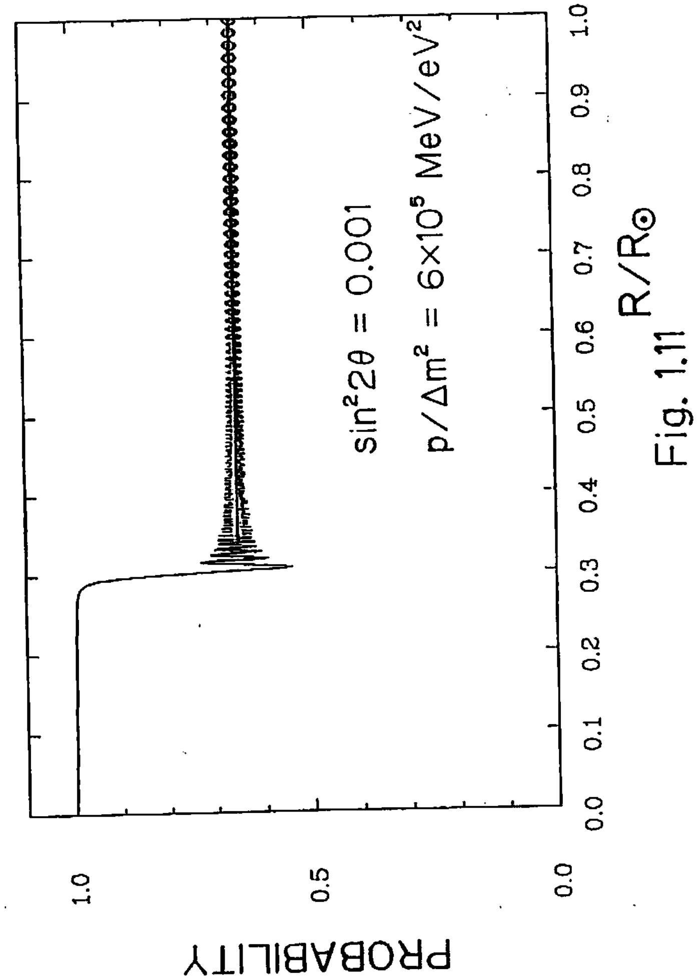

Fig. 1.11

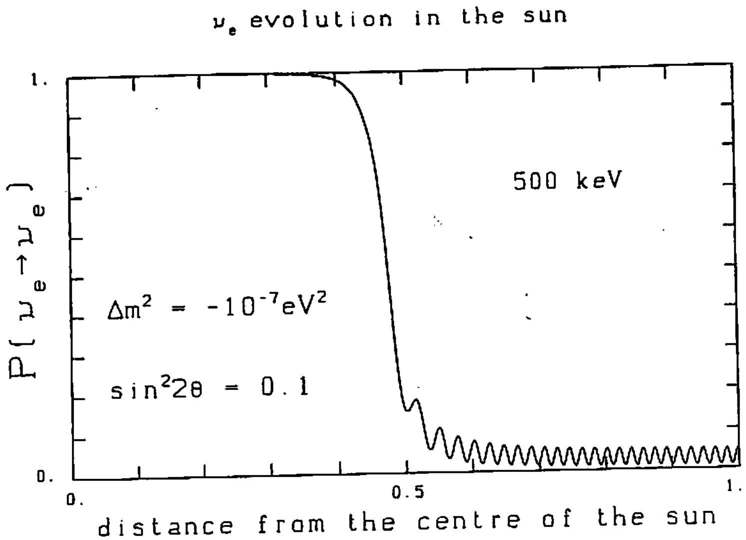

Fig. 4

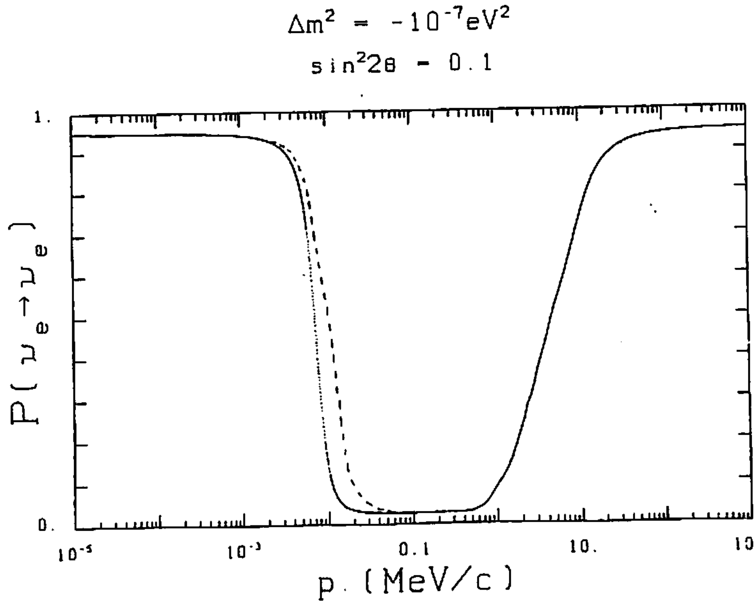

Fig. 5

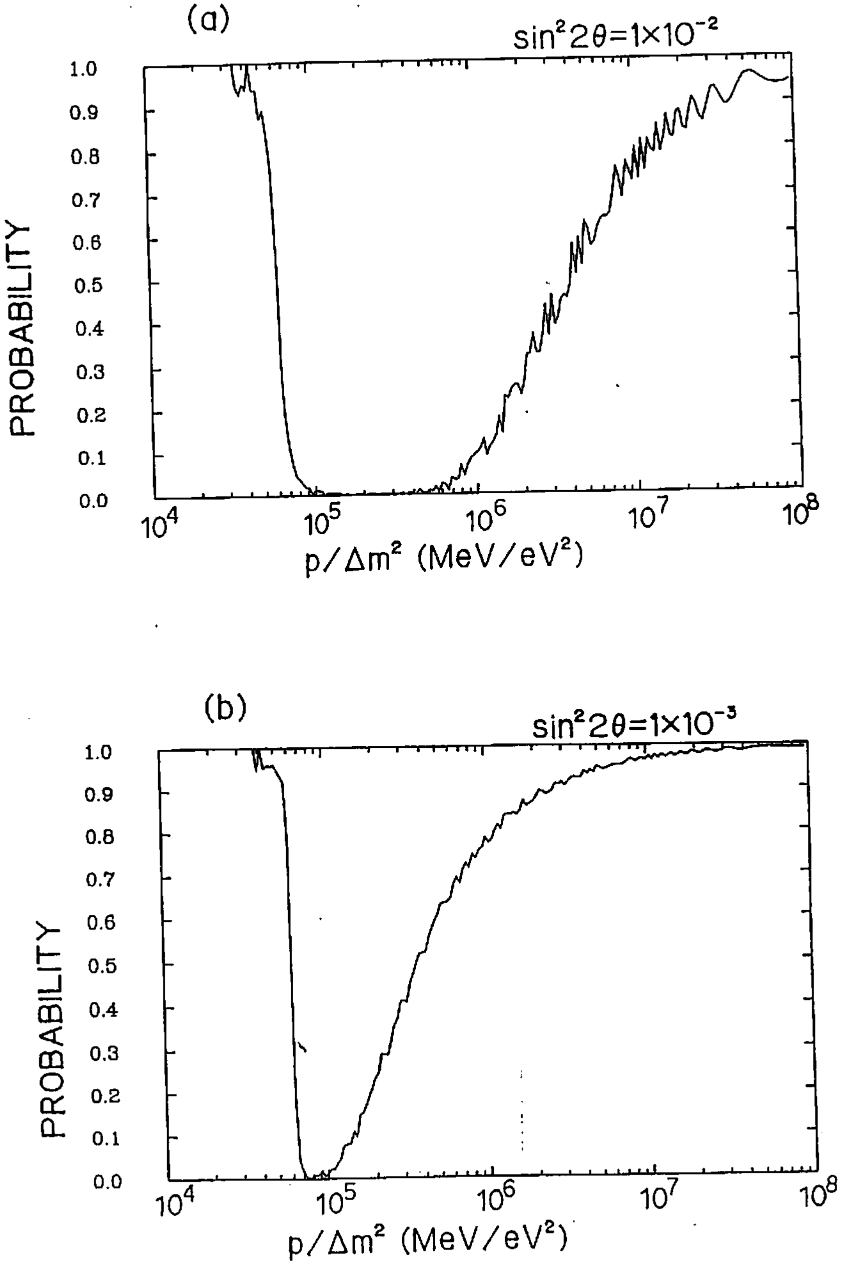

Fig. 1.12

νmass experiment

νmassの直接測定実験

$$T \to {}^3He^+ + e^- + \overline{\nu_e}$$

$$E_0 = 18.6\text{keV}, \quad \tau_{\frac{1}{2}} = 12\text{yr}.$$

$$\frac{dN}{dE} = \text{const} \times P \times E(E_0 - E)^2 \times \left(1 - \frac{m_\nu^2 C^4}{(E_0 - E)^2}\right)^{-\frac{1}{2}}$$

near the end point

$$\frac{dN}{dE} \sim (E_0 - E)^2 - m_\nu^2 C^4 / 2$$

Kurie plot

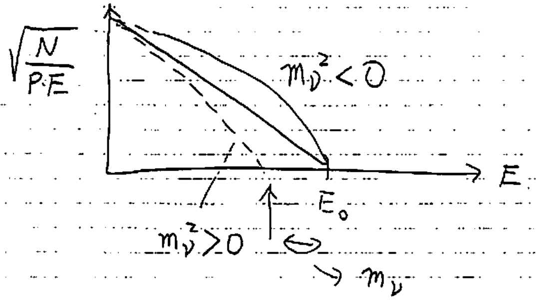

M_ν^2 from Tritium Beta Decay Measurements

M_ν limit (95% C.L.)

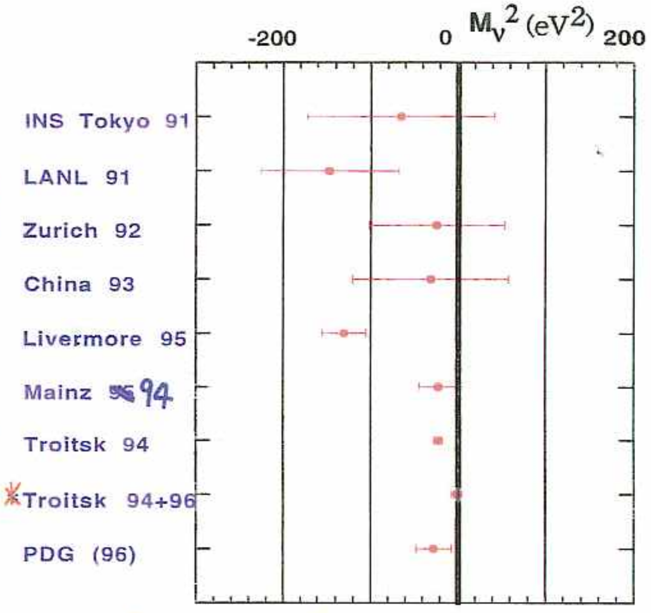

magnetic spectro-meter

⇑

⇓

electro-static

13.1

9.3

11.7

12.4

7

5.6

4.35

3.5

*) Accounting for anomaly

INS Tokyo 91 : $-65\pm85\pm65$ eV^2 , Phys. Lett. B256, 105 (1991).
LANL 91 : $-147\pm68\pm41$ eV^2 , Phys. Rev. Lett. 67, 957 (1991).
Zurich 92 : $-24\pm48\pm61$ eV^2 , Phys. Lett. B287, 381 (1992).
China 93 : $-31\pm75\pm48$ eV^2 , CJNP 15, 261(1993).
Livemore 95 : $-130\pm20\pm15$ eV^2 , Phys. Rev. Lett. 75, 3237 (1995).
Mainz 95 : $-22\pm17\pm14$ eV^2 , Neutrino 96.
Troitsk 94 : -22 ±4.8 eV^2 ,Phys. Lett. B350, 263 (1995).
Troitsk 94+96 : -1 ±6.3 eV^2 ,Neutrino 96.
PDG (96) : -27 ± 20 eV^2 ,Average by Particle Data Group, Phys. Rev. D54, 280 (1996).

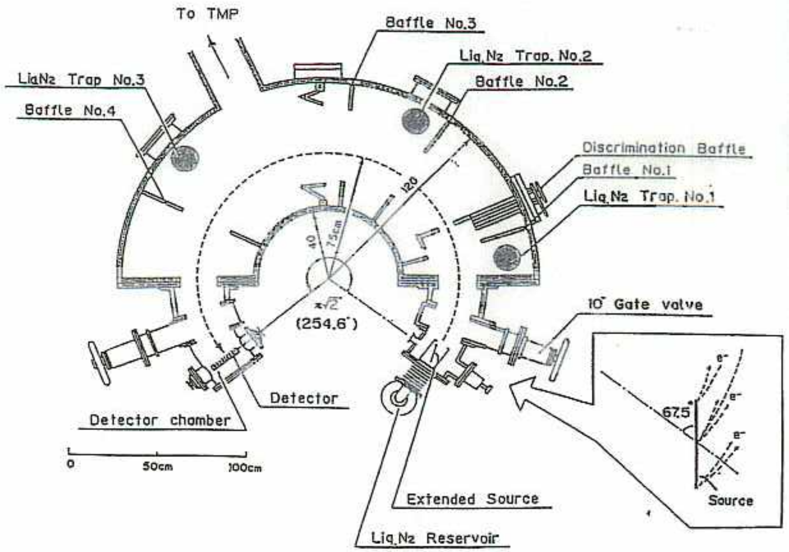

Figure 14: Schematic top view of the INS $\pi\sqrt{2}$ spectrometer.

calculation was performed for the latter case up to 3rd order approximation and the tilt angles were determined to be 67.6° for the source and 4.2° (almost normal incidence) for the detector [87]. The calculation was confirmed by measurements of iso-aberration contours for three different momenta of $\Delta p/p = 0\%$ and $\pm1.5\%$ with the use of the ^{207}Bi K-conversion line (975 keV). From this study, a baffle slit of $\Delta p/p = 0.01\%$ (FWHM) was designed for the wide extended source and expected line shapes were calculated [88].

The applicability of the non-equipotential method was tested with the use of 5 narrow ^{109}Cd strip sources, each separated 45.5 mm along the source plane with the tilt angle of 67.5°. With the optimized potentials on the individual sources, 5 separated K-line (62 keV) peaks without potential (Fig.15(a)), were well unified into one (Fig.15(b)). The dotted histogram in Fig.15(c) is a sum of the five spectra added by lining up their peak positions and the solid histogram is the spectrum observed with the potentials; no appreciable difference was found. It worked quite satisfactorily with an accuracy of 5×10^{-5} in momentum [89], much better than the required precision.

The non-equipotential was formed by source electrodes and an electrode cage surrounding the extended source as shown in Fig.16, where the exit side of the cage was kept at the ground potential. The 500 μm wide electrodes were vertically printed at every 45 mm interval on a surface of a high purity alumina substrate plate with high-resistive RuO$_2$ coating . Optimized electric voltage applied on the source electrodes exhibited an approximately parabolic distribution just as predicted by the orbit calculation.

Dire

Fig sour the sum solid

Fig whi

e third
:tively.
of the
(taken

181.7
: 170.1
: 180.6
± 165.5
±380.7

ıfers to
.etector
adratic
:rs thus
/pically
keV.
; neigh-
ı have a
he *FSS*
:o those
d in the
ropriate

ıe corre-
a,b) and
rve, and
dividual
ι. Using
not only
ained by
lting m_ν^2

nd *SUO*
shift the
FSS was
Arafune
basis set
and final
phasized
f. [42], ω_i

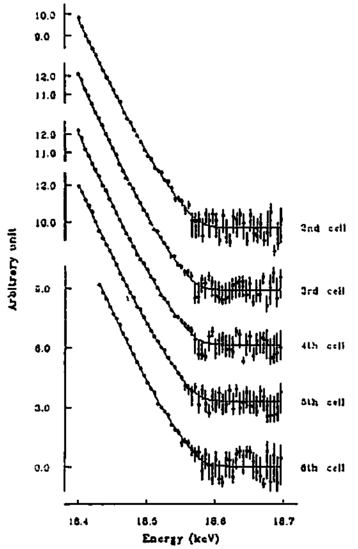

Figure 20: Observed data and the best fit curves are shown for the energy region from 18.4 to 18.7 keV in the form of Kurie plots. The detection efficiency η was corrected for and overlapping data were summed up in the figure. (taken from ref. [27].)

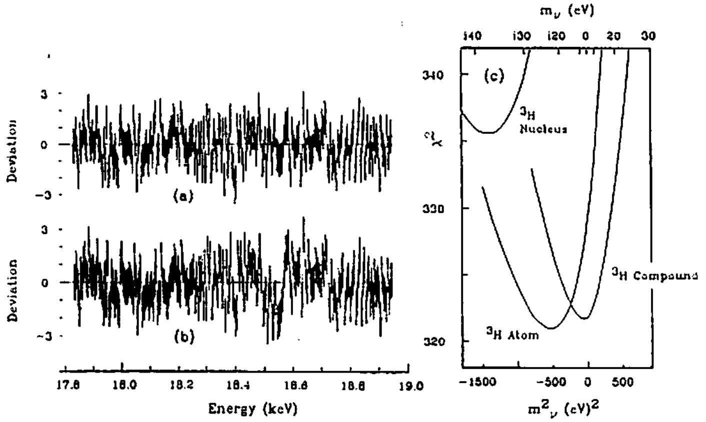

Figure 21: Deviation of the data from the fit divided by the error on each data point, and the relation between χ^2 and m_ν^2 for the case of the fourth cell. (a) shows the best fit case for all eight free parameters including the m_ν^2. (b) The case for the seven free parameters with m_ν^2 fixed at (30 eV)^2. (c) shows χ^2 obtained as a function of m_ν^2 for the full fit to seven free parameters, assuming the *FSS* for the ^{3}H nucleus, ^{3}H atom, and ^{3}H compound as calculated by ref. [41]. (taken from ref. [27].)

ents. The
· a 100 eV
unts. The
individual

[27]

ıg.

30

ıte
)₂)₂Cd
n

40

tr.
o. ctr.
e div.)

150K

1
1.0(sys.)

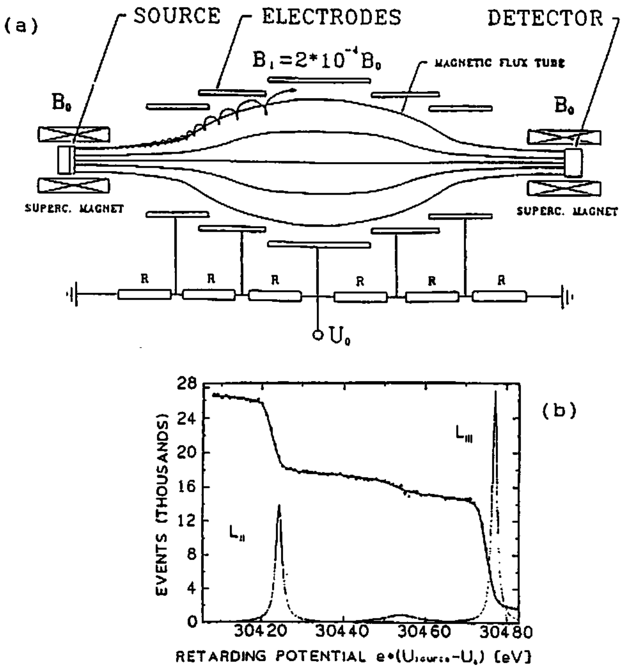

Figure 9: (a) Schematic view of the Mainz spectrometer. (b) Observed integrated spectrum of L conversion lines of ^{83m}Kr. (taken from A. Picard et al. [75])

rather than a differential spectrum, was measured in this way. The sharpness of this discrimination (see Fig. 9(b)) determined the energy resolution, which was given by $\Delta E = (B_1/B_0)E$; $\Delta E =$ (a few) eV was obtained by differentiating the observed spectra of ^{83m}Kr conversion lines. The spectrometer provided a large solid angle of $\Omega/4\pi = 40\%$ because only the solenoidal coil is a limiting factor and the acceptable polar angle is $\leq 78^o$. The signal-to-noise ratio was 1 : 1 at 30 eV below E_0.

The first result has been published in 1993 as

$$m_\nu^2 = -39 \pm 34(\text{stat.}) \pm 15(\text{sys.}) \quad (\text{eV})^2, \tag{21}$$

or $m_\nu < 7.2$ eV with 95% C.L, and $E_0 = (18,574.8 \pm 0.6)$ eV. A χ^2 fit was carried out by changing the lower limit (E_{low}) of the fitting energy interval with five free parameters, A_0, E_0, m_ν^2 and two parameters representing the background, and also with four free parameters by fixing α_1 to be the pre-determined value of $(6.7 \pm 1.7) \times 10^{-5}$ (eV)$^{-1}$. A significant dependence of m_ν^2 and E_0 on $E_{\rm low}$ was found: m_ν^2 were distributed around -100 (eV)^2 with statistical uncertainty of ±20

Solenoid retarding spectrometer

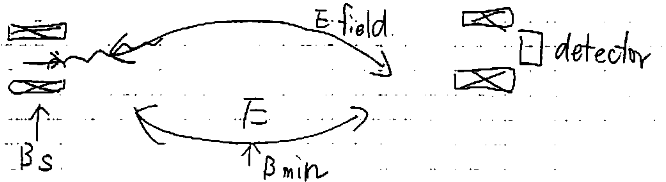

adiabatic : guiding field の relative change が cyclotron orbit よりも小さい。

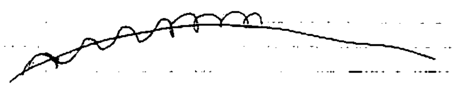

・ 角運動量 $\vec{\mu}$ は保存する。

・ $-\vec{\mu}\cdot\vec{B} = E_\perp$ transverse energy は 中心に行く ほど 弱くなる。すべての energyが $E_{//}$ に向く。

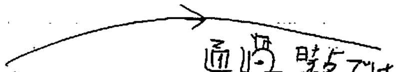

通過時点では ほとんど $E_{//}$

だから energyの resolutionは、

$$\delta E = E \times \frac{B_{min}}{B_S}$$ となる。

$\uparrow$ 18.6keV $\quad$ $\uparrow$ $\sim \frac{1}{3000}$

〜 数 ~~m~~eVの resolution。

Troitzk , Mainz の 実験

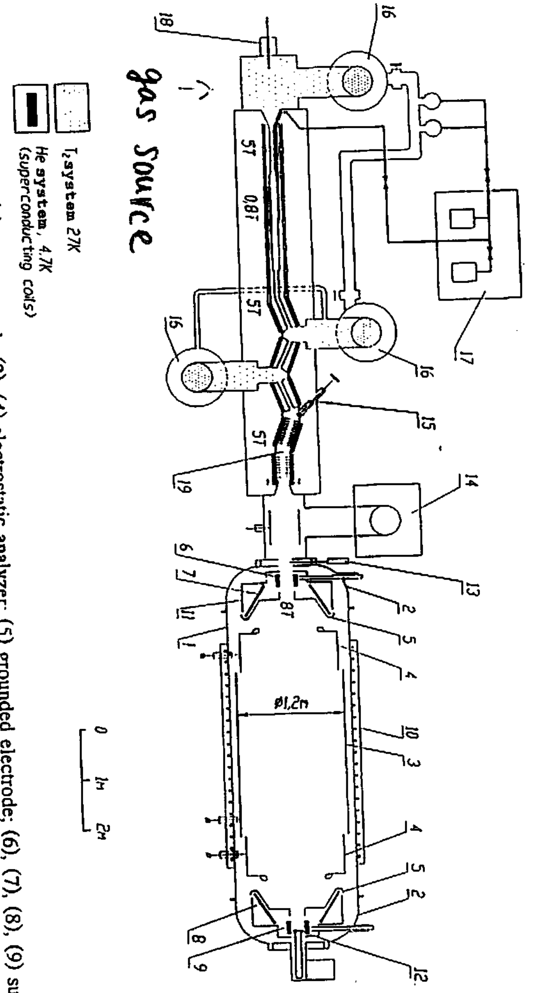

Fig. 1. Experimental setup. (1), (2) vacuum tank; (3), (4) electrostatic analyzer; (5) grounded electrode; (6), (7), (8), (9) superconducting solenoids; (10) warm coil; (11) liquid-N_2 jacket; (12) detector; (13) fast shutter; (14) Ti-pump; (15) cold valve; (16) Hg diffusion pump; (17) T_2 purification system; (18) electron gun; (19) argon pump.

Troitzk

T-41

Mainz Neutrino Mass Experiment since 1997

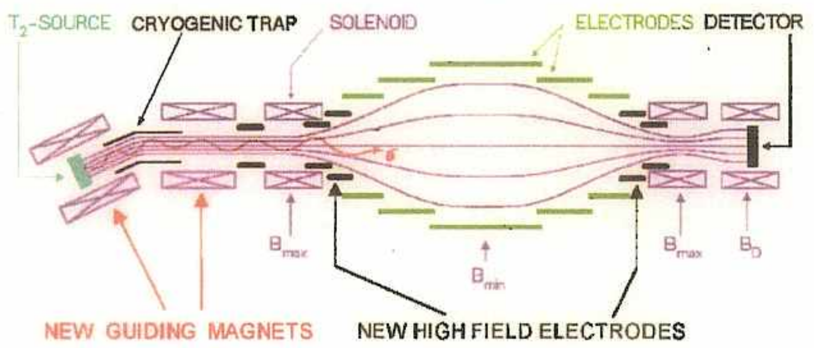

Magnetic Adiabatic Collimation + Electrostatic Filter (MAC–E–Filter)

⇒ sharp integrating transmission function without tails:

$\Delta E = E \cdot B_{min}/B_{max} = E \cdot A_{s,eff}/A_{analysis} \approx 4.8\mathrm{eV}$

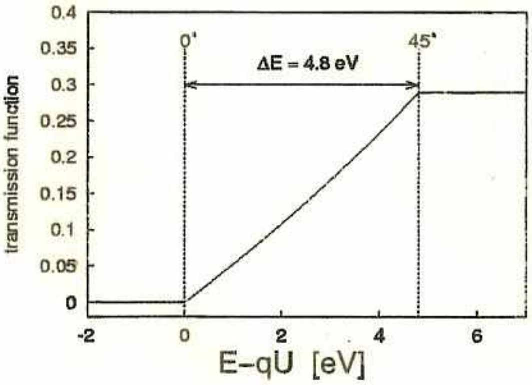

T-40

The Troitsk Neutrino Mass Experiment

Gaseous T_2 source

MAC–E–Filter

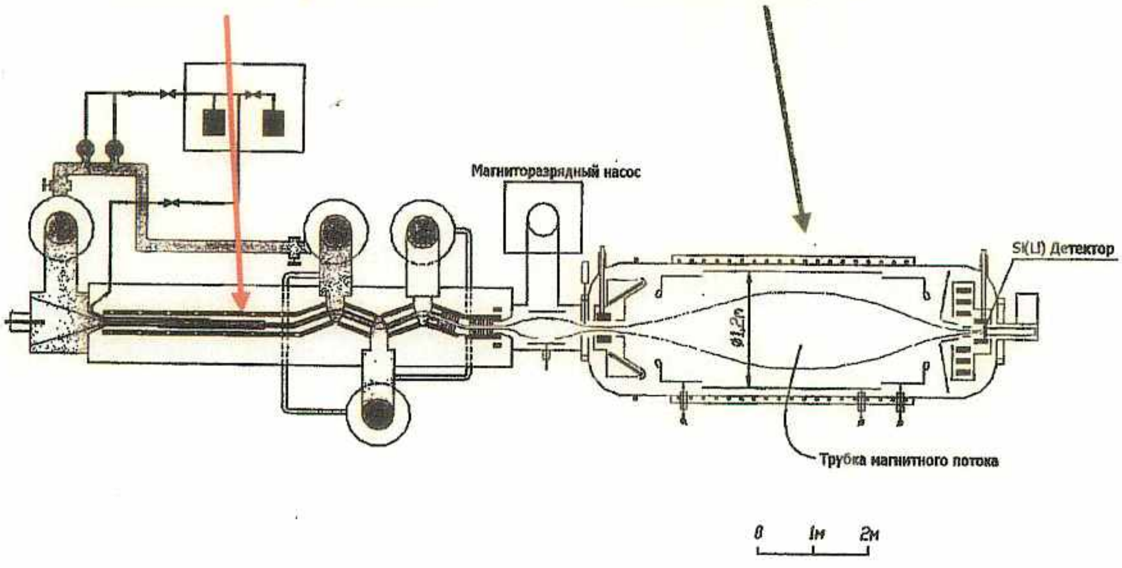

column density: 10^{17} cm^{-2}

luminosity: L = 0.6cm^2

($L = \Delta\Omega/2\pi * A_{source}$)

energy resolution: $\Delta E = 3.5\mathrm{eV}$

3 electrode system in 1.5m

diameter UHV vessel ($p<10^{-9}$ mbar)

Results of 1998/1999, 2001 data

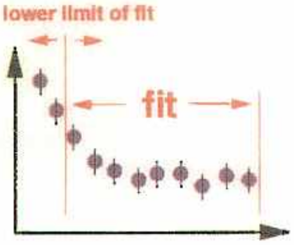

(see poster E2)

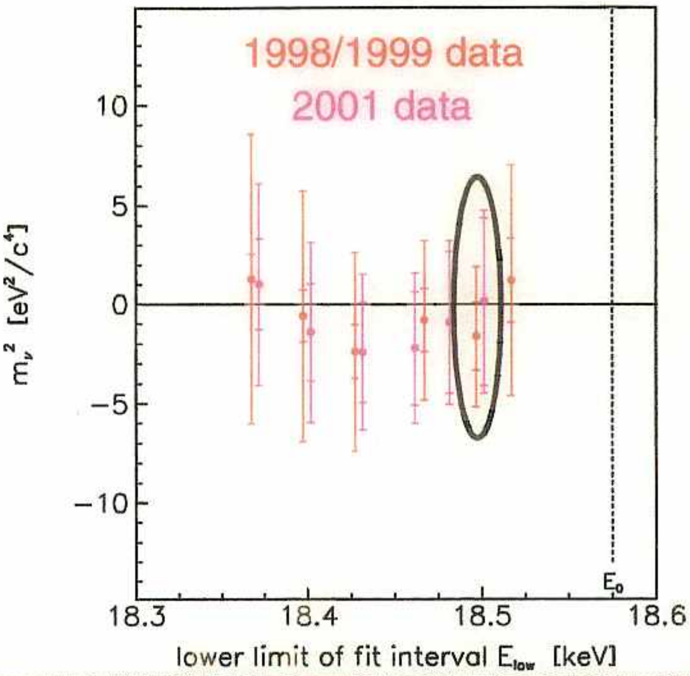

1998/1999: $m^2(\nu) = -1.6 \pm 2.5 \pm 2.1$ eV² ⇒ m(ν)< 2.2 eV (95% C.L.)

2001: $m^2(\nu) = +0.1 \pm 4.2 \pm 2.0$ eV²

1998/1999/2001: $m^2(\nu) = -1.2 \pm 2.2 \pm 2.1$ eV² ⇒ m(ν)< 2.2 eV (95% C.L.)

⇒ **Mainz sensitivity limit reached, final analysis of all Mainz data soon**

Mainz data of 1998,1999

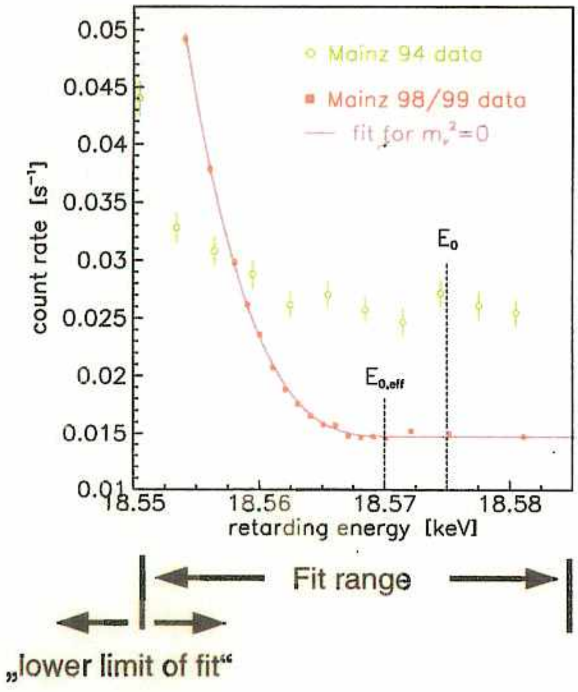

1998+1999: Signal/background 10 x higher

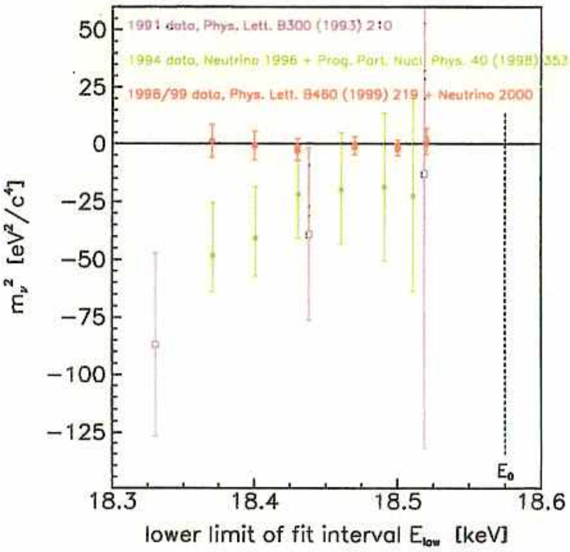

1998+1999: roughening transition avoided by T < 2 K

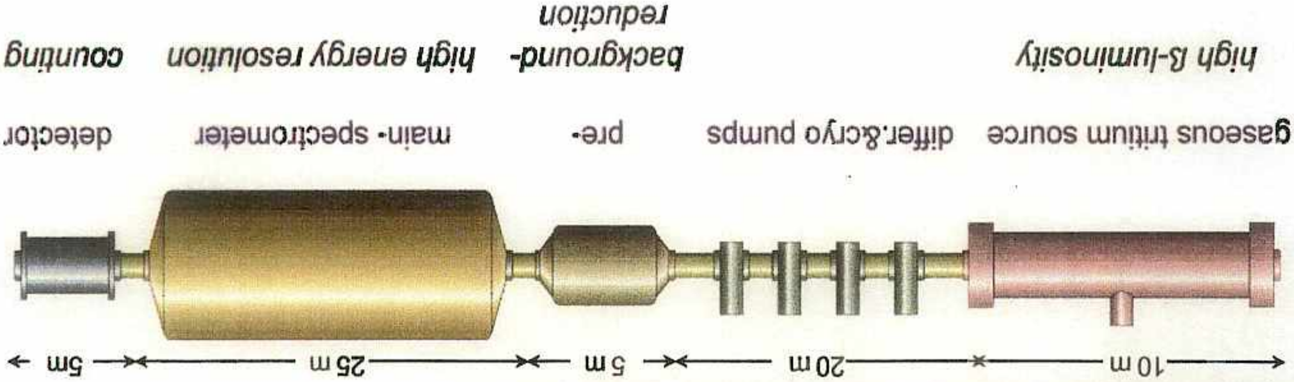

KATRIN Layout

KATRIN will be located on the site of FZK at *Tritium Laboratory Karlsruhe*

TLK is worldwide unique, for ITER tritium fuel cycle

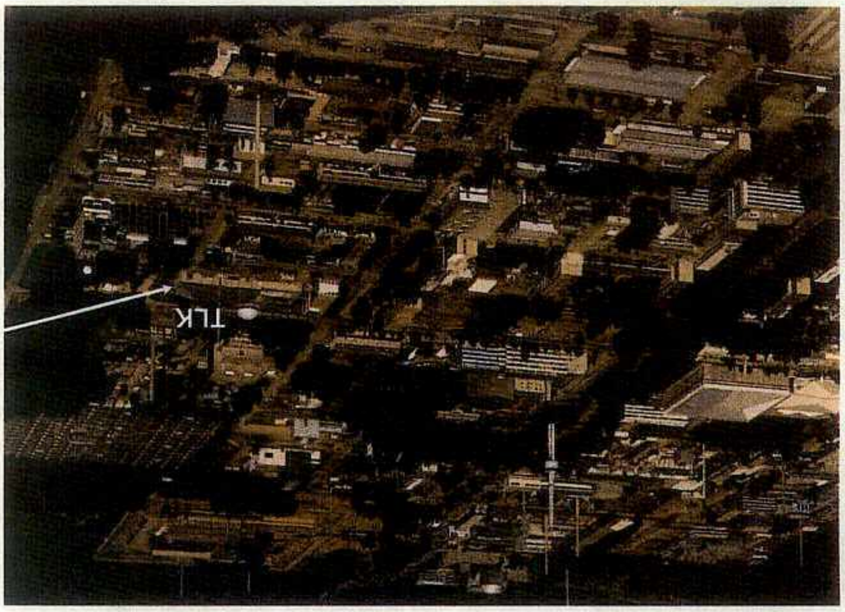

---

scaling factors for next-generation experiment

experimental observable in ß-decay is m_ν^2

aim : improve m_ν by one order of magnitude (2 eV → 0.2 eV)

requires : improve $\acute{m}_\nu^2$ by two orders of magnitude (4 eV^2 → 0.04 eV^2)

problem : count rate close to ß-end point drops very fast (~δE^3)

last 10 eV : 2 x 10^{-10} / last 1 eV : 2 x 10^{-13} of total ß-activity

- improve statistics :
- stronger tritium source (factor 80) (& larger analysing plane, Ø=10m)
- longer measuring period (~100 days → ~1000 days)
- improve energy resolution :
- large electrostatic spectrometer with ΔE=1 eV (factor 4 improvement)
- reduce systematic errors :
- better control of systematics, energy losses (reduce to less than 1/10)

electrostatic spectrometers: *tandem design*

electrostatic pre-filtering & analysis of **tritium ß-decay electrons**

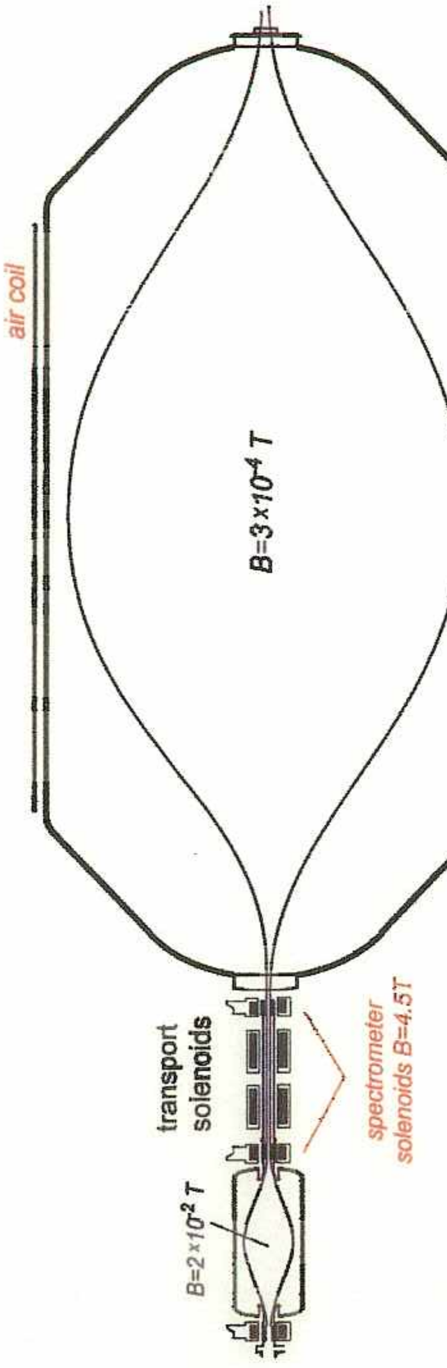

main spectrometer
variable retarding potential 18.5-18.6 kV
Ø = 10 m / L = 22 m
ΔE = 1 eV

pre-spectrometer
fixed retarding potential 18.5-18.6 kV
Ø = 1.7 m / L = 3.5 m
ΔE = 70 eV

ν_μ mass measurement K. Assamagan, Phys. Rev. D 53 (1996) 6065.
PSIの, Switzerland.

$\pi^+ \to \mu^+ \nu_\mu$

105.658389 ± 0.000034 MeV

(139.56995 ± 0.00035) MeV

spectrometerで μ^+の momentumをはかる。

$P_{\mu^+} = 29.79200 \pm 0.00011$

$m_{\nu_\mu}^2 = (-0.016 \pm 0.023)$

$m_{\nu_\mu} <$ 0.17 MeV (90% C.L.)

ν_τ mass measurement

$e^+ + e^- \to \tau^+\tau^-$

τの mass : $1777 \pm^{0.30}_{0.27}$ MeV

なるべく多くの π へ行く modeを使う。

$\pi^\pm$ 139.6 MeV

$\tau \to 5\pi^\pm(\pi^0)\nu_\tau$

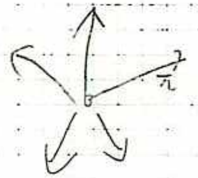

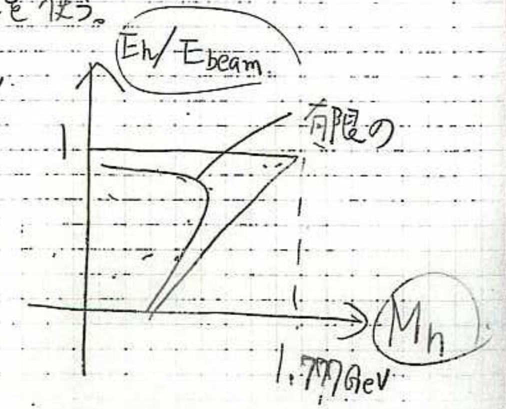

ν_τ mass limit from ALEPH

(M. Girone, PA10, 1003)

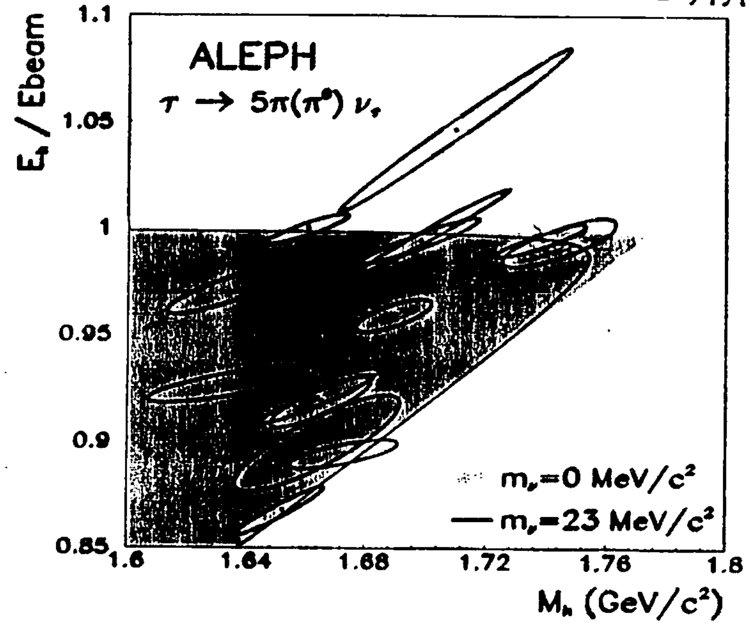

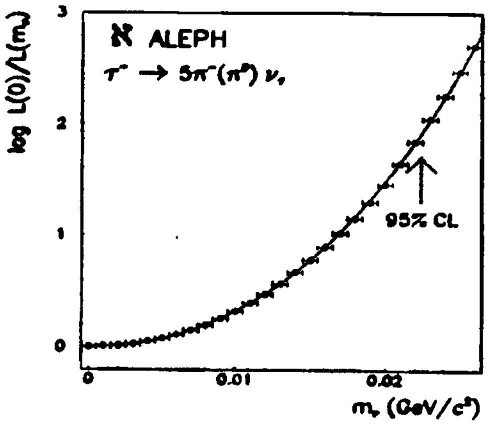

$5\pi^\pm(\pi^0)\nu_\tau$: $m_\nu < 22.3$ MeV/c^2 @ 95% C.L.

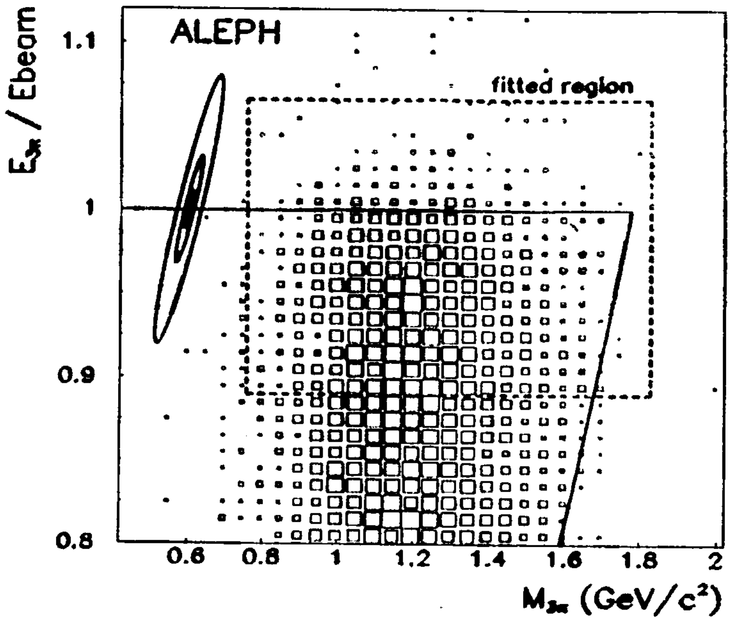

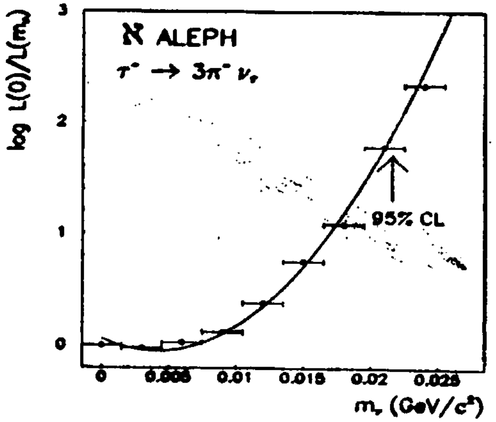

$3\pi^\pm\nu_\tau$: $m_\nu < 21.5$ MeV/c^2 @ 95% C.L.

Combine $5\pi^\pm(\pi^0)$ and $3\pi^\pm\nu_\tau$

$\underline{m_{\nu_\tau} \leq 18.2 \text{ MeV}/c^2}$ at 95% C.L.

Double ββ decay

原子核の binding energy の負
あるAに着目して

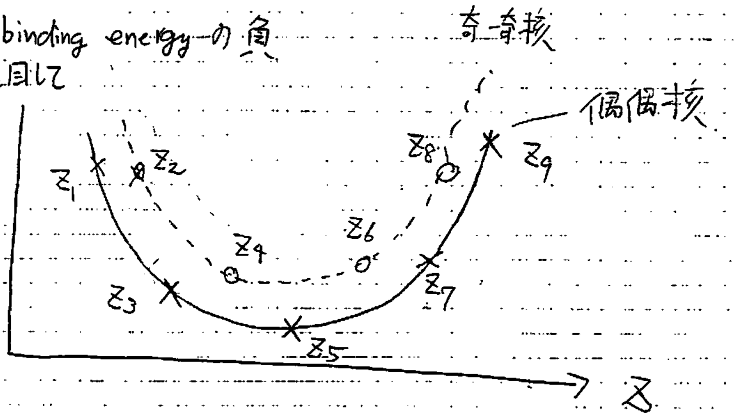

$Z_2 \to Z_3$ …… β decay

$Z_8 \to Z_7$ …… β^+ decay

Z_3 は Z_4 とかに decay しないが、virtual に Z_4 を経由して Z_5 に行く $Z_3 \to Z_5$ が ββ decay である。

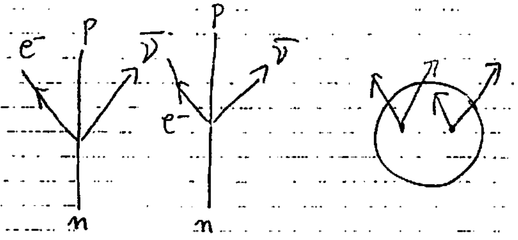

2ν modeの lifetimeは $10^{19} \sim 10^{24}$ year

10.6.4 Electron-capture neutrinos

Finally, a neutrino oscillation experiment has been suggested in which a beam of monoenergetic neutrinos is formed from electron capture in ^{65}Zn. In this case, the smearing of L/E would be caused only by the finite source or detector. This experiment is of special interest because of indications from tritium β decay that $m_{\nu_e} =$ 30 eV/c^2 and therefore that neutrino oscillations (if they are visible at all) might be in the $L/E = 0.1-1.0$ m/MeV range (see Section 10.8).

10.7 Double β decay

10.7.1 Double-β-decay rates

Nuclei exist for which ordinary β decay is energetically forbidden or highly suppressed by conservation of angular momentum but

Table 10.2. *Possible $\beta^-\beta^-$ transitions*

Transition	A	Z	Isotopic abundance (%)	Transition energy (MeV)	Intermediate transition energy $(A,Z)-(A,Z+1)$ (MeV)
Ca–Ti	46	20	0.0033	0.985	−1.382
Ca–Ti	48	20	0.185	4.267	+0.289
Zn–Ge	70	30	0.62	1.008	−0.653
Ge–Se	76	32	7.67	2.045	−0.923
Se–Kr	80	34	49.82	0.138	−1.871
Se–Kr	82	34	9.19	3.003	−0.089
Kr–Sr	86	36	17.37	1.240	−0.054
Zr–Mo	94	40	2.80	1.230	−0.921
Zr–Mo	96	40	17.40	3.364	+0.215
Mo–Ru	100	42	9.62	3.034	−0.335
Ru–Pd	104	44	18.5	1.321	−1.145
Pd–Cd	110	46	12.7	2.004	−0.868
Cd–Sn	114	48	28.86	0.547	−1.439
Cd–Sn	116	48	7.58	2.811	−0.517
Sn–Te	122	50	4.71	0.349	−1.622
Sn–Te	124	50	5.98	2.263	−0.653
Te–Xe	128	52	31.79	0.872	−1.268
Te–Xe	130	52	34.49	2.543	−0.407
Xe–Ba	134	54	10.44	0.731	−1.328
Xe–Ba	136	54	8.87	2.718	−0.112
Ce–Nd	142	58	11.07	1.379	−0.777
Nd–Sm	148	60	5.71	1.936	−0.514
Nd–Sm	150	60	5.60	3.390	−0.036
Sm–Gd	154	62	22.61	1.260	−0.718
Gd–Dy	160	64	21.75	1.782	−0.029
U–Pu	238	92	99.275	1.173	−0.117

26種類

もし、ν が majorana ν とすると

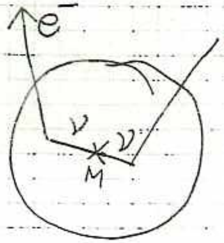

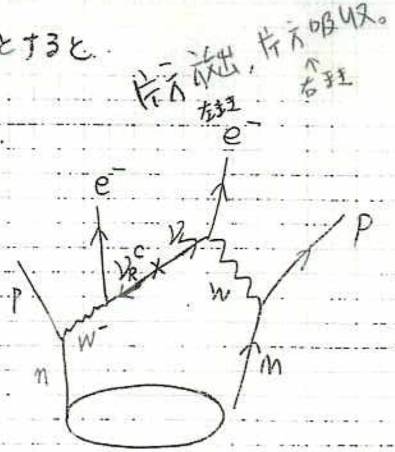

$0\nu\beta\beta$

M. Fukugita
Physics and Astrophysics of Neutrinos

$$\Gamma \propto (G_F \cos\theta)^4 \, G_{0\nu} \left(\frac{m_\nu}{m_e}\right)^2 \times |M|^2$$

Phasespace factor

原子核の form factor

$$G_{0\nu} = \frac{m_e^7}{8\pi^5}\left(\frac{t_0^5}{30} + \frac{t_0^4}{3} + \frac{4}{3}t_0^3 + 2t_0^2 + t_0\right)$$

$$t_0 = T_0/m_e$$

$2\nu\beta\beta$ $\Gamma \propto (G_F \cos\theta)^4 g_A^4 G_{2\nu} |M_{GT}|^2$

Fermi 遷移　$\Delta J = 0$, No parity change
のcontribution は少ないので、上は G.T のみ書いた。
Gamow-teller：$|\Delta J| = 1$, No parity change

^{76}Ge, ^{82}Se, ^{100}Mo では direct に $2\nu\beta\beta$ がはかられている。

1.4×10^{21}年　8.9×10^{19}年　8×10^{18}年

DBD & Neutrino Properties

Theoretical description ...

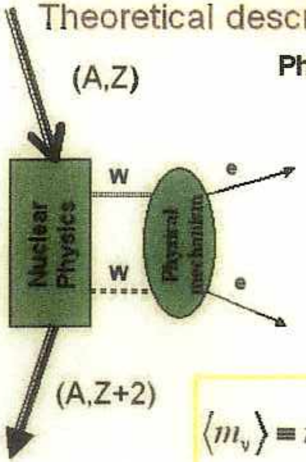

Phase space: high Q

Nuclear matrix element:
Relevant uncertainty source (h)

$$\left(T^{0\nu}_{1/2}\right)^{-1} = \sum_k G_k(Q,Z) M_k^2 \, \omega_k^2$$

Physical mechanism

$$\boxed{G(Q,Z)M^{\,2}\langle m_\nu\rangle^2}$$

Neutrino mass

±1 if CP conserved

$$\langle m_\nu\rangle \equiv m_{ee} = \left|\sum_k U_{ek}^2 m_k\right| = \left|\sum_k |U_{ek}|^3 e^{i\alpha_{ek}} m_k\right|$$

Pontecorvo-Maki-Nakagawa-Sakata mixing matrix: →

$$\begin{pmatrix} \nu_e \\ \nu_\mu \\ \nu_\tau \end{pmatrix} = \begin{pmatrix} U_{e1} & U_{e2} & U_{e3} \\ U_{\mu1} & U_{\mu2} & U_{\mu3} \\ U_{\tau1} & U_{\tau2} & U_{\tau3} \end{pmatrix} \begin{pmatrix} \nu_1 \\ \nu_2 \\ \nu_3 \end{pmatrix}$$

I-59

2ν2β Experimental situation

2nd order weak process

Severe test for nuclear matrix elements calculations

Weighted average of the most recent experiments
i) average asymmetryc bars
ii) add systematic errors in quadrature

$$\left[T^{2\nu}_{1/2}(0^+ \rightarrow 0^+)\right]^{-1} = G^{2\nu}(Q,Z)\left|M^{2\nu}_{GT}\right|^2$$

Phase Space Integral
Exactly Calculable

Isotope	$T_{1/2}^{2\nu}$(y)	$M_{GT}^{2\nu}$ (MeV^{-1})
^{48}Ca	$(4.25 \pm 1.6) \times 10^{19}$	0.05
^{76}Ge	$(1.38 \pm 0.14) \times 10^{21}$	0.15
^{82}Se	$(8.9 \pm 1.0) \times 10^{19}$	0.10
^{96}Zr	$(1.43^{+3.4}_{-0.8}) \times 10^{19}$	0.12
^{100}Mo	$(8.2 \pm 0.6) \times 10^{18}$	0.22
^{100}Mo(0^{+*})	$(6.8 \pm 1.2) \times 10^{20}$	0.1
^{116}Cd	$(3.2 \pm 0.3) \times 10^{19}$	0.12
^{128}Te	$(7.2 \pm 0.3) \times 10^{24}$	0.025
^{130}Te	$(2.7 \pm 0.1) \times 10^{21}$	0.017
^{136}Xe	$> 8.1 \times 10^{20}$	<0.03
^{150}Nd	$(7.0^{+12.0}_{-1.0}) \times 10^{18}$	0.07
^{238}U	$(2.0 \pm 0.6) \times 10^{21}$	0.05

Elliott and Vogel 2002

Nuclear structure effects
cause variations by a
factor ~10
on the matrix elements
i.e. a factor ~100
on the lifetime

Calculated values span a range of
3-4 orders of magnitude
around the experimental value

Tretyak and Zdesenko 2002

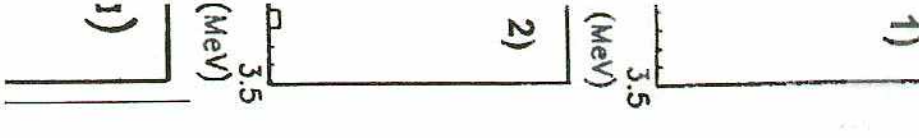

2νββ

NEMO-2

V are quoted in Tables 1 and 2). A new variant of ELEGANTS is searching for the double beta decay of ^{48}Ca.

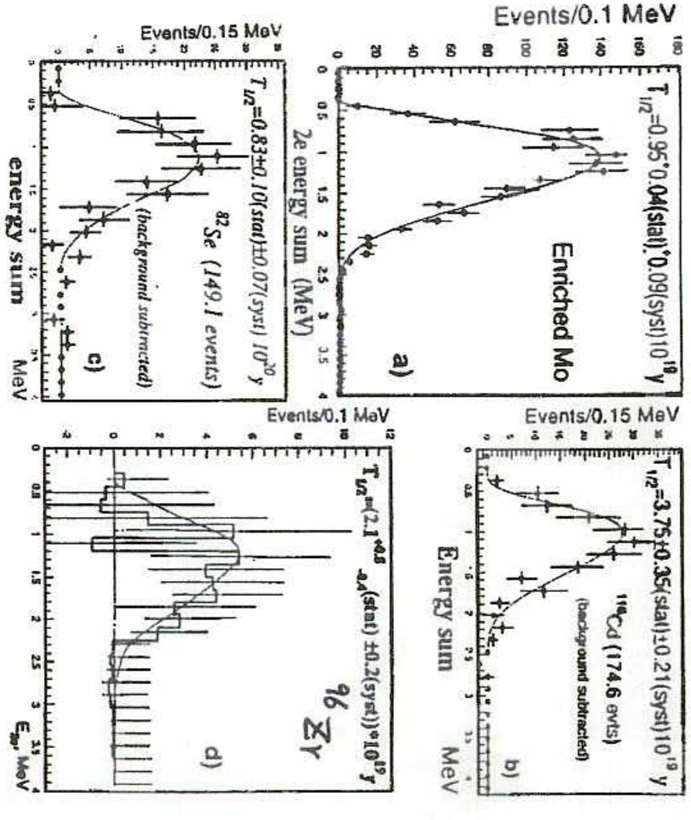

Figure 4.

The Caltech/PSI/Neuchatel Collaboration [8] investigates the double beta decay of ^{136}Xe in the

That imp
tained in
pressure)
mode.

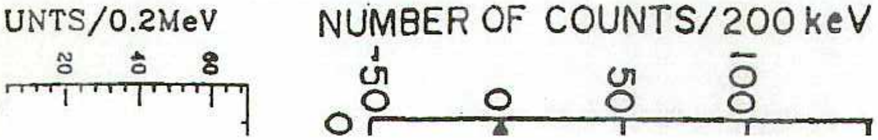

ββ では.

(1) T_0 : Q valueの大きい原子核が有理

(2) Matrix elementがあるていどわかっている。

(3) detectorにできる。

Detection Method

(1) Total energy absorption

例えば. Ge Semiconductor Detector

^{76}Ge ββ : 7.8% of natural Ge → enriched 86%

$Q_{\beta\beta} = 2.041$ MeV

Heidelberg / Moscow collab.

~~12.2~~ 11.5 kg ^{76}Ge total 5コ

(2) source and tracking device

0ν2β Experimental Situation

2 main experimental approaches:

- Active Source
- Passive Source

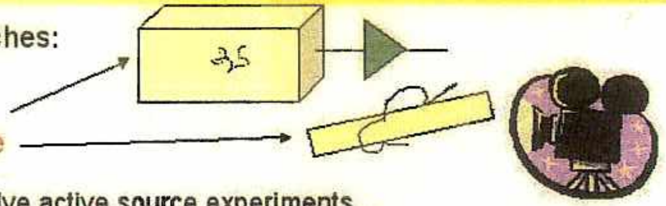

Best 0ν2β results involve active source experiments

Experiment	Isotope	$T_{1/2}^{0\nu}$ (y)	$<m_\nu>$ (eV)
You Ke et al. 1998	^{48}Ca	> 9.5 × 10^{21} (76%)	< 8.3
Klapdor-Kleingrothaus 2001	^{76}Ge	> 1.9 × 10^{25}	< 0.35
Aalseth et al 2002		> 1.57 × 10^{25}	< 0.33 - 1.35
Elliott et al. 1992	^{82}Se	> 2.7 × 10^{22} (68%)	< 5
Ejiri et al. 2001	^{100}Mo	> 5.5 × 10^{22}	< 2.1
Danevich et al. 2000	^{116}Cd	> 7 × 10^{22}	< 2.6
Bernatowicz et al. 1993	$^{130/128}$Te*	(3.52 ±0.11) × 10^{-4}	< 1.1 – 1.5
Bernatowicz et al. 1993	^{128}Te*	> 7.7 × 10^{24}	< 1.1 – 1.5
Mi DBD – ν 2002	^{130}Te	> 2.1 × 10^{23}	< 0.85 – 2.1
Luescher et al. 1998	^{136}Xe	> 4.4 × 10^{23}	< 1.8 – 5.2
Belli et al. 2001	^{136}Xe	> 7 × 10^{23}	< 1.4 – 4.1
De Silva et al. 1997	^{150}Nd	> 1.2 × 10^{21}	< 3
Danevich et al. 2001	^{160}Gd	> 1.3 × 10^{21}	< 26

Heidelberg-Moscow

Klapdor-Kleingrothaus HV et al. Eur. Phys. J. 12 (2001) 147

Max-Planck-Institut für Kernphysik
Russian Science Center Kurchatov Institute

since 1990

Gran Sasso underground laboratory

- Five Ge diodes (overall mass 10.9 kg) isotopically enriched (86%) in ^{76}Ge
- Lead box and nitrogen flushing of the detectors
- Digital Pulse Shape Analysis (factor 5 reduction)

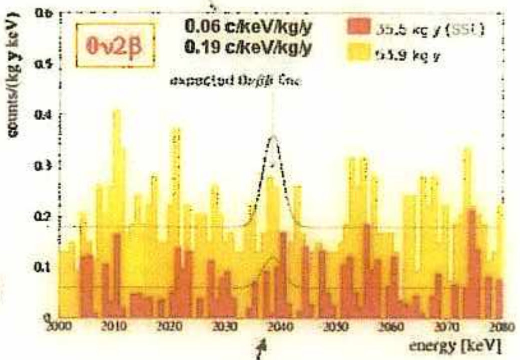

$T_{1/2}^{0\nu} > 1.9 \times 10^{25}$ (90 % C.L.)
$<m_\nu> < 0.35$ (0.3-1.24) eV

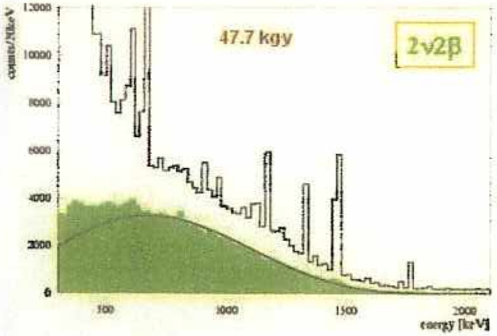

Accurate background model:
$T_{1/2}^{2\nu} > (1.55 \pm 0.01(\text{stat})\ ^{+0.19}_{-0.15}\ (\text{syst})) \times 10^{21}$

Neutrinoless Experiment with MOlibdenum III
or Neutrino Ettore Majorana Observatory

Large Collaboration: 13 groups from Europe, USA and Japan

Passive source - Spectroscopic approach

$0\nu 2\beta$ sensitivity:
T ~ 10^{24} y
$<m\nu> \sim 0.1$ eV

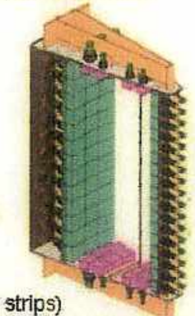

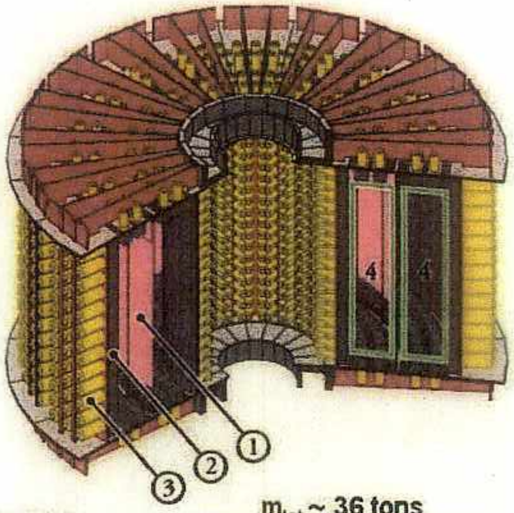

Detector structure: 20 sectors

1 Source:
up to 10 kg of $\beta\beta$ isotopes
(metal film or powder glued to mylar strips)
cylindrical surface: 20 m² x 40-60 mg/cm²

2 Tracking volume:
open octagonal drift cells (6180)
operated in Geiger mode
(σ_r=0.5 mm,σ_Z=1 cm)

3 Calorimeter:
1940 plastic scintillators coupled to low activity PMs:
FWHM(1 MeV) ~ 11-14.5 %

$m_{tot} \sim 36$ tons
Low activity materials

Magnetic Field (30 G) + Iron Shield (20 cm) + Neutron Shield (30 cm H_2O)

②

Kamiokande
Super-kamiokande
detector

Water Cherenkov detector

$\xrightarrow{\beta = \frac{v}{c}}$ particle

if $v_{particle} > v_{light}$

$v_{light} = \frac{c}{n}$

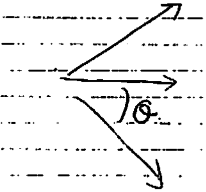

$\cos\theta = \frac{1}{n\beta}$

$n = 1.34$

$$\frac{dN}{dx\,d\lambda} = 2\pi\alpha\left(1 - \frac{1}{(n\beta)^2}\right)\frac{1}{\lambda^2}$$

↑ 単位長さ

↑ fine structure constant

$\lambda = 300 - 600$ nm, $n = 1.34$, $\beta = 1$ とすると

1cm あたり 340 photon 出る。

↑ relativistic particle だと ~ 1cm あたり 2MeV

したがって 1MeV あたり $340 \times \frac{1}{2} \times 0.4 \times (0.1 \sim 0.2) \times e^-$

↑ photo coverage

$\cong 7$ p.e./MeV

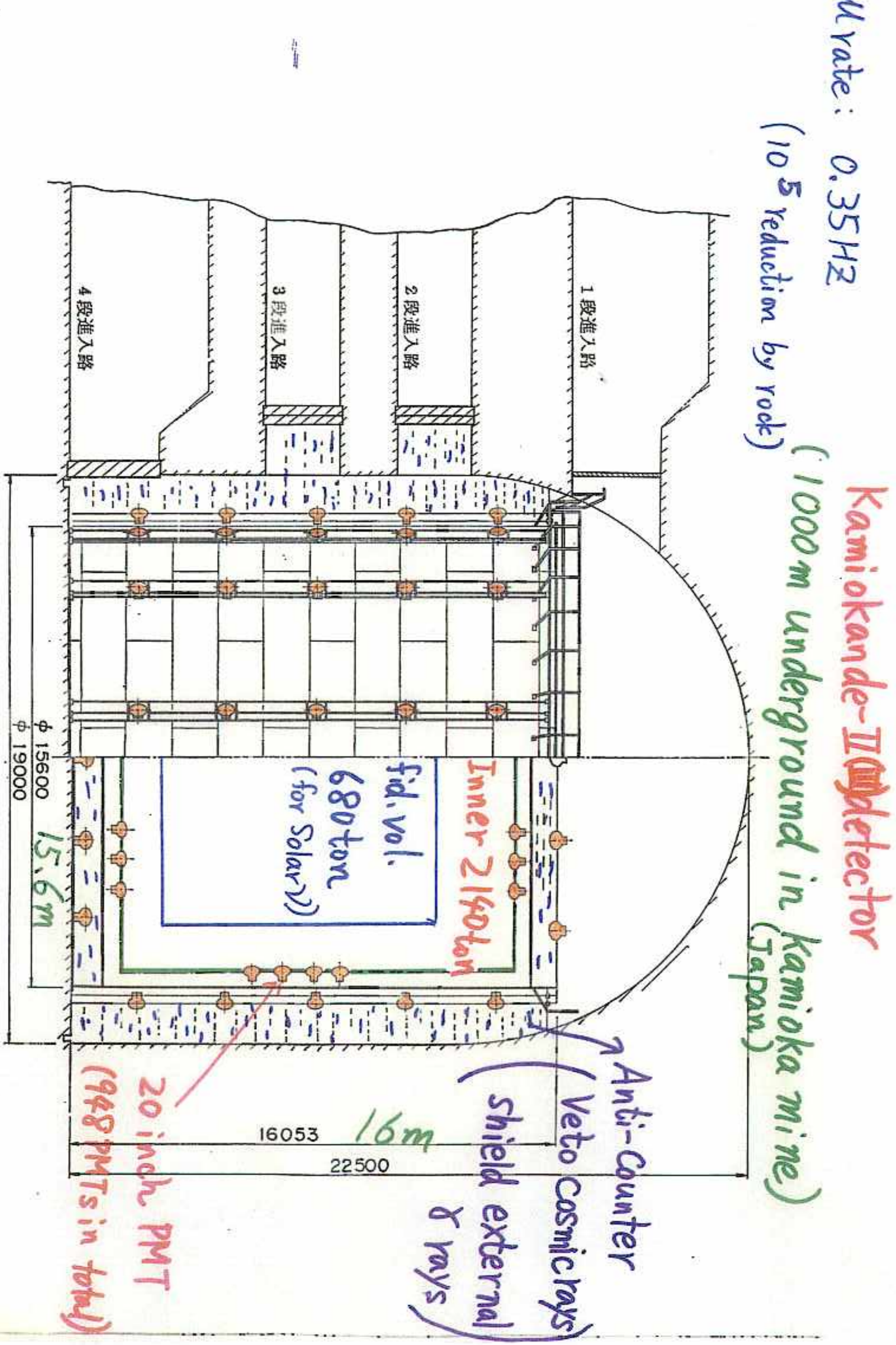

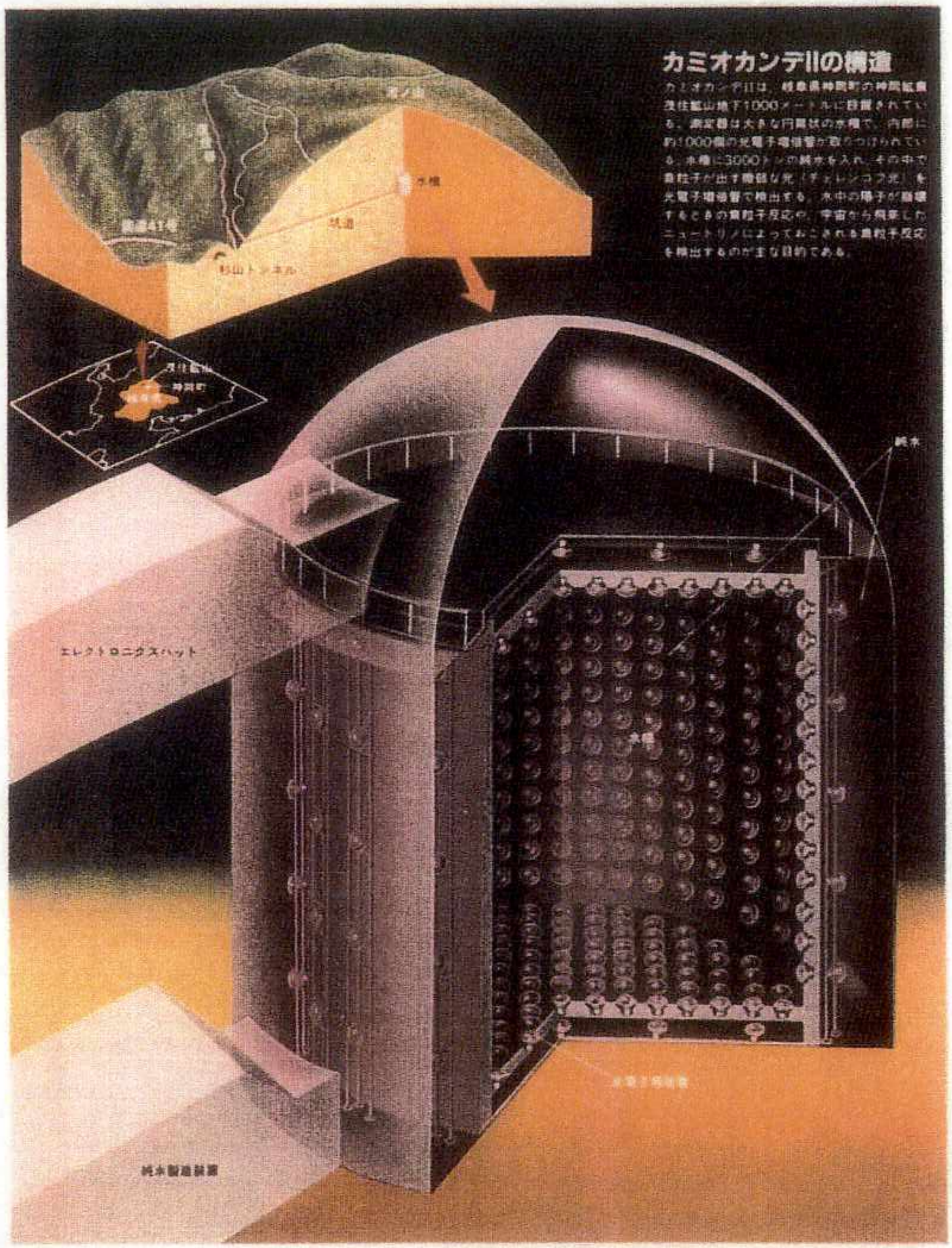

カミオカンデIIの構造

カミオカンデIIは、岐阜県神岡町の神岡鉱業茂住鉱山地下1000メートルに設置されている。測定器は大きな円筒状の水槽で、内部に約1000個の光電子増倍管が取りつけられている。水槽に3000トンの純水を入れ、その中で素粒子が出す微弱な光（チェレンコフ光）を光電子増倍管で検出する。水中の陽子が崩壊するときの素粒子反応や、宇宙から飛来したニュートリノによっておこされる素粒子反応を検出するのが主な目的である。

Super Kamiokande vs Kamiokande

Paramters	Super-Kamiokande	Kamiokande-3
Total size Total mass	41mh × 39mϕ 50000t	16mh × 19mϕ 4500t
Fiducial mass supernova ν proton decay solar ν	 32000t 22000t 22000t	 2140t 1040t 680t
Tickness of anti-counter	2m	1.2m~1.5m
Number of PMTs	11146	947
Photosensitive coverage	40%	20% × 1.27 (light reflector)
PMT timing resoluton @1p.e.	2.5nsec	4nsec
Energy resolution	16%/√E/10MeV	19%/√E/10MeV
Position resolution @10MeV	50cm	1m
Analysis threshold	5MeV	7MeV

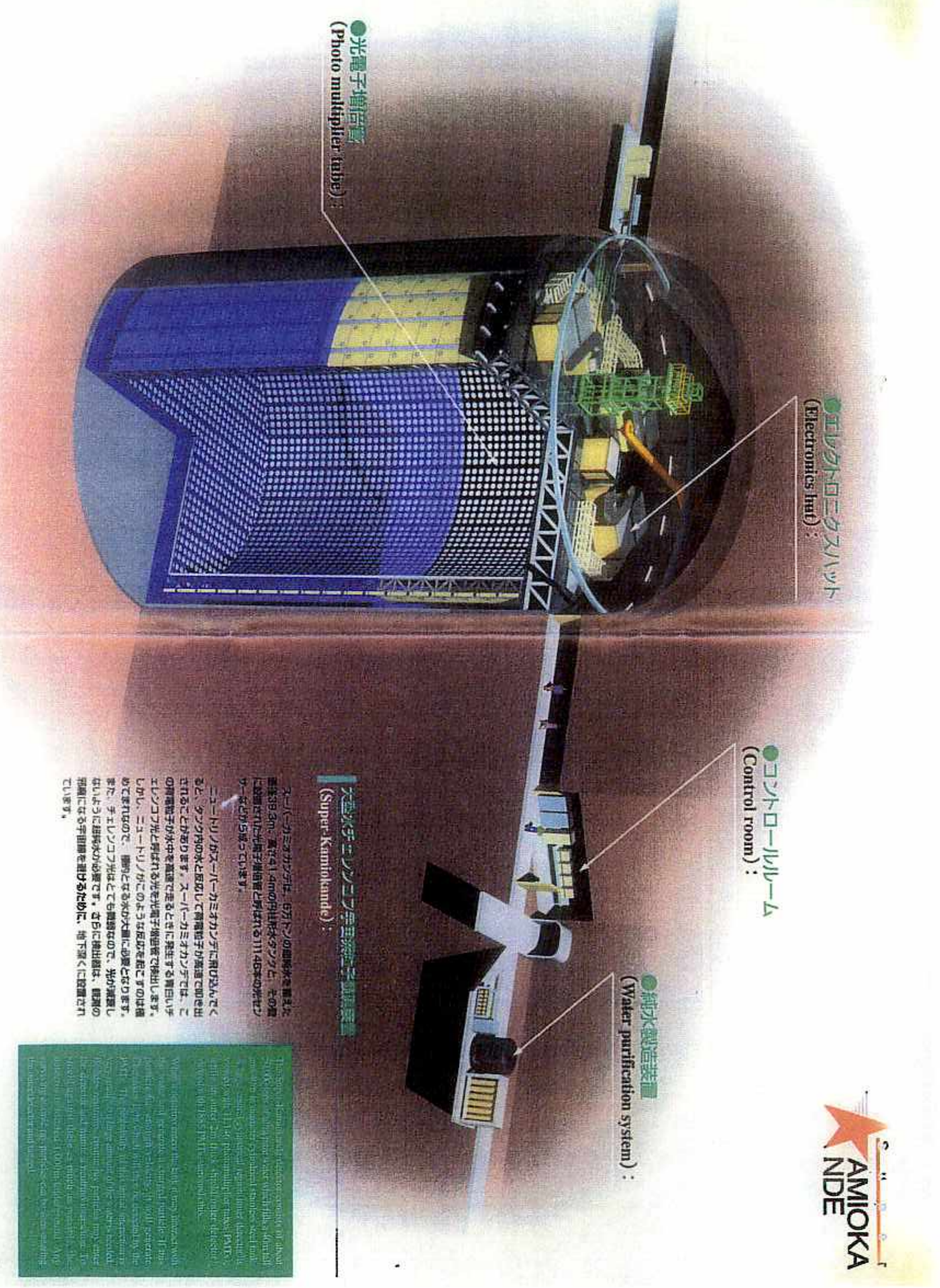

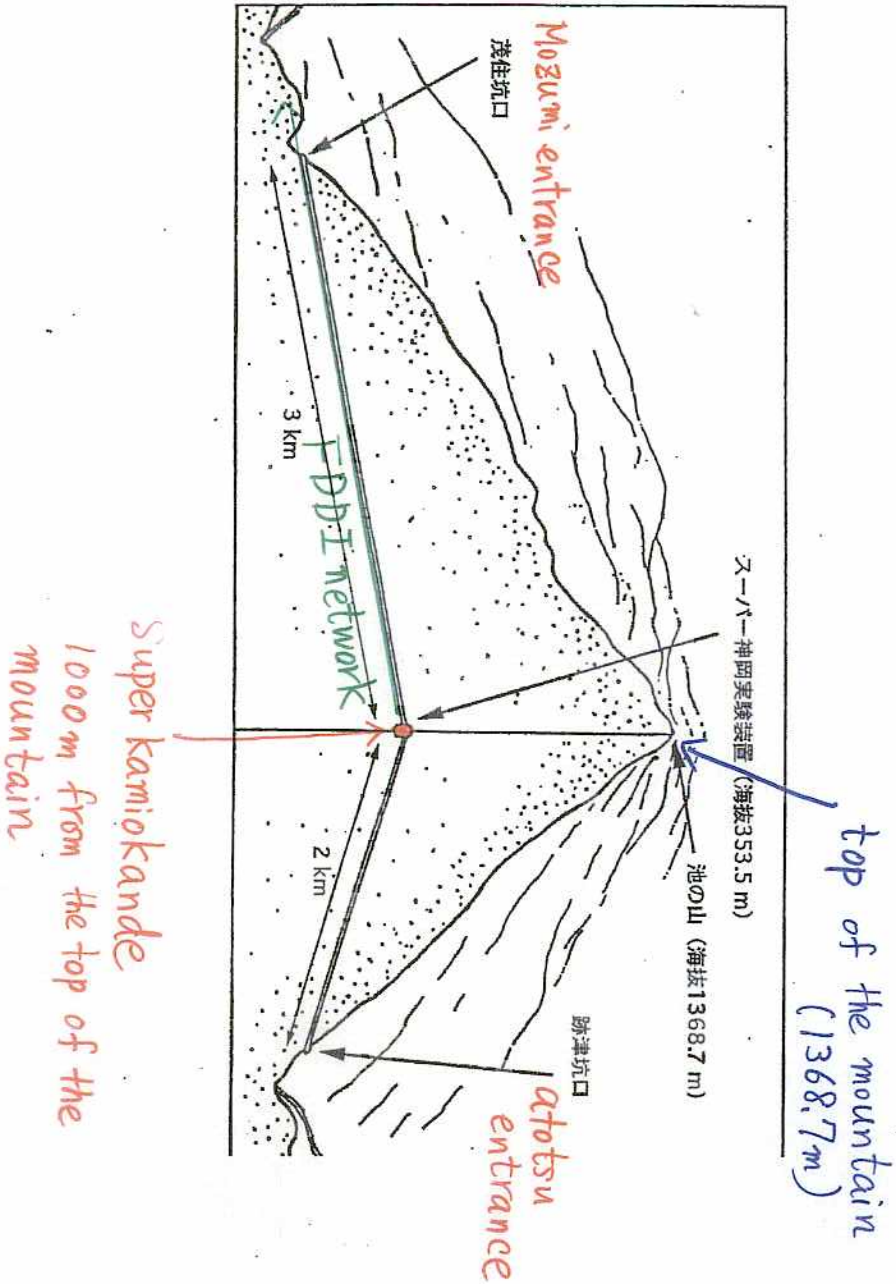

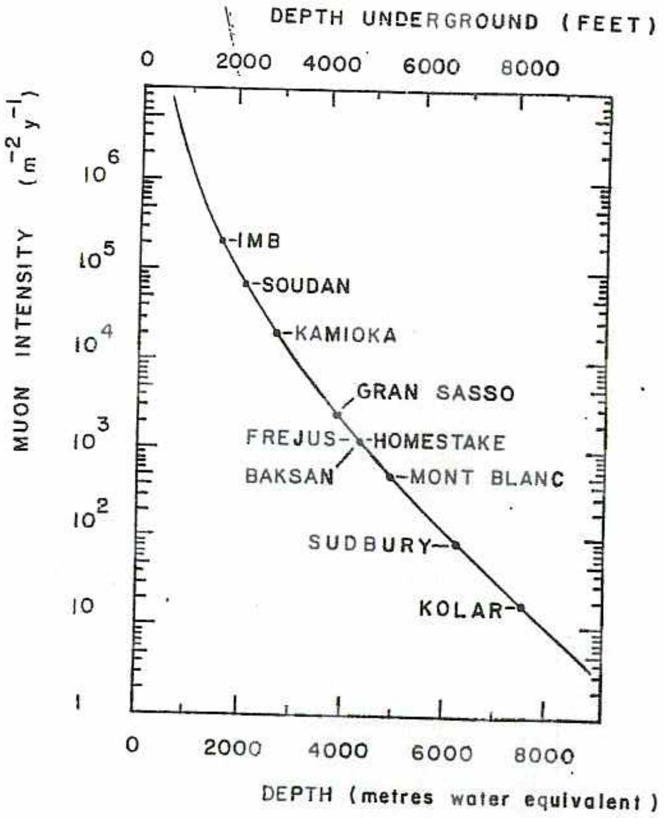

Figure III.5 Cosmic ray muon intensity as a function of overburden (mwe) or depth underground (feet in standard rock).

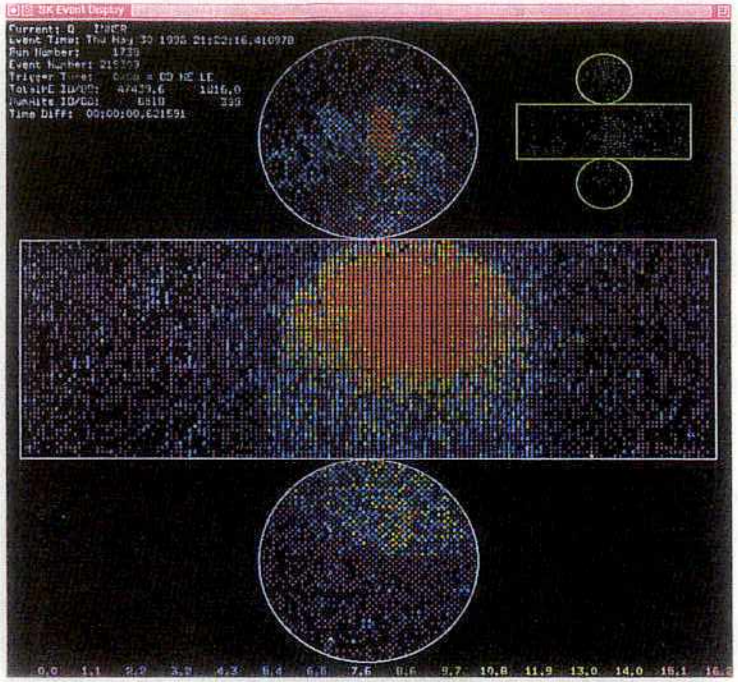

Typical cosmic ray muons

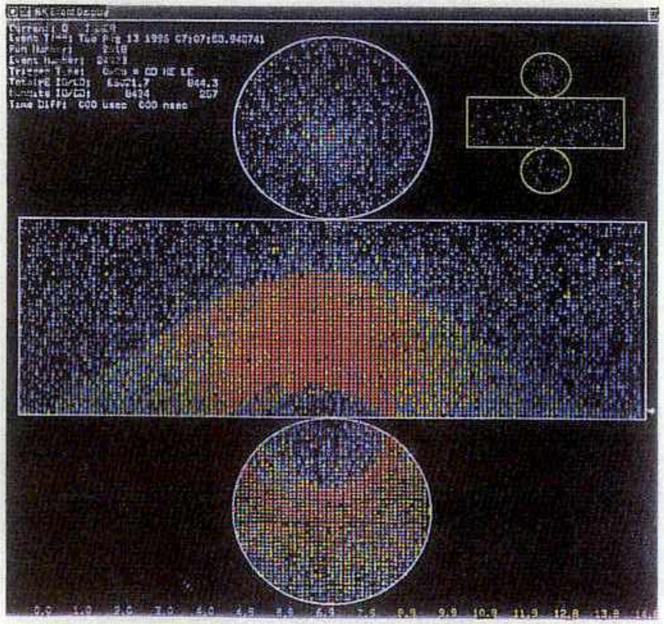

Trigger

≧ 29 PMT hits / 200nsecr
rate ~10Hz

- Super-Low-Energy (SLE) trigger since May 29, 1997

≧ 24 PMT hits / 200nsec
raw rate ~120Hz (most of them are close to the ID wall)
⇒ on-line fid. vol. cut ⇒ 20Hz

Trigger efficiency measured by Ni(n,γ)Ni source

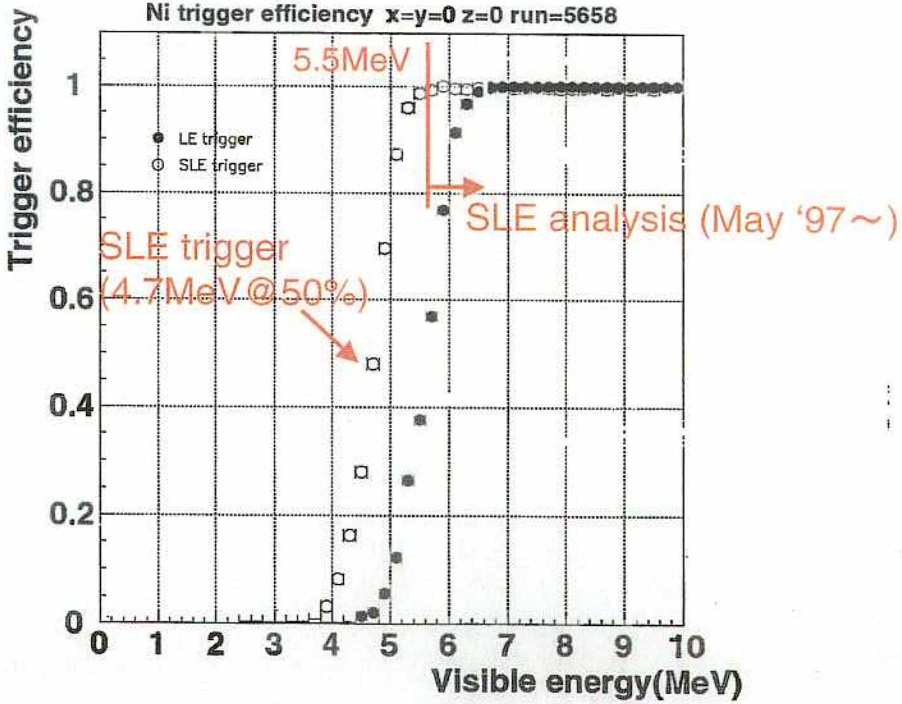

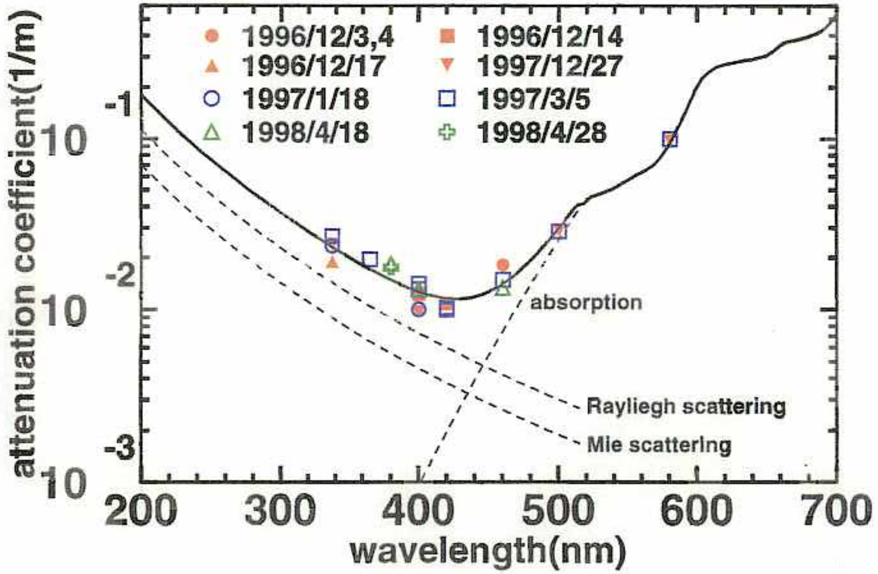

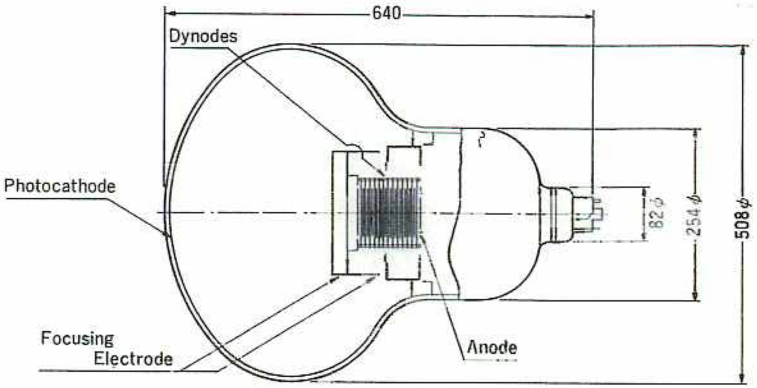

Fig. 2. The construction of the 20" PMT.

dynodes of 13 stages are installed to obtain a large photoelectron collection area as well as high current amplification. The structure and the arrangement of the focusing electrodes, which strongly affect the photoelectron collection efficiency and the timing property, are carefully designed on the basis of electron trajectory analysis. Fig. 4 shows the simulation of the electron trajectories from the photocathode to the first dynode with a voltage difference of 800 V. Photoelectro traced under an initial energy of 0.5 eV and em angles of 0° and ±90°.

3. The PMT characteristics

Several characteristics of the PMT and mea methods are discussed in this section. The foll

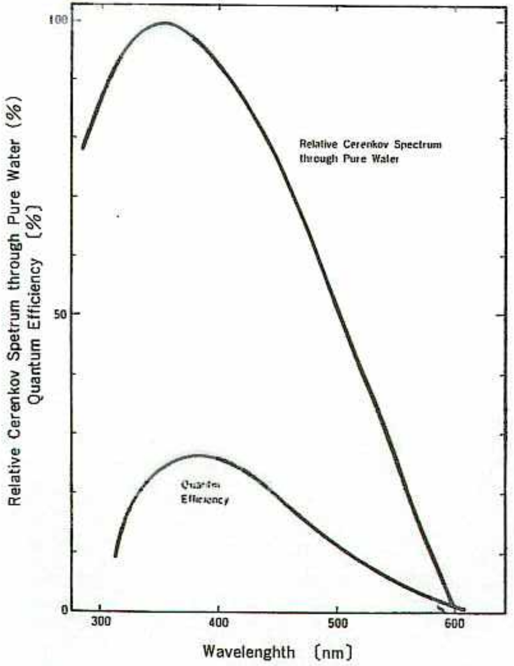

Fig. 3. Spectrum of Cherenkov light and measured photocathode quantum efficiency.

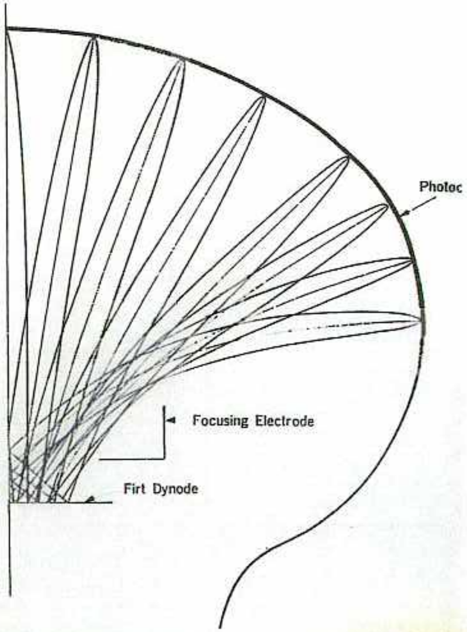

Fig. 4. Computer simulation of electron trajectories.

KSK-20

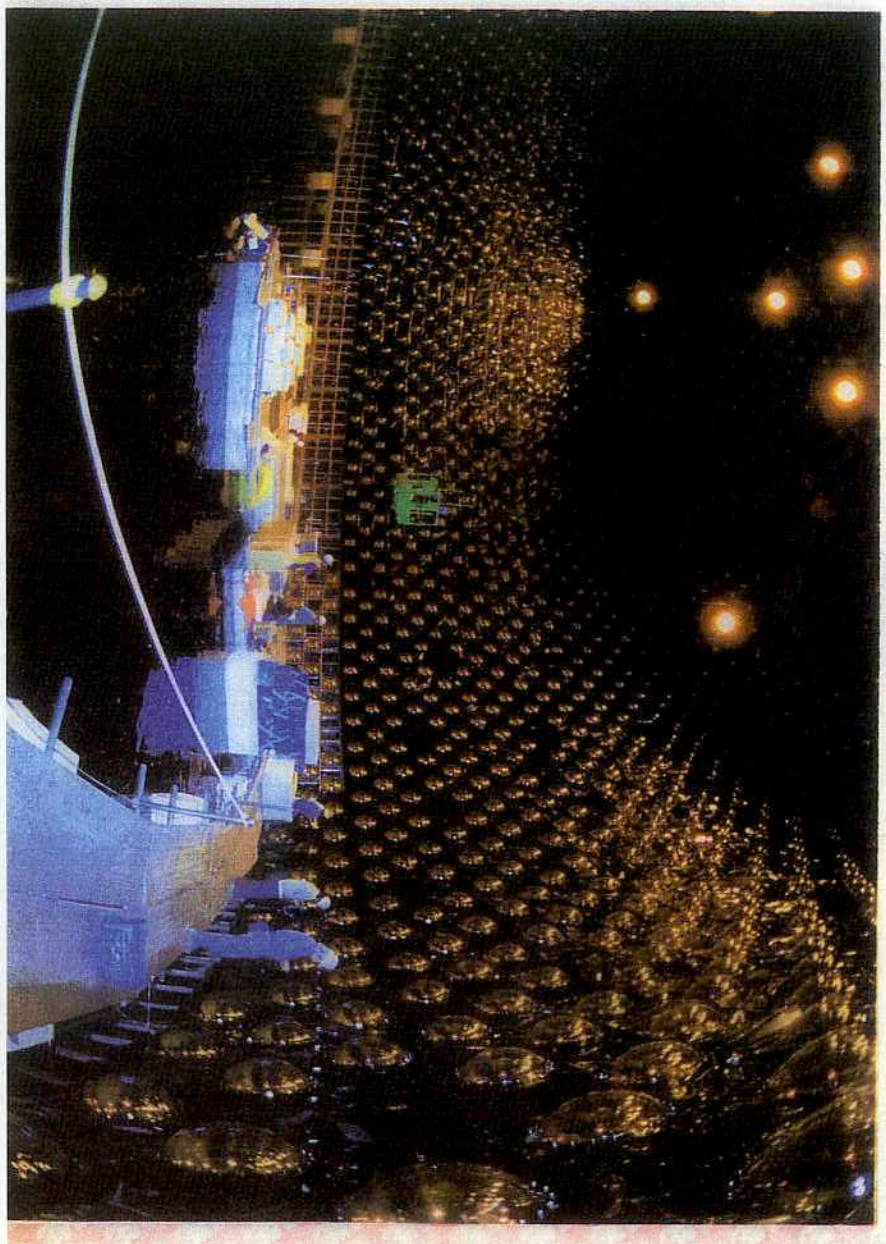

KSK-19

③

Atmospheric neutrinos

Introduction

- production
- Detection

⋮

- primary cosmic ray

H (proton) ~90.6%, He ~9.0%, CNO ~0.4%

above 100 MeV/nucleon

P ~95.2%, He ~4.5%, CNO ~0.3% above ~2GeV/nucleon

other component Ne, S, Fe 等は negligible for atm. ν

>2GeV/nucleon
- He carry ~15% のnucleon
- CNO ~3.6% のnucleon

- 数GeV 以下の nucleon は 太陽活動と反相関。

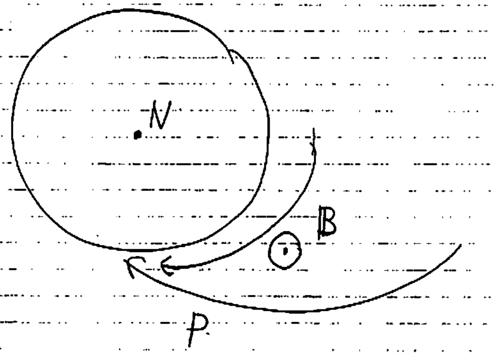

- これ以上 入って来れない energy : geomagnetic cut off

1日 drift

Atm-2

Atm-5

Calculation of Low-Energy Atmospheric Neutrino Fluxes

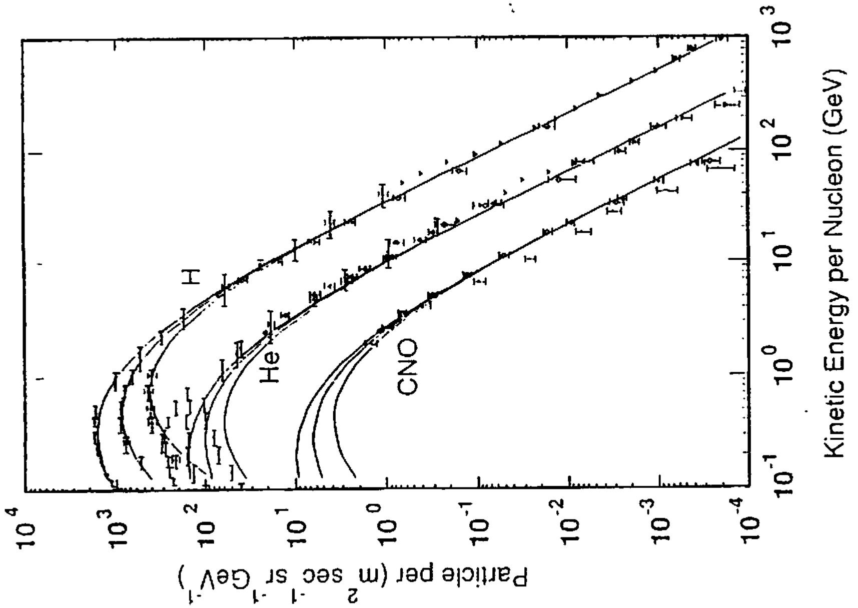

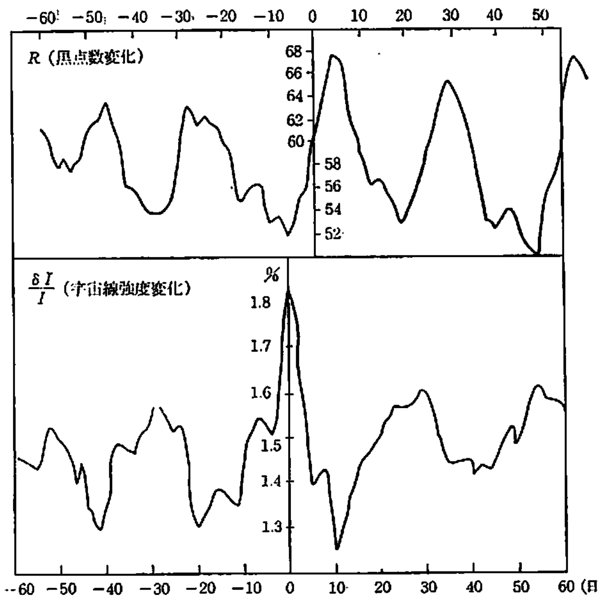

9-4 図　太陽黒点数の変化と宇宙線硬成分強度の変化の相関を示す例．図によれば太陽黒点数が最大になった日より～6日遅れて宇宙線強度の最小になっている．
観測場所：Huancayo. 1940～41 年における平均値

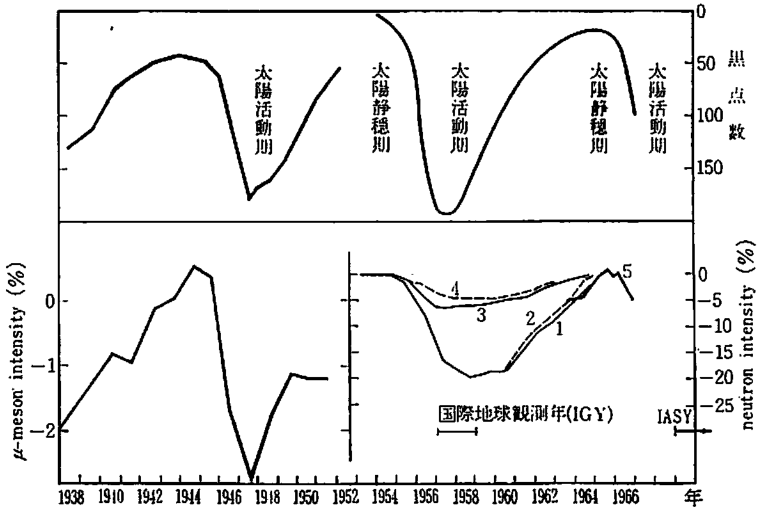

9-5 図　太陽活動と地上で測った宇宙線強度との関係をほぼ3サイクル（11 年周期）にわたって示す．1938～1951 の期間に対しては Godhavn, Cheltenham, Christchurch, Huancayo における μ 中間子強度の観測値の平均を与えてある．1953～1964 には各地に neutron monitor が完成したのでそのデータの中から 1) Mt. Washington, 2) Climax, 3) 乗鞍, 4) Huancayo の結果を示してある．5) は Deep River の大型 neutron monitor によるものである．

40

atm-7

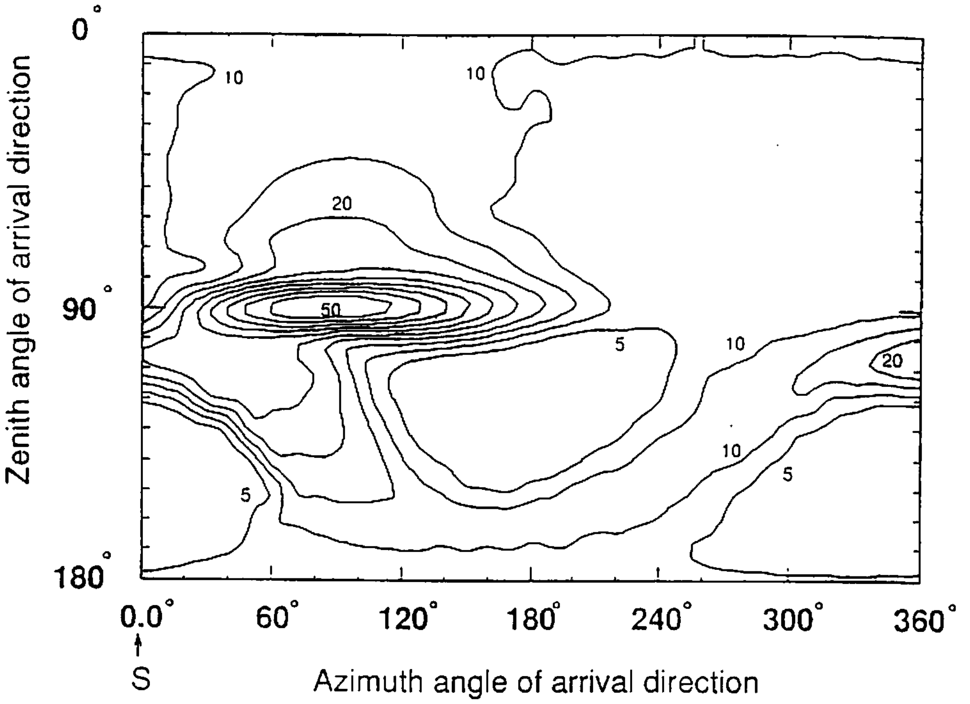

Figure 3: Contour map of the cutoff-rigidity for the ν arrival direction at Kamiok Azimuth angles of 0°, 90°, 180°, and 270° show the directions of south, east, north, a west, respectively.

Atm-7

41

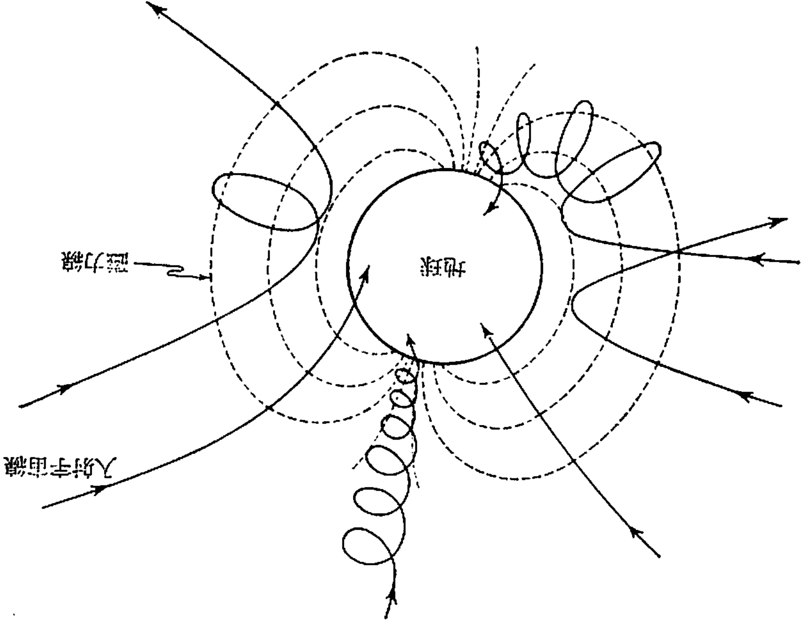

8-1 図　宇宙線に対する地球磁場の影響
遠方から飛んでくる荷電粒子が地球磁場の中に入るとそのエネルギーとはじめの入射方向に応じて，いろいろな軌道を描き，あるものは地球表面に触れずに遠ざかっていく．

すなわち，pc は eV 単位）．磁場がすべての場所について与えられていれば，粒子の運動の軌道を追跡すること

BESS 97, 98

- Simple Cylindrical Shape → large SΩ ($0.3\,m^2sr$)
  easy to determine
- Up to 28 ($= \underset{JET}{24} + \underset{IDC}{2\times2}$) points /track → fig
  - MDR = 20 GV
  - Interaction can be seen
  - High E

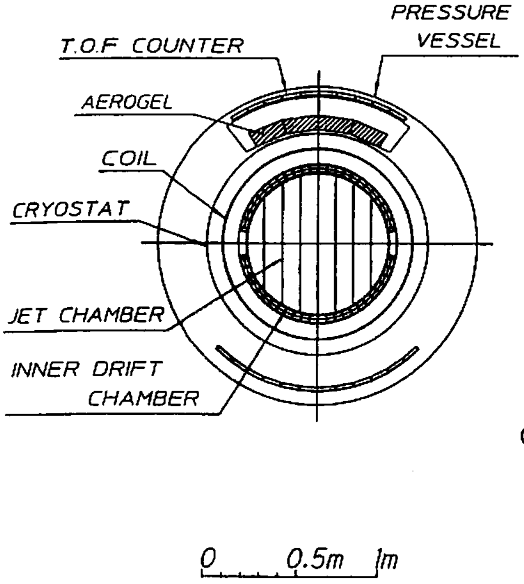

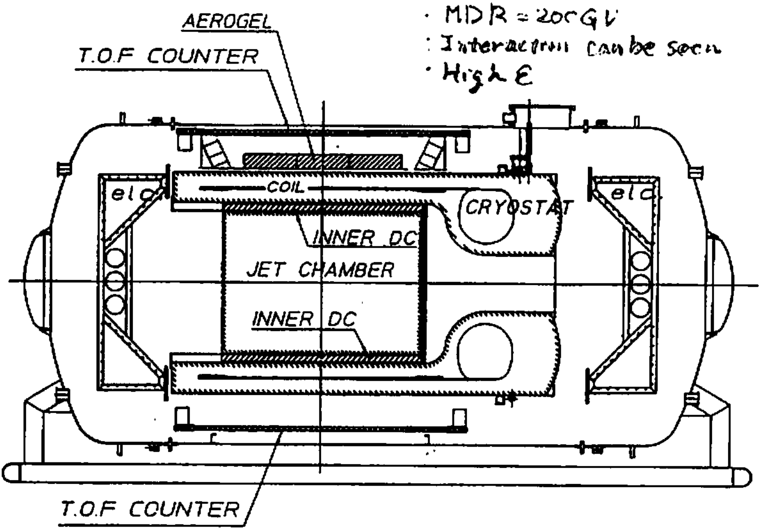

- thin Superconducting Solenoidal Magnet ($\underset{g}{0.2}X_0$)
  Uniform 1 Tesla $\mathbb{B}$ $0.8m\phi \times 1m$ → fig
- Fast DAQ (multi CPU) Live time ~85%

Uniform $\mathbb{B}$

LEAP, MASS. IMAX. CAPRICE

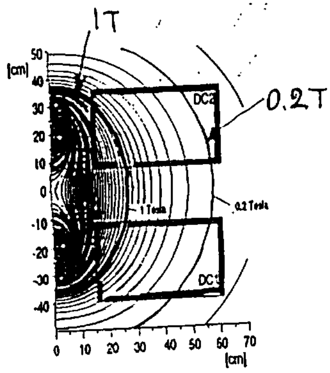

BESS

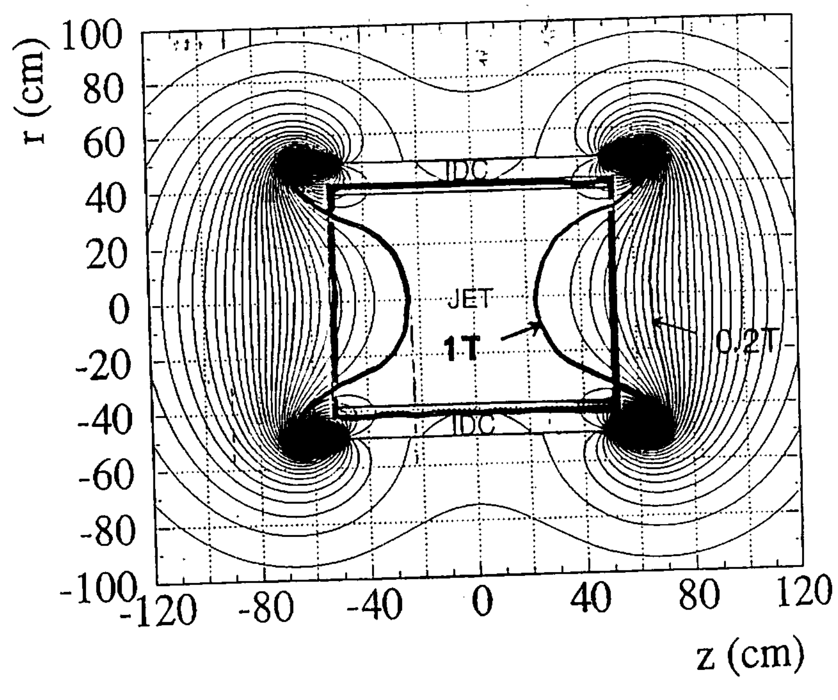

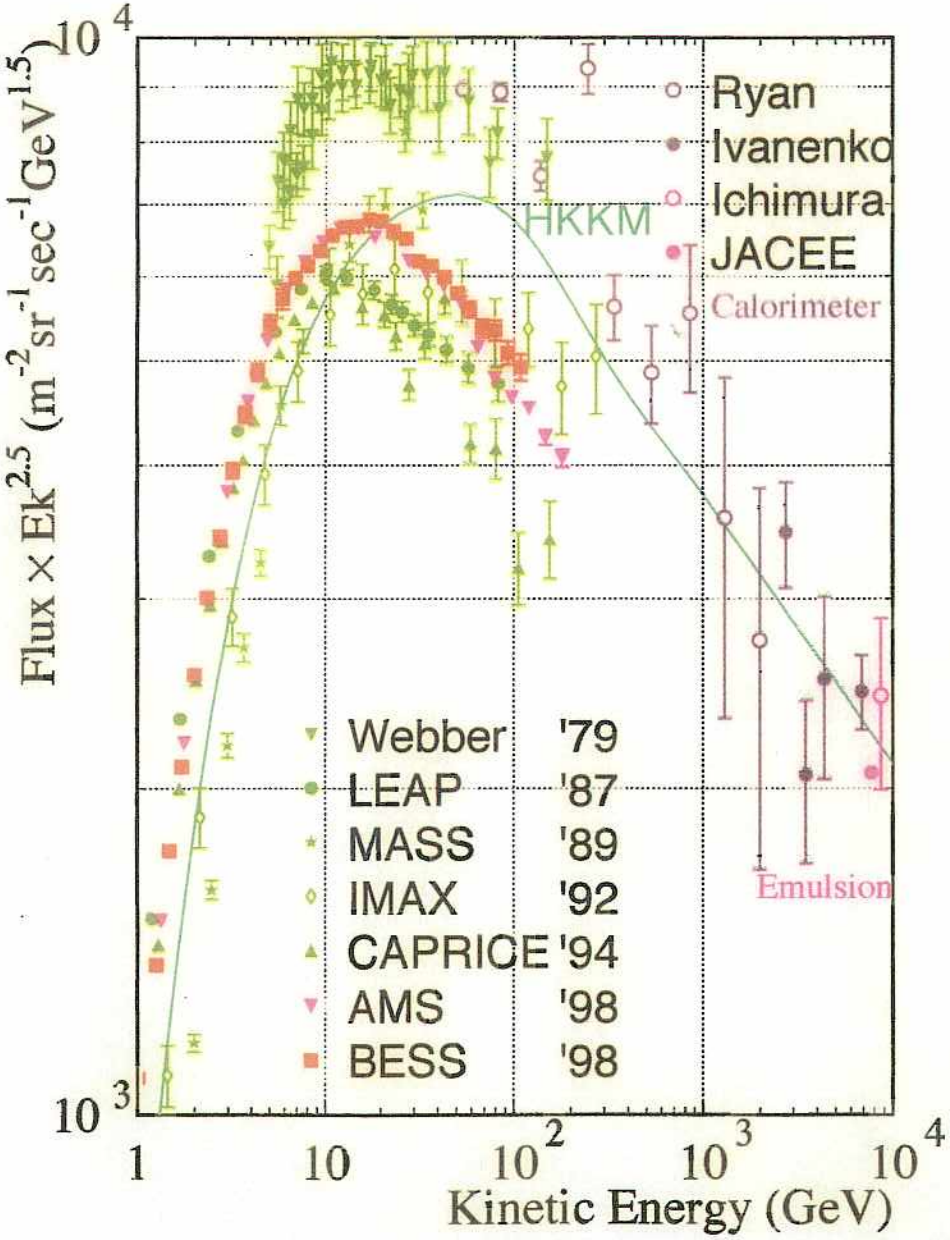

Flux × Ek$^{2.5}$ (m^{-2}sr^{-1}sec^{-1}GeV$^{1.5}$)
10 4
10 3
1
10
10 2
10 3
10 4
Kinetic Energy (GeV)
HKKM
Ryan
Ivanenko
Ichimura
JACEE
Calorimeter
Emulsion
Webber '79
LEAP '87
MASS '89
IMAX '92
CAPRICE '94
AMS '98
BESS '98

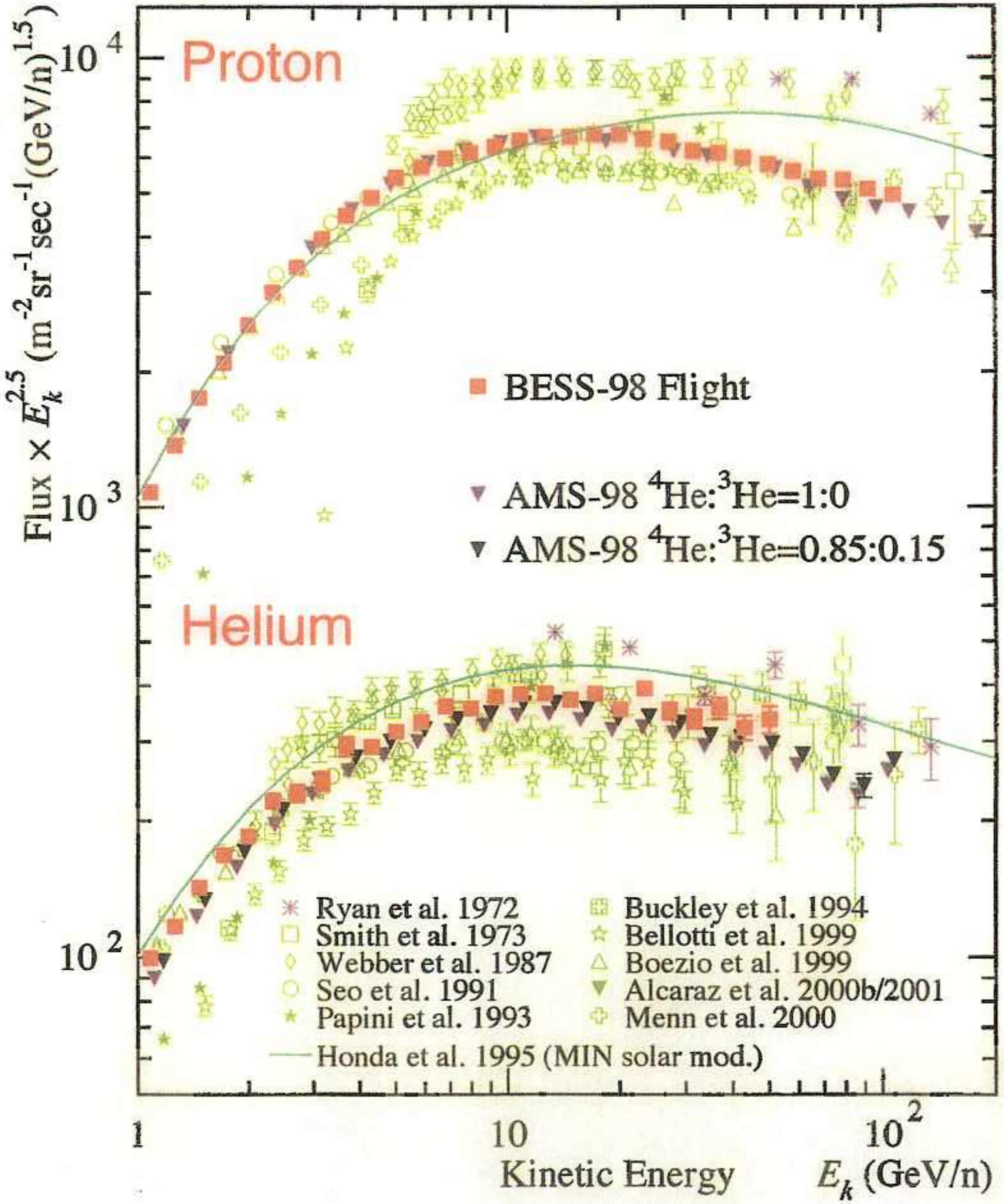

Flux × $E_k^{2.5}$ (m^{-2}sr^{-1}sec^{-1}(GeV/n)$^{1.5}$)
10 4
10 3
10 2
1
10
10 2
Kinetic Energy E_k (GeV/n)
Proton
Helium
BESS-98 Flight
AMS-98 ^{4}He:^{3}He=1:0
AMS-98 ^{4}He:^{3}He=0.85:0.15
Ryan et al. 1972
Smith et al. 1973
Webber et al. 1987
Seo et al. 1991
Papini et al. 1993
Buckley et al. 1994
Bellotti et al. 1999
Boezio et al. 1999
Alcaraz et al. 2000b/2001
Menn et al. 2000
Honda et al. 1995 (MIN solar mod.)

Chapter 3

Balloon Observations

This chapter describes four balloon observations, BESS-'97, '98, '99 and 2000, which have been successfully carried out.

3.1 Performance of the Balloon Flights

The BESS scientific balloon flights were carried out in northern Canada from Lynn Lake((56°48'N,101°25'W), the geomagnetic cutoff rigidity is 0.4 GV), Manitoba to near Peace River((56°15'N,117°18'W)), Alberta in summer of '97 '98, '99 and 2000. Table 3.1 gives summaries of the four flights, and the trajectories of the balloons in each year are shown in Figure 3.1.

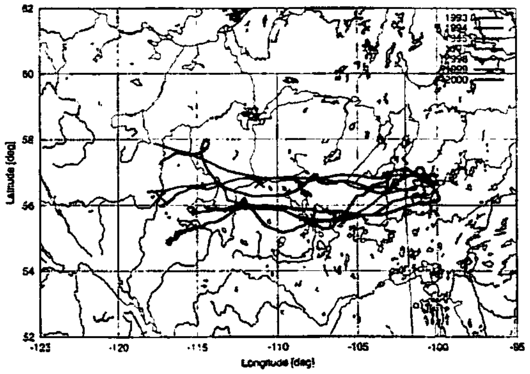

Figure 3.1: Flight trajectories for BESS-'97, '98, '99 and 2000 together with for BESS-'93, '94 and '95.

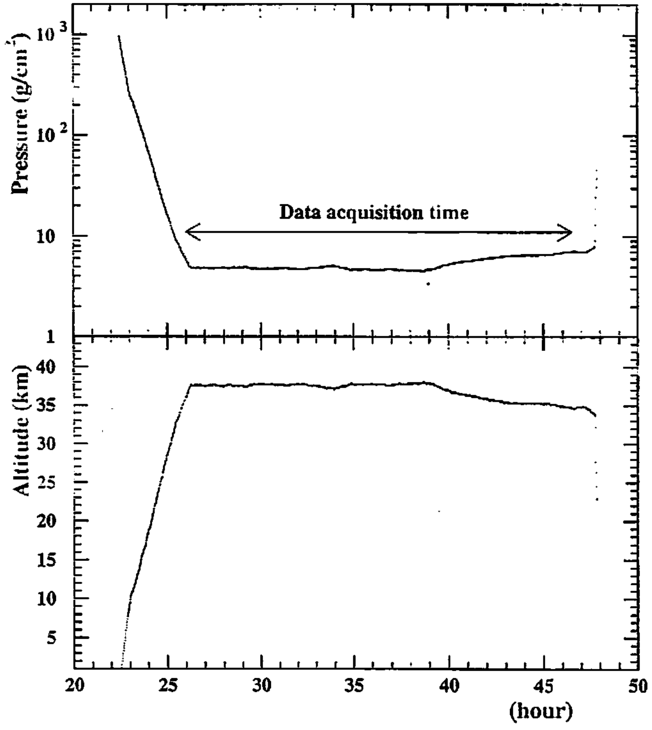

Figure 3.2: The altitude and pressure data during the BESS '97 flight.

atm-11

$$\rho(\text{cm}) = \frac{1}{300}\boxed{\frac{pc}{Ze}}\frac{1}{H}$$

↑ gauss

Volt単位 pc は eV 単位

- rigidity

Nuclear interaction

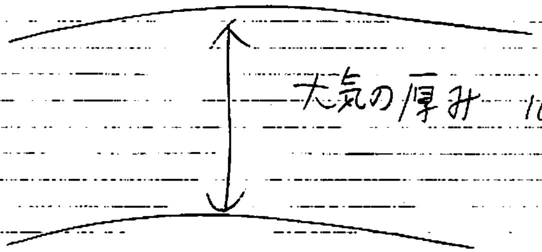

nuclear interaction の m.f.p. の 10倍程度

40mb

$$\boxed{40\times10^{-3}\times10^{-24}\text{cm}^2\times6\times10^{23}\times1000 = 24\text{回}}$$

radiation length of air : 36.7g/cm²

→ 27回

atm-12

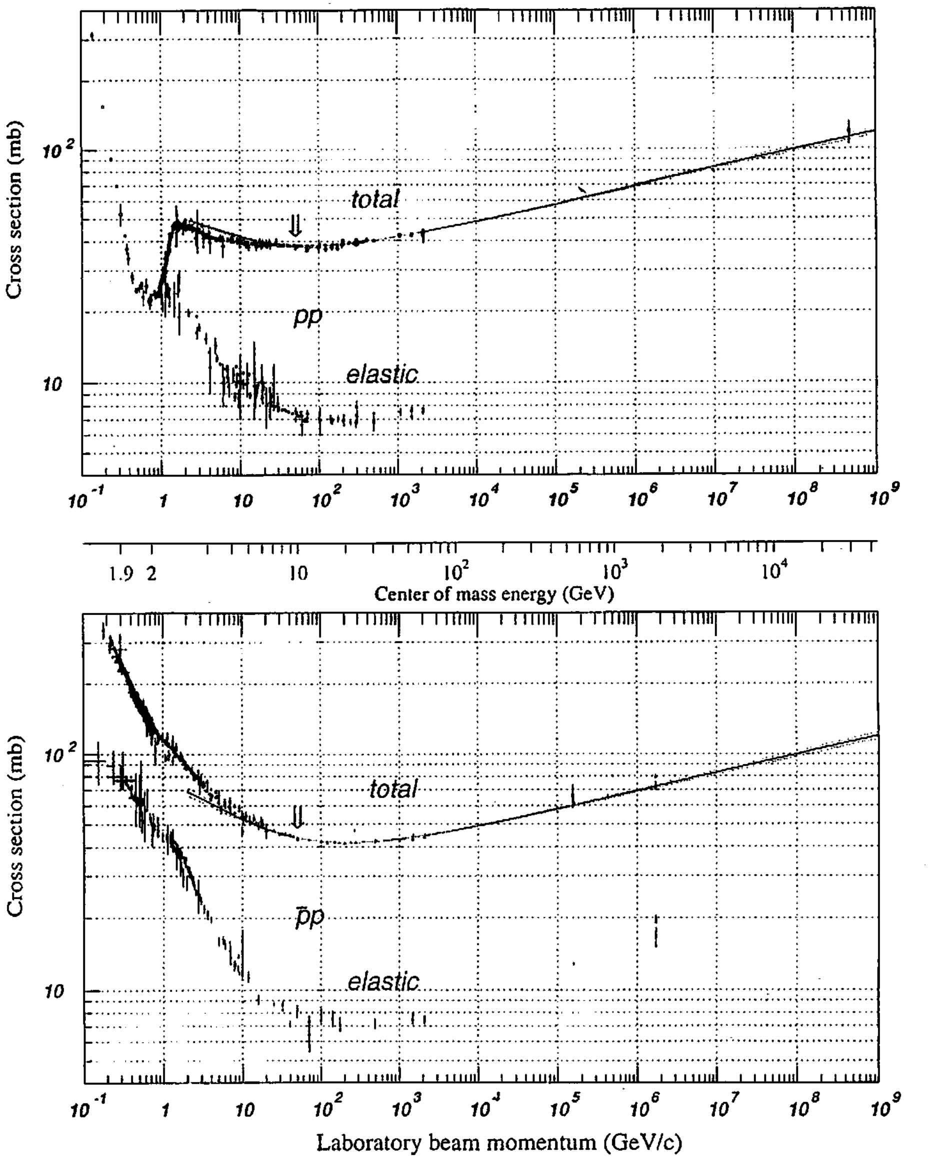

Figure 36.18: Total and elastic cross sections for pp and $\bar{p}p$ collisions as a function of laboratory beam momentum and total center-of-mass energy. Computer-readable data files may be found at `http://pdg.lbl.gov/xsect/contents.html` (Courtesy of the COMPAS Group, IHEP, Protvino, Russia, 1996.)

production in the three interaction models is compared with data on light nuclei (beryllium) in Fig. 5. These data [31,32] are for beam momenta in the range 19–24 GeV/c, which is the median energy for production of ~ GeV neutrinos [29].

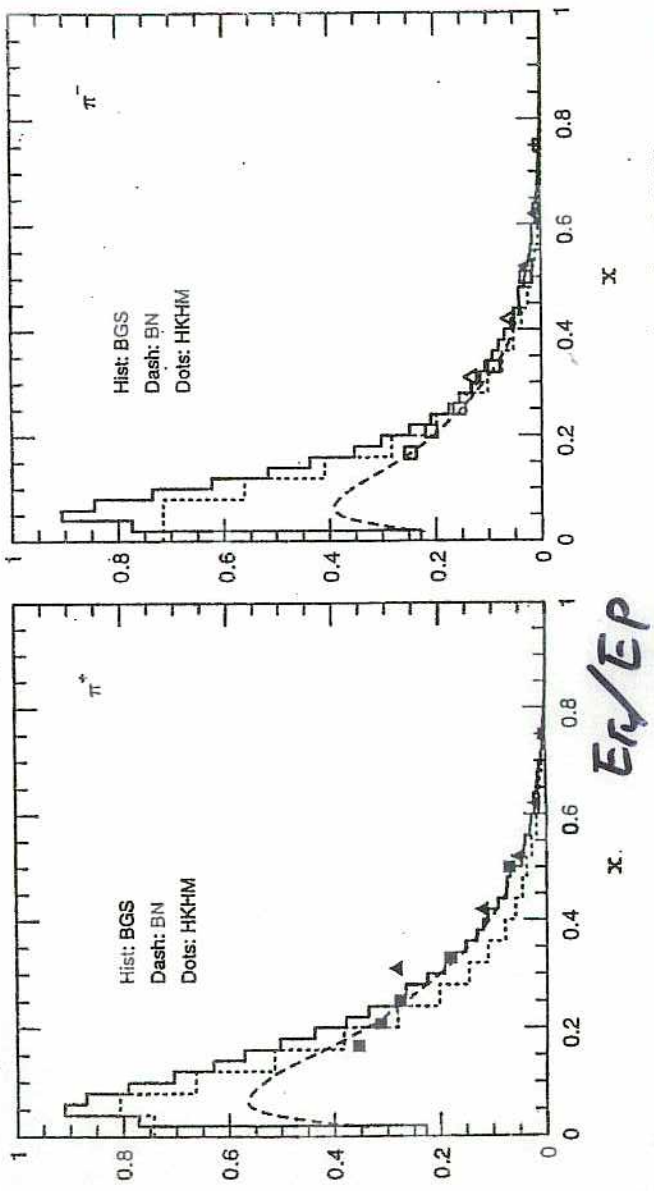

FIG. 5. Distributions of fractional momentum ($dn/d\ln x$) of charged pions produced in interactions of ≈20 GeV/c momentum protons with light nuclei. Models are shown for target=air, data [31,32] for target=Be. π^+ and π^- are shown separately.

---

[3] We are grateful to D. H. Perkins for pointing out this reference to us and making this comparison [36].

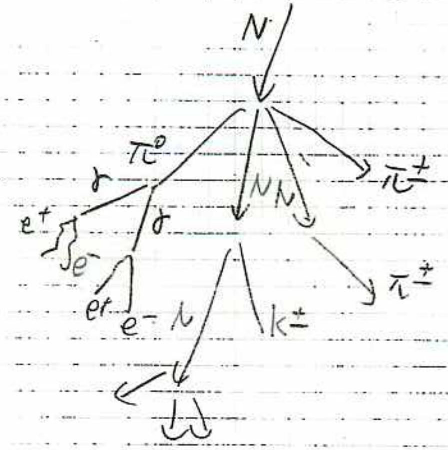

$\nu_\mu : \nu_e = 2 : 1$

$$\pi^+ \to \mu^+ \nu_\mu$$

$$\mu^+ \to e^+ + \nu_e + \overline{\nu_\mu}$$

$$\pi^- \to \mu^- \overline{\nu_\mu}$$

$$\hookrightarrow e^- + \overline{\nu_e} + \nu_\mu$$

問題

π^+

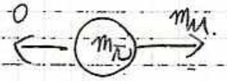

$$m_\pi = E_\mu + E_\nu$$

$$E_\nu = P_\nu = P_\mu$$

$$m_\pi = \sqrt{m_\mu^2 + P_\nu^2} + E_\nu$$

$$(m_\pi - E_\nu)^2 = m_\mu^2 + E_\nu^2$$

$$m_\pi^2 - 2m_\pi E_\nu + \cancel{E_\nu^2} = m_\mu^2 + \cancel{E_\nu^2}$$

$$E_\nu = \frac{m_\pi^2 - m_\mu^2}{2m}$$

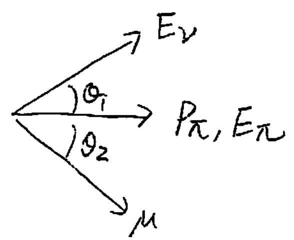

$$E_\nu \sin\theta_1 = P_\mu \sin\theta_2 \quad — ①$$

$$E_\nu \cos\theta_1 + P_\mu \cos\theta_2 = P_\pi \quad — ②$$

$$E_\pi = E_\nu + E_\mu \quad — ③$$

$$E_\nu^2 \sin^2\theta_1 = P_\mu^2 \sin^2\theta_2$$

$$+ \quad (E_\nu \cos\theta_1 - P_\pi)^2 = P_\mu^2 \cos^2\theta_2$$

$$P_\mu^2 = E_\nu^2 - 2E_\nu \cos\theta_1 P_\pi + P_\pi^2 \quad — ④$$

$$③ \rightarrow \quad E_\mu^2 = (E_\pi - E_\nu)^2 = E_\pi^2 - 2E_\pi E_\nu + E_\nu^2 \quad — ⑤$$

$$⑤ - ④ \quad m_\mu^2 = m_\pi^2 - 2E_\pi E_\nu + 2E_\nu \cos\theta P_\pi$$

$$2E_\nu (E_\pi - P_\pi \cos\theta) = m_\pi^2 - m_\mu^2$$

$$E_\nu = \frac{m_\pi^2 - m_\mu^2}{2(E_\pi - P_\pi \cos\theta)}$$

重心系

Lab系 $\pi^+ \longrightarrow$

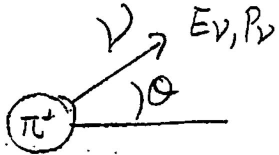

$E_\nu = P_\nu$

$$\gamma = \frac{E_{\pi^+}}{m_{\pi^+}}, \quad \gamma = \frac{1}{\sqrt{1-\beta^2}}$$

Lab系での ニュートリノエネルギーは、

$$E_\nu' = \gamma E_\nu + \gamma\beta P_\nu \cdot \cos\theta$$

$$= E_\nu(\gamma + \gamma\beta\cos\theta) = \gamma E_\nu(1+\beta\cos\theta)$$

$$P_{/\!/}' = \gamma\beta E_\nu + \gamma P_\nu \cos\theta = E_\nu(\gamma\beta + \gamma\cos\theta)$$
$$= \gamma E_\nu(\beta + \cos\theta)$$

$$P_\perp' = E_\nu \sin\theta, \quad P' = \gamma E_\nu\left(\sqrt{(\beta+\cos\theta)^2 + \frac{1}{\gamma^2}\sin^2\theta}\right)$$

$$= \gamma E_\nu \sqrt{(\beta+\cos\theta)^2 + (1-\beta^2)\sin^2\theta}$$

$$= \gamma E_\nu \sqrt{(\beta^2 + 2\beta\cos\theta + 1 - \beta^2\sin^2\theta)} = \gamma E_\nu(1+\beta\cos\theta)$$

最大ν energy : $\dfrac{m_\pi^2 - m_\mu^2}{2(E_\pi - P_\pi)}$

$$P_\pi = \sqrt{E_\pi^2 - m_\pi^2}$$

$E_\pi \gg m_\pi$のとき、 $= E_\pi - \dfrac{1}{2}\dfrac{m_\pi^2}{E_\pi}$

$$\sqrt{} = \frac{m_\pi^2 - m_\mu^2}{\frac{m_\pi^2}{E_\pi}} = E_\pi \times \frac{m_\pi^2 - m_\mu^2}{m_\pi^2}$$

$$\sqrt{1-\delta}$$

$$E_\pi\left(\sqrt{\cancel{1} - \frac{m_\pi^2}{E_\pi^2}}\right) = 0.43 E_\pi$$

$$= 1 - \frac{1}{2}\delta$$

$\mu^+ \to e^+ \nu_e \overline{\nu_\mu}$

e^+に着目　$\overline{\nu_\mu}$に着目

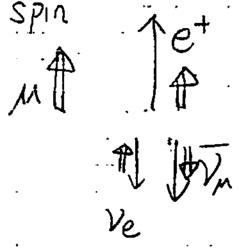

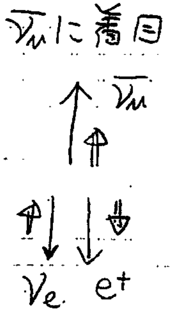

$\overline{\nu_\mu}$とe^+のspectrumは同じ。(e mass を neg.って

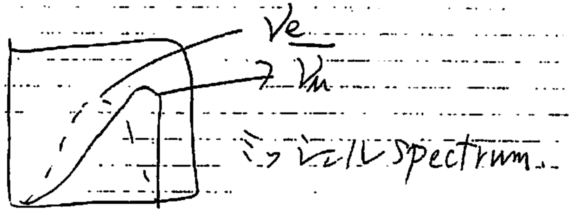

$\mu^- \to e^- \overline{\nu_e}\, \nu_\mu$ は.

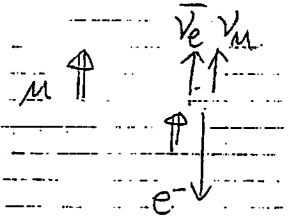

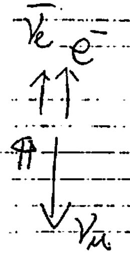

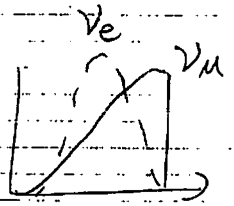

Thus, ISIS represents a ν-source with identical intensities for ν_μ, ν_e
cally ($\Phi_\nu = 6.37 \cdot 10^{13}\,\nu$/s per flavor for p-beam current $I_p = 200\,\mu$A
the ν's are well defined due to the decay at rest of both the π^+ and μ

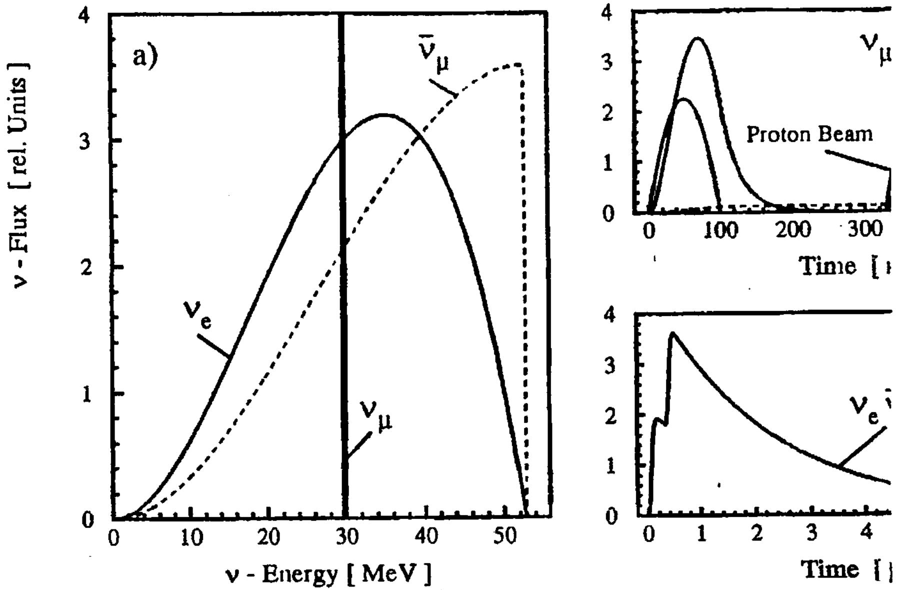

Fig. 1. Neutrino energy spectra (a) and production times (b)

π^+–decay are monoenergetic (E_ν=30 MeV), the continous energy dist
to 52.8 MeV can be calculated using the V–A theory. Since π^+ and μ^+
beam dump target, the ν production region is essentially limited to
to the proton beam and ±10 cm along the beam axis. With a mean di
$L = 17.6$ m and including the spatial resolution of the detector, the un
flight path is less than 1%. ISIS therefore ensures that the important
L and E_ν for ν–oscillations are determined with high precision.

Two parabolic proton pulses of 100 ns basis width and a gap of 22
repetition frequency of 50 Hz (fig. 1b). The different lifetimes of pio
($\tau = 2.2\,\mu$s) allow a clear separation in time of the ν_μ-burst from th
Furthermore the accelerator duty cycle allows effective suppression
background by four to five orders of magnitude.

2. The KARMEN Detector

The neutrinos are detected in a 56 t liquid scintillation calorimeter

Atmospheric ν flux

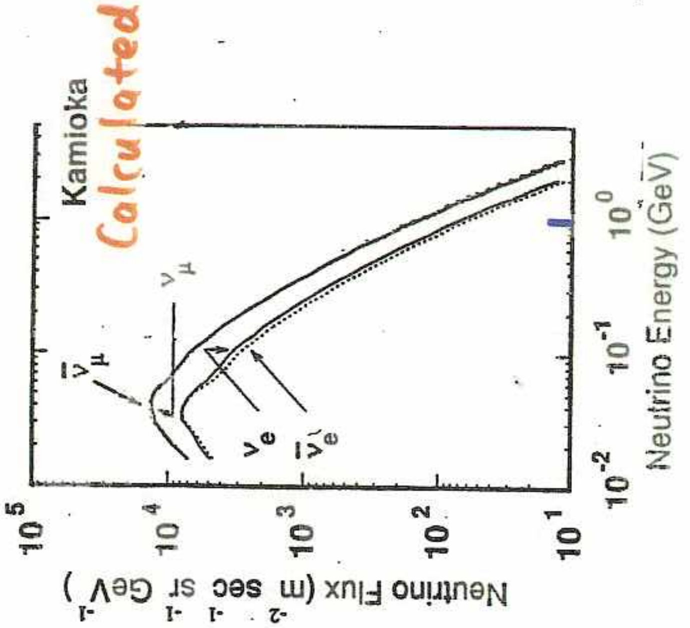

Primary Cosmic Ray flux

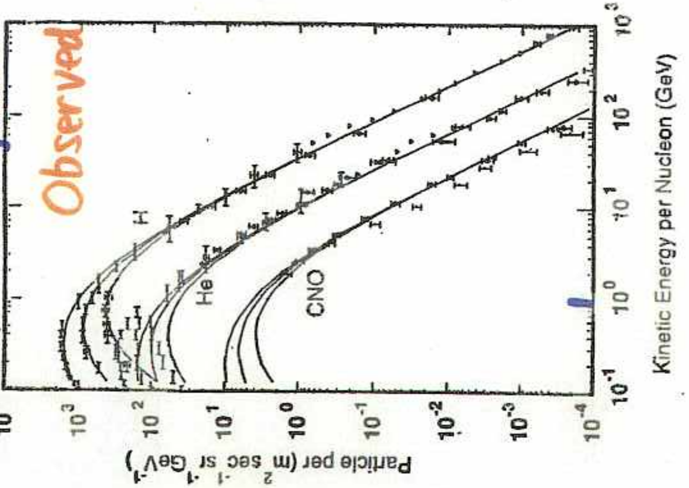

Atmospheric ν で ν oscillation を議論するのた
何が普遍的な量であるか。

$$\pi^+ \rightarrow \mu^+ \nu_\mu$$
$$\hookrightarrow e^+ \nu_e \bar{\nu}_\mu$$

$$\pi^- \rightarrow \mu^- \bar{\nu}_\mu$$
$$\hookrightarrow e^- \bar{\nu}_e \nu_\mu$$

たとえ少し $K^\pm$ がまじっていても

$K^+ \rightarrow$	$\mu^+\nu_\mu$	63.5%
	$\pi^+\pi^0$	21.2%
	$\pi^+\pi^+\pi^-$	5.6%

結論は同じで

$$\frac{\nu_\mu + \bar{\nu}_\mu}{\nu_e + \bar{\nu}_e}$$ は、いつも 2。

integrate all Energy

Atmospheric neutrino spectrum

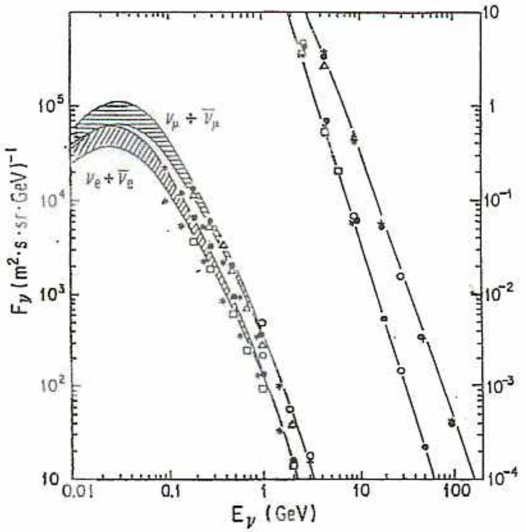

Energy dependence of ν_μ/ν_e ratio

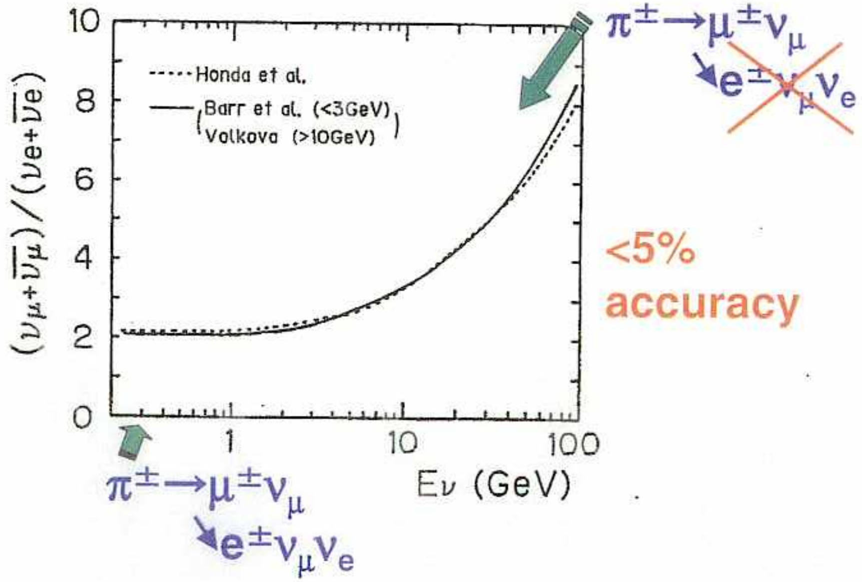

<5% accuracy

② High energy

μ-life time 2.2μsec.

Cで速ったとすると 3×10^8 m/sec

660m でdecay

atmspheric νは、

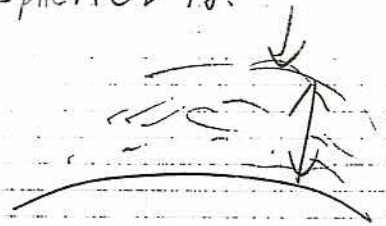

10~30km の所でうまれる。

したがって γ factorが 40位以上になると、decayせずに地表におちる。

$$E_\mu \simeq \gamma m_\mu = 40\times105.7\,\mathrm{MeV}$$
$$\simeq 4\,\mathrm{GeV}$$

νのenergyにして 2GeV位から $\dfrac{\overline{\nu_\mu+\nu_\mu}}{\nu_e+\overline{\nu_e}}$ からずれてくる。

しかし、この比は、μの decay kinematicによるので、Modelによるちがいは小さい。そこで

$$\left(\frac{\nu_\mu+\overline{\nu_\mu}}{\nu_e+\overline{\nu_e}}\right)_{Data} \Bigg/ \left(\frac{\nu_\mu+\overline{\nu_\mu}}{\nu_e+\overline{\nu_e}}\right)_{MC}$$ を使う。

double ratio

Zenith angle distribution

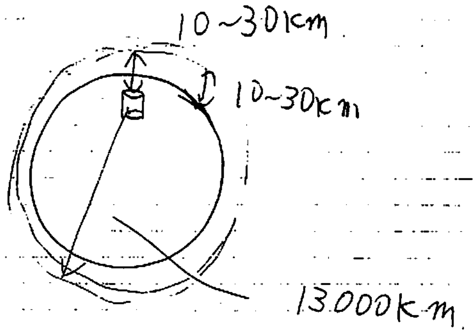

ν oscは

$$1-\sin^2 2\theta \sin^2\left(1.27\times\frac{L}{E_\nu}\Delta m^2\right)$$

例えば $\Delta m^2 = 3\times10^{-3}\,eV^2$とすると

$L=$ ~km, $E_\nu =$ GeV 単位なので

$\frac{L}{E_\nu}\Delta m^2$は 下向き 0.06

1GeVのνに対して上向きは 39

ν-flux

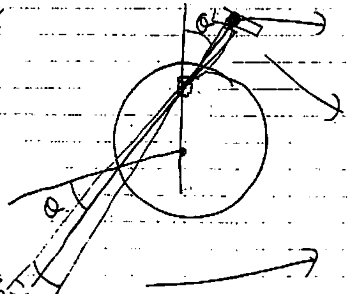

微小体積 大気の厚み

$(\Delta\theta\times L_1)^2\times\Delta D$

$(\Delta\theta\times L_2)^2\times\Delta D$

入射角度は同じ。detectorで観測されるための acceptance

$\propto \frac{1}{L_1^2}$, $\propto \frac{1}{L_2^2}$

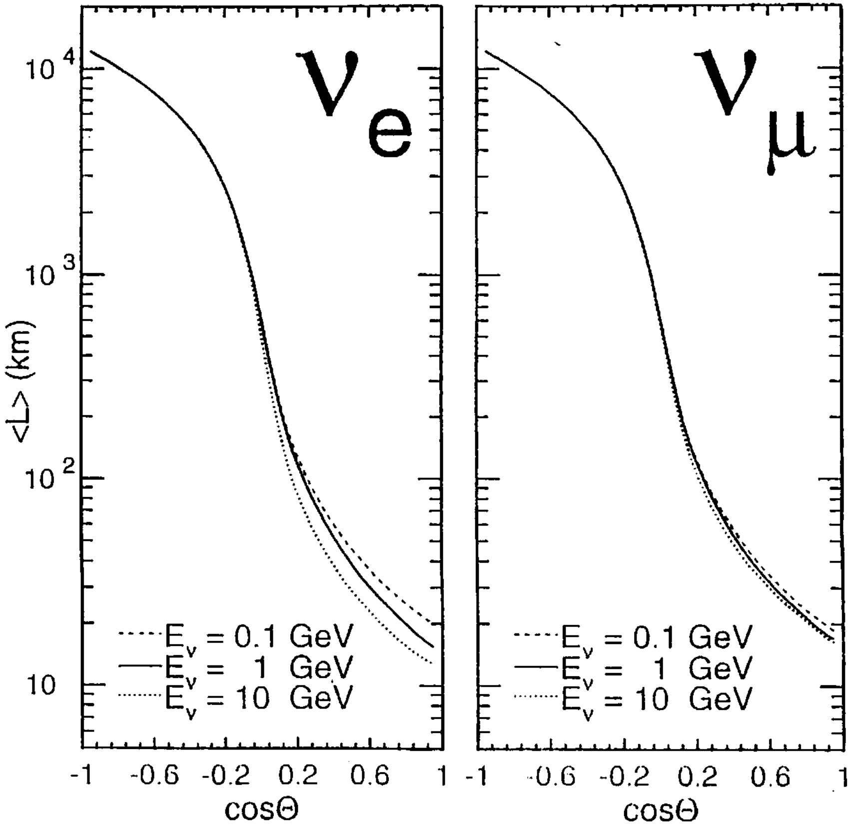

したがって flux は $\propto \Delta\Theta^2 \times \Delta D$ に比例し、 atm-32
下向きと 上向きの flux は、かわらない。
したがって 上、下 対称に なる。

Energy の 高い所では 横方向が 多い。
なぜか、

$\pi^\pm$の life time ; $\tau \doteq 26$ n-sec

$c\tau \doteq 7.8$ m

Interaction length は、 $\doteq 90$ g/cm²
1気圧の時

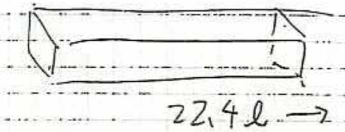

平均分子量 29位 29 g

$$\frac{\ell x}{22400} \times 29 = 90 ;$$

$\ell \doteq 700$ m

したがって $\pi^\pm$の energy が 数10GeV以上 位以上に なると

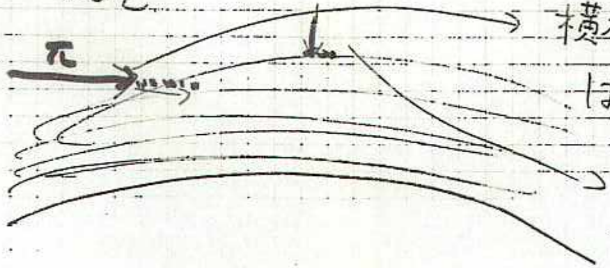

→ 横方向は、大気のうすい所を長 はしる。

→ すぐ こいところに なる。

したがって 横方向 が多くな

Zenith angle distribution

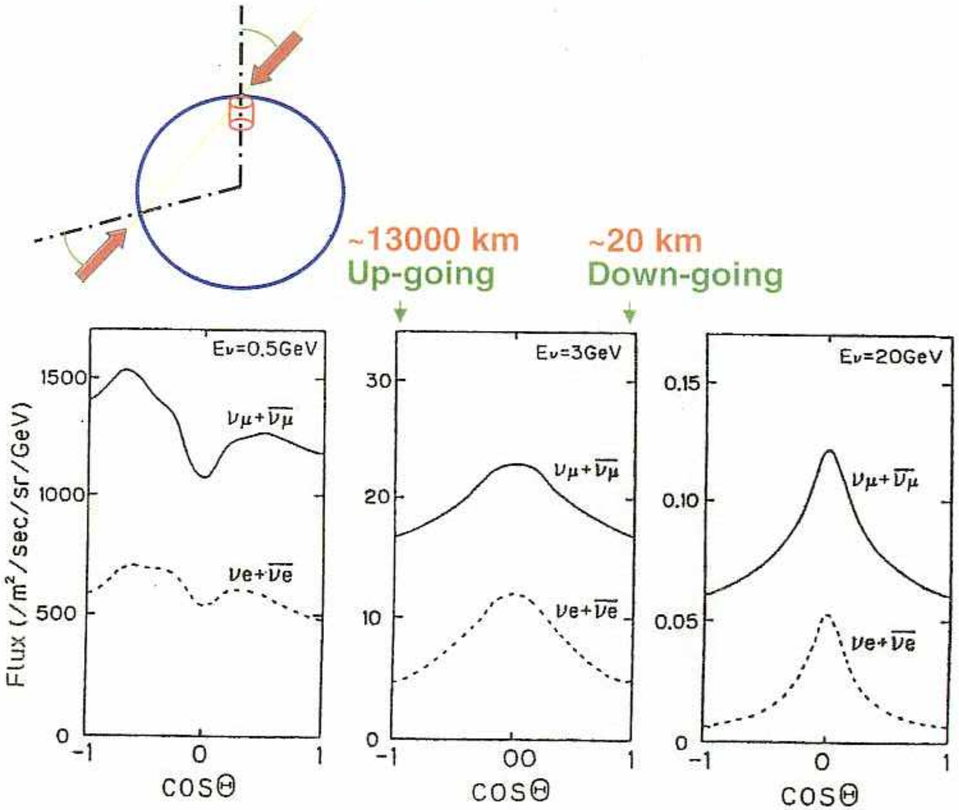

For E_ν > a few GeV,

Upward / downward = 1 (within a few %)

⬇

Up/Down asymmetry for neutrino oscillations

ν-interaction

How to detect ν

CC:

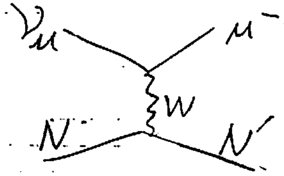

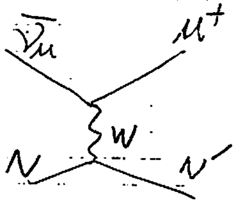

NC:

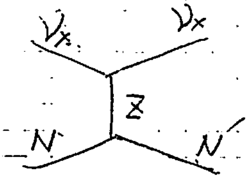

CC: flavor を保存する。

(1)

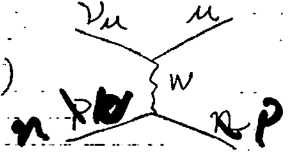

ν_μ + ~~p~~ n → μ^- + ~~n~~ p quesi-elastic

(2)

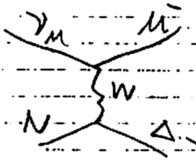

Δ → N+π

$\nu_\mu + N \Rightarrow \mu^- + N + \pi$

single π production

(3)

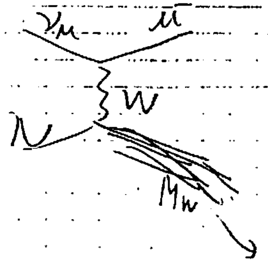

Multi-π production

deep-inelastic scattering

W → many π production

the final state are determined from the q^2 ($q = p_\nu - p_{lepton}$;

dependence of the cross section. This cross section is calculated [12] using the standard $V - A$ theory. Neutral-current (NC) quasi-elastic interactions are almost always invisible in water Cerenkov detectors unless a final-state proton recoils with sufficient energy ($p_p \gtrsim 1.5$ GeV/c) to emit Cerenkov radiation, or pions are produced by nucleon interactions off water nuclei. Fig. 2 shows the calculated cross sections for CC quasi-elastic interactions off free nucleons. The data from the Argonne 12-foot bubble-chamber experiment are also shown. The calculated cross section seems to be slightly higher than that from the Argonne data. This is because a parameter appearing in the formula of the cross section M_A, called axial-vector mass, measured by the Argonne experiment was 0.95 ± 0.09 GeV, while the value inputted in our calculation was 1.01 GeV, based on more recent measurements. Very roughly, the cross section of neutrino is proportional to the M_A value.

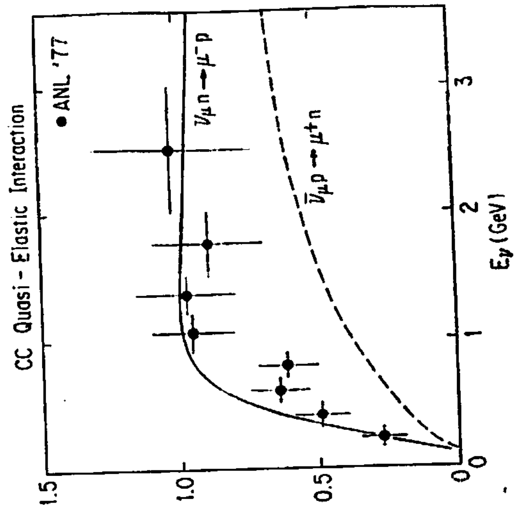

Figure 2: Cross section of charged-current quasi-elastic interactions off a free nucleon. The curves represent the calculation and the black circles with error bars represent the data [13]. The curve tends to have a larger cross section, because the value of M_A used in the simulation (1.01 GeV) is larger than the best-fit value of this experiment

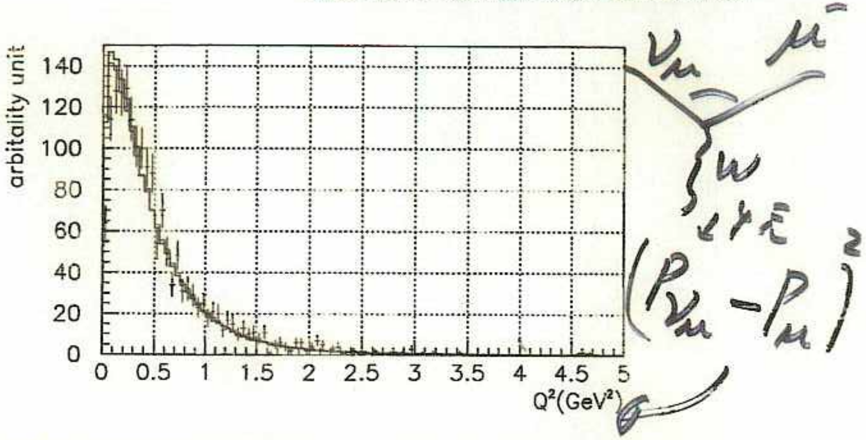

Figure 7.1: Differential cross section $d\sigma/dq^2$ for $\nu_\mu + n \rightarrow \mu^- + p$ interaction. Solid line is our calculation and points show experimental data from BNL bubble chamber experiment [102].

cross sections:

$$\sigma(\nu p \rightarrow \nu p) = 0.153 \times \sigma(\nu n \rightarrow e^- p) \quad (7.7)$$
$$\sigma(\bar{\nu} p \rightarrow \bar{\nu} p) = 0.218 \times \sigma(\bar{\nu} p \rightarrow e^+ n) \quad (7.8)$$
$$\sigma(\nu n \rightarrow \nu n) = 1.5 \times \sigma(\nu p \rightarrow \nu p) \quad (7.9)$$
$$\sigma(\bar{\nu} n \rightarrow \bar{\nu} n) = 1.0 \times \sigma(\bar{\nu} p \rightarrow \bar{\nu} p) \quad (7.10)$$

These numerical factors are taken from Ref. [108, 109].

7.2.3 Single meson productions via baryon resonances ($\nu + N \rightarrow l(\nu) + N' +$ meson)

The single-meson productions via resonances are the dominant hadron production processes in the region where the invariant mass of the hadron system (W) is less than about 2.0 GeV/c^2.

We simulate the single-meson productions via resonances based on Rein and Sehgal's theory [110]. The Rein & Sehgal's theory was originally developed for single-pion productions, but we extended their methods in order to include η and K meson productions.

In this theory, single-meson production is considered in 2 steps:

Resonance production	$\nu + N \rightarrow l(\nu) + N^*$
Resonance decay	$N^* \rightarrow N' + \pi(\eta, K)$

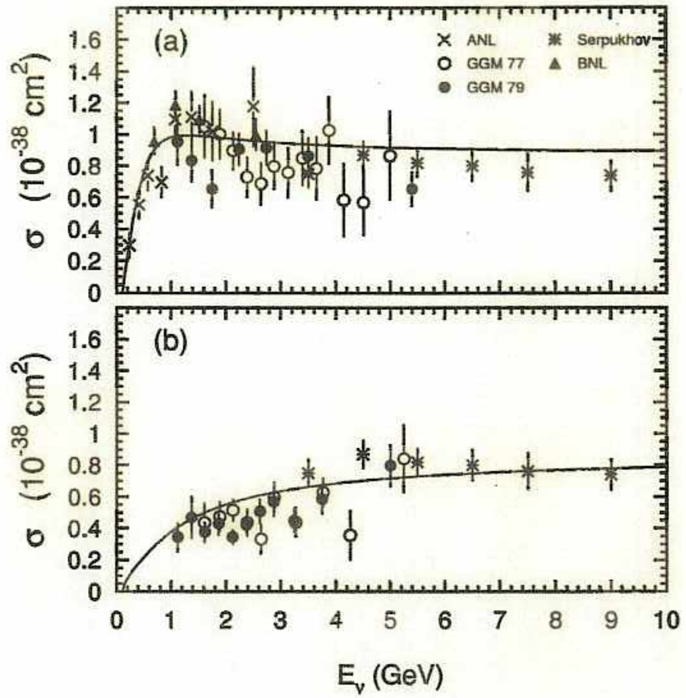

Figure 7.2: Cross section for (a) $\nu_\mu + n \rightarrow \mu^- + p$ interaction and (b) $\overline{\nu}_\mu + p \rightarrow \mu^+ + n$ interaction. Solid lines show our calculation and points show experimental data from ANL 12' [103], Gargamelle [104, 105], BNL 7' [106] bubble chambers and a spark chamber experiment at Serpukhov [107].

乏数 GeV Bjorken scaling

$$\frac{d\sigma^{\nu N,\bar\nu N}}{dx\,dy} = \frac{G_F^2 M E_\nu}{\pi}\left\{(1-y+\tfrac{1}{2}y^2)F_2(x) \pm y(1-\tfrac{1}{2}y)xF_3(x)\right\}$$

$$x = \frac{-q^2}{2M(E_\nu - E_{lepton})}, \quad y = (E_\nu - E_{lepton})/E_\nu$$

↑ target parton がどの位の momentum をもっているか。

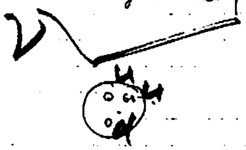

↓ ハドロンへどの位 energy を transfer したか。

$$F_2 = x \times (u + \bar u + d + \bar d + s + \bar s)$$

$$-xF_3 = x((u+d) - (\bar u + \bar d) - - -)$$

$$\frac{\sigma(\nu_\mu + N \to \nu_\mu + X)}{\sigma(\nu_\mu + N \to \mu^- + X)} \cong 0.26$$

$$\frac{\sigma(\bar\nu_\mu + N \to \bar\nu_\mu + X)}{\sigma(\bar\nu_\mu + N \to \mu^+ + X)} \cong 0.39$$

$F_2(x')$ （文献 3-7より）

H. Deden et al., Charge-changing interactions

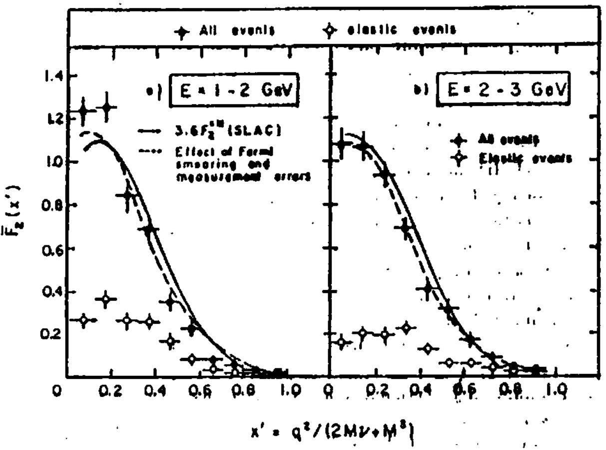

Fig. 3a, b.

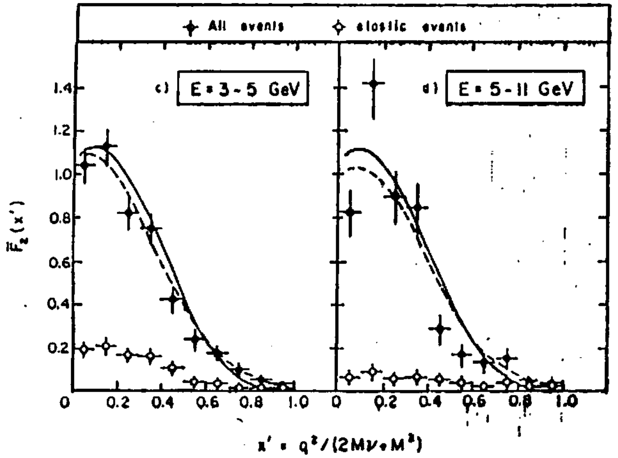

Fig. 3. $\bar F_2^{\nu N}(x', E)$ deduced from eq. (4) by replacing $x = q^2/2M\nu$ by the Bloom-Gilman variable $x' = q^2/(2M\nu + M^2)$, and without any cuts in q^2 or W^2. In each energy range, the SLAC curve of 3.6 $F_2^{eN}(x')$ is given, together with the modification expected from Fermi smearing and measurement errors.

図 3-11

$x'F_3(x')$ 分布（文献3-7より）

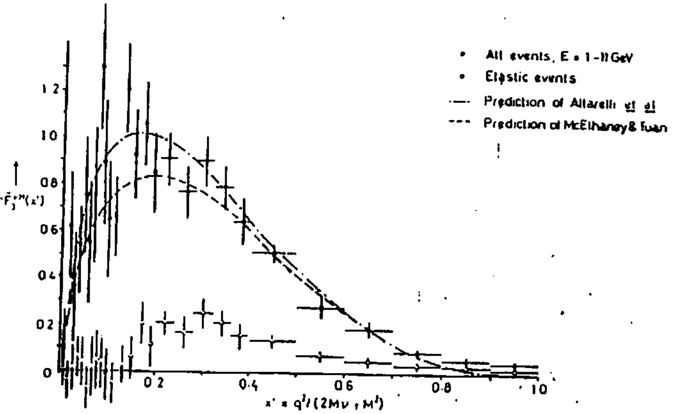

Fig. 5. Values of $x'F_3^{\nu N}(x')$ computed for all events, without cuts in q^2 or W^2. The curves show typical predictions, based on empirical fits of quark momentum distributions to electron scattering data.

図 3-12

$\nu P \to \mu^- P \pi^+$ 全断面積（文献3-8より）

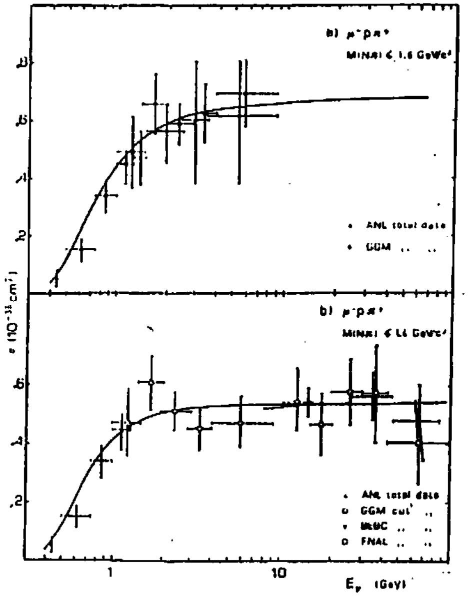

図 3-13

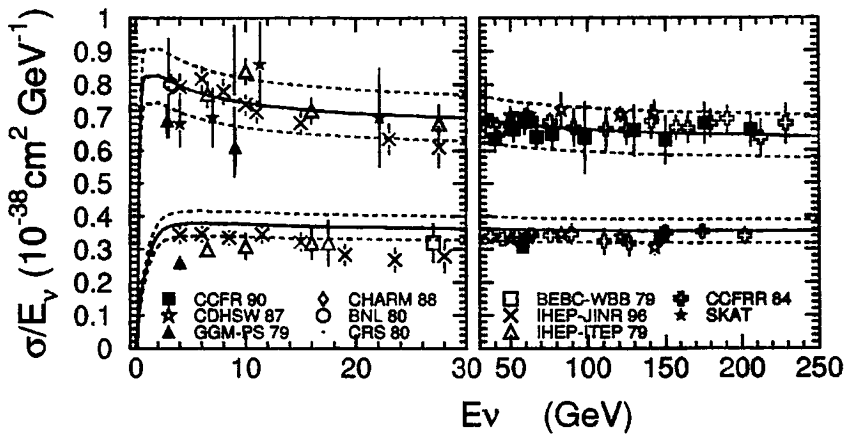

Figure 7.8: Cross sections for CC inclusive interactions on iso-scalar target for (a) $\nu_\mu + N \to \mu^- + X$, and (b) $\overline{\nu}_\mu + N \to \mu^+ + X$. Solid lines are the sum of the cross sections of all interaction modes described in the text, and dashed lines show ± 10% scaled lines. Points show experimental data from CCFR [132], CDHSW [133], Gargamelle [134, 135], CHARM [136], BNL [137], CRS [138], BEBC-WWB [139], IHEP-JINR [140], IHEP-ITEP [141], CCFRR [142], SKAT [143].

Fig. 7.8 shows the total cross section as a function of neutrino energy compared with experimental data. The total cross section is calculated as σ(Q.E.) + σ(Single meson) + σ(coherent π) + σ(DIS). The experimental data are the cross sections of the inclusive neutrino and antineutrino interactions $\nu_\mu(\overline{\nu}_\mu) + N \to \mu^\pm + X$ taken from Ref. [132, 133, 134, 135, 136, 137, 138, 139, 140, 141, 142, 143].

7.2.6 Fermi motion of a nucleon

A nucleon bound in a nucleus has a non-zero momentum (Fermi momentum). We use the Fermi momentum distribution in ^{16}O which was estimated from electron scattering experiment on ^{12}C target [144], taking into account that 4 nucleons (2 protons and 2 neutrons) are in the 1S state and the other 12 nucleons are in the 1P state. The distributions of the Fermi momentum are shown in Figure 7.9.

σ of ν 1GeVで $\sim 10^{-38}\,\mathrm{cm}^2$

13000km $\rho = 5.5\,\mathrm{g/cm^3}$

$= 1.3\times 10^{9}\,\mathrm{cm}$ 1g中に 6×10^{23}コの核子

$10^{-38}\times 1.3\times 10^{9}\times 5.5\times 6\times 10^{23}$

$=$ 4×10^{-5} の probability で interaction

$10^{-34} \sim 10^{-33}\,\mathrm{cm}^2$ 位でまま出す。

おれまがり $\boxed{E_\nu \cong 100\,\mathrm{TeV}}$

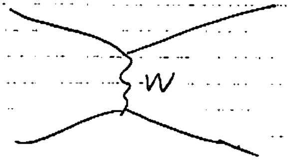

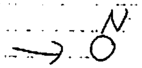

重心系のE $\sqrt{2m_p E_\nu}$

Wのmass ; 80.3GeV

$M_W = \sqrt{2 m_p E_\nu}$ となると

$E_\nu = 3\,\mathrm{TeV}$

propagator

$\propto \dfrac{1}{-q^2+M_W^2}$ small q^2では $\propto \dfrac{1}{M_W^2}$

$E_\nu \sim$

---

for calculating event rates in proposed detectors. We have gathered in Tables 1 and 2 the charged-current and neutral-current cross sections and values of $\langle y\rangle$, for νN and $\bar{\nu}N$ collisions, respectively.

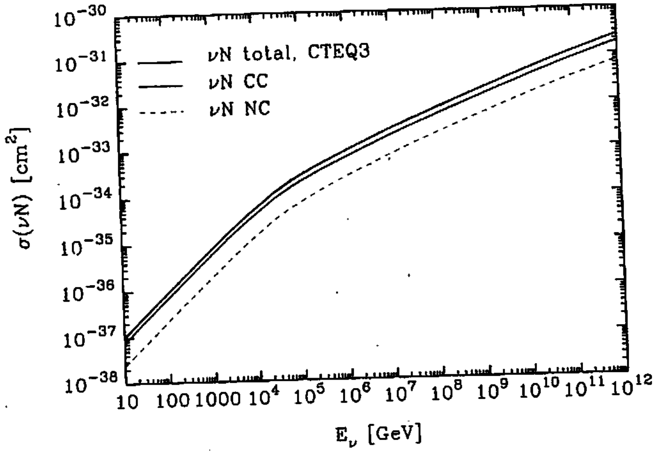

Fig. 8. Cross sections for νN interactions at high energies: dotted line, $\sigma(\nu N \to \nu + \text{anything})$; thin line, $\sigma(\nu N \to \mu^- + \text{anything})$; thick line, total (charged-current plus neutral-current) cross section.

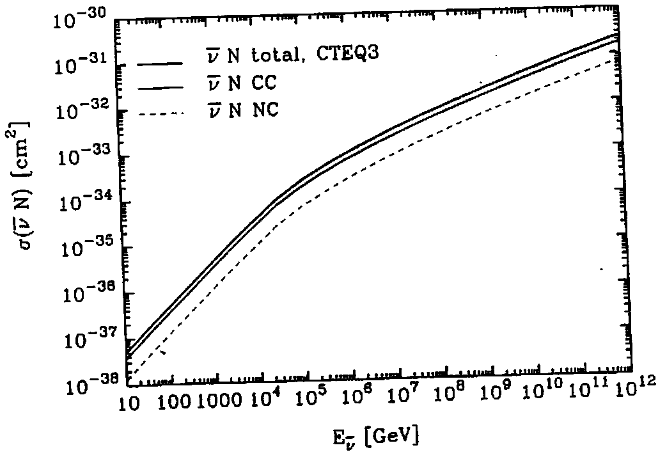

Fig. 9. Cross sections for $\bar{\nu}N$ interactions at high energies: dotted line, $\sigma(\bar{\nu}N \to \bar{\nu} + \text{anything})$; thin line, $\sigma(\bar{\nu}N \to \mu^+ + \text{anything})$; thick line, total (charged-current plus neutral-current) cross section.

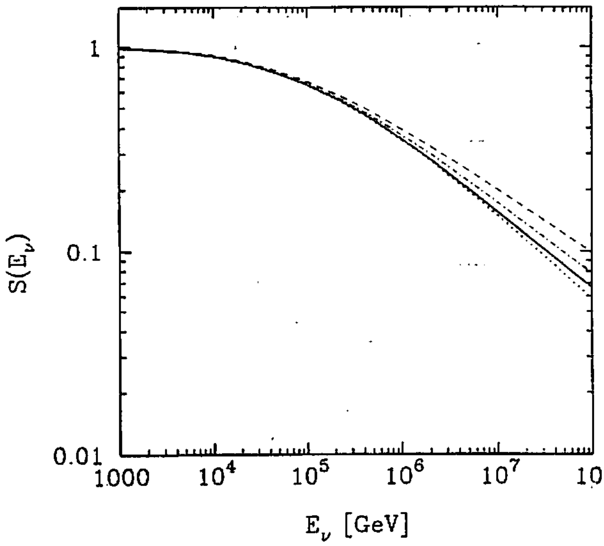

Fig. 20. The shadow factor $S(E_\nu)$ for upward-going neutrinos assuming that $\sigma = \sigma_{\rm tot}$ in (35) for CTEQ-DIS (solid line), CTEQ-DLA (dot-dashed) and D$_-$ (dotted) parton distribution functions. Also shown is the shadow factor using the EHLQ cross sections (dashed line).

For the case of isotropic fluxes, such as the AGN and cosmic neutrino fluxes presented in §8.1, the attenuation can be represented by a shadow factor that is equivalent to the effective solid angle for upward muons, divided by 2π:

$$S(E_\nu) = \frac{1}{2\pi}\int_{-1}^{0} d\cos\theta \int d\phi \exp\left[-z(\theta)/\mathcal{L}_{\rm int}(E_\nu)\right] . \qquad (35)$$

The interaction length $\mathcal{L}_{\rm int}(E_\nu)$ is shown in Figures 11 and 12 for νN and

---

弱

$\sim 10^4$ ν /m²/sec/str/GeV として

$\sigma = 10^{-38}$ cm² とすると

0.05 × 2π

0.5 0.6

$10^4 \times 10^{-4} \times 4\pi$ /cm²/sec/GeV

$\simeq$ 10 /cm²/sec/GeV

22 kton 中の核子数

$22 \times 10^3 \times 10^6 \overset{g}{} \times 6 \times 10^{23}$

23+9+1 33

$\simeq 1.3 \times 10^{33}$ コ

10^{-38} cm² × 10/cm²/sec/GeV × 1.3×10^{33} ×0

$\simeq \sim 10^{-4}$ /sec

1日は 0.86×10^5 sec

$\approx$ 10 ev./day

④

Atmospheric neutrinos

SK data

How to detect atmospheric neutrinos

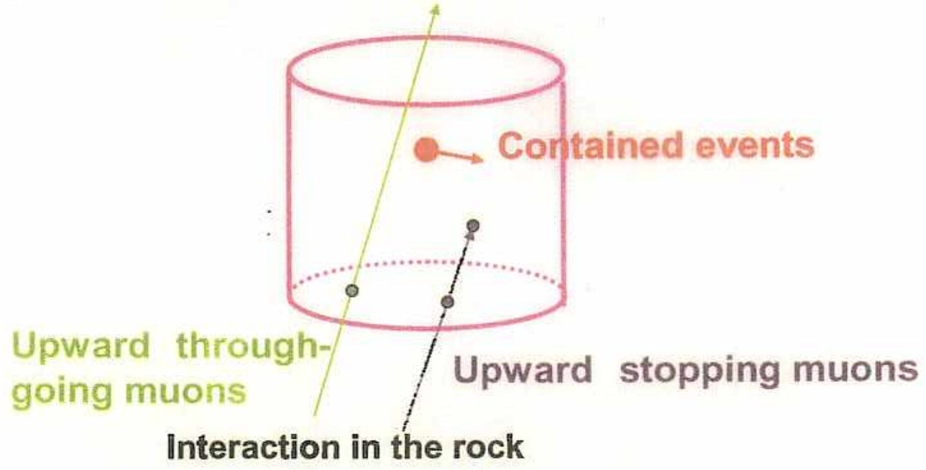

Initial neutrino energy spectrum

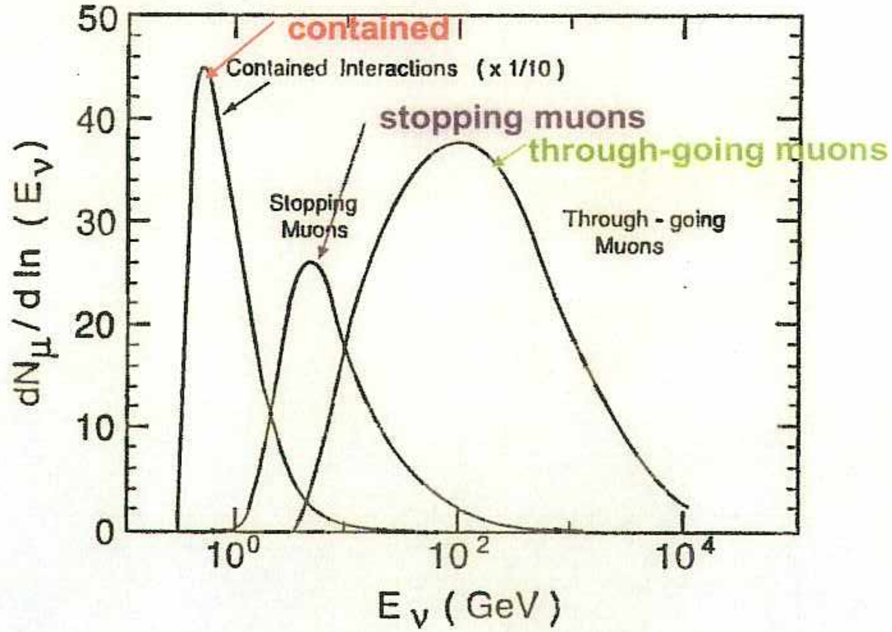

atmSK-3

Contained event analysis

Fully Contained (FC)

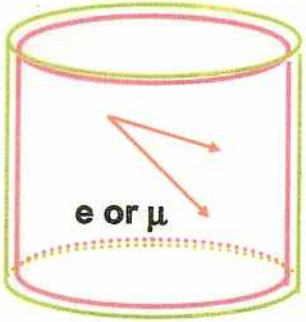

No hit in Outer Detector

Partially Contained (PC)

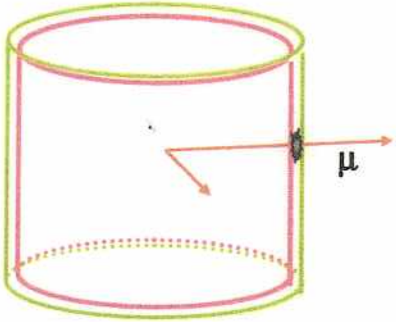

One cluster in Outer Detector

Reduction

Automatic ring fitter
Particle ID
Energy reconstruction

Fiducial volume (>2m from wall, 22 ktons)
E_{vis} > 30 MeV (FC), > 3000 p.e. (~350 MeV) (PC)

Final sample:
FC: 8.2 ev./day, PC: 0.55 ev./day

E_{vis} < 1.33 GeV : Sub-GeV
E_{vis} > 1.33 GeV : Multi-GeV

---

atmsk-4

PARTICLE IDENTIFICATION

700 MeV muon (Monte Carlo)

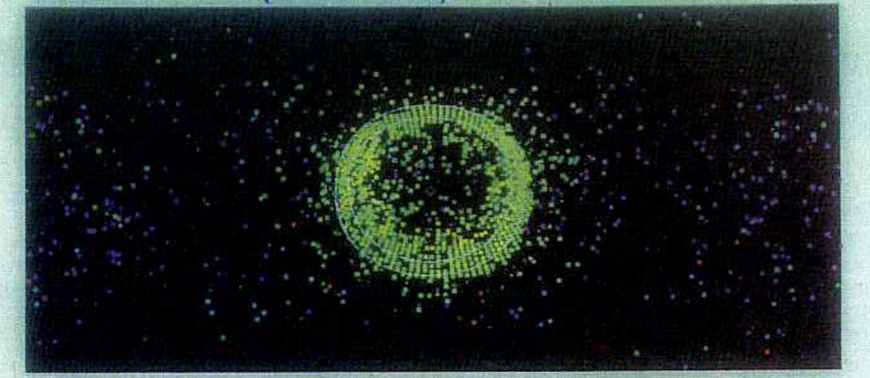

4023 photoelectrons, 1553 hits non-showering

500 MeV electron (Monte Carlo)

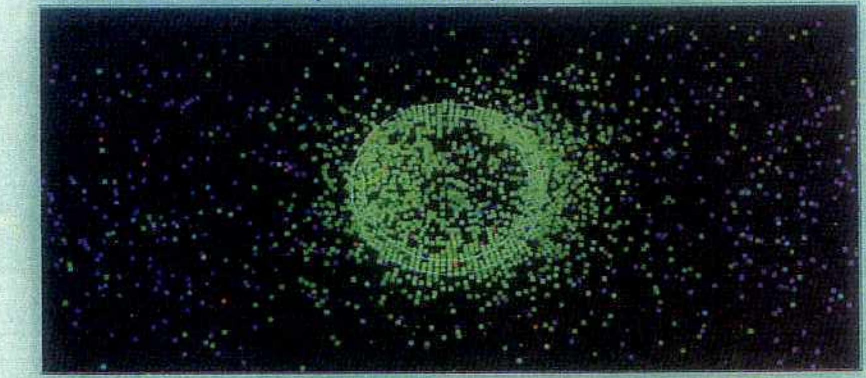

3917 photoelectrons, 2086 hits showering

projected view of detector as seen from fit vertex
color represents residual time from vertex

atmsk-6

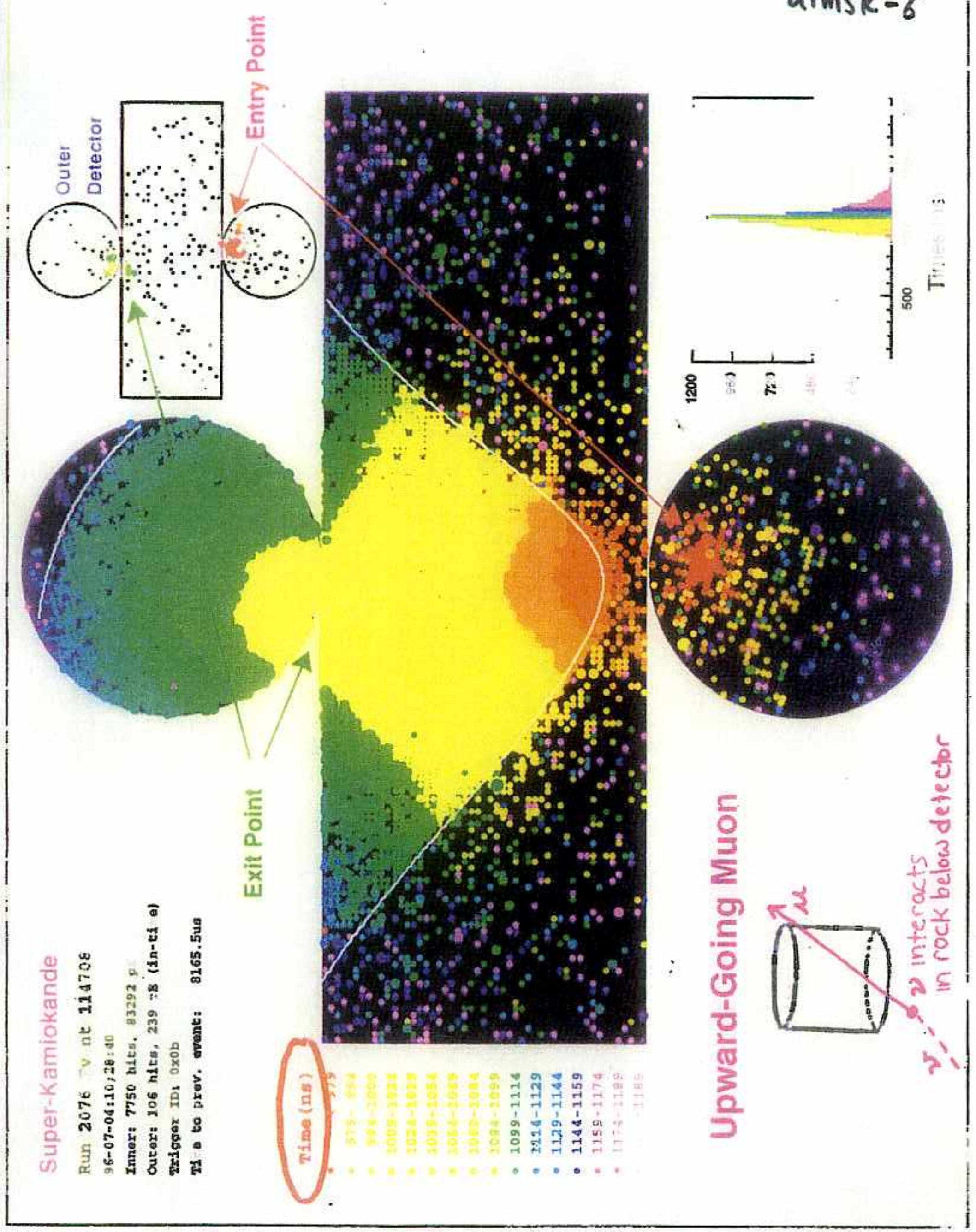

atmsk-7

Likelihood for particle identification

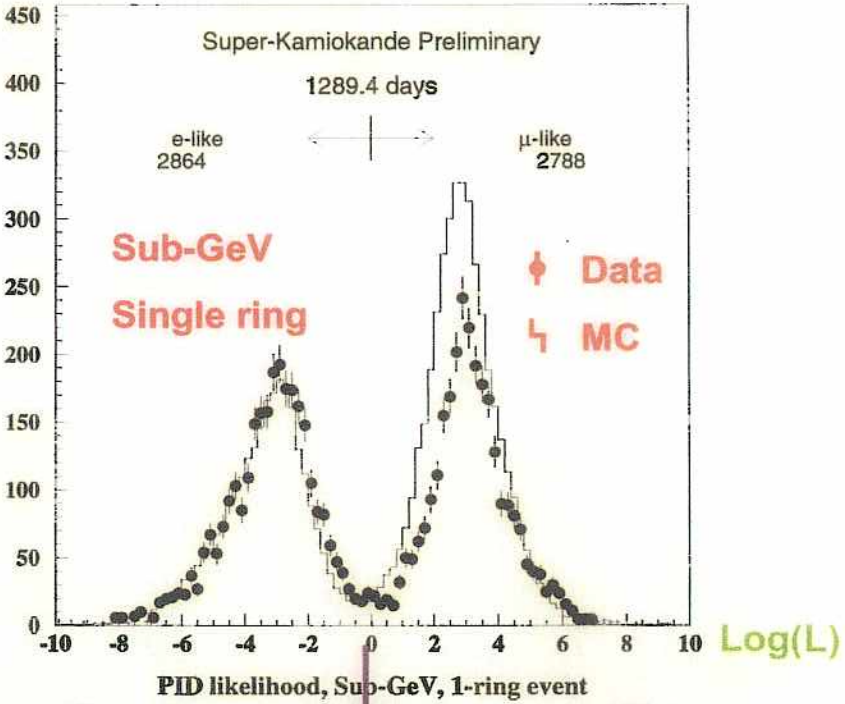

e-like ⇔ μ-like

Mis-identification: 0.6 ± 0.1 % for sub-GeV
~ 2 % for multi-GeV

Checked by e/μ beam at KEK (E261A)

Source of e-like/μ-like events (M.C. simulation)

- Sub-GeV 1-ring

			e-like			μ-like		
ν_e	$\nu_e,\bar{\nu}_e$ CC	QE (quasi-elastic)	10002	67.02%	87%	55	0.24%	
		non-QE	2962	19.85%		22	0.10%	
ν_μ	$\nu_\mu,\bar{\nu}_\mu$ CC	QE	122	0.82%		16603	73.89%	95%
		non-QE	374	2.51%		4797	21.35%	
	NC		1463	9.80%		992	4.41%	
	TOTAL		14923	100.0%		22469	100.0%	

- Multi-GeV 1-ring

			e-like			μ-like		
ν_e	$\nu_e,\bar{\nu}_e$ CC	QE	1237	35.39%	80%	3	0.07%	
		non-QE	1572	44.98%		14	0.34%	
ν_μ	$\nu_\mu,\bar{\nu}_\mu$ CC	QE	27	0.77%		2098	50.41%	99%
		non-QE	291	8.33%		2032	48.82%	
	NC		368	10.53%		15	0.36%	
	TOTAL		3495	100.0%		4162	100.0%	

- Partially Contained (PC)

			e-like		μ-like		
ν_e	$\nu_e,\bar{\nu}_e$ CC	QE	–	–	9	0.33%	
		non-QE	–	–	41	1.51%	
ν_μ	$\nu_\mu,\bar{\nu}_\mu$ CC	QE	–	–	415	15.29%	98%
		non-QE	–	–	2233	82.28%	
	NC		–	–	16	0.59%	
	TOTAL		–	–	2714	100.0%	

QE : $\nu N \rightarrow \ell^{\pm} N'$

non QE : $\nu N \rightarrow \ell^{\pm} N' \pi \ldots$

ν- lepton angular correlation

Bubble chamber data (BNL)

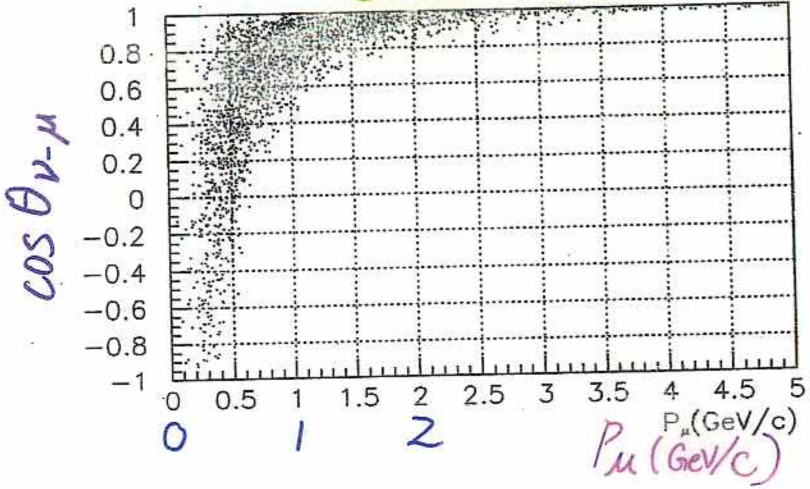

SK Monte Carlo for BNL

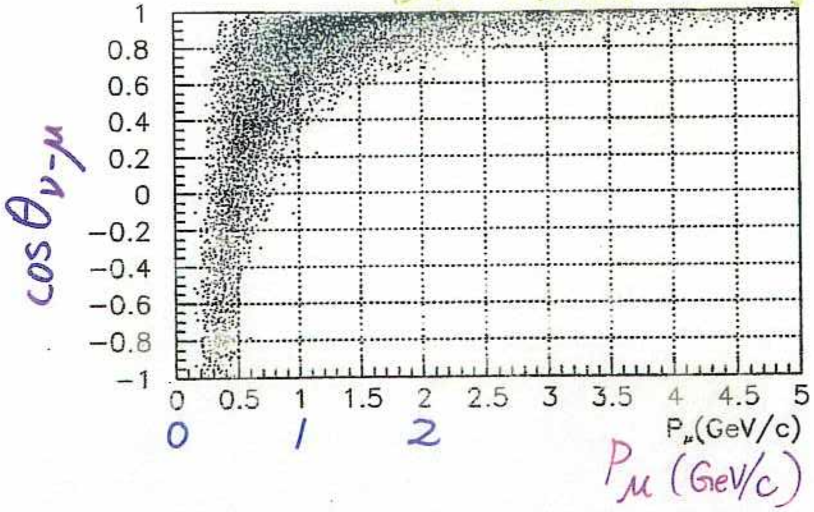

~flat $\cos\theta_{\nu\text{-}\mu}$ for $P_\mu < 0.4$ GeV

Sub-GeV Data

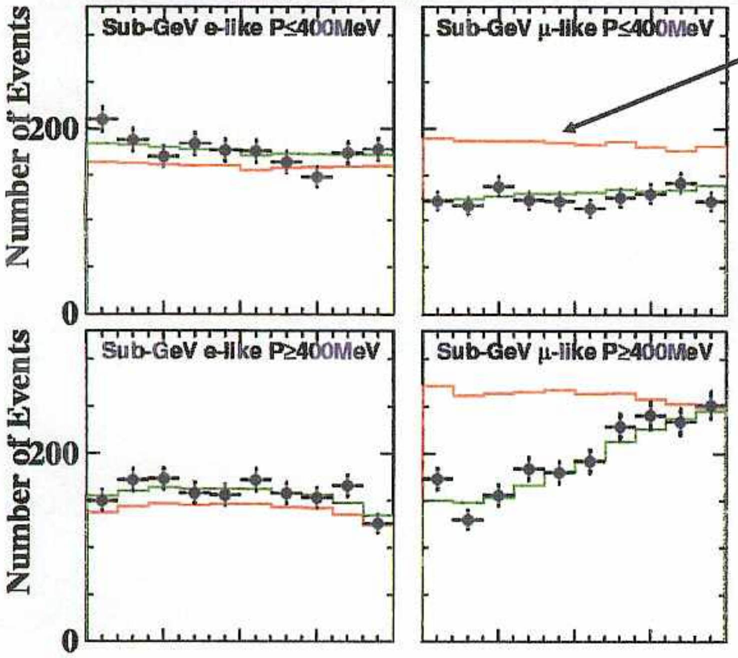

(note no "3D" horizon peak)
No cos(θ) shape information at the lowest energies, only flavor ratio is useful

	e-like	μ-like
Sub-GeV (<1.33 GeV)	3353 (Data) 3013.9 (MC)	3227 (Data) 4466.9 (MC)

$$\text{Sub GeV } \frac{(\mu / e)_{data}}{(\mu / e)_{MC}} = 0.649 \pm \underset{\text{(stat.)}}{0.016} \pm \underset{\text{(syst.)}}{0.051}$$

At higher energies, ν→μ directionality better preserved plus shorter L ν_μ no longer oscillate: cos(θ) shape information very useful

Key:
-- Data
-- MC (no osc.)
-- MC (best fit)

28th ICRC, 2 Aug.
2003 , Tsukuba

Multi-GeV data

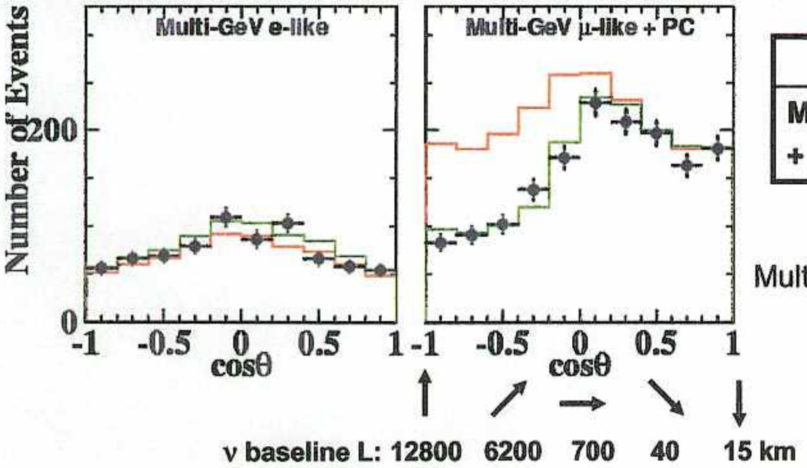

	e-like	μ-like
Multi-GeV + PC	746 (Data) 700.4 (MC)	1562 (Data) 2098.0 (MC)

$$\text{Multi GeV+PC } \frac{(\mu / e)_{data}}{(\mu / e)_{MC}} = 0.699 \underset{\text{(stat.)}}{\pm^{0.032}_{0.030}} \underset{\text{(syst.)}}{\pm 0.083}$$

At even higher energies, ν flux up/down symmetric and low-L ν_μ do not have time to disappear.

$$A = \left(\frac{N_{up} - N_{down}}{N_{up} + N_{down}}\right)_{\mu\text{-like}} = -0.289 \pm \underset{\text{(stat.)}}{0.028} \pm \underset{\text{(syst.)}}{0.004}$$

Compare to $A_{e\text{-like}}$= -0.020±0.043±0.005
MC $A_{\mu\text{-like}}$= -0.003±0.005±0.009
Observed $A_{\mu\text{-like}}$ 9.5σ from no-oscillation prediction!

Key:
-- Data
-- MC (no osc.)
-- MC (best fit)

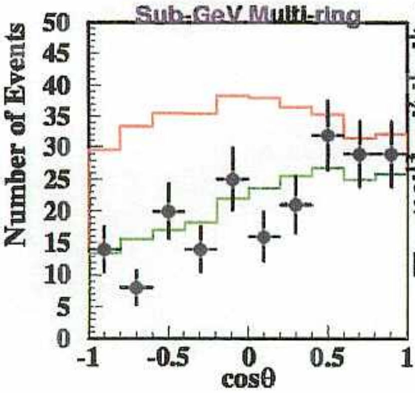

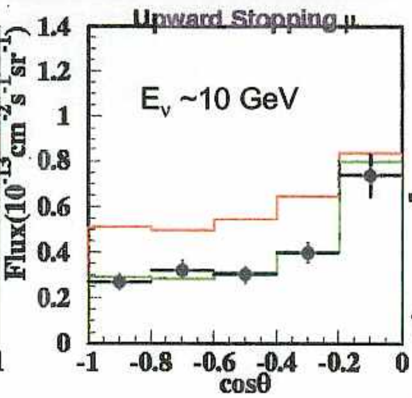

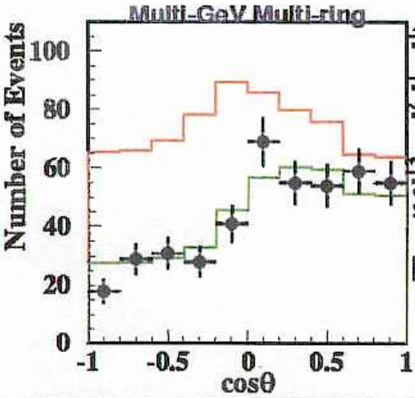

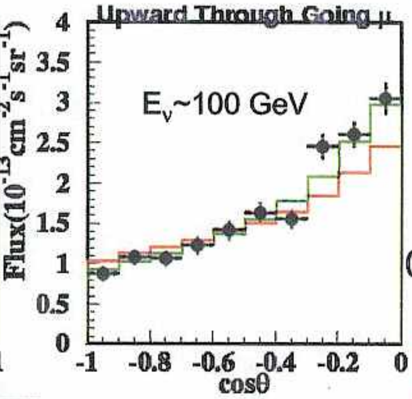

More Data

Up through going μ –

Measured flux:

$1.70\pm0.02\pm0.04\times10^{-13}$ cm^{-2}s^{-1}sr^{-1}
(stat.) (syst.)

Theoretical calc:

$1.57\pm0.35\times10^{-13}$ cm^{-2}s^{-1}sr^{-1}
(theo.)

Up stopping μ –

Measured flux:

$0.41\pm0.02\pm0.02\times10^{-13}$ cm^{-2}s^{-1}sr^{-1}
(stat.) (syst.)

Theoretical calc:

$0.61\pm0.14\times10^{-13}$ cm^{-2}s^{-1}sr^{-1}

(theo.)

	Data	MC
Sub-GeV Multi-ring μ	208	346.4
Multi-GeV Multi-ring μ	439	739.4

Key:
-- Data
-- MC (no osc.)
-- MC (best fit)

- More ν_μ, different E_ν and systematics

Sub-Sample Consistency

S K

- This low energy sub-sample's only handle on oscillations is the μ/e flavor ratio
- Used to be high (alone!), is now consistent with other sub-samples

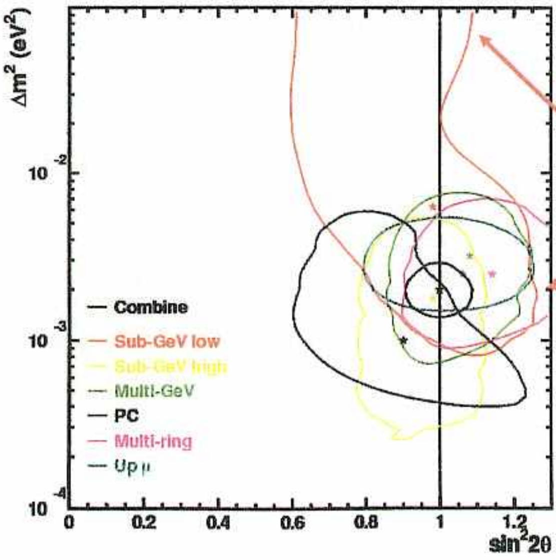

Note open-ended "swoosh" shape of a one-parameter flavor ratio fit to two osc. parameters (lowest E event sub-sample)

New Oscillation Results

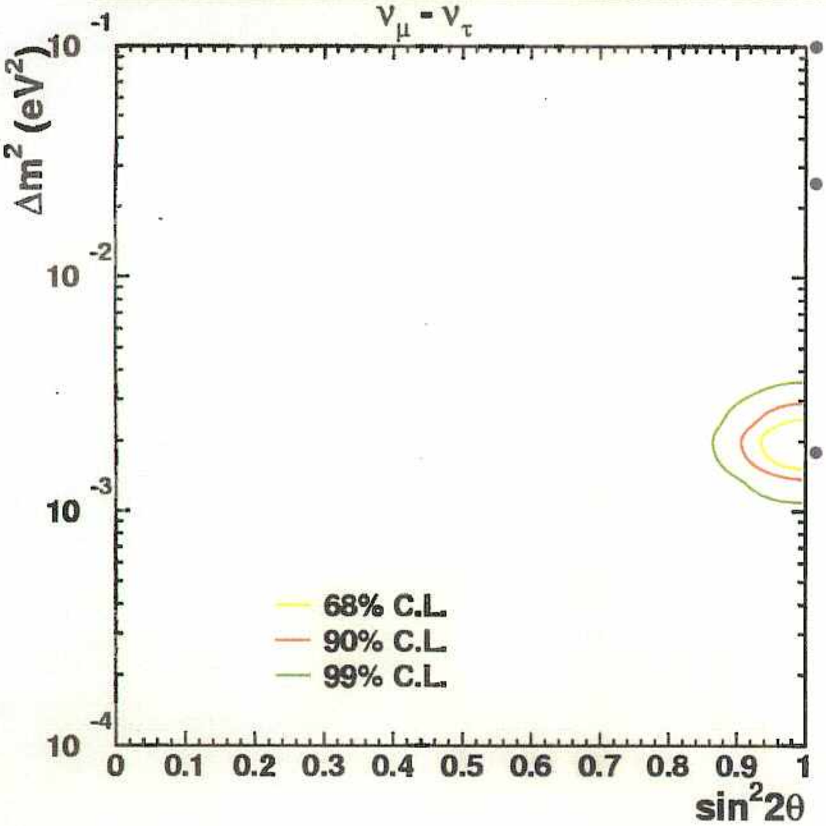

- For $\nu_\mu \leftrightarrow \nu_\tau$ oscillation:
- Best fit: $\sin^2(2\theta)=1.0$, $\Delta m^2=2.0\text{x}10^{-3}$ eV^2
  - χ^2 = 170.8/170 dof
- 90% c.l. region:
  - $\sin^2(2\theta)>0.9$
  - $1.3 <\Delta m^2<3.0\text{x}10^{-3}$ eV^2

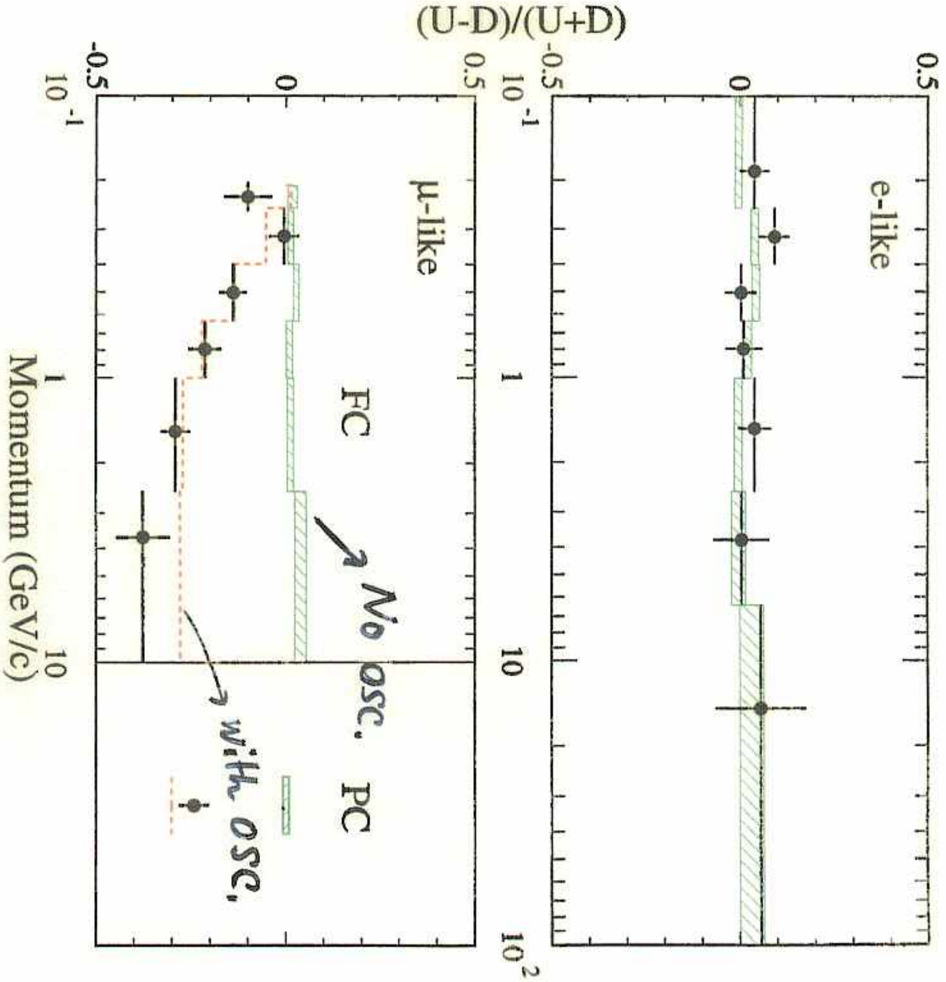

atmSK-16

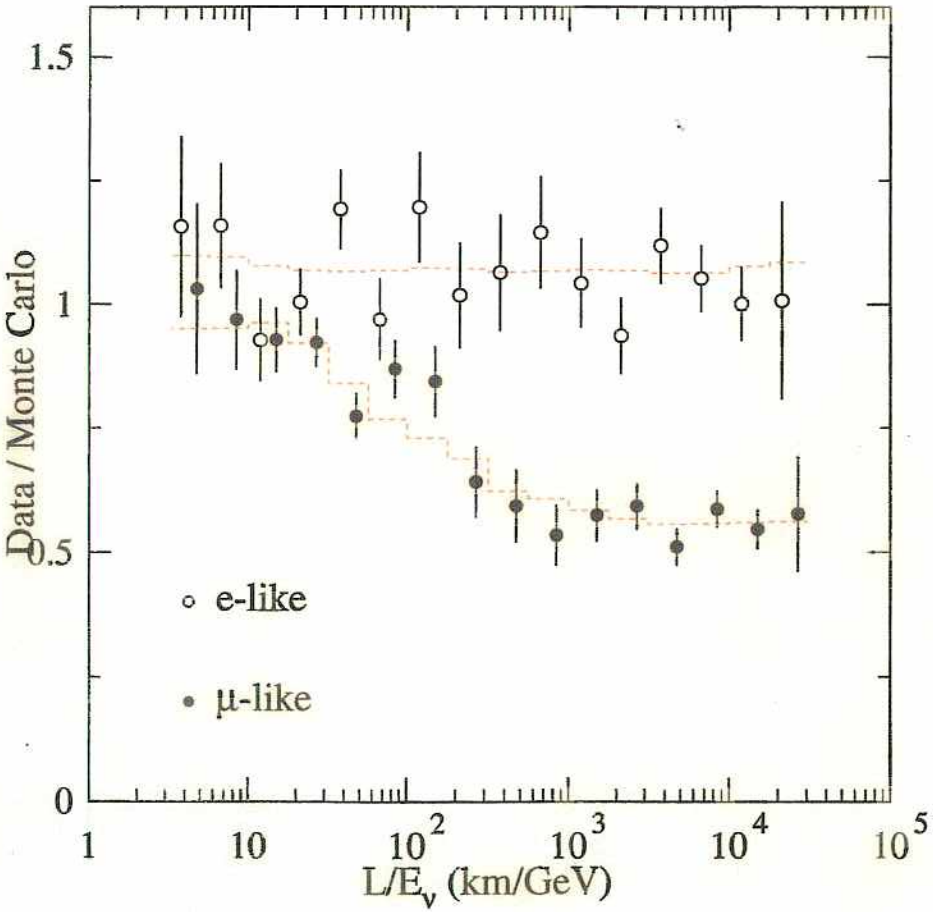

atmSK-17

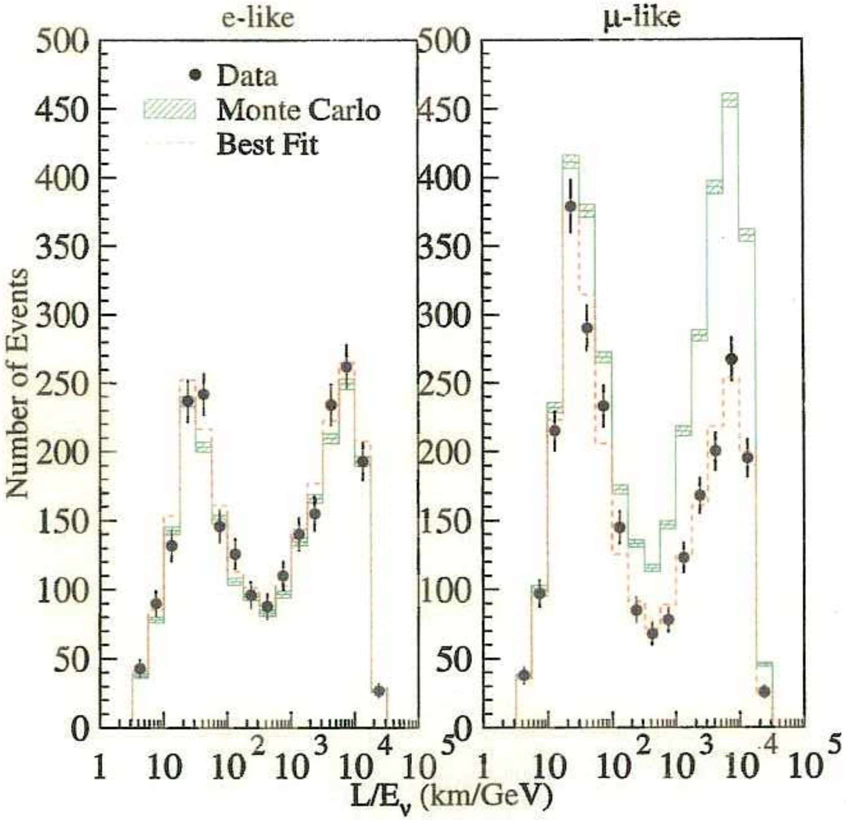

ν_τ cross sections

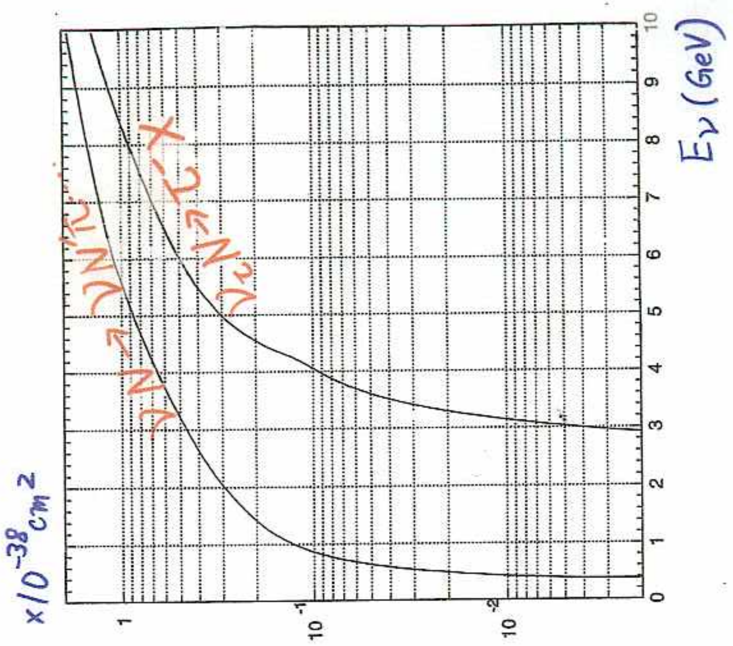

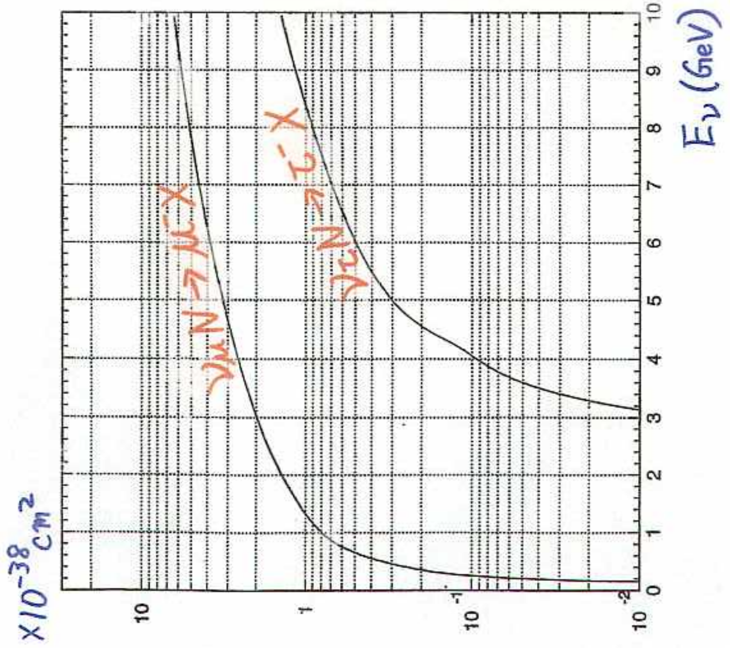

Event rate of τ production

(assuming $\nu_\mu \to \nu_\tau$ oscillation)

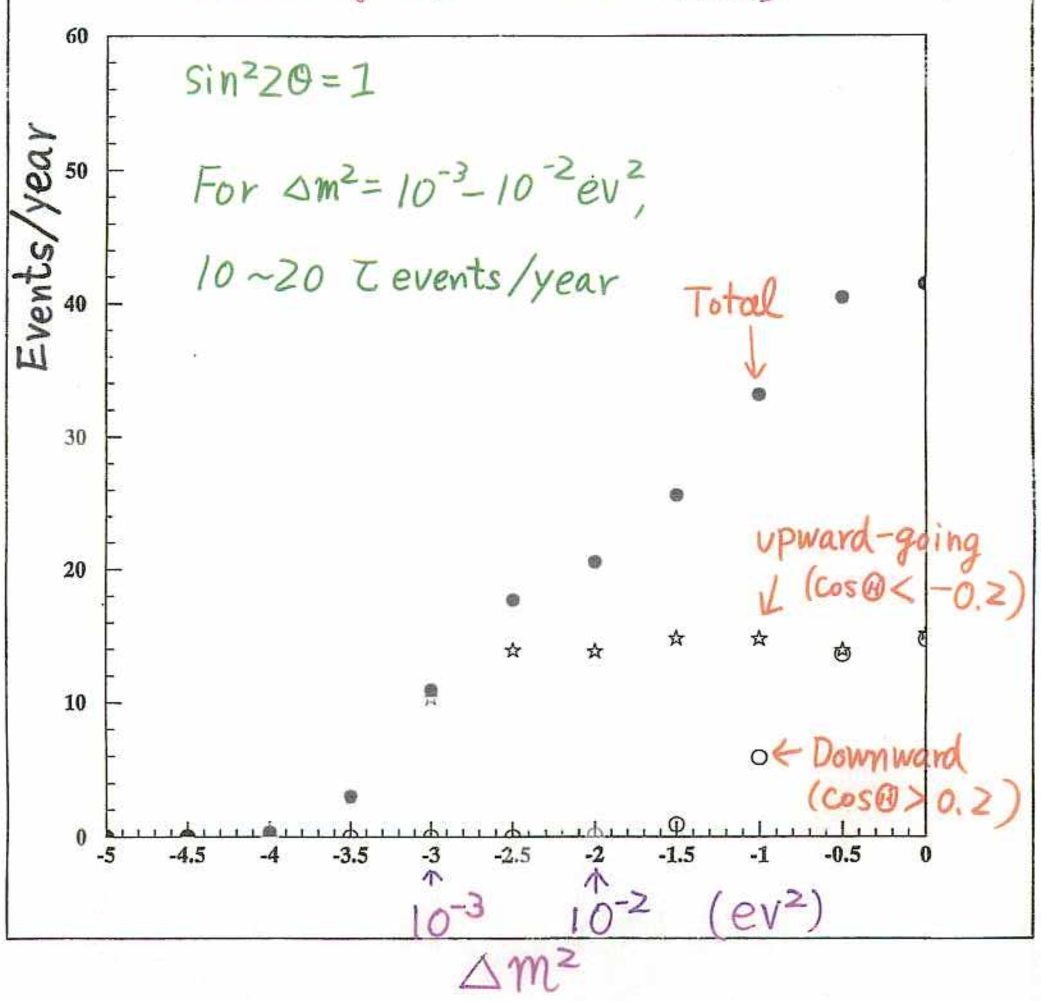

$\sin^2 2\theta = 1$

For $\Delta m^2 = 10^{-3} - 10^{-2} eV^2$,

10 ~ 20 τ events/year

反応しない

$\nu_\mu \rightarrow \nu_\tau$ or $\nu_\mu \rightarrow \nu_{sterile}$?

Using MSW effect and enriched NC sample

$\nu_\mu \rightarrow \nu_\tau$: No matter effect

$\nu_\mu \rightarrow \nu_s$: With matter effect

Neutrino oscillation in matter:

$$\begin{pmatrix} \nu_\mu \\ \nu_s \end{pmatrix} = \begin{pmatrix} \cos\theta_m & \sin\theta_m \\ -\sin\theta_m & \cos\theta_m \end{pmatrix} \begin{pmatrix} \nu_1 \\ \nu_2 \end{pmatrix}$$

$$\sin^2 2\theta_m = \frac{\sin^2 2\theta}{(\zeta - \cos 2\theta)^2 + \sin^2 2\theta}$$

$$\zeta = -\sqrt{2}\, G_F n_n E_\nu / \Delta m^2$$

For $\sin^2 2\theta = \sim 1$ $\quad \sin^2 2\theta_m \sim \dfrac{1}{\zeta^2 + 1}$

And for E_ν = 30~100 GeV ⇒ $\zeta \gg 1$ and

$\sin^2 2\theta_m \ll 1$

Suppression !

Strategy:

Obtained allowed region using lower energy events (Fully contained sample)

Then,

Test zenith angle of NC enriched events, high energy PC and through-going muon events.

Zenith angle of high energy PC events

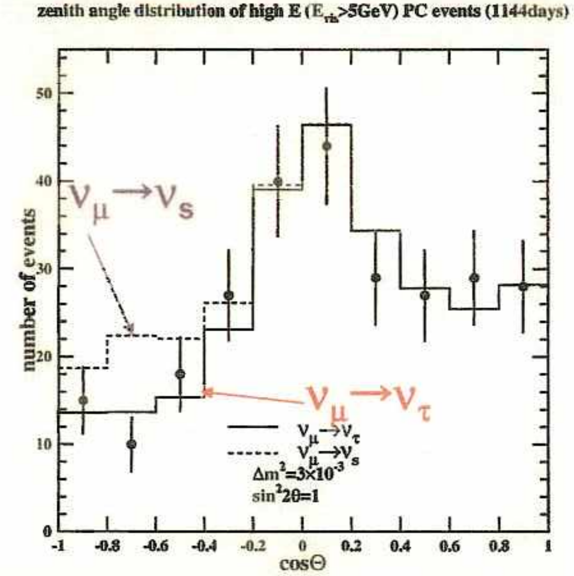

> 45000 p.e.
(E> ~ 5 GeV)

<E>=~25 GeV

$\Delta m^2 = 3\ \mathrm{x}10^{-3} eV^2$

$\sin^2 2\theta = 1$

Zenith angle of upward-going muon

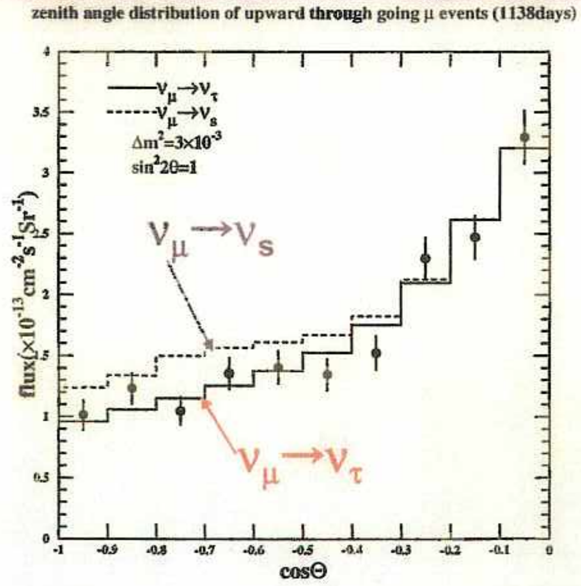

$\Delta m^2 = 3\ \mathrm{x}10^{-3} eV^2$

$\sin^2 2\theta = 1$

uımsk = 24

Zenith angle of NC enriched events

Criteria

> 400 MeV visible energy

Multi-ring event

e-like ring is the most energetic ring

Contents

NC : 29 %

ν_e CC : 46 %

ν_μ CC : 25 %

zenith angle distribution of N.C. enriched multi-ring events (1144days)

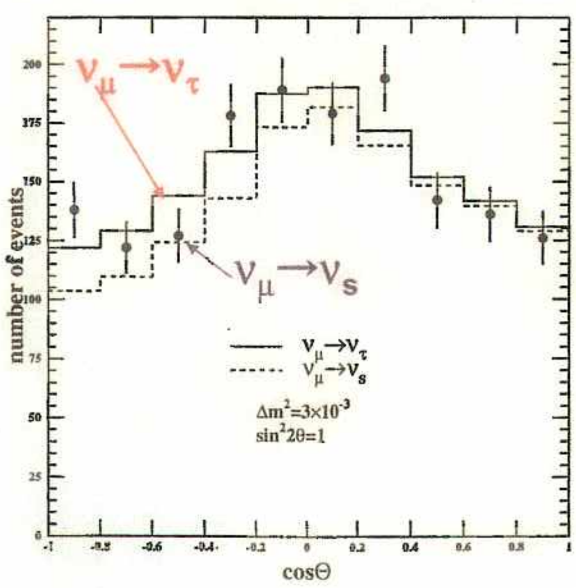

$\Delta m^2 = 3 \times 10^{-3} eV^2$

$\sin^2 2\theta = 1$

ν_μ to $\nu_{sterile}$?

- High energy ν experience matter effects which suppress oscillations to sterile ν
  - Matter effects not seen in up-μ or high-energy PC data
  - Reduction in neutral current interactions also not seen
  - constrains ν_s component of ν_μ disappearance oscillations
- Pure $\nu_\mu \leftrightarrow \nu_s$ disfavored
  - ν_s fraction < 20% at 90% c.l.

Limit On ν_μ-ν_s Admixture

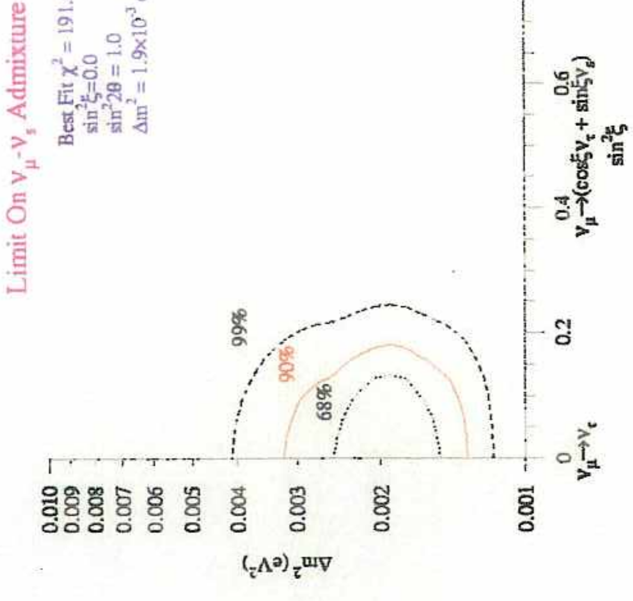

28th ICRC, 2 Aug. 2003, Tsukuba

Alec Habig

$\nu_\mu \rightarrow \nu_\tau$ appearance search

Neutrino CC cross sections

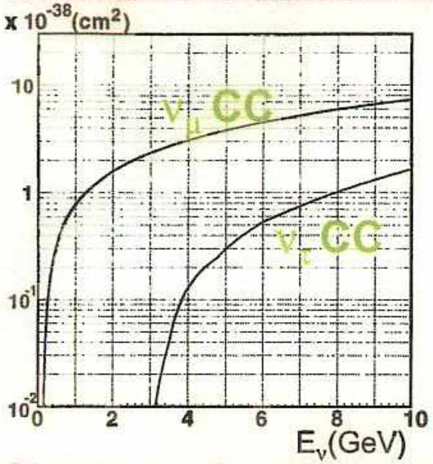

Expected τ events

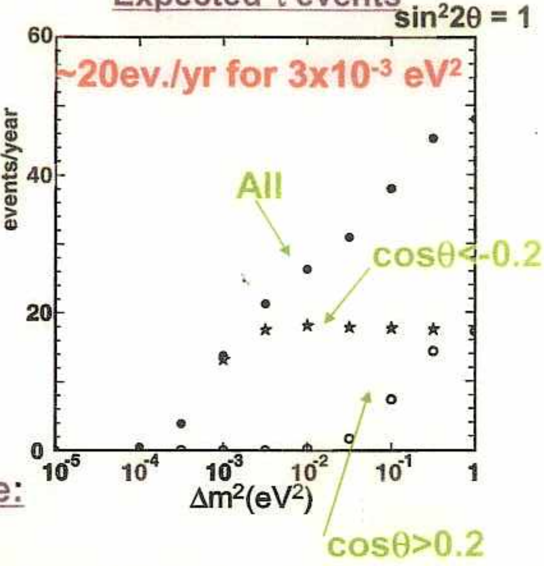

Signature of τ appearance:

$\nu_\tau + N \rightarrow \tau + N' + \pi + \pi$ .....
↳ $\mu\nu\nu$, $e\nu\nu$, ν+hadrons(π,π,....)

- Higher multiplicity of Cherenkov rings
- More $\mu \rightarrow e$ decay signals
- More spherical event pattern

Search for τ appearance (3 methods) :

(1) Energy flow and event shape analysis

(2) Likelihood method using # of rings, $\mu \rightarrow e$, max p.e. ring and etc.

(3) Neural network method

Each method is optimized using only downward going events and then looks at upward going events.

(I.e. blind method to disable systematic bias.)

τ detection in atmospheric ν

Selection Criteria
- multi-GeV, multi-ring
- most energetic ring is e-like
- log(likelihood) > 1 (single-ring)
  > 0 (multi-ring)

τ likelihood is defined using;
- total energy
- number of rings
- number of decay electrons
- max(Ei)/ Σ Ei
- distance between ν interaction point and decay-e point
- max(P_μ)
- Pt/$Evis^{3/4}$
- PID likelihood of most energetic ring

τ–like selection; effτ=44%, S/N=8%

observed τ–like events; 506

MC expectation; CC ν_τ37 events,
BG 461 events ($CC\nu_e$ 43.1%, $CC\nu_\mu$ 24.5%, NC 32.4%)

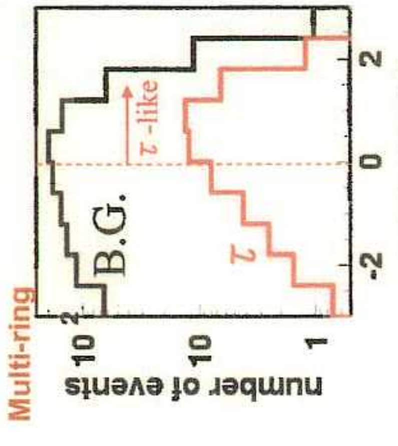

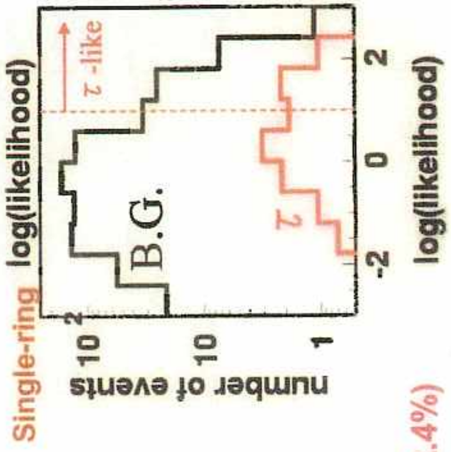

zenith angle dist. of τ-like events

$$\chi^2 = \sum_{\cos\Theta}^{5} \left(\frac{N_{data} - (\alpha N^{\tau}_{MC} + \beta N^{BG}_{MC})}{\sigma} \right)^2$$

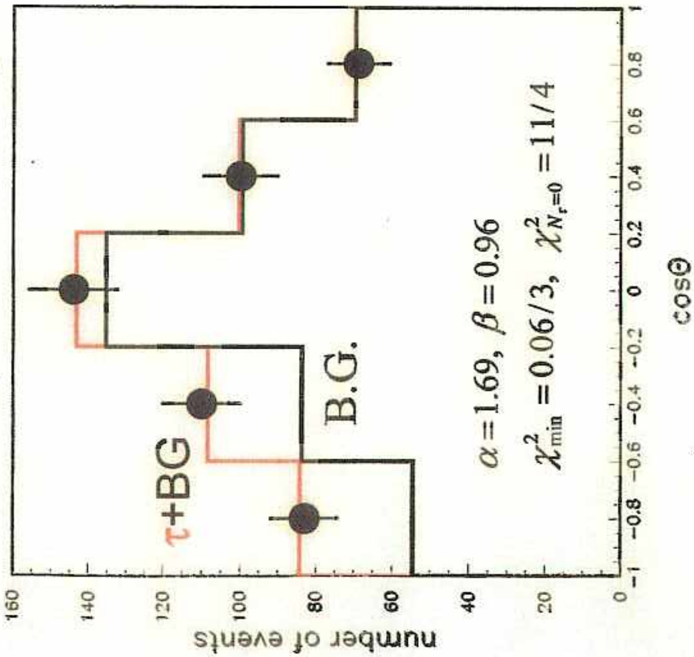

- $N^{FC}_{\tau} = \alpha N^{\tau}_{MC}/(\text{eff.}=0.44)$
  =145+-44(stat.)
  +11/-16(sys.)

  N_{exp}=86
- consistent with $\nu_\mu \leftrightarrow \nu_\tau$
- another analysis gives similar results:
  *analysis-2(neural network)
  N^{FC}_{τ}=99+-39(stat.)
  +-13(Δm^2)
  +0/-16(3-flavor)

Three-Flavor Analysis

$$\begin{pmatrix} \nu_e \\ \nu_\mu \\ \nu_\tau \end{pmatrix} = \begin{pmatrix} U_{e1} & U_{e2} & U_{e3} \\ U_{\mu 1} & U_{\mu 2} & U_{\mu 3} \\ U_{\tau 1} & U_{\tau 2} & U_{\tau 3} \end{pmatrix} \begin{pmatrix} \nu_1 \\ \nu_2 \\ \nu_3 \end{pmatrix}$$

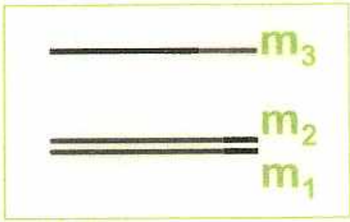

Assuming $m_3 \gg m_1, m_2$

Oscillation can be expressed by

Δm^2 (=$m_3^2 - m_{1,2}^2$), U_{e3}^2, $U_{\mu 3}^2$, $U_{\tau 3}^2$ (=1− U_{e3}^2 − $U_{\mu 3}^2$)

U (Maki-Nakagawa-Sakata Matrix) =

$$\begin{pmatrix} c_{12}c_{13} & s_{12}c_{13} & s_{13}e^{-i\delta} \\ -s_{12}c_{23}-c_{12}s_{13}s_{23}e^{-i\delta} & c_{12}c_{23}-s_{12}s_{13}s_{23}e^{-i\delta} & c_{13}s_{23} \\ s_{12}s_{23}-c_{12}s_{13}c_{23}e^{-i\delta} & -c_{12}s_{23}-s_{12}s_{13}c_{23}e^{-i\delta} & c_{13}\overset{c}{s}_{23} \end{pmatrix}$$

$s_{ij}=\sin\theta_{ij}$、$c_{ij}=\cos\theta_{ij}$

θ_{13} = 0 pure $\nu_\mu \leftrightarrow \nu_\tau$

θ_{23} = $\pi/2$ pure $\nu_e \leftrightarrow \nu_\mu$

θ_{23} = 0 pure $\nu_e \leftrightarrow \nu_\tau$

Active 3 flavor oscillation analysis

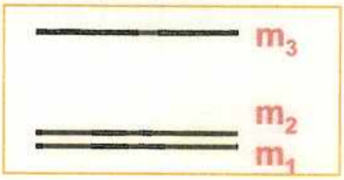

assuming $\Delta m^2_{23} = \Delta m^2_{atm} \sim O(10^{-3})$ eV^2
$\Delta m^2_{12} = \Delta m^2_{sol} < O(10^{-4})$ eV^2 << Δm^2_{atm}

neutrino oscillations in vacuum are described as;

$P(\nu_e \to \nu_\mu) = \sin^2(2\theta_{13})$ x $\sin^2\theta_{23}$ x $\sin^2(1.27\Delta m^2 L/E)$
$P(\nu_\mu \to \nu_\tau) = \cos^4\theta_{13}$ x $\sin^2(2\theta_{23})$ x $\sin^2(1.27\Delta m^2 L/E)$
$P(\nu_\tau \to \nu_e) = \sin^2(2\theta_{13})$ x $\cos^2\theta_{23}$ x $\sin^2(1.27\Delta m^2 L/E)$

3 parameters; $\Delta m^2(=m^2_3 - m^2_2)$, θ_{13} ($\sin^2\theta_{13}$<0.026), θ_{23} ($\sim\pi/4$)

Oscillation effect of ν_e flux is cancelled out @ low energy (E_ν<1GeV)
However, possible matter effect @ high energy (E_ν> 3 GeV)

nonzero θ_{13}

resonance happens at $E_\nu \sim$ 8 GeV (Mantle)
$E_\nu \sim$ 3 GeV (core) (for $\Delta m^2 = 3\times10^{-3}$eV^2)

Allowed region for active 3-flavor oscillations

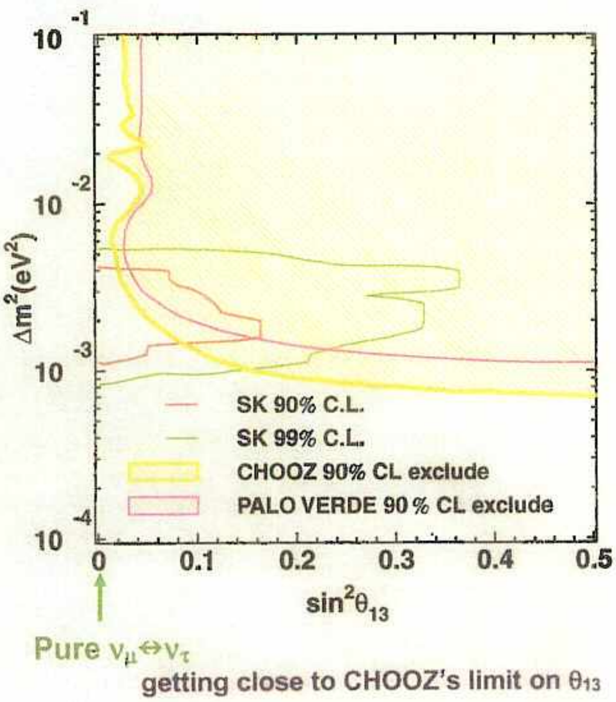

getting close to CHOOZ's limit on θ_{13}

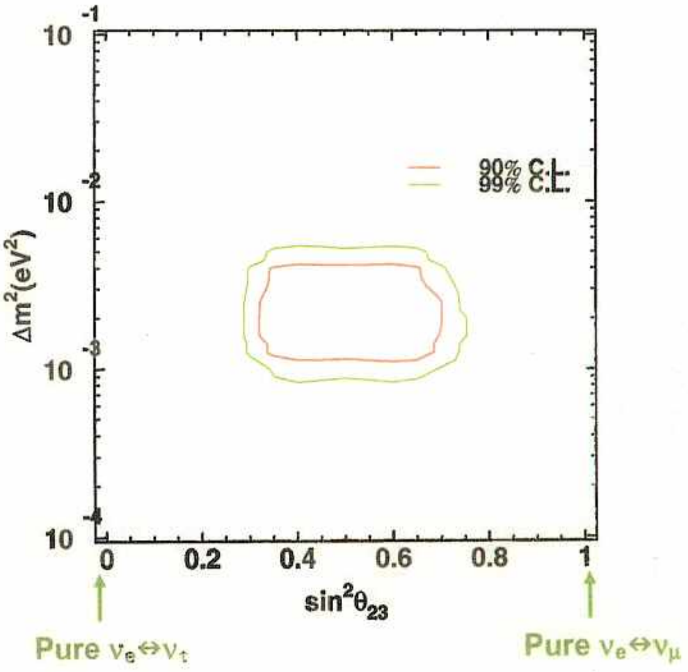

consistent with CHOOZ's excluded region

atmSK-32

Triangular plot for three flavor analysis

ref.: Fogli, Lisi, Marrone and Scioscia,
Phys. Rev. D59, 33001(1998); hep-ph/9904465.

$\boxed{\nu_3 = U_{e3}\nu_e + U_{\mu3}\nu_\mu + U_{\tau3}\nu_\tau}$

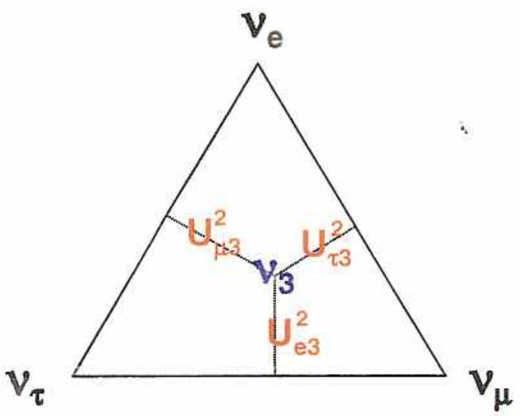

Unitarity is automatically satisfied by the triangular representation.

$$U_{e3}^2 + U_{\mu3}^2 + U_{\tau3}^2 = 1$$

For example, maximal pure $\nu_\mu \rightarrow \nu_\tau$ oscillation ($U_{\mu3}^2 = U_{\tau3}^2 = 1/2$) is

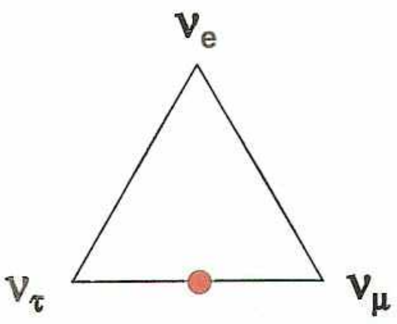

---

atmSK-33

Allowed region for each Δm^2

(Fogli et al., hep-ph/9904465)

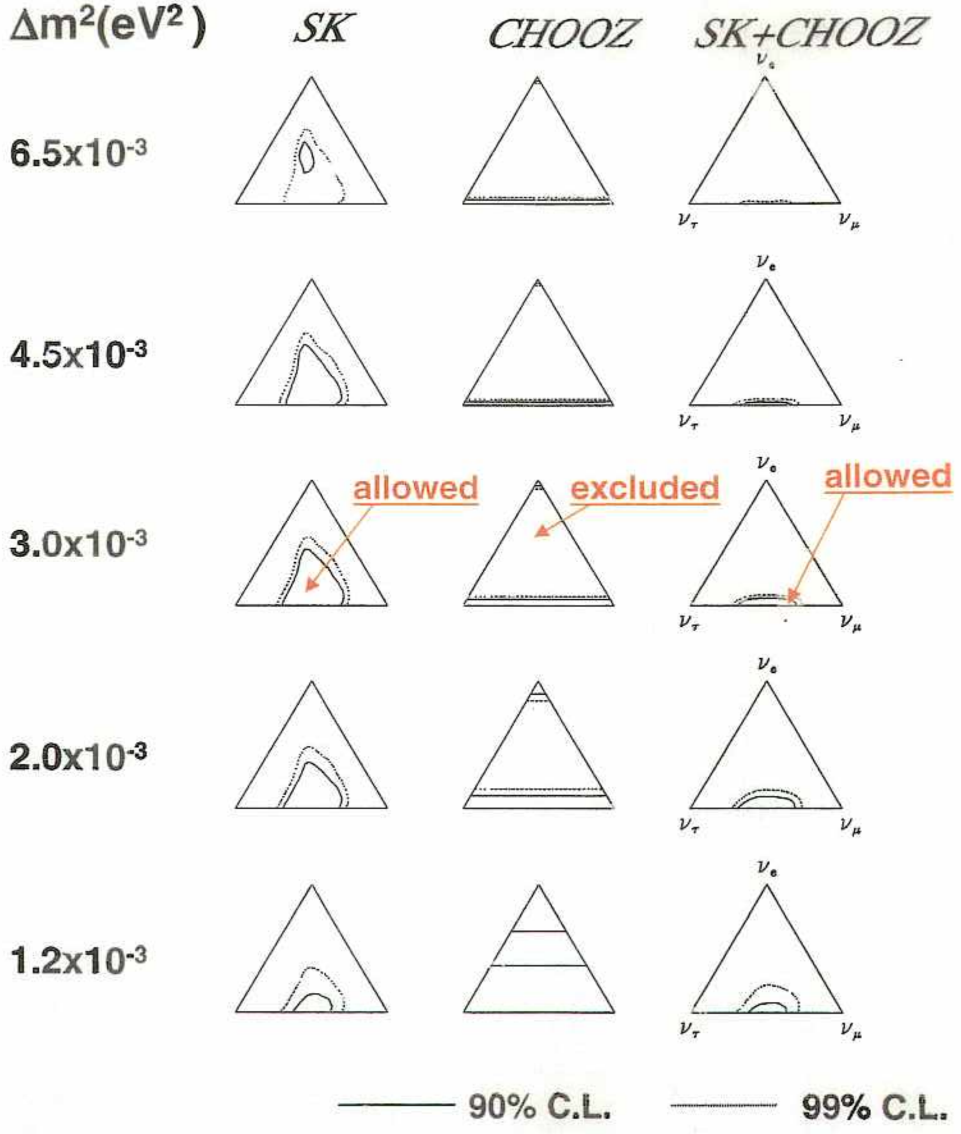

East/West effect of atmospheric neutrinos

Trajectory of cosmic-rays in earth magnet

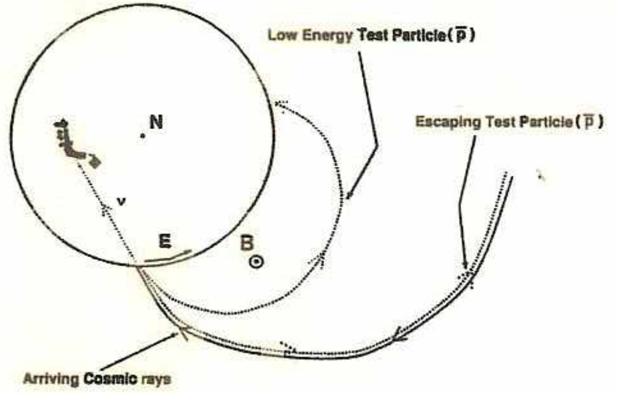

Cutoff rigidity

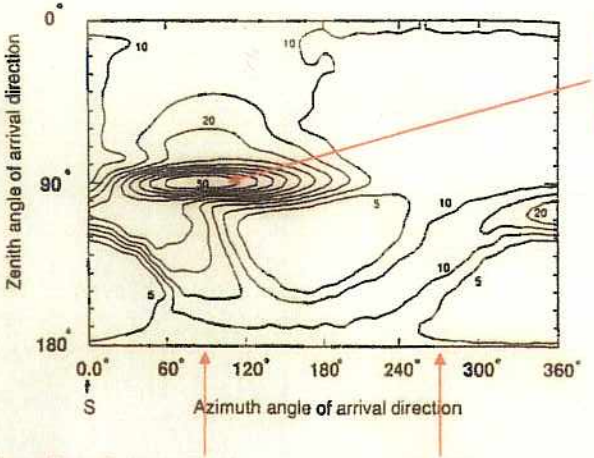

Suppress primary cosmic Rays for this direction P > 50 GeV

Coming from east (going to west)

west

East/West effect data from SK

Azimuth angle distribution

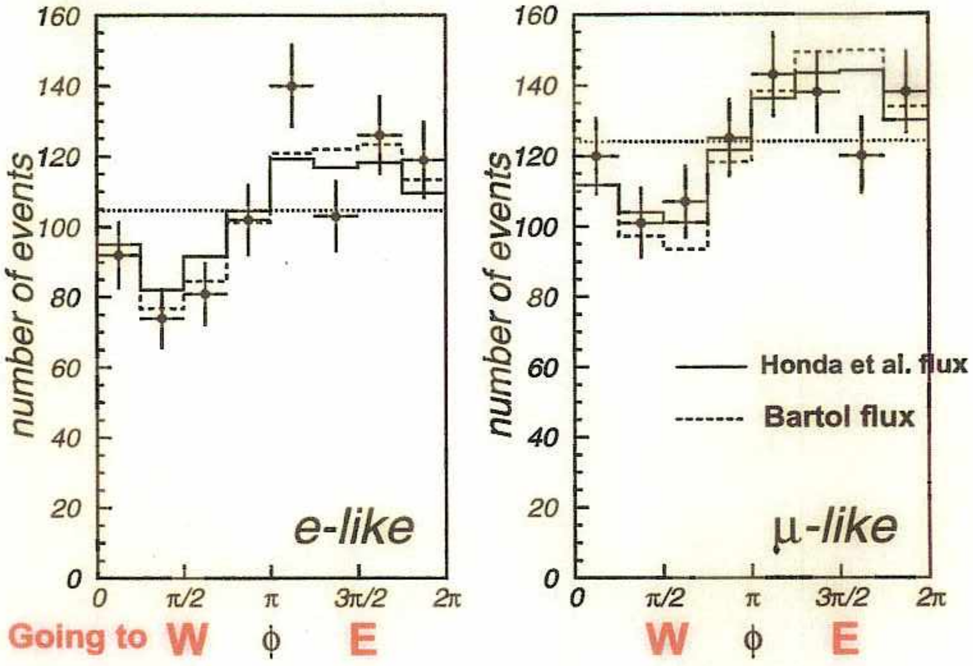

Event selection criteria

$-0.5 < \cos\theta < 0.5$

400 MeV/c < p < 3000 MeV/c

⑤

Atmospheric neutrinos

Other experiments

SOUDAN-2
MACRO
⋮

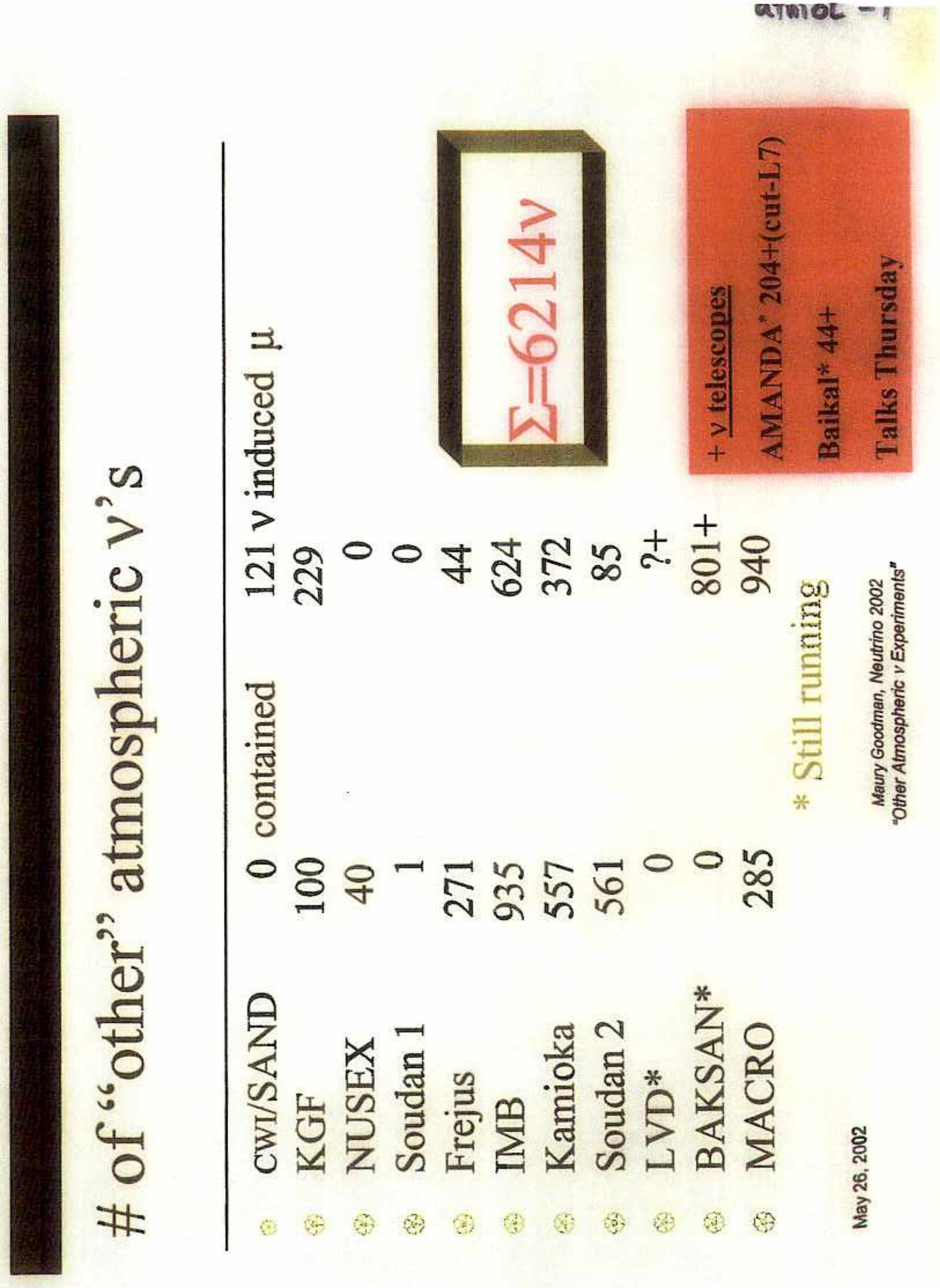

of "other" atmospheric ν's

CWI/SAND	0 contained	121 ν induced μ
KGF	100	229
NUSEX	40	0
Soudan 1	1	0
Frejus	271	44
IMB	935	624
Kamioka	557	372
Soudan 2	561	85
LVD*	0	?+
BAKSAN*	0	801+
MACRO	285	940

Σ=6214ν

+ ν telescopes
AMANDA* 204+(cut-L7)
Baikal* 44+
Talks Thursday

* Still running

May 26, 2002

Maury Goodman, Neutrino 2002
"Other Atmospheric ν Experiments"

$R(=\frac{(\mu/e)_{Data}}{(\mu/e)_{MC}})$ measured by experiments

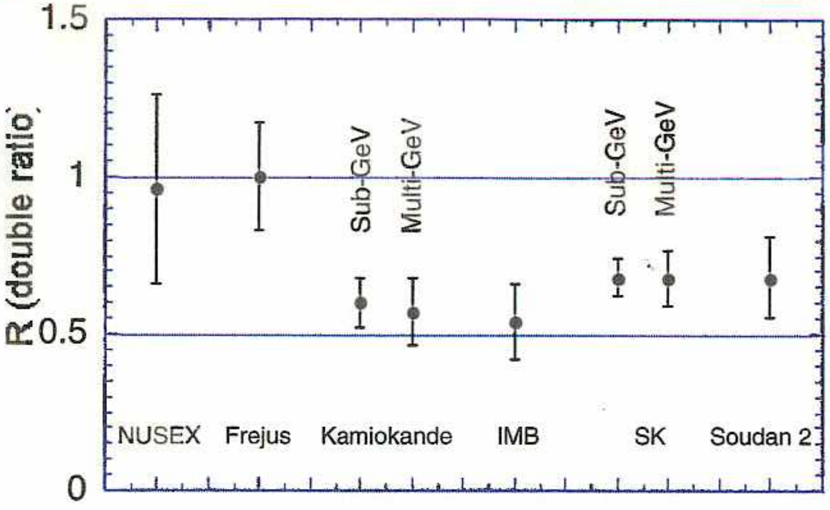

experiment	kt·yr	ev #	R(data/MC)
NUSEX	0.74	50	0.96 +0.32/-0.28
Frejus	2.0	200	1.00±0.15±0.08
Kam sub-GeV	7.7	482	0.60 +0.06/-0.05±0.05
Kam multi-GeV	8.2	233	0.57 +0.08/-0.07±0.07
IMB	7.7	610	0.54±0.05±0.11
SK sub-GeV	52.3	5134	0.68±0.02±0.05
SK multi-GeV	52.3	2122	0.68±0.04±0.08
Soudan 2	4.6	220	0.68±0.11±0.06

The Soudan 2 Detector:

Slow-drift time projection chamber

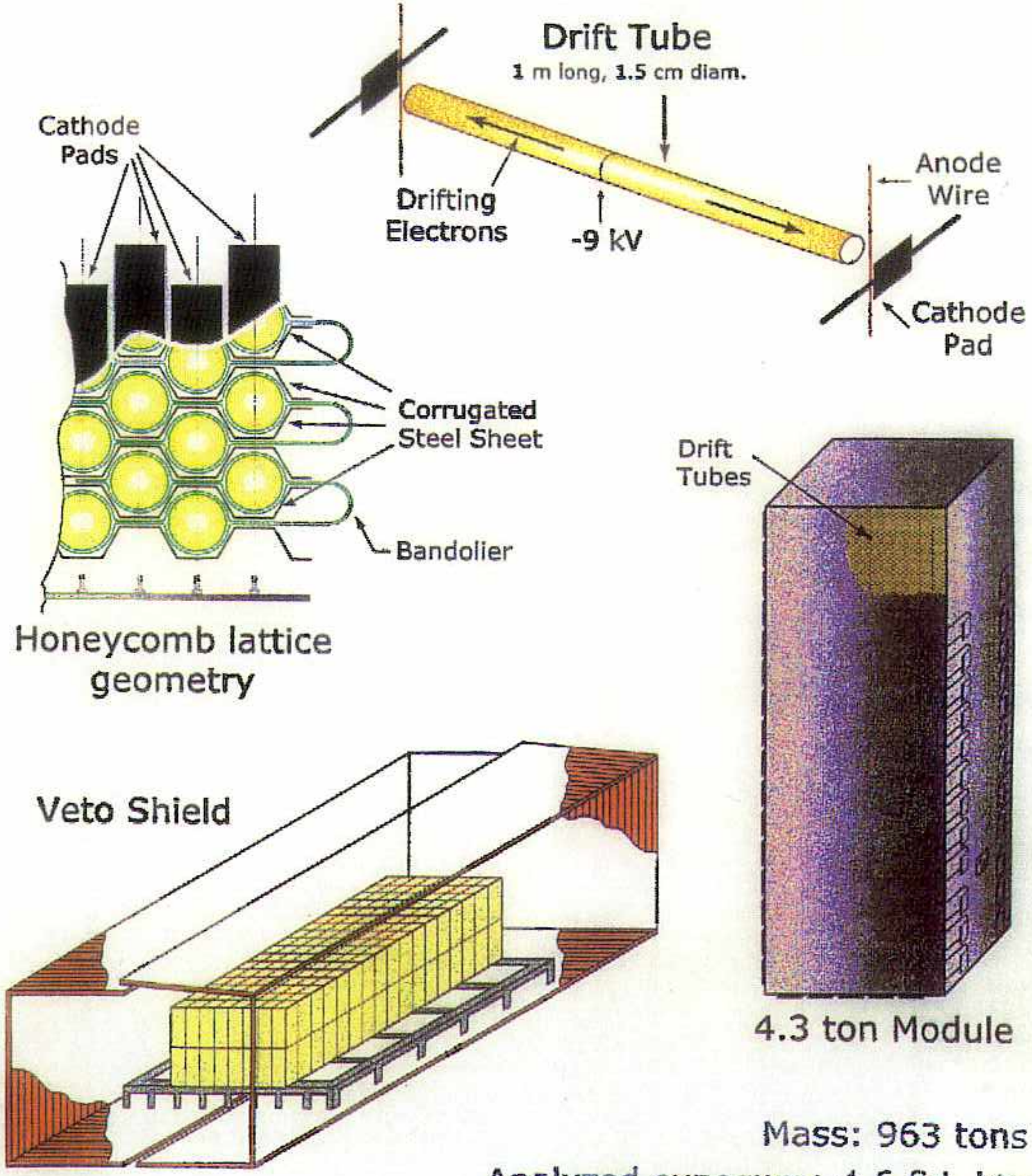

Mass: 963 tons
Analyzed exposure: 4.6 fid. kty

Soudan 2

Track, Shower, Multiprong Events in Soudan 2:

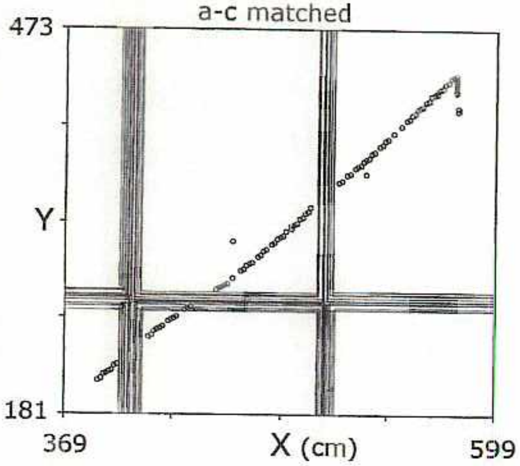

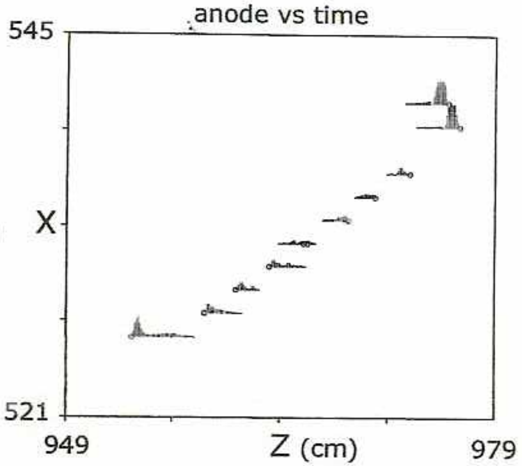

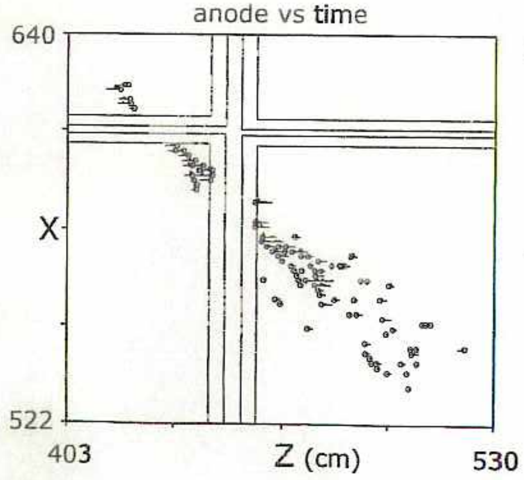

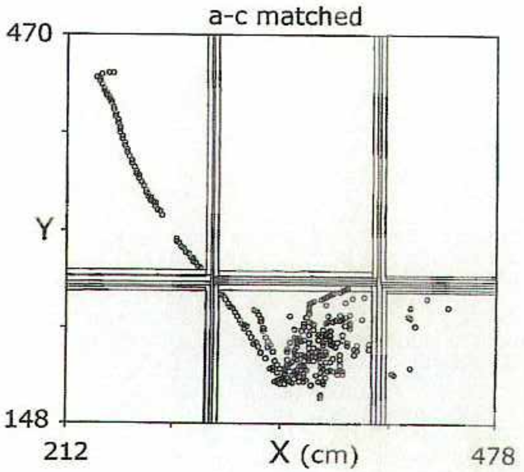

Soudan 2; Azimuth & Zenith plots

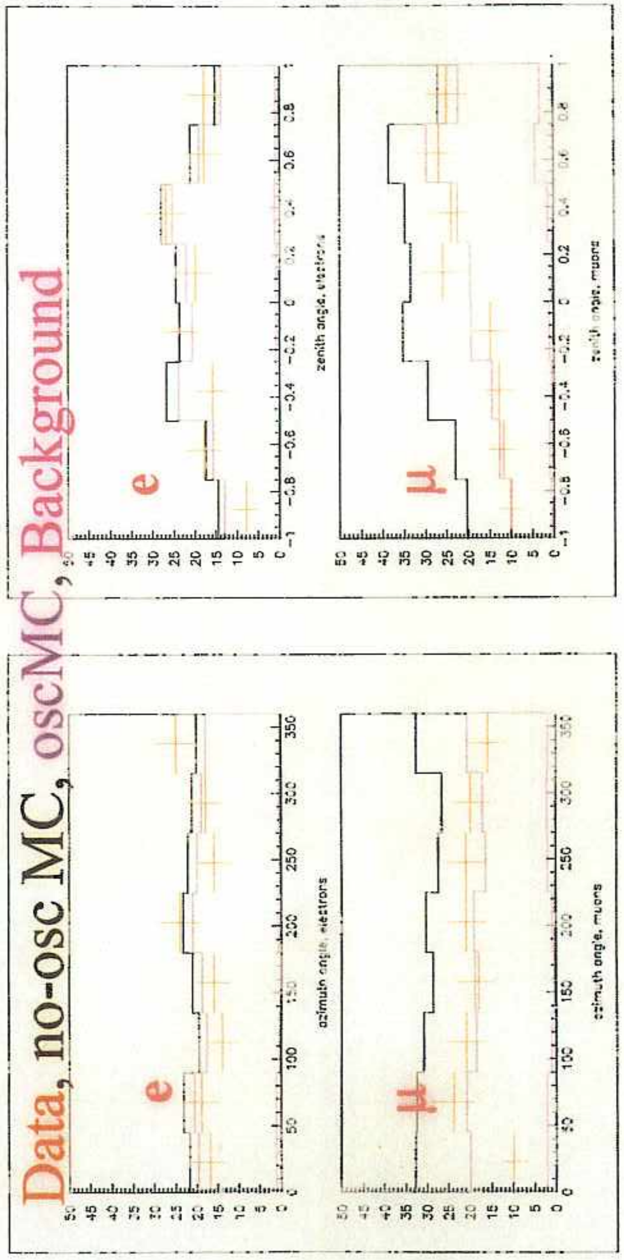
Data, no-osc MC, oscMC, Background

Soudan 2 Data sets, 5.90 kt years

R values

no cut
- all 0.768 ± 0.098
- hires 0.681 ± 0.096
- lowres t/s 0.807 ± 0.278
- lowres m 0.826 ± 0.224

300 Mev cut
- all 0.708 ± 0.092
- hires 0.643 ± 0.105
- lowres t/s 0.641 ± 0.260
- lowres m 0.851 ± 0.167

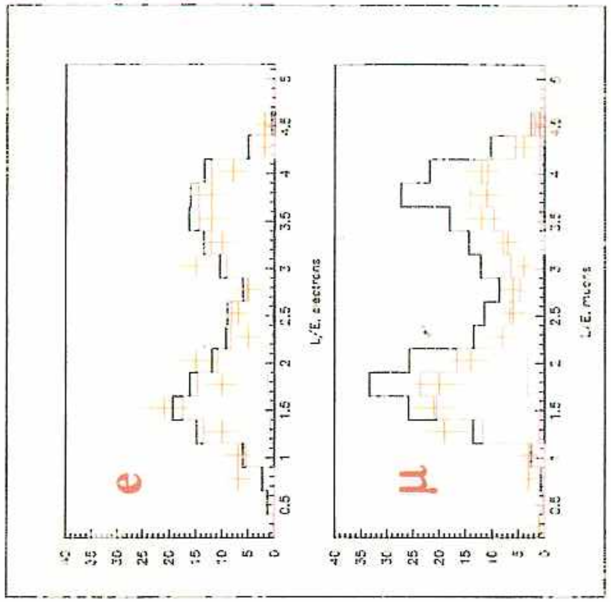

L/E

MACRO detector

(In Gran Sasso)

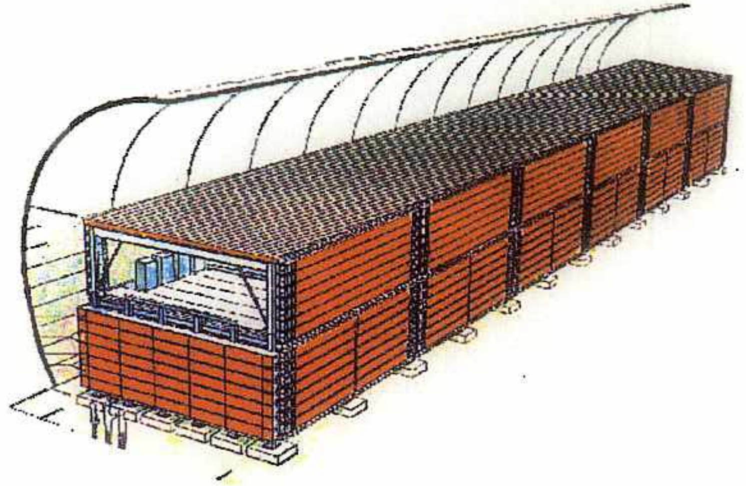

Tracking calorimeter: 76.6m x 12m x 9.3 m

Tracking: Streamer tubes with 3cm cells, wire and 27 deg. stereo strip readout.

Angular resolution < 1 deg.

Timing for directionality:
Liquid scintillation counters

3 horizontal planes and vertical walls

Timing resolution 0.5 nsec.

Total Mass: ~5.3 kilotons

MACRO ν_μ event topology

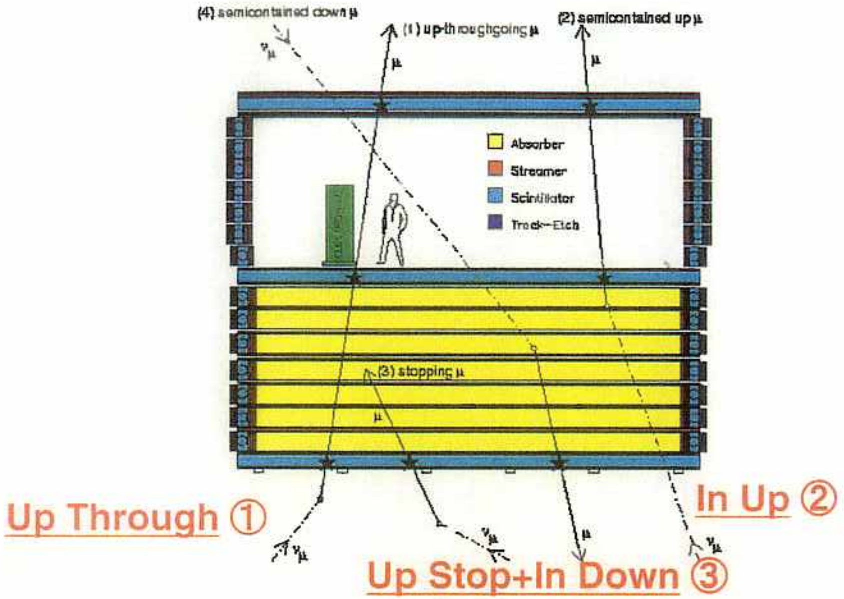

Up Through ①

In Up ②

Up Stop+In Down ③

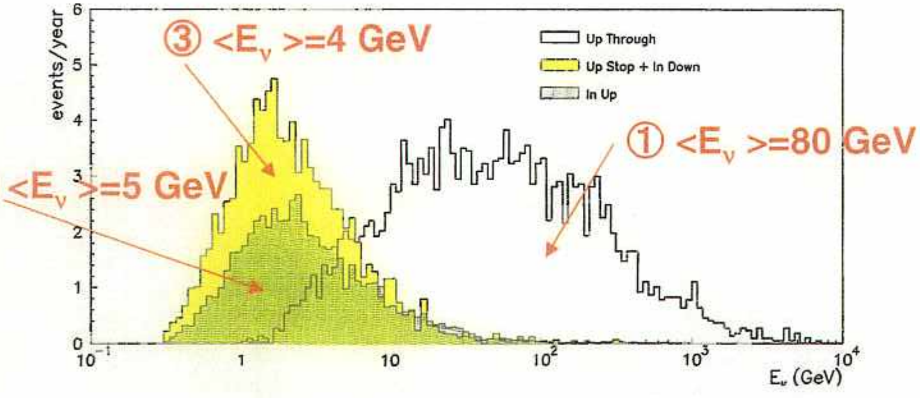

Parent neutrino energy

Macro High Energy Events

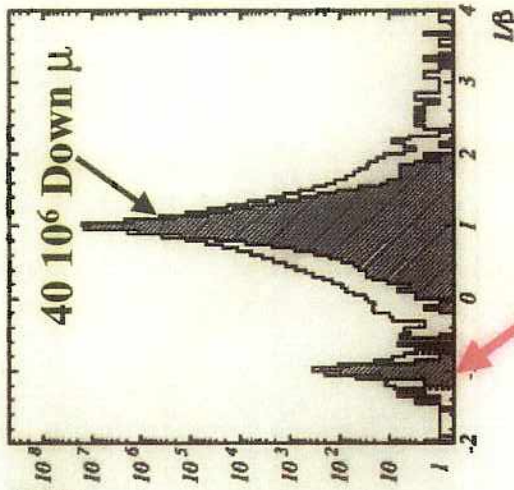

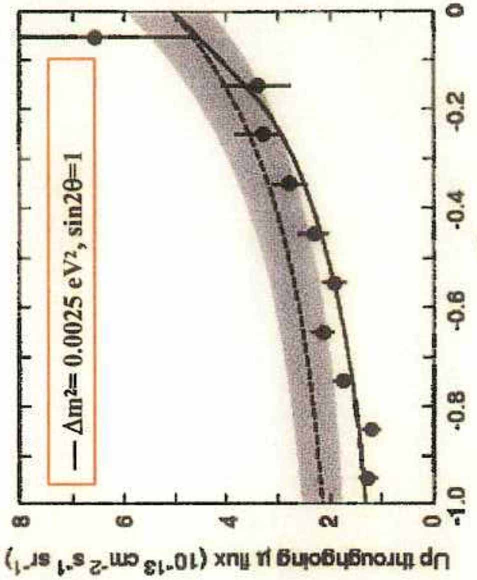

$\Delta m^2 \sin^2(2\theta)$ Comparison

color code:

Soudan

Macro HE

Macro LE

Super-Kamiokande

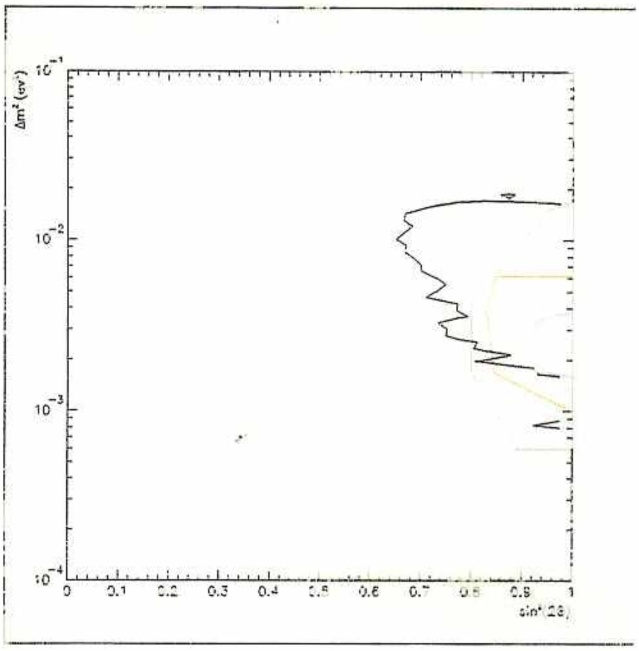

ATMOT-10

Macro Low Energy Events

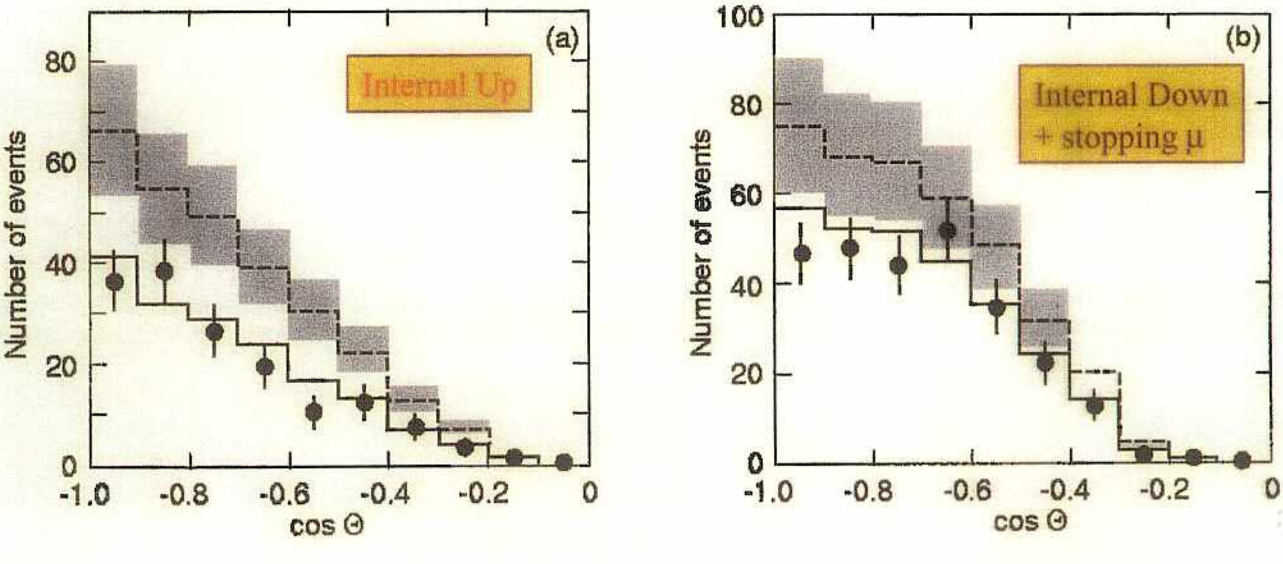

ATMOT-10

⑥

K2K long baseline experiment

K2K long baseline neutrino experiment

どれだけのミューニュートリノが到達するかを調べる。またニュートリノ振動で生まれたタウニュートリノの反応を観測する。

陽子シンクロトロンでつくった陽子ビームを標的に衝突させると、パイ中間子が生じる。パイ中間子はパイプを飛行する間に崩壊し、ミューニュートリノがつくられる。ミューニュートリノの数は前置装置で測定される。

Super-Kamiokande

250 km

Front detectors

KEK PS

~400 ν events

(no oscillation)

ν_μ beam

$\langle E_\nu \rangle$ = ~1.5 GeV

10^{20} pot

12 GeV

KEK-1

K2K Experiment

- Accelerator: 12 GeV proton synchrotron
  - beam intensity: 6×10^{12} protons/pulse
  - repetition: 1 pulse / 2.2 sec
  - pulse width: 1.1 μsec (9 bunches)
- Front (near) detector: 300m from the target
- Far detector (Super-Kamiokande): 250 km from the target

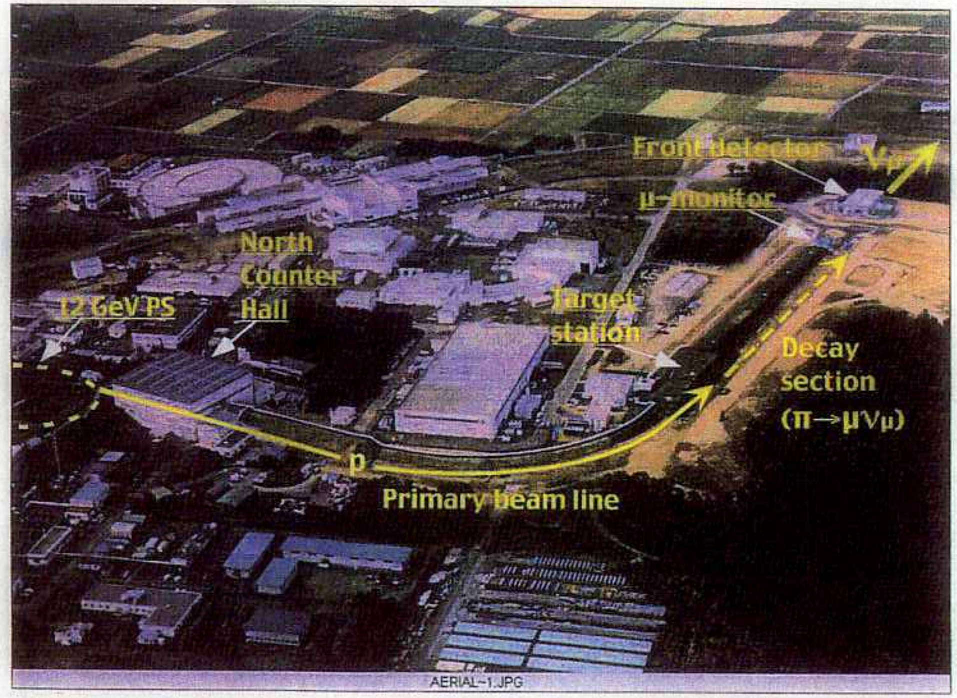

K2K

Neutrino flux at Front Detector (KEK)

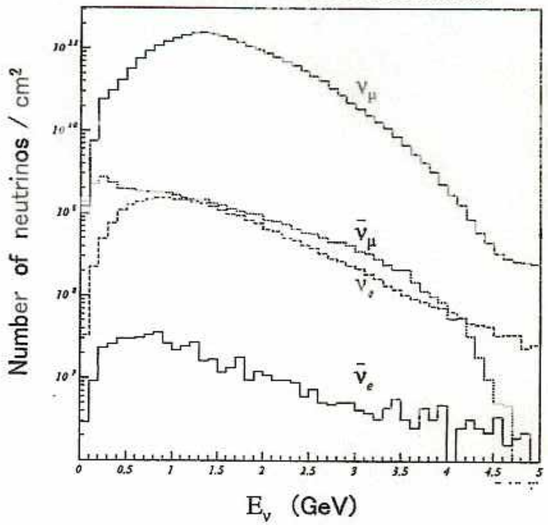

Neutrino flux at Super-Kamiokande

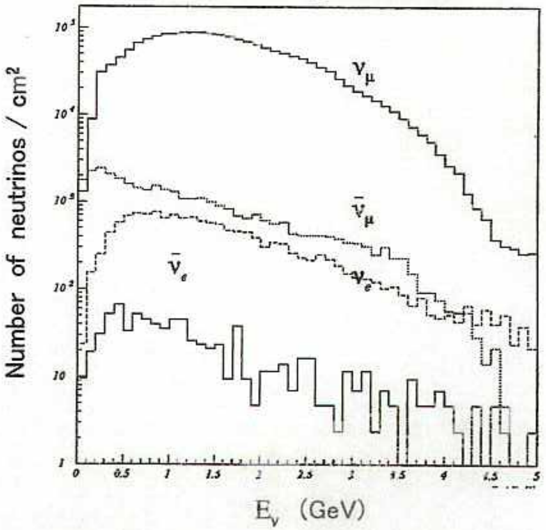

Neutrino oscillation @ K2K

Oscillation probability

$$\mathbf{prob.} = \sin^2 2\theta \cdot \sin^2\left(\frac{1.27\Delta m^2 \, L}{E_\nu}\right)$$

constatnt (250km)

⇩

- reduction of number of events
- Spectrum distortion

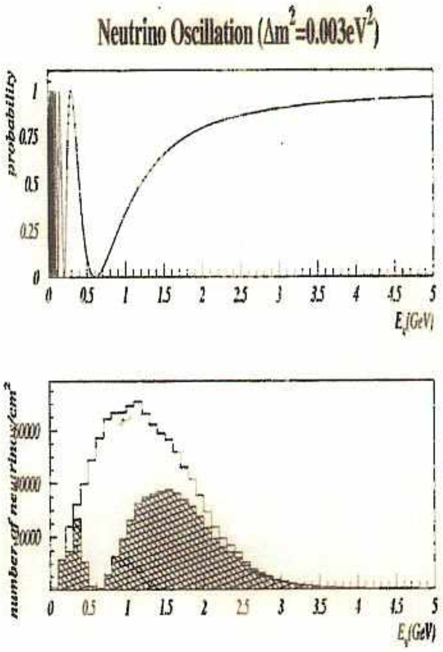

- measure neutrino flux @ ND
- Near to Far extrapolation
- compare number of events and spectrum shape @ SK

K2K-4

83

Overview of experiment

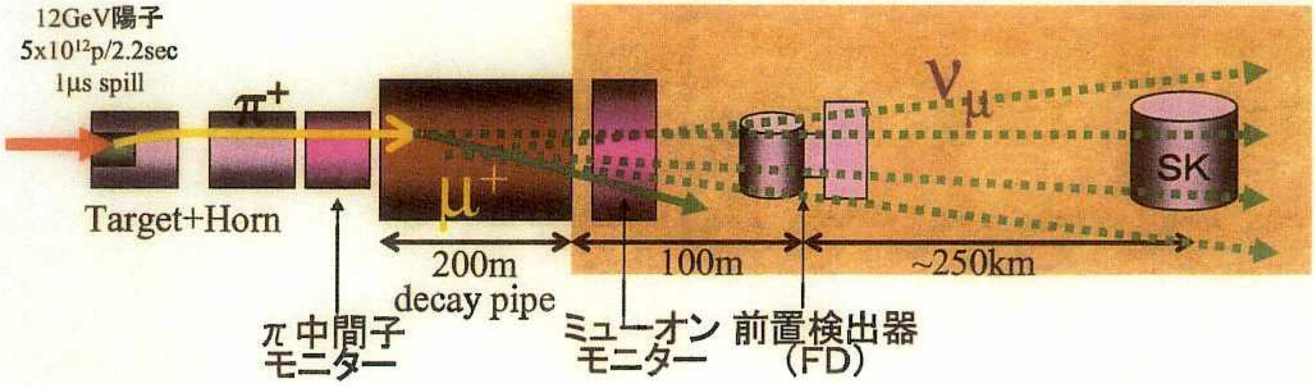

生成時のν_μスペクトル

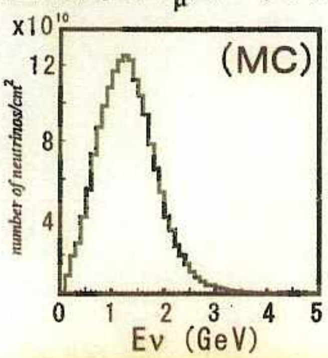

前置検出器で測定

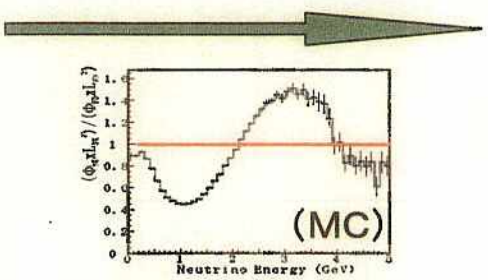

スペクトルの比≠1

π中間子モニターで測定

SK到達時のν_μスペクトル

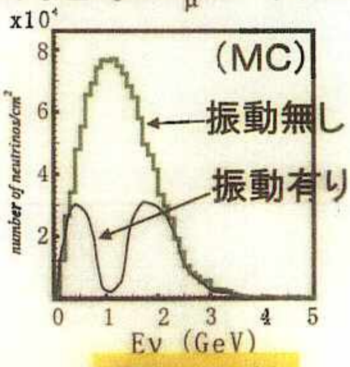

観測と比較

K2K-5

K2K

Magnetic horn system

Maximum current: 250 kA

Neutrino flux: intensified by a factor of 14

Magnetic Horn system

(for Long Baseline Neutrino Oscillation Experiment)

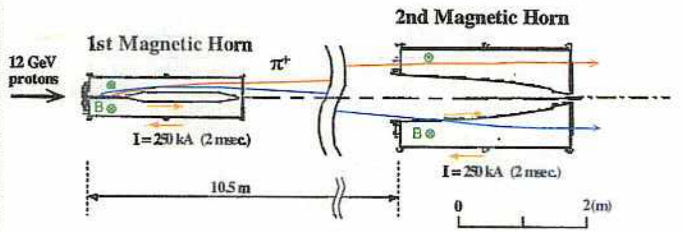

Design	• Optical	Higher ν-flux
	• Mechanical	Maxwell stress
	• Electrical	R, L

		1st Horn	2nd Horn
Length	(mm)	2400	2650
Outer Diam.	(mm)	620	1520
Inner conducter	(mm)	3	3
Outer conducter	(mm)	10	10
Material		A6061-T6	A6061-T6 & T651

K2K

Horn Magnet / Target system
1st - HORN

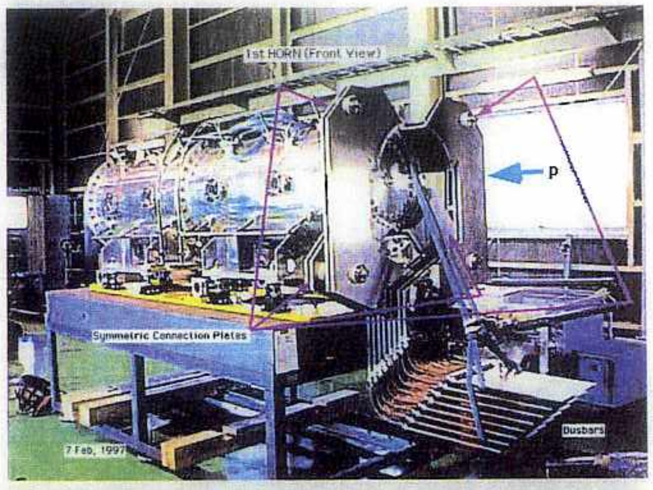

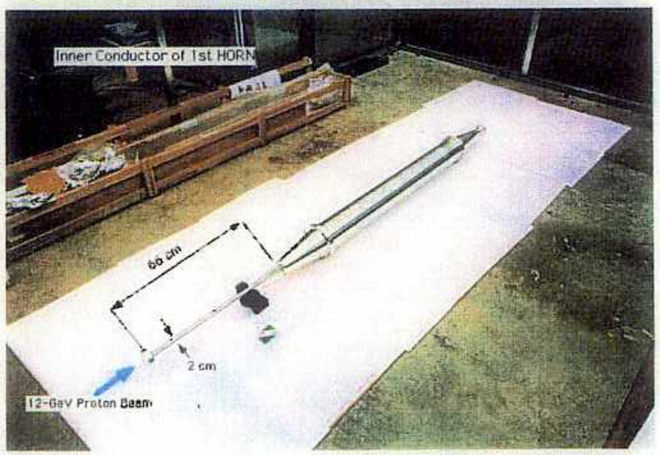

K2k-8

GPS system

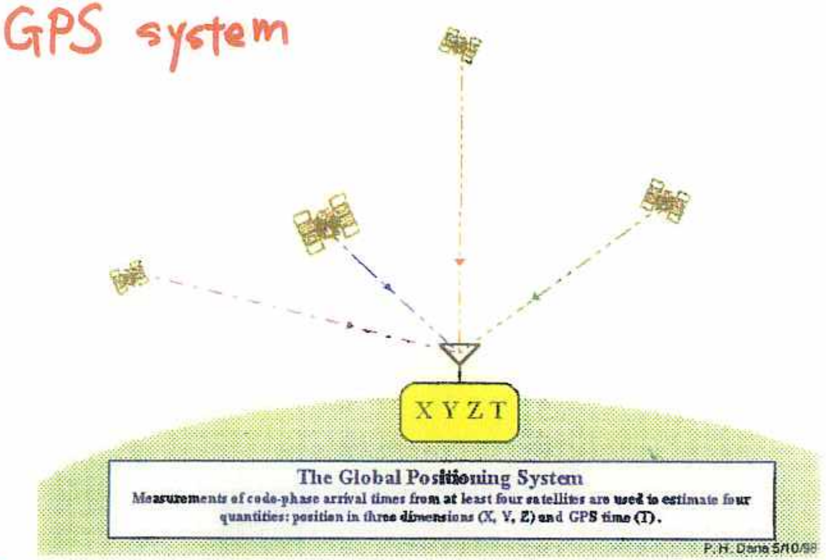

The Global Positioning System

Measurements of code-phase arrival times from at least four satellites are used to estimate four quantities: position in three dimensions (X, Y, Z) and GPS time (T).

P. H. Dana 5/10/98

# of Observed Satelites

KEK →

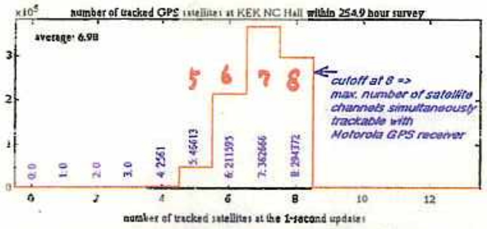

SK →

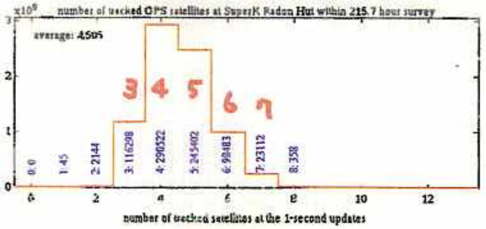

GPS time resolution ⇒

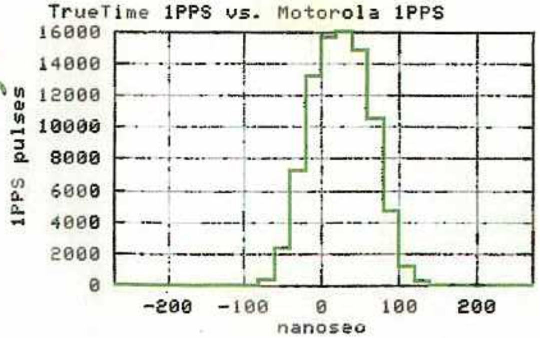

K2K-7

K2K

Front detector

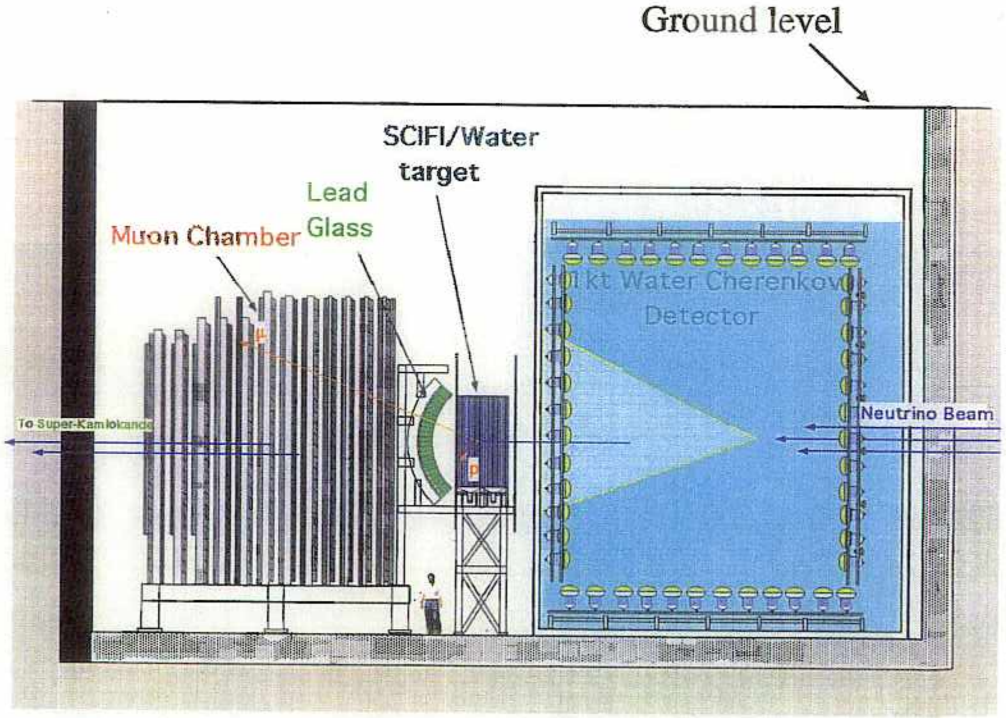

K2K

A neutrino event in the 1 kton water Cherenkov detector

Shown here is a Cherenkov ring produced by a muon which was created by a ν_μ interacted in the water tank. Upper right corner shows that there was no activity in the anticounter.

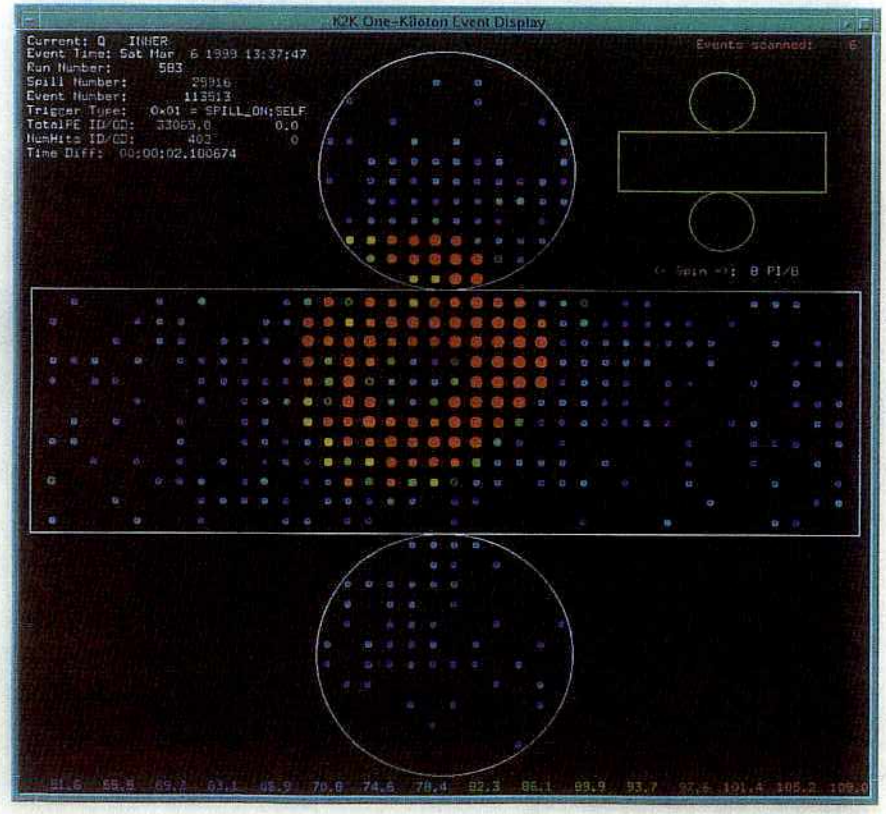

```
Current: Q   INNER
Event Time: Sat Mar  6 1999 13:37:47
Run Number:        583
Spill Number:          25916
Event Number:         113513
Trigger Type:   0x01 = SPILL_ON:SELF
TotalPE ID/OD:   33065.0         0.0
NumHits ID/OD:        402          0
Time Diff:  00:00:02.100674
```

K2K

A candidate for a two-prong neutrino event, $\nu_\mu + n \rightarrow \mu^- + p$

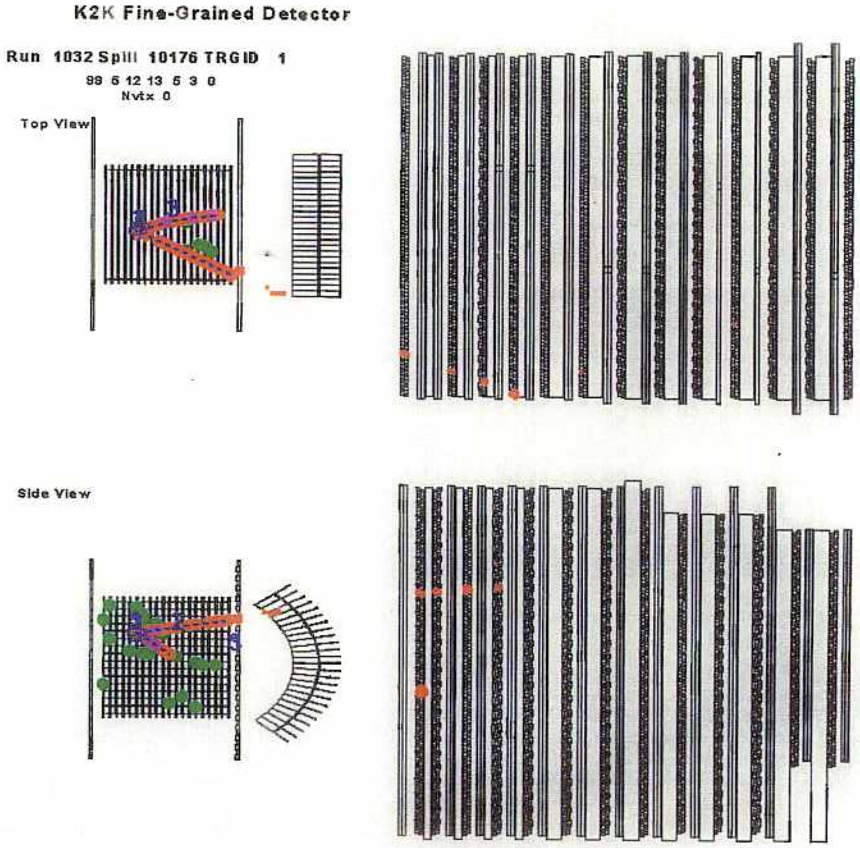

K2K

Goal of the experiment

10^{20} protons on target in 3 ~ 4 years

(All our plots and tables are normalized to this number)

Detector	Fine grained	1 kt water Cherenkov	Super-Kamiokande
Fiducial mass	water 4tons	water 21 tons	water 22.5 ktons
Integrated flux	$2.6 \times 10^{12}/\mathrm{cm}^2$	$2.4 \times 10^{12}/\mathrm{cm}^2$	$1.84 \times 10^{6}/\mathrm{cm}^2$ (before cuts)
ν_μ CC	63208	325526	281
Quasi-elastic	21969	114216	93
single-π	18812	97283	79
multi-π	21031	106784	103
ν_μ NC	22530	116226	99
single-π^0	4642	24006	20
ν_μ total	85744	441710	381

K2K

E_ν Distribution at Super-Kamiokande for the case of $\nu_\mu \rightarrow \nu_\tau$

(E_ν is calculated assuming quasi-elastic scattering)

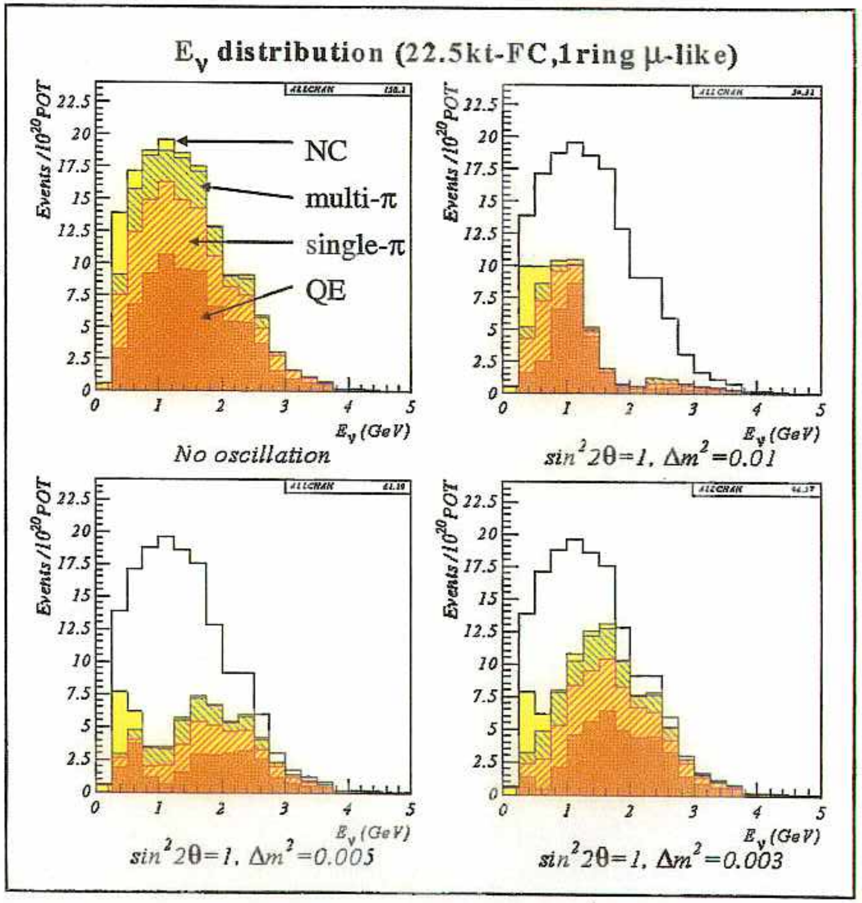

Neutrino Energy E_ν Reconstruction

CC quasi elastic (QE)

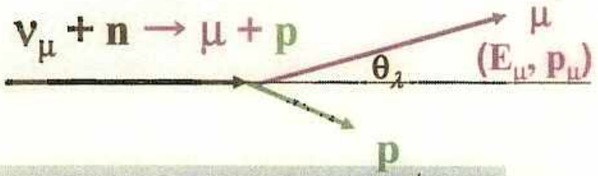

$\nu_\mu + n \rightarrow \mu + p$

$$E_\nu = \frac{m_N E_\mu - m_\mu^2/2}{m_N - E_\mu + p_\mu \cos\theta_\mu}$$

Rate(Eν,Near) → <u>φ(Eν,Near)</u>
↑
σ(QE), σ(nonQE)

CC inelastic

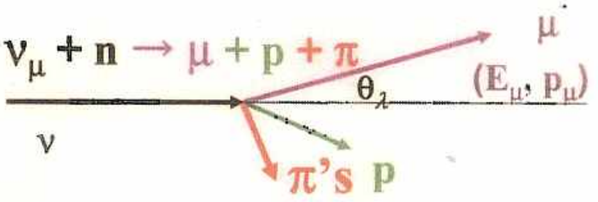

$\nu_\mu + n \rightarrow \mu + p + \pi$

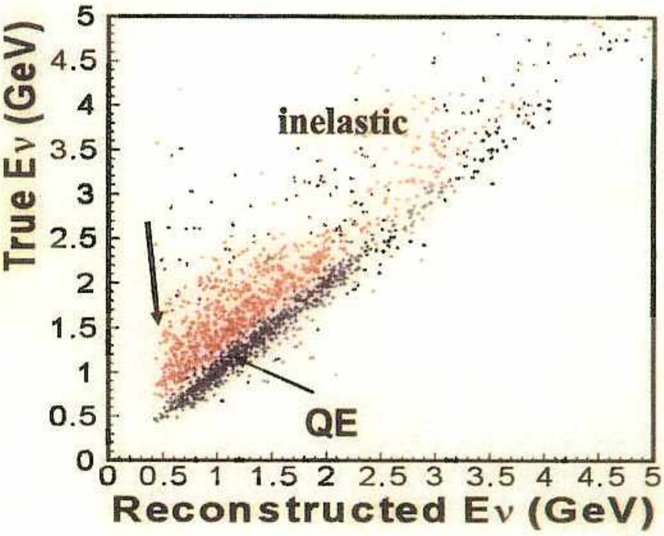

88

Delivered Protons on Target (POT)

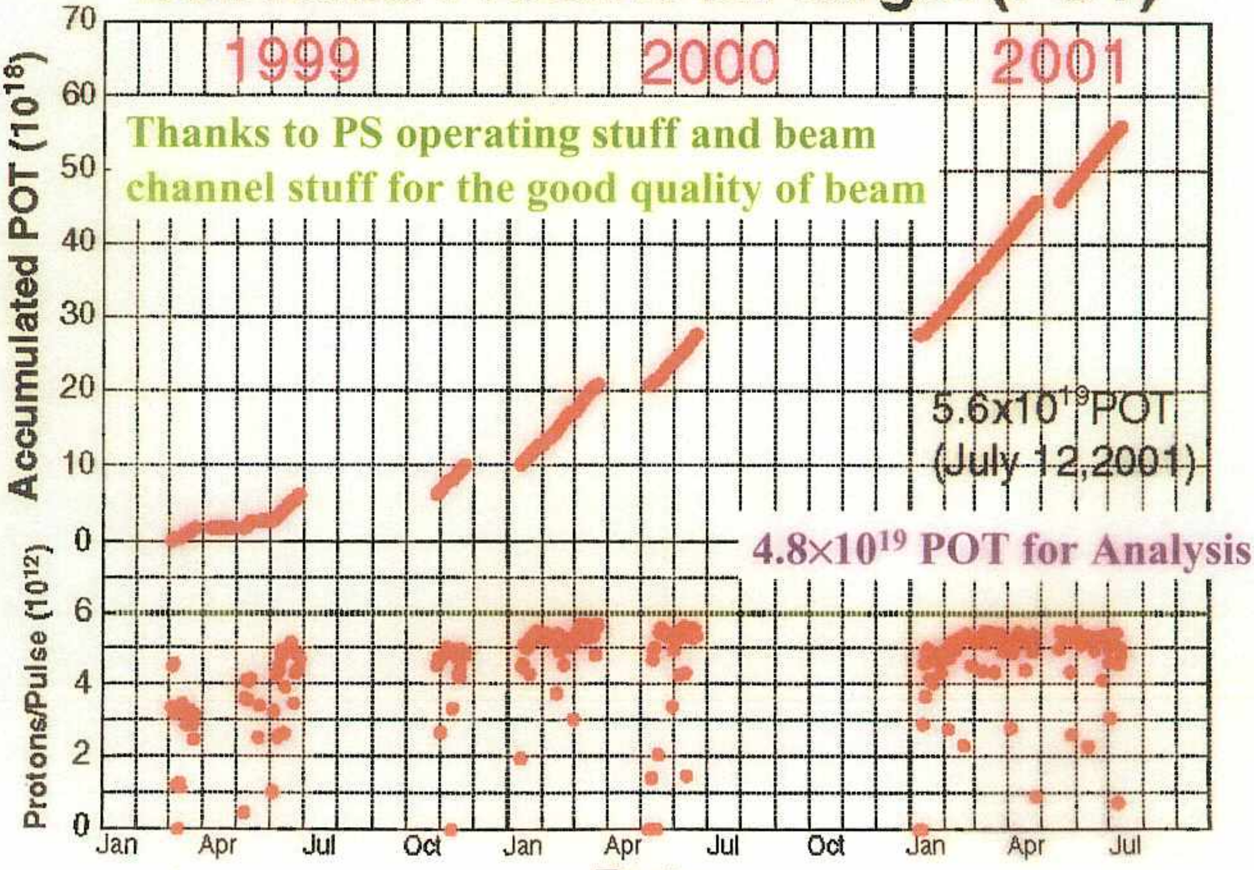

Thanks to PS operating stuff and beam channel stuff for the good quality of beam

5.6x10^{19}POT (July 12,2001)

4.8×10^{19} POT for Analysis

Spectrum at near detector

1kt 1Rμ sample

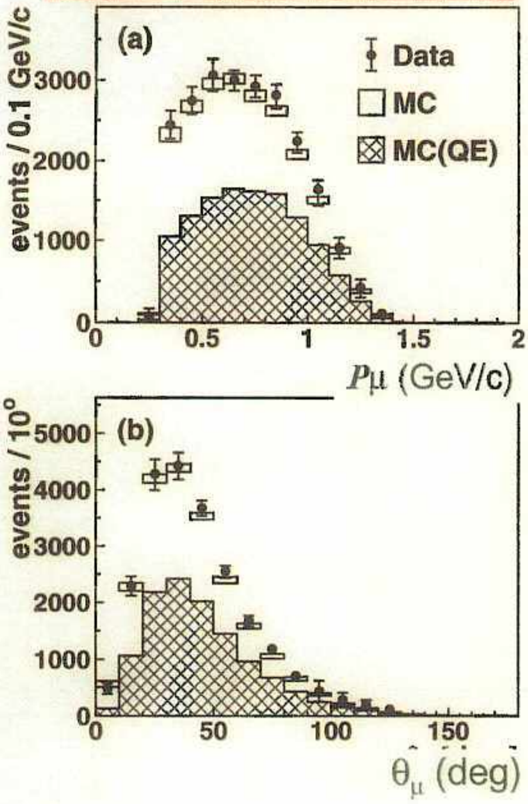

Scifi

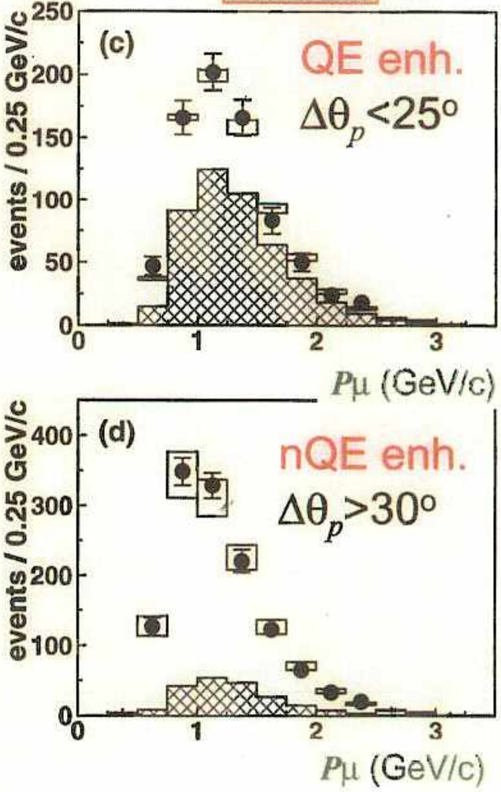

89

Event selection @ SK

Event time distribution

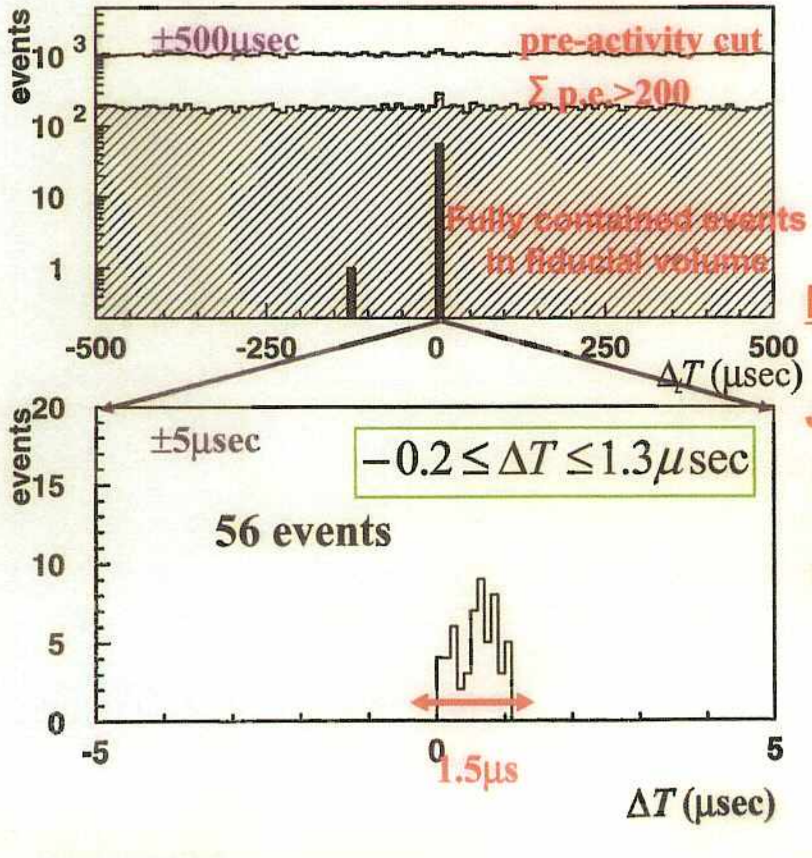

$-0.2 \leq \Delta T \leq 1.3 \mu\text{sec}$

N_{SK} (number of events) analysis

Jun 99-Jul 01

fully contained events

56 events observed

$80.1^{+6.2}_{-5.4}$ events expected w/o oscillation

null oscillation prob. 1.3%

Best fit 1ring μ-like spectrum & N_{SK}

reconstructed Eν

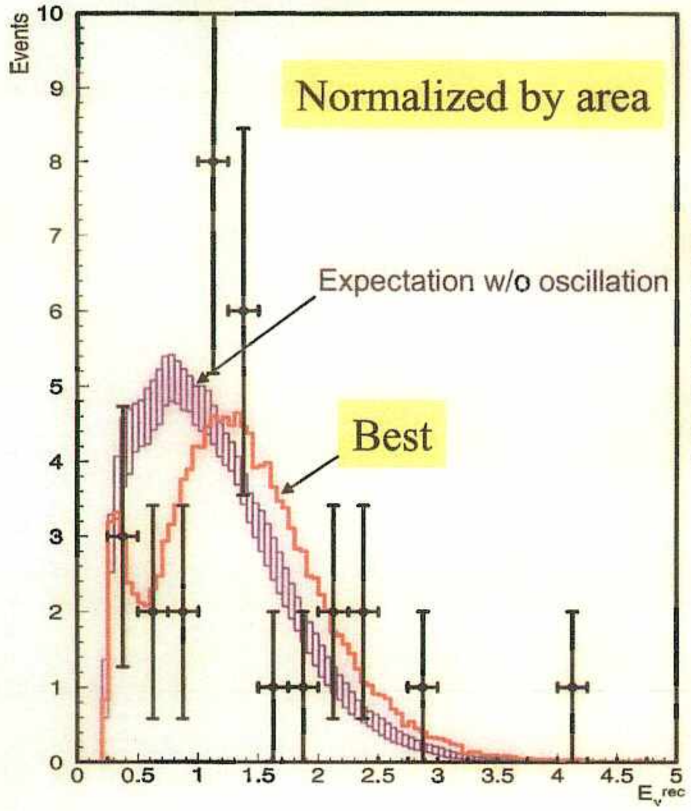

Best fit point
($\sin^2 2\theta$, Δm^2)
= (1.0, 2.8×10^{-3}eV^2)

KS test (shape):79%

for N_{SK}
56ev obs. / 54ev exp.

Both Shape & N_{SK} agree with best fit expectation

Allowed region (Shape+N_{SK})

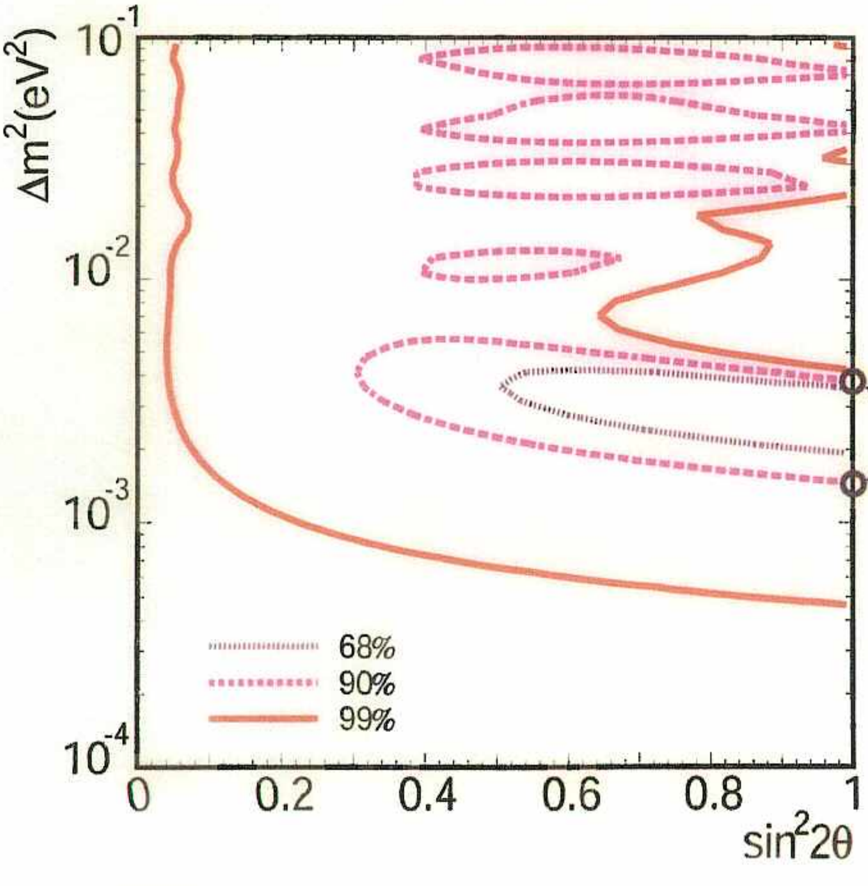

Δm^2=
1.5~3.9x10^{-3}eV^2
@ $\sin^2 2\theta$=1
@90%CL

Comparison of K2K-I result and new result of atmospheric neutrinos in SK-I

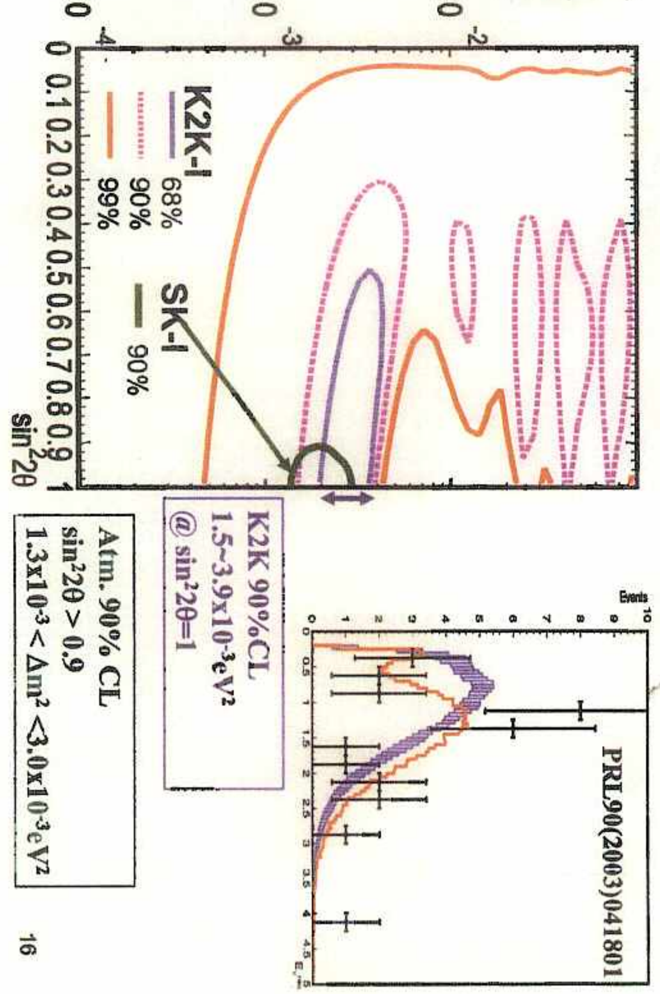

K2K 90%CL
$1.5\sim3.9\times10^{-3}$ eV²
@ $\sin^2 2\theta=1$

Atm. 90% CL
$\sin^2 2\theta > 0.9$
$1.3\times10^{-3} < \Delta m^2 < 3.0\times10^{-3}$ eV²

SK Data Summary K2K-II

	K2K-II (Jan.-Apr. '03)	(K2K-I)
• #spills:	2.8×10^6	9.2×10^6
• POT:	1.5×10^{19}	4.8×10^{19}
• Observed:	16 (23 incl out of FV)	56 (91)
• Expected:		
– 1kt	$26.4^{+2.3}_{-2.1}$	$80.1^{+6.2}_{-5.4}$

- **Obs/Exp(1kt)** **0.61 ± 0.15(stat) ↔ 0.70 ± 0.09(stat)**

Consistent rate reduction

Calibration of SK-II (new configuration of PMTs)

Upgrade of near detector with fine segmented scintillator detector

SK is back ! Updated SK events in K2K-II

FC K2K-II Preliminary *FC 22.5kt*

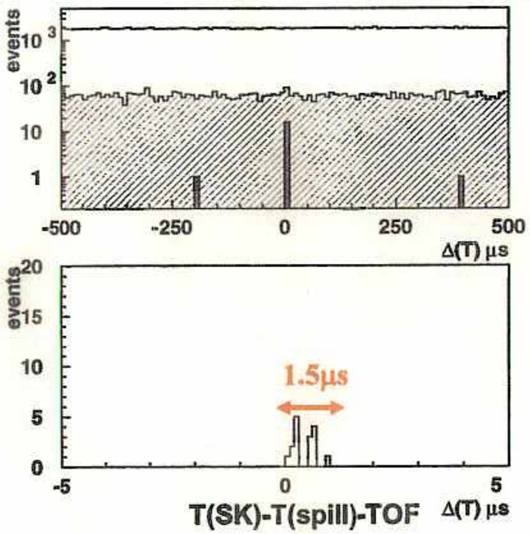

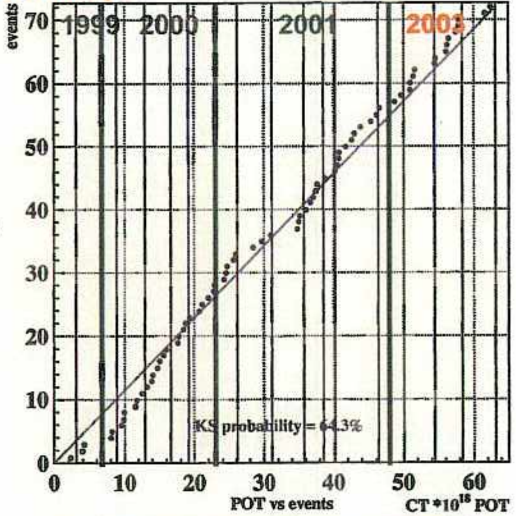

Full water on 10-Dec.-2002

⑦

Solar ν

- Introduction
- Experiments
  - ^{37}Cl
  - Kamiokande
  - Ga experiments
  - SK
  - SNO

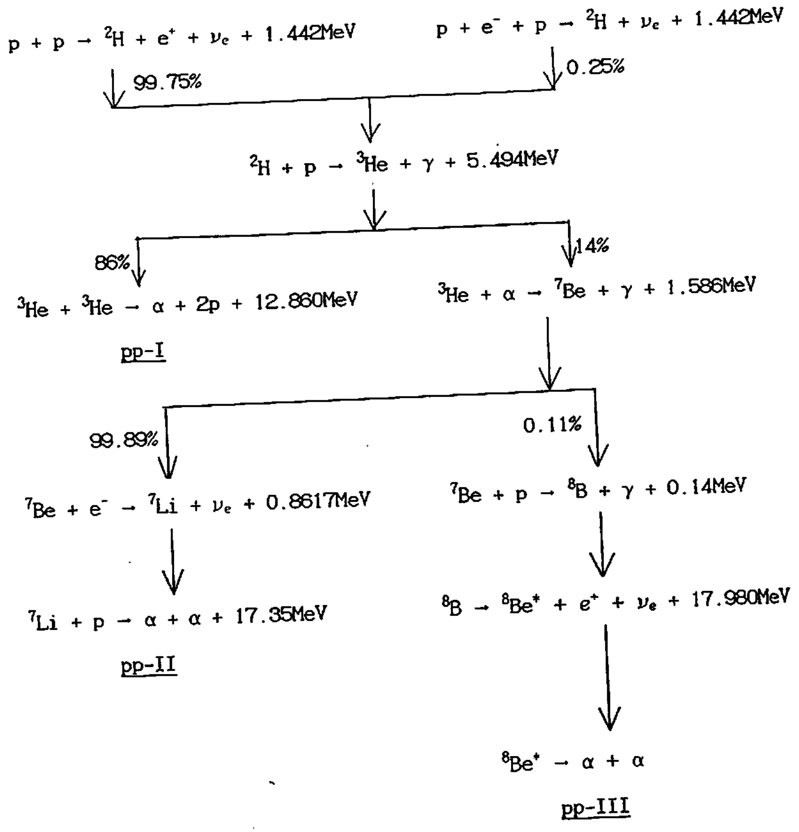

Fig. 1.1

The CNO cycle

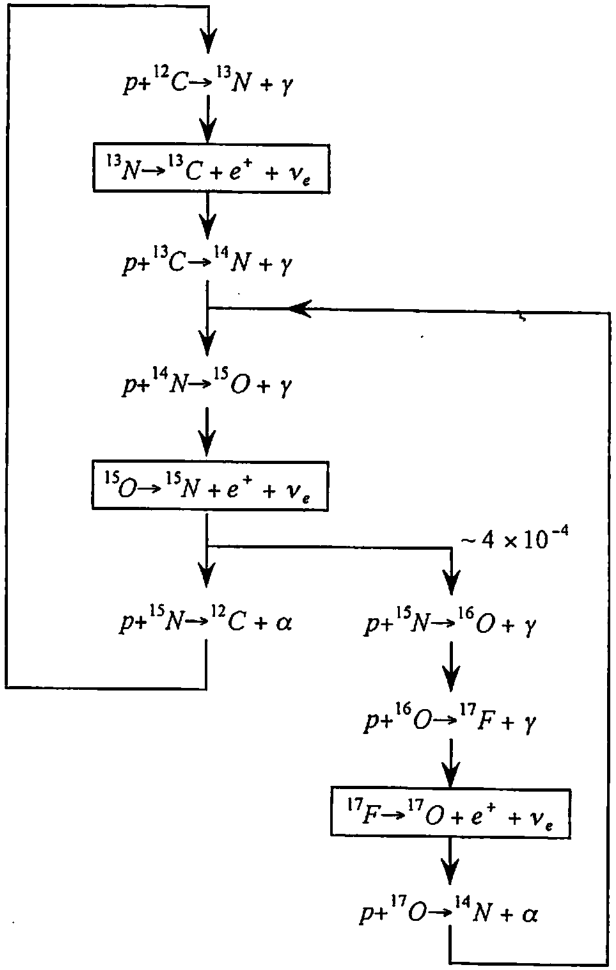

Fig. 1.2

$$4p \rightarrow {}^{4}He + 2e^{+} + 2\nu_e$$

$$\phi = 2 \times \frac{L}{Q} \times \frac{1}{4\pi R^2}$$

Q : PP-I 26.2 MeV

-II 25.6 MeV

-III 19.7 MeV

Luminosity

$L = 3.86 \times 10^{33}$ erg/sec

R : earth orbit 1.5×10^{1}

Q : local の平均 ~26 MeV

$\phi = 6.6 \times 10^{10}\ \nu_e/\mathrm{cm}^2/\mathrm{sec}$

ν fluxの計算

Standard solar model

(1) Hydrostatic equilibrium

$$\frac{dP}{dr} = -\rho \times \frac{GM(r)}{r^2}$$

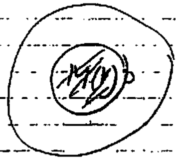

(2) Mass continuity

$$\frac{dM(r)}{dr} = 4\pi r^2 \rho$$

(3) Energy conservation

$$\frac{dL(r)}{dr} = 4\pi r^2 \rho \times \varepsilon$$

ε : energy release from nuclear process

$L(r)$ Luminosity

(4) Energy transportation

$$-\frac{dT}{dr} = \frac{3}{4ac}\frac{\kappa\rho}{T^3}\frac{L(r)}{4\pi r^2} \quad \text{(radiation)}$$

輻射

or

$$-\frac{dT}{dr} = -\left(1-\frac{1}{\gamma}\right)\frac{T}{P}\frac{dP}{dr} \quad \text{(convection)}$$

κ : absorption coefficient

a : Stefan-Bolzman constant

c : light verocity

γ : ratio of the specific heats $= C_p/C_v$

Convection

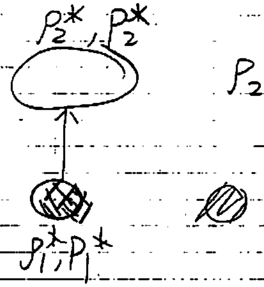

$\rho_1^* = \rho_1$, $P_1^* = P_1$

$P_2^* = P_2$ ~~のとき~~ である $\rho_2^* = \rho_1^* \times \left(\frac{P_2^*}{P_1^*}\right)^{\frac{1}{\gamma}}$

$\gamma = \frac{5}{3}$ for highy ionized gas

$\rho_2^* > \rho_2$ なら gratitational force によりもどされる

したがって安定。

しかし $\rho_2^* < \rho_2$ なら convection がおこる

"Structure and evolution of the star"
~~Ma~~ Martin Schwarzschild 1957

ρとP,Tの関係

$P = P(\rho, T, X, Y, Z)$ Equation of state

hydrogen Helium other (massでの割合)

$\rho, M(r), L(r), T$ の4つの分布を4つの方程式でと

Boundary condition :

$M_\odot = 1.99 \times 10^{33}$ g

$R_\odot = 6.96 \times 10^{10}$ cm

$T_\odot$ Age $= 4.6 \times 10^9$ year

$L_\odot$ surface Luminosity : 3.86×10^{33} erg/sec

注意：中心温度、density などは input ではない。計算から出るもの。

Assumptions

(1) t=0の時 太陽は chemically homogeneous

(2) Heより大きい element について 現在の太陽表面での abundance は initial abundance と同じである。

$Z = 0.020$ only 2%

total Z= 0.020

TABLE II. Fractional abundances of heavy elements.

Element	Number fraction (Grevesse, 1984)	Number fraction (Aller, 1986)	Number fraction (Ross-Aller, 1976)
C	0.29661	0.27983	0.30279
N	0.05918	0.05846	0.06326
O	0.49226	0.49761	0.50249
Ne	0.06056	0.06869	0.02699
Na	0.00129	0.00125	0.00138
Mg	0.02302	0.02552	0.02892
Al	0.00179	0.00198	0.00241
Si	0.02149	0.02672	0.03244
P	0.00017	0.00018	0.00023
S	0.00982	0.01040	0.01151
Cl	0.00019	0.00019	0.00023
Ar	0.00230	0.00227	0.00073
Ca	0.00139	0.00134	0.00163
Ti	0.00006	0.00007	0.00008
Cr	0.00028	0.00035	0.00037
Mn	0.00017	0.00016	0.00019
Fe	0.02833	0.02382	0.02297
Ni	0.00108	0.00114	0.00138
Total	1.000	1.000	1.000

TABLE III. Rosseland mean opacities (cm^2g^{-1}). Here $E-X=10^{-X}$.

$\rho/(T6)^3$ T6	2.818E-2	3.981E-2	5.623E-2	2.818E-2	3.981E-2	5.623E-2	2.818E-2	3.981E-2	5.623E-2	2.818E-2	3.981E-2	5.623E-2
1.000	4.659E+1	5.802E+1	7.116E+1	4.407E+1	5.557E+1	6.892E+1	4.886E+1	6.085E+1	7.463E+1	4.609E+1	5.813E+1	7.208E+1
1.218	4.122E+1	5.168E+1	6.421E+1	3.823E+1	4.850E+1	6.075E+1	4.326E+1	5.424E+1	6.738E+1	4.002E+1	5.078E+1	6.359E+1
1.483	3.931E+1	4.931E+1	6.083E+1	3.592E+1	4.528E+1	5.681E+1	4.136E+1	5.188E+1	6.399E+1	3.772E+1	4.752E+1	5.963E+1
1.807	3.262E+1	4.050E+1	5.009E+1	2.989E+1	3.694E+1	4.555E+1	3.434E+1	4.267E+1	5.280E+1	3.140E+1	3.883E+1	4.791E+1
2.200	2.728E+1	3.286E+1	3.889E+1	2.464E+1	3.004E+1	3.588E+1	2.879E+1	3.470E+1	4.109E+1	2.595E+1	3.167E+1	3.786E+1
2.680	1.921E+1	2.214E+1	2.496E+1	1.760E+1	2.048E+1	2.335E+1	2.030E+1	2.342E+1	2.641E+1	1.859E+1	2.164E+1	2.468E+1
3.264	1.267E+1	1.433E+1	1.606E+1	1.160E+1	1.326E+1	1.494E+1	1.340E+1	1.515E+1	1.698E+1	1.226E+1	1.402E+1	1.579E+1
3.975	8.107E+0	9.145E+0	1.036E+1	7.404E+0	8.393E+0	9.451E+0	8.553E+0	9.644E+0	1.092E+1	7.814E+0	8.855E+0	9.966E+0
4.841	5.236E+0	5.940E+0	6.731E+0	4.703E+0	5.358E+0	6.115E+0	5.502E+0	6.238E+0	7.062E+0	4.947E+0	5.633E+0	6.422E+0
5.896	3.527E+0	4.017E+0	4.597E+0	3.137E+0	3.584E+0	4.118E+0	3.687E+0	4.197E+0	4.798E+0	3.284E+0	3.749E+0	4.303E+0
7.181	2.528E+0	2.895E+0	3.341E+0	2.205E+0	2.553E+0	2.957E+0	2.627E+0	3.008E+0	3.468E+0	2.295E+0	2.655E+0	3.074E+0
8.746	1.941E+0	2.240E+0	2.604E+0	1.680E+0	1.952E+0	2.279E+0	2.007E+0	2.315E+0	2.689E+0	1.739E+0	2.020E+0	2.356E+0
10.652	1.620E+0	1.875E+0	2.192E+0	1.397E+0	1.624E+0	1.910E+0	1.668E+0	1.930E+0	2.256E+0	1.440E+0	1.674E+0	1.968E+0
12.973	1.434E+0	1.666E+0	1.938E+0	1.237E+0	1.434E+0	1.672E+0	1.473E+0	1.712E+0	1.991E+0	1.272E+0	1.475E+0	1.720E+0
15.800	1.306E+0	1.484E+0	1.719E+0	1.122E+0	1.285E+0	1.474E+0	1.340E+0	1.523E+0	1.762E+0	1.153E+0	1.321E+0	1.514E+0
19.243	1.130E+0	1.285E+0	1.429E+0	9.754E-1	1.086E+0	1.242E+0	1.156E+0	1.313E+0	1.459E+0	1.000E+0	1.114E+0	1.270E+0
23.436	9.526E-1	1.053E+0	1.176E+0	8.077E-1	8.932E-1	1.000E+0	9.707E-1	1.072E+0	1.196E+0	8.246E-1	9.111E-1	1.019E+0
	X=0.7300, Z=0.0195			X=0.3500, Z=0.0195			X=0.7300, Z=0.0208			X=0.3500, Z=0.0208		

Thermo nuclear reaction

2種類の原子核の反応 rateは.

$$I_{12} = n_1 n_2 \int \sigma(\vec{v_1}-\vec{v_2})\,|\vec{v_1}-\vec{v_2}|\,N_1(\vec{v_1})N_1(\vec{v_2})\,d\vec{v_1}d\vec{v}.$$

$n_1 n_2$ ↗ density

N : Maxwell-Bortzmann 分布

$$\left(\frac{m_i}{2\pi kT}\right)^{\frac{3}{2}} \exp\left(-\frac{m_i v_i^2}{2kt}\right)$$

$I_{12} = n_1 n_2 \langle\sigma v\rangle$ とかく。

$\boxed{\sigma}$ 原子核反応の時には Coulomb barrierをこえないといけない。

$$V \equiv \frac{Z_1 Z_2 e^2}{R} = \frac{1.44\, Z_1 Z_2}{R(fm)}\, MeV$$

Maxwell-Boltzmannの平均 energyは、

$$KT = 8.62\times10^{-8}\, T\, keV$$

太陽中心 1.55×10^7 K で KT は、1.3keV である

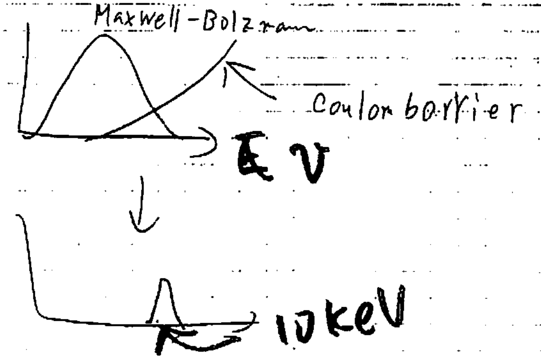

Coulomb barrier のトンネル効果の確率

$$\propto \exp\left(-\frac{2\pi z_1 z_2 e^2}{\hbar v}\right)$$

cross section は通常 geometrical factor $\propto \pi\lambda^2$ に比例

$\uparrow$ de Broglie ド・ブロ~~イ~~波長

$$\pi\lambda^2 \propto \left(\frac{1}{p}\right)^2 \propto \frac{1}{E}$$

したがって

$\sigma(E)$ は $\propto \frac{1}{E} \exp(- \quad)$

そこで $\sigma(E) = \frac{S(E)}{E} \exp\left(-\frac{2\pi z_1 z_2 e^2}{\hbar v}\right)$ とかく。

S(E) は原子核に固有の反応の強さ

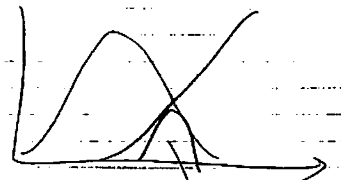

ガモフ peak : $E_0 \simeq (akT/2)^{\frac{2}{3}}$

$\Delta E_0 = \sqrt{4E_0kT/3}$

$a = \sqrt{2}\pi \frac{z_1 z_2 e^2 \sqrt{\mu}}{\hbar} =$

$\mu = \frac{m_1 m_2}{m_1 + m_2}$

~~mean~~ reduced mass

$E_0 \simeq$ 数10 keV

例: S_{17}

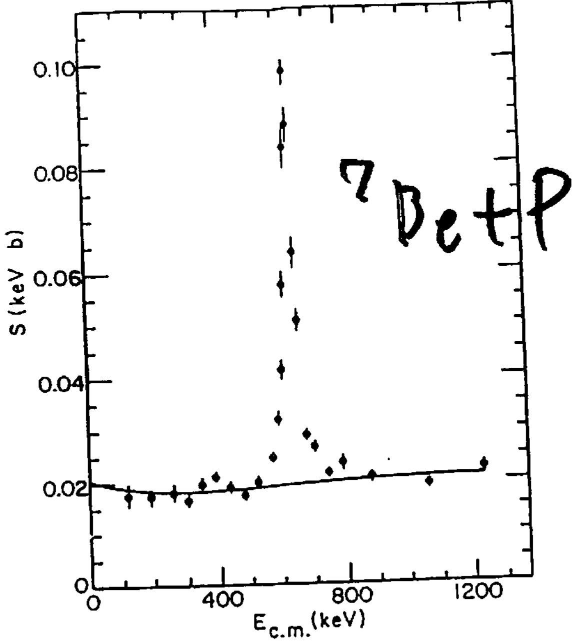

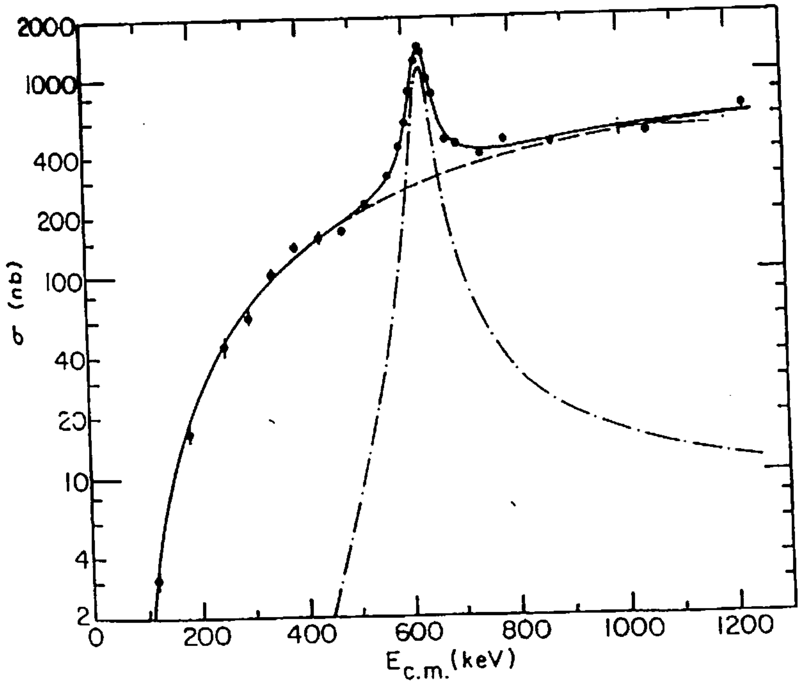

TABLE I. Some important nuclear cross-section factors.[a]

Reaction	No.	Recent Refs.	BP[b] (1992)	This work[b] (1994)	Comment
$^1H(p,e^+\nu_e)^2H$	1	c	$4.00^{+0.06}_{-0.04}\times 10^{-22}$	$3.89(1\pm 0.011)\times 10^{-22}$	improved matrix element; vac. polarization
$^1H(p+e^-,\nu_e)^2H$	2		Eq. (3.17)	Eq. (3.17)	see note (a)
$^3He(^3He,2p)^4He$	3	d	$5.0(1\pm 0.06)\times 10^3$	$4.99(1\pm 0.06)\times 10^3$	vac. polarization
$^3He(^4He,\gamma)^7Be$	4	d	$0.533(1\pm 0.032)$	$0.524(1\pm 0.032)$	vac. polarization
$^7Be(e^-,\nu_e)^7Li$	5	e	Eq. (3.18)	Eq. (3.18)	improved plasma screening
$^7Be(p,\gamma)^8B$	6	d,e	$0.0224(1\pm 0.093)$	$0.0224(1\pm 0.093)$	small vac. polarization
$^{14}N(p,\gamma)^{15}O$	7	d	$3.32(1\pm 0.12)$	$3.29(1\pm 0.12)$	vac. polarization

[a] The tabulated values of $S(0)$ are expressed in keV barn. Other recommended nuclear parameters are given in Tables 3.2 and 3.4 of Bahcall (1989), which is also the source of "Eq. (3.17)" and "Eq. (3.18)."

[b] The uncertainties for the cross-section factors are indicated in parentheses; they represent 1 σ errors in the experimental values (see Parker and Rolfs, 1991).

[c] Kamionkowski and Bahcall (1994a).

[d] Kamionkowski and Bahcall (1994b).

[e] Johnson *et al.* (1992).

.ne observed flux of ^8B neutrinos is 0.45 of the standard model rate including diffusion and 0.61 of the standard model without diffusion.

The present paper is organized as follows. In Sec. II, we describe improved input data and compare with the parameters that were used in earlier solar model calculations. In Sec. III, we describe and compare the various prescriptions for element diffusion. We present our principal results on a series of solar models in Sec. IV. We describe in Sec. V how we calculate uncertainties in the predicted fluxes and event

A. Nuclear reaction rates

The principal progress on the nuclear reaction rates since 1992 has been theoretical, including a recalculation of the nuclear matrix element for the *p-p* reaction (Kamionkowski and Bahcall, 1994a) and a self-consistent evaluation of the effects of vacuum polarization on the rates of the other important solar nuclear reactions (Kamionkowski and Bahcall, 1994b). Two recent reviews summarize the experimental situation (Parker, 1994) and the theoretical situation

---

~150 g/cm³

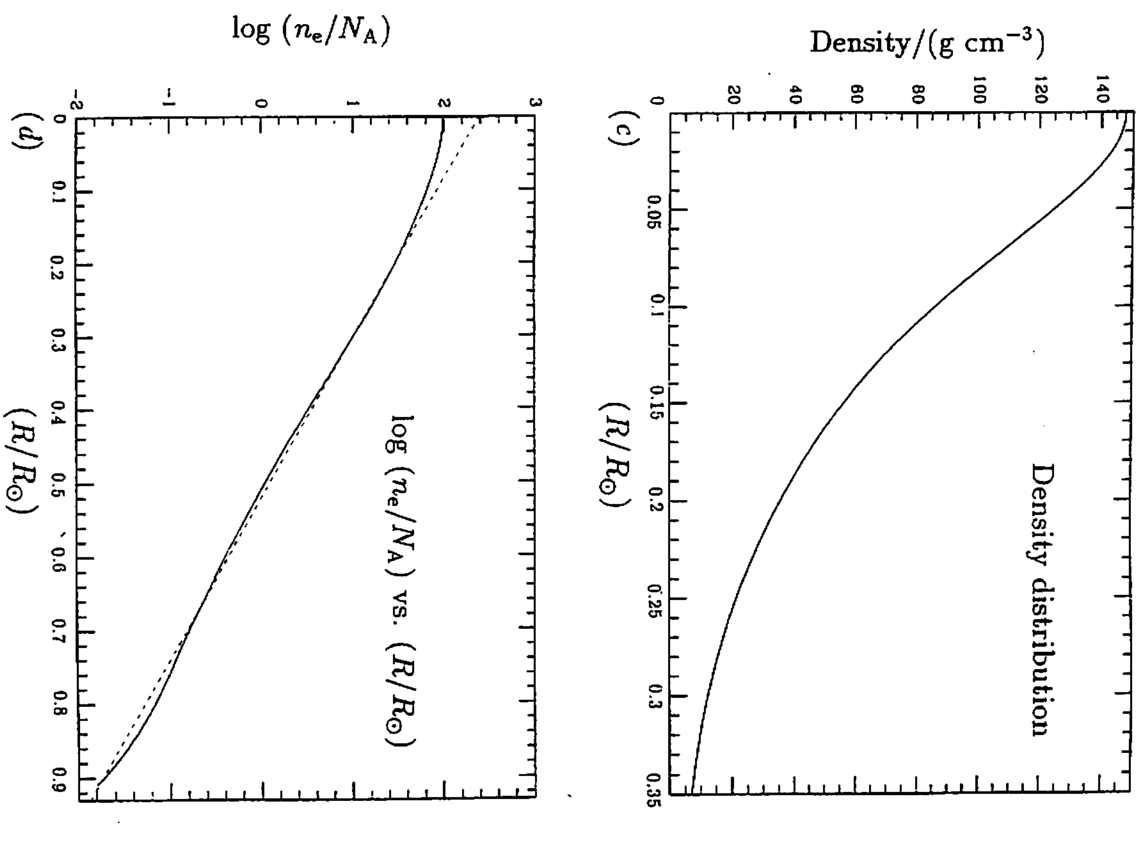

Figure 4.1 (c,d) Radial profiles of physical parameters (con't) Figure 4.1*c* illustrates the density distribution in the standard solar model. Figure 4.1*d* shows as a solid line the logarithm of the electron number density, N_e, divided by Avogadro's number, N_A, as a function of solar radius. The dotted line is an exponential fit to the density distribution, the parameters of which are given in the text [from Bahcall and Ulrich (1988)].

nominal (cf. paper I, Sec. III.B)
effective temperature has increased by 3%.

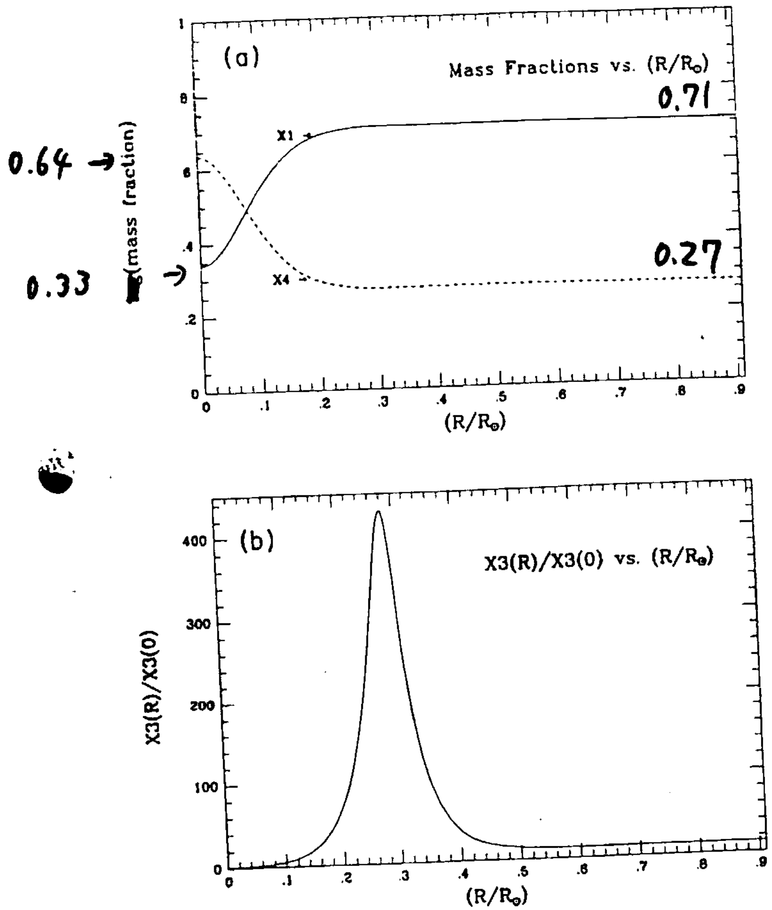

FIG. 7. Mass fractions as a function of radius: (a) logarithm of the hydrogen and helium mass fractions as a function of position in the sun; (b) dependence of the ^{3}He abundance upon position in the sun; (b) dependence of the ^{3}He abundance upon position. The figures shown here illustrate the values obtained for the standard solar model described in Sec. V.B and Table X.

sol.12

Our best estimates fo
gether with the theor
Table XIII. The fluxe
solar model. The tota
was evaluated using
cussed in Sec. II and t
to input parameters th
XV and Eqs. (15) and
Table XIII gives the
Columns 3–9 give the
of the indicated param

What information a
vidual neutrino fluxes
the sun the *p-p*, ^{8}B, ^{7}B
comparison with Fig
give the physical con
this figure allows on
imprinted on the neu
region in which the *p*
that of the total ener
occurs in both distri
tion, $0.09R_\odot$ and *T*
tions for the *p-p* p
respect to the energy

Because of its str
production is peake
$T=15\times10^6$ K, and
$0.02R_\odot$ to $0.07R_\odot$.
termediate between
$0.06R_\odot$ and spreadi
$0.10R_\odot$.

The hep distribu
(half-peak points) fr
$0.13R_\odot$ and $T=1$
neutrinos are produ
lar core is that the
outward from the
lower temperatures

sol-13

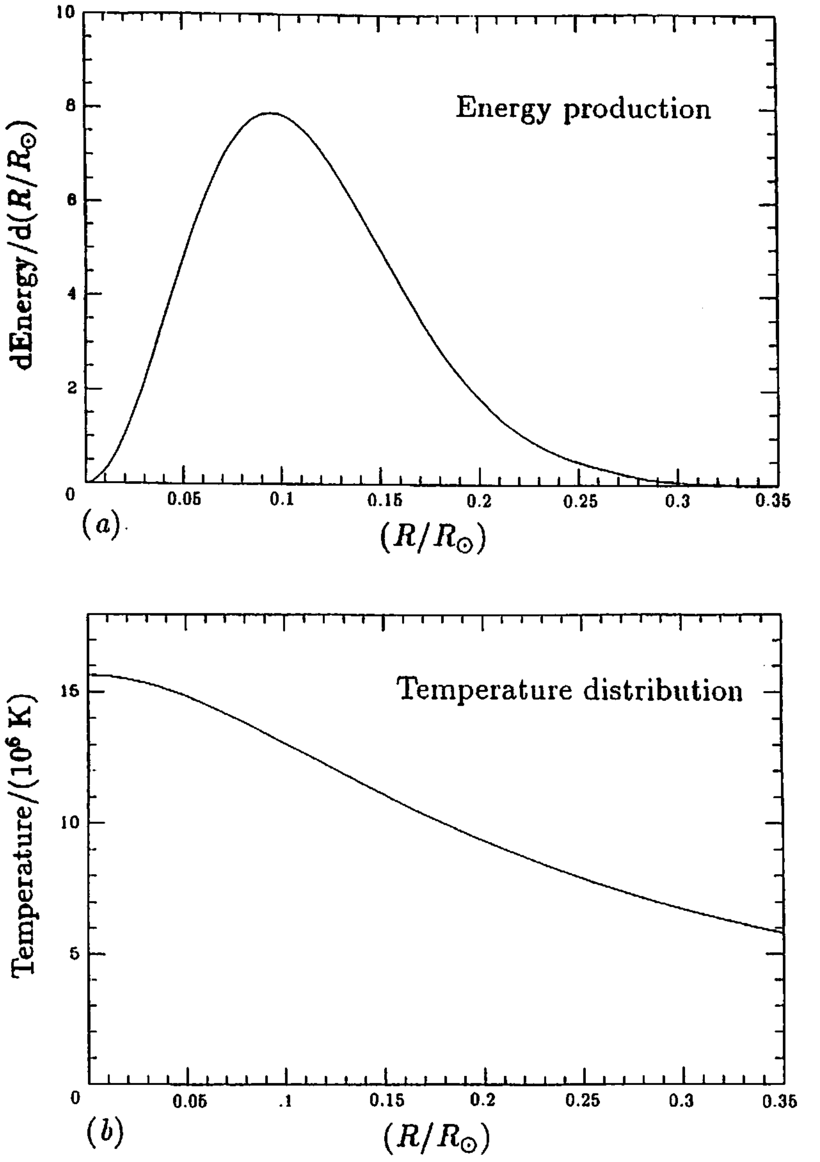

Figure 4.1 (a,b) Radial profiles of physical parameters Figure 4.1*a* shows the fraction of the energy generation that is produced at each position in the standard solar model. Figure 4.1*b* illustrates the temperature distribution in the standard solar model.

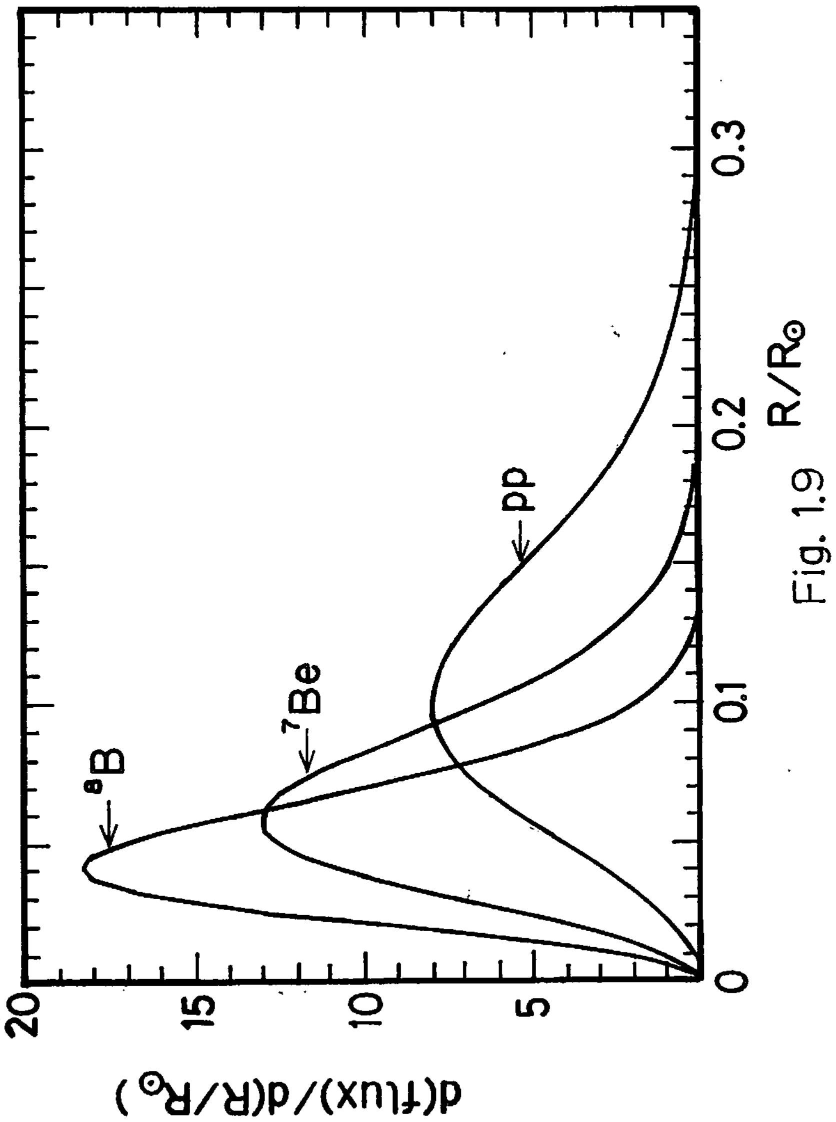

Fig. 1.9

Iben (1967,1974) and Demarque & Guenther (1991) summarize in comprehensive presentations the evolution of solar parameters in models that were calculated prior to the inclusion of element diffusion in solar evolutionary codes. These discussions did not encounter the problem of semiconvection discussed here in § 3.3 because this phenomenon is caused by effects of diffusion near the base of the convective zone.

The solar radius and luminosity (or equivalently, the solar effective temperature and luminosity) constitute precise constraints on the possible geological histories of the earth. We quantify these constraints in the following subsection and specify upper limits to the allowed discrepancies from the standard solar model profile of solar luminosity versus age.

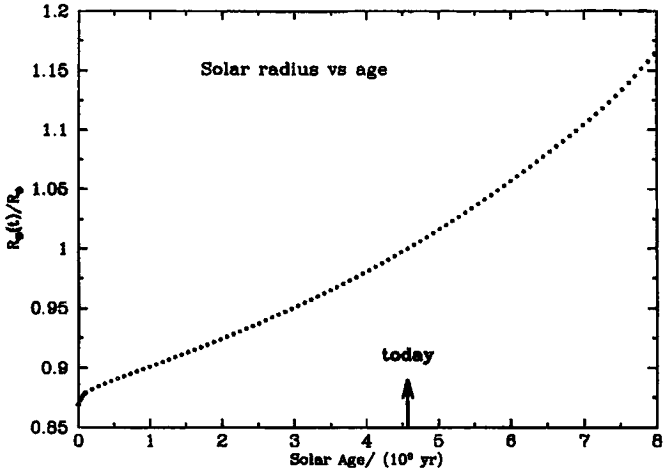

Fig. 1.— The calculated radius, $R_\odot(t)$, as a function of age for the standard solar model, Bahcall-Pinsonneault (2000). The solar age is measured in units of 10^9 yr. The present age of the sun, 4.57×10^9 years, is indicated by an arrow in Figure 1. The radius increases from $0.87R_\odot$ at the zero age main sequence to $1.0R_\odot$ at the present epoch and $1.18R_\odot$ at a solar age of 8 billion years.

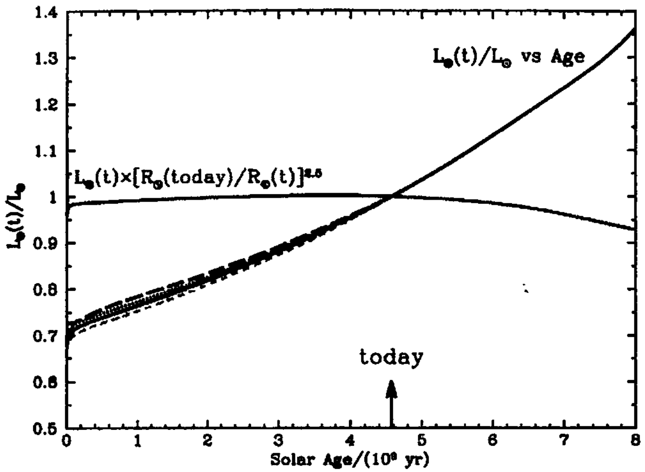

Fig. 2.— The normalized solar luminosity, $L_\odot(t)/L_\odot$(today) versus solar age for the Standard solar model (solid curve) and for three 'deficient' solar models: the No Diffusion model (dotted curve), the $S_{34} = 0$ model (short dashes), and the Mixed model (long dashes). The luminosity evolution of the sun is essentially the same in all solar models we have investigated, including deficient solar models. The rms deviation of the deviant models from the standard solar model luminosity is only 1% over the history of the sun from the zero-age main sequence to the current epoch (see text for more details). The product $L_\odot(t) \times R_\odot(t)^{-2.5}$ varies by ±4% over the entire period from the zero age main sequence to a solar age of 8 billion years, while the solar luminosity itself varies by slightly more than a factor of two during this period. In the period between 4 billion years to 8 billion years, the relation $L_\odot(t) \propto R_\odot(t)^2$ is satisfied to ±1/2%. The solar luminosity has increased by 48% from the zero main sequence to the present epoch. The present age of the sun is indicated by an arrow at 4.59 × 10^9 years.

risen monotonically from a zero-age value of $0.677L_\odot$.

The time evolution of the solar luminosity is robust. We also show in Figure 2 the solar luminosity as a function of time for the three most deficient solar models that are described in the following section, § 4. The rms difference between the standard luminosity and the luminosity of the deviant models is 1.6% for the mixed model (1.2% ignoring the first Gyr), 0.7% for the no diffusion model (0.5% ignoring the first Gyr), and 0.9% for the $S_{34} = 0$ model (0.8% ignoring the first Gyr). The largest deviations occur for the zero-age main sequence models and are 2.5% for

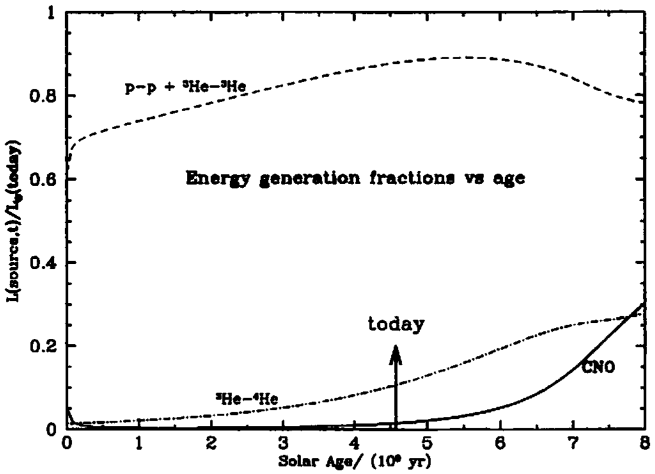

Fig. 3.— The fraction in the Standard model of the solar luminosity produced by different nuclear fusion reactions versus solar age. The luminosity generated by the $p - p$ nuclear fusion branch that is terminated by the ^{3}He-^{3}He reaction is marked by a dashed curve in the figure and the luminosity produced by the $p - p$ branches that proceed through the ^{3}He-^{4}He reaction is denoted by a dot-dashed curve. The luminosity generation by the CNO cycle is indicated by a solid line. The unit of luminosity is the present-day total solar luminosity. At the present epoch, the $p - p$ + ^{3}He-^{3}He reactions produce 87.8% of the solar luminosity and the branches terminating through the ^{3}He-^{4}He reaction generate 10.7% of the solar luminosity. The CNO cycle produces 1.5% of the present-epoch luminosity.

3.2. Energy fractions

Figure 3 shows, for the Standard model, the energy generated by different nuclear fusion reactions as a function of solar age. The present-day total solar luminosity, $L_\odot$(today), is the unit of luminosity in Figure 3.

The branch of the $p - p$ chain that is denoted in Figure 3 by $p - p + {}^3$He-^{3}He (the dashed curve) proceeds primarily through the reactions $p(p, e^+ \nu_e)^2$H$(p,\gamma)^3$He$(^3$He$, 2p)^4$He. For simplicity, we include all $p - p$ reactions in this sum but do not show explicitly the pep reactions in the above scheme. The small energy contribution due to pep reactions is included in the calcugradient is nearly constant in time, the equations of stellar structure imply that the quantity $\kappa PL/MT^4$ will be approximately constant at the base of the convective zone. From Figure 6, we see that both the opacity and the temperature decrease slowly at the base of the convective zone. Solar models therefore compensate for the increase of the luminosity by the decrease of the pressure at the boundary between radiative and convective equilibrium.

3.4. Central values of Temperature, Density, and Pressure

Figure 7 shows the time dependence of the central values for the temperature, density, and pressure of the Standard solar model. The results are normalized to the computed values for the present epoch.

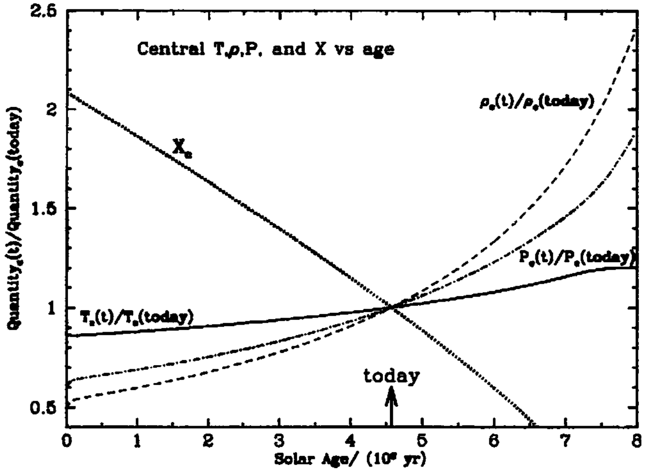

Fig. 7.— The temporal evolution of the central temperature, density, pressure, and hydrogen mass fraction. The figure shows the computed values for the Standard solar model of the central temperature (solid line), pressure (dot-dash line), density (dash line), and hydrogen mass fraction (dotted line).

Over the 8 billion years shown in Figure 7, the central temperature increases by about 39%.

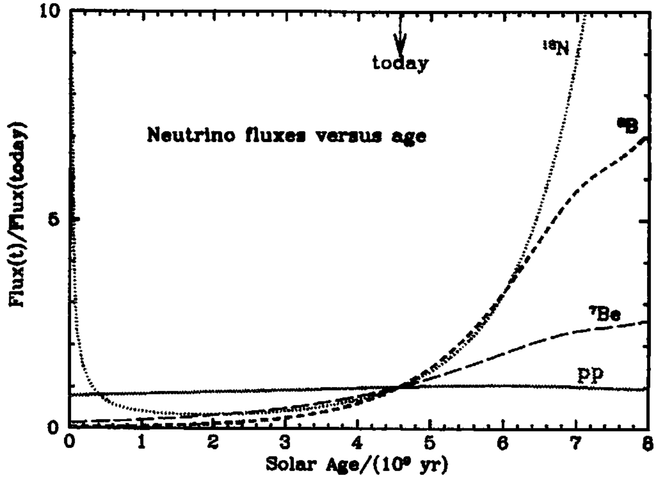

Fig. 10.— The pp, ^{7}Be, ^{8}B, and ^{13}N neutrino fluxes as a function of solar age. The figure shows the Standard model ratios of the fluxes divided by their values at 4.57×10^9 yr. The pp flux is represented by a solid line, the ^{7}Be flux by a line of long dashes, the ^{8}B flux by short dashes, and the ^{13}N flux by a dotted line.

The ^{7}Be and ^{8}B neutrino fluxes increase monotonically and by larger amounts than the pp flux. Both the ^{7}Be and the ^{8}B fluxes begin with very low fluxes relative to their current values, 14% and 3%, respectively, of their intensities at 4.57×10^7 yr. At a solar age of 8 billion years, the ^{7}Be neutrino flux is 2.6 times larger than it is today and the ^{8}B neutrino flux is 7.1 times larger than today. At the current epoch, the ^{7}Be flux is increasing by about 65% per billion years and the ^{8}B flux is increasing faster, about 120% per billion years.

The ^{13}N neutrino flux has the most interesting time dependence. In the first 10^8 y on the main sequence, the ^{13}N flux is much larger than its current value because ^{12}C has not yet been burned to the equilibrium value appropriate for the CNO cycle. The reaction ^{12}C$(p,\gamma)^{13}$N occurs relatively often in this early stage of solar evolution and the neutrino flux from ^{13}N beta-decay has a peak value of about 11 times its current flux. The minimum ^{13}N flux, 33% of its present value, is attained at a solar age of 1.8 billion years. Thereafter, the ^{13}N flux increases steadily as the central

SSMの結果から.

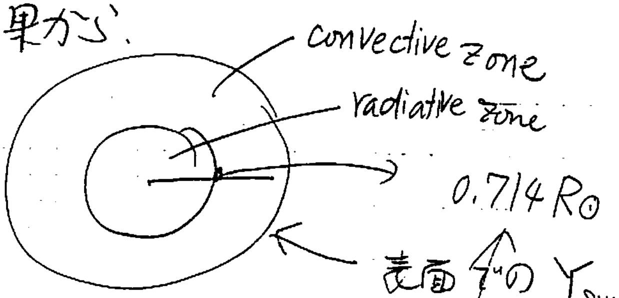

表面での $Y_{surf} = 0.243$
↑
model

実測値 : $(0.714 \pm 0.001) R_\odot$

$Y_{surf} = (0.249 \pm 0.003)$

とconsistent。

$\boxed{\text{sum : } 6.55 \times 10^{10}\ \text{cm}^{-2}\text{s}^{-1}}$

(1 ± 0.01)

PP 5.95×10^{10} $\text{cm}^{-2}\text{sec}^{-1}$ $E_{max} = 0.42$ MeV

pep 1.40×10^{8} $(1 + 0.01)$ $E = 1.44$ MeV

hep 9.3×10^{3} $E_{max} = 18.8$ MeV

^{7}Be 4.77×10^{9} (1 ± 0.10) $E = 0.862$ MeV

0.384 MeV
で 10.4%

^{8}B 5.05×10^{6} $(1 \pm^{0.20}_{0.16})$ $E_{max} = \sim 14$ MeV

^{13}N 5.48×10^{-8} $(1.00 \pm^{0.21}_{0.17})$

^{15}O 4.80×10^{8} $(1.00 \pm^{0.25}_{0.19})$

^{17}F 6.33×10^{-4} $(1.00 \pm^{0.12}_{0.11})$

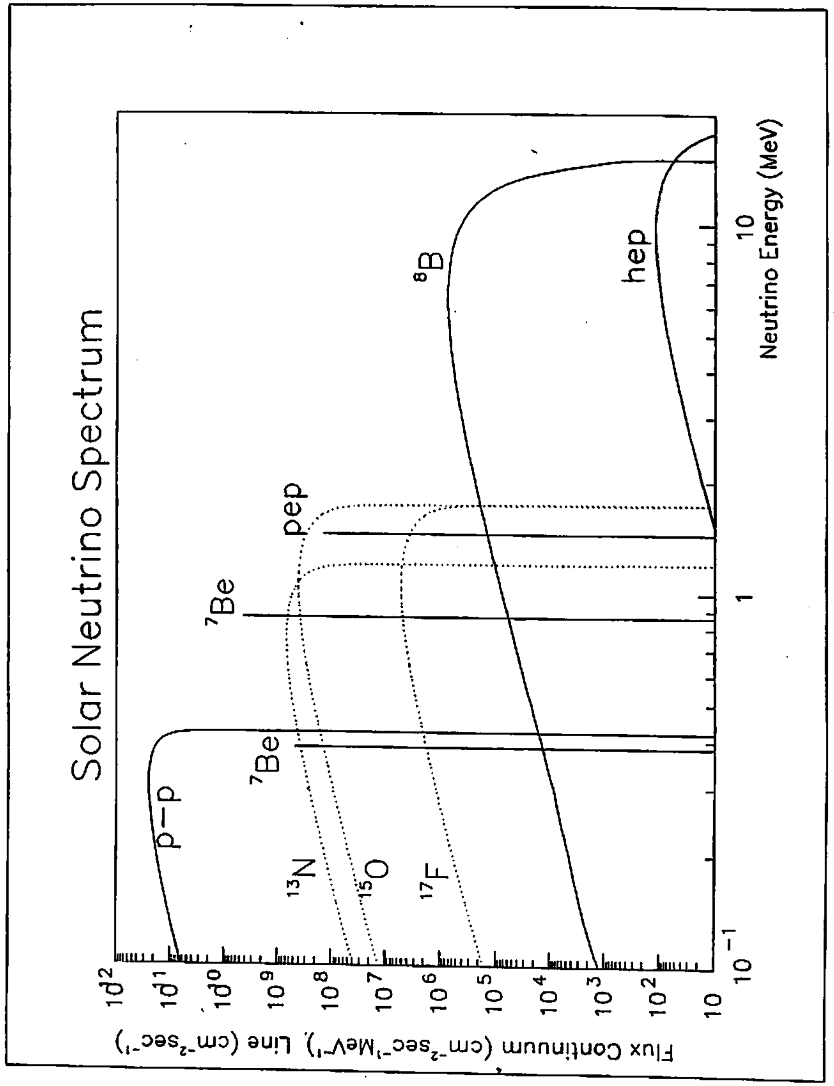

Fig. 1.3

Test SSM by helioseismology 日震学

Sound speed $c^2 = \Gamma_1 \frac{P}{\rho}$ $\Gamma_1 = \frac{C_P}{C_V} = \frac{5}{3}$

Helium voice   air → Helium

ρが小さくなる。

Cが大きくなって $\frac{c}{\quad} = \nu$

$c = \lambda\nu$. λは同じでも νが大きくなる。

Heliumの割合がわかる。

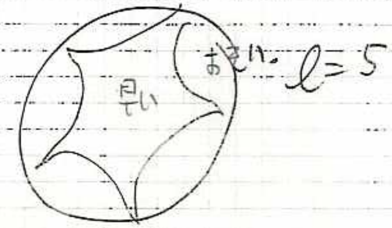

Solar modelと 0.5%以内の精度でよく あっている。

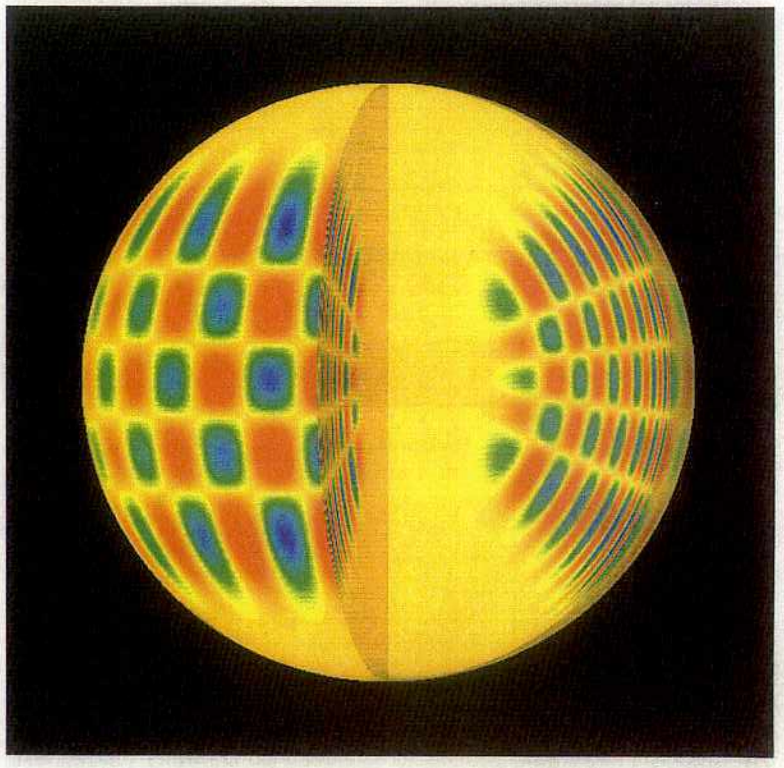

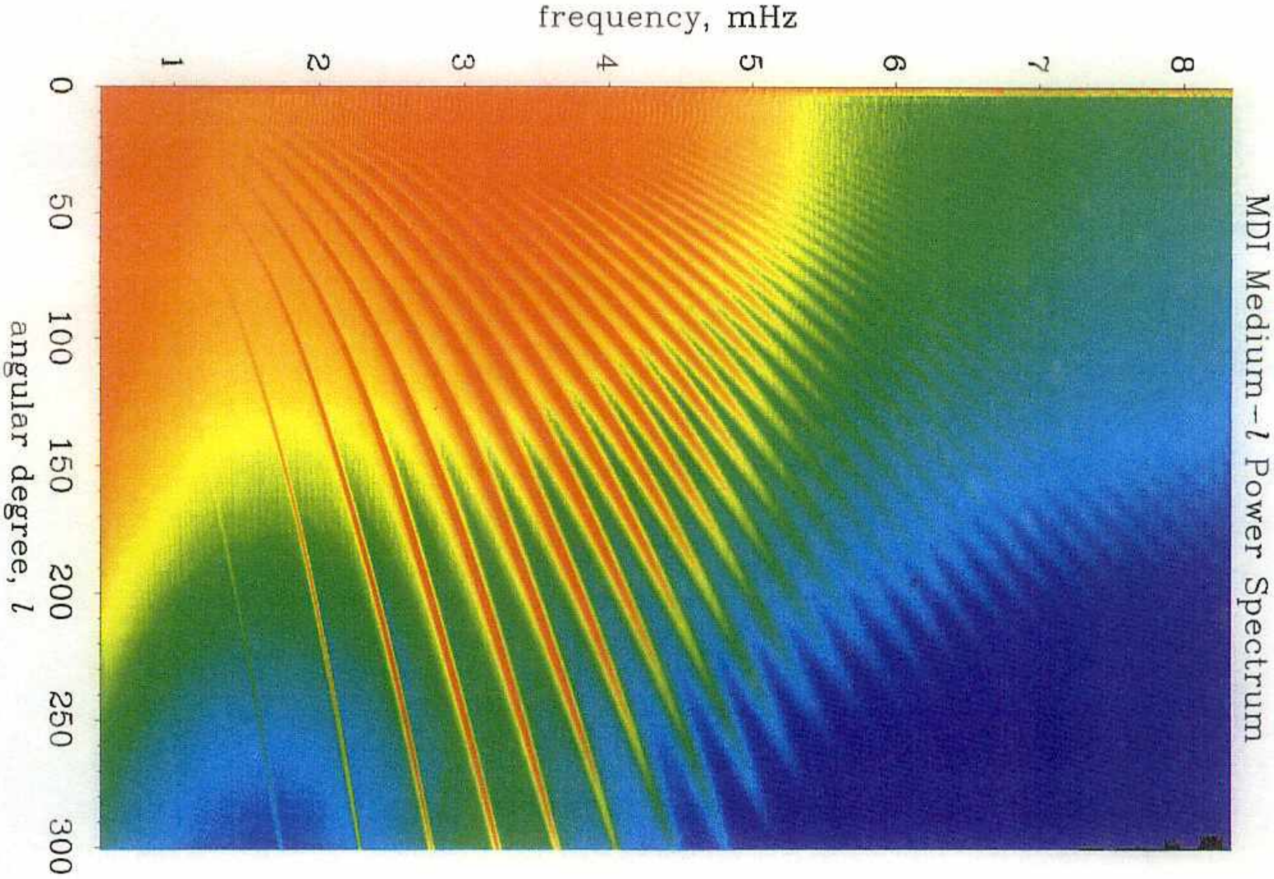

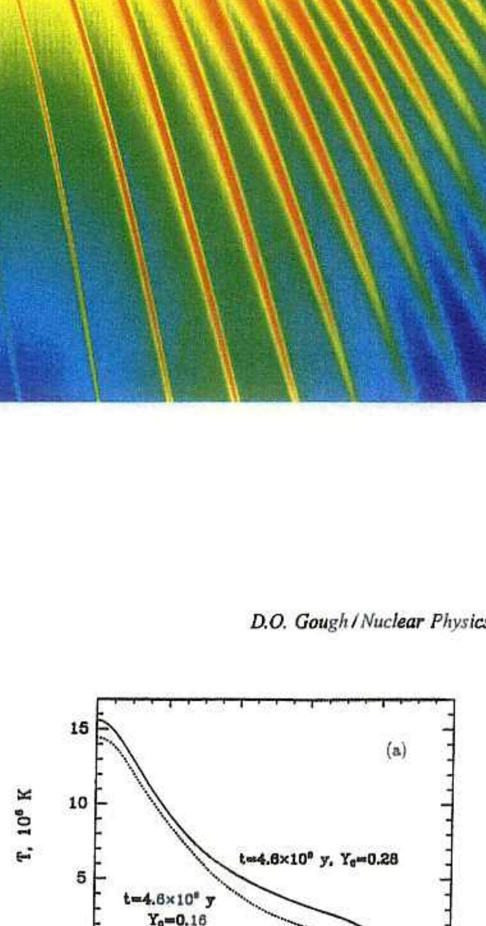

Fig. 5. (a) temperature $T(r)$ of two solar models with initial helium abundances $Y_0 = 0.28$ (solid curve) and $Y_0 = 0.14$ (dotted curve). (b) squares of sound speeds, $c^2(r)$, of the two models of (a); the dashed curve represents c^2 at zero age in the model with $Y_0 = 0.28$. A sound-speed inversion of solar data is included also as a continuous curve.

difficulty lies in explaining three different measure-

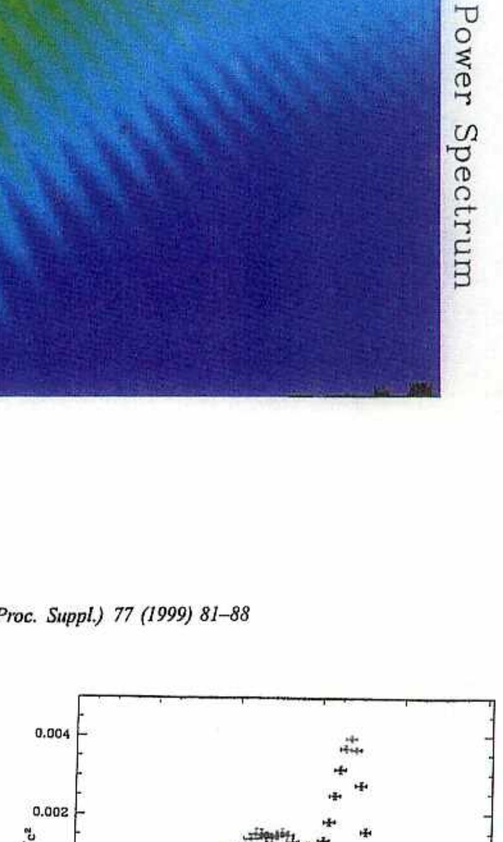

Fig. 6. Localized averages of the relative difference $\delta c^2/c^2$ between the squared sound speeds in the Sun and in the standard solar model of Christensen-Dalsgaard *et al.* (1996). The horizontal bars represent the characteristic widths of the averaging kernels A, such as are illustrated in Figure 4; the vertical bars are standard errors (which are correlated).

But would merely removing the discrepancy be scientifically sufficient? Certainly not. Firstly, it is important to be sure that the model really does represent the spherically averaged structure of the Sun, which involves investigating more than just the sound speed. Secondly, we need also to investigate the asphericity, which, as Haxton has pointed out, may not be small in all respects.

3. 4 DIGRESSION ON ROTATION

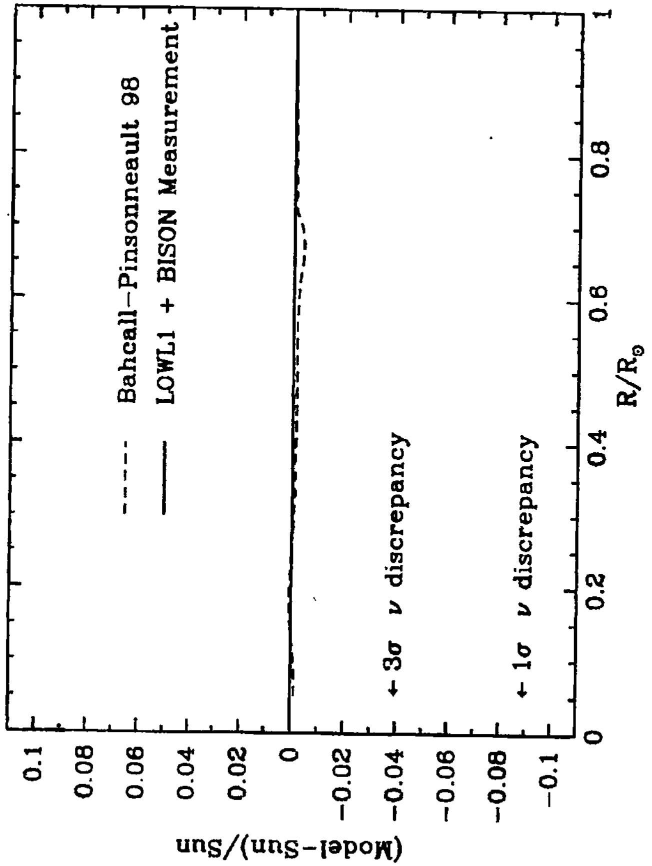

Figure 2. Predicted versus Measured Sound Speeds. This figure shows the excellent agreement between the calculated (solar model BP98, Model) and the measured (Sun) sound speeds, a fractional difference of 0.001 rms for all speeds measured between $0.05R_\odot$ and $0.95R_\odot$. The vertical scale is chosen so as to emphasize that the fractional error is much smaller than generic changes in the model, 0.03 to 0.08, that might significantly affect the solar neutrino predictions.

106

Solar ν experiments

① Davis exp. 1970~

② Kamiokande $\nu e^- \to \nu e^-$ → SKでくわしく。

③ Gallium experiment GALLEX
SAGE

④ SK

Davis exp.

He gas purge で Ar をとり出す。

ext. efficiency は 95.8% 回収前に known amount の ^{36}Ar, ^{38}Ar を入れて それの回収率を見る。

$$^{37}Cl + \nu_e \to {}^{37}Ar + e^-$$

24.2% abundance

$E_{thr} = 0.814\,MeV$

$\tau_{\frac{1}{2}}(^{37}Ar) = 35\,days$

expose : ~80 days

SSM expected production rate ~1.4 atms/day

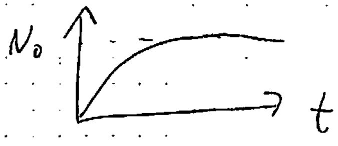

$N_0(1 - e^{-\frac{t}{\tau}})$

$1.4\,atms \times \frac{\tau_{\frac{1}{2}}}{\ln 2} \approx 71\,atm$ 平衡

^{37}Cl detector

1480m underground

615 tons of C_2Cl_4

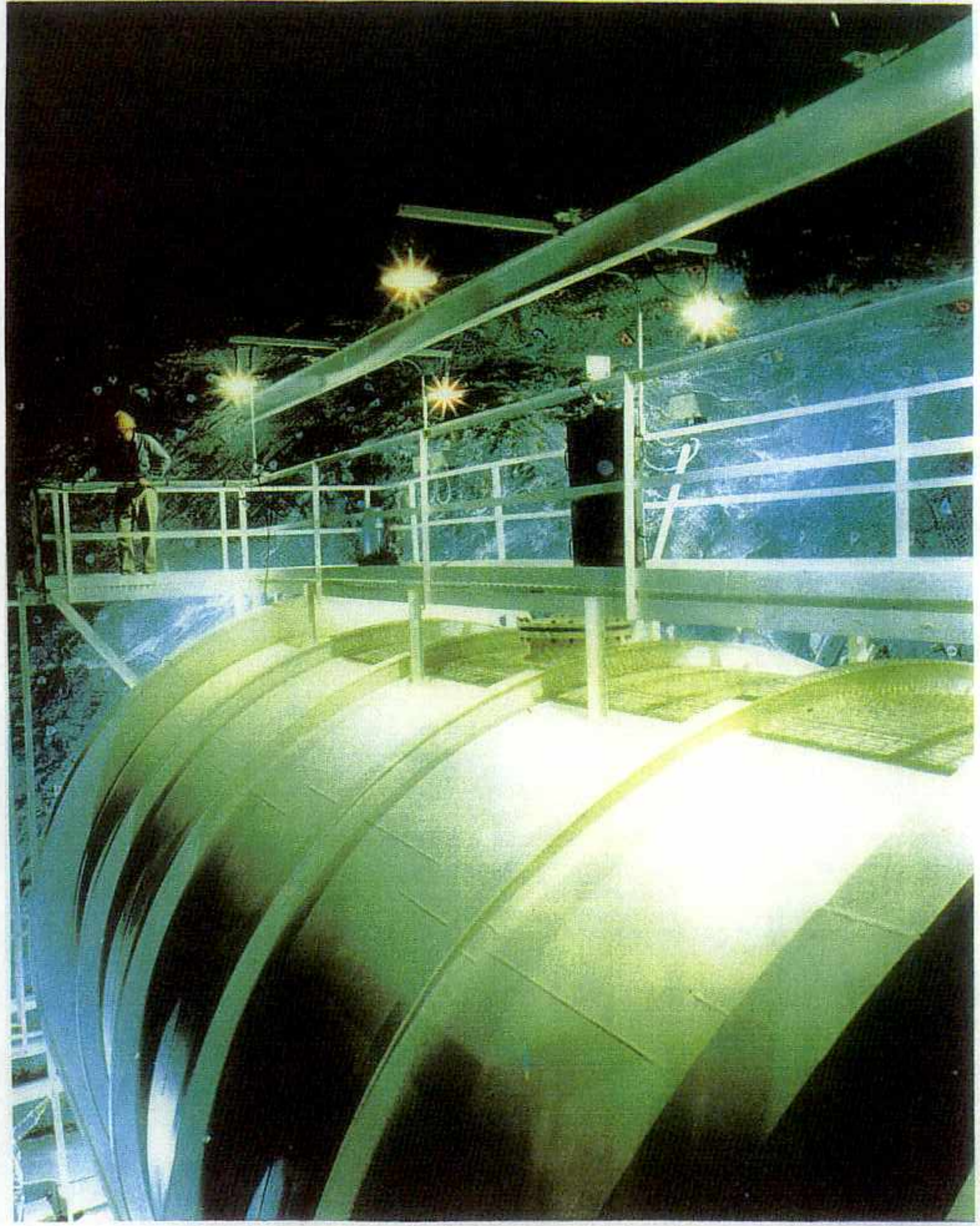

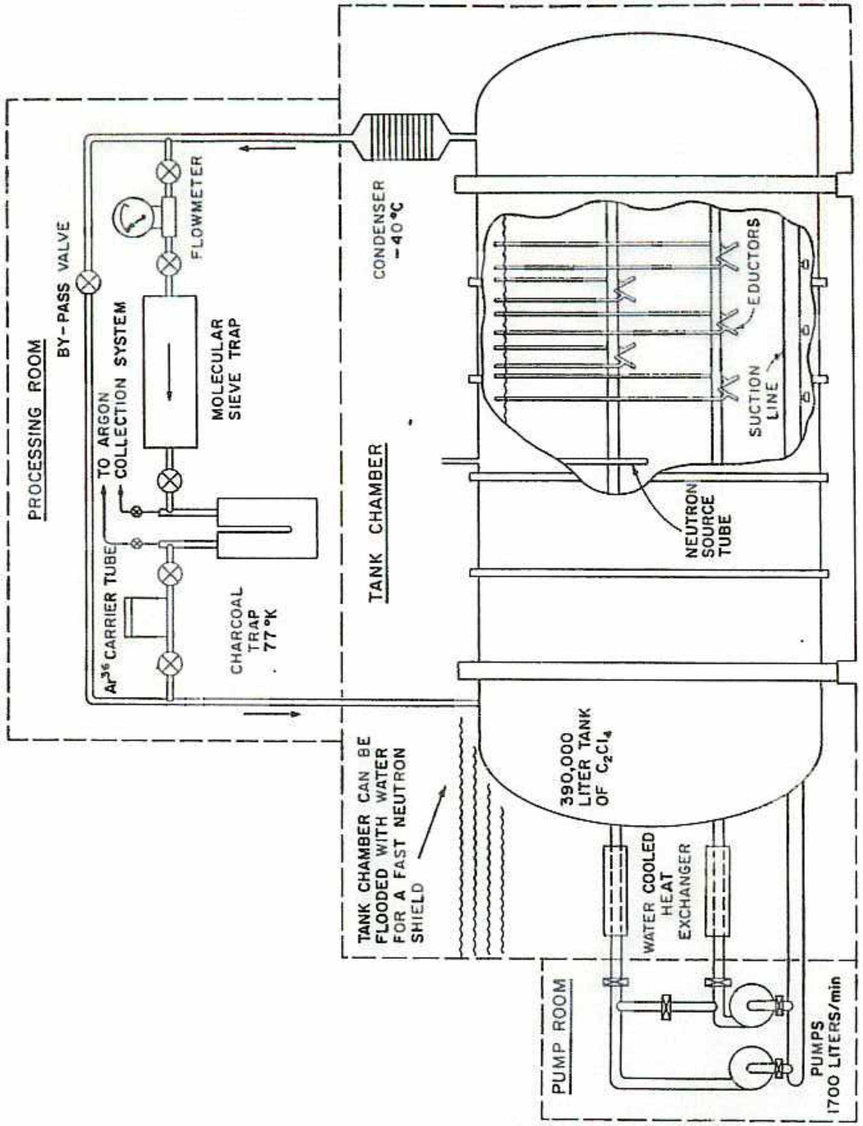

FIG. 1. Schematic arrangement of the Brookhaven solar neutrino dector.

50/-30

Each contribution (SSM prediction)

SNU

PP	0.0	
Pep	0.22	
^{7}Be	1.15	← 15%
^{8}B	5.76	← 76%
^{13}N	0.09	
^{15}O	0.33	
^{17}F	0.0	

他から8%

Davis 1.4 Ar/day

$7.6 ^{+1.3}_{-1.1}$

SNU: 10^{-36} captures/atms/sec

^{37}Ar は electron capture decay

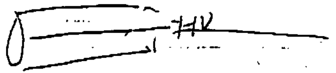

small proportional counter

2.82 keV の Auger electron

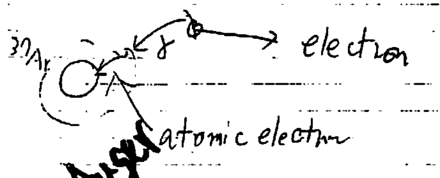

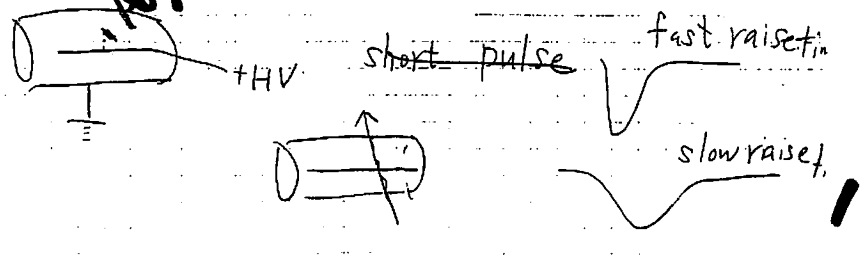

501-31

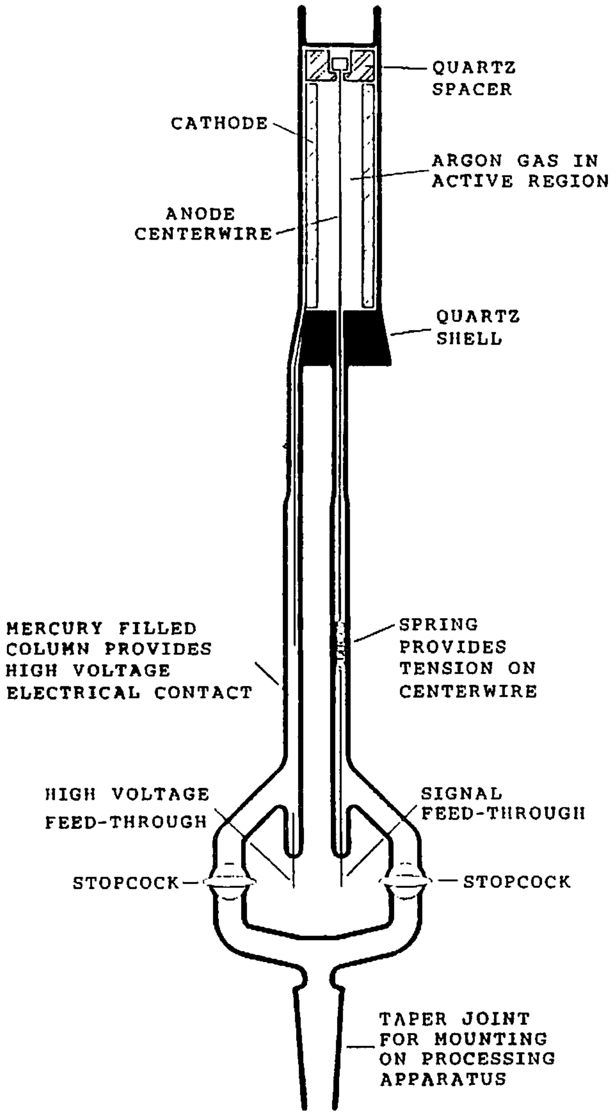

FIG. 7.—Proportional counter geometry. Sketch of the miniature proportional counters used to observe ^{37}Ar decays. Counters typically have an overall length of 20 cm, with an active region 30 mm long and 4.5 mm in diameter.

This seal assures that no gas is lost by leakage through the valve.

Since the counters are baked out at temperatures in excess of 200° C, a space must be left between the cathode and the counter shell to allow for differential thermal

extracted from the tank t
argon to fill the counter
methane. The methane u
is very low in tritium.
^{37}Ar decays in the mi
distinguished from back
their distinct energy and
nant decay mode of ^{37}Ar
its 2.82 keV of energy i
Auger electrons from at
range of these electrons
that the approximately 1
Auger electrons are high
the electrons thus have
center wire, resulting in
than 5 ns). Background
interacting with an at
Compton scattering; the
deposits energy compar
looking for, will have a
the counter and will thus
wide region, leading to a
The signal from the
directly coupled to a fas
preamplifier output is th
a standard shaping amp
than the pulse rise time
converter to measure th
going into a timing filter
time. This timing ampli
and then integrates the
short time constant (5
into a pulse stretcher tha
the ADP signal, for "an
which has appropriate
analog-to-digital conve
portional to energy and
time of the pulse from th
In an ADP versus c
narrow band (Fig. 8),
broad region below this

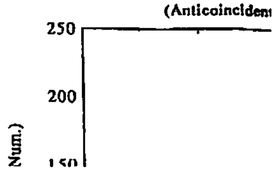

^{37}Cl experiment

Signal: Events occurring less than 50 days after time of extraction

49 runs, 1065 events, 6.41 years of counting

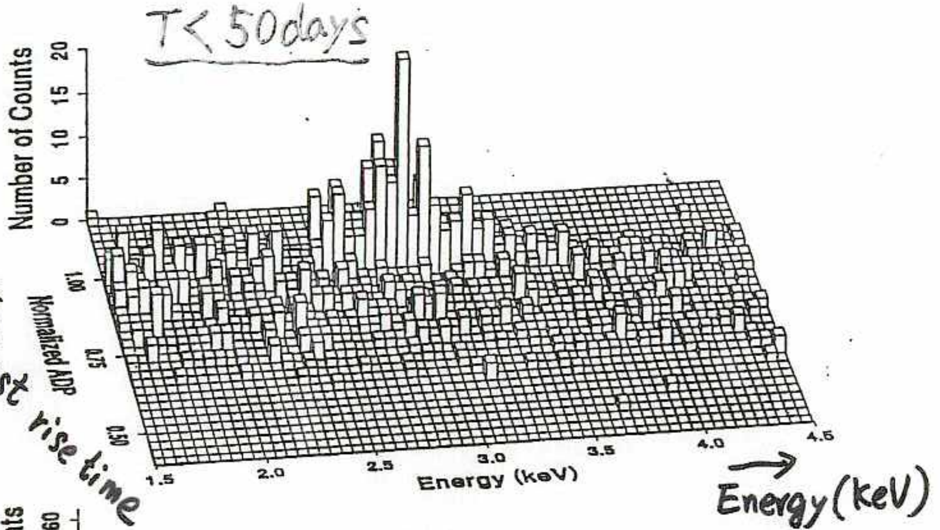

Background: Events occurring more than 150 days after time of extraction

49 runs, 2132 events, 20.51 years of counting

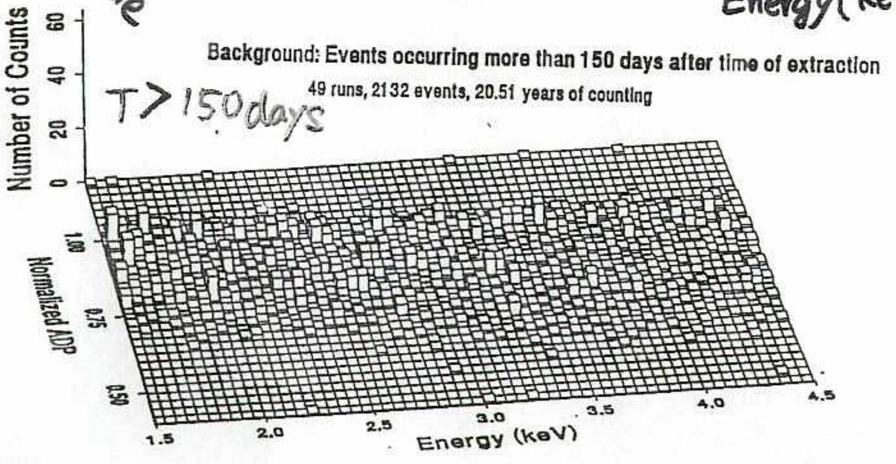

109

The method of maximum likelihood is also used to combine the results of all 108 observations to find the production rate that is most likely to have produced the entire data set. The average production rate for several runs is found by multiplying the likelihood functions of these runs together and searching parameter space for the most likely

WSS

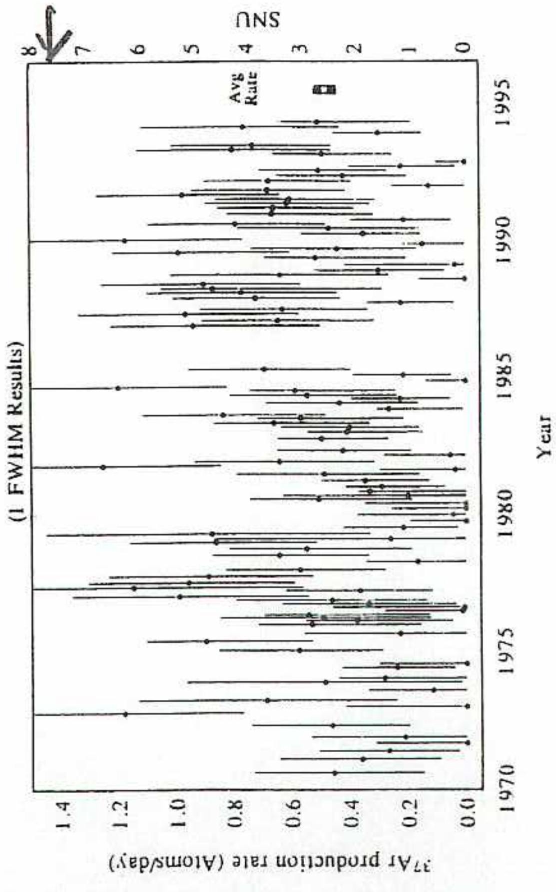

FIG. 13.—Homestake Experiment—one FWHM results. Results for 108 individual solar neutrino observations made with the Homestake chlorine detector. The production rate of ^{37}Ar shown has already had all known sources of nonsolar ^{37}Ar production subtracted from it. The errors shown for individual measurements are statistical errors only and are significantly non-Gaussian for results near zero. The error shown for the cumulative result is the combination of the statistical and systematic errors

^{37}Cl result : 2.56 ± 0.16 ± 0.16 SNU

$\updownarrow$ ratio 0.34

7.6 SNU SSM

Gallium exp.

GALLEX 1991 〜 1997 それ以降 GNO

SAGE 1990 〜

$^{71}Ga + \nu_e \rightarrow {}^{71}Ge + e^-$

$E_{thr.} = 0.233$ MeV

$\tau_{\frac{1}{2}}(^{71}Ge) = 11.4$ days

回収 : 〜20 days

SSM expectation

pp	69.7	← 54%
pep	2.8	
^7Be	34.2	← 27%
^8B	12.1	← ~9%
^{13}N	3.4	
^{15}O	5.5	
^{17}F	0.1	
total	128^{+9}_{-7} SNU	

GALLEX detector

Gran Sasso (3100 m.w.e.)

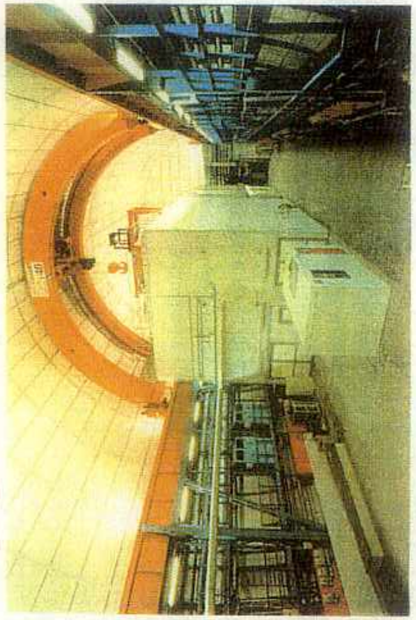

Fig. 9. GALLEX process building in hall A of the LNGS underground laboratory

are passed through scrubbers and continuously monitored for HCl.

A general overview of the technical equipment is given in Figure 11. The detector tanks are two 70 m³ vessels of vinyl ester resin reinforced with fiberglass, with an inner lining of 4 mm of PVDF; the outer dimensions are 3.9 m diameter and 7.8 m overall height. These dimensions just barely allow the tanks to be transported inside the tunnel (Fig. 12). The central tube to accommodate a calibration neutrino source exists only in tank A. The sparging system in tank A has been designed for a gas flow of 250 m³/h and is made up of four concentric pipe rings perforated at the bottom. The sparging system in tank B consists of only one pipe ring and has been designed for ten times lower gas throughputs. The

Fig. 12.: Transportation of a detector tank into the Gran Sasso tunnel

GALLEX 30.3 tons of Ga in $GaCl_3$ solution

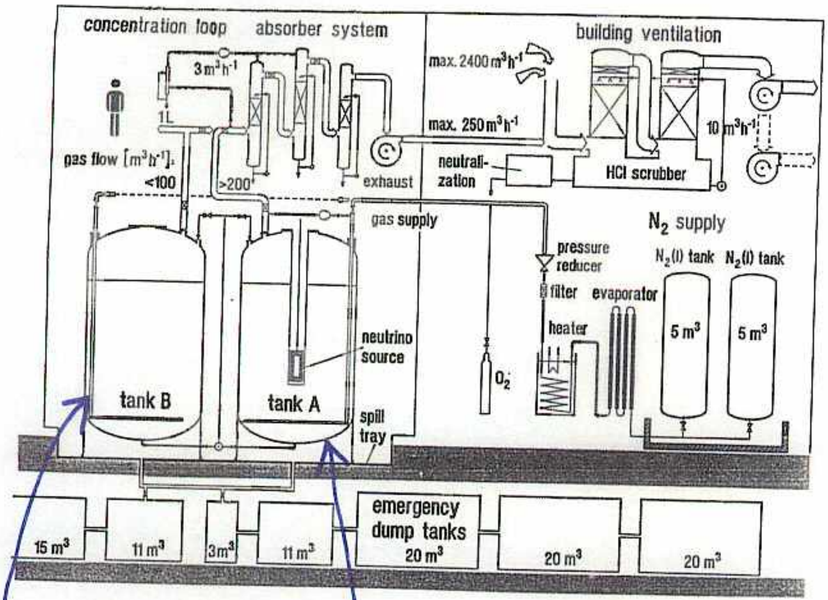

Fig. 11. Simplified flowsheet and survey of the technical equipment of the GALLEX facility.

Angew. Chem. Int. Ed. Engl. 1992, *31*, 1283–1297

GALLEX-I GALLEX-II

4. The $GaCl_3$ Detector Solution

4.1. Supply and Specification

Purchasing the very large quantity of 30.3 t of a highly concentrated $GaCl_3$ solution that met spe criteria was difficult to achieve in a relatively shor time. The $GaCl_3$ solution was prepared at a Rhôr facility in Salindres (France) and delivered to I tween December 1988 and May 1990; a total of of roughly 2.2 t each arrived in specially designe casks. All batches were carefully examined for we position, and critical impurities before they were the contents of the interim storage tanks in the ou imental hall. All of the batches met GALLEX a criteria. The chemical analyses performed in three laboratories yielded results which were in surprisi agreement. The specifications and the measured me

sol-36

SAGE detector ~7ton × 8 Ga reactors (metalic Ga)

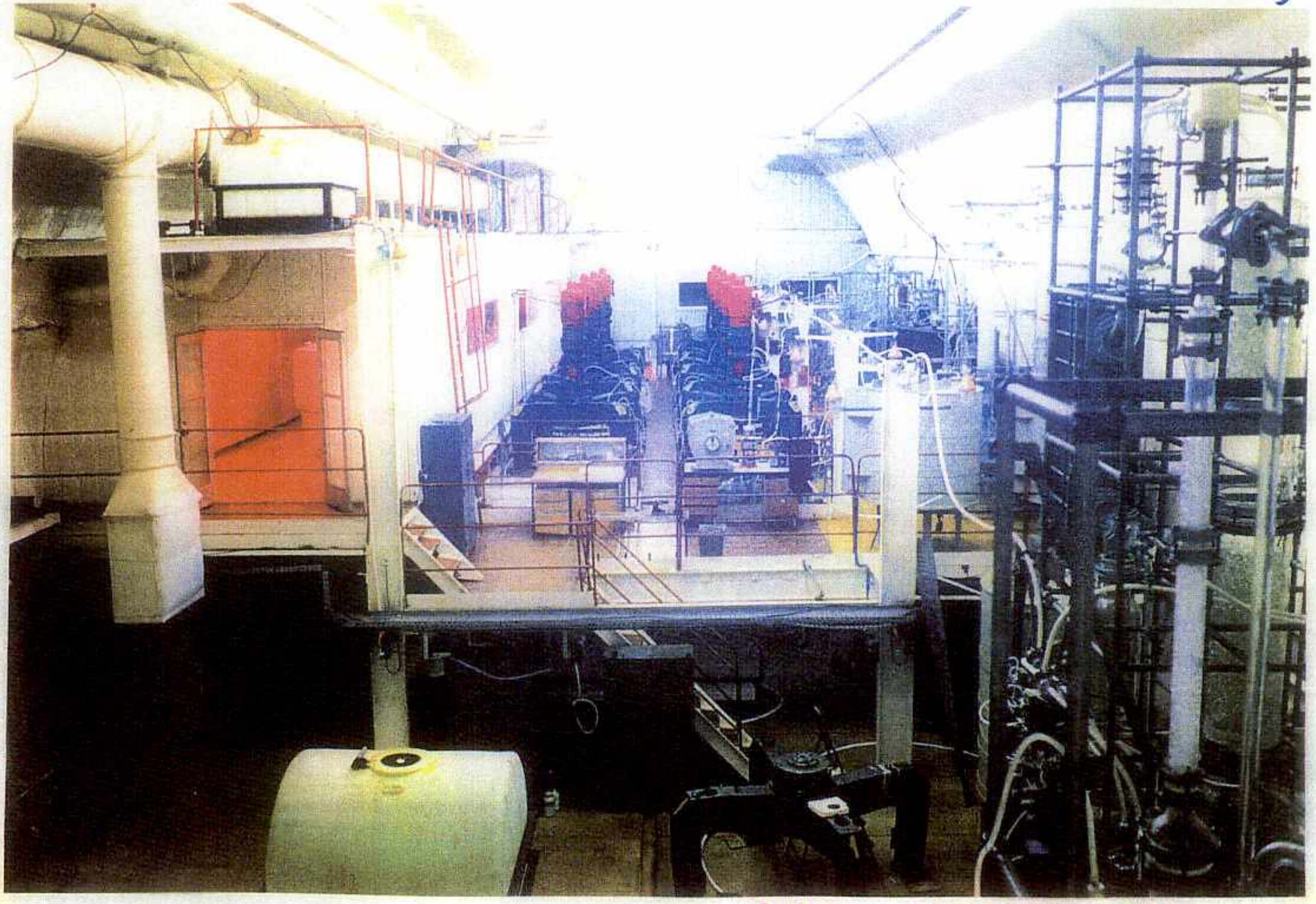

Baksan (4715 m.w.e)

SAGE Experiment Overview

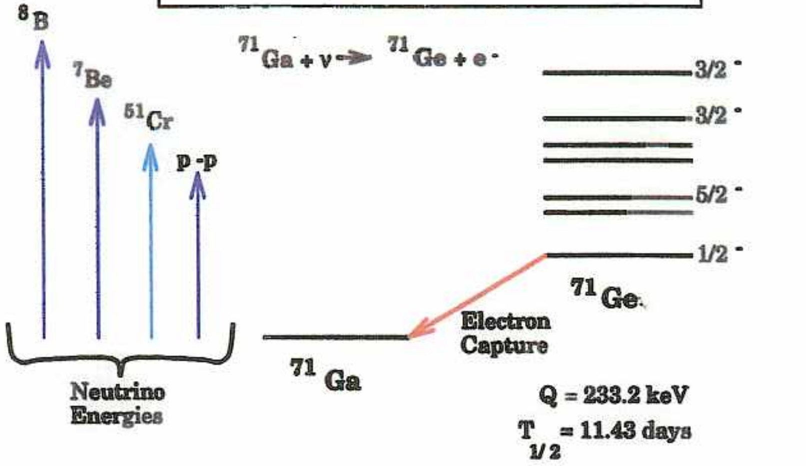

Q = 233.2 keV

$T_{1/2}$ = 11.43 days

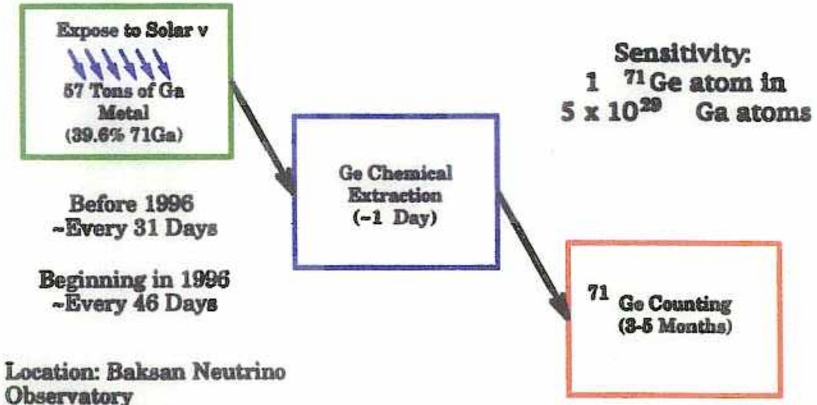

Sensitivity:
1 ^{71}Ge atom in
5 x 10^{29} Ga atoms

Before 1996
~Every 31 Days

Beginning in 1996
~Every 46 Days

Location: Baksan Neutrino Observatory
Mount Andyrchi
Caucasus Mountains,
Russia

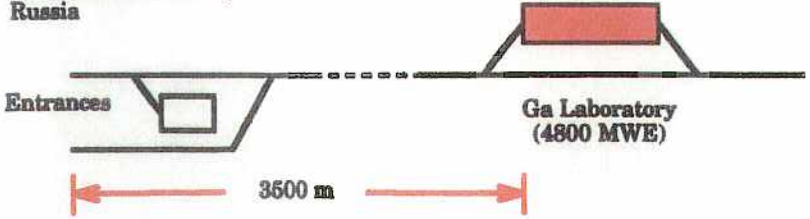

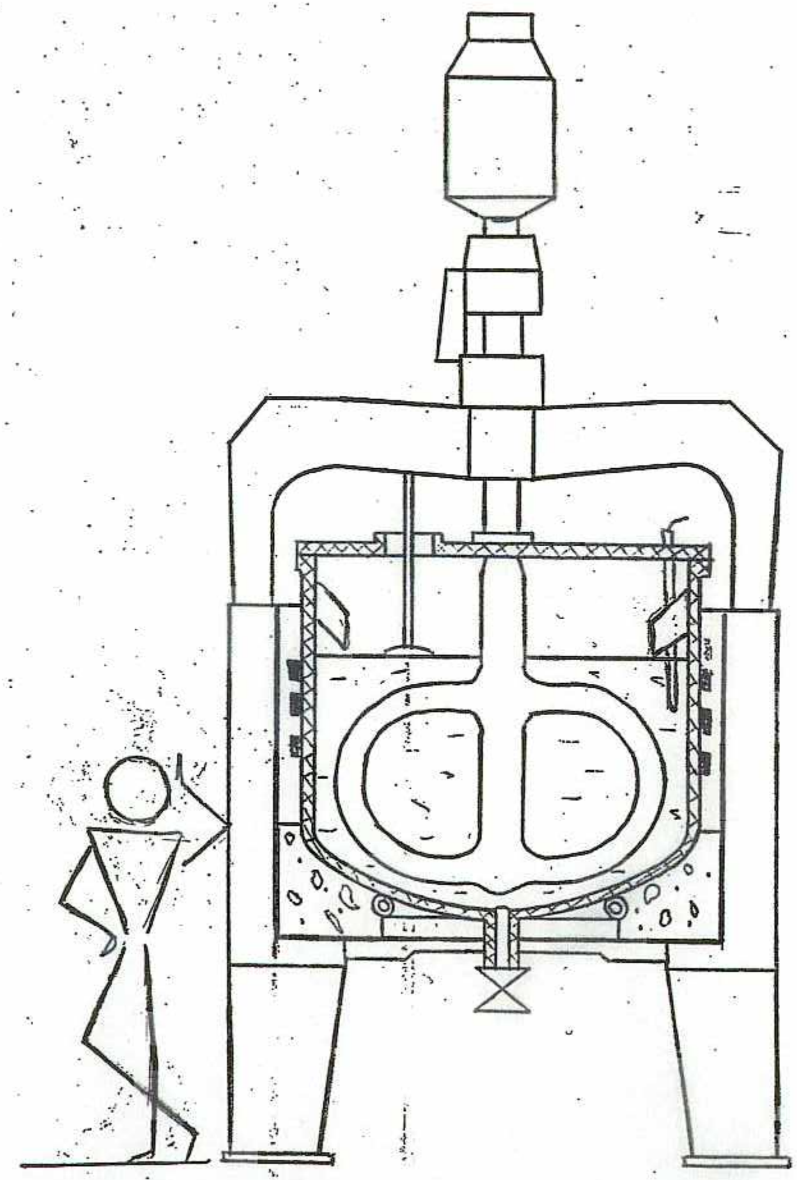

SAGE Extraction Chemistry
(SAGE III)

• Add Ge carrier (~700 μg Ge) to 50 tons of Ga	Metallic Ga is in liquid form
• Extract Ge with (H_2O_2+HCl) aqueous solution (double step procedure)	Oxidize < 0.1% Ga Dissolve Ge in HCl Check Ga concentration
• Separate Ge from the Ga solution by distillation	
• Sweep out $GeCl_4$ from the acidified condensate	
• Trap Ge in small amount (~1 l) of H_2O	Check Ge concentration by atomic absorption
• Extract $GeCl_4$ into CCl_4	
• Back extract $GeCl_4$ into 50 cm^3 low tritium H_2O	Check Ge concentration by atomic absorption
• Synthesize GeH_4 (germane gas)	
• Fill counter with GeH_4 (~20%) and Xe (~80%)	Check Ge concentration by volume measurement

---

GALLEX I

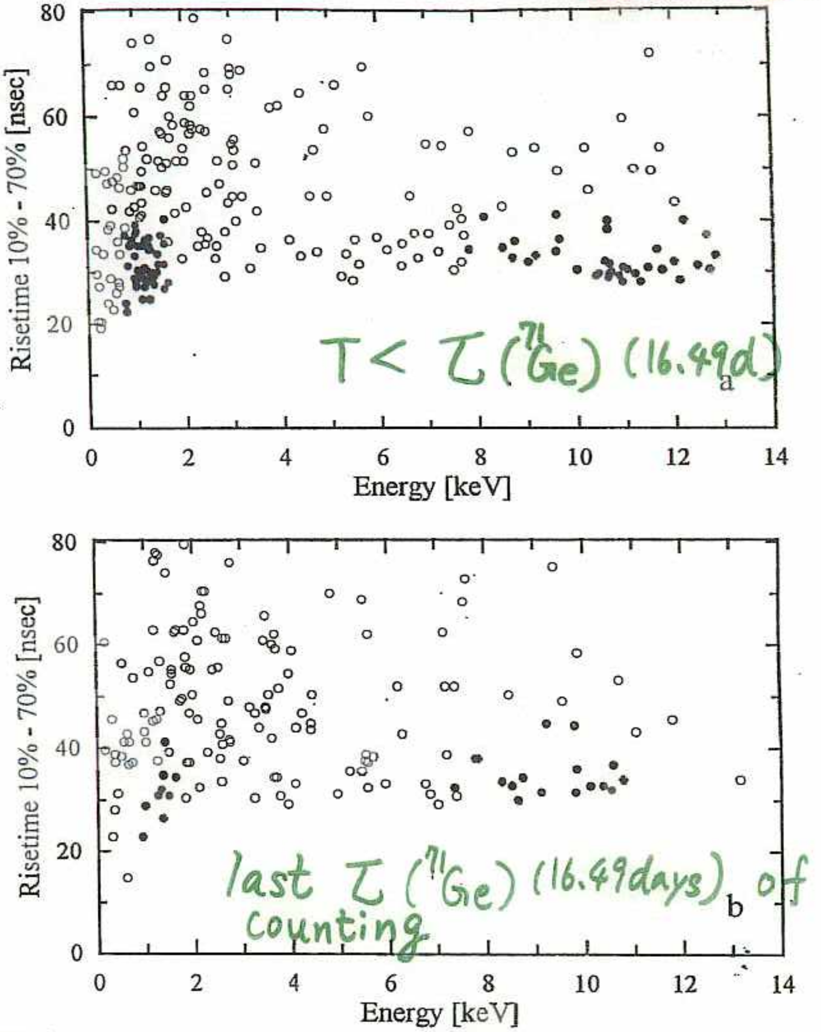

Figure 1

a Rise time versus energy for all unvetoed events observed in GALLEX I solar runs during the first 16.49 live days of counting, taken onwards from the start of counting of each run, respectively (16.49 days is one mean life of ^{71}Ge).

b As above, but for the last 16.49 live days of counting taken backwards from the end of counting for each run, respectively.

Solid dots mark counts within the L- or K- energy and rise time windows, open dots mark counts outside the windows. The population of solid dots defines no sharp window boundaries since counts come from many similar, yet not identical windows. Enrichments in L- and K- windows of (a) are apparent. No significant differences between (a) and (b)are seen outside the windows. This is quantified in table 2.

Calibration spectrum (SAGE)

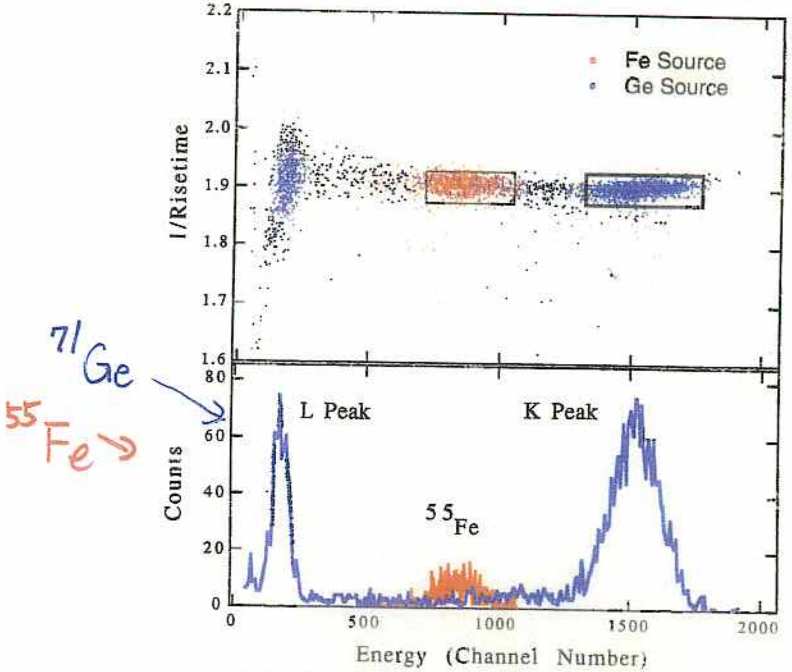

Fig. 1. Calibration spectrum using external ^{55}Fe and internal ^{71}Ge sources.

background channels in 60 t of Ga metal show that:

(i) As the laboratory is lined with low-background concrete, the external neutron background is low and has been measured to be $(4.56 \pm 1.62) \times 10^{-3}$ fast neutrons/cm^2/d [21]. The (n, p) cross sections on the Ga isotopes are small and this results in a production rate of less than 0.001 ^{71}Ge atoms/d.

(ii) The background from internal radioactivity is mainly determined by the concentrations of U, Th, and ^{226}Ra in the Ga. These concentrations have been measured [22] to be less than 3.0×10^{-10} gm U/gm Ga, 4.2×10^{-10} gm Th/gm Ga and less than 1.0×10^{-16} gm ^{226}Ra/gm Ga. These limits, combined with measured yields of ^{71}Ge from alpha particles [16], indicate that less than 0.015 ^{71}Ge atoms/d are produced.

(iii) The measured muon flux in the underground laboratory [23] is $(2.23 \pm 0.07) \times 10^{-9}$ muon/cm^2/s corresponding to a depth of 4715 mwe. With this flux the production rates of the Ge isotopes from cosmic ray muons have been calculated [24] to be 0.007 ^{71}Ge 0.020 ^{69}Ge, and 0.013 ^{68}Ge atoms/d.

Thus, the total background production rate of all Ge activities from all sources (if all sources were at the measured limits) has been determined to be less than 1.0% (i.e., 1.3 SNU) of the SSM production rate.

3. Extraction history

The experiment began operation in May 1988 when purification of the 30 t of Ga commenced. Long-lived

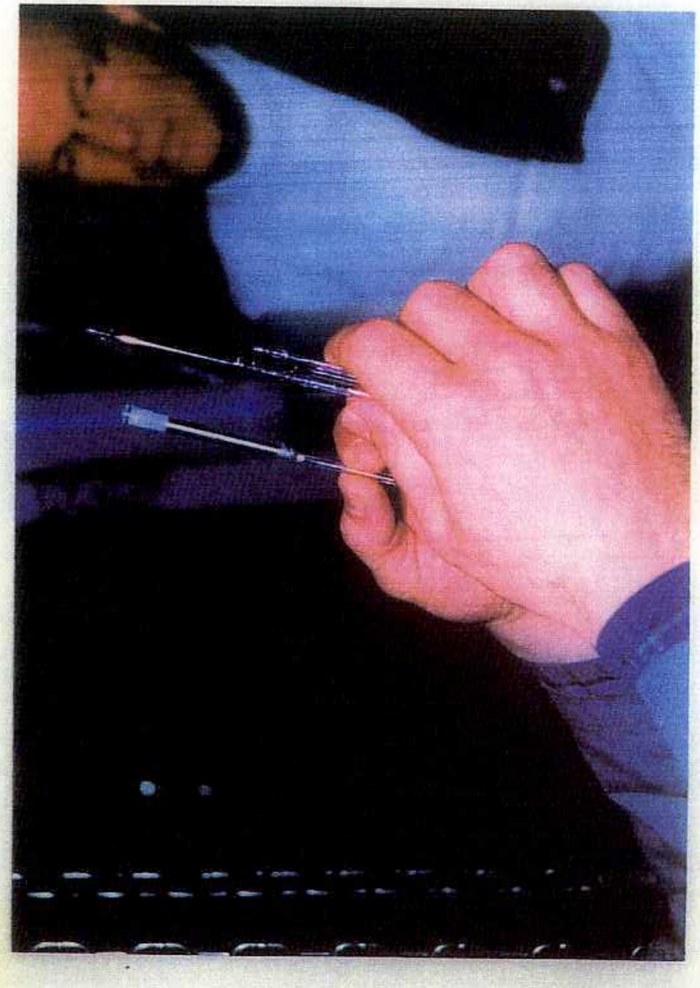

SAGE proportional counter

301 ÷ 45
5

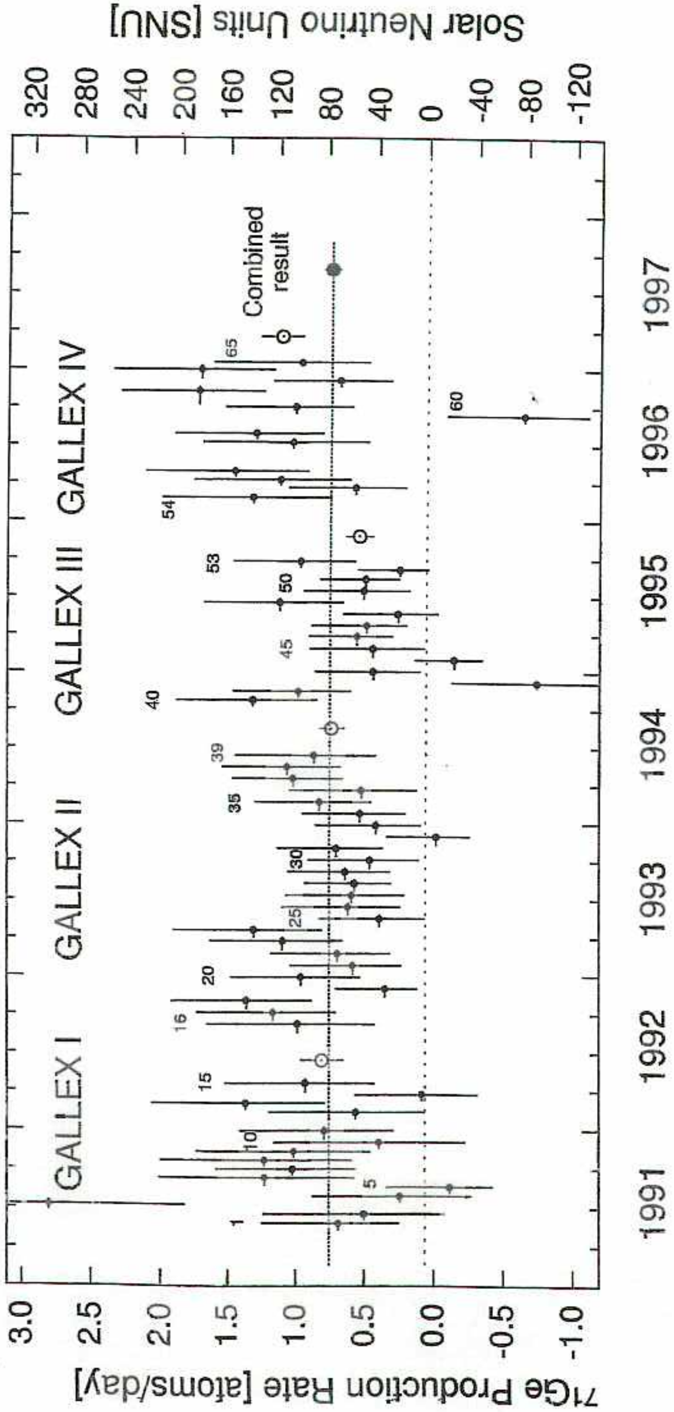

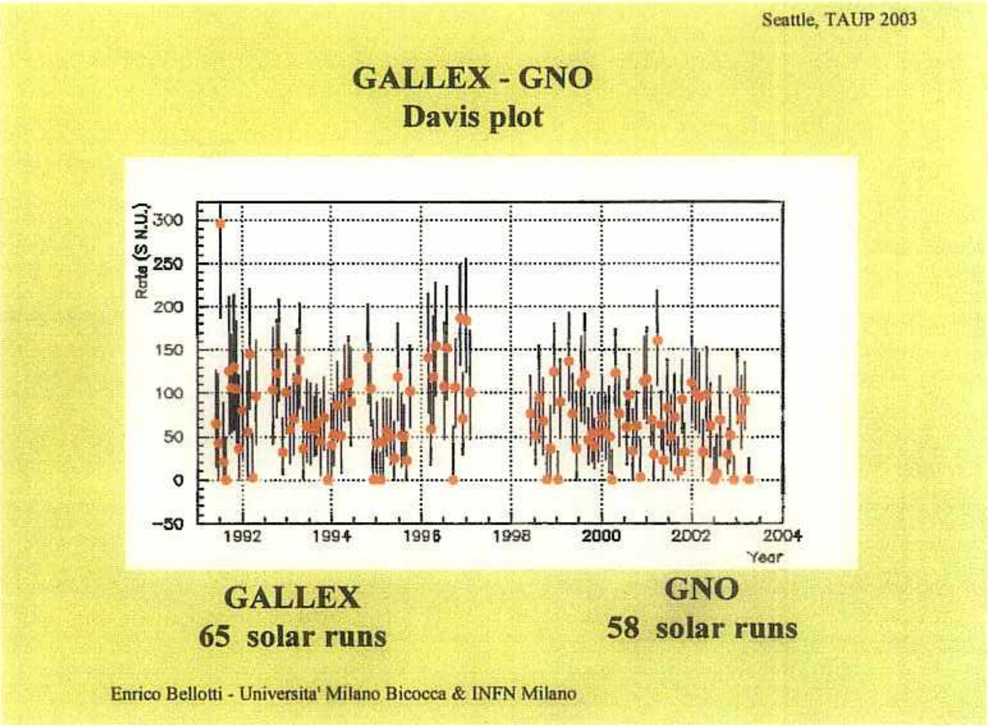
Seattle, TAUP 2003

GALLEX - GNO
Davis plot

GALLEX
65 solar runs

GNO
58 solar runs

Enrico Bellotti - Universita' Milano Bicocca & INFN Milano

115

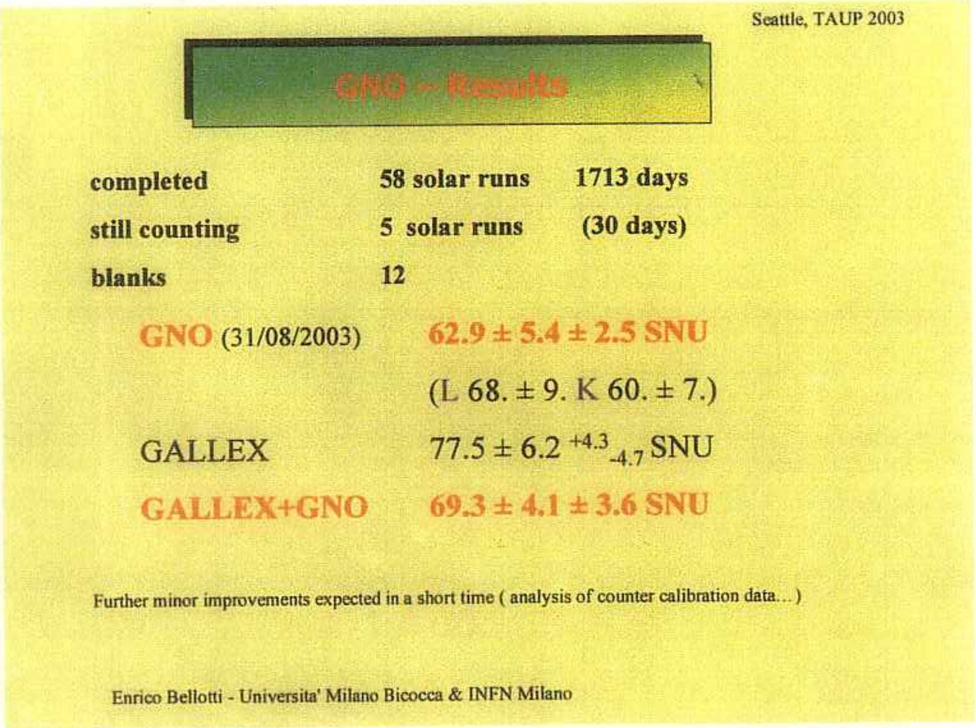

Seattle, TAUP 2003

GNO – Results

completed	**58 solar runs**	**1713 days**
still counting	**5 solar runs**	**(30 days)**
blanks	**12**	

GNO (31/08/2003) 62.9 ± 5.4 ± 2.5 SNU

(L 68. ± 9. K 60. ± 7.)

GALLEX 77.5 ± 6.2 $^{+4.3}_{-4.7}$ SNU

GALLEX+GNO 69.3 ± 4.1 ± 3.6 SNU

Further minor improvements expected in a short time (analysis of counter calibration data…)

Enrico Bellotti - Universita' Milano Bicocca & INFN Milano

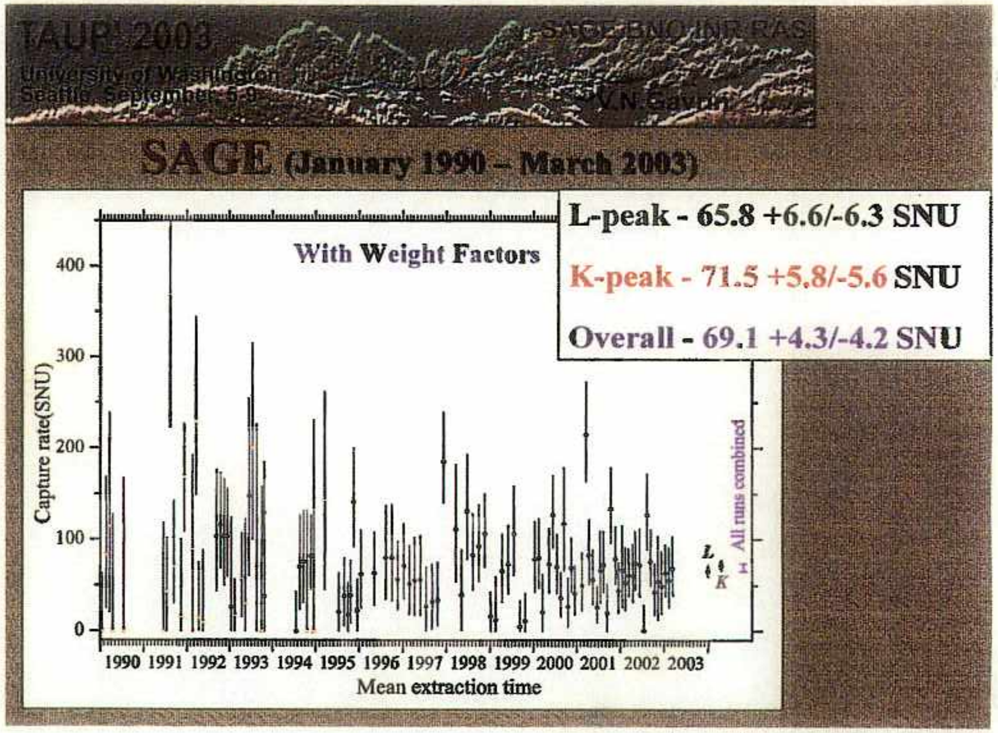

TAUP 2003
University of Washington
Seattle, September 5-9

SAGE BNO INR RAS

V.N.Gavrin

SAGE (January 1990 – March 2003)

L-peak - 65.8 +6.6/-6.3 SNU

K-peak - 71.5 +5.8/-5.6 SNU

Overall - 69.1 +4.3/-4.2 SNU

systematic error $^{+3.8}_{-3.4}$ SNU

⇒ overall

$69.1 \pm^{5.7}_{5.4}$ SNU

20)

239

$$^{50}\mathrm{Cr}\,(n,\gamma)\,^{51}\mathrm{Cr} \xrightarrow[27.7\ \mathrm{d}]{\mathrm{E.C.}} {}^{51}\mathrm{V} + \nu$$

(746 keV)

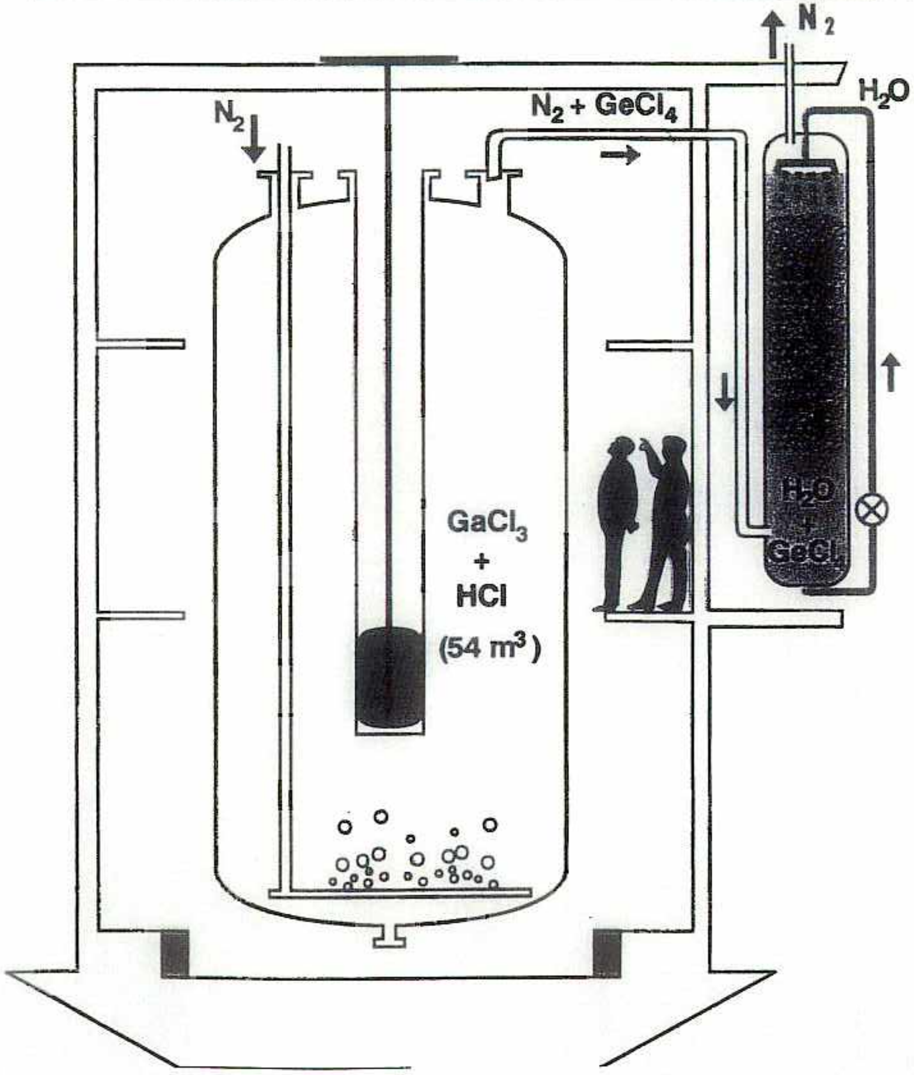

^{51}Cr ニュートリノ線源

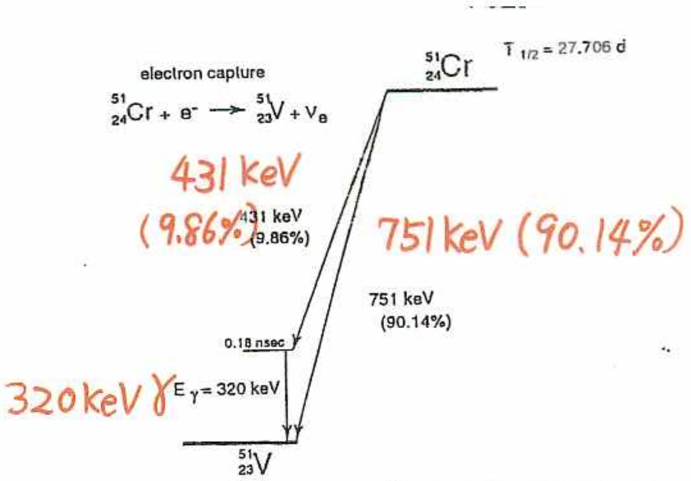

Fig. 1. Characteristics of the decay of ^{51}Cr. The "751 keV" line combines the 746 and 751 keV lines and the "431 keV" line combines the 426 and 431 keV lines.

Enriched Cr ソース

	σ_{therm} [barn]	$i_{natural}$ %	i_{Gallex} %	
^{50}Cr	15.9	4.35	38.6	$+n \rightarrow {}^{51}$Cr
^{51}Cr	30	-	-	burn-up < 1%
^{52}Cr	0.76	83.8	60.7	
^{53}Cr	18.2	9.5	0.7	
^{54}Cr	0.36	2.35	<0.3	

GALLEX : Calibration by neutrino

Cr Source Time Table

^{51}Cr : 746 keV ν

- **irradiation of the source at the Siloé reactor (Grenoble)**
  27. May - 20. June 1994
- **exposure of the GALLEX target to the source at the LNGS**
  23. June - 19. October 1994
- **first preliminary result expected in November 1994**
- **end of counting planned for April 1995**
- **final result expected for early summer 1995**

The Chromium Source

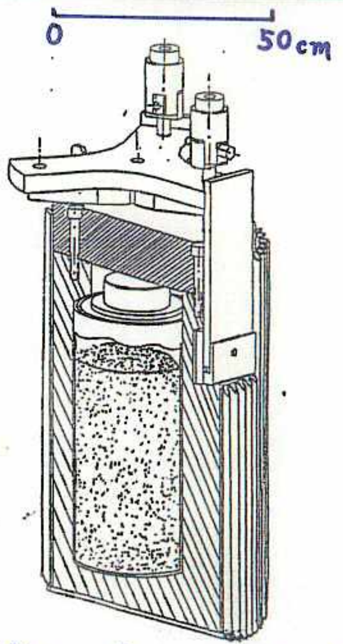

6.2×10^{16} Bq
(~2 MCi)

~200 ^{71}Ge decays

36kg of enriched Cr

501-51

GALLEX ^{51}Cr ν- SOURCES

Source strengths:

1: 1.71 ± $^{.03}_{.04}$ MCi; 2: 1.87 ± $^{.09}_{.06}$ MCi

Measured rate:

$$R = \frac{\text{OBSERVED}}{\text{EXPECTED}} = \mathbf{0.93 \pm 0.08}$$

[1.01 ± 0.10 and 0.84 ± 0.11]

Phys.Lett B 420 (1998) 114

with new value for solar "background"
after GALLEX IV (=77.5 SNU):

$$R = \mathbf{0.91 \pm 0.08}$$

EXPERIMENTAL PROOF OF THE RADIOCHEMICAL METHOD

Solar ν measurement by Kamiokande and SK.

$\nu e^- \rightarrow \nu e^-$ scattering.

$E_{thr.} \cong 5\,\mathrm{MeV}$ ⇒ only ^8B solar ν measurement

Advantage:

- real time experiment
- 方向性.
- Energy information

$\nu_e e^- \rightarrow \nu_e e^-$

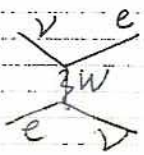

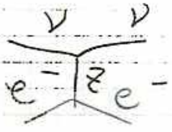

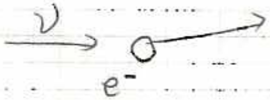

$$\frac{d\sigma(E)}{dT} = \frac{2G_F^2 m_e^2}{\pi\hbar^4}\left[g_L^2 + g_R^2\left(1 - T/E_\nu\right)^2 - (g_L g_R)\left(\frac{T m_e}{E_\nu^2}\right)\right]$$

T; kinetic energy of electron

$$g_L = (\pm\tfrac{1}{2} + \underbrace{\sin^2\theta_W}_{0.23}) \;,\; g_R = \sin^2\theta_W$$

$+$: $\nu_e e^-$

$-$: $\nu_\mu e^-$

A Typical low-energy event

- Timing information — vertex position
- Ring pattern — direction
- number of hit PMTs — energy

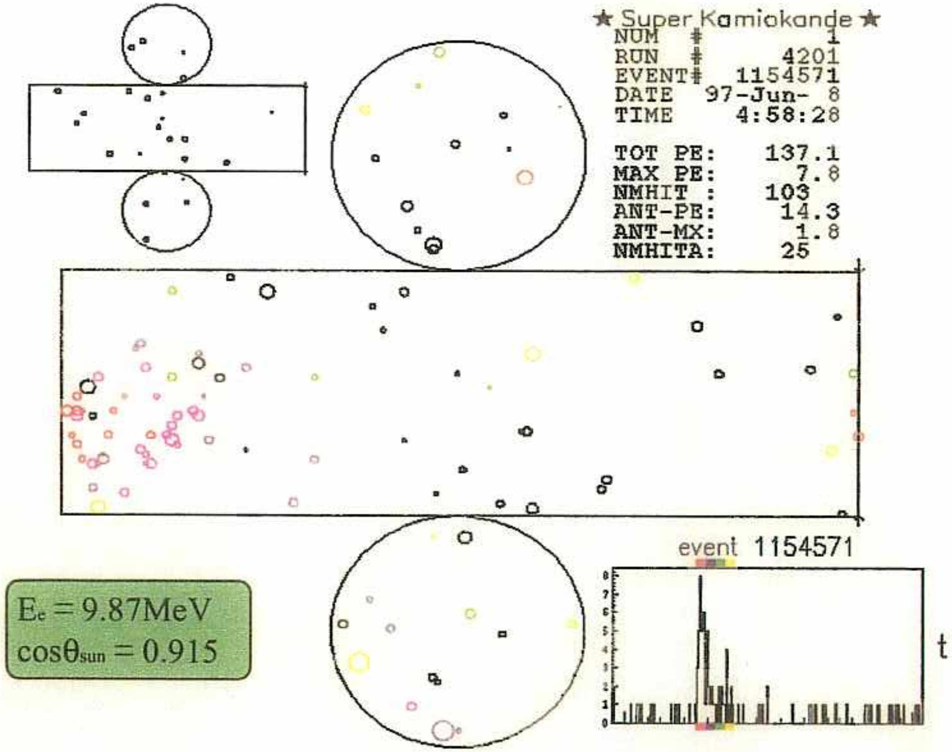

```
★ Super Kamiokande ★
NUM   #          1
RUN   #       4201
EVENT#     1154571
DATE    97-Jun- 8
TIME       4:58:28

TOT PE:      137.1
MAX PE:        7.8
NMHIT :      103
ANT-PE:       14.3
ANT-MX:        1.8
NMHITA:       25
```

$E_e = 9.87\,\mathrm{MeV}$
$\cos\theta_{sun} = 0.915$

Detect solar neutrinos by

$\nu + e \rightarrow \nu + e$ scattering

$\xrightarrow{\nu}$ -e^- maximum erergy

$$y_{max} = \frac{T}{E_\nu} = \frac{2E_\nu}{2E_\nu + m_e}$$

$m_e \approx 0$としてみると

$$\sigma_{total\ \nu_e + e^-} = 0.95 \times 10^{-44}\, E_\nu\,(MeV)$$

$$\sigma_{total\ \nu_\mu + e^-} = 0.16 \times 10^{-44}\, E_\nu\,(MeV)$$

$\sim \frac{1}{6}$ of $\sigma_{\nu_e + e^-}$

$$\cos\theta = \frac{y\left(1 + \frac{m_e}{E_\nu}\right)}{\sqrt{y^2 + 2\frac{m_e}{E_\nu}y}}$$

$\theta \lesssim 8°$ で小さい。

$g_L^2 = 0.53, \quad g_R^2 = 0.05$

(V-A) classical V-A での $\nu_e e^-$ scattering

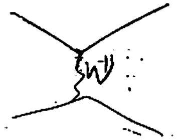

only

ν_e

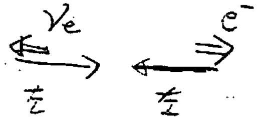

total angular momentum = 0

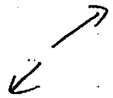

Go to any angle

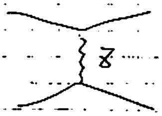

により $(1-\gamma_5)$ でない部分が入る。

$$-M(\nu_\mu e) = \left[\frac{-ig}{4\cos\theta_W}\, \overline{u_{\nu_2}}\, \gamma^\lambda (1-\gamma_5) u_{\nu_1}\right] \frac{g_{\lambda\sigma} - q_\lambda q_\sigma / m_Z^2}{q^2 - m_Z^2}$$

$$\times \left[\frac{-ig}{2\cos\theta_W}\, \overline{u_{e_2}}\, \gamma_\sigma (g_V - g_A \gamma_5)\, u_{e_1}\right]$$

$$g_V = 2\sin^2\theta_W - \frac{1}{2}$$

$$g_A = -\frac{1}{2}$$

Any way, $g_L^2 = 0.53$, $g_R^2 = 0.05$ なので、

y分布 $\left(\frac{T}{E_\nu}\right)$ は ほぼ flat。

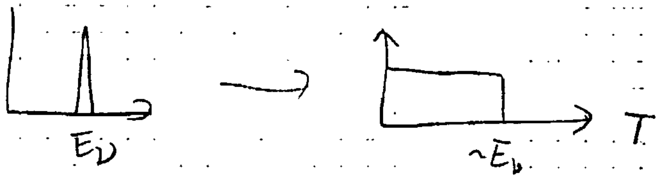

νe scattering kinematics

νe →νe scattering

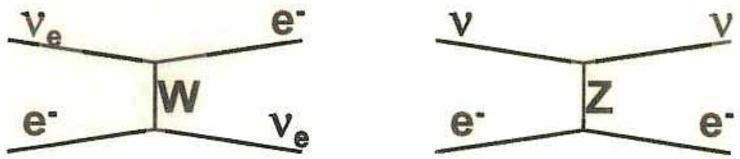

$$\frac{d\sigma}{dT} = \frac{2G_F^2 m_e}{\pi}\left[g_L^2 + g_R^2(1-T/E_\nu)^2 - g_L g_R m_e T/E_\nu^2\right]$$

T: kinetic energy of recoil electron
g_L= (±1/2 + $\sin^2\theta_W$) for ν_e and $\nu_{\mu(\tau)}$
g_R= $\sin^2\theta_W$

e.g. dσ/d*T* for 10 MeV neutrino

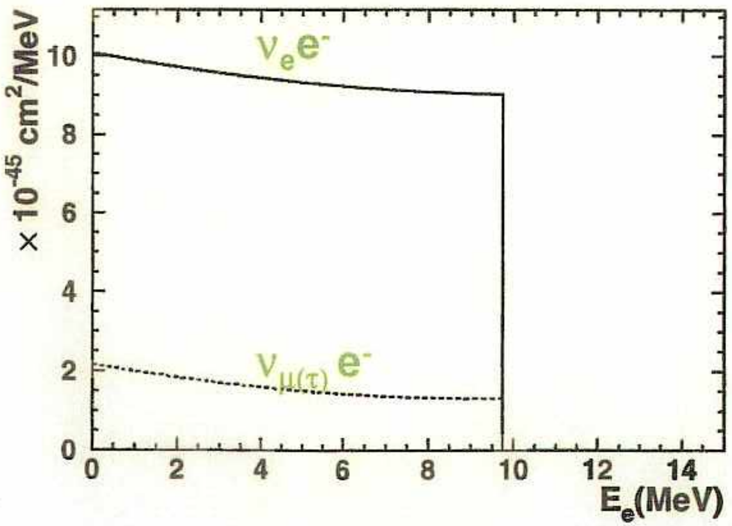

νe scattering kinematics

^{8}B solar neutrino spectrum

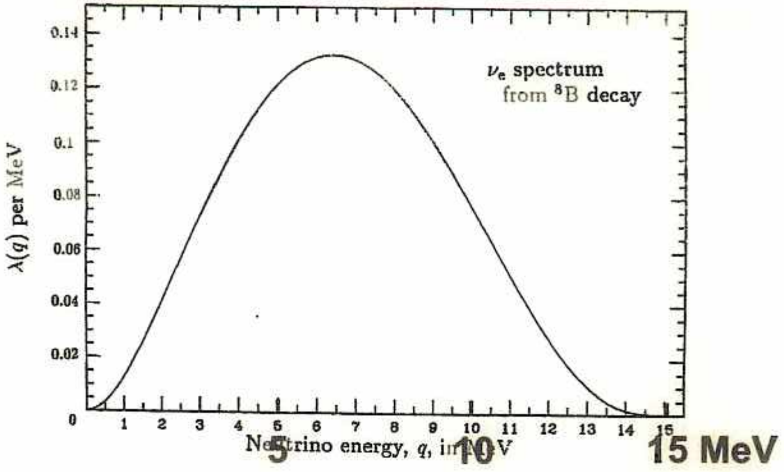

Total cross section for ^{8}B neutrinos

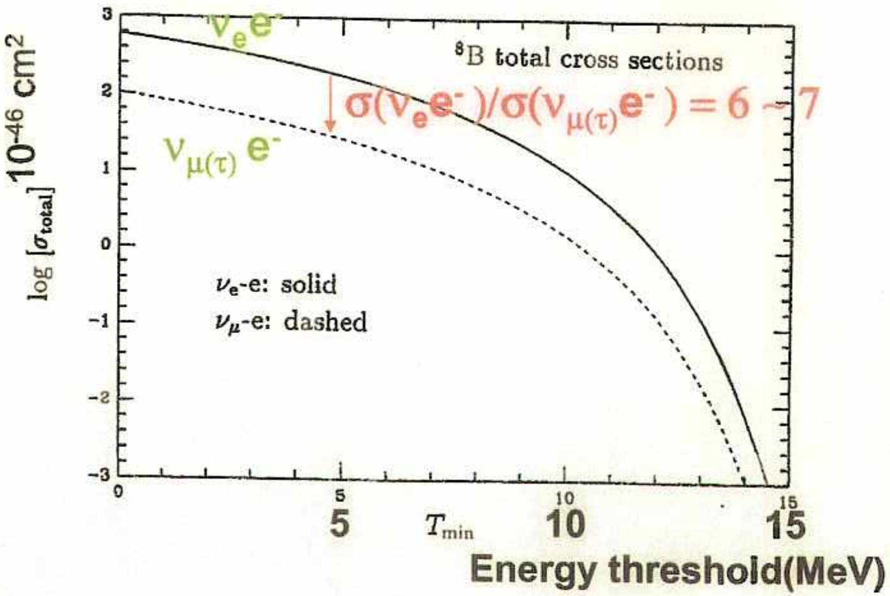

Recoil electron energy spectrum

SSM prediction

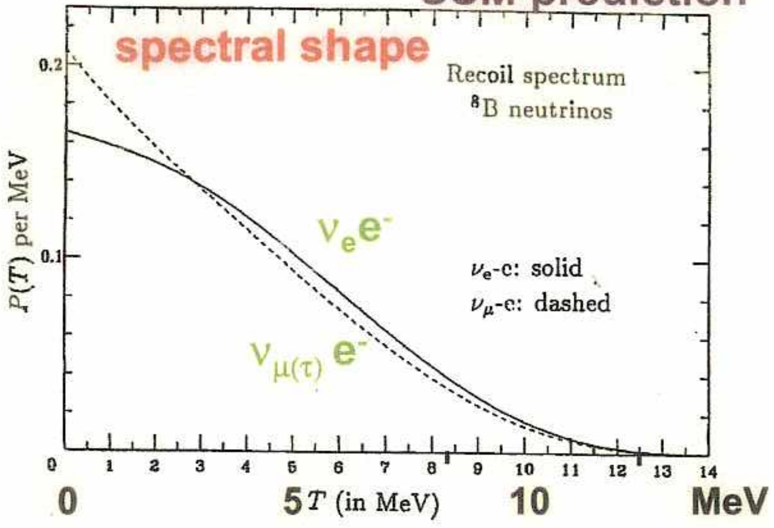

となる。

SKの結果 flux : $(2.35 \pm 0.02 \pm 0.08] \times 10^{6}/\mathrm{cm}^2/\mathrm{s}$

SSM : $5.05 \times 10^{6}\ /\mathrm{cm}^2/\mathrm{sec}.$

$$\frac{\text{Data}}{\text{SSM}} = 0.465 \pm 0.005 \pm^{0.016}_{0.015}$$

約半分 //

^{37}Cl vs. SK

実験値 : 2.56 SNU

pp 0.0

pep 0.22

^{7}Be 1.15

^{8}B 5.76 → SKの結果から 0.465倍すると 2.7 SNU

^{13}N 0.09

^{15}O 0.33

^{17}F 0.0

他からのcontributionは0に近い。

^{7}Beとかは0！

7.6 SNU

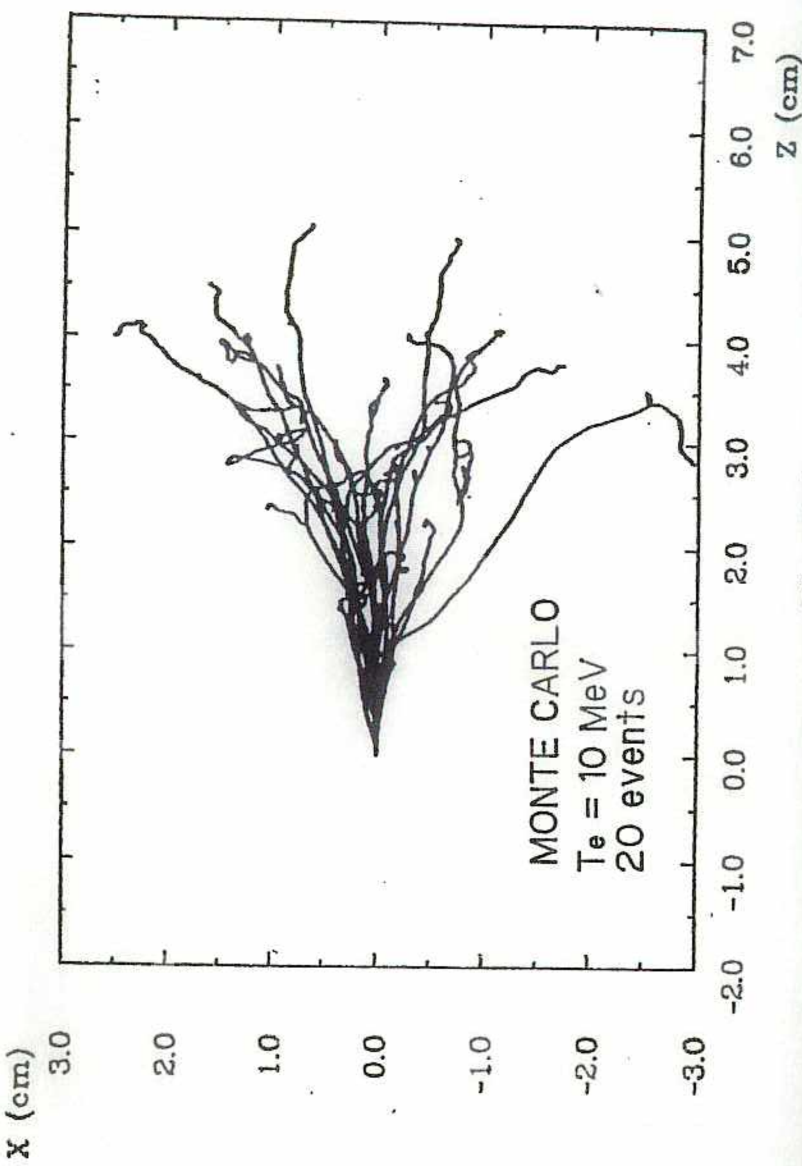

Fig. 5.6

The Sun by Neutrinograph

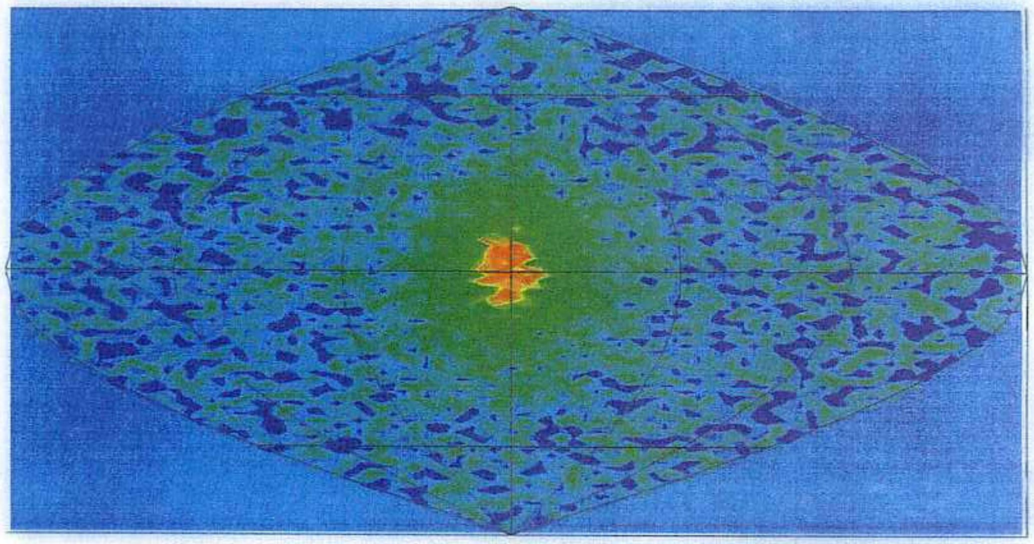

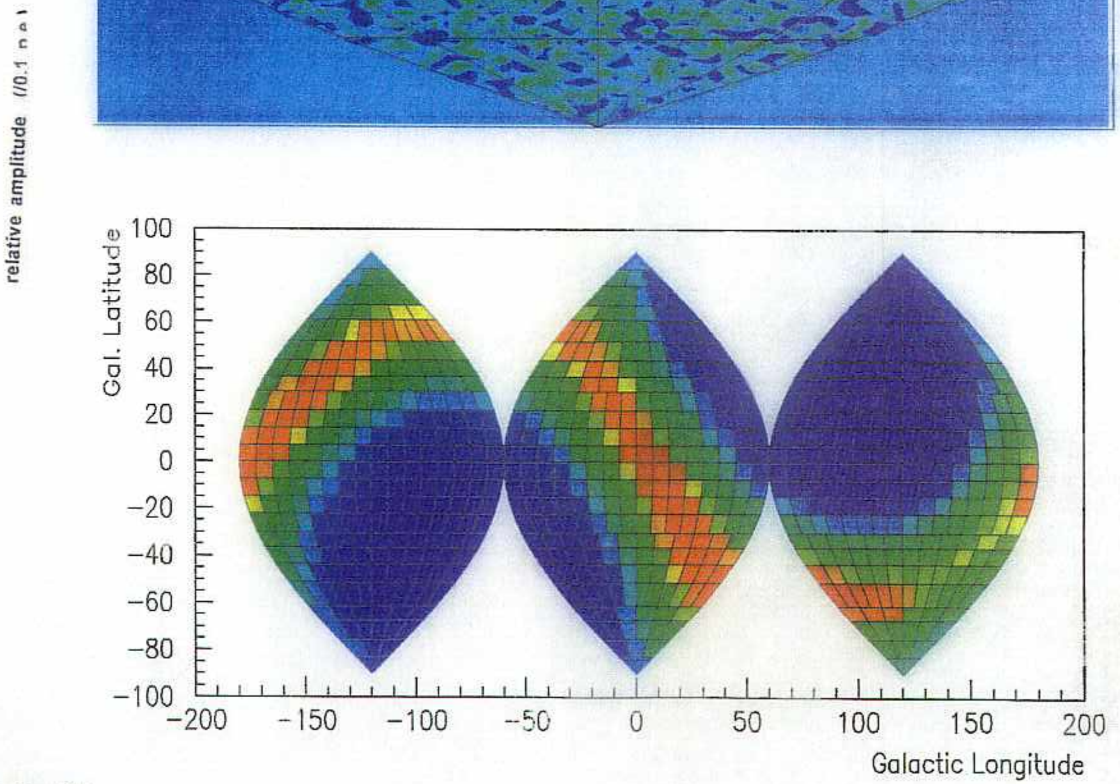

Direction to the Sun

May 31, 1996 – July 13, 2001
1496 days

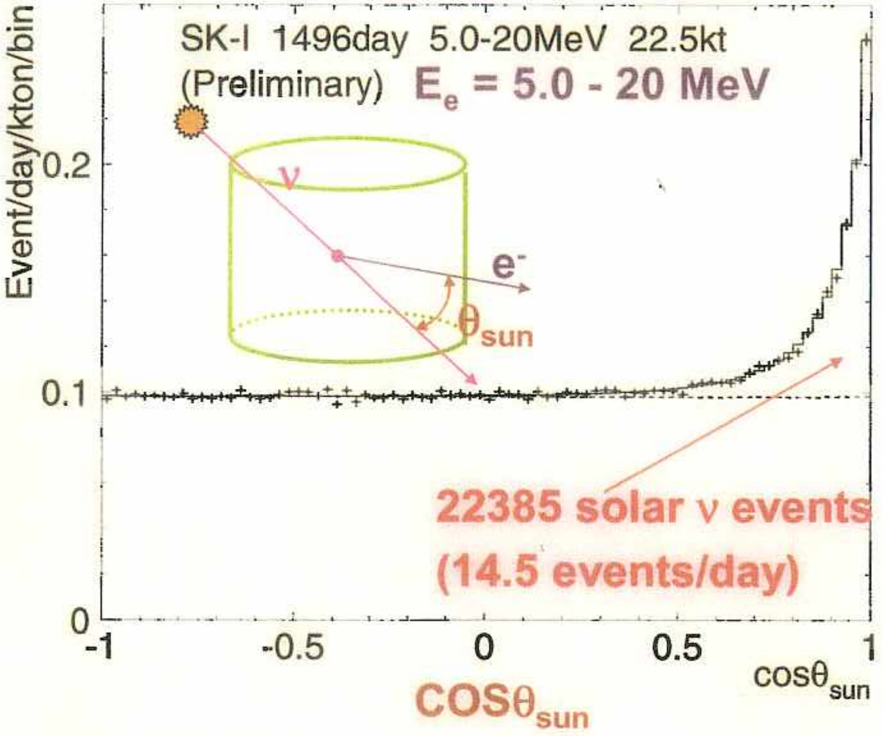

22385 solar ν events
(14.5 events/day)

^{8}B flux : $2.35 \pm 0.02 \pm 0.08$ [x 10^6 /cm^2/sec]

$$\frac{\text{Data}}{\text{SSM(BP2000)}} = 0.465 \pm 0.005 \,{}^{+0.016}_{-0.015}$$

(BP2000: 5.05 x 10^6 /cm^2/sec)

(using Ortiz et al. spectrum shape(nucl-ex/0003006))

Time Dependence of SK Rate

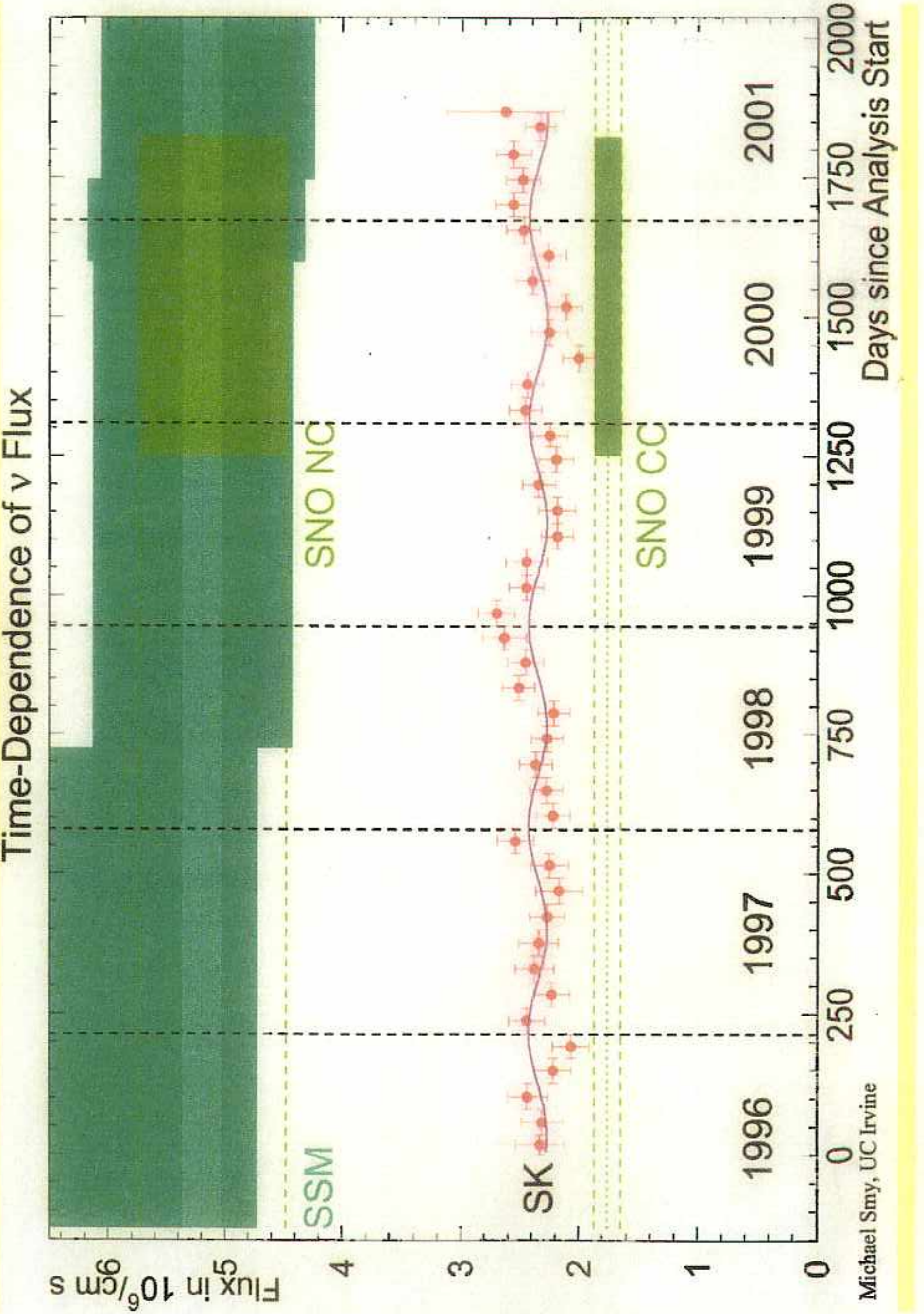

Yearly Variation of SK Rate

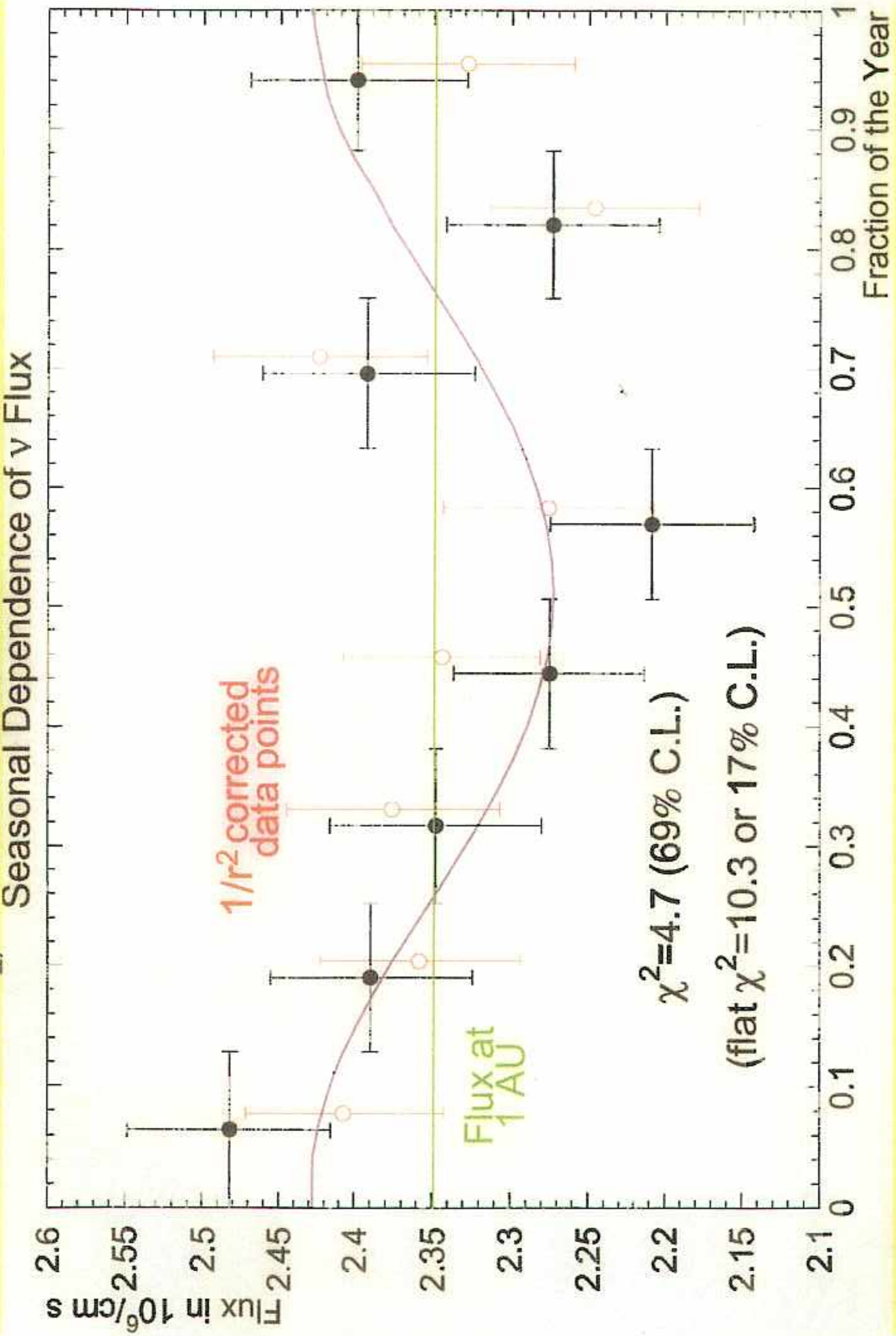

Michael Smy, UC Irvine

LINAC calibration

Precise calibration of absolute energy scale, energy resolution, and angular resolution using electron LINAC.

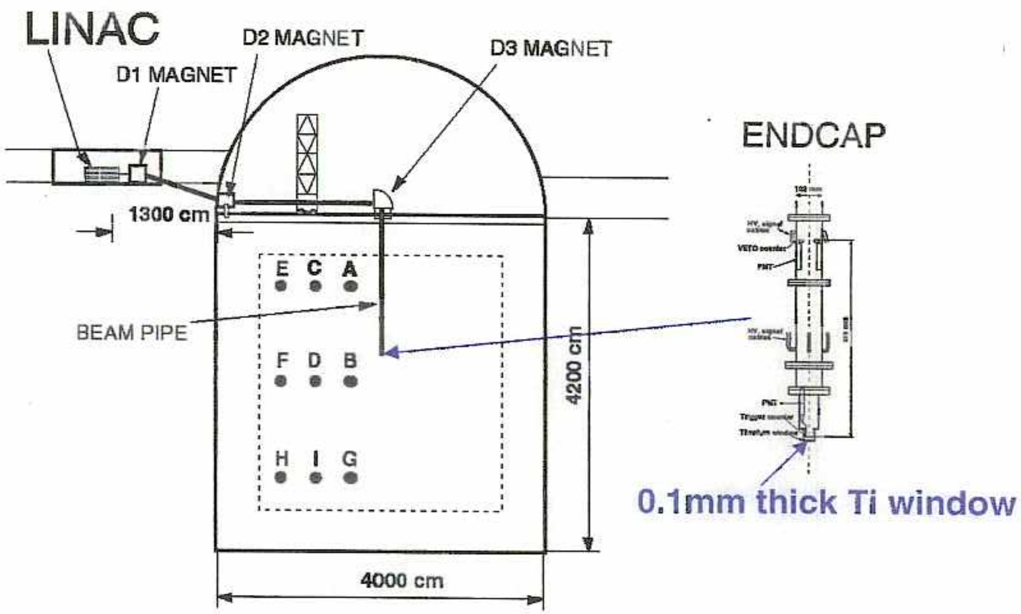

- Beam energy: 5 ~ 16 MeV/c
- Beam energy spread: < 0.5 %
- Data taking at 9 typical positions in SK
- Beam energy determined by Ge detector (<20 keV accuracy)

Energy spectrum of LINAC calibration

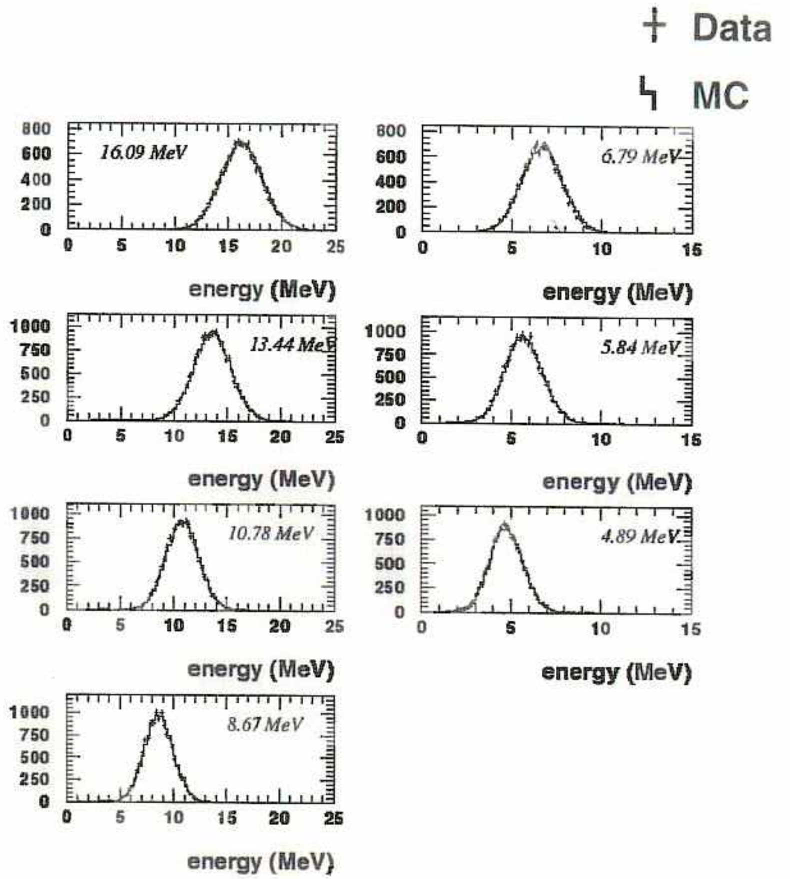

Energy scale and resolution are precisely calibrated.

Systematic error of the absolute energy scale is 0.64 %.

Error in energy scale or resolution ?

LINAC calibration

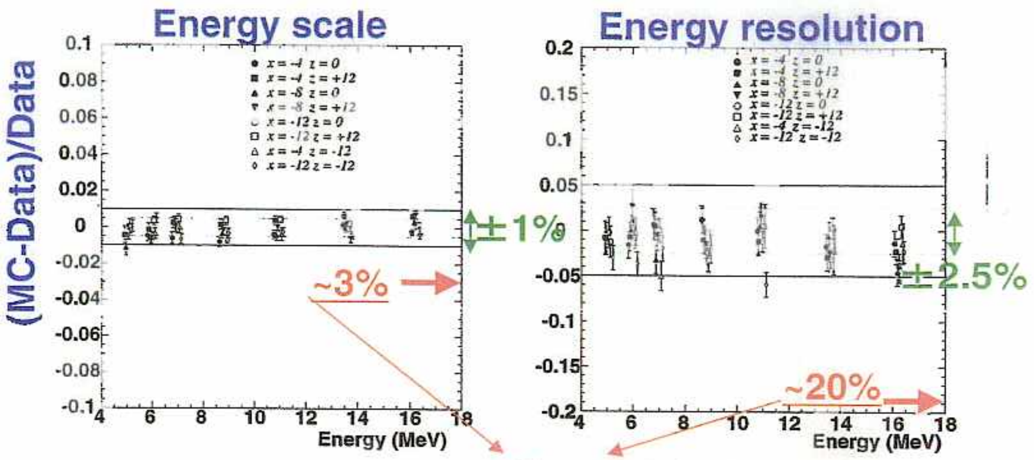

To explain the raise

Resolution tail ?

LINAC 10.78 MeV data

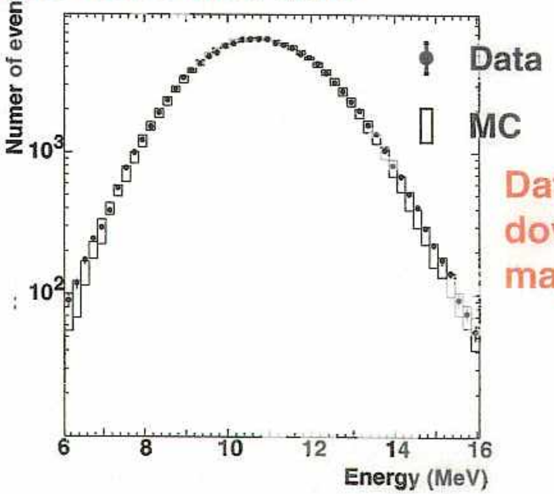

Data and MC agree down to 2 orders of magnitudes

The raise is not due to wrong calibration.

^{16}N calibration

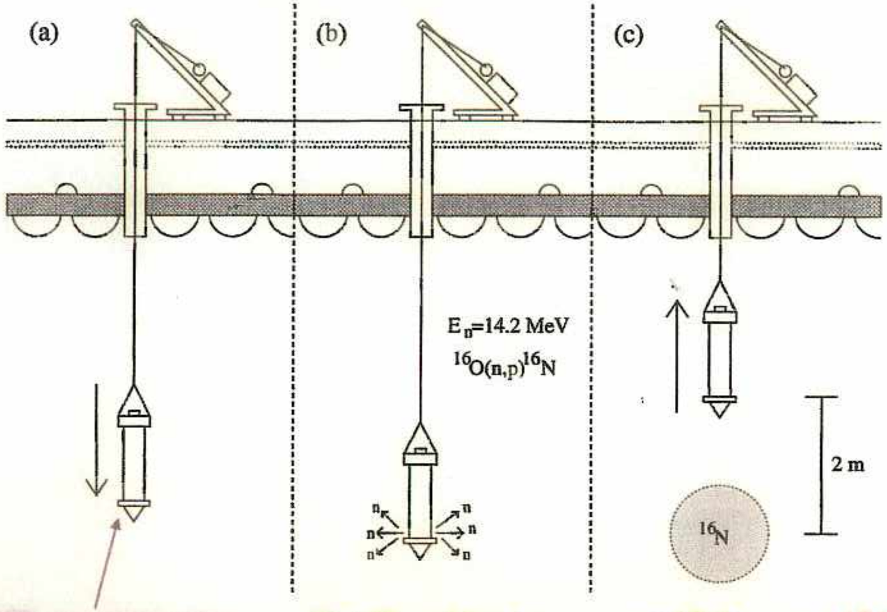

DT generator

D+T→He+n (14.2 MeV)

n+^{16}O→p+^{16}N

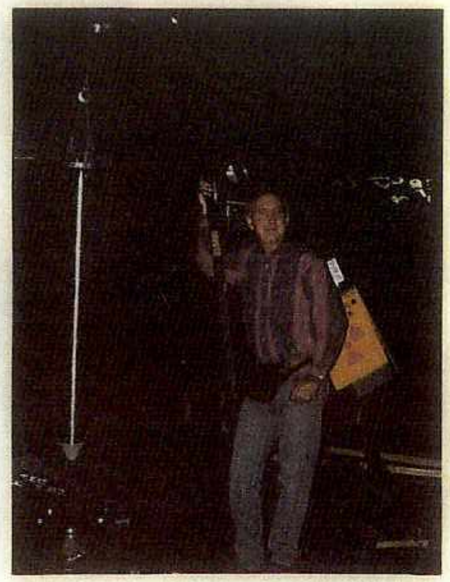

- ~10^6 n /pulse
- ~1% of n creates ^{16}N
- ^{16}N decay is precisely known.
  - 66.2% 6.129MeVγ + 4.29MeVβ
  - 28.0% 10.419 MeV β, and etc.
- Data taken at various positions in the detector.
- Uniform direction complementary to LINAC calibration.

---

^{16}N calibration data

Event time after fire

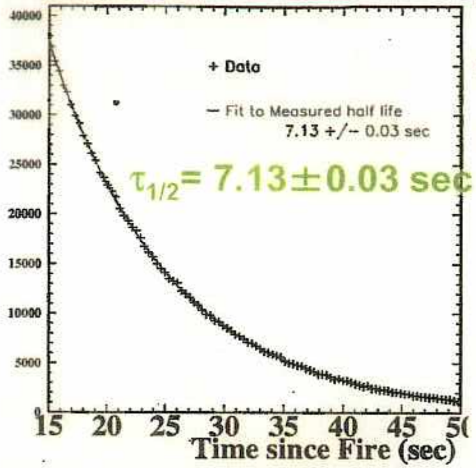

$\tau_{1/2}$= 7.13±0.03 sec

Energy spectrum

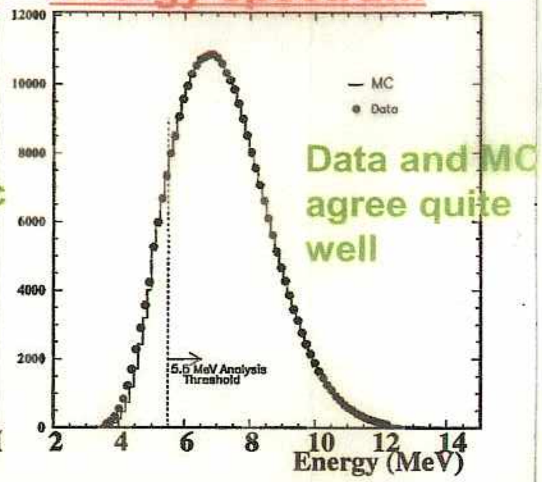

Data and MC agree quite well

Direction dependence of energy scale

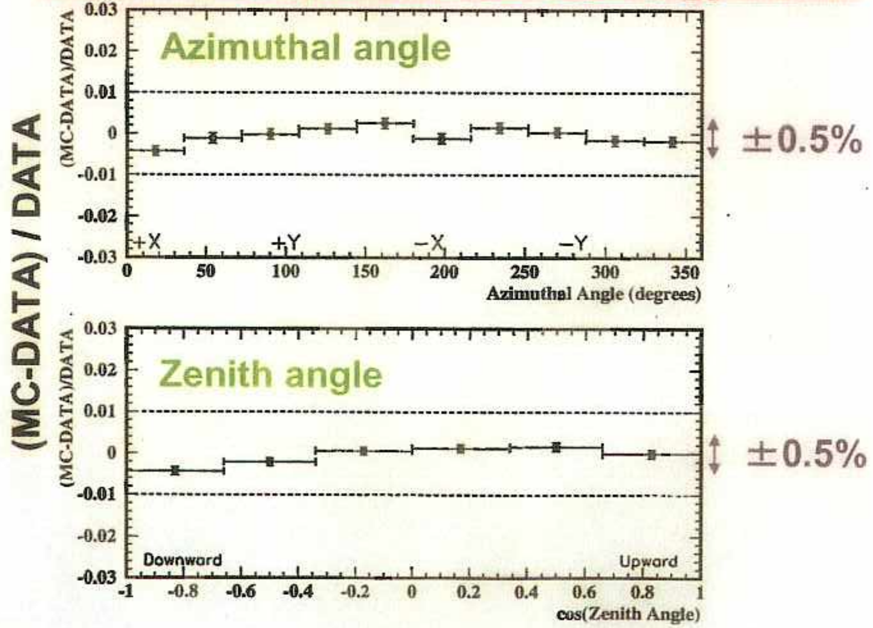

Azimuthal angle ±0.5%

Zenith angle ±0.5%

⑧

Solar ν

neutrino oscillation

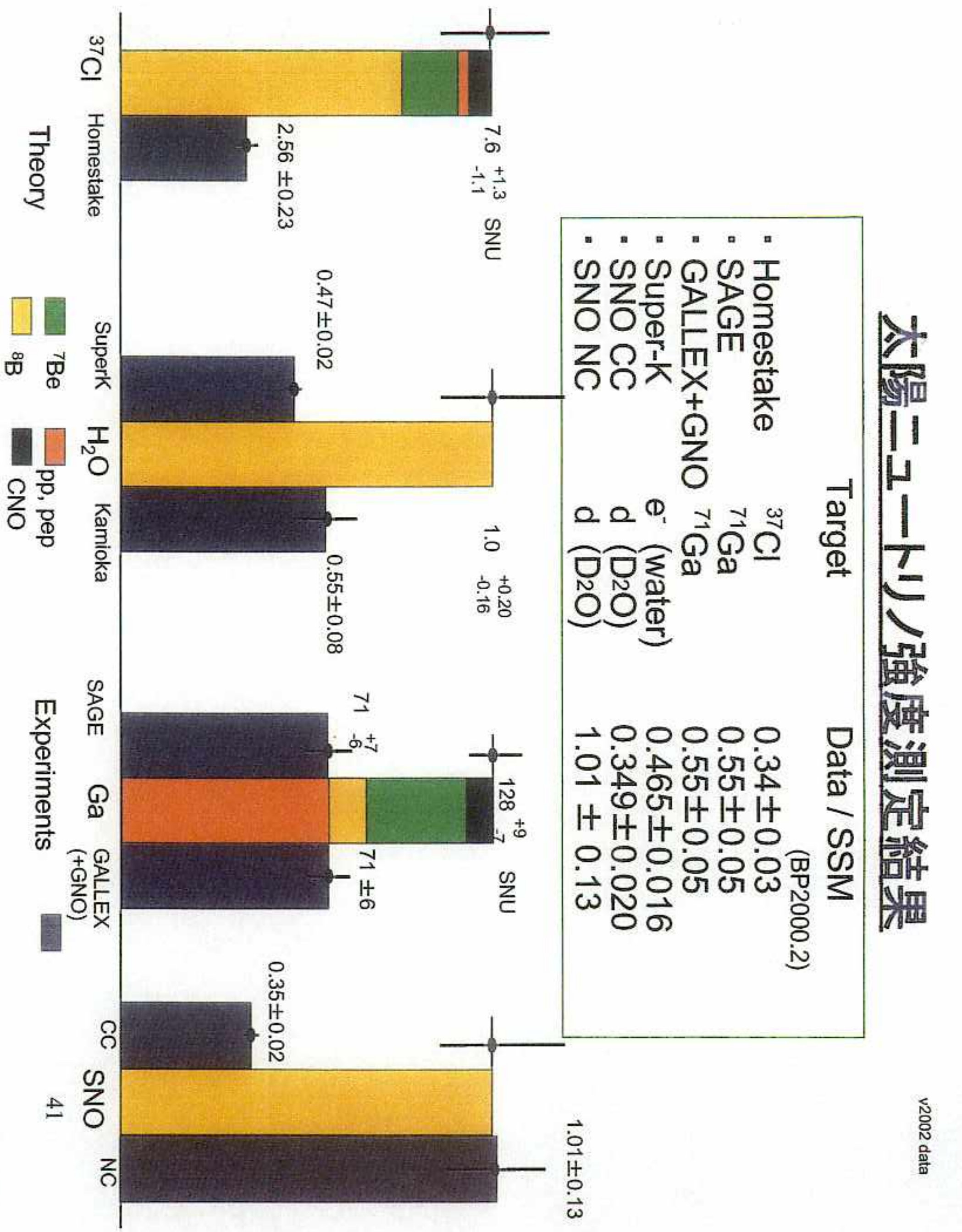

太陽ニュートリノ強度測定結果

	Target	Data / SSM (BP2000.2)
Homestake	^{37}Cl	0.34±0.03
SAGE	^{71}Ga	0.55±0.05
GALLEX+GNO	^{71}Ga	0.55±0.05
Super-K	e^- (water)	0.465±0.016
SNO CC	d (D_2O)	0.349±0.020
SNO NC	d (D_2O)	1.01 ± 0.13

Solar Neutrinos

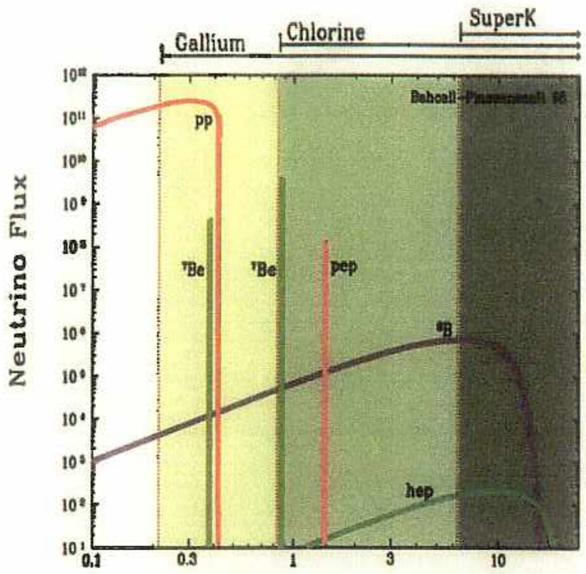

Neutrino Energy (MeV) http://www.sns.ias.edu/~jnb/

pp-chain

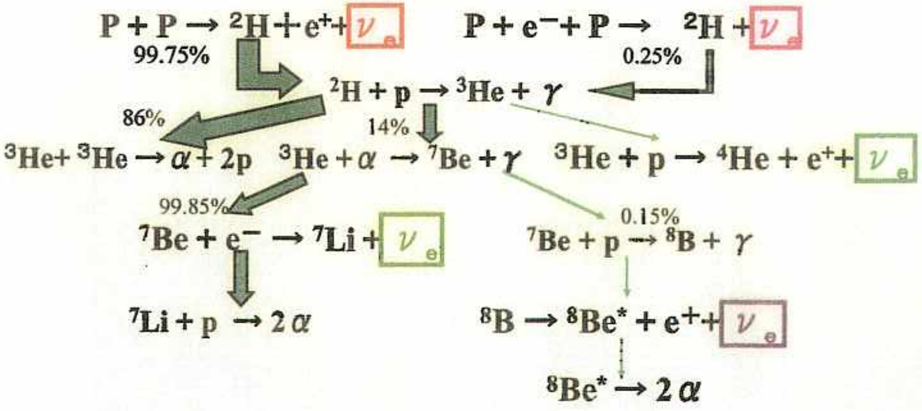

$P + P \rightarrow {}^2H + e^+ + \nu_e$ 99.75%

$P + e^- + P \rightarrow {}^2H + \nu_e$ 0.25%

${}^2H + p \rightarrow {}^3He + \gamma$

86% ${}^3He + {}^3He \rightarrow \alpha + 2p$

14% ${}^3He + \alpha \rightarrow {}^7Be + \gamma$

${}^3He + p \rightarrow {}^4He + e^+ + \nu_e$

99.85% ${}^7Be + e^- \rightarrow {}^7Li + \nu_e$

0.15% ${}^7Be + p \rightarrow {}^8B + \gamma$

${}^7Li + p \rightarrow 2\alpha$

${}^8B \rightarrow {}^8Be^* + e^+ + \nu_e$

${}^8Be^* \rightarrow 2\alpha$

Ga 実験 vs SK.

PP 54%

${}^7Be$ 27%

${}^8B$ 9% ── ${}^8B \times SK$ 5%位。

Gallex, SAGEの平均値は

55% ± 4% (GALLE + SAGE)

PPだけでほとんどせつめいがついてほ

${}^7Be \simeq 0$ と consistent。

Solar modelの問題か。

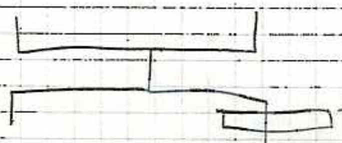

${}^3He + {}^4He \rightarrow {}^7Be + \gamma$

${}^7Be + e^- \rightarrow {}^7Li + \nu_e$ +0.8

${}^7Be\ \nu$

${}^7Be + P \rightarrow {}^8B + \gamma$

$\downarrow$

${}^8B \rightarrow {}^8Be^* + e^+ + \nu_e$

ν ${}^7Be$だけ無くして ⟷ ${}^8B$を半分は不可能と思われる。

実験結果で ${}^8B$, ${}^7Be$を freeにして fitする。

Solar modelの変更では説明がつかない。

⇒ ν oscillation

^{8}B vs. ^{7}Be flux compared with standard solar models

Hata and Langacker (Neutrino 98)

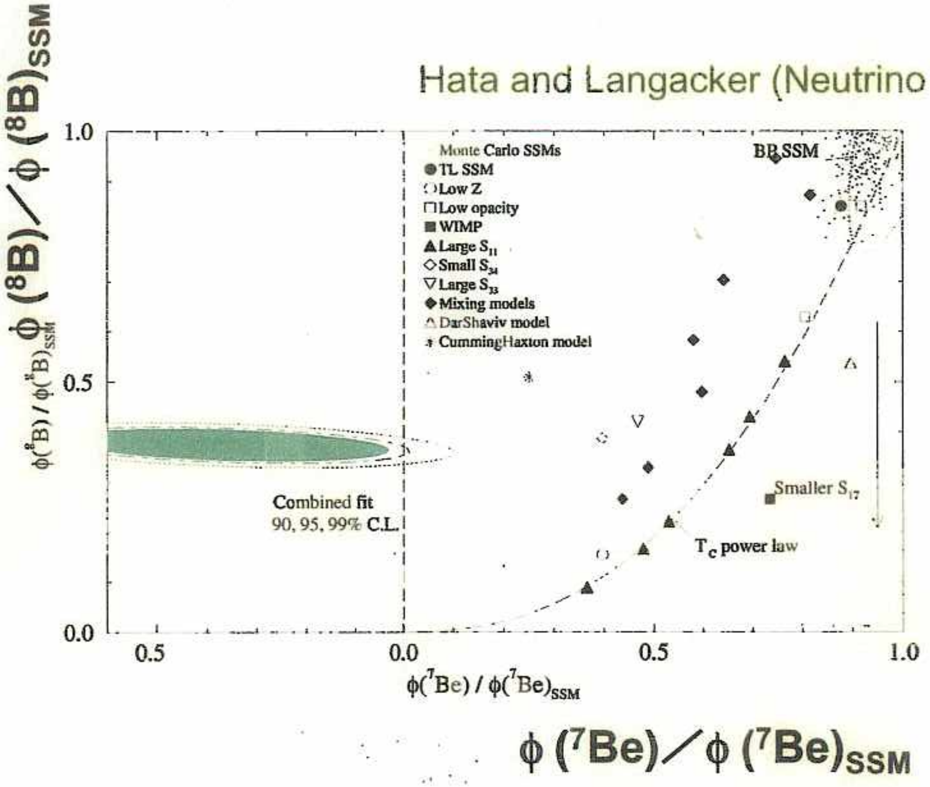

Astrophysical solution has difficulty to explain solar neutrino problem.

Solar ν oscillation

$\nu_e \longrightarrow \nu_\mu$ or ν_τ

^{37}Cl : $\nu_e + {}^{37}\mathrm{Cl} \rightarrow e^-$ - - -

^{71}Ga : $\nu_e + {}^{71}\mathrm{Ga} \rightarrow e^-$ - - -

ν_eのみに対して sensitive

$\nu_e e^- \rightarrow \nu_e e^-$

↓

$\nu_\mu e^- \rightarrow \nu_\mu e^-$ は cross sectionが $\frac{1}{7}$

例えば ν_eが全て ν_μになると $\frac{1}{7}$になってしまう。

① ν vacuum oscillation

$$1 - \sin^2 2\theta \sin^2\left(1.27 \times \frac{\overset{m}{L}}{\underset{\text{MeV}}{E_\nu}} \Delta m^2\right)$$

Δm^2が大きいとすると〜 $\frac{1}{2}$

$$1 - \frac{1}{2}\underset{\substack{\uparrow\\ \text{最大でも}1}}{\sin^2 2\theta}$$

→ $\nu_e \rightarrow \nu_e$ は $\frac{1}{2} \sim 1$ の間

もし ^{37}Cl で $\frac{1}{3}$ というのが有意だとすると

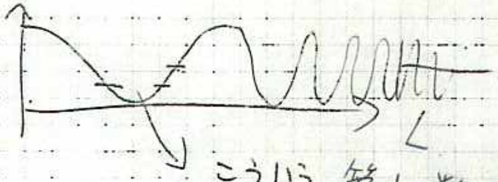

こういう 第1,数 周期位に ないといけない。

これを Just-So という。

のΔm^2は $\frac{L(m)}{E_\nu}\Delta m^2$ が 1のorder

L : 1.5×10^{11}m

E_ν : 数MeV

$$\Delta m^2 \simeq \underline{10^{-11}\sim10^{-10}\,\mathrm{eV}^2}$$

② MSW solution

MSW resonance effectをおこすためには

Resonance 条件

$$\frac{L_\nu}{L_0} = \cos2\theta$$

$$L_0 = 2\pi/\sqrt{2}GN = 1.6\times10^7 m/\rho$$

ρ は /cm³ での

$\rho = N/6\times10^{23}$ electron density

太陽中心 ; ~100 $\rho \fallingdotseq 100$

$\cos2\theta$ $\theta\sim0$のとき $\cos2\theta=1$

$$L_\nu \fallingdotseq 1.6\times10^5 m$$

$$L_\nu = 2.48m\times\left(\frac{P}{1\,\mathrm{MeV}}\right)\left(\frac{\Delta m^2}{}\right)^{-1}$$

⇒ $\Delta m^2 = 10^{-4}\sim10^{-5}\,\mathrm{eV}^2$ あたりでおこる。

$P(\nu_e\to\nu_e)$がある値 例: $0.4\pm\delta$

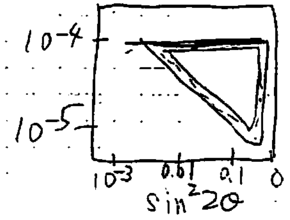

Adiabatic 条件をみたしていると

太陽から出てきた時は heavier state に近い。

$$\nu_2 = \sin\theta\,\nu_e + \cos\theta\,\nu_{\mu \text{ or } \tau}$$

ν_eの probability は $\sin^2\theta$

$\sin^2 2\theta$ が小さいとき $\sin^2\theta$ も小さい ほとんど0に近い。

したがって ^{7}Be が0になることもありうる。

MSWをおこすための条件

(1) Resonance をおこす density が太陽中心の electron density 以下

$$\frac{L_\nu}{L_0} = \cos2\theta$$

$$L_\nu = 2.5m\times\left(\frac{E}{\Delta m^2}\right)$$

$$L_0 = 1.6\times10^7/\rho$$

$$\frac{\left(2.5\times\frac{E}{\Delta m^2}\right)}{1.6\times10^7/\rho} = \cos2\theta$$

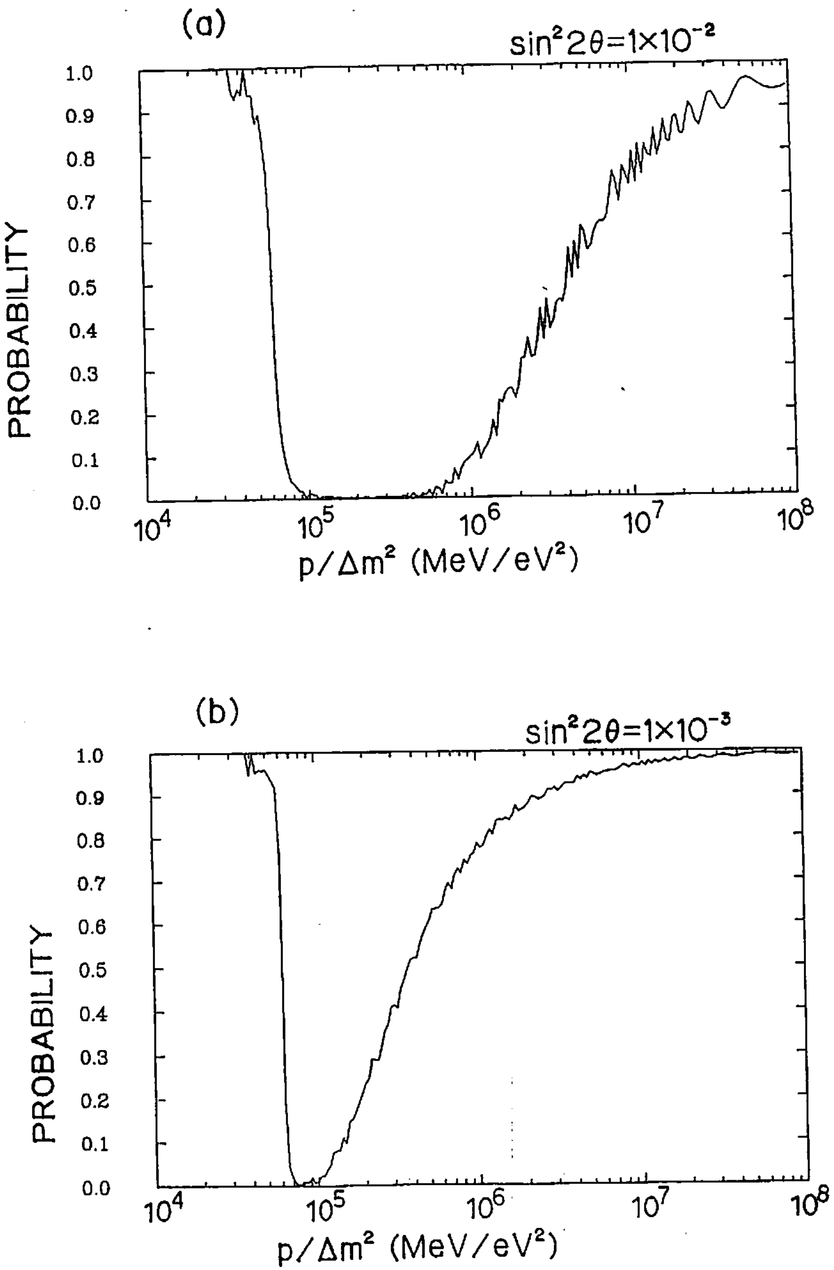

Fig. 1.12

$$\rho = \frac{\cos 2\theta}{2.5 \times \frac{E}{\Delta m^2}} \times 1.6 \times 10^7$$

$$\cong \frac{\Delta m^2}{E} \times \cos 2\theta \times 10^7 < 100$$

$$\frac{\Delta m^{2} \rightarrow eV^2}{\underset{\uparrow MeV}{E}} < 10^{-5}$$

$E = 10 MeV$ とすると

$$\underline{\Delta m^2 < 10^{-4} eV^2}$$

(2) Adiabatic 条件

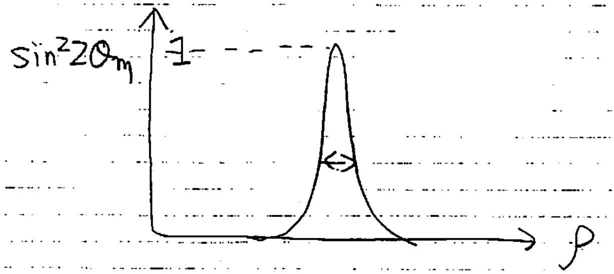

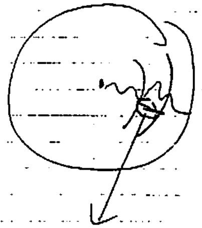

$$\sin^2 2\theta_m = \frac{\sin^2 2\theta}{\sin^2 2\theta + (L_\nu/L_0 - \cos 2\theta)^2}$$

$\sin^2 2\theta_m$ が大きい間に何度か振動すること。

matter中での oscillation length

$$L_m = \frac{L_\nu}{\sqrt{1 - 2\left(\frac{L_\nu}{L_0}\right)\cos 2\theta + \left(\frac{L_\nu}{L_0}\right)^2}}$$

$\frac{L_\nu}{L_0} = \cos 2\theta$ を入れると

$$L_m = \frac{L_\nu}{\sin^2 2\theta}$$

$$L_m \ll \left(\frac{1}{\rho}\frac{d\rho}{dR}\right)^{-1} \simeq 10^8$$

$$L_\nu = 2.48 \times \frac{P}{\Delta m^2}$$

$$2.48 \times \frac{P}{\Delta m^2 \times \sin^2 2\theta} < 10^8$$

$$\underline{\underline{\Delta m^2 \times \sin^2 2\theta \gtrsim 10^{-8} \times P}}$$

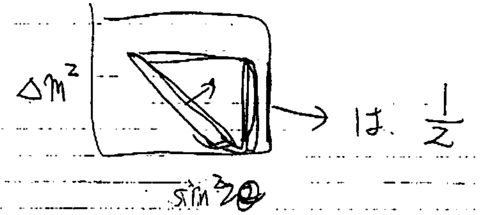

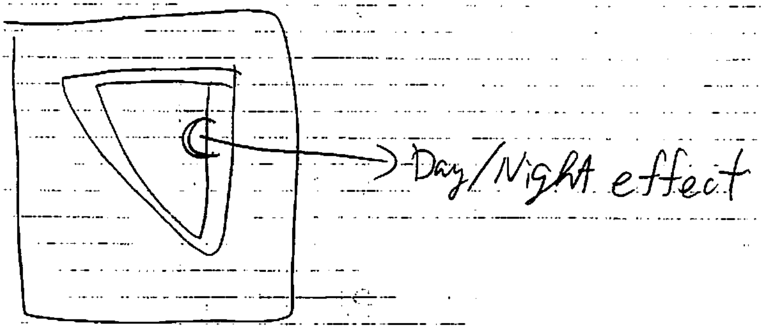

地球のdensity ~ 5 g/cm^2

なくなった ν_e が regenerationにより もどる。

5 g/cm^3 を入れると

$\frac{L_\nu}{L_0} = \cos 2\theta$ に入れると $10^{-6} \sim 10^{-5}$ eV^2
(P = 10MeVに対して)

地球の物質effectで regeneration

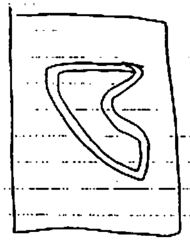

となる。

Gallex, SAGEでは、 $\frac{\text{Data}}{\text{SSM}} > 0.5$ なので、

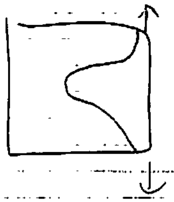

$\sin^2 2\theta$ が1のあたりも許される。

Combineすると 3つの solutionが許される。

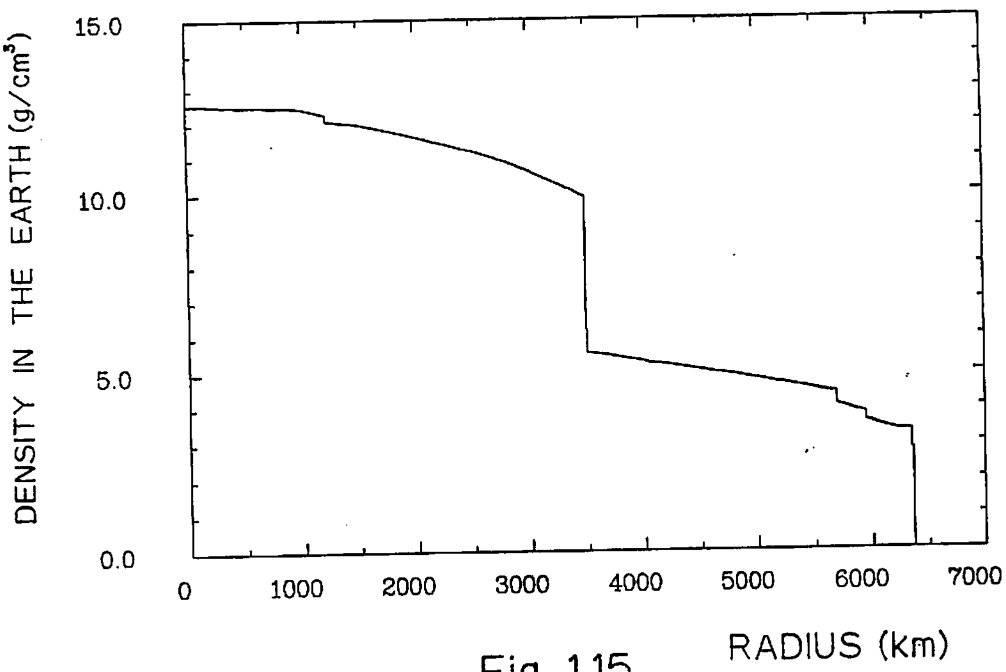

Fig. 1.15

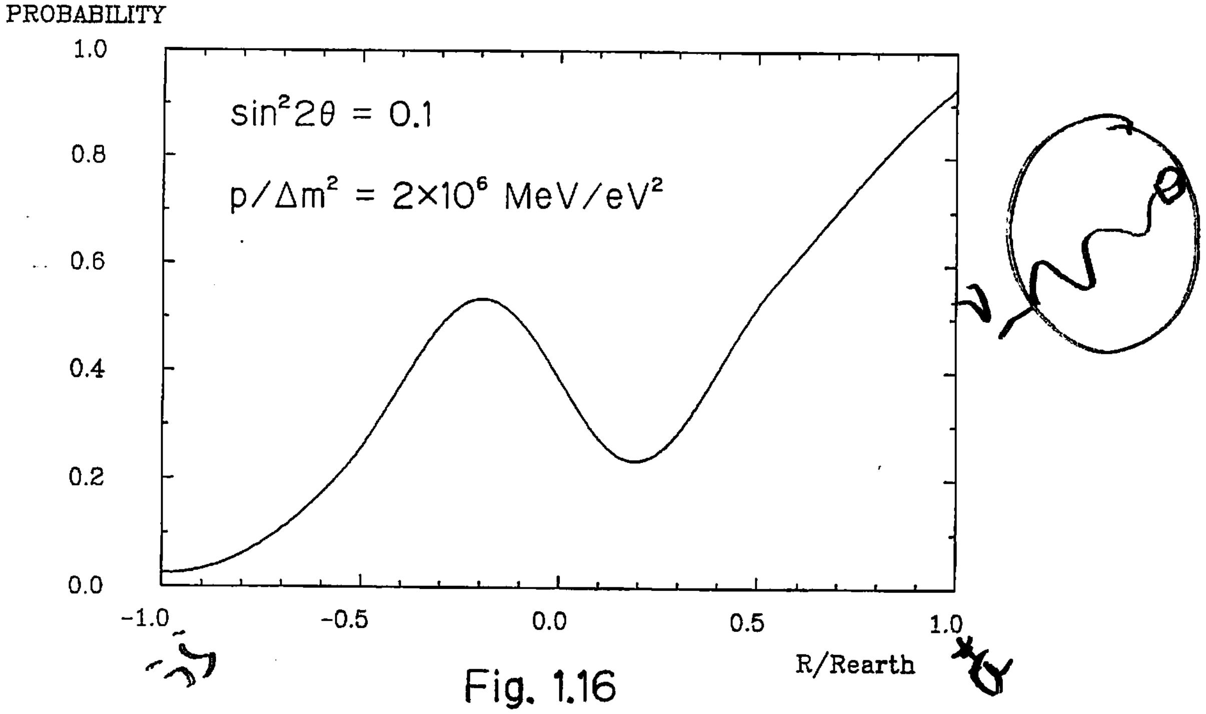

$\sin^2 2\theta = 0.1$

$p/\Delta m^2 = 2\times10^6$ MeV/eV^2

Fig. 1.16

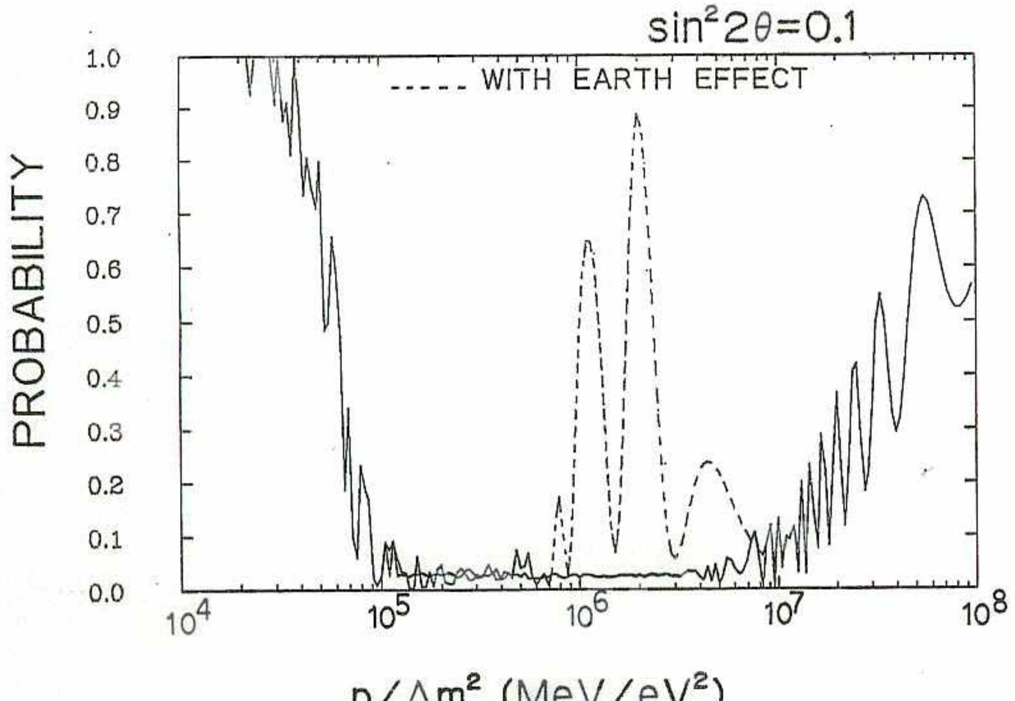
sin²2θ=0.1
----- WITH EARTH EFFECT
PROBABILITY
1.0
0.9
0.8
0.7
0.6
0.5
0.4
0.3
0.2
0.1
0.0
10⁴
10⁵
10⁶
10⁷
10⁸
p/Δm² (MeV/eV²)

Fig. 1.17

Cl & Ga

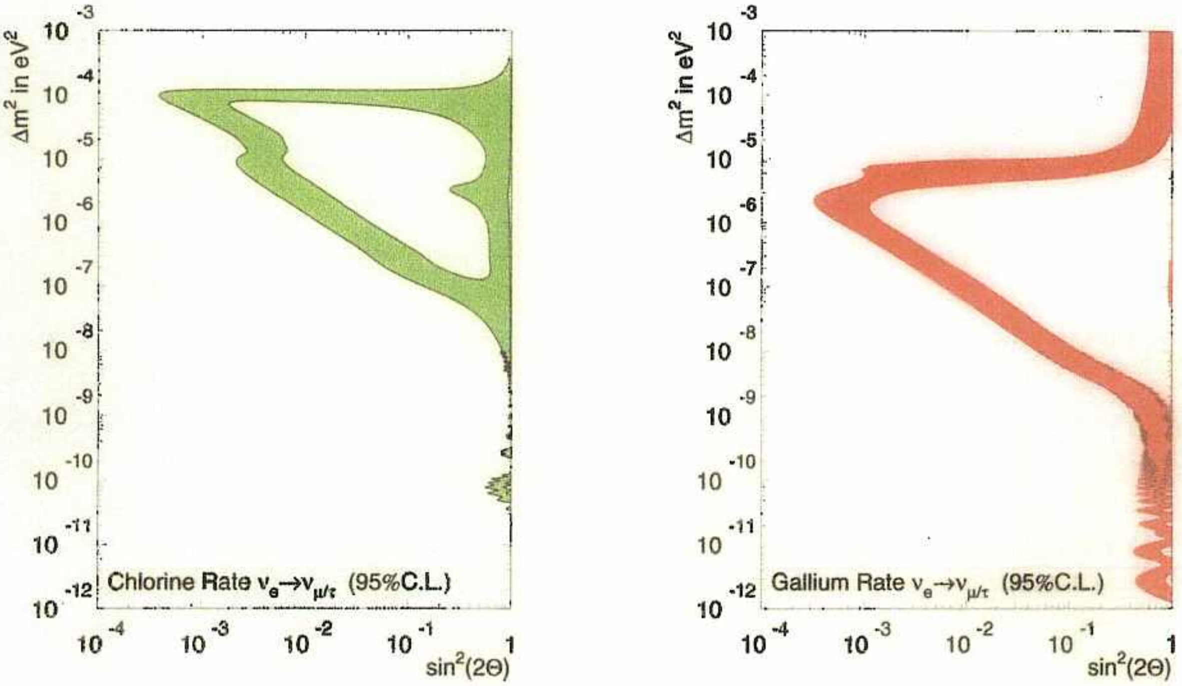
Δm² in eV²
10⁻³
10⁻⁴
10⁻⁵
10⁻⁶
10⁻⁷
10⁻⁸
10⁻⁹
10⁻¹⁰
10⁻¹¹
10⁻¹²
Chlorine Rate νe→νμ/τ (95%C.L.)
10⁻⁴
10⁻³
10⁻²
10⁻¹
1
sin²(2Θ)
Δm² in eV²
10⁻³
10⁻⁴
10⁻⁵
10⁻⁶
10⁻⁷
10⁻⁸
10⁻⁹
10⁻¹⁰
10⁻¹¹
10⁻¹²
Gallium Rate νe→νμ/τ (95%C.L.)
10⁻⁴
10⁻³
10⁻²
10⁻¹
1
sin²(2Θ)

SNO & SK

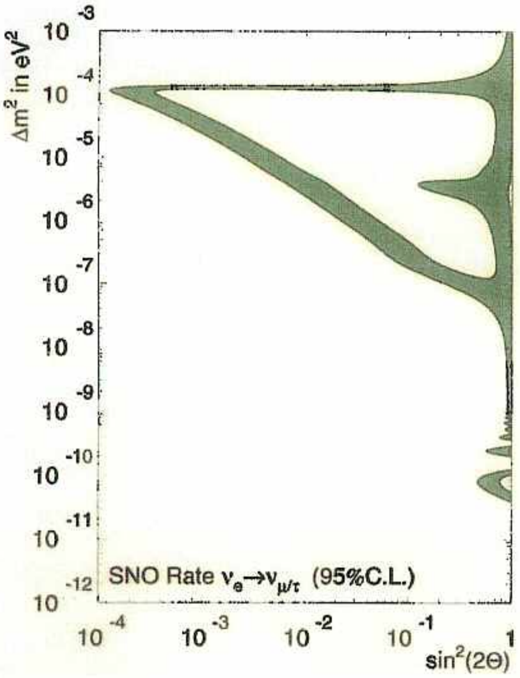

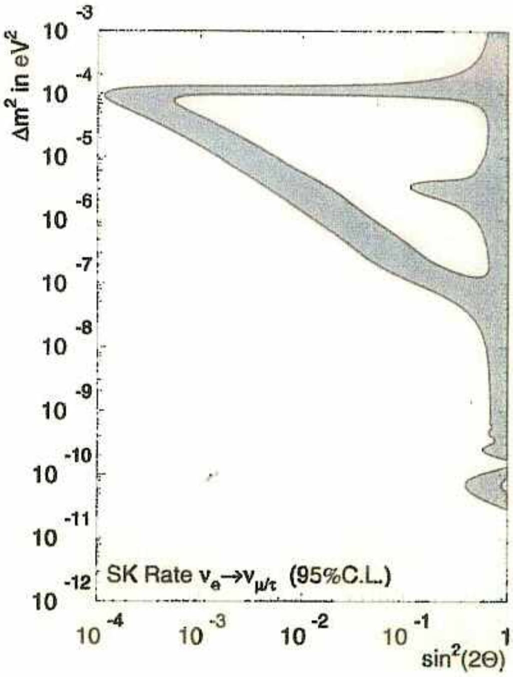

SOLOSC-16

Flux (Rate)-global analysis (guide for the solution)

$\nu_e \rightarrow \nu_\mu(\nu_\tau)$ **95% C.L.**

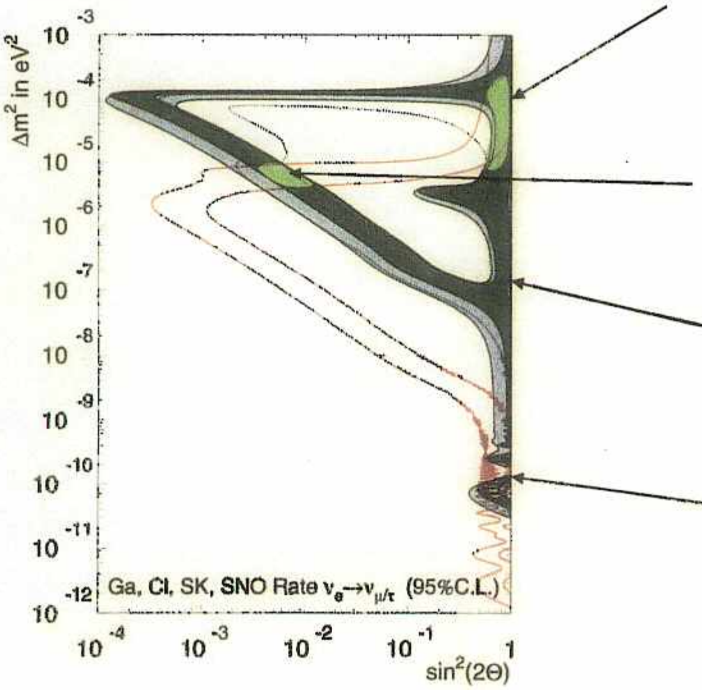

MSW Large Mixing Angle

Small Mixing Angle

LOW

(Ga does not like this solution)

Vacuum

SolOSC-17

Oscillation parameters based on flux of Homestake, GALLEX, SAGE, SK and SNO

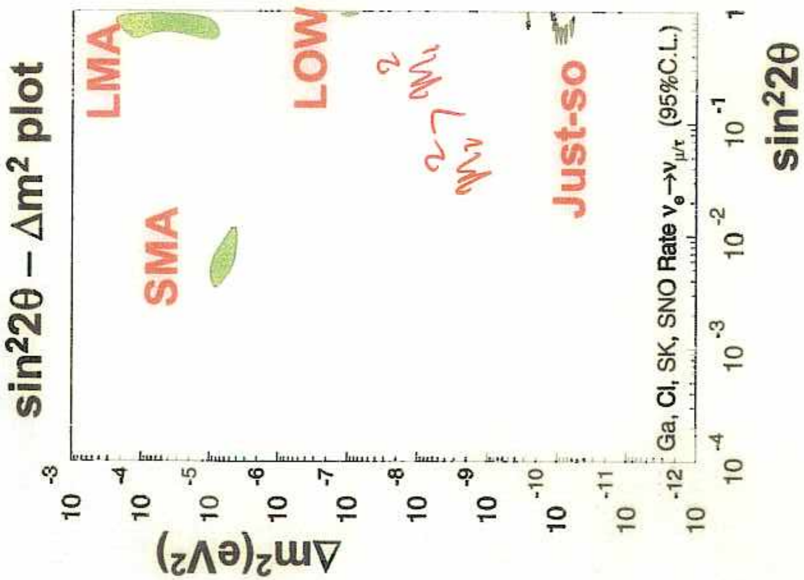

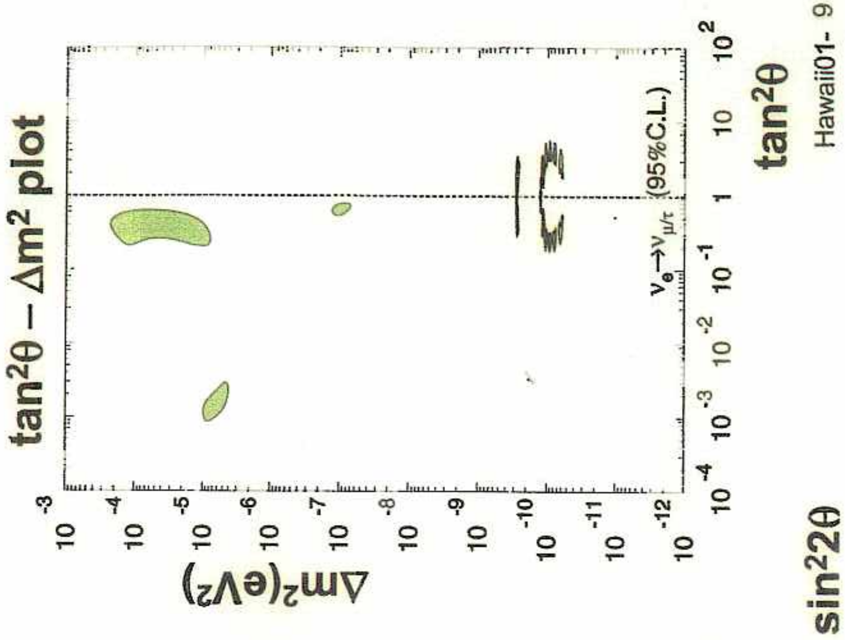

Oscillation probability for each solution

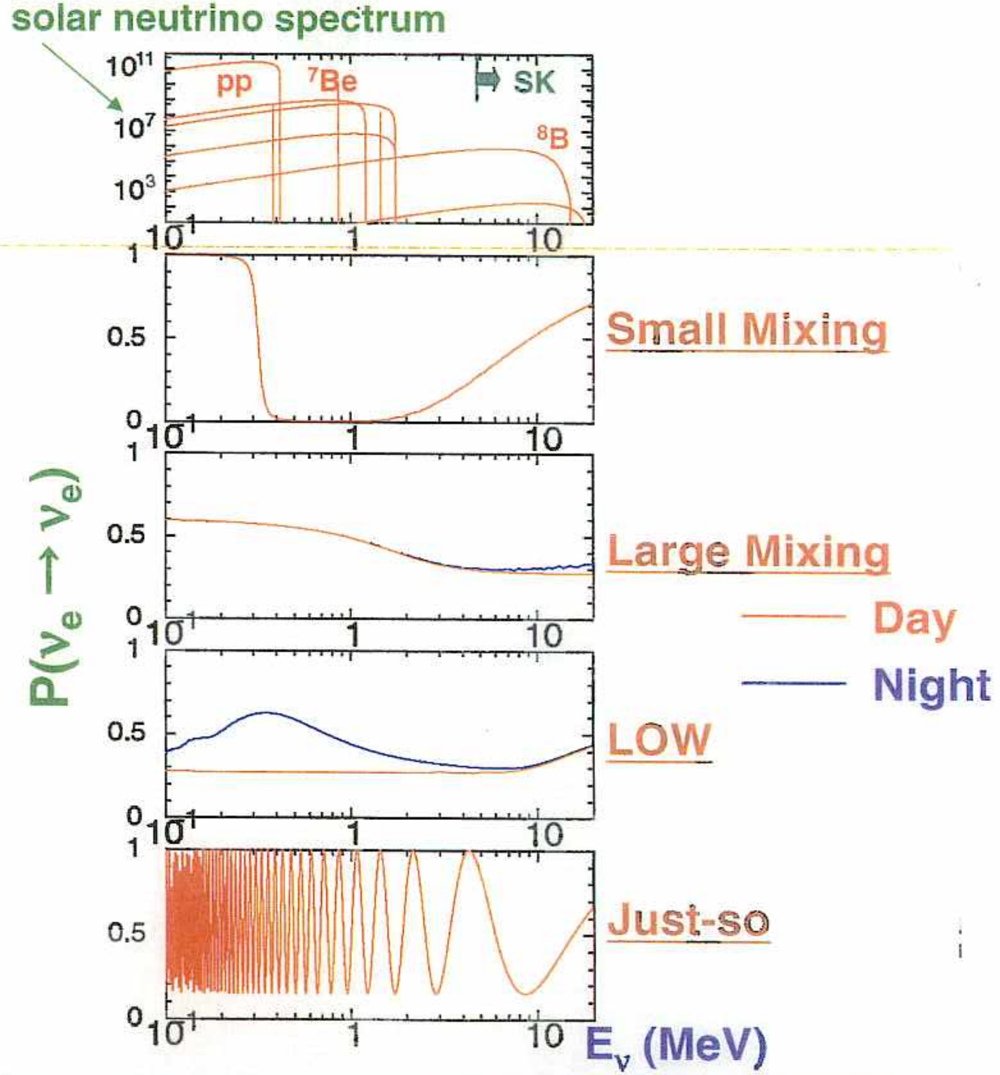

Spectral shape and Day/night analysis

Model independent test of ν oscillation

重水(D_2O)を用いたカナダのSNO実験

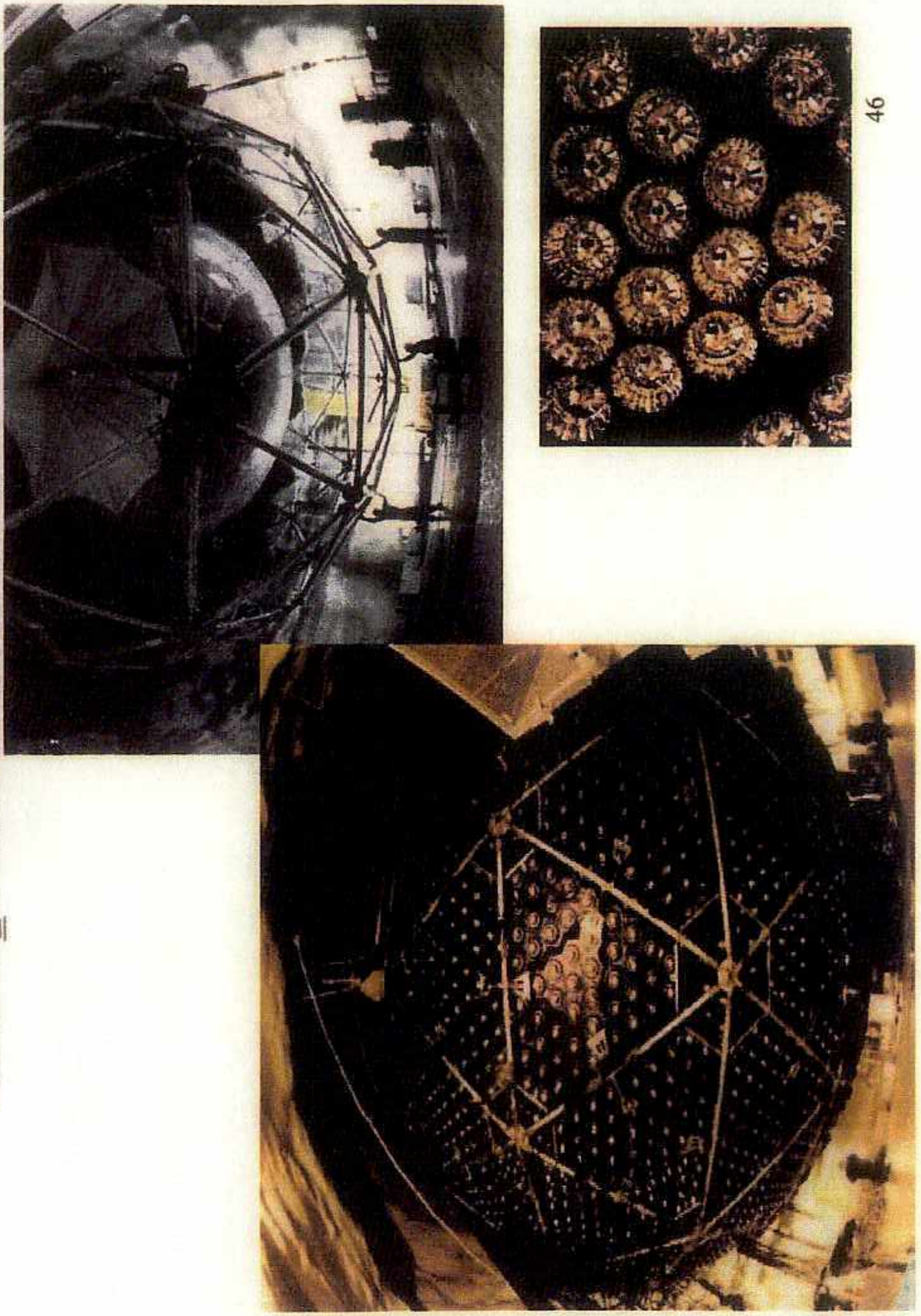

SNO

http://www.sno.phy.queensu.ca/

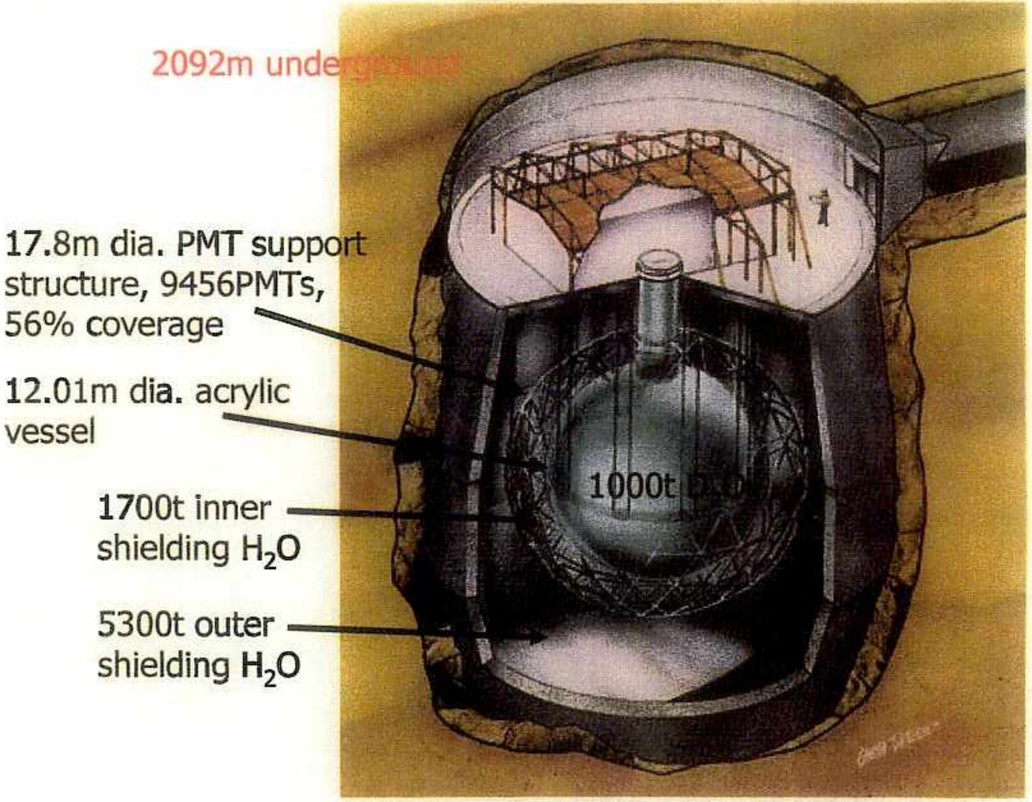

- 5.5m radial fiducial volume for solar neutrino analysis
- 5MeV energy threshold
- Energy scale uncertainty 1.2%
- Energy resolution 14% at 10MeV

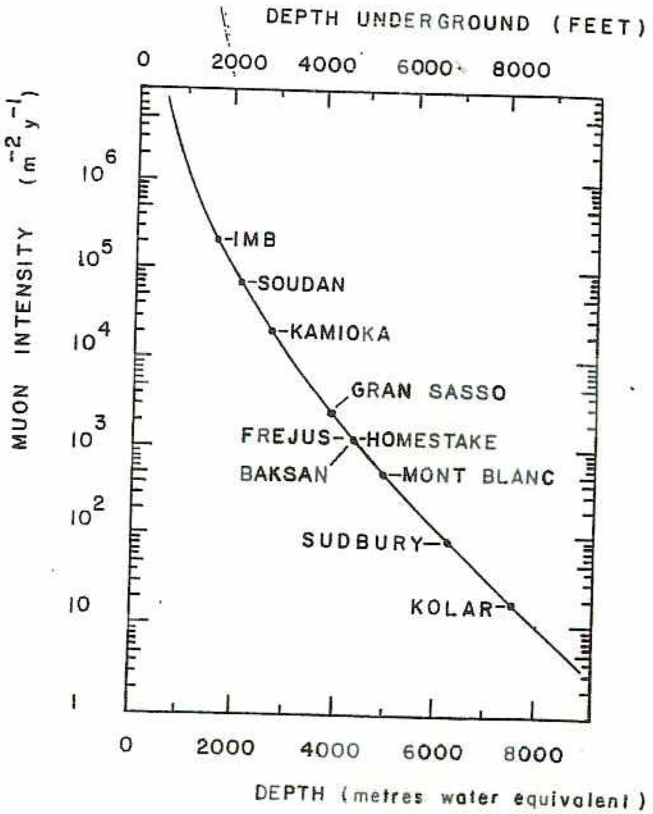

Figure III.5 Cosmic ray muon intensity as a function of overburden (mwe) or depth underground (feet in standard rock).

ν Reactions in SNO

CC $\nu_e + d \Rightarrow p + p + e^-$

- **-Good measurement of ν_e energy spectrum**
- **-Weak directional sensitivity ∝ 1-1/3cos(Θ)**
- **- ν_e only.**

NC $\nu_x + d \Rightarrow p + n + \nu_x$

- **- Equal cross section for all ν types**
- **- Measure total ^{8}B ν flux from the sun.**

ES $\nu_x + e^- \Rightarrow \nu_x + e^-$

- **-Low Statistics**
- **-Mainly sensitive to $\nu_{e,}$, some sensitivity to ν_μ and ν_s**
- **-Strong directional sensitivity**

Neutron Capture Efficiency & Uncertainties

Capture Efficiency

Total	29.90 +/- 1.10 %
With threshold & fiducial cut	14.38 +/- 0.53 %

Flux Uncertainty

ΔNC/NC

−4.0,+3.6 %

Response vs Radius

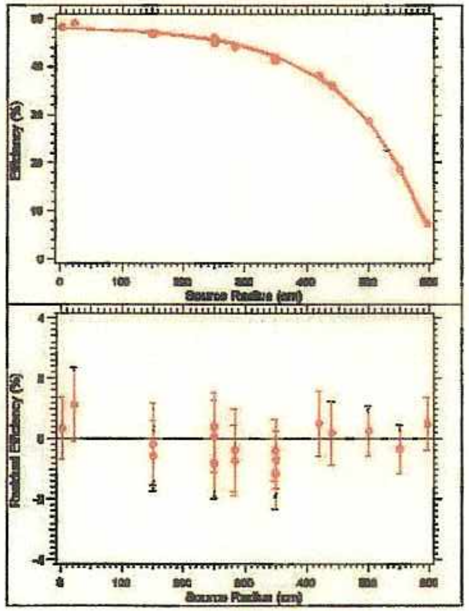

The Pure D_2O Phase Dataset

- Livetime: 306.4 days (November 2, 1999 ➡ May 27, 2001)
  Day: 128.5 days Night: 177.9 days
- Energy Threshold: 5 MeV Kinetic
- Fiducial Volume Cut: 550 cm
- Total Number of Events after cuts: 2928
  Neutron Bkg 78^{+12}_{-12} Cherenkov Bkg 45^{+18}_{-12}

Shape Constrained Signal Extraction Results

#EVENTS

CC	$1967.7^{+61.9}_{+60.9}$
ES	$263.6^{+26.4}_{+25.6}$
NC	$576.5^{+49.5}_{+48.9}$

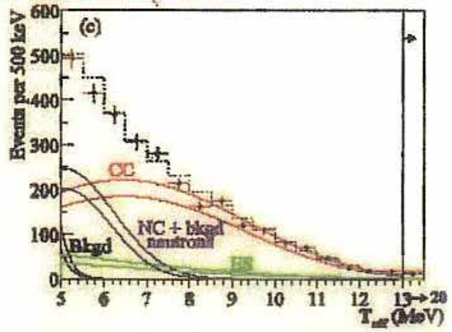

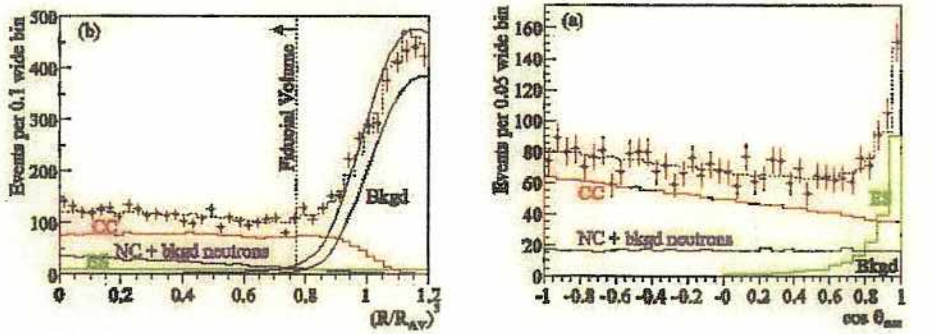

The latest results

Nov.2,1999~May.28,2001
total: 306.4days, 2928events

nucl-ex/0204008

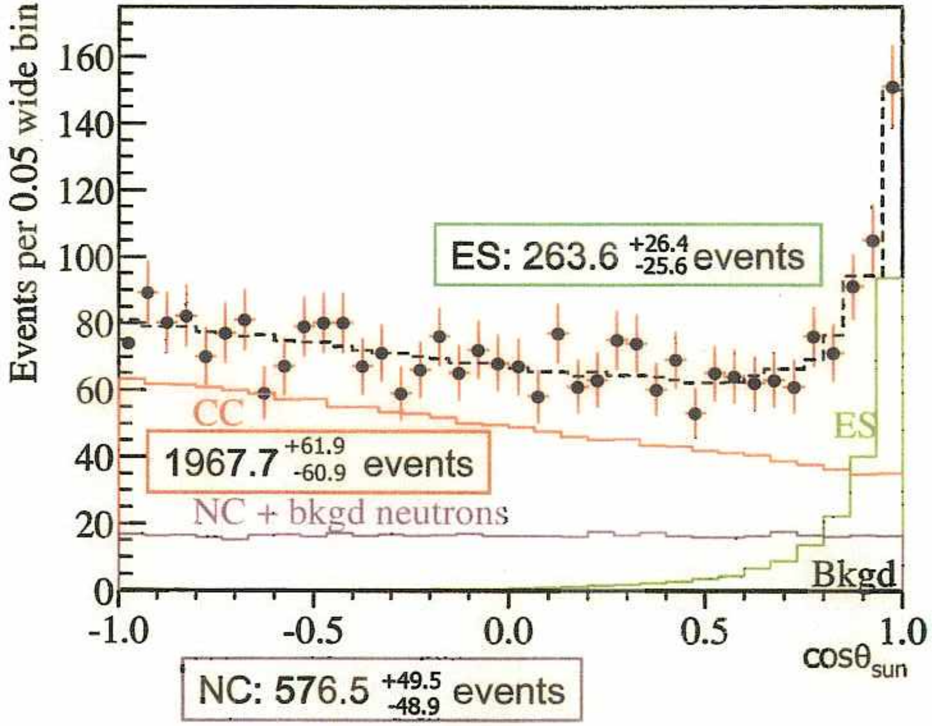

↓

$[\times 10^6/\mathrm{cm}^2/\mathrm{s}]$

$$\phi_{CC} = 1.76\,^{+0.06}_{-0.05}\,(\text{stat.}) \pm 0.09 (\text{syst.})$$

$$\phi_{ES} = 2.39\,^{+0.24}_{-0.23}\,(\text{stat.}) \pm 0.12 (\text{syst.})$$

$$\phi_{NC} = 5.09\,^{+0.44}_{-0.43}\,(\text{stat.})\,^{+0.46}_{-0.43}\,(\text{syst.})$$

SKとSNO CCとの比較から求めたニュートリノ成分

SNO $\phi_{CC} = 1.76 \pm 0.11$ [x10^6/cm^2/s] $\phi_{CC} = \phi_e$

SK $\phi_{ES} = 2.35 \pm 0.09$ $\phi_{ES} = \phi_e + 0.15\,\phi_{\mu,\tau}$

⇧ $\phi_{\mu,\tau} = 3.9 \pm 0.9$

$\phi_x = 5.7 \pm 0.9$ **(total active ^{8}B neutrino flux)**

(ϕ_{SSM} = 5.05+1.01/-0.81)

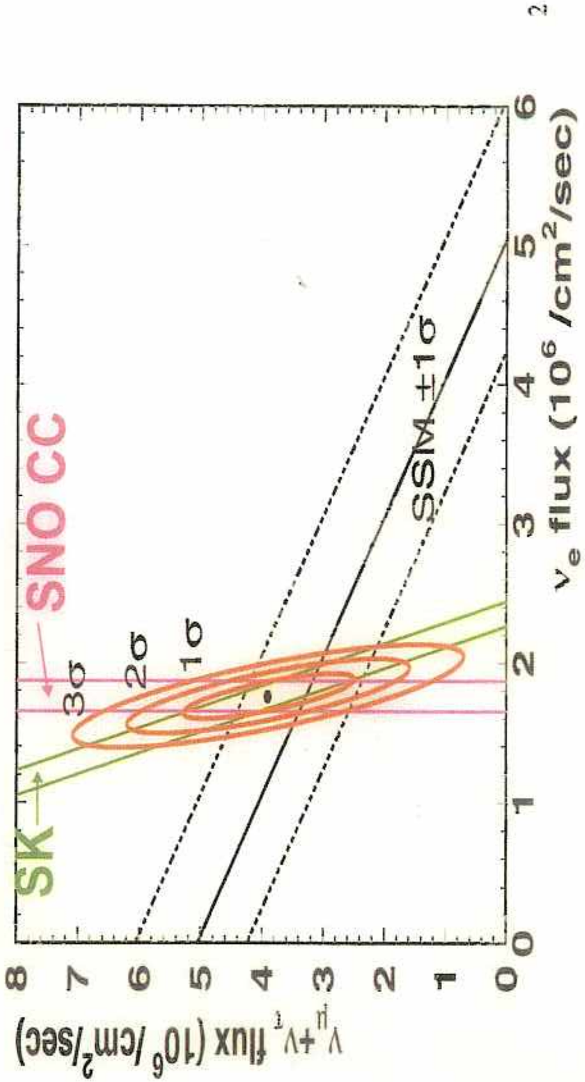

Present and Future of SNO

The Salt Phase

$n + {}^{35}Cl \rightarrow {}^{36}Cl + \Sigma\gamma \ldots \rightarrow e^-$ ($E_{\Sigma\gamma}$ = 8.6 MeV)

- Higher n-capture efficiency
- Higher event light output
- Event isotropy differs from e$^-$
- Running since June 2001

Neutral Current Detectors

$n + {}^3He \rightarrow p + t$

- Event by event separation

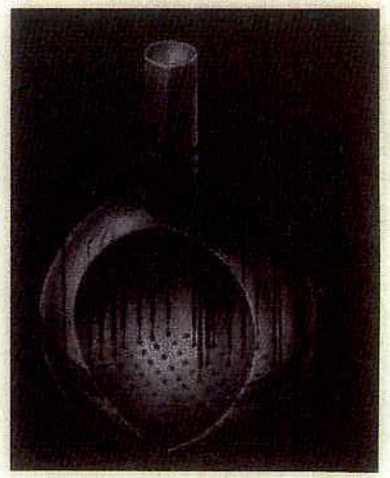

Advantages of NaCl for Neutron Detection

- Higher capture cross section
- Higher energy release
- Many gammas

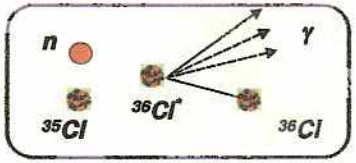

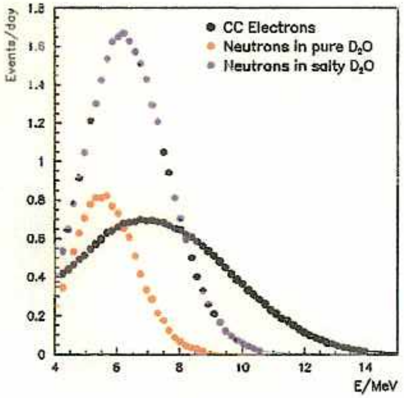

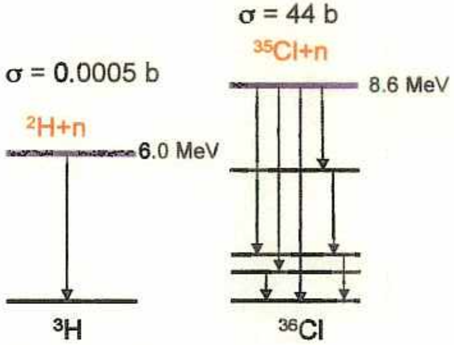

Neutron Capture Efficiency in SNO

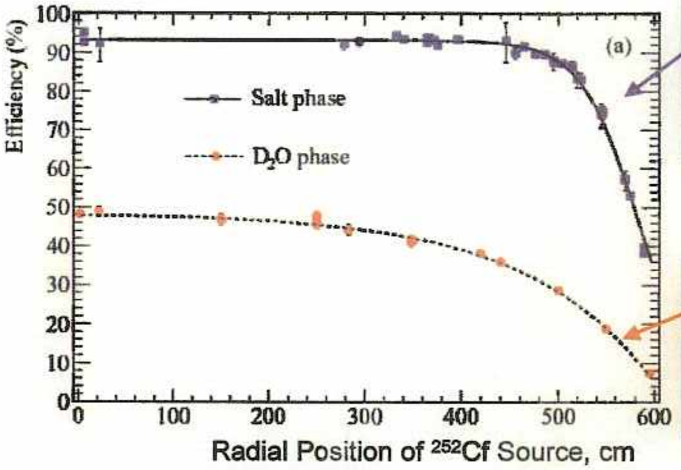

$^{35}Cl(n,\gamma)^{36}Cl$
Average Eff. =
0.399
$T_e \geq 5.5$ MeV and
$R_\gamma \leq 550$ cm

$^2H(n,\gamma)^3H$
Average Eff. =
0.144
$T_e \geq 5.0$ MeV and
$R_\gamma \leq 550$ cm

Cherenkov light and β_{14}

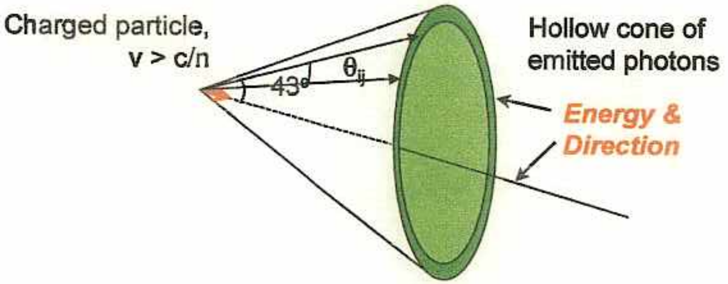

Energy &
Direction

Wate

$$\beta_1 = \frac{2}{N(N-1)} \sum_{i=1}^{N-1} \sum_{j=i+1}^{N} cos\theta_{ij}$$

$$\beta_4 = \frac{2}{N(N-1)} \sum_{i=1}^{N-1} \sum_{j=i+1}^{N} \frac{1}{64}(9 + 20cos2\theta_{ij} + 35cos4\theta_{ij})$$

$\beta_{14} = \beta_1 + 4\beta_4$

β_{14} Distributions for SNO Salt Data

Data from July 26, 2001 to Oct. 10, 2002

254.2 live days

3055 candidate events:

1339.6 $^{+63.8}_{-61.5}$ CC

1344.2 $^{+69.8}_{-69.0}$ NC

170.3 $^{+23.9}_{-20.1}$ ES

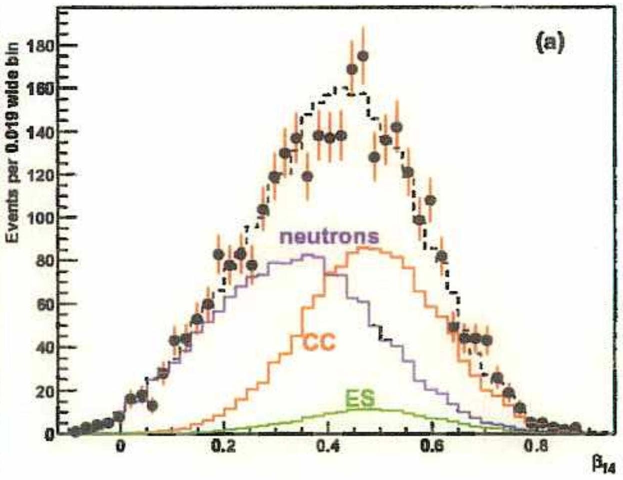

Sun-angle distributions

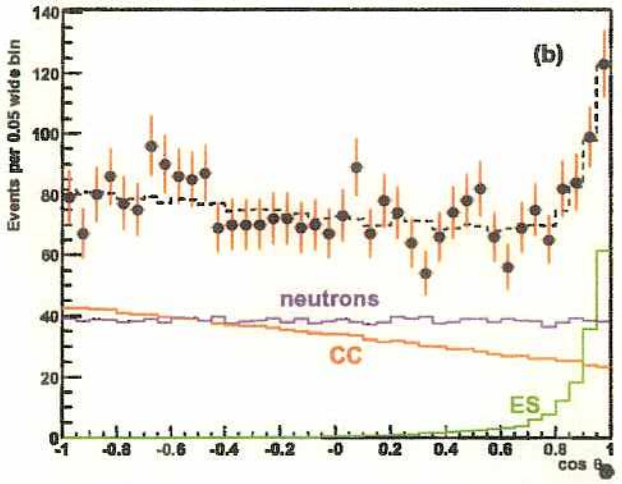

Toward sun

Away from sun

Energy spectra

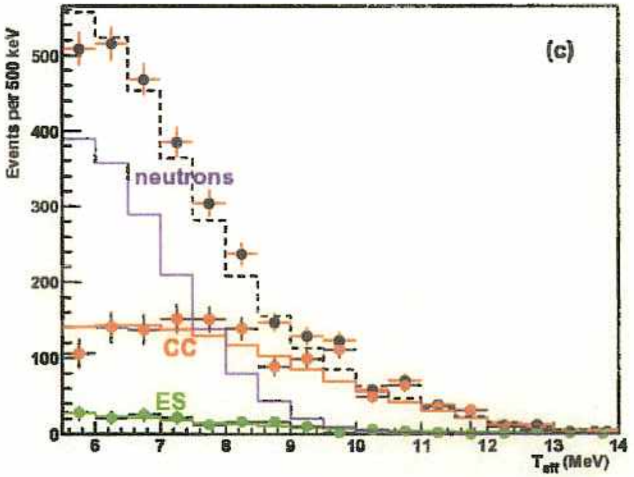

Electron kinetic energy

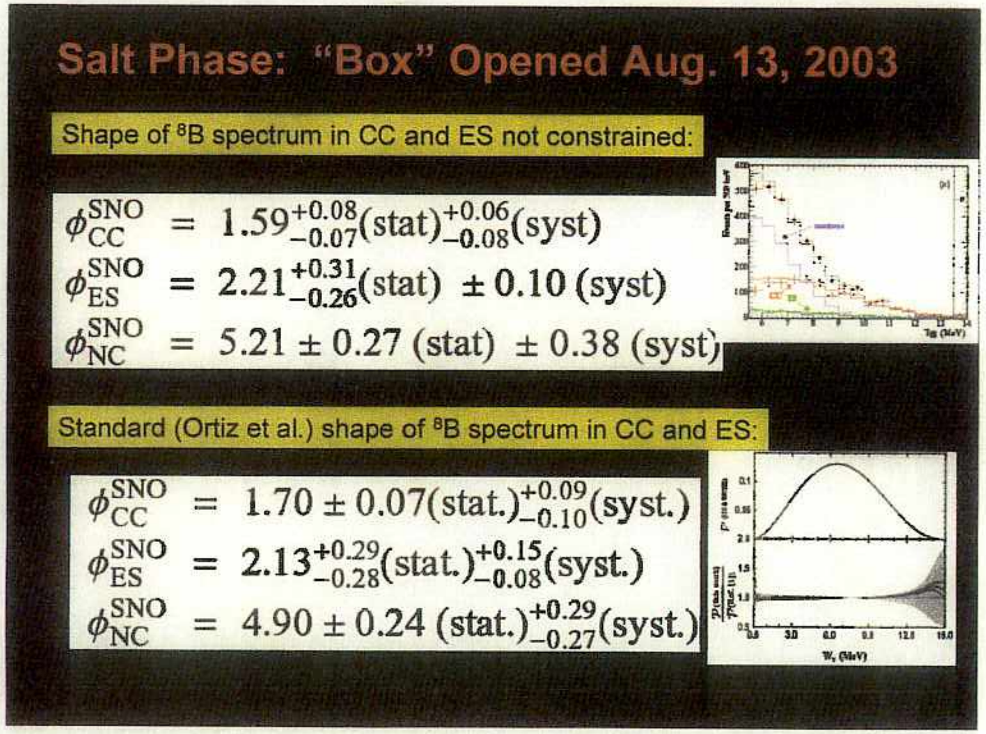

Salt Phase: "Box" Opened Aug. 13, 2003

Shape of ^{8}B spectrum in CC and ES not constrained:

$$\phi_{CC}^{SNO} = 1.59^{+0.08}_{-0.07}(\text{stat})^{+0.06}_{-0.08}(\text{syst})$$
$$\phi_{ES}^{SNO} = 2.21^{+0.31}_{-0.26}(\text{stat}) \pm 0.10\,(\text{syst})$$
$$\phi_{NC}^{SNO} = 5.21 \pm 0.27\,(\text{stat}) \pm 0.38\,(\text{syst})$$

Standard (Ortiz et al.) shape of ^{8}B spectrum in CC and ES:

$$\phi_{CC}^{SNO} = 1.70 \pm 0.07(\text{stat.})^{+0.09}_{-0.10}(\text{syst.})$$
$$\phi_{ES}^{SNO} = 2.13^{+0.29}_{-0.28}(\text{stat.})^{+0.15}_{-0.08}(\text{syst.})$$
$$\phi_{NC}^{SNO} = 4.90 \pm 0.24\,(\text{stat.})^{+0.29}_{-0.27}(\text{syst.})$$

ν_e flux and $\nu_\mu+\nu_\tau$ flux from SK and SNO

SK $\phi_{ES} = 2.35\pm0.09$ [x10^6/cm^2/s] $\phi_{ES} = \phi_e + 0.15\,\phi_{\mu,\tau}$

SNO $\phi_{CC} = 1.68\pm0.09$ $\phi_{CC} = \phi_e$

SNO $\phi_{NC} = 5.21\pm0.47$ $\phi_{NC} = \phi_e + \phi_\mu + \phi_\tau$

Obtained total flux: $\phi_{exp} = 5.4\pm0.3$ (cf. $\phi_{SSM} = 5.05+1.01/-0.81$)

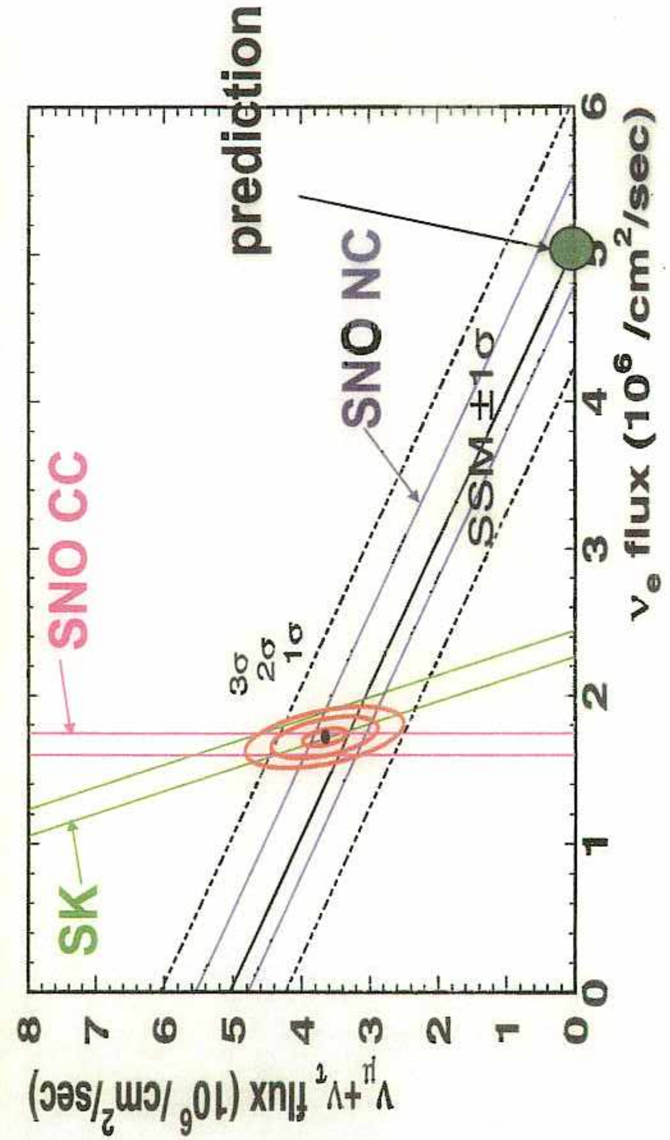

Day/Night Effect

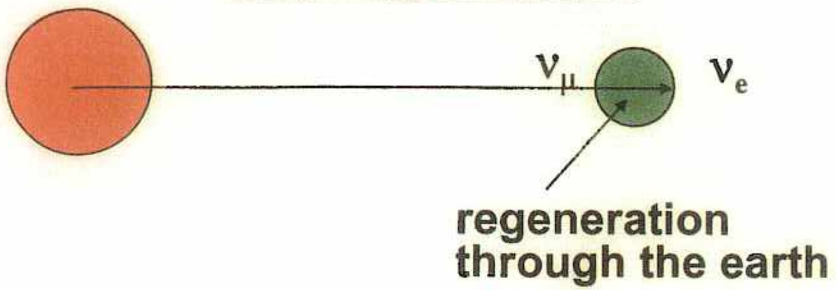

Earth density: ρ=5g/cm² (average), 13(at core)

Affect to oscillations for $\Delta m^2 = 10^{-6} - 10^{-4}$ eV²

SK

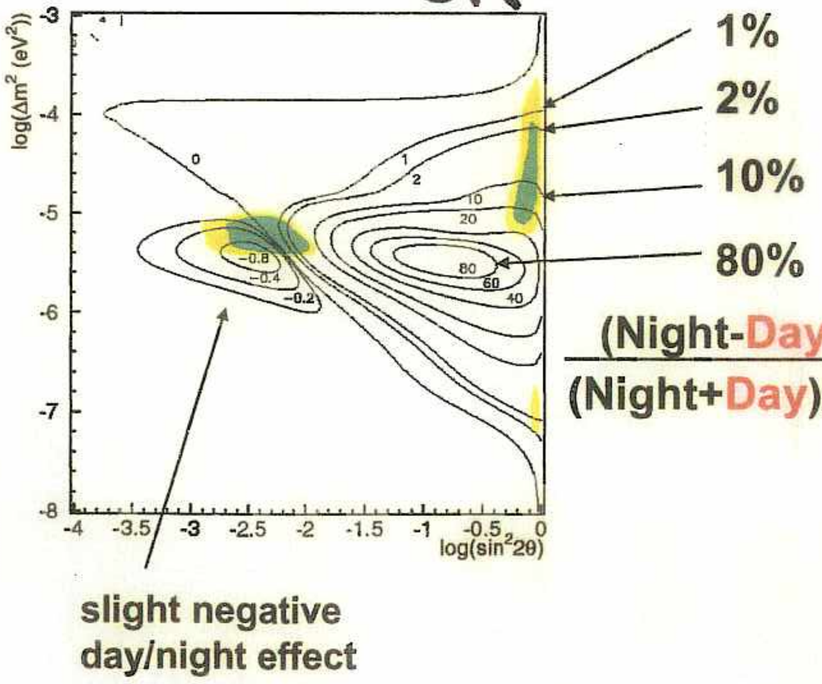

$$\frac{(\text{Night}-\text{Day})}{(\text{Night}+\text{Day})/2}$$

Day/Night analysis (SK)

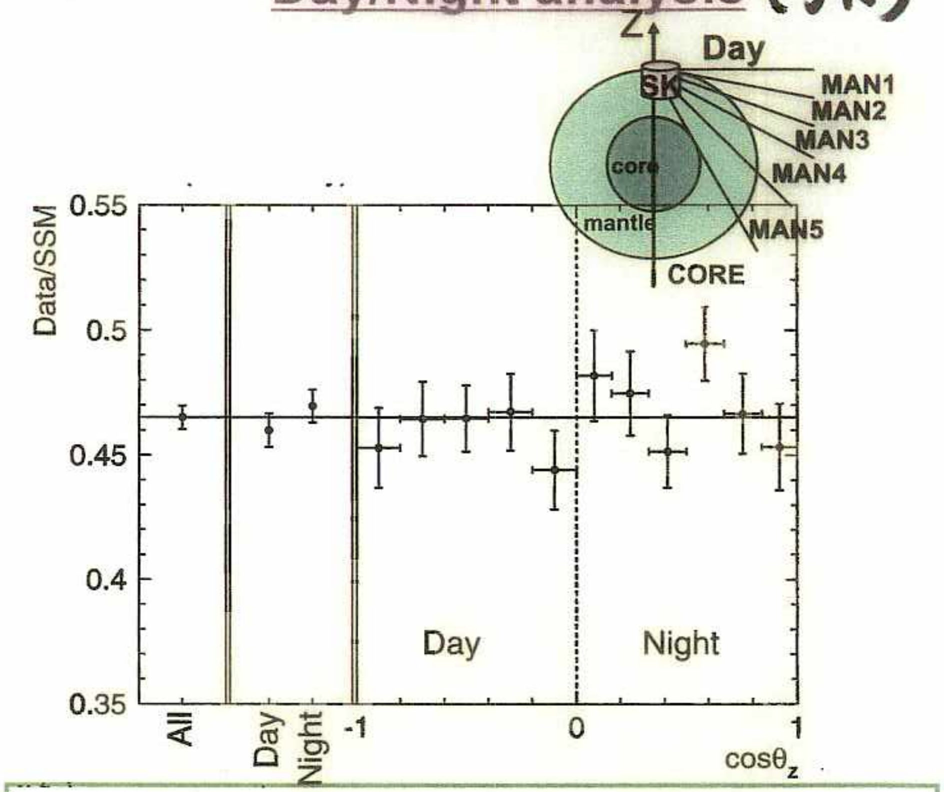

Day: 733 effective days
$f(^8B) = 2.32 \pm 0.03 \pm^{0.08}_{0.07}$ [×10⁶/cm²/s]

Night: 763 effective days
$f(^8B) = 2.37 \pm 0.03 \pm 0.03$ [×10⁶/cm²/s]

$$\frac{N-D}{(N+D)/2} = 0.021 \pm 0.020(\text{stat.}) \pm {}^{0.013}_{0.012}(\text{sys.})$$

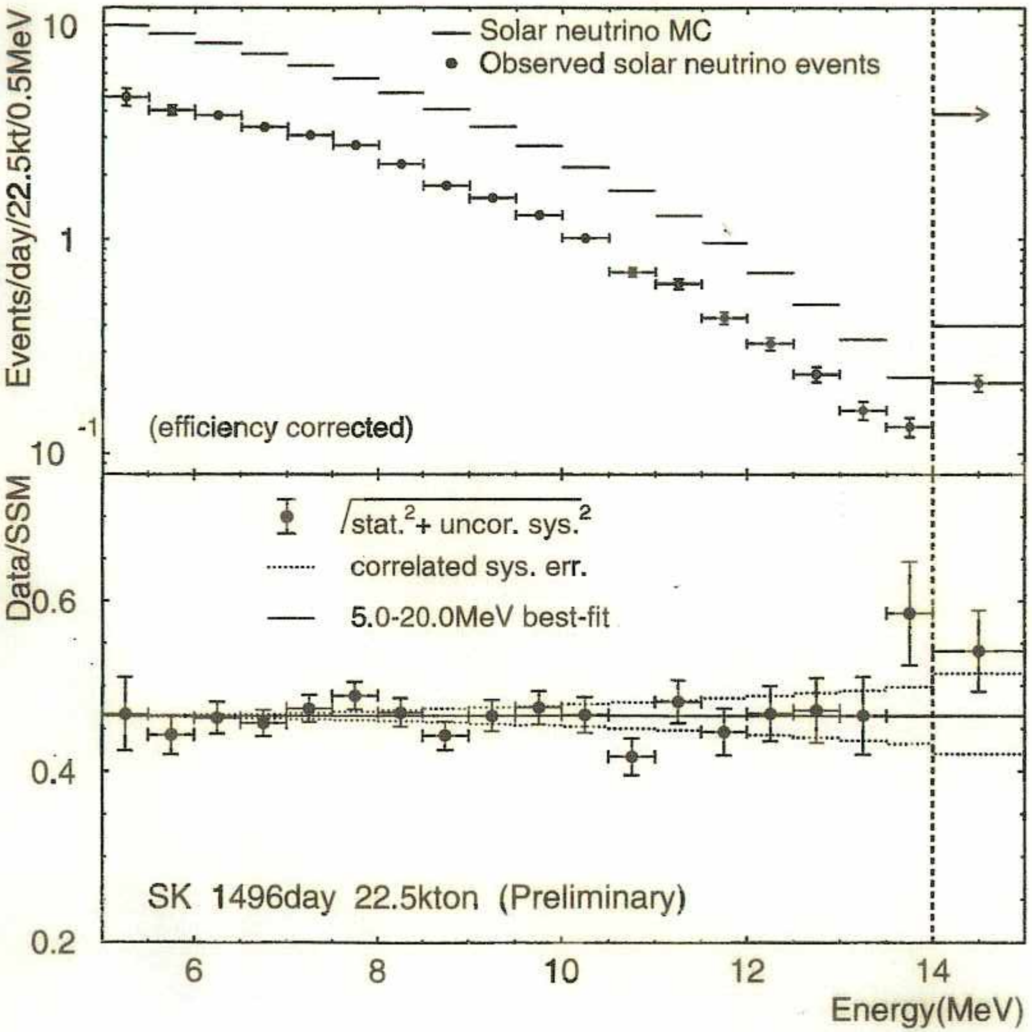

Oscillation analysis

Spectrum shape comparison

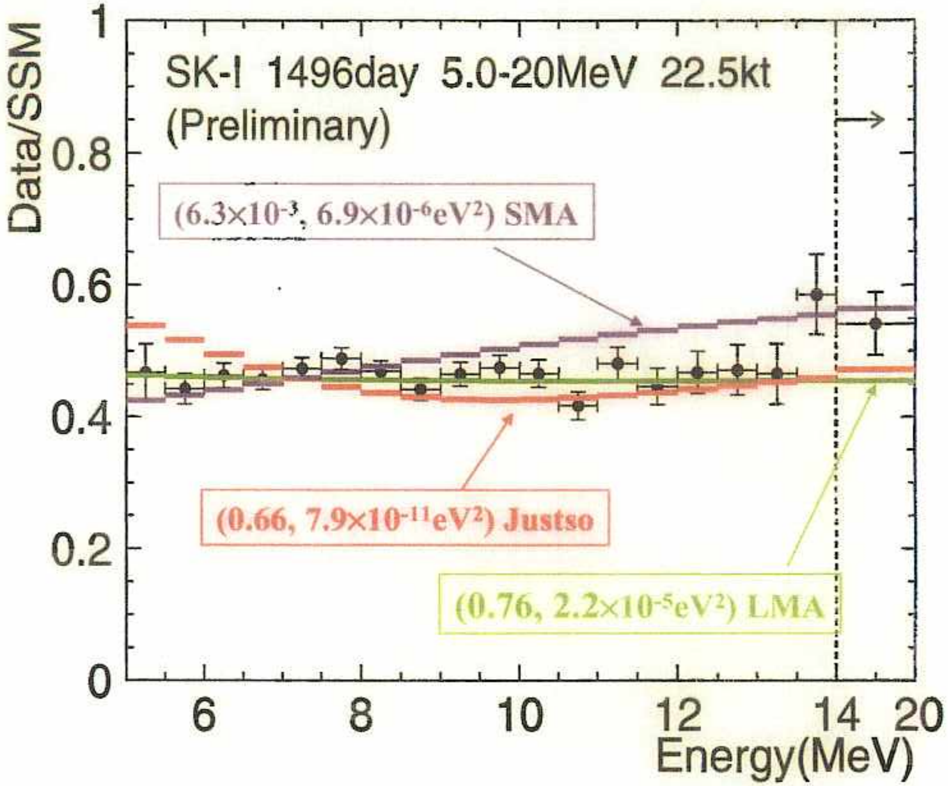

Bad fit for SMA and Just-so solutions.

Excluded region from SK zenith-spectrum

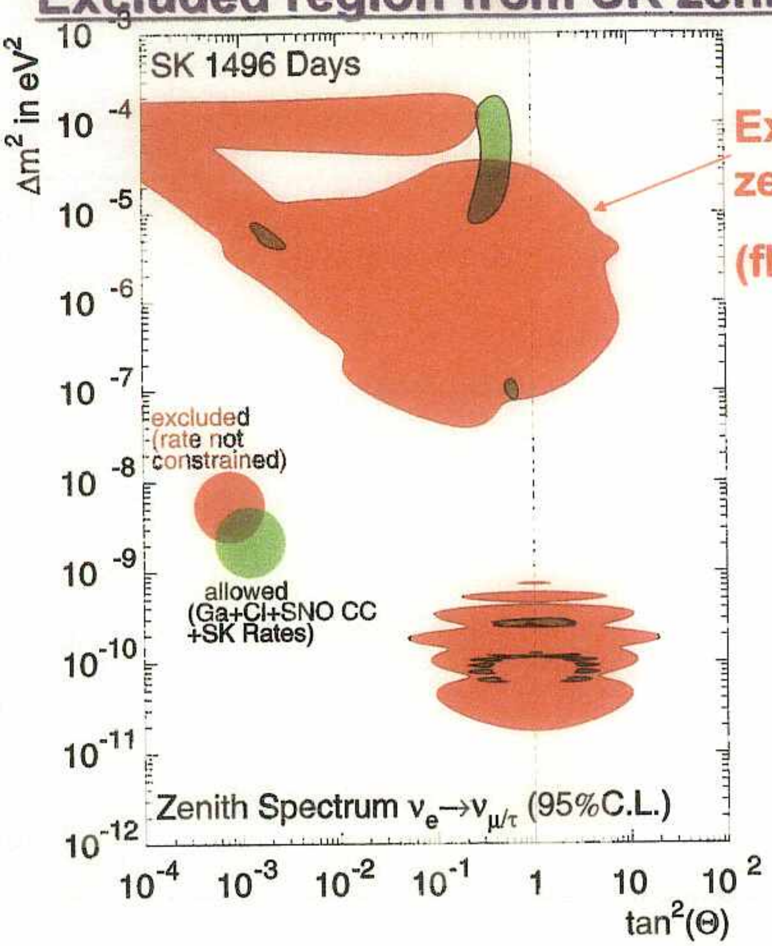

Excluded by SK zenith-spectrum

(flux independent)

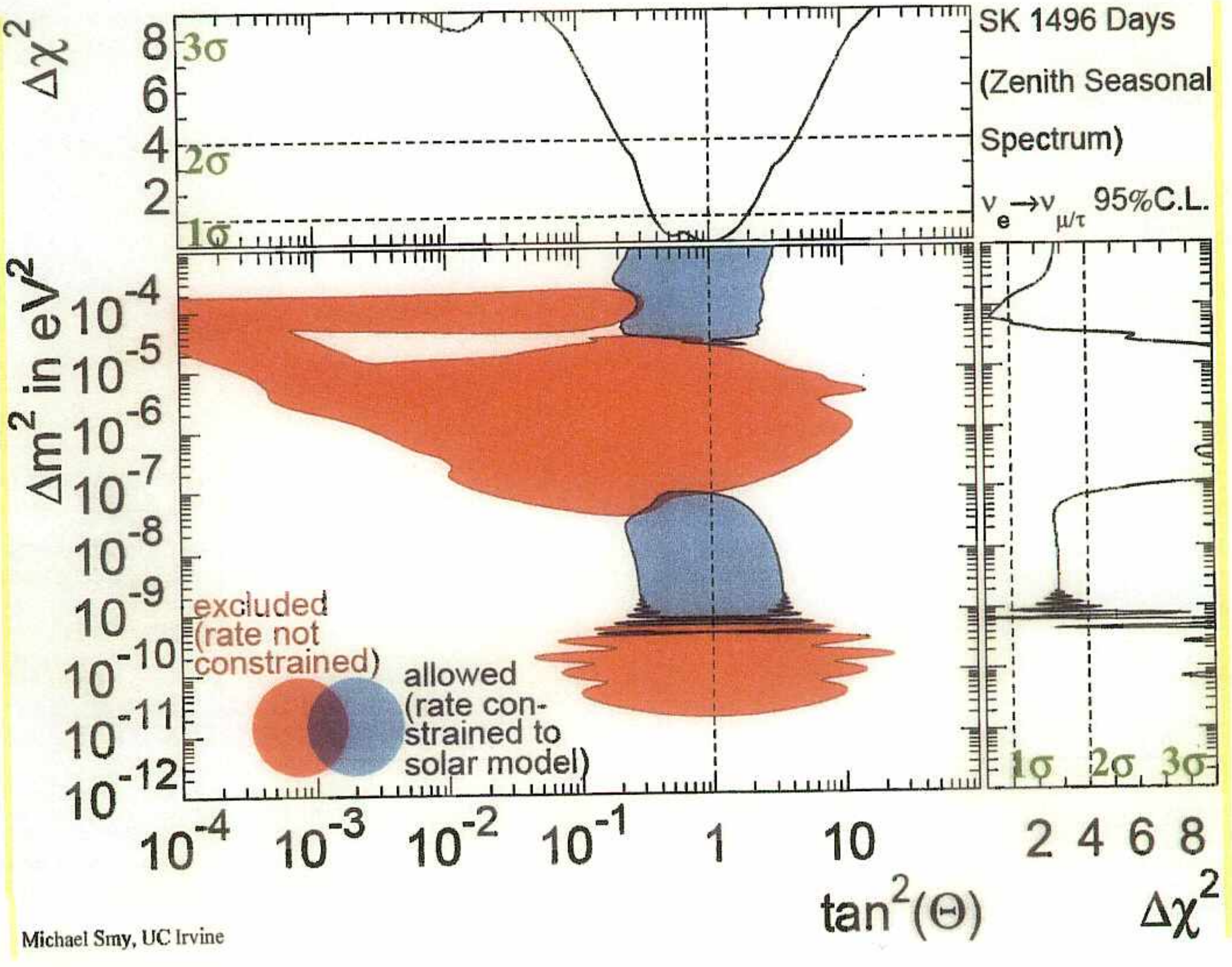

Michael Smy, UC Irvine

Combined analysis with all solar ν experiments

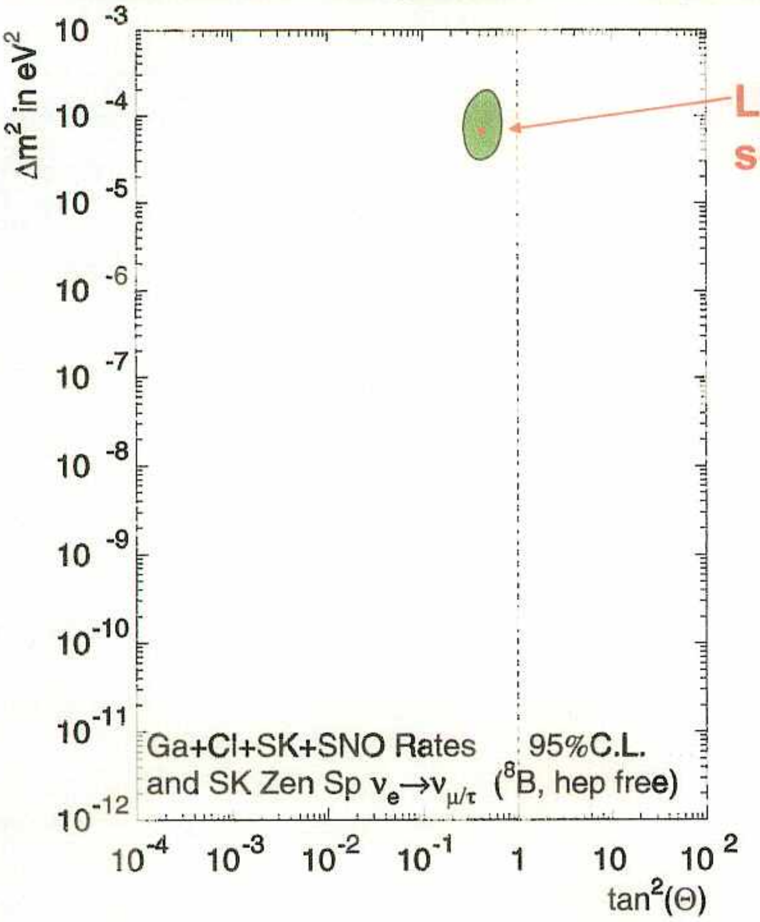

LMA is the only solution with 98% C.L.

Phys.Lett.B539(2002)179.

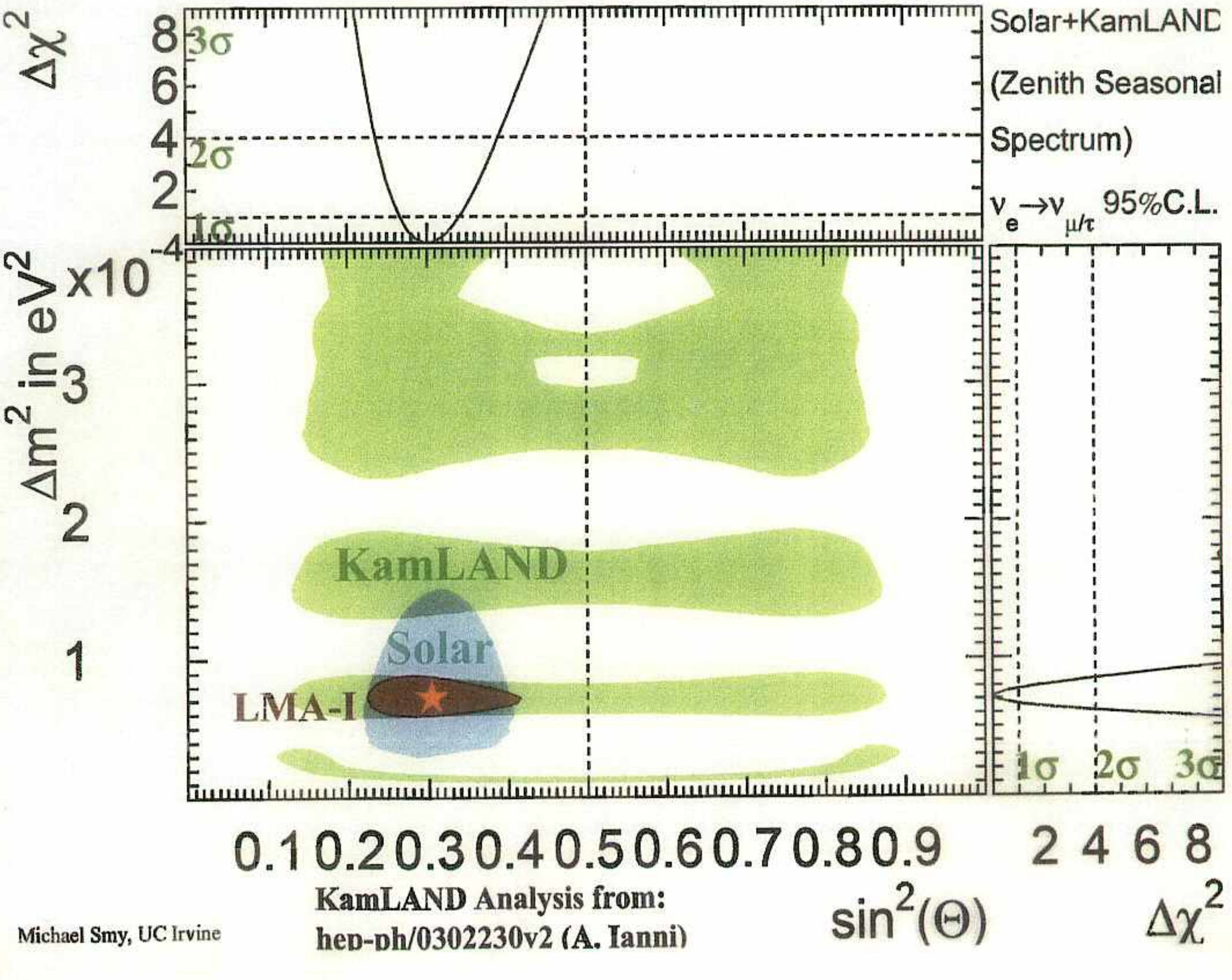

KamLAND Analysis from:
hep-ph/0302230v2 (A. Ianni)

⑨

Recent results from

KamLAND

KamLAND Schematics

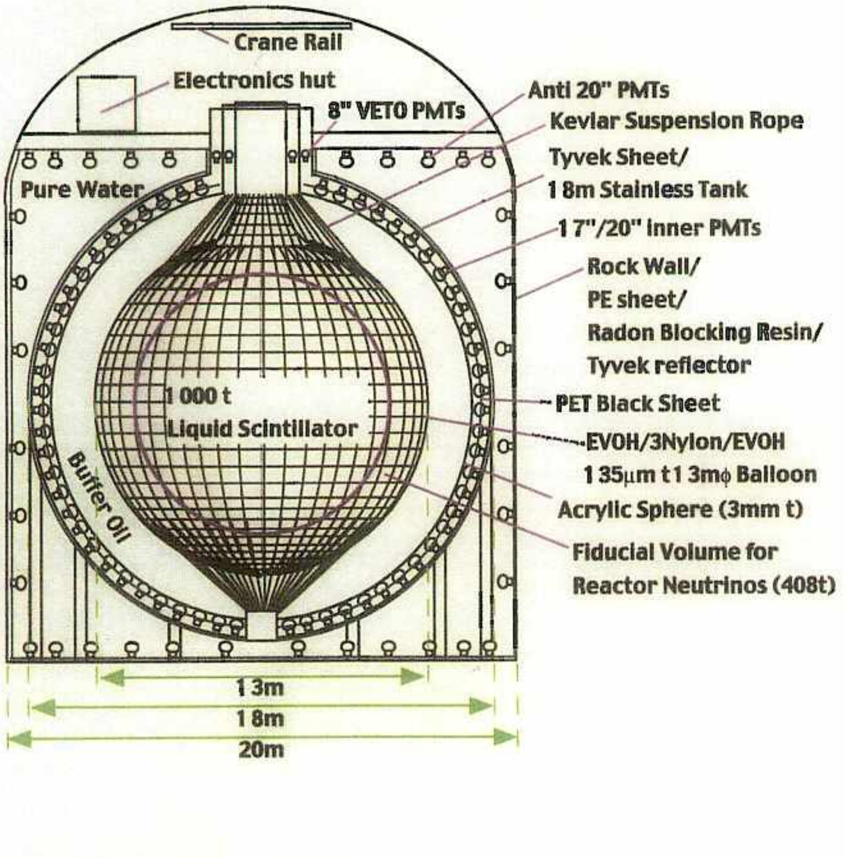

Liquid Scintillator

20% PseudoCumene
80% dodecane
1.5g/l PPO
8,000 photons/MeV
L=10 m @400 nm
ρ_{LS}=0.780 g/cm^3

Buffer Oil

50% dodecane
50% isoparaffin
ρ_{LS}/ρ_{BO}=1.0004

PMTs

1325 17"PMTs σ~1 nsec
22% coverage
(554 20"PMTs σ~5 nsec)
(34% coverage)

Energy Resolution

σ/E ~ 7.5%/√E (MeV) ~320p.e./MeV
(σ/E ~ 6%/√E (MeV)) (~500p.e./MeV)

Vertex Resolution

σ~25 cm @1 MeV

KL-1

KL-5

Detector

KL-6

80% of contribution comes from reactors located at ~200km from Kamioka.

If adopted for oscillation search

$$P=1-\sin^2 2\theta \sin^2(1.27\Delta m^2 L/E_\nu)$$
$$= \pi/2$$

Typical distance 175km
Typical energy 5MeV

→ Sensitive @ $\Delta m^2 \sim 4x10^{-5}eV^2$

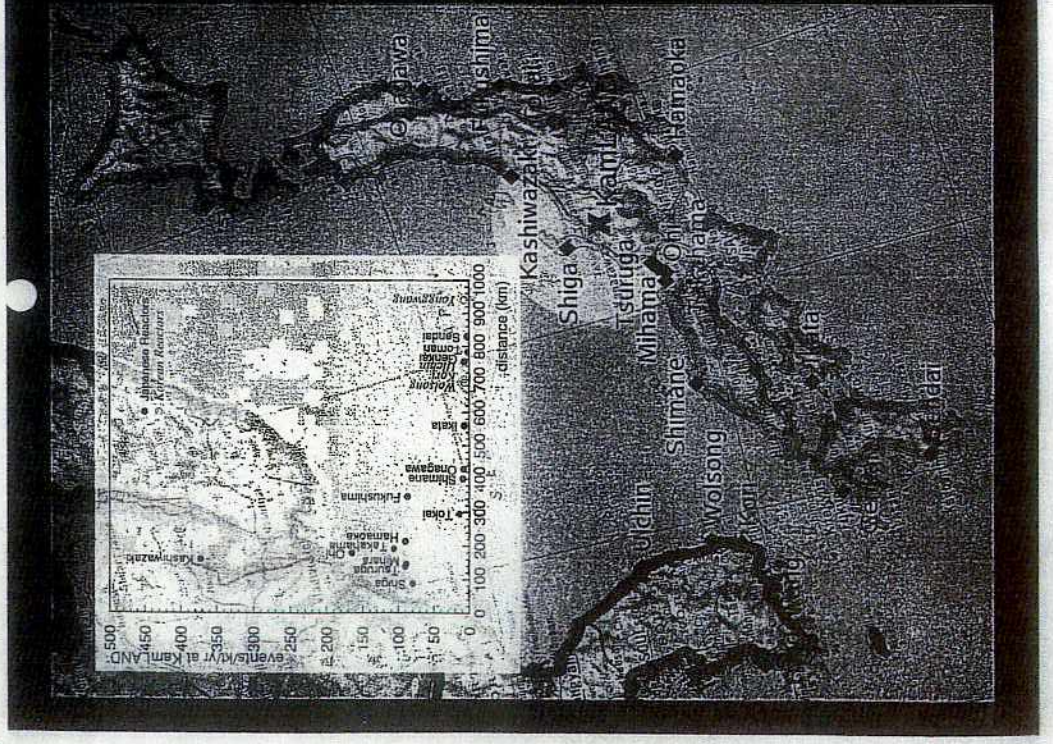

KL-7

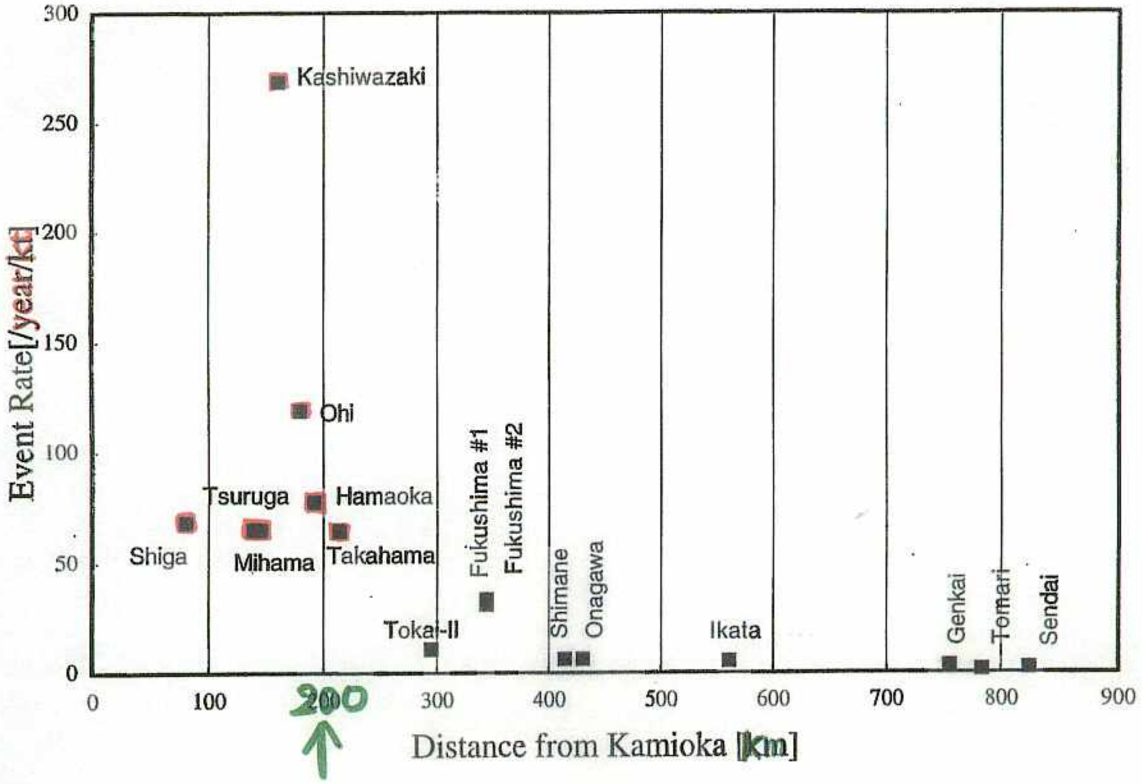

KL-8

Total man-made thermal output with nuclear power reactors in the world amounts to ~1.1 TW.

Japan	152 GW
Asia w/o Japan	60 GW
Europe	521 GW
North America	333 GW
Others	11 GW

It corresponds to 2×10^{23} anti electron neutrino creation / sec.

70 GW (7% of world total) is generated at 175±30 km distance from Kamioka site.

This high population provides $5 \times 10^{6}/cm^{2}/sec$ of neutrino flux at Kamioka and it is measurable amount with an O(kiloton) underground detector.

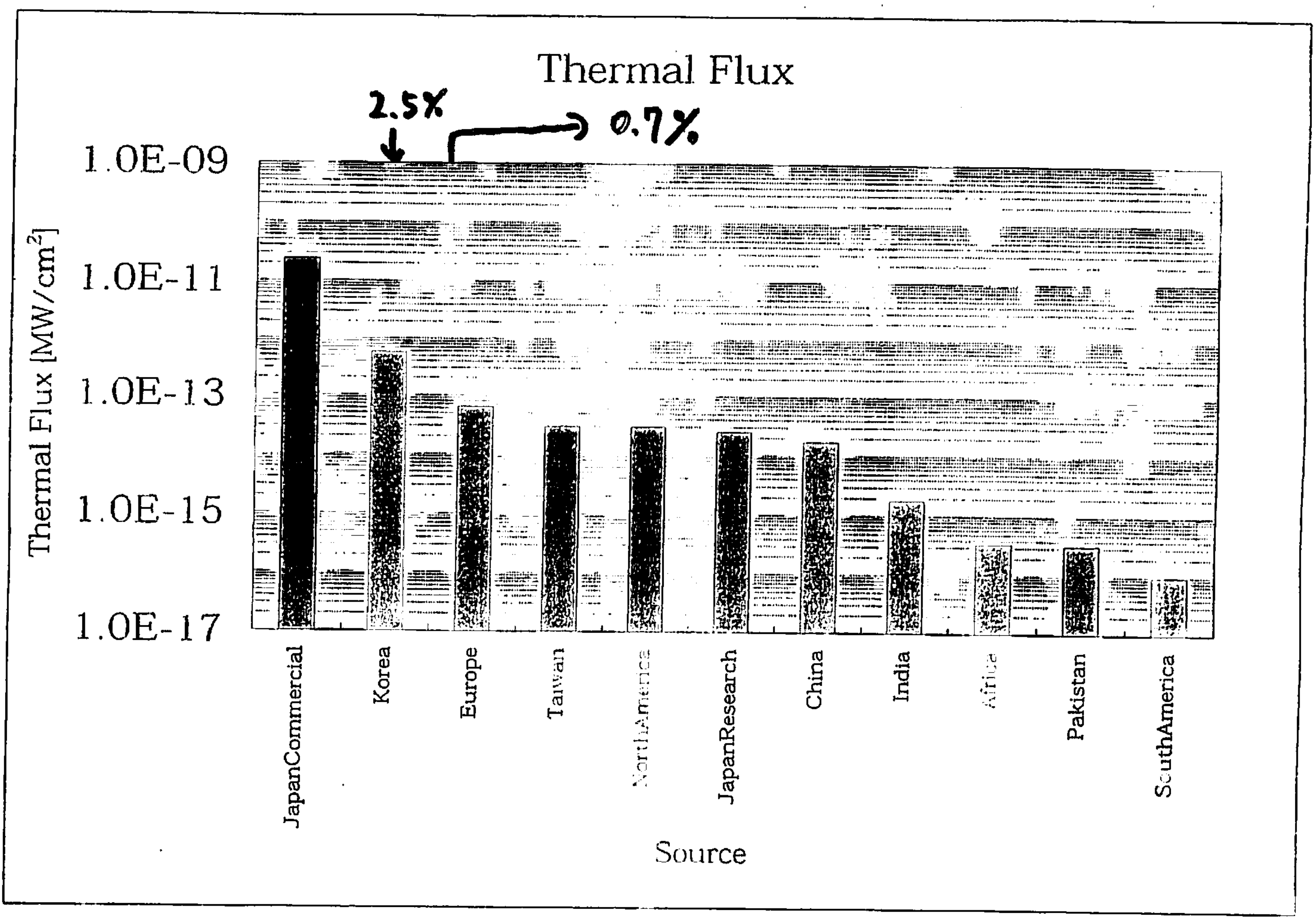

KL-9

Fission Rate

Only 4 fissile nuclei contribute to reactor power outputs.

^{235}U	201.8 MeV
^{238}U	205.0 MeV
^{239}Pu	210.3 MeV
^{241}Pu	212.6 MeV

Normalization to the total fission rate is well defined by the measured at much better than level.

Contribution of each nuclei evolves as fuel burns (burn up effect). can be accurately calculated knowing history of thermal power, fraction of new fuel and ^{235}U enrichment.
Systematic error to the neutrino event rate is much smaller than .

KL-10

KL-11

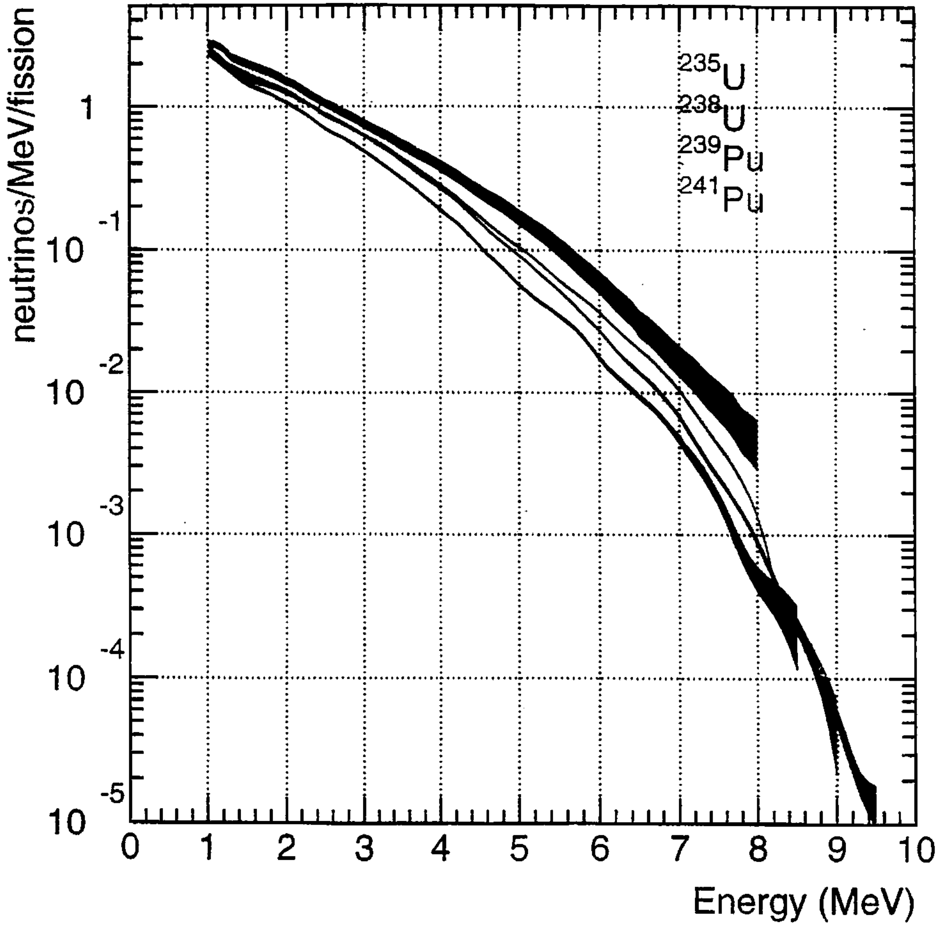

KL-12

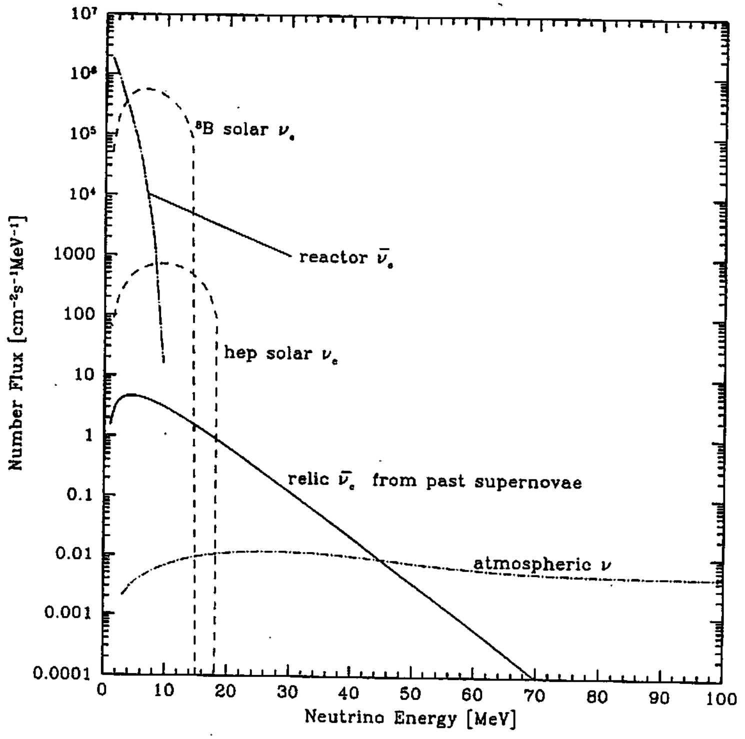

Figure 4:

KL-14

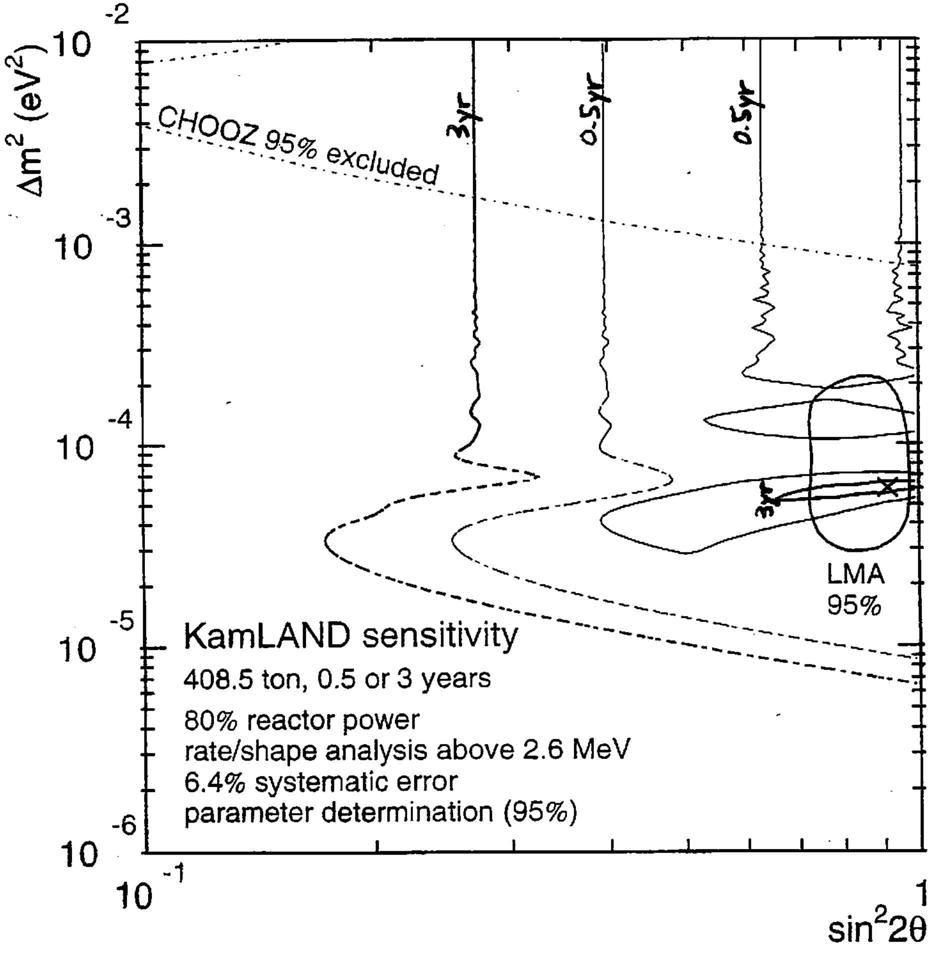

KamLAND sensitivity
408.5 ton, 0.5 or 3 years
80% reactor power
rate/shape analysis above 2.6 MeV
6.4% systematic error
parameter determination (95%)

KL-15

Clear 2 fold delayed coincidence Signature

$\bar{\nu}_e + p \to e^+ + n \quad \Rightarrow \quad n + p \to D + \gamma\,(2.22437\,MeV)$

Capture time 210 μsec (KamLAND)

Theoretical uncertainty of neutrino cross section calculation is only 0.2% for the entire reactor neutrino energy spectrum.

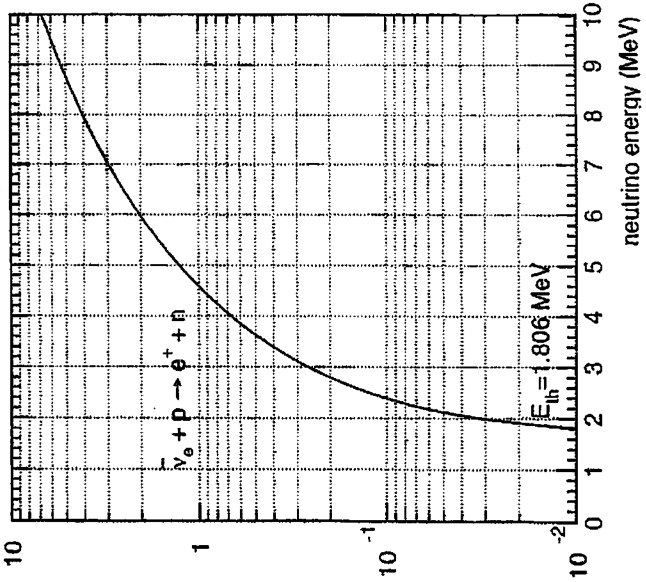

Order(1/M) calculation

P.Vogel and J.F.Beacom hep-ph/9903553

Outer Radiative Correction

A.Kurylov, M.J.Ramsey-Musolf and P.Vogel

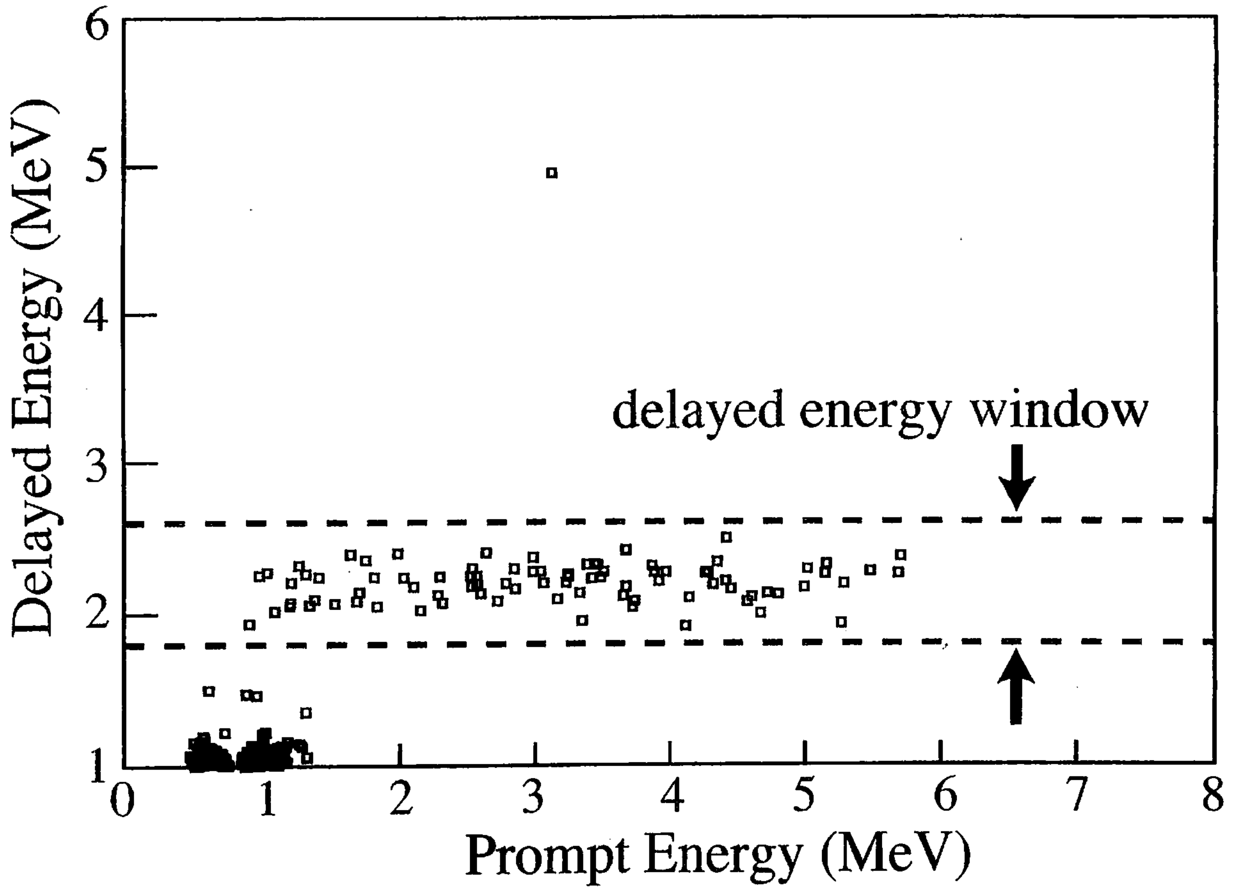

Delayed Energy (MeV)
1
2
3
4
5
6
delayed energy window
0
1
2
3
4
5
6
7
8
Prompt Energy (MeV)

KL-16

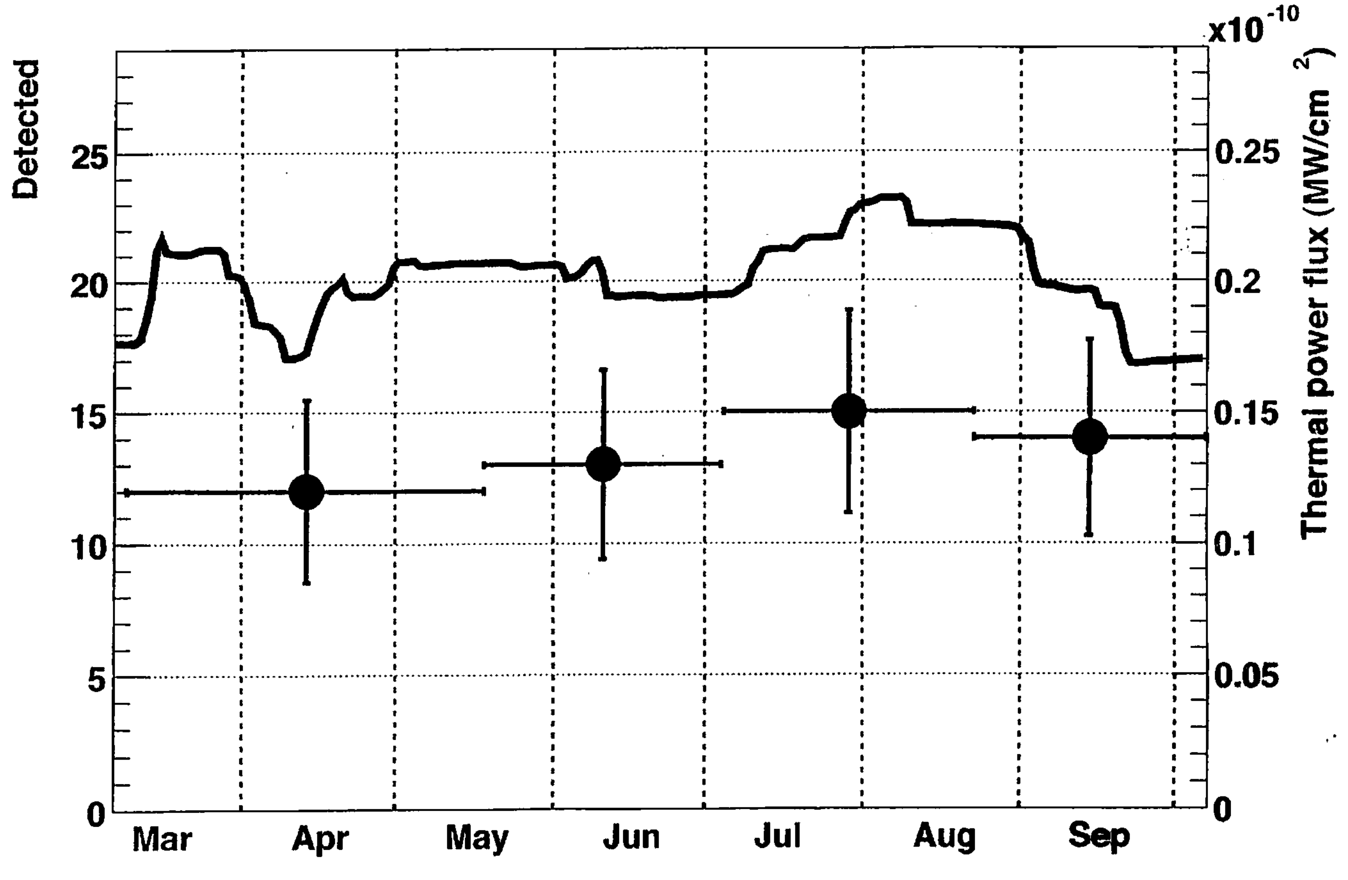

Detected
0
5
10
15
20
25
x10^-10
Thermal power flux (MW/cm 2)
0
0.05
0.1
0.15
0.2
0.25
Mar
Apr
May
Jun
Jul
Aug
Sep

KL-17

Data Summary

from March 4 through October 6, 2002
(145.1 live days)

E_{prompt} > 2.6 MeV

Expected neutrino: 86.8±5.6
Expected BG: 0.95±0.99
Observed: 54

R=0.611±0.085(stat)±0.041(syst)

99.95% CL. disappearance

E_{prompt} > 0.9 MeV

Expected neutrino: 124.8±7.5
Expected BG: 2.91±1.12 (+ ~9 geo-nu)
Observed: 85

R=0.586

KL-18

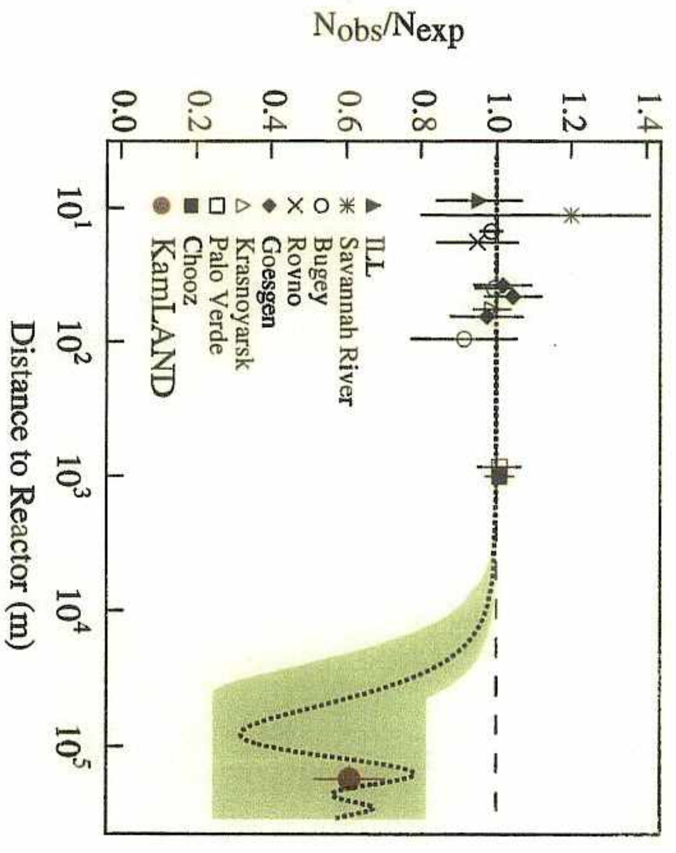

KL-17

KL-30

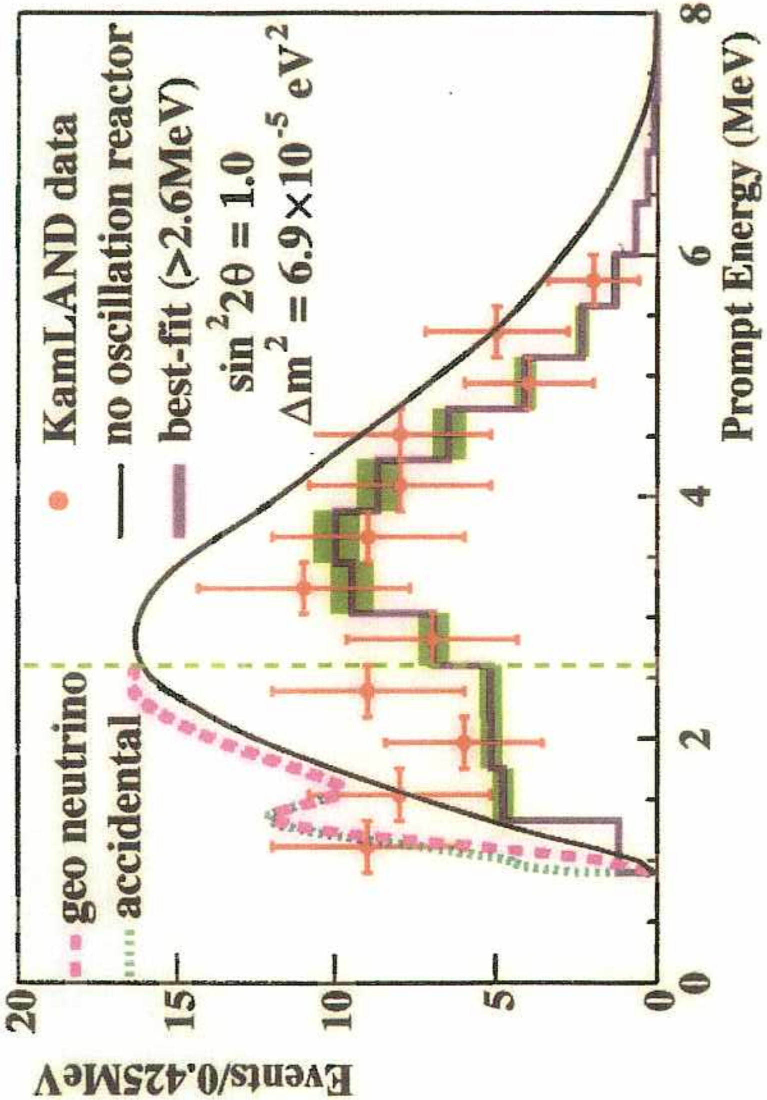
KamLAND data
no oscillation reactor
best-fit (>2.6MeV)
$\sin^2 2\theta = 1.0$
$\Delta m^2 = 6.9\times10^{-5}$ eV^2
geo neutrino
accidental
Events/0.425MeV
Prompt Energy (MeV)
0
5
10
15
20
0
2
4
6
8

KL-32

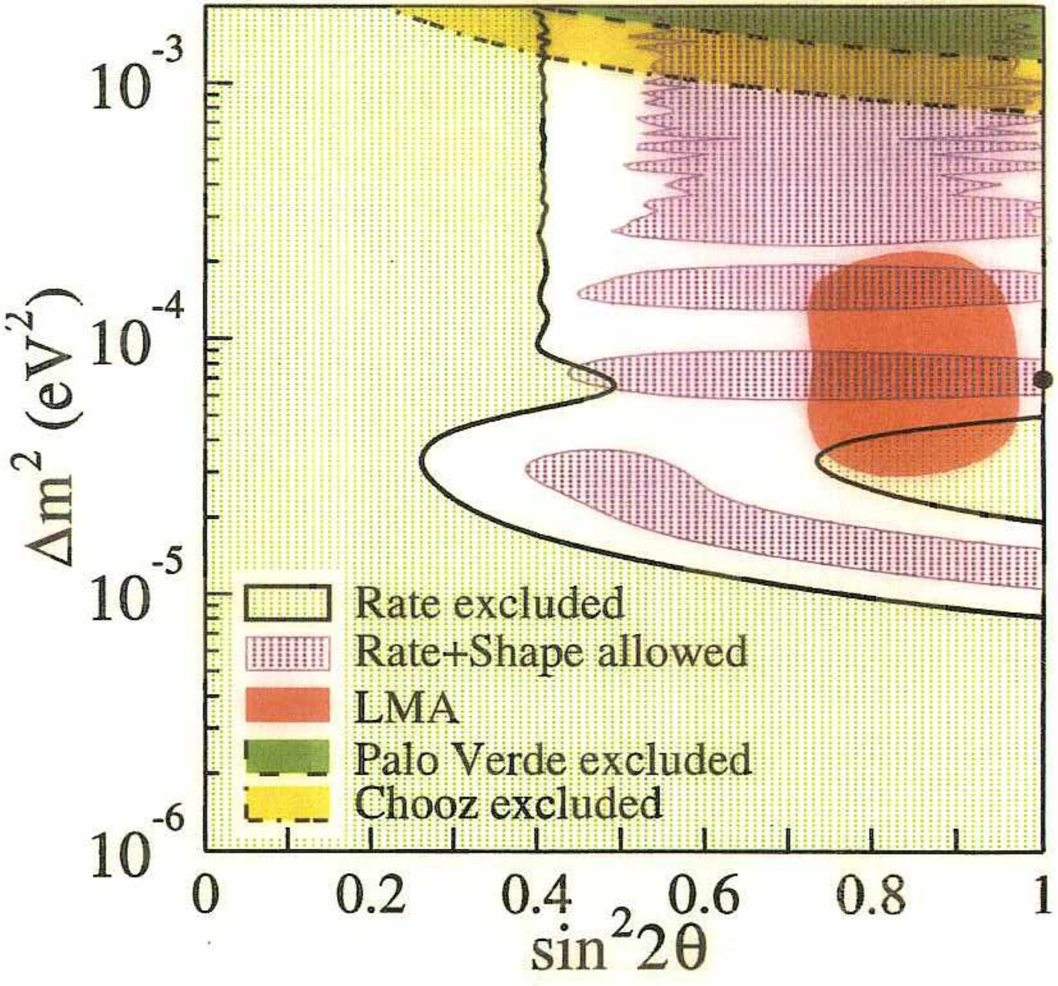
Δm^2 (eV^2)
10^{-3}
10^{-4}
10^{-5}
10^{-6}
$\sin^2 2\theta$
0
0.2
0.4
0.6
0.8
1
Rate excluded
Rate+Shape allowed
LMA
Palo Verde excluded
Chooz excluded

⑩

Other reactor ν experiments

Reactor ν experiments

$\overline{\nu_e}$: energy ～数 MeV

したがって $\Delta m^2 \simeq 3 \times 10^{-3}\, eV^2$ とすると

$$L_\nu = 2.5m \times \frac{E}{\Delta m^2}$$

～ 1 km 位になる。

Long baseline reactor experiment

通常 $\overline{\nu_e}$ は $\overline{\nu_e} + P \Rightarrow e^+ + n$

$\hookrightarrow$ capture on Gd $\rightarrow \gamma$

$P \rightarrow 2.2 MeV$

でとらえる。

$$\sigma(\overline{\nu_e} P) = 0.88 \times 10^{-43}\, E_e \cdot P_e\ cm^2$$

$$E_e = E_\nu - (m_n - m_p) = E_\nu - 1.3 MeV$$

σ は $\nu_e e^-$ の約 100 倍

CHOOZ, Palo Verde, Kam-Land

C. Bemporad (PAl0, 1010)

CHOOZ

ackground : ~2.5 events/day

Data taking : 1997 spring ~

Results will be published in a few months.

Palo Verde

750m away

● detector

↓ 46 m.w.e.

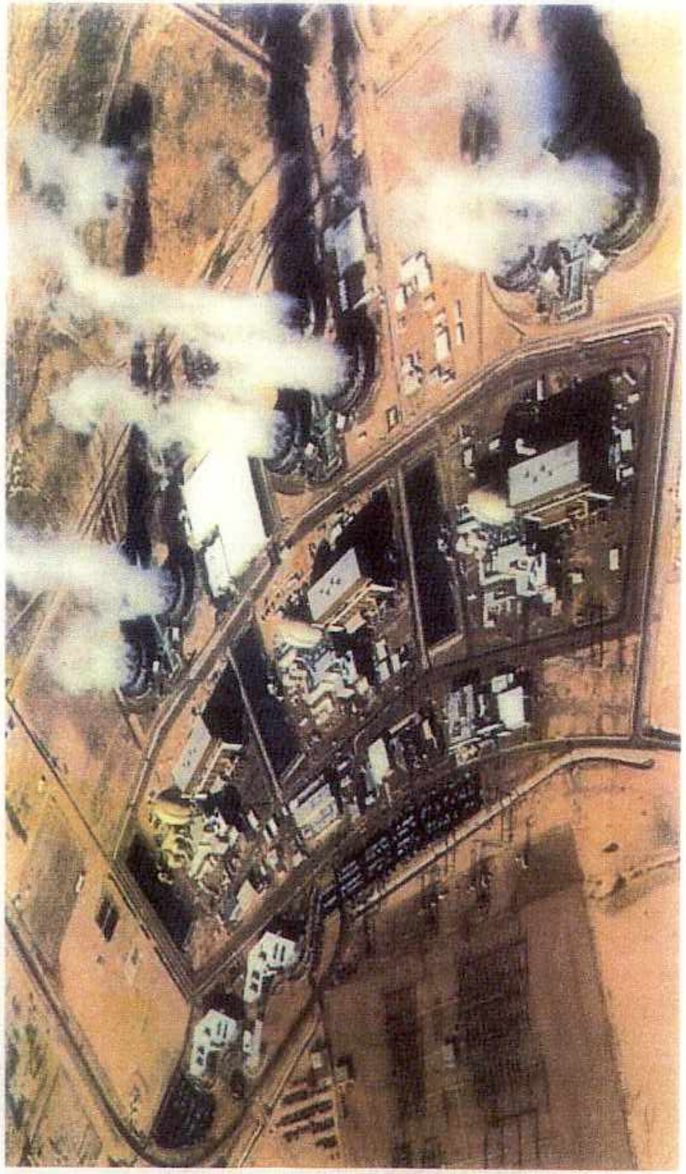

3×3.6GWth

Y.Wang (PA10, 1011)

Palo Verde

46 m.w.e.

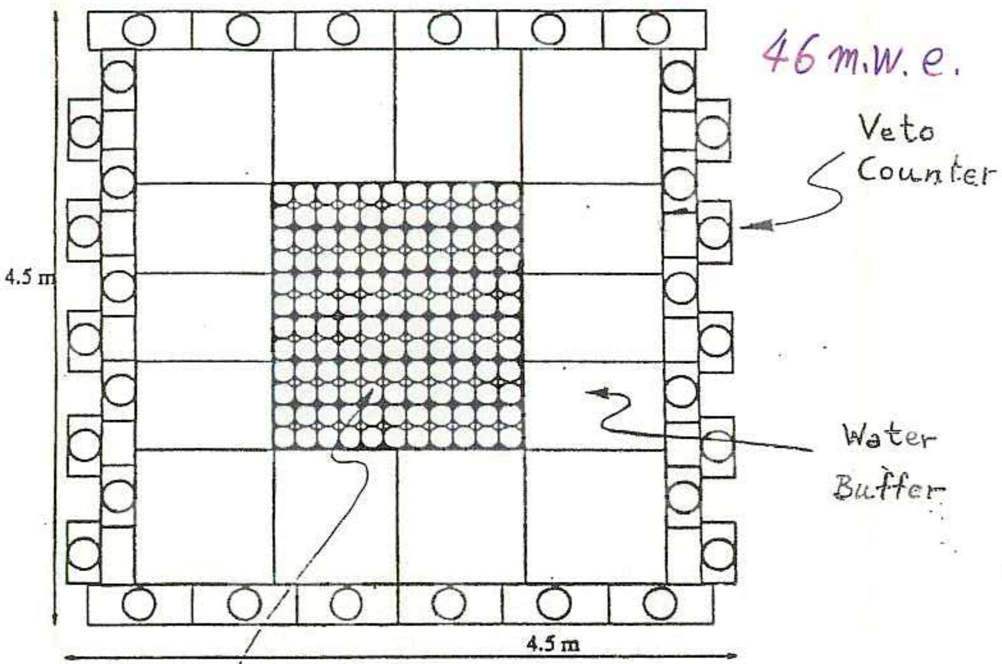

Central detector 9m × 66 modules
(12tons liq. scinti. total)
with 0.1% Gd

event rate ~50 ev./day (20% eff.)

4 fold coincidence :

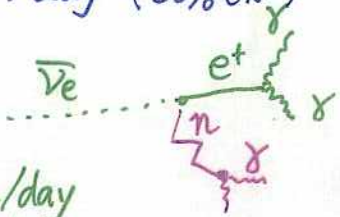

Background : ~50 ev./day
(correlated : 34 ev./day
uncorrelated : 15 ev/day)

Start data taking in fall 1997.

162

① TARGET

$\bar{\nu}_e + p \to e^+ + n$
$n + Gd$

0.1%

Gd LOADED SCINTILLATOR

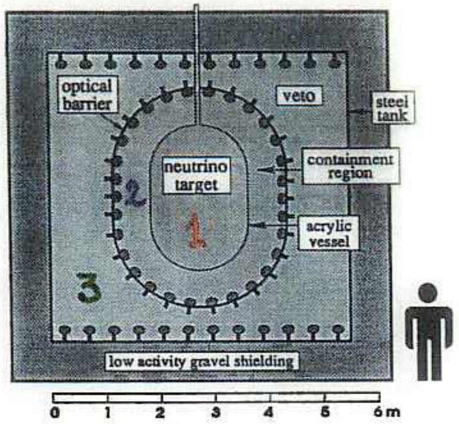

CHOOZ PARAMETERS

Region 1 size:	180 cm x 280 cm
Region 2 size:	320 cm x 420 cm
Region 1 volume, cu. m	5.6
Region 2 volume, cu. m	19.6
Region 3 volume, cu. m	105
Total volume, cu. m	131
Region 1 mass, tons	4.7
Region 2 mass, tons	16.7
Region 3 mass, tons	90
Total mass, tons	111
No. of PMT's viewing target	192
PMT coverage	15 %
Photoelectrons/MeV	125
Energy resolution @ 1 MeV σ_E/E	12 %

"CALORIMETER"

100 Positron Events

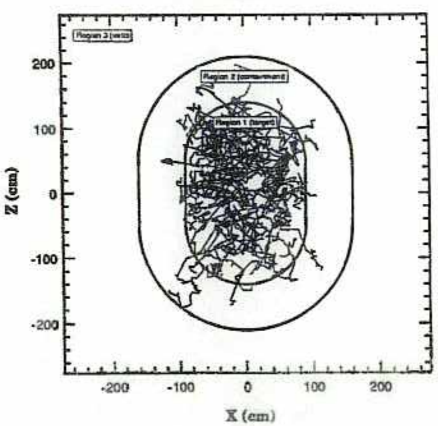

100 Gd Neutron Capture Events

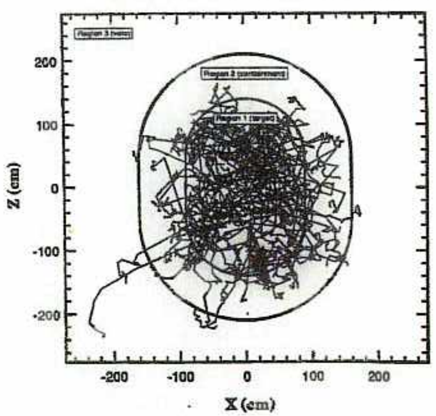

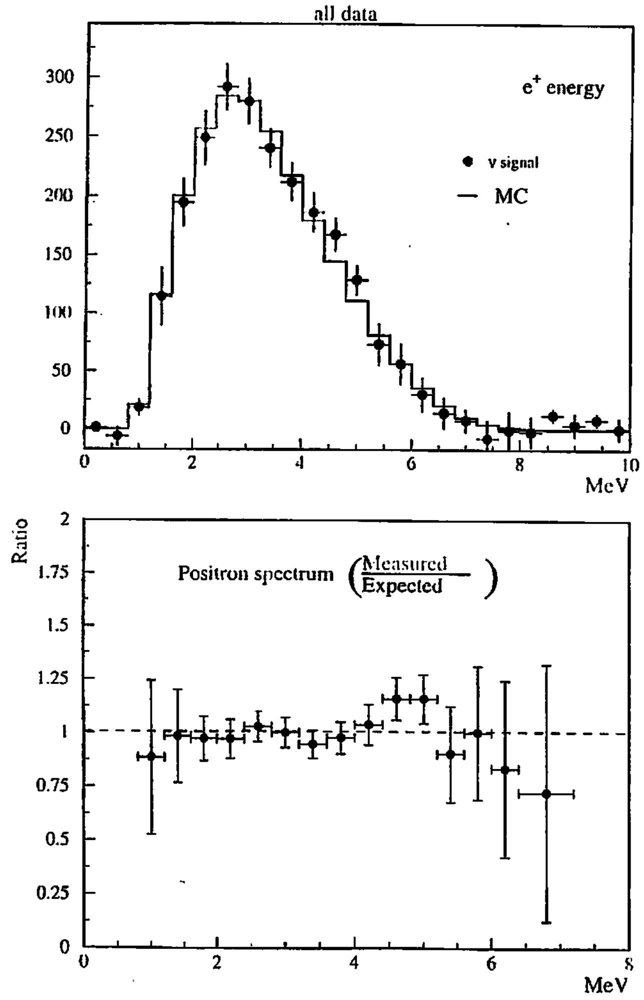

Figure 7: (above) Expected positron spectrum for the case of no oscillations, superimposed on the measured positron spectrum obtained from the subtraction of reactor-ON and reactor-OFF spectra; (below) measured vs. expected ratio. The errors shown are statistical.

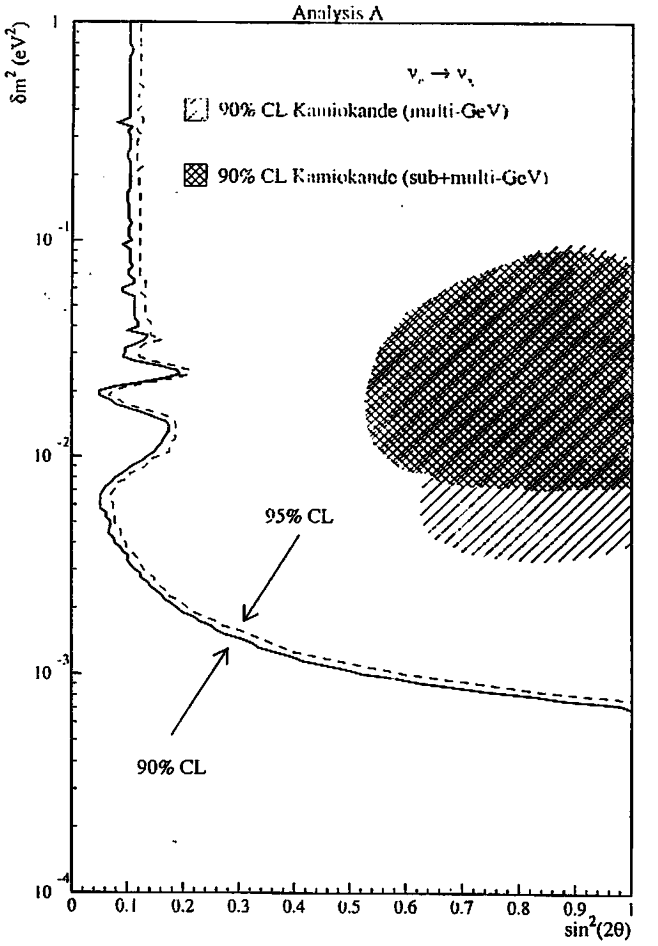

Figure 9: Exclusion plot for the oscillation parameters based on the absolute comparison of measured vs. expected positron yields.

Assume $m_3^2 \gg m_1^2 \simeq m_2^2$

$\Delta m^2 \simeq \Delta m_{13}^2 \simeq \Delta m_{23}^2$, $\Delta m_{12} \simeq 0$

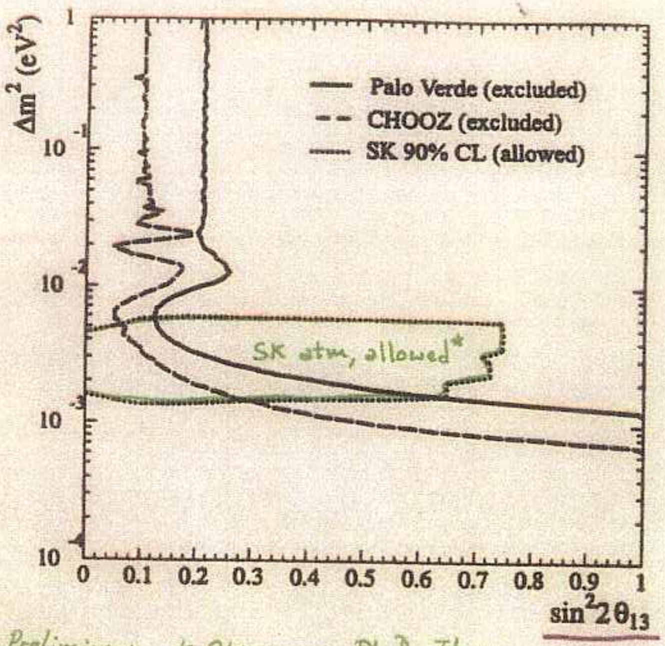

* Preliminary, K. Okumura PhD Thesis
U. of Tokyo

⑪

Short base line accelerator experiments

LSND

KARMEN

Mini BooNE

LSND and KARMEN

Neutrino source:
High intensity low energy
(800 MeV) proton beam
into beam stop target.

Small $\overline{\nu}_e$ flux

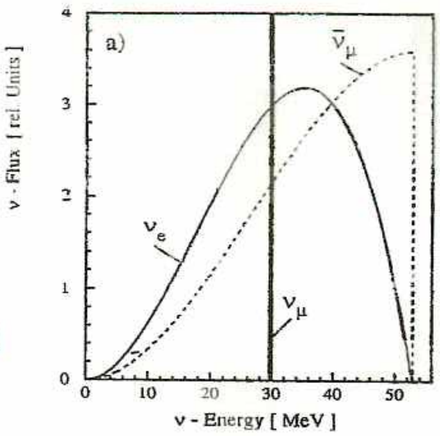

	LSND	KARMEN
Accelerator	LAMPF	ISIS
Proton E	800 MeV	800 MeV
Proton current	~ 1mA	~ 0.2 mA
Beam pulse	500 μsec	2×100nsec
Detector	liquid scintillator + ch~~a~~erenkov	liquid scintillator (segmented)
Mass	180 tons	56 tons
Distance from source	29 m	17 m
Angle to beam axis	17 deg.	90 deg.

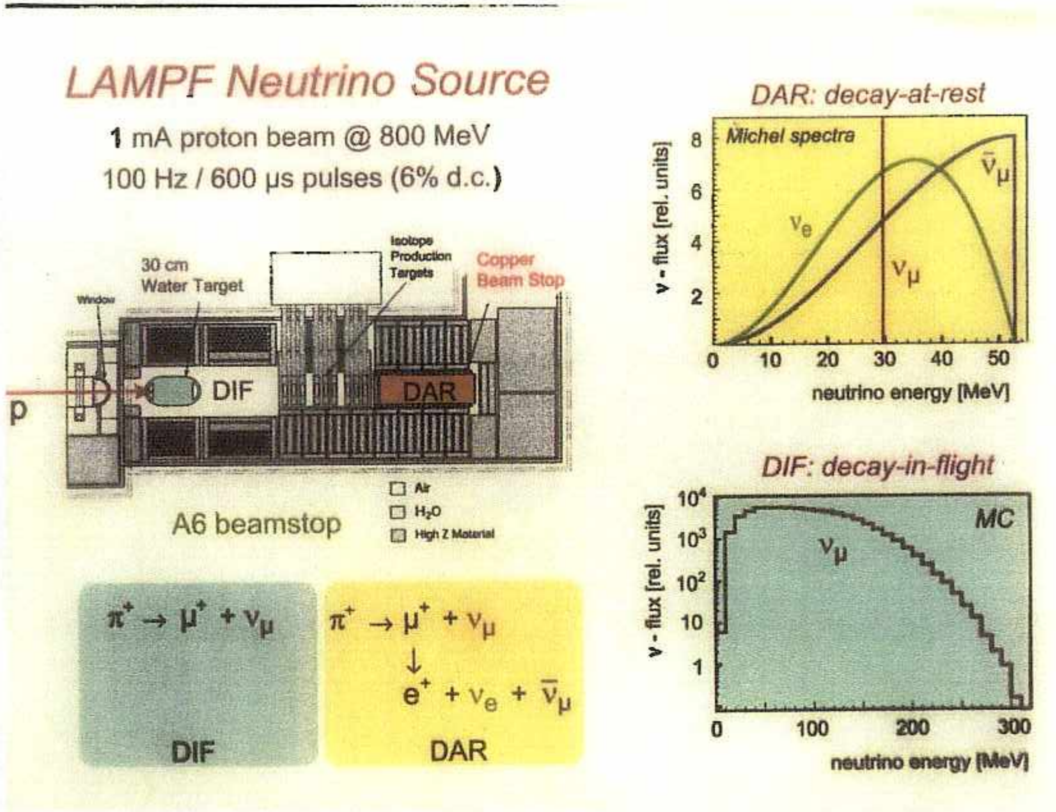

LAMPF Neutrino Source

1 mA proton beam @ 800 MeV

100 Hz / 600 μs pulses (6% d.c.)

DIF

$\pi^+ \to \mu^+ + \nu_\mu$

DAR

$\pi^+ \to \mu^+ + \nu_\mu$

$\downarrow$

$e^+ + \nu_e + \bar{\nu}_\mu$

$\overline{\nu_\mu} \to \overline{\nu_e}$ search in LSND

(LSND collaboration, Phys.Rev.C54, 2685 (1996))

$\overline{\nu_\mu}$ from decay at rest (DAR)

LAMPF neutrino beam

$P(800\mathrm{MeV}) \xrightarrow{89\%} \pi^+ \xrightarrow[\text{DIF}]{3\%} \mu^+\nu_\mu \longrightarrow e^+\nu_e\overline{\nu_\mu}$

$\pi^+ \xrightarrow[\text{DAR}]{97\%} \mu^+\nu_\mu \longrightarrow e^+\nu_e\overline{\nu_\mu}$

$P(800\mathrm{MeV}) \xrightarrow{11\%} \pi^- \xrightarrow[\text{DIF}]{5\%} \mu^-\overline{\nu_\mu} \xrightarrow{12\%} e^-\boxed{\overline{\nu_e}}\nu_\mu$

$\mu^-\overline{\nu_\mu} \xrightarrow{88\%} \text{captured } \nu_\mu$

$\pi^- \xrightarrow{95\%} \text{stop (absorbed)}$

$\overline{\nu_e}/\overline{\nu_\mu}=7.8\times10^{-4}$ (NIM A291,621(1990),A368, 416(1996))

signature: $\overline{\nu}_e + p \to \underline{e^+} + n$

$n + p \to d\underline{\gamma}$ (2.2 MeV)

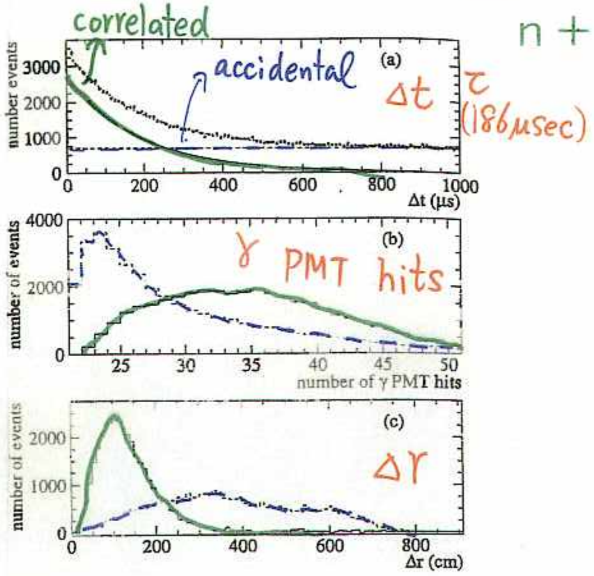

$L = P(\text{hits}) \times P(\Delta r) \times P(\Delta t)$

$$R = \frac{L(\text{correlated})}{L(\text{accidental})}$$

LSND

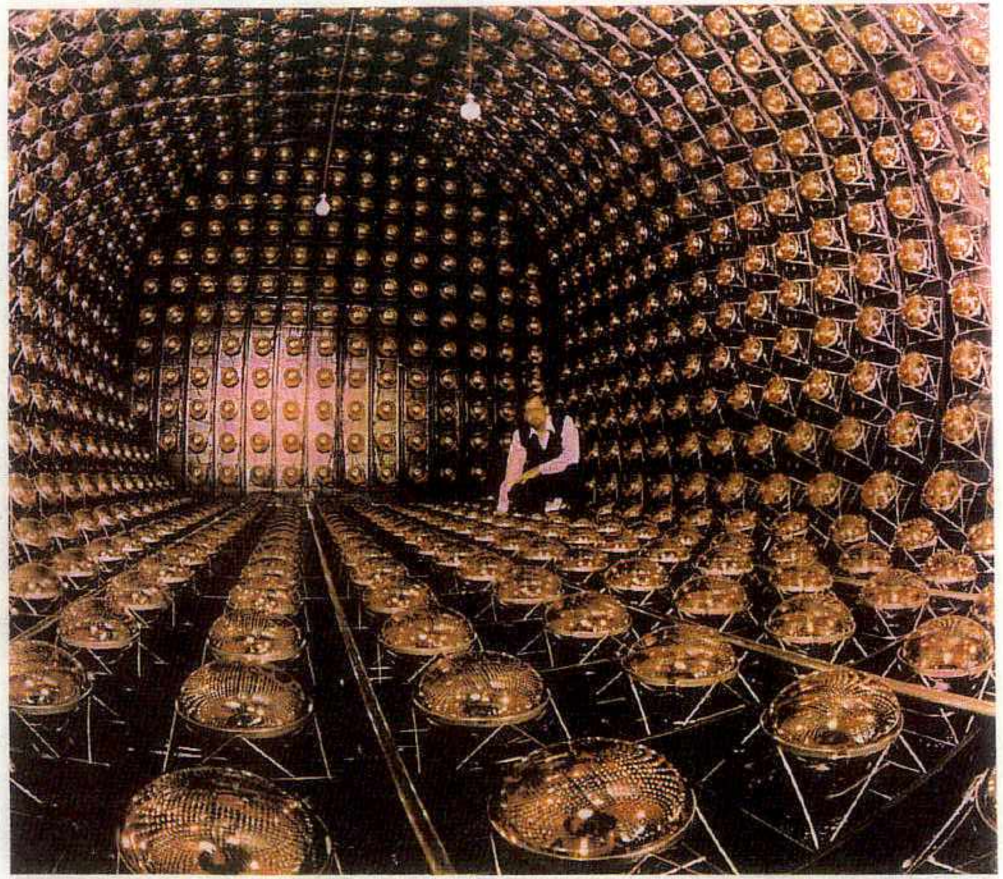

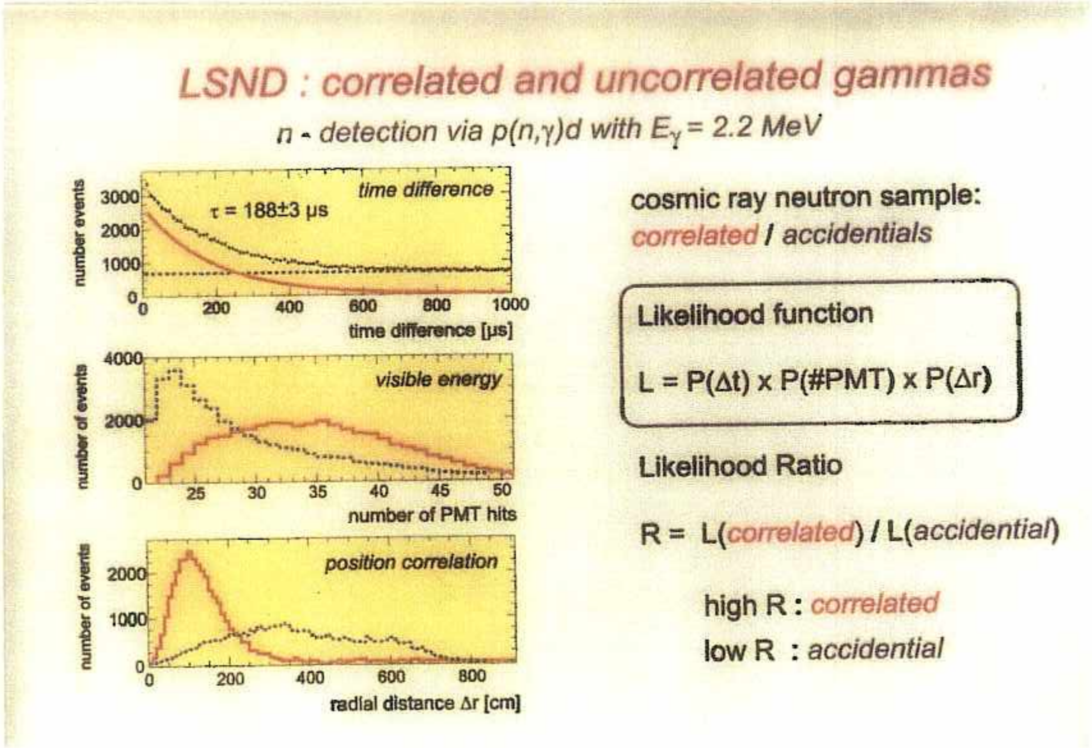

LSND : correlated and uncorrelated gammas

n - detection via p(n,γ)d with $E_\gamma = 2.2$ MeV

cosmic ray neutron sample:
correlated / *accidentials*

Likelihood function

L = P(Δt) x P(#PMT) x P(Δr)

Likelihood Ratio

R = L(*correlated*) / L(*accidential*)

high R : *correlated*
low R : *accidential*

SB-5

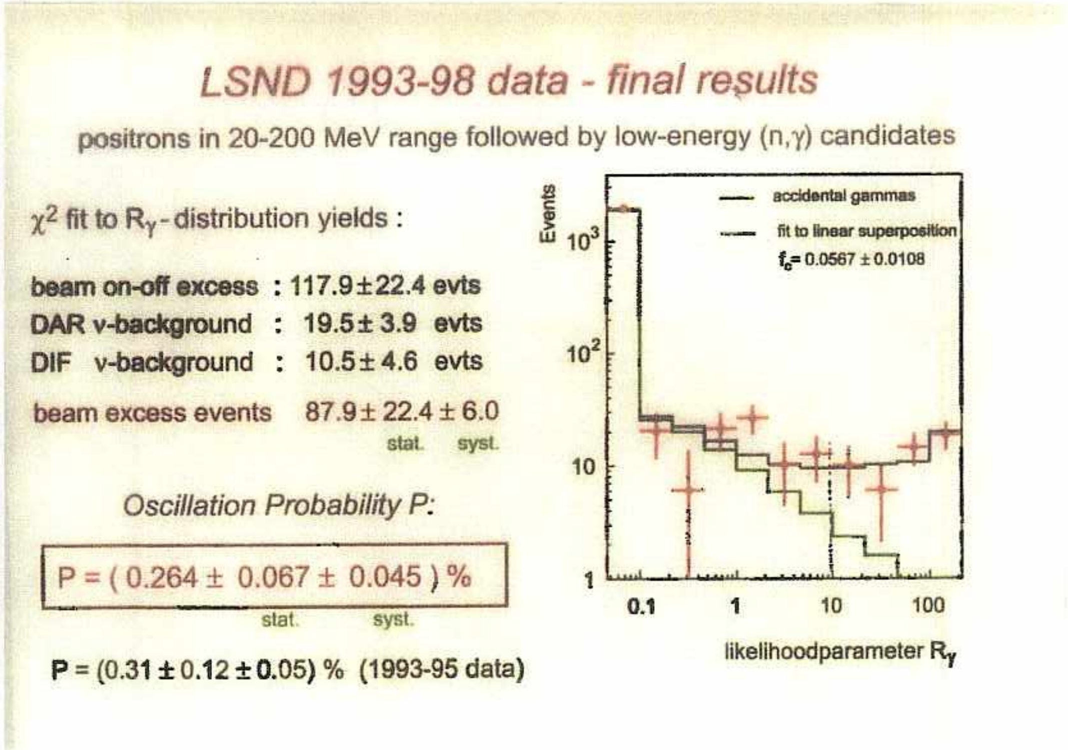

LSND 1993-98 data - final results

positrons in 20-200 MeV range followed by low-energy (n,γ) candidates

χ^2 fit to R_γ - distribution yields :

beam on-off excess : 117.9±22.4 evts
DAR ν-background : 19.5±3.9 evts
DIF ν-background : 10.5±4.6 evts
beam excess events 87.9±22.4±6.0
stat. syst.

Oscillation Probability P:

P = (0.264 ± 0.067 ± 0.045) %
stat. syst.

P = (0.31±0.12±0.05) % (1993-95 data)

SB-6

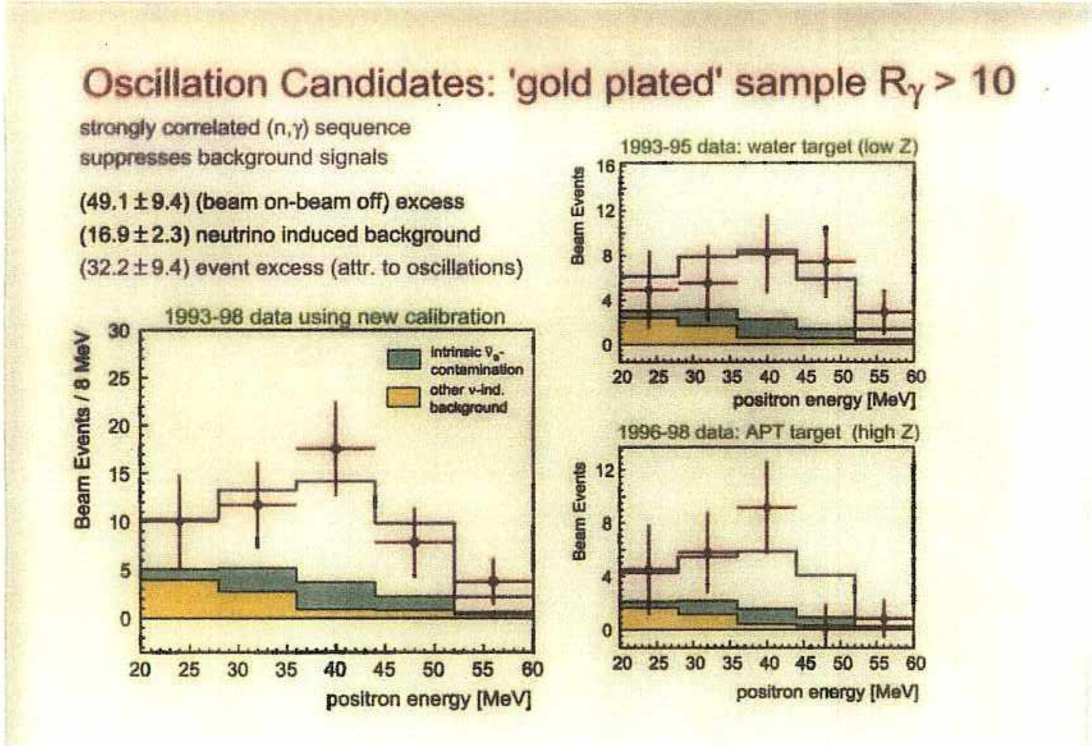

Oscillation Candidates: 'gold plated' sample $R_\gamma > 10$

strongly correlated (n,γ) sequence
suppresses background signals

(49.1±9.4) (beam on-beam off) excess
(16.9±2.3) neutrino induced background
(32.2±9.4) event excess (attr. to oscillations)

LSND event based maximum likelihood analysis

A. Aguilar et al. (LSND Collab.), Phys. Rev. **D64** (2001) 112007

LSND favoured regions (90%CL)

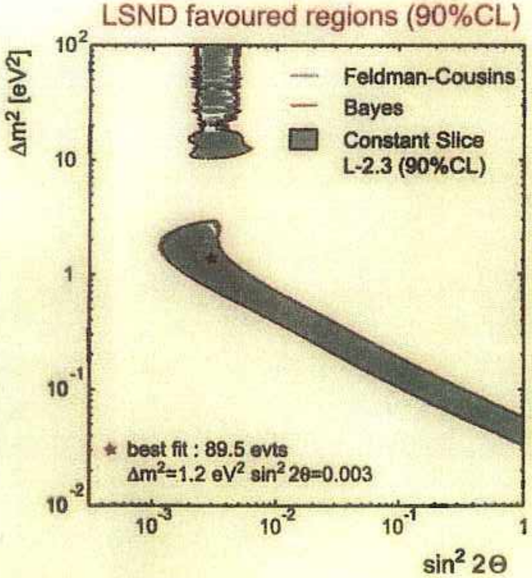

5697 candidate events
with 4 fit variables (3600 bins) :

electron energy E_e
scattering angle $\cos \Theta_\nu$
distance along axis z
likelihood ratio R_γ

'combined' LSND likelihood
contour for DAR *and* DIF data

electron energy range : 20-200 MeV

global $\bar{\nu}_\mu$ - $\bar{\nu}_e$ *and* ν_μ - ν_e analysis

---

ISIS Spallation Neutron Source

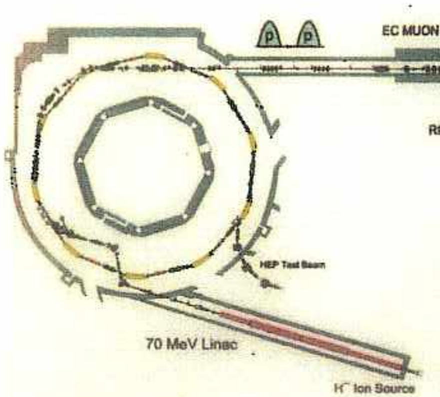

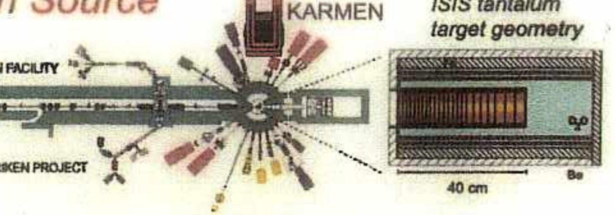

DAR: $\pi^+ \rightarrow \mu^+ + \nu_\mu$, $\mu^+ \downarrow e^+ + \nu_e + \bar{\nu}_\mu$

ISIS rapid cycling synchrotron
800 MeV protons
200 μA current
50 Hz extraction
10^{-5} duty cycle
6.4×10^{-4} $\bar{\nu}_e$ contamination

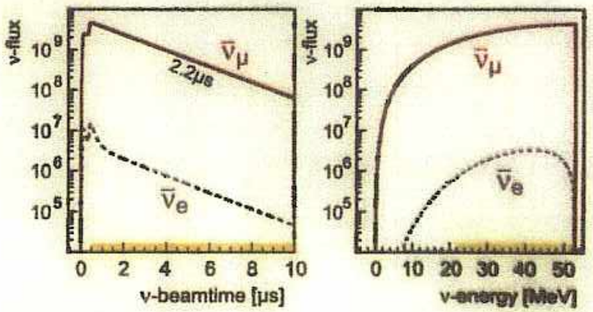

ν - production at ISIS

$$\pi^+ \to \mu^+ + \nu_\mu \qquad \tau_\pi = 26\text{ ns}$$

$$\downarrow$$

$$e^+ + \nu_e + \bar{\nu}_\mu \qquad \tau_\mu = 2.2\ \mu\text{s}$$

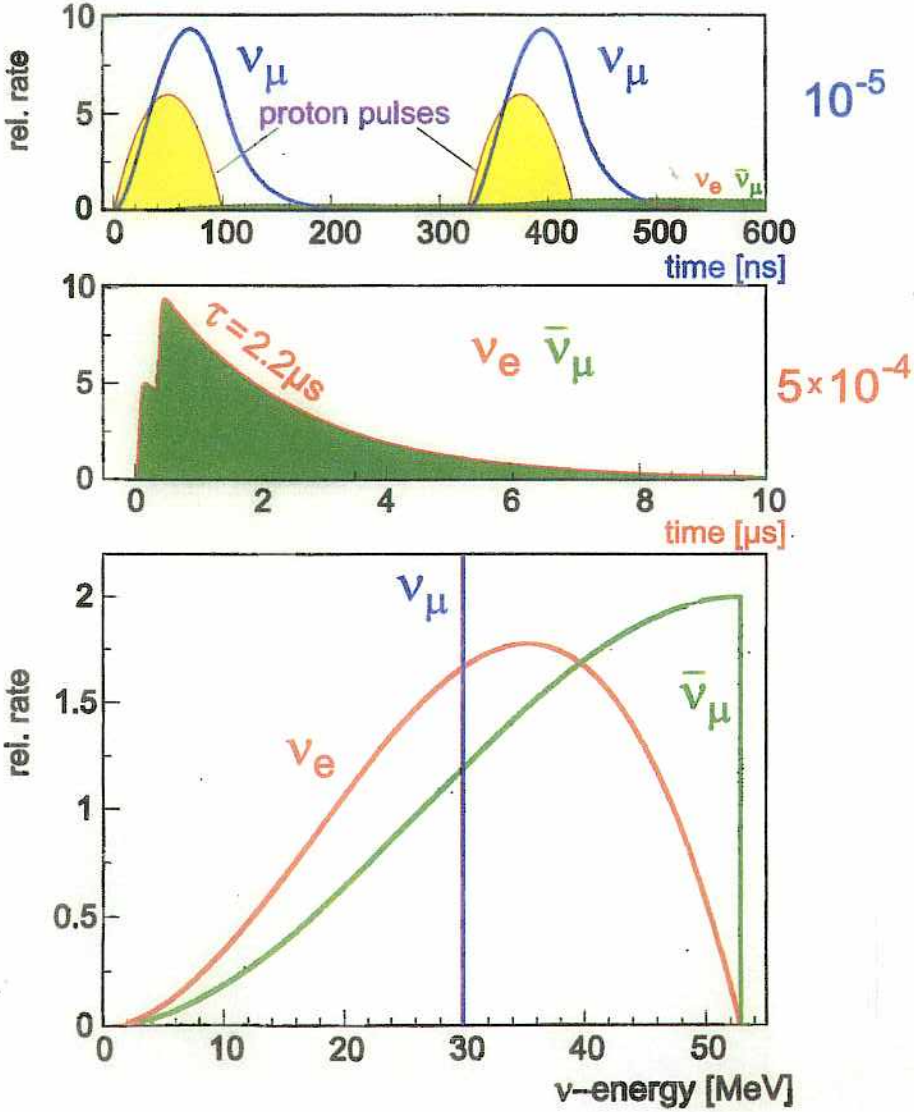

KARMEN detector

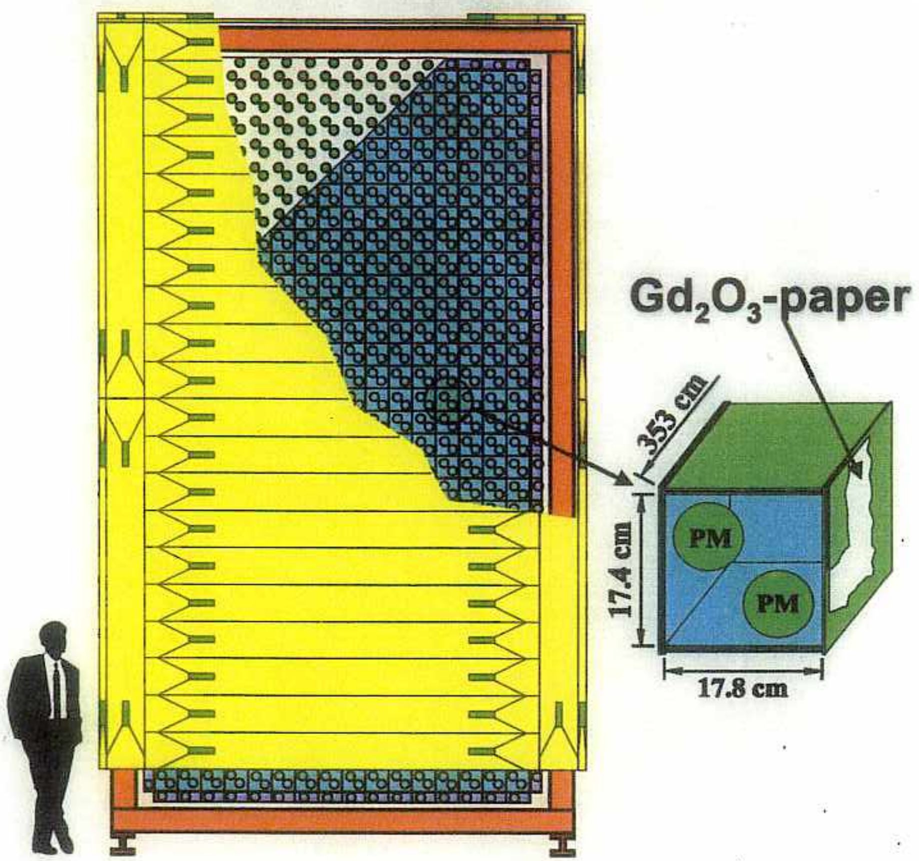

96% active volume of ^{12}C and p

$$\sigma_E = \frac{11.5\%}{\sqrt{E[\text{MeV}]}} \qquad \Delta t_{ISIS} \leq \pm 2\text{ns}$$

$\bar{\nu}_\mu \to \bar{\nu}_e$ oscillation signature

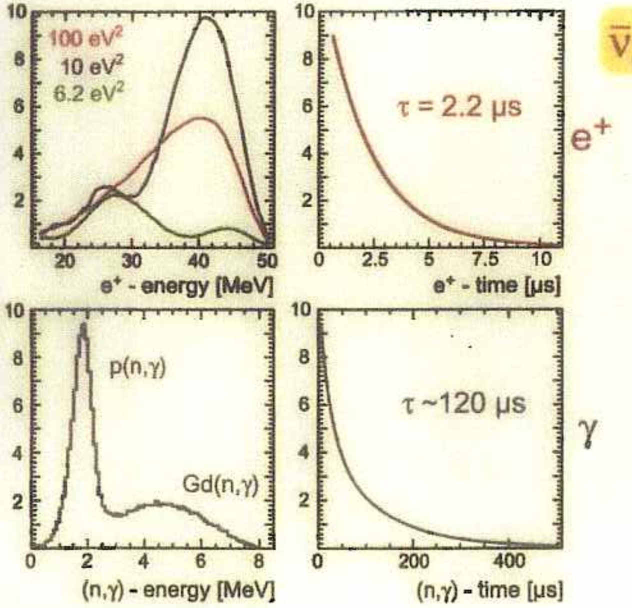

$\bar{\nu}_e + p \to n + e^+$

Q = -1.8 MeV

therm. + capt.

→ Gd(n,γ)

$\Sigma E_\gamma = 8$ MeV

→ p(n, γ)

$E_\gamma = 2.2$ MeV

spatially correlated delayed coincidence

$\langle\sigma\rangle = 0.93 \times 10^{-40}$ cm^2

final KARMEN2 candidate event ensemble

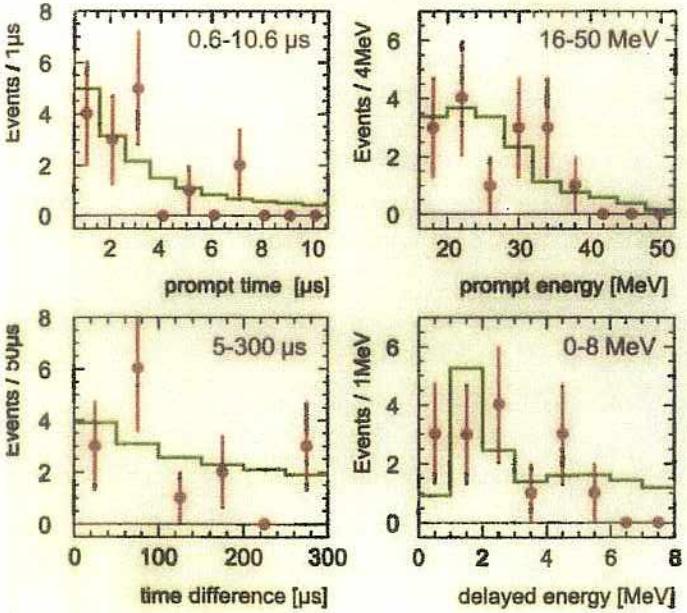

15 candidate events

(15.8 ± 0.5) background events are expected

cosmic background : 3.9 ± 0.2 evts
ν_e-induc. excl. CC : 5.1 ± 0.2 evts
ν_e-ind. CC & rand. γ : 4.8 ± 0.3 evts
intrin. contamination : 2.0 ± 0.2 evts

no oscillation excess

Final KARMEN2 limit and final LSND regions

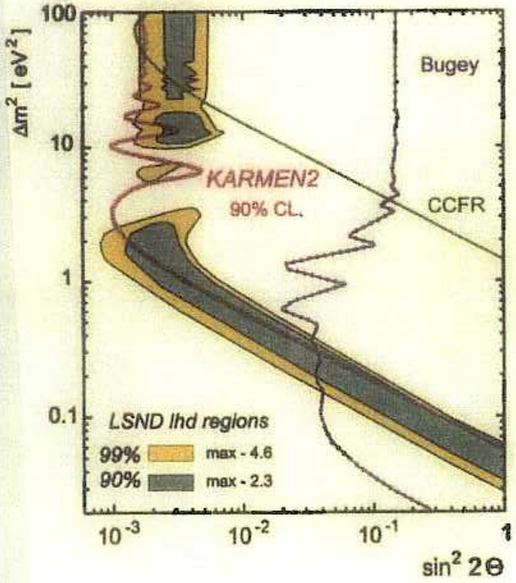

4y KARMEN2 data taking 2/97 - 2/02

unified (frequentist) approach Feldman-Cousins

oscillation limit :

$\sin^2 2\theta < 1.7 \times 10^{-3}$ (90% CL.)

large Δm^2

oscillation sensitivity :

$\sin^2 2\theta < 1.6 \times 10^{-3}$ (90% CL.)

KARMEN2 excludes a significant part of the LSND parameter space

---

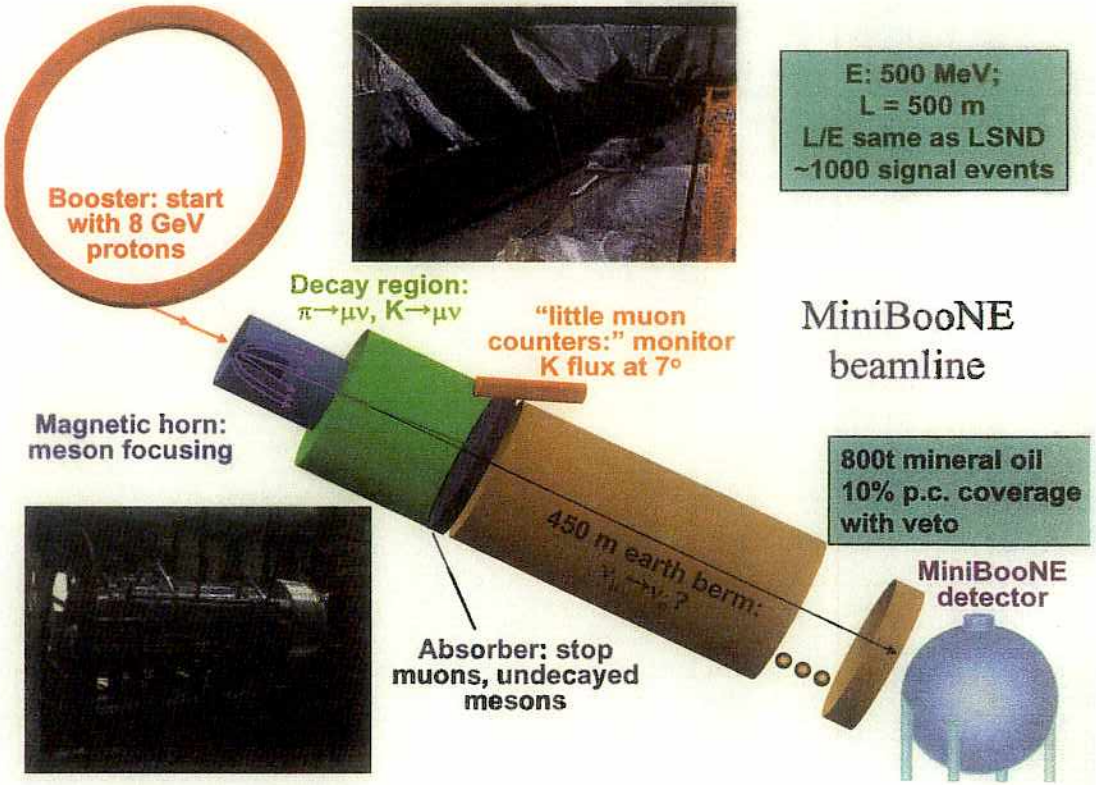

MiniBooNE beamline

E: 500 MeV;
L = 500 m
L/E same as LSND
~1000 signal events

Booster: start with 8 GeV protons

Decay region: $\pi \to \mu\nu$, $K \to \mu\nu$

"little muon counters:" monitor K flux at 7°

Magnetic horn: meson focusing

800t mineral oil
10% p.c. coverage
with veto

450 m earth berm: $\nu_\mu \to \nu_e$?

MiniBooNE detector

Absorber: stop muons, undecayed mesons

MiniBooNE Particle ID

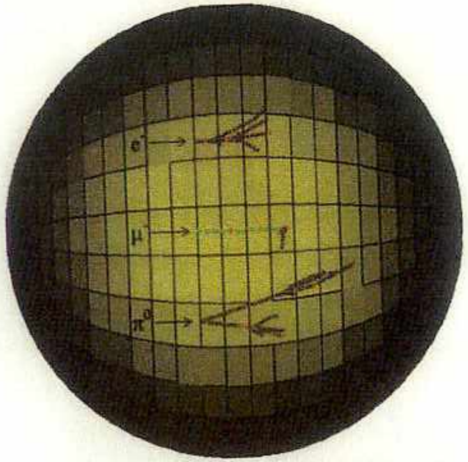

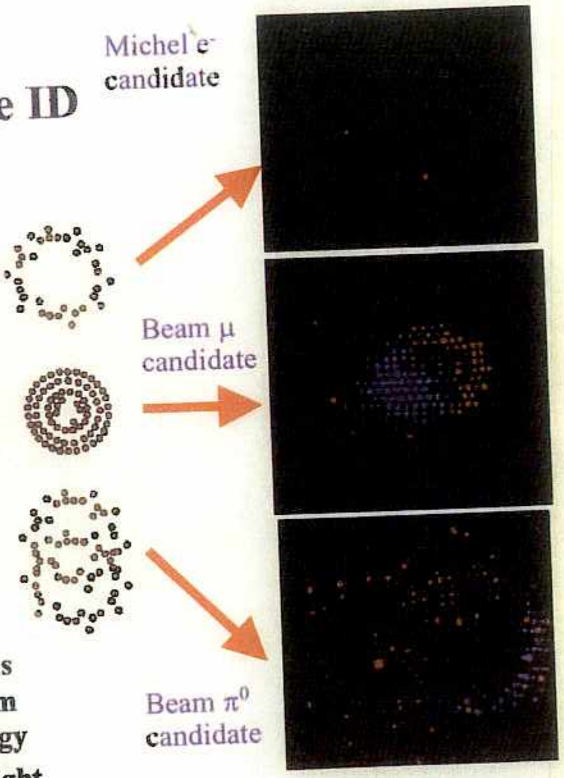

Identify electrons (and thus candidate ν_e events) from characteristic hit topology of mineral oil Cherenkov light

---

Overall MiniBooNE Status

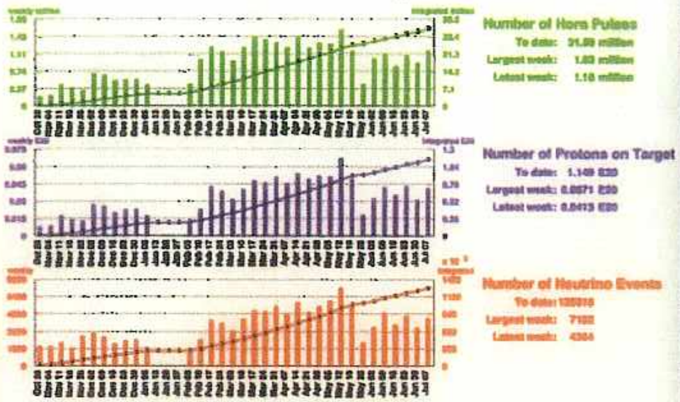

Steadily taking data

- **Currently at ~10% of $1x10^{21}$ POT goal**
- **Have collected >125,000 ν events**
- **Detector performing well**
- **Still need more beam!**

- Proton rate delivered by Booster has dramatically improved over time

- Further Booster upgrades in the works to reach intended rate
- Detector works beautifully!
- Expect first physics results in the Fall

173

⑫

3 (4) flavor
ν oscillation
MNS matrix

MNS matrix

Solar ν best fit $\tan^2\theta_{12} = 0.42$

$\theta_{12} = 33^\circ$

atmospheric ν $\sin^2 2\theta_{23} \simeq 1$

$\theta_{23} \simeq 45^\circ$

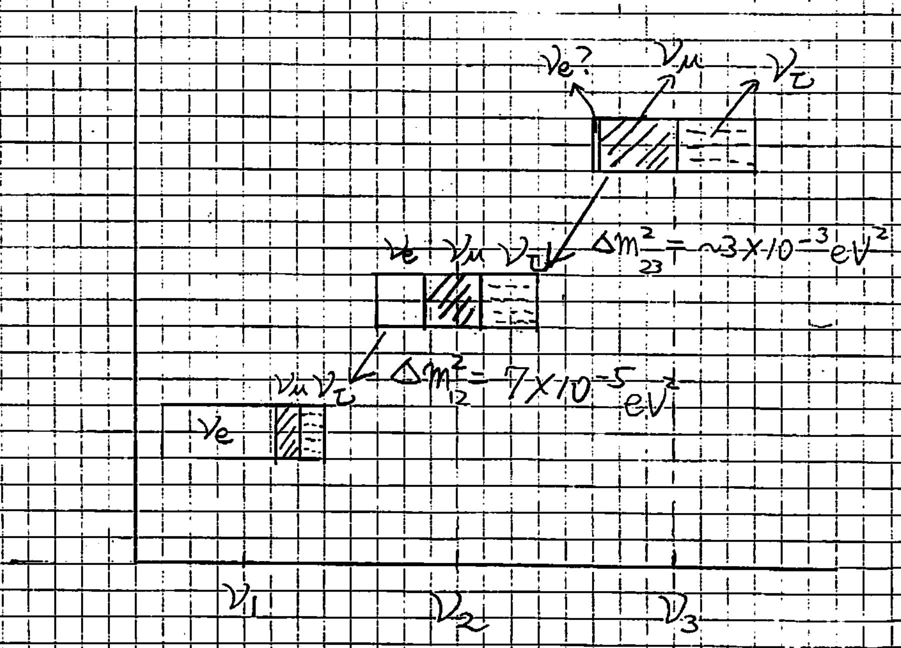

mass hierarcy を仮定すると

$m_3 \simeq \sqrt{\Delta m^2_{23}} = 0.05\,eV$

$m_2 = \sqrt{\Delta m^2_{12}} = 0.008\,eV$

大気ニュートリノも太陽ニュートリノも混合が大きい

- ニュートリノの混合はクォークに比べて何故こんなに大きいのか？
  - ニュートリノ

$$\begin{pmatrix} U_{e1} & U_{e2} & U_{e3} \\ U_{\mu 1} & U_{\mu 2} & U_{\mu 3} \\ U_{\tau 1} & U_{\tau 2} & U_{\tau 3} \end{pmatrix} =$$

0.74-0.90	0.45-0.65	< 0.16
0.22-0.61	0.46-0.77	0.57- $1/\sqrt{2}$
0.14-0.55	0.36-0.68	$1/\sqrt{2}$- 0.82

Fukugita, Tanimoto, PL B515(2001)30

  - クォーク

$$\begin{pmatrix} U_{d1} & U_{d2} & U_{d3} \\ U_{s1} & U_{s2} & U_{s3} \\ U_{b1} & U_{b2} & U_{b3} \end{pmatrix} =$$

0.974- 0.976	0.219- 0.226	0.002- 0.005
0.219- 0.225	0.973- 0.975	0.037- 0.043
0.004- 0.014	0.035- 0.043	0.9990- 0.9993

Particle Data Group, EPJ C15(2000)1

53

MNS-2

- **MNS(Maki-Nakagawa-Sakata) Matrix**

$$U=\begin{bmatrix} c_{12}c_{13} & s_{12}c_{13} & \overset{\downarrow}{s_{3}}e^{-i\delta} \\ -s_{12}c_{23}-c_{12}s_{13}s_{23}e^{-i\delta} & c_{12}c_{23}-s_{12}s_{13}s_{23}e^{-i\delta} & c_{13}s_{23} \\ s_{12}s_{23}-c_{12}s_{13}c_{23}e^{-i\delta} & -c_{12}s_{23}-s_{12}s_{13}c_{23}e^{-i\delta} & c_{13}\overset{c}{s_{23}} \end{bmatrix}$$

$s_{ij}=\sin\theta_{ij}$、$c_{ij}=\cos\theta_{ij}$

$\Delta m_{ij}^2= \Delta m_i^2-\Delta m_j^2$

	Δm_{12}^2	Δm_{23}^2	θ_{12}	θ_{23}	θ_{13}	δ
solar ν and reactor ν	○		○			
LBL and atm. ν (MINOS, CERN, JHF-SK)		○ (size)		○	○	
Future LBL (ν factory or JHF-ν -II)		○ (sign)				○

MNS-3

The general expression for the oscillation probability in vacuum is

$$\begin{aligned} P(\nu_\alpha \to \nu_\beta; L) &= \delta_{\alpha\beta} - 4\sum_{j<k} \mathrm{Re}\left(U_{\alpha j}U^*_{\beta j}U^*_{\alpha k}U_{\beta k}\right)\sin^2\left(\frac{\Delta E_{jk}L}{2}\right) \\ &\quad +2\sum_{j<k}\mathrm{Im}\left(U_{\alpha j}U^*_{\beta j}U^*_{\alpha k}U_{\beta k}\right)\sin\left(\Delta E_{jk}L\right), \end{aligned}$$

where $\Delta E_{jk} \equiv \sqrt{m_j^2+p^2} - \sqrt{m_k^2+p^2} = \Delta m^2_{jk}/2E$. The CP violating term is rewritten as

$$\begin{aligned} & 2\sum_{j<k}\mathrm{Im}\left(U_{\alpha j}U^*_{\beta j}U^*_{\alpha k}U_{\beta k}\right)\sin\left(\Delta E_{jk}L\right) \\ = \;& 2\ J_{\alpha\beta}\left[\sin\left(\Delta E_{12}L\right)+\sin\left(\Delta E_{23}L\right)+\sin\left(\Delta E_{31}L\right)\right] \\ = \;& 4\ J_{\alpha\beta}\left[\sin\left(\frac{\Delta E_{12}L}{2}\right)\sin\left(\frac{\Delta E_{23}L}{2}\right)\sin\left(\frac{\Delta E_{31}L}{2}\right)\right] \end{aligned}$$

where

$$J_{\alpha\beta} \equiv \mathrm{Im}\left(U_{\alpha 1}U^*_{\beta 1}U^*_{\alpha 2}U_{\beta 2}\right)$$

is the Jarlskog factor, and

$$\mathrm{Im}\left(U_{\alpha 1}U^*_{\beta 1}U^*_{\alpha 2}U_{\beta 2}\right) = \mathrm{Im}\left(U_{\alpha 2}U^*_{\beta 2}U^*_{\alpha 3}U_{\beta 3}\right) = \mathrm{Im}\left(U_{\alpha 3}U^*_{\beta 3}U^*_{\alpha 1}U_{\beta 1}\right)$$

is used. In the case of diappearance experiment, only the CP conserving term survives and

$$\begin{aligned} & P(\nu_e \to \nu_e; L) = P(\bar\nu_e \to \bar\nu_e; L) \\ = \;& 1 - 4|U_{e1}|^2|U_{e2}|^2\sin^2\left(\frac{\Delta m^2_{21}L}{4E}\right) \\ & -4|U_{e1}|^2|U_{e3}|^2\sin^2\left(\frac{\Delta m^2_{31}L}{4E}\right) - 4|U_{e2}|^2|U_{e3}|^2\sin^2\left(\frac{\Delta m^2_{32}L}{4E}\right) \qquad (1) \end{aligned}$$

Assuming $\Delta m^2_{21} = \Delta m^2_\odot = 3\times 10^{-5}\mathrm{eV}^2$, $\Delta m^2_{32} = \Delta m^2_{\mathrm{atm}} = 3\times 10^{-3}\mathrm{eV}^2$, $\Delta m^2_{31} = \Delta m^2_{32} + \Delta m^2_{21} \simeq \Delta m^2_{32}$ is correct with 1% accuracy, and using the standard parametrization for the MNSP matrix

$$U = \begin{pmatrix} c_{12}c_{13} & s_{12}c_{13} & s_{13}e^{-i\delta} \\ -s_{12}c_{23} - c_{12}s_{23}s_{13}e^{i\delta} & c_{12}c_{23} - s_{12}s_{23}s_{13}e^{i\delta} & s_{23}c_{13} \\ s_{12}s_{23} - c_{12}c_{23}s_{13}e^{i\delta} & -c_{12}s_{23} - s_{12}c_{23}s_{13}e^{i\delta} & c_{23}c_{13} \end{pmatrix},$$

(1) becomes

$$\begin{aligned} & P(\nu_e \to \nu_e; L) = P(\bar\nu_e \to \bar\nu_e; L) \\ \simeq \;& 1 - 4|U_{e1}|^2|U_{e2}|^2\sin^2\left(\frac{\Delta m^2_{21}L}{4E}\right) \\ & -4|U_{e3}|^2\left(1-|U_{e3}|^2\right)\sin^2\left(\frac{\Delta m^2_{32}L}{4E}\right) \\ = \;& 1 - c^4_{13}\sin^2 2\theta_{12}\sin^2\left(\frac{\Delta m^2_{21}L}{4E}\right) - \sin^2 2\theta_{13}\sin^2\left(\frac{\Delta m^2_{32}L}{4E}\right) \end{aligned}$$

In the case of KamLAND, since the energy is low ($|\Delta m^2_{32}L/4E| \gg 1$), we have $\sin^2\left(\Delta m^2_{32}L/4E\right) \to 1/2$ and

$$\begin{aligned} & P(\nu_e \to \nu_e; L) = P(\bar\nu_e \to \bar\nu_e; L) \\ \simeq \;& 1 - c^4_{13}\sin^2 2\theta_{12}\sin^2\left(\frac{\Delta m^2_{21}L}{4E}\right) - \frac{1}{2}\sin^2 2\theta_{13} \end{aligned}$$

In the three flavor case, it has been known that the following expression holds[1]:

$$P^{(3)}(\nu_e \to \nu_e; A(x)) = (1-|U_{e3}|^2)^2 P^{(2)}(\nu_e \to \nu_e; (1-|U_{e3}|^2)A(x)) + |U_{e3}|^4,$$

where $A(x) \equiv \sqrt{2}G_F N_e(x)$ is the matter effect.

References

[1] C.-S. Lim, Proc. of the BNL Neutrino Workshop on Opportunities for Neutrino Physics at BNL, Upton, N.Y., February 5-7, 1987, ed. by M. J. Murtagh, p111; A. Yu. Smirnov, Proc. of the Int Symposium on Neutrino Astrophysics, Takayama/Kamioka 19 - 22 October 1992, ed. by Y. Suzuki and K. Nakamura, p.105.

1 Preliminaries

From the general expression for the oscillation probability in vacuum

$$\begin{aligned} P(\nu_\alpha \to \nu_\beta; L) &= \delta_{\alpha\beta} - 4\sum_{j<k} \mathrm{Re}\left(U_{\alpha j}U^*_{\beta j}U^*_{\alpha k}U_{\beta k}\right)\sin^2\left(\frac{\Delta E_{jk}L}{2}\right) \\ &\quad +2\sum_{j<k} \mathrm{Im}\left(U_{\alpha j}U^*_{\beta j}U^*_{\alpha k}U_{\beta k}\right)\sin\left(\Delta E_{jk}L\right), \end{aligned}$$

the disappearance probability in four neutrino schemes is given by

$$\begin{aligned} &P(\nu_e \to \nu_e; L) = P(\bar{\nu}_e \to \bar{\nu}_e; L) \\ = \;& 1 - 4|U_{e1}|^2|U_{e2}|^2\sin^2\left(\frac{\Delta m^2_{21}L}{4E}\right) - 4|U_{e1}|^2|U_{e3}|^2\sin^2\left(\frac{\Delta m^2_{31}L}{4E}\right) \\ & -4|U_{e2}|^2|U_{e3}|^2\sin^2\left(\frac{\Delta m^2_{32}L}{4E}\right) - 4|U_{e1}|^2|U_{e4}|^2\sin^2\left(\frac{\Delta m^2_{41}L}{4E}\right) \\ & -4|U_{e2}|^2|U_{e4}|^2\sin^2\left(\frac{\Delta m^2_{42}L}{4E}\right) - 4|U_{e3}|^2|U_{e4}|^2\sin^2\left(\frac{\Delta m^2_{43}L}{4E}\right) \qquad (1) \end{aligned}$$

There are two kinds of four neutrino schemes, (2+2) [1, 2] and (3+1) [3]. Here I use a parametrization [1] for the MNSP matrix

$$\begin{aligned} & U_{\mathrm{MNSP}} \\ \equiv\;& R_{34}(\frac{\pi}{2} - \theta_{34})R_{24}(\theta_{24})R_{23}(\frac{\pi}{2})U_{23}(\theta_{23},\delta_1)U_{14}(\theta_{14},\delta_3)U_{13}(\theta_{13},\delta_2)R_{12}(\theta_{12}) \\ \equiv\;& \begin{pmatrix} U_{e1} & U_{e2} & U_{e3} & U_{e4} \\ U_{\mu 1} & U_{\mu 2} & U_{\mu 3} & U_{\mu 4} \\ U_{\tau 1} & U_{\tau 2} & U_{\tau 3} & U_{\tau 4} \\ U_{s1} & U_{s2} & U_{s3} & U_{s4} \end{pmatrix} \\ =\;& \left(\begin{array}{ll} \multicolumn{2}{l}{c_{12}c_{13}c_{14}} \\ \multicolumn{2}{l}{-c_{12}c_{23}c_{24}s_{13}e^{-i\delta_2} + c_{24}s_{12}s_{23}e^{i\delta_1} - c_{12}c_{13}s_{14}s_{24}e^{-i\delta_3}} \\ \multicolumn{2}{l}{-c_{12}c_{13}c_{24}c_{34}s_{14}e^{-i\delta_3} + c_{12}c_{23}c_{34}s_{13}s_{24}e^{-i\delta_2} - c_{34}s_{12}s_{23}s_{24}e^{i\delta_1} + c_{23}s_{12}s_{34} + c_{12}s_{13}s_{23}s_{34}e^{-i(\delta_1+\delta_2)}} \\ \multicolumn{2}{l}{-c_{23}c_{34}s_{12} - c_{12}c_{34}s_{13}s_{23}e^{-i(\delta_1+\delta_2)} - c_{12}c_{13}c_{24}s_{14}s_{34}e^{-i\delta_3} + c_{12}c_{23}s_{13}s_{24}s_{34}e^{-i\delta_2} - s_{12}s_{23}s_{24}s_{34}e^{i\delta_1}} \\ \\ \multicolumn{2}{l}{c_{13}c_{14}s_{12}} \\ \multicolumn{2}{l}{-c_{23}c_{24}s_{12}s_{13}e^{-i\delta_2} - c_{12}c_{24}s_{23}e^{i\delta_1} - c_{13}s_{12}s_{14}s_{24}e^{-i\delta_3}} \\ \multicolumn{2}{l}{-c_{13}c_{24}c_{34}s_{12}s_{14}e^{-i\delta_3} + c_{23}c_{34}s_{12}s_{13}s_{24}e^{-i\delta_2} + c_{12}c_{34}s_{23}s_{24}e^{i\delta_1} - c_{12}c_{23}s_{34} + s_{12}s_{13}s_{23}s_{34}e^{-i(\delta_1+\delta_2)}} \\ \multicolumn{2}{l}{c_{12}c_{23}c_{34} - c_{34}s_{12}s_{13}s_{23}e^{-i(\delta_1+\delta_3)} - c_{13}c_{24}s_{12}s_{14}s_{34}e^{-i\delta_3} + c_{23}s_{12}s_{13}s_{24}s_{34}e^{-i\delta_2} + c_{12}s_{23}s_{24}s_{34}e^{i\delta_1}} \\ \\ c_{14}s_{13}e^{i\delta_2} & s_{14}e^{i\delta_3} \\ c_{13}c_{23}c_{24} - s_{13}s_{14}s_{24}e^{i(\delta_2-\delta_3)} & c_{14}s_{24} \\ -c_{24}c_{34}s_{13}s_{14}e^{i(\delta_2-\delta_3)} - c_{13}c_{23}c_{34}s_{24} - c_{13}s_{23}s_{34}e^{-i\delta_1} & c_{14}c_{24}c_{34} \\ c_{13}c_{34}s_{23}e^{-i\delta_1} - c_{24}s_{13}s_{14}s_{34}e^{i(\delta_2-\delta_3)} - c_{13}c_{23}s_{24}s_{34} & c_{14}c_{24}s_{34} \end{array}\right) \\ & \qquad (2) \end{aligned}$$

where $U_{23}(\theta_{23},\delta_1) \equiv e^{2i\delta_1\lambda_3}R_{23}(-\theta_{23})e^{-2i\delta_1\lambda_3}$, $U_{14}(\theta_{14},\delta_3) \equiv e^{\sqrt{6}i\delta_3\lambda_{15}/2}R_{14}(\theta_{14})\, e^{-\sqrt{6}i\delta_3\lambda_{15}/2}$, $U_{13}(\theta_{13},\delta_2) \equiv e^{2i\delta_2\lambda_8/\sqrt{3}}R_{13}(\theta_{13})e^{-2i\delta_2\lambda_8/\sqrt{3}}$, $R_{jk}(\theta) \equiv \exp\left(iT_{jk}\theta\right)$, $(T_{jk})_{\ell m} = i\left(\delta_{j\ell}\delta_{km} - \delta_{jm}\delta_{k\ell}\right)$, $2\lambda_3 \equiv \mathrm{diag}(1,-1,0,0)$, $2\sqrt{3}\lambda_8 \equiv \mathrm{diag}(1,1,-2,0)$, $2\sqrt{6}\lambda_{15} \equiv \mathrm{diag}(1,1,1,-3)$ are 4×4 matrices (λ_j are elements of the $su(4)$ generators).

As in the three flavor case, it has been known that the following expression holds in the four neutrino case (there is some typo in [1]):

$$\begin{aligned} & P^{(4)}\left(\nu_e \to \nu_e; A(x)\right)_\odot \\ =\;& P^{(2)}\left(\nu_e \to \nu_e; (1 - |U_{e3}|^2 - |U_{e4}|^2)A(x)\right)_\odot \left(1 - |U_{e3}|^2 - |U_{e4}|^2\right)^2 \\ & +|U_{e3}|^4 + |U_{e4}|^4, \\ =\;& c^4_{13}c^4_{14}P^{(2)}\left(\nu_e \to \nu_e; c^2_{13}c^2_{14}A(x)\right)_\odot + s^4_{13}c^4_{14} + s^4_{14}, \qquad (3) \end{aligned}$$

where $A(x) \equiv \sqrt{2}G_F N_e(x)$ is the matter effect. (3) shows that $P^{(4)}$ is similar to $P^{(2)}$ as long as $|\theta_{13}|$ and $|\theta_{14}|$ are small, and θ_{12} plays a role of the solar mixing angle.

In the discussions below, I always average out rapid oscillations ($\sin^2\left(\Delta m^2 L/4E\right) \to 1/2$ if $|\Delta m^2 L/4E| \gg 1$) and ignore negligible oscillation terms ($\sin^2\left(\Delta m^2 L/4E\right) \to 0$ if $|\Delta m^2 L/4E| \ll 1$).

2 (3+1)-scheme

Without loss of generality I assume that one distinct mass eigenstate is ν_4 (See Fig. 1 (b) or (c) in [4]), the largest mass squared difference is $\Delta m^2_{43} \equiv \Delta m^2_{\mathrm{LSND}}$, $\Delta m^2_{32} \equiv \Delta m^2_{\mathrm{atm}}$, and $\Delta m^2_{21} \equiv \Delta m^2_\odot$.

There are two important constraints from the reactor data. From the Bugey result [5], I have

$$\begin{aligned} P(\bar{\nu}_e \to \bar{\nu}_e; L)_{\mathrm{Bugey}} &= 1 - 4|U_{e4}|^2(1 - |U_{e4}|^2)\sin^2\left(\frac{\Delta m^2_{43}L}{4E}\right)\Bigg|_{\mathrm{Bugey}} \\ &= 1 - \sin^2 2\theta_{14}\sin^2\left(\frac{\Delta m^2_{43}L}{4E}\right)\Bigg|_{\mathrm{Bugey}} \end{aligned}$$

Since only three values for $\Delta m^2_{\mathrm{LSND}}$ are allowed by the constraints [3, 4] ($\Delta m^2_{43} = 0.9, 1.7, 6.0\mathrm{eV2}$), I have

$$\sin^2 2\theta_{14} \lesssim 0.1$$

(See, e.e, Fig. 2 in [4]). From the Chooz result [6], I have

$$\begin{aligned} P(\bar{\nu}_e \to \bar{\nu}_e; L)_{\mathrm{Chooz}} &= 1 - 2|U_{e4}|^2(1 - |U_{e4}|^2) - 4|U_{e2}|^2|U_{e3}|^2\sin^2\left(\frac{\Delta m^2_{32}L}{4E}\right)\Bigg|_{\mathrm{Chooz}} \\ &= 1 - \frac{1}{2}\sin^2 2\theta_{14} - s^2_{12}c^4_{14}\sin^2 2\theta_{13}\sin^2\left(\frac{\Delta m^2_{32}L}{4E}\right)\Bigg|_{\mathrm{Chooz}}. \end{aligned}$$

Since θ_{12} has to be of order one (assuming the LMA MSW solution), I have

$$\sin^2 2\theta_{13} \lesssim 0.1$$

Now the disappearance probability in KamLAND is

$$P(\bar{\nu}_e \to \bar{\nu}_e; L)_{\mathrm{KamLAND}}$$

$$
\begin{aligned}
&\simeq 1-4|U_{e1}|^2|U_{e2}|^2\sin^2\left(\frac{\Delta m^2_{21}L}{4E}\right)\bigg|_{\mathrm{KamLAND}} - 2|U_{e3}|^2(1-|U_{e3}|^2-|U_{e4}|^2) - 2|U_{e4}|^2(1-|U_{e4}|^2)\\
&= 1-c^4_{13}c^4_{14}\sin^2 2\theta_{12}\sin^2\left(\frac{\Delta m^2_{21}L}{4E}\right)\bigg|_{\mathrm{KamLAND}} - \frac{1}{2}c^4_{14}\sin^2 2\theta_{13} - \frac{1}{2}\sin^2 2\theta_{14}
\end{aligned}
$$

3 (2+2)-scheme

Without loss of generality I assume that the largest mass squared difference is $\Delta m^2_{42} \equiv \Delta m^2_{\mathrm{LSND}}$ (See Fig. 1 (a) in [4]), $\Delta m^2_{43} \equiv \Delta m^2_{\mathrm{atm}}$, and $\Delta m^2_{21} \equiv \Delta m^2_{\odot}$.

From the Bugey result [5], I have

$$
\begin{aligned}
P(\bar{\nu}_e \to \bar{\nu}_e; L)_{\mathrm{Bugey}} &= 1-4(|U_{e3}|^2+|U_{e4}|^2)(1-|U_{e3}|^2-|U_{e4}|^2)\sin^2\left(\frac{\Delta m^2_{42}L}{4E}\right)\bigg|_{\mathrm{Bugey}}\\
&= 1-4c^4_{13}c^4_{14}(1-c^4_{13}c^4_{14})\sin^2\left(\frac{\Delta m^2_{42}L}{4E}\right)\bigg|_{\mathrm{Bugey}}
\end{aligned}
$$

Since $0.2\mathrm{eV}^2 \lesssim \Delta m^2_{\mathrm{LSND}} \lesssim 0.3\mathrm{eV}^2$ is necessary to satisfy the constraints of the CDHSW [7] (See, e.e, Fig. 2 in [4]), and the atmospheric neutrinos [8, 9] I have

$$
4(|U_{e3}|^2+|U_{e4}|^2) = 4(1-c^4_{13}c^4_{14}) \lesssim 0.04, \tag{4}
$$

which leads $s^2_{13} \lesssim 0.01$ and $s^2_{14} \lesssim 0.01$. The constraint from the Chooz result [6] in this scheme gives trivial result, i.e., it follows from (4).

Now the disappearance probability in KamLAND is

$$
\begin{aligned}
&P(\bar{\nu}_e \to \bar{\nu}_e; L)_{\mathrm{KamLAND}}\\
&\simeq 1-4|U_{e1}|^2|U_{e2}|^2\sin^2\left(\frac{\Delta m^2_{21}L}{4E}\right)\bigg|_{\mathrm{KamLAND}} - 2(|U_{e3}|^2+|U_{e4}|^2)(1-|U_{e3}|^2-|U_{e4}|^2) - 2|U_{e3}|^2|U_{e4}|^2\\
&= 1-c^4_{13}c^4_{14}\sin^2 2\theta_{12}\sin^2\left(\frac{\Delta m^2_{21}L}{4E}\right)\bigg|_{\mathrm{KamLAND}} - 2c^2_{13}c^2_{14}(1-c^2_{13}c^2_{14}) - \frac{1}{2}s^2_{13}\sin^2 2\theta_{14}
\end{aligned}
$$

References

[1] N. Okada and O. Yasuda, Int. J. Mod. Phys. **A 12**, 3669 (1997).

[2] S.M. Bilenky, C. Giunti and W. Grimus, hep-ph/9609343; Eur. Phys. J. **C1**, 247 (1998).

[3] V. Barger, B. Kayser, J. Learned, T. Weiler and K. Whisnant, Phys. Lett. **B489**, 345 (2000).

[4] O. Yasuda, hep-ph/0102166.

[5] Bugey Collaboration, B. Ackar et al., Nucl. Phys. **B434** (1995) 503.

[6] CHOOZ Collaboration, M. Apollonio et al., Phys. Lett. **B420**, 397 (1998); Phys. Lett. **B466**, 415 (1998).

[7] CDHSW Collaboration, F. Dydak et al., Phys. Lett. **134B** (1984) 281.

[8] O. Yasuda, hep-ph/0006319.

[9] M. C. Gonzalez-Garcia, M. Maltoni and C. Pena-Garay, hep-ph/0105269.

⑬

Future long baseline accelerator experiments

- MINOS
- CERN → G.S.
- JHF

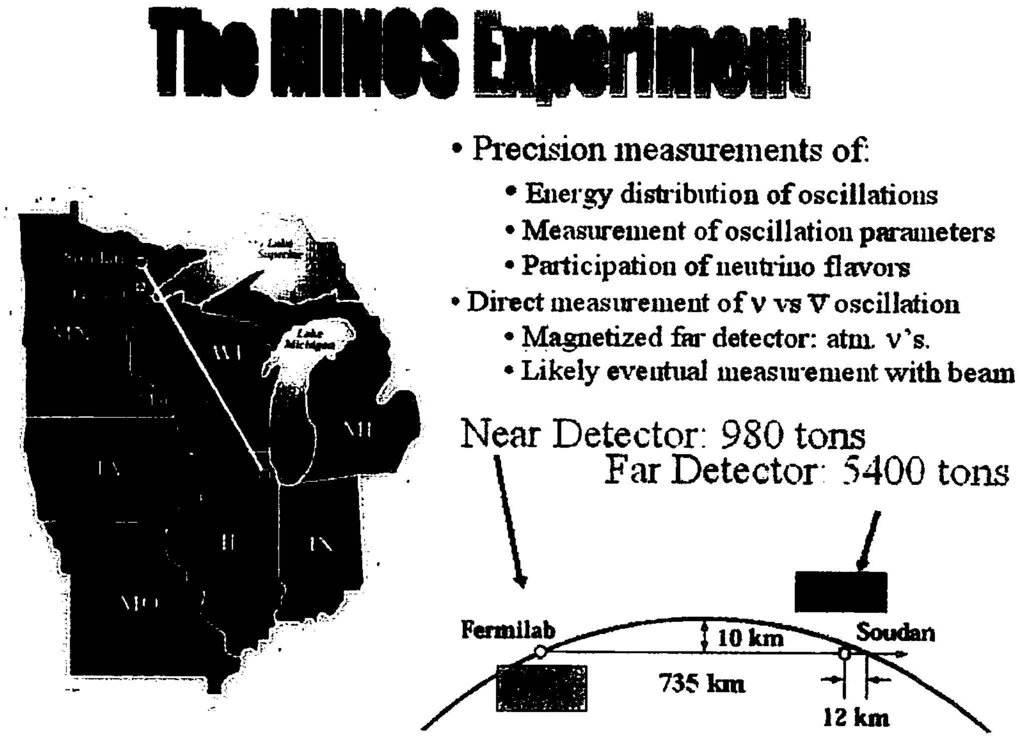

The MINOS Experiment

- Precision measurements of:
  - Energy distribution of oscillations
  - Measurement of oscillation parameters
  - Participation of neutrino flavors
- Direct measurement of ν vs $\bar{\nu}$ oscillation
  - Magnetized far detector: atm. ν's.
  - Likely eventual measurement with beam

Near Detector: 980 tons
Far Detector: 5400 tons

The NuMI Neutrino Energy Spectra

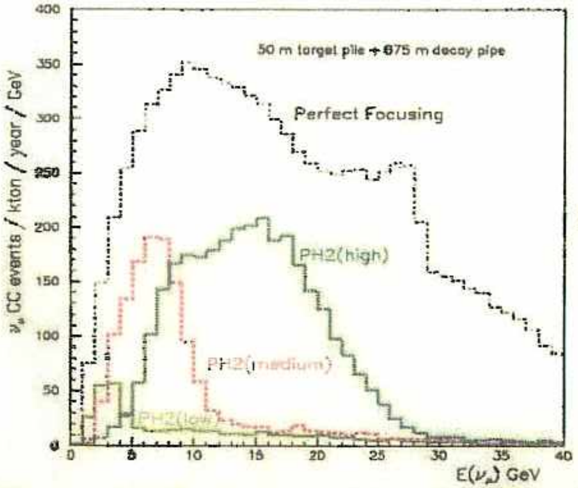

ν_μ CC Events/kt/year

Low	Medium	High
470	1270	2740

ν_μ CC Events/MINOS/2 year

Low	Medium	High
5080	13800	29600

$4x10^{20}$ protons on target/year
$4x10^{13}$ protons/1.9 seconds

By moving the horns and target, different energy spectra are available using the NuMI beamline. The energy can be tuned depending on the specific oscillation parameters expected/observed.

MINOS (Main Injector Neutrino Oscillation Search)

Far Detector

38,700 m ² Active Detector Planes
4 cm wide solid scintillator strips
WLS fiber readout

Magnetized Fe Plates
730 Layers x 2.54 cm Fe
8.1 kT Total Mass

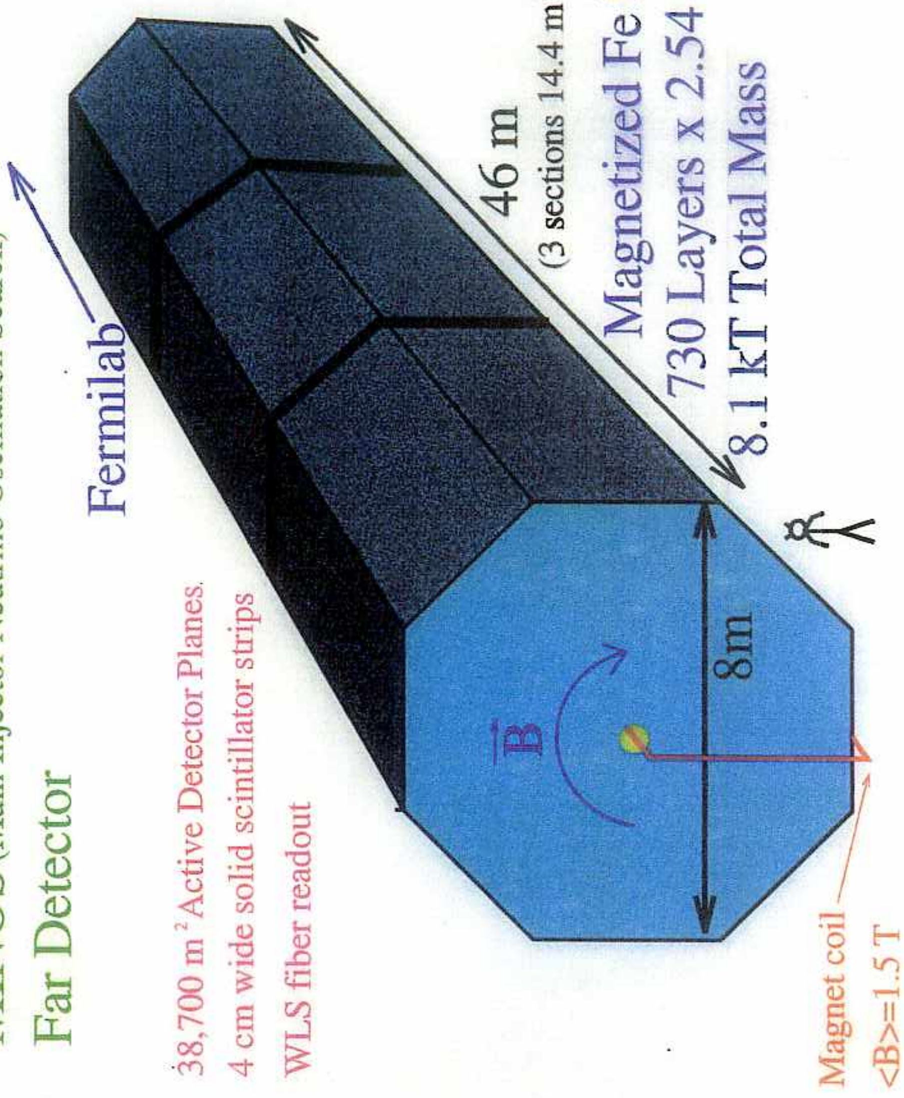

Detector Technology

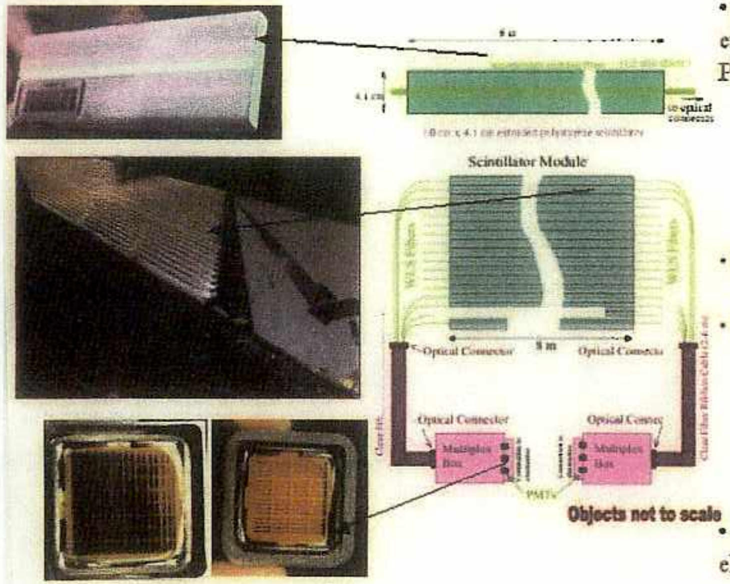

- Scintillator strips are extruded polystyrene (Itasca Plastic)
  - PPO (1%) and POPOP (0.03%) fluors
  - Co-extruded TiO_2 reflective coating
  - Fiber groove
- Kuraray 1.2mm WLS Fibers
  - (Y-11 175ppm)
- PMTs:
  - Far Detector: Hamamatsu R6000-M16 multi-anode PMTs (16 channels), 8 fibers/pixel.
  - Near Detector: "M64", one fiber per pixel.
- Viking "VA"-based front-end electronics.

CERN to Gran Sasso Neutrino Beam

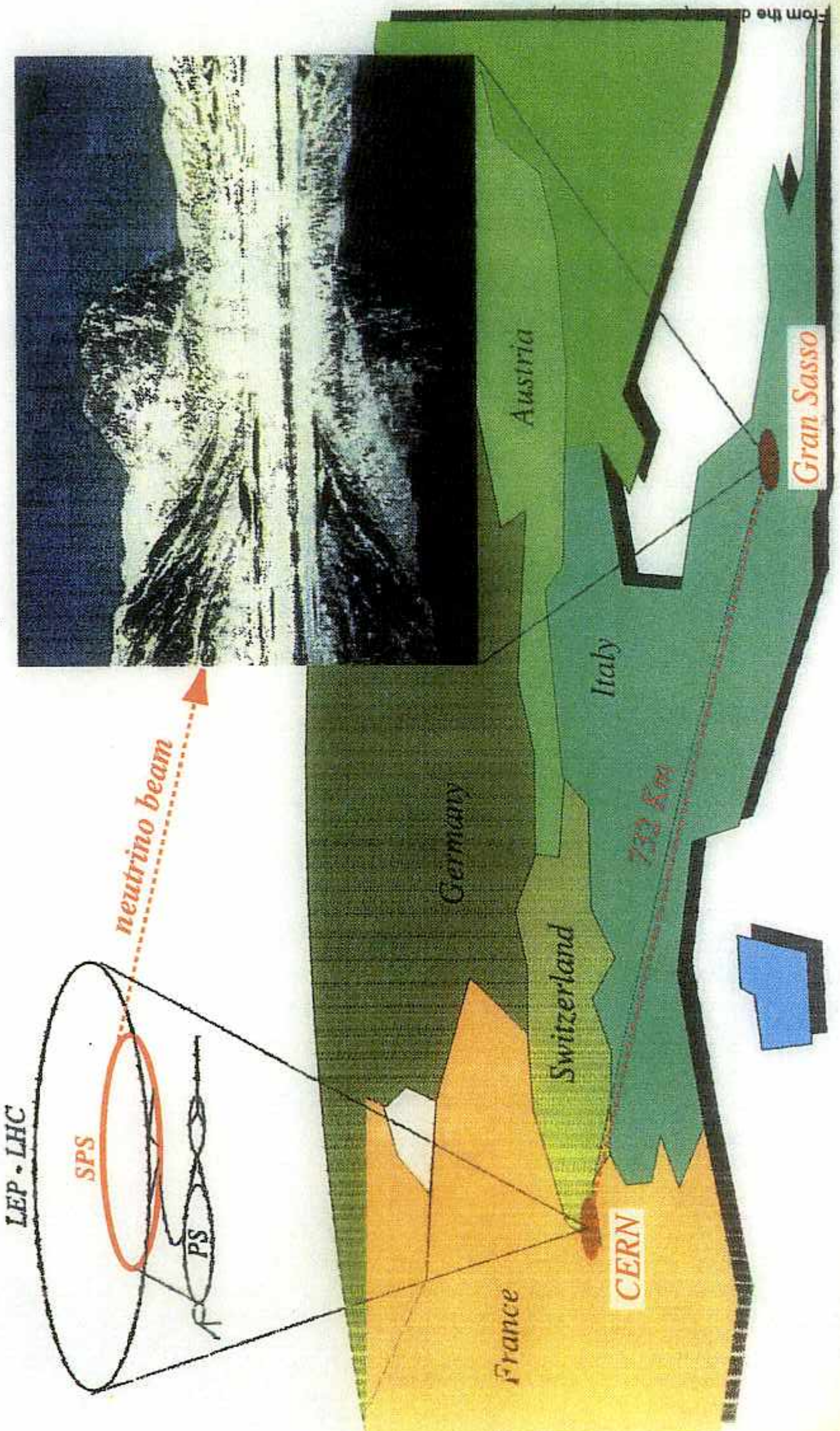

2 ways of detecting τ appearance

ν_μ ….. ν_τ → $\tau^- + X$

oscillation

CC interaction

$\mu^- \ \nu_\tau \ \bar{\nu}_\mu$	BR 18 %
$h^- \ \nu_\tau \ n\pi^0$	50 %
$e^- \ \nu_\tau \ \bar{\nu}_e$	18 %
$\pi^+ \ \pi \ \pi \ \nu_\tau \ n\pi^0$	14%

<u>OPERA</u>: Observation of the decay topology of τ *(à la CHORUS)*
In photographic emulsion
(~ **μm** granularity)
A digital Cloud chamber

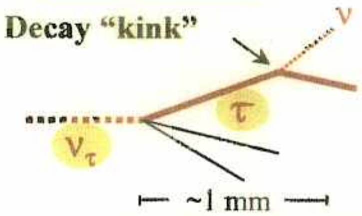

<u>ICARUS</u>: detailed TPC image in liquid argon and kinematic criteria *(à la NOMAD)*
(~ **mm** granularity)
A digital Bubble chamber

But also: ν_μ … $\nu_e \rightarrow e^- + X$

The smallest OPERA element

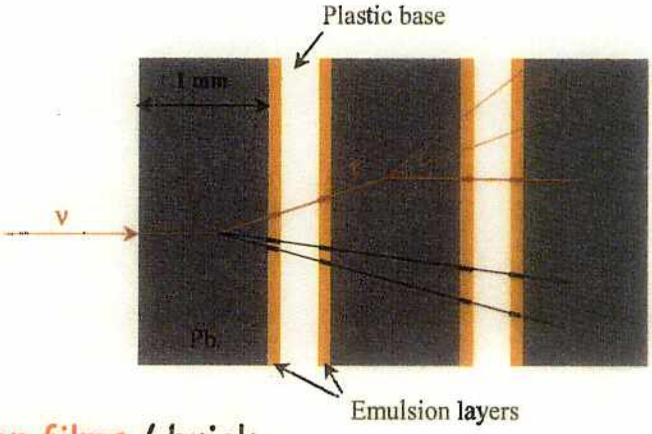

56 emulsion films / brick

- To the full detector:
  2 supermodules
  31 walls / supermodule
  52 x 64 bricks /wall
  200 000 bricks

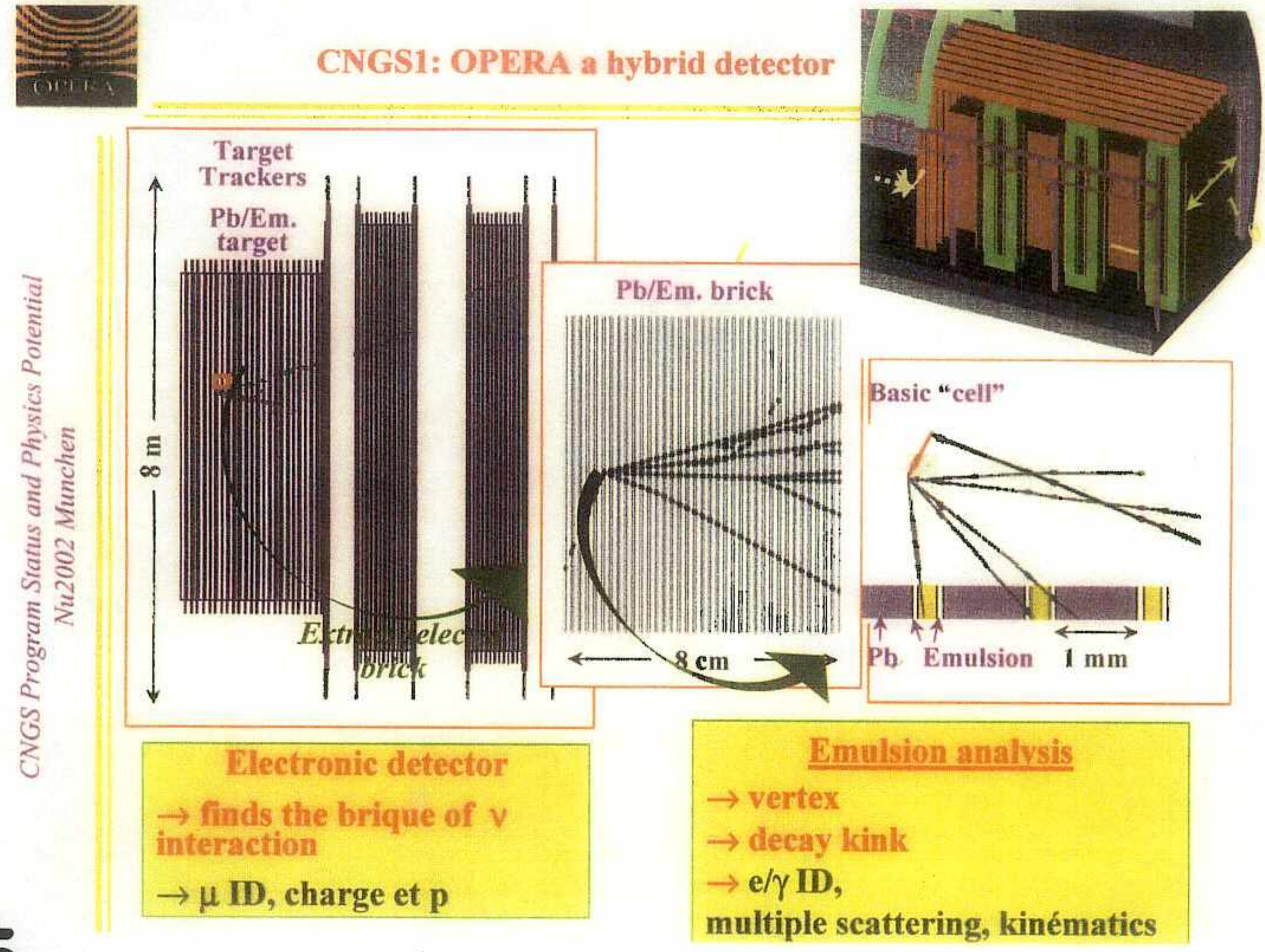

CNGS1: OPERA a hybrid detector

Electronic detector

- → finds the brique of ν interaction
- → μ ID, charge et p

Emulsion analysis

- → vertex
- → decay kink
- → e/γ ID,

multiple scattering, kinématics

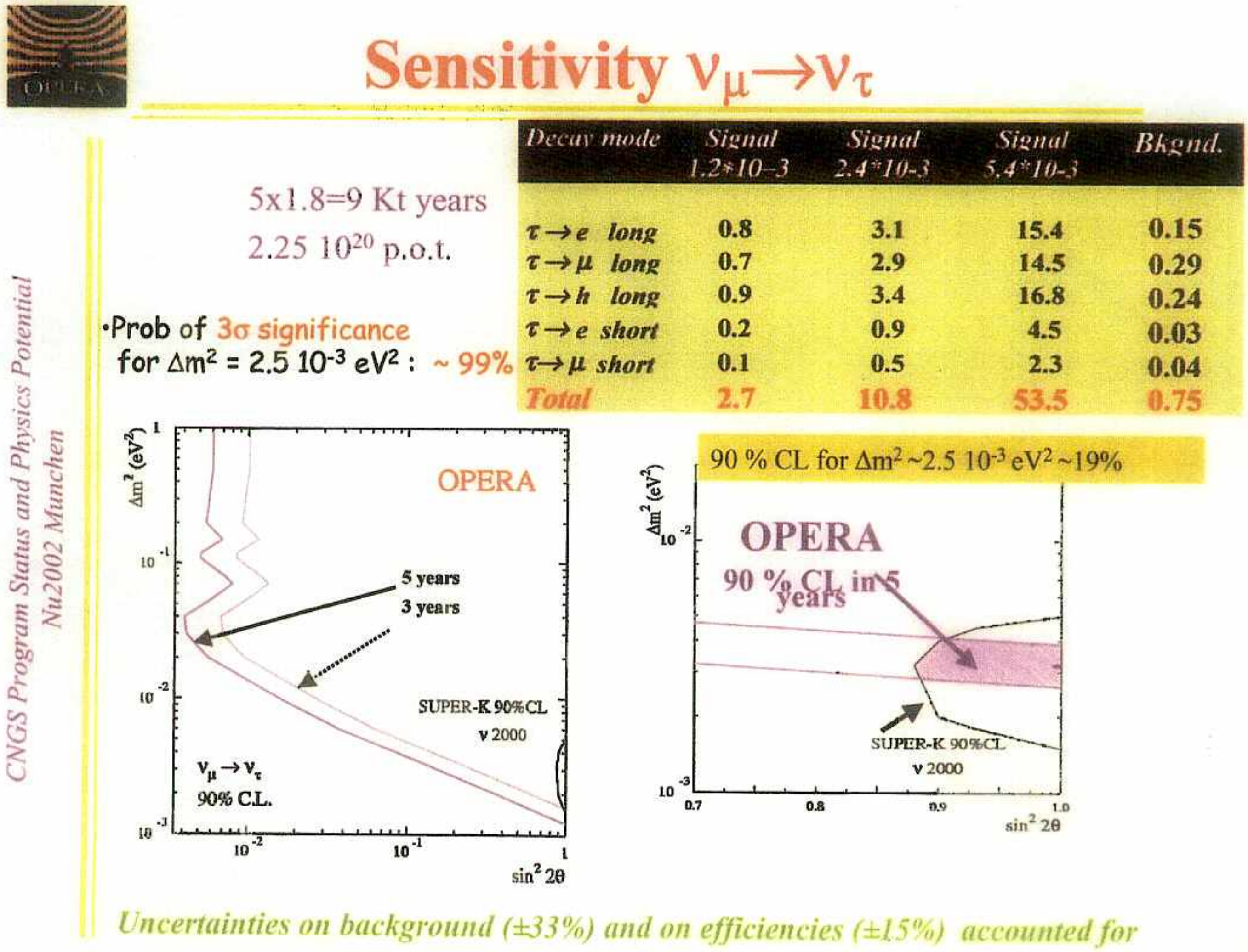

Sensitivity $\nu_\mu \rightarrow \nu_\tau$

5x1.8=9 Kt years

2.25 10^{20} p.o.t.

- Prob of 3σ significance for $\Delta m^2 = 2.5\ 10^{-3}\ eV^2$: ~ 99%

Decay mode	Signal $1.2*10^{-3}$	Signal $2.4*10^{-3}$	Signal $5.4*10^{-3}$	Bkgnd.
$\tau \rightarrow e$ long	0.8	3.1	15.4	0.15
$\tau \rightarrow \mu$ long	0.7	2.9	14.5	0.29
$\tau \rightarrow h$ long	0.9	3.4	16.8	0.24
$\tau \rightarrow e$ short	0.2	0.9	4.5	0.03
$\tau \rightarrow \mu$ short	0.1	0.5	2.3	0.04
Total	2.7	10.8	53.5	0.75

90 % CL for $\Delta m^2 \sim 2.5\ 10^{-3}\ eV^2 \sim 19\%$

Uncertainties on background (±33%) and on efficiencies (±15%) accounted for

ICARUS T3000 (proposed)

T3000 Detector in Hall B of LNGS (cloning of T600)

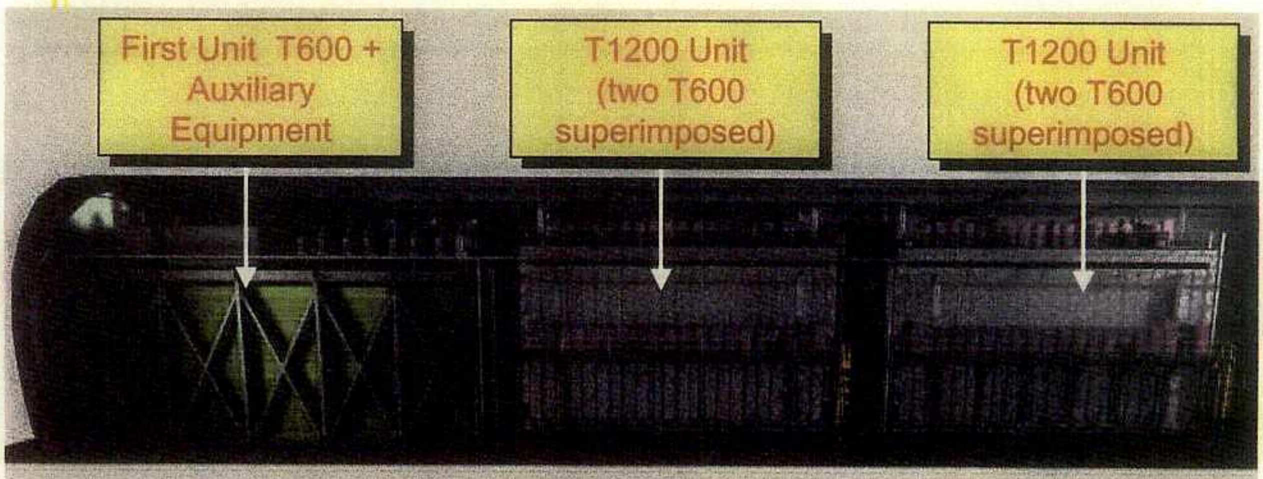

First Unit T600 + Auxiliary Equipment

T1200 Unit (two T600 superimposed)

T1200 Unit (two T600 superimposed)

Improved statistics for:

≈ 70 Metres

Future extension to additional modules

1. **Solar neutrinos**
2. **Atmospheric neutrinos**
3. **Supernova neutrinos**
4. **CERN-NGS neutrinos**
5. **Proton decay**

T600: installed in LNGS in 2003

T3000: operational by summer 2006

184

ICARUS $\nu_\mu \rightarrow \nu_\tau$

Golden channel $\tau \rightarrow e$ (good e/π^0 separation) but also ($\tau \rightarrow \rho$)

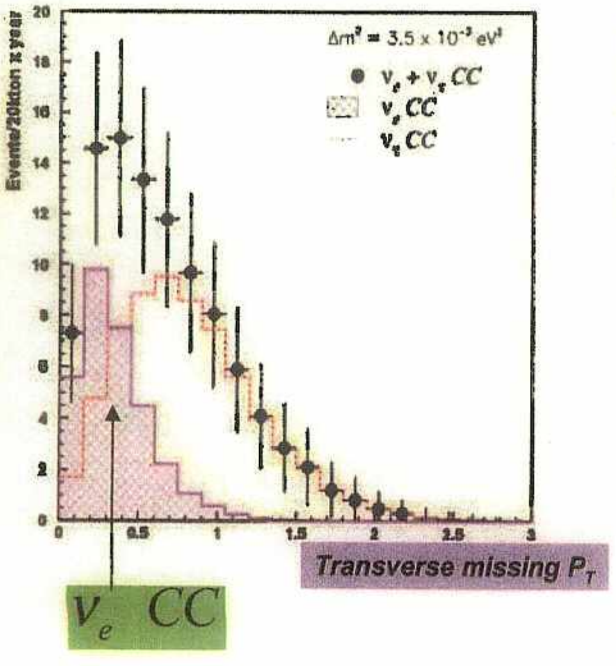

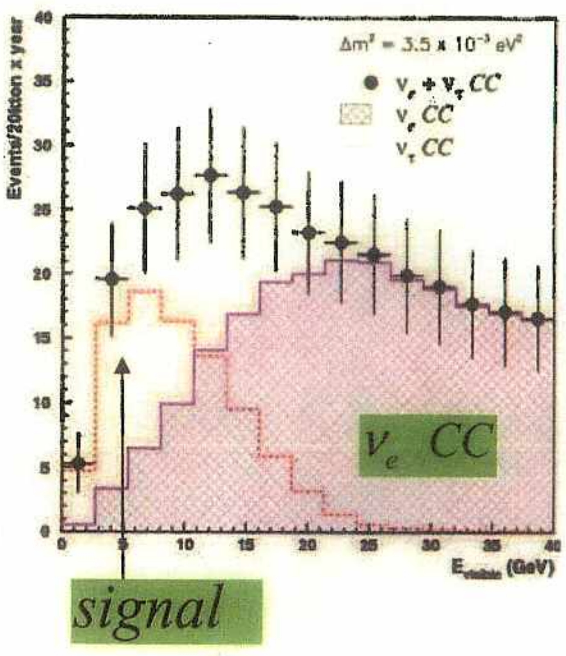

JHF プロジェクト

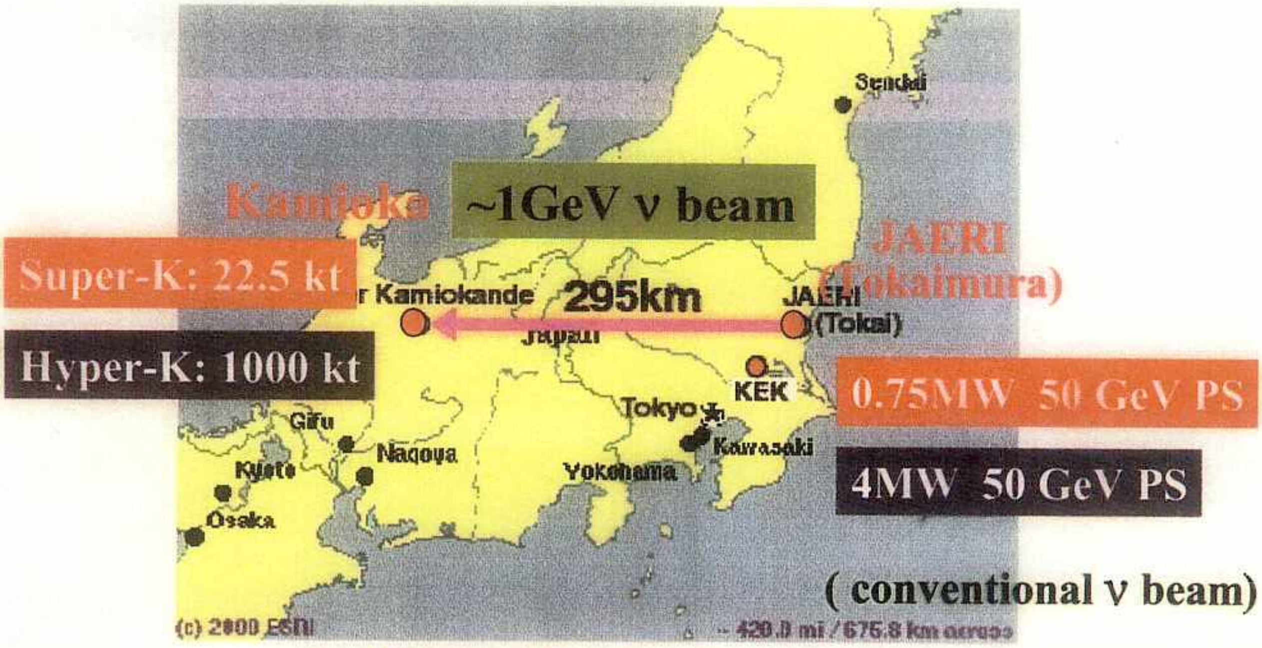

実験前期最初の5年間 (0.77MW + Super-K)
実験後期 (4MW+Hyper-K) ~ 前期 <u>×200</u>

JHF ν beam Facility

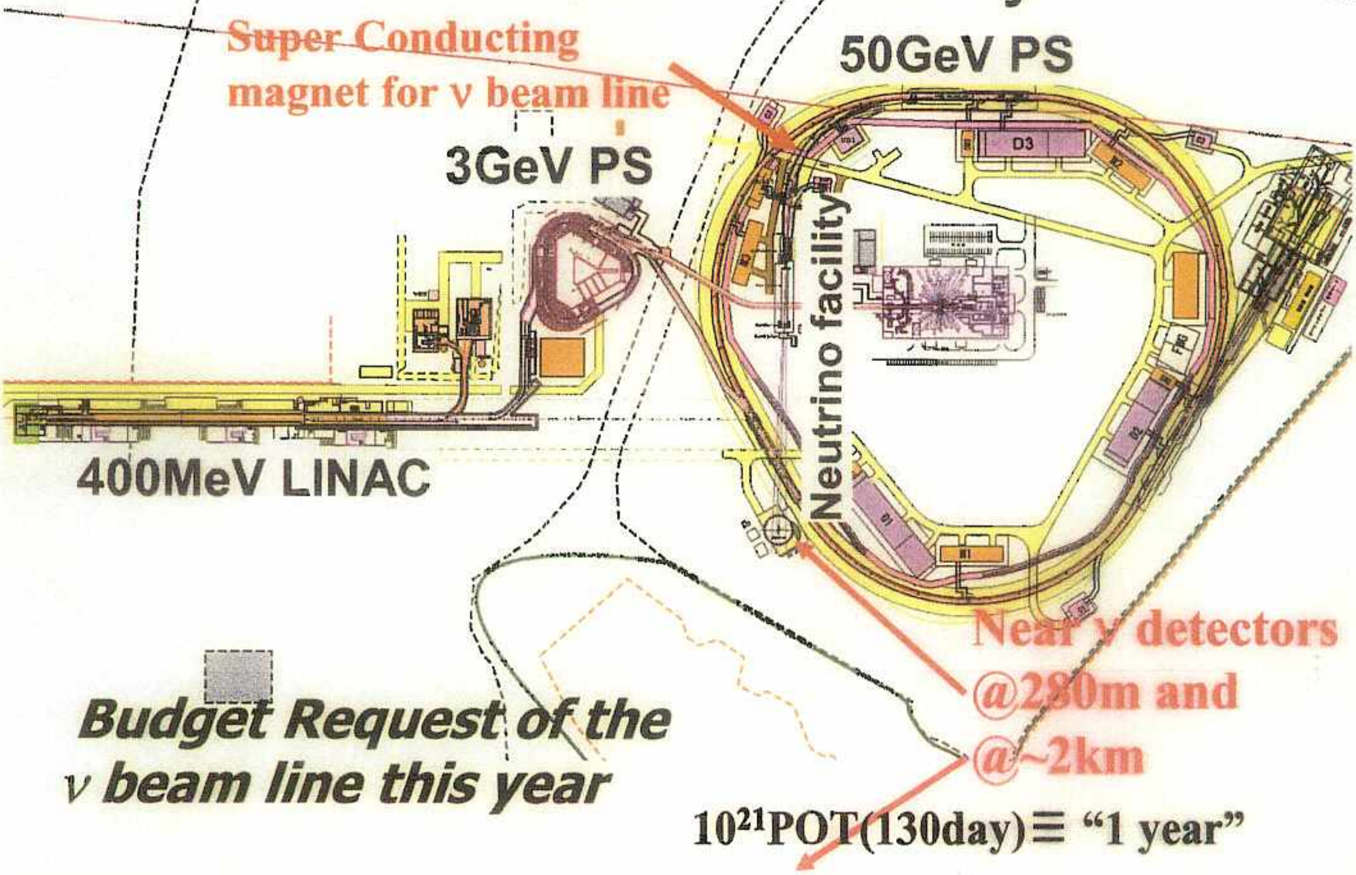

Budget Request of the
ν beam line this year

10^{21}POT(130day)≡ "1 year"

$\nu_\mu \rightarrow \nu_\mu$ disappearance

Observation / Null-Oscillation

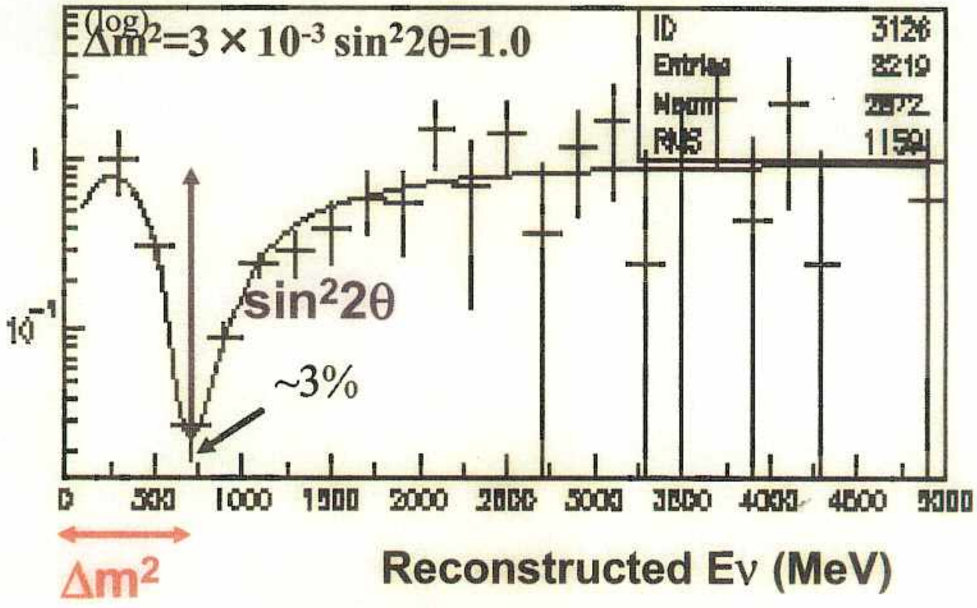

$\delta \sin^2 2\theta_{23} \sim 0.01$ (=1%)

$\delta \Delta m_{23}{}^2 \quad < 1 \times 10^{-4} \mathrm{eV}^2$

JHFニュートリノの感度

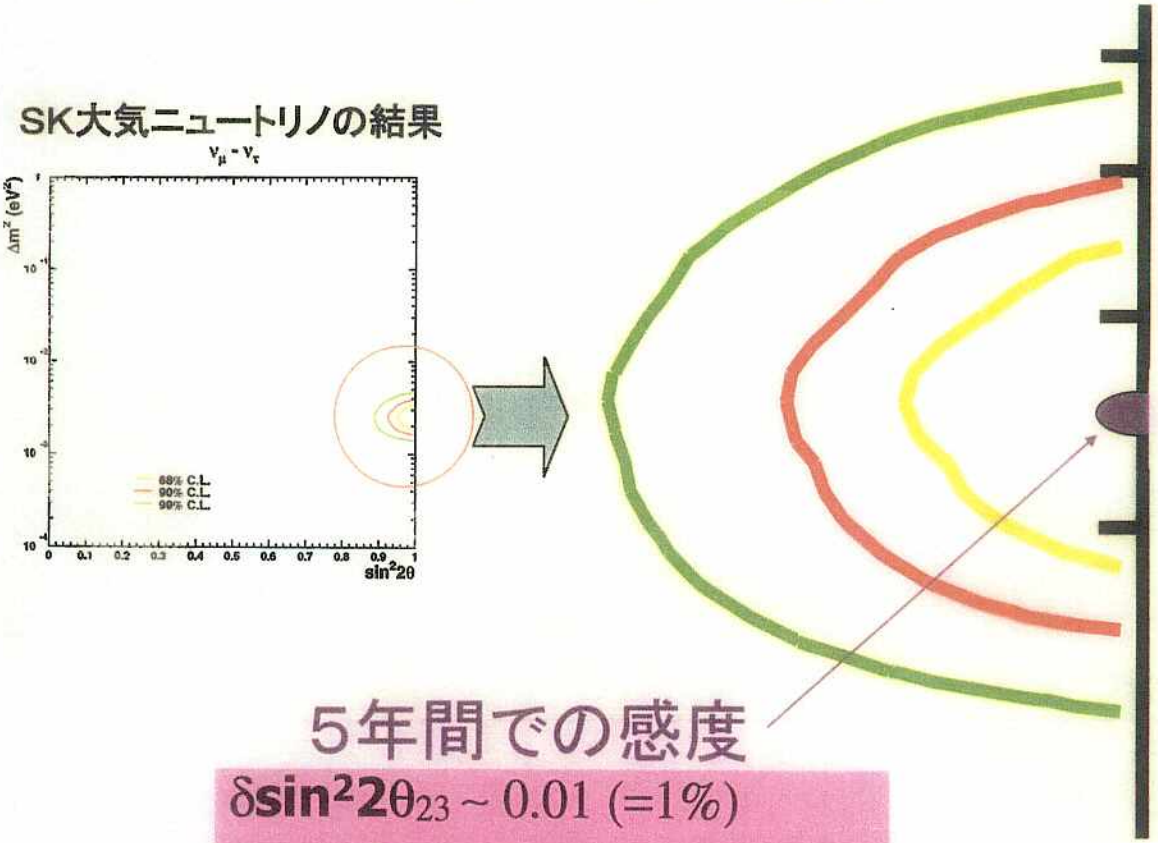

5年間での感度

$\delta \sin^2 2\theta_{23} \sim 0.01$ (=1%)

$\delta \Delta m_{23}{}^2 \quad < 1 \times 10^{-4} \mathrm{eV}^2$

$\nu_\mu \rightarrow \nu_e$ appearance

$\sin^2 2\theta_{\mu e}=0.05$ ($\sin^2 2\theta_{\mu e} \equiv 0.5\sin^2 2\theta_{13}$)

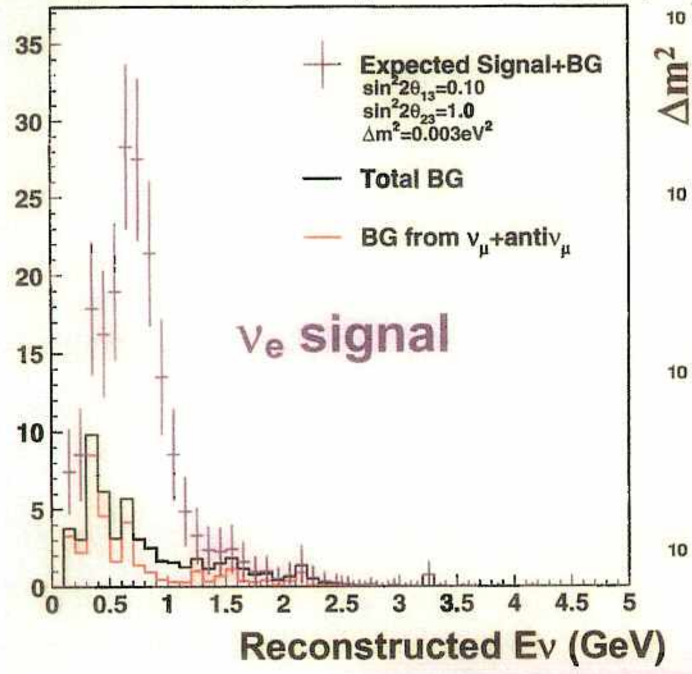

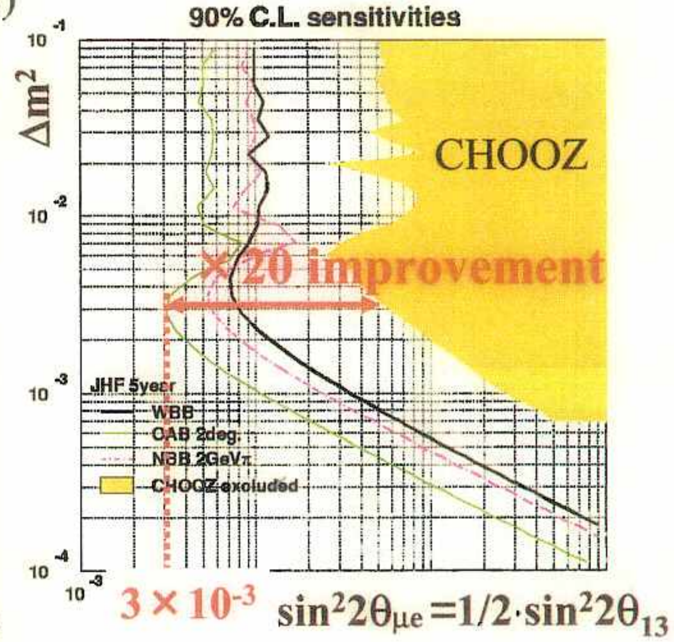

$\sin^2 2\theta_{13} < 0.006$ (90% C.L.)

$\nu_\mu \rightarrow \nu_e$ oscillation probability (1)

$$P(\nu_\mu \rightarrow \nu_e) = \boxed{4C_{13}^2 S_{13}^2 S_{23}^2 \sin^2 \frac{\Delta m_{31}^2 L}{4E}}$$ Dominant

$$+8C_{13}^2 S_{12} S_{13} S_{23} (C_{12} C_{23} \cos\delta - S_{12} S_{13} S_{23}) \cos\frac{\Delta m_{32}^2 L}{4E} \sin\frac{\Delta m_{31}^2 L}{4E} \sin\frac{\Delta m_{21}^2 L}{4E}$$

$$\boxed{-8C_{13}^2 C_{12} C_{23} S_{12} S_{13} S_{23} \sin\delta \sin\frac{\Delta m_{32}^2 L}{4E} \sin\frac{\Delta m_{31}^2 L}{4E} \sin\frac{\Delta m_{21}^2 L}{4E}}$$ **CPV**

$$+4S_{12}^2 C_{13}^2 \{C_{12}^2 C_{23}^2 + S_{12}^2 S_{23}^2 S_{13}^2 - 2C_{12} C_{23} S_{12} S_{23} S_{13} \cos\delta\} \sin^2\frac{\Delta m_{21}^2 L}{4E}$$

$$-8C_{13}^2 S_{13}^2 S_{23}^2 \cos\frac{\Delta m_{32}^2 L}{4E} \sin\frac{\Delta m_{31}^2 L}{4E} \frac{aL}{4E} (1 - 2S_{13}^2)$$

$\delta \rightarrow -\delta$, $a \rightarrow -a$ for $\overline{\nu}_\mu \rightarrow \overline{\nu}_e$

Matter effect:

$$a = 7.56\times10^{-5}[\mathrm{eV}^2]\cdot\left(\frac{\rho}{[\mathrm{g/cm}^3]}\right)\cdot\left(\frac{E}{[\mathrm{GeV}]}\right)$$

$$\boxed{A_{CP} \equiv \frac{P-\overline{P}}{P+\overline{P}} \approx \frac{\Delta m_{12}^2 L}{E} \cdot \frac{\sin 2\theta_{12}}{\sin\theta_{13}} \cdot \sin\delta}$$

$\nu_\mu \rightarrow \nu_e$ oscillation probability (2)

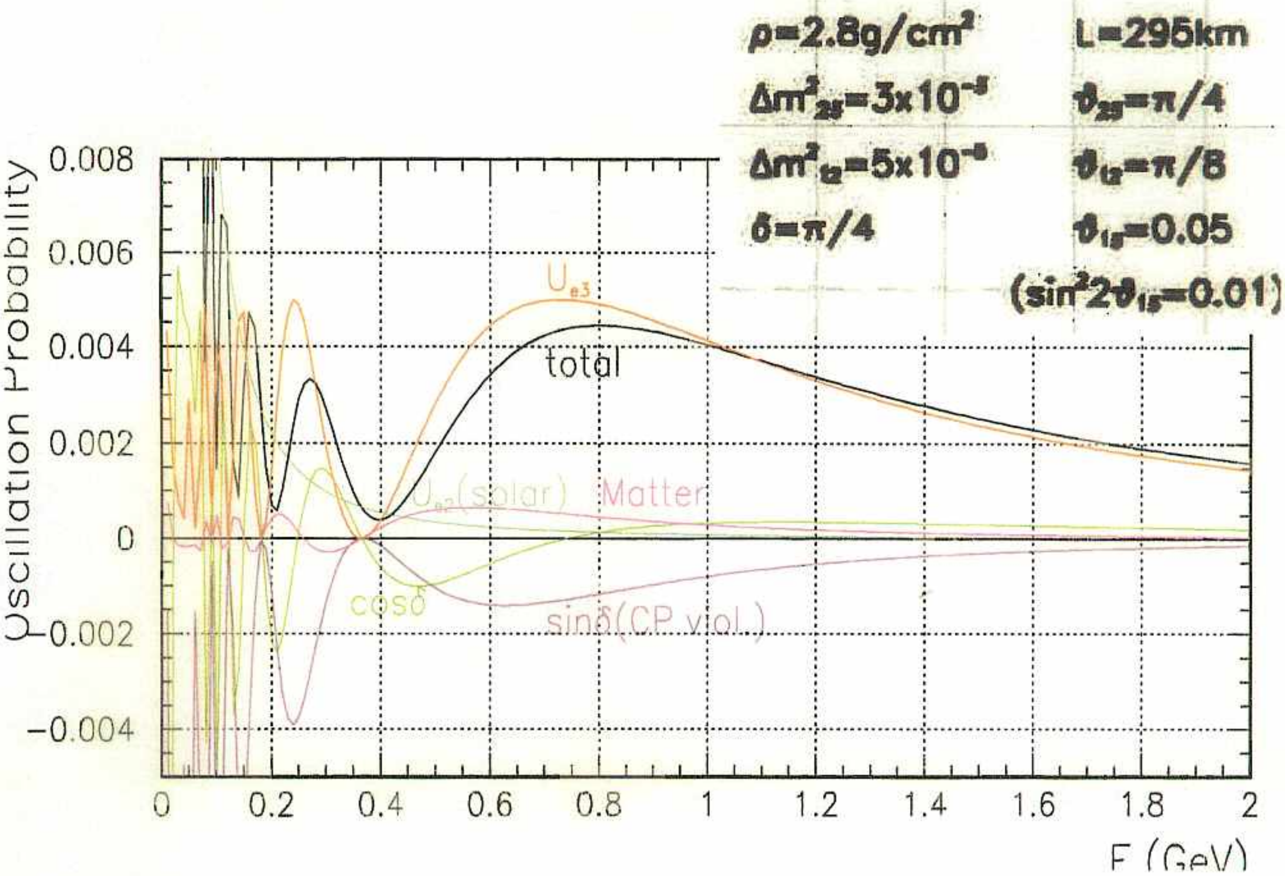

$\nu_\mu \rightarrow \nu_e$ oscillation probability (3)

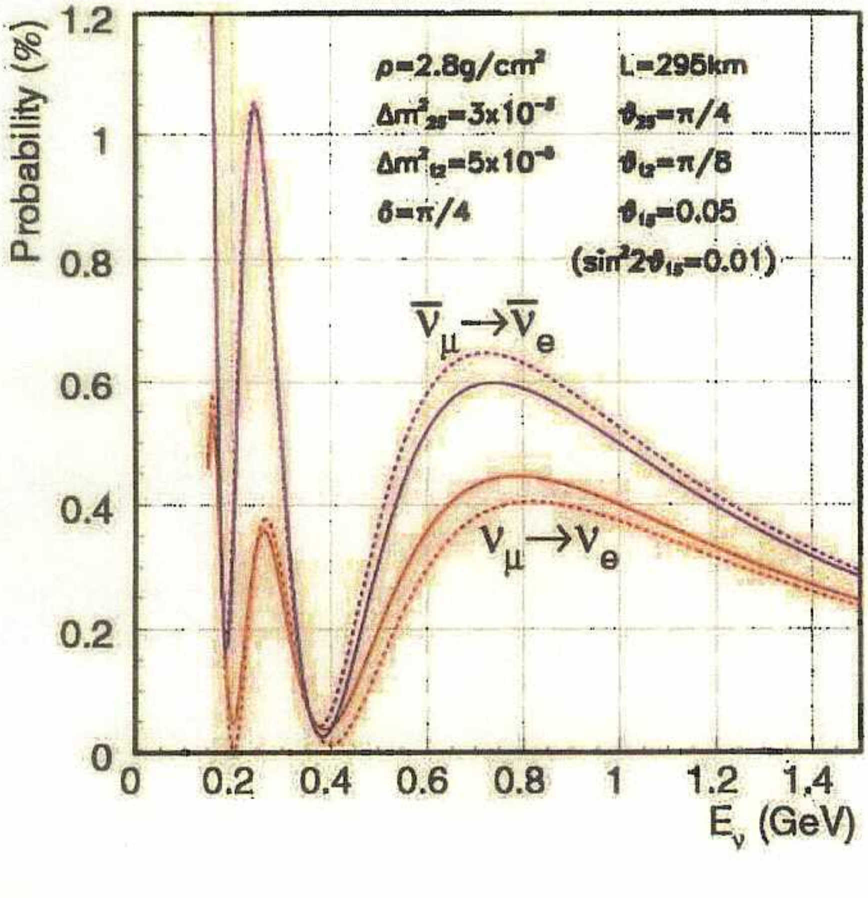

295km

Solid line: w/ matter
Dashed line: w/o matt

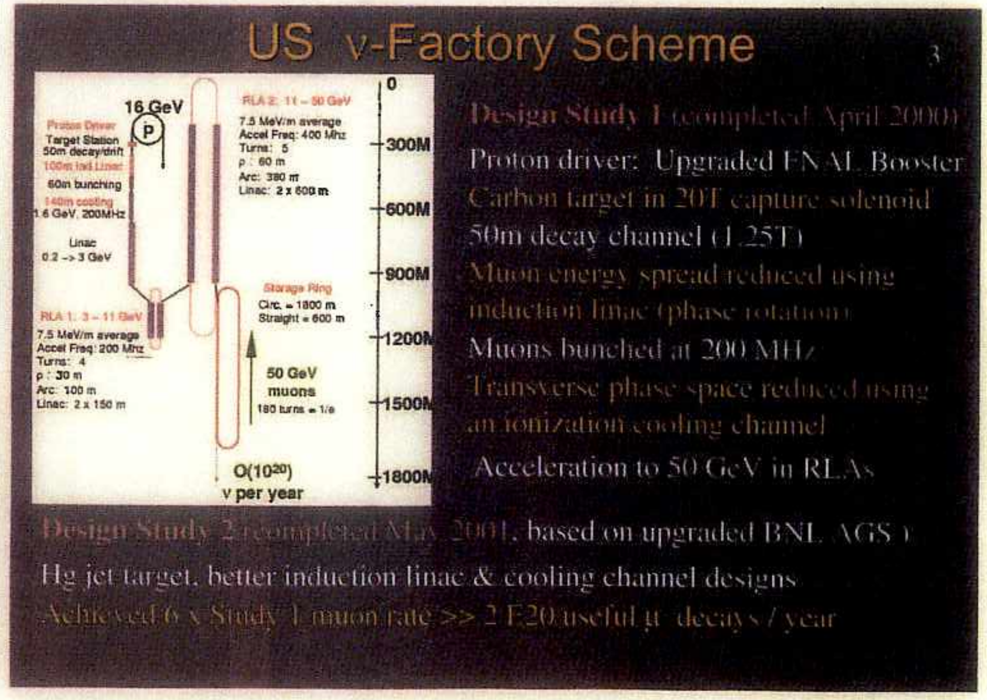

US ν-Factory Scheme

Design Study 1 (completed April 2000)

Proton driver: Upgraded FNAL Booster

Carbon target in 20T capture solenoid

50m decay channel (1.25T)

Muon energy spread reduced using induction linac (phase rotation)

Muons bunched at 200 MHz

Transverse phase space reduced using an ionization cooling channel

Acceleration to 50 GeV in RLAs

Design Study 2 (completed May 2001, based on upgraded BNL AGS)

Hg jet target, better induction linac & cooling channel designs

Achieved 6 x Study 1 muon rate >> 2 E20 useful μ decays / year

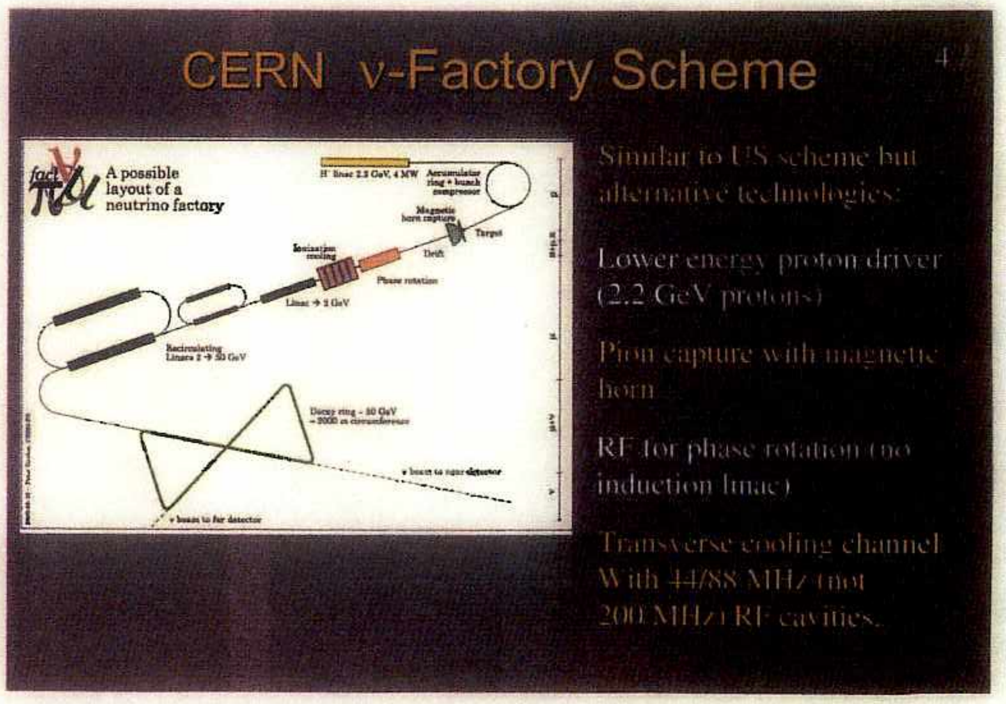

CERN ν-Factory Scheme

Similar to US scheme but alternative technologies:

Lower energy proton driver (2.2 GeV protons)

Pion capture with magnetic horn

RF for phase rotation (no induction linac)

Transverse cooling channel With 44/88 MHz (not 200 MHz) RF cavities.

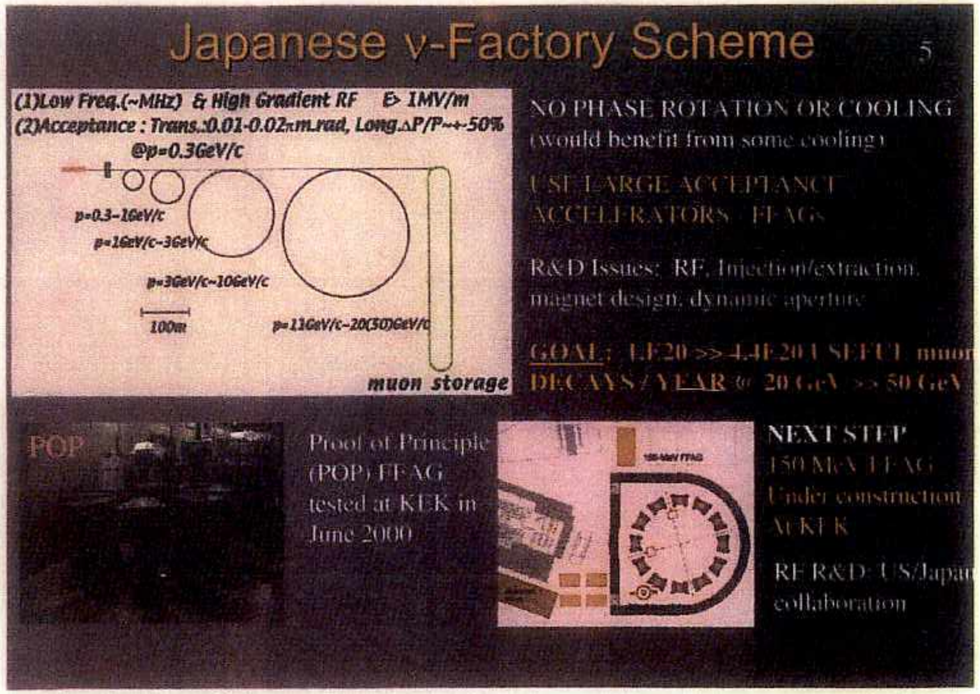

Japanese ν-Factory Scheme

(1)Low Freq.(~MHz) & High Gradient RF E> 1MV/m
(2)Acceptance : Trans.:0.01-0.02πm.rad, Long.ΔP/P~+-50%
@p=0.3GeV/c

NO PHASE ROTATION OR COOLING (would benefit from some cooling)

USE LARGE ACCEPTANCE ACCELERATORS - FFAGs

R&D Issues: RF, Injection/extraction, magnet design, dynamic aperture

GOAL: 1E20 >> 4.4E20 USEFUL muon DECAYS/YEAR @ 20 GeV >> 50 GeV

Proof of Principle (POP) FFAG tested at KEK in June 2000

NEXT STEP
150 MeV FFAG
Under construction
At KEK

RF R&D: US/Japan collaboration

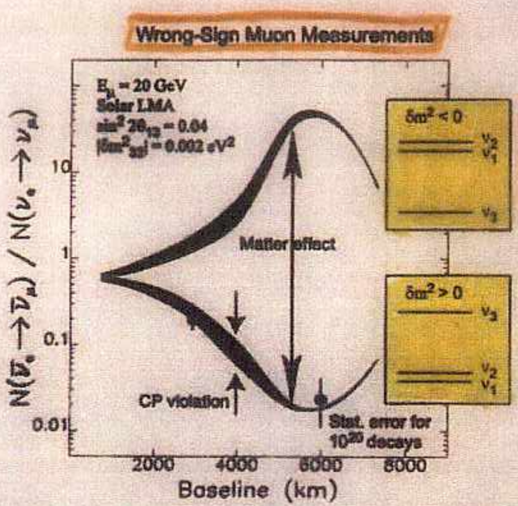

$$\frac{\mu^+ \text{ in } \mu^- \text{ BEAM}}{\mu^- \text{ in } \mu^+ \text{ BEAM}}$$

Figure I: Predicted ratios of $\bar{\nu}_e \to \bar{\nu}_\mu$ to $\nu_e \to \nu_\mu$ rates at a 20 GeV neutrino factory. The upper (lower) band is for $\delta m^2_{32} < 0$ ($\delta m^2_{32} > 0$). The range of possible CP violation determines the widths of the bands. The statistical error shown corresponds to 10^{20} muon decays of each sign and a 50 kt detector. Results are from Ref. 51.

↳ PRESUMABLY BARGER/GEER/RAJA/WHISNANT

ℓ-24

CERVERA et al

COMPREHENSIVE STUDY

CURRENT LIMIT 0.05

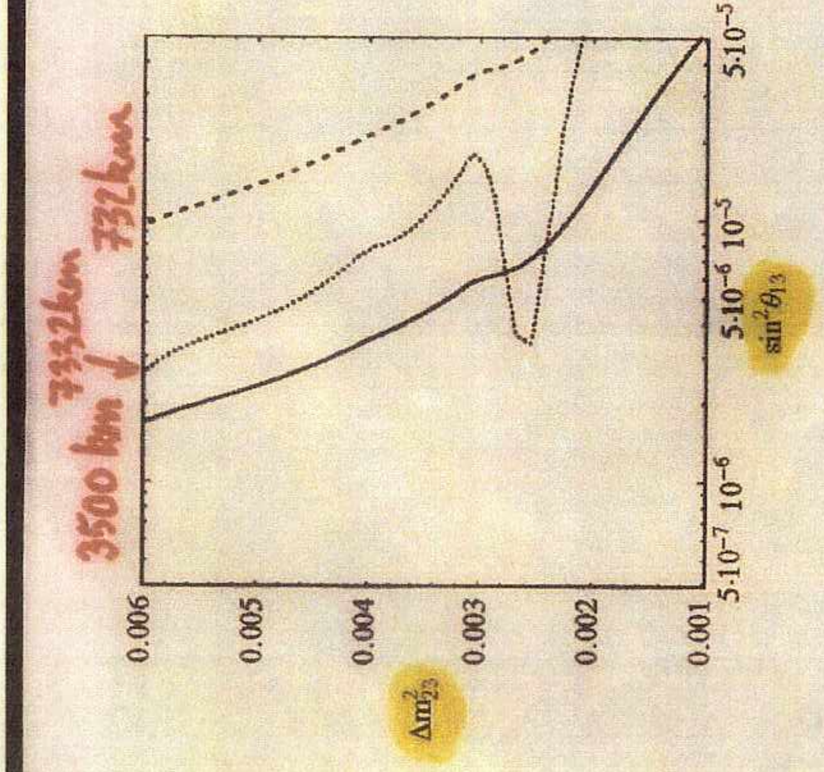

As in Fig. [12], including as well background errors and detection efficiencies.

ℓ-25

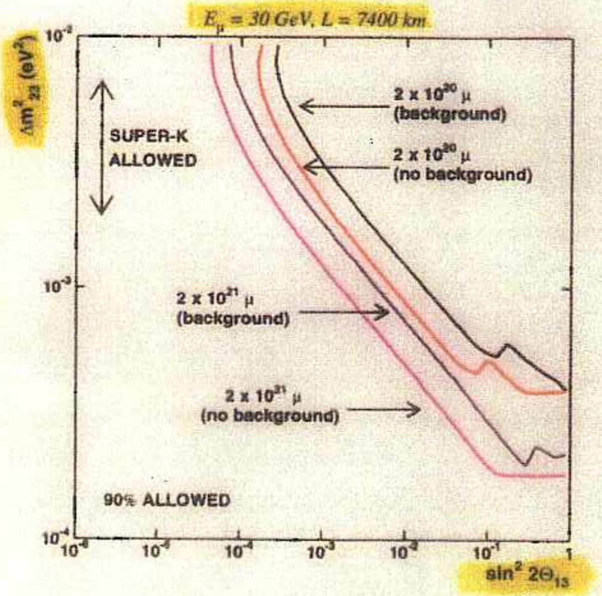

Figure 9: Sensitivity on θ_{13}

Bueno et al.
ICANOE

⑭

Supernova neutrinos

超新星の分類

- Ⅰ型：スペクトル中に水素線がない。
- Ⅱ型：スペクトル中に水素線がある。

Ⅰ型は、さらに

- Ⅰa：Siの吸収線あり。
- Ⅰb：Heの吸収線あり。
- Ⅰc：Si, Heも見えない。

Ⅰa　連星系をなす $3M_\odot \sim 8M_\odot$ の星が進化の過程で質量放出によって水素の外層を失って、中心に残った炭素の白色矮星が爆発的に燃える現象：

C+Oでできた白色矮星からFeを作る。

爆発エネルギー：(C+Oの原子核の束縛エネルギー) −

(Feの 〃)

＋星の重力による束縛エネルギー

$= \sim 10^{51}$ erg.

超新星が光る熱源：

$^{56}Ni \rightarrow {}^{56}Co \rightarrow {}^{56}Fe$

半減期 ~7日 ~77日

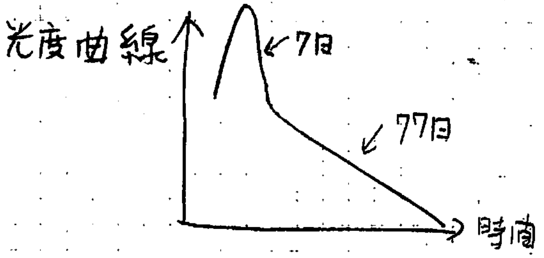

分類

I型

II型

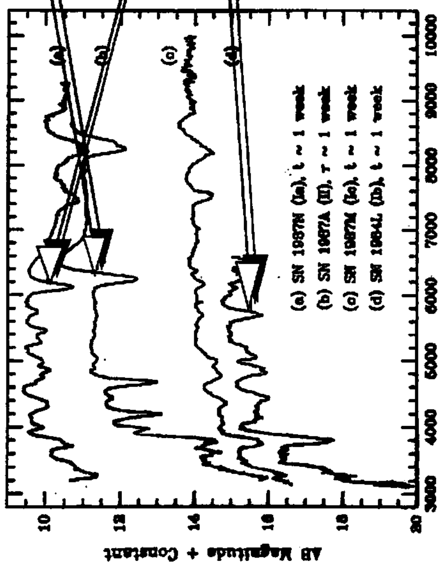

水素のHα 線 6563 → II型

Si 吸収線 → Ia型

He 吸収+輝線 → Ib型

鈴木英之氏修論

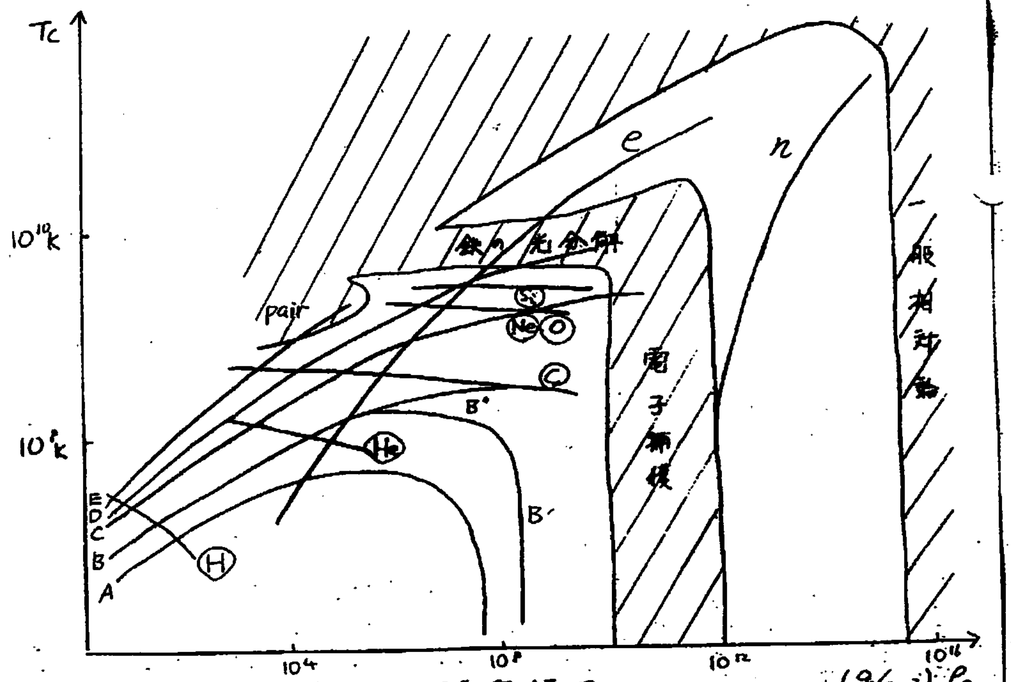

図 2.2 星の進化と不安定領域

A： M<3M⊙, B：3M⊙～8M⊙ , C：8～(10-12) M⊙

D： (10~12)M⊙～(50~100)M⊙ , E：(50～100)M⊙ 以上

電子の縮退

星の中心が高密度になってくると、電子の縮退圧を考えないといけない。
位相空間体積と量子状態数の

$$\boxed{2\times\frac{\left(\frac{4\pi}{3}\right)p_F^3\,V}{(2\pi\hbar)^3}=N_e}$$

$V \longrightarrow$ 体積

N_e ← 電子数

p_F : Fermi momentum

$$n_e=\frac{N_e}{V}$$ ：電子密度

$$=\frac{\rho}{m_N\times\mu_e}$$

m_N ← 核子質量　μ_e ← $\frac{\text{核子数}}{\text{電子数}}=\sim 2$

$$\Rightarrow\ p_F=2\pi\hbar\times\left(\frac{3}{8\pi}\right)^{\frac{1}{3}}\times\left(\frac{\rho}{m_N\mu_e}\right)^{\frac{1}{3}}\quad\text{----} ①$$

Fermi energy は、

$$\varepsilon_F=\frac{1}{2m_e}p_F^2=\frac{2\pi\hbar}{2m_e}\times\left(\frac{3}{8\pi}\right)^{\frac{2}{3}}\times\left(\frac{\rho}{m_N\mu_e}\right)^{\frac{2}{3}}$$

ρ を g/cm³ 単位で書いて

$\rho=1\,\mathrm{g/cm^3}$ 中に m_N が 6×10^{23}

$\hbar c=197\,\mathrm{MeV\cdot fm}=1.97\times10^{-5}\,\mathrm{eV\cdot cm}$

$$\varepsilon_F=\frac{2\pi}{2\times0.5\times10^6}\times(6\times10^{23})^{\frac{2}{3}}\times\left(\frac{3}{8\pi}\right)^{\frac{2}{3}}\times(1.97\times10^{-5})^2\times\frac{1}{\mu_e^{\frac{2}{3}}}\times\left(\frac{\rho}{[\mathrm{g/cm^3}]}\right)^{\frac{2}{3}}\mathrm{eV}$$

$$=4\times\frac{1}{(\mu_e)^{\frac{2}{3}}}\times\left(\frac{\rho}{[\mathrm{g/cm^3}]}\right)^{\frac{2}{3}}\mathrm{eV}$$

Fermi 縮退圧力：

内部エネルギー $U_F=n_e\times\varepsilon_F$

$$=\frac{\rho}{m_N\times\mu_e}\times\frac{4}{(\mu_e)^{\frac{2}{3}}}\times\rho^{\frac{2}{3}}$$

$$\propto\rho^{\frac{5}{3}}$$

$$P_F=\frac{d(U_F/\rho)}{d(1/\rho)}=\frac{\rho}{m_N\mu_e}\times\frac{2}{3}\varepsilon_F\propto\rho^{\frac{5}{3}}\quad\text{----} ②$$

以上は非相対論的計算だったが
$p_F>m_ec$ の相対的場合は、
$\varepsilon_F=\sqrt{m_e^2c^4+p_F^2c^2}-m_ec^2$ として計算すると
$p_F\gg m_ec$ の時、$P_F=\frac{\rho}{m_N\mu_e}\times\frac{1}{3}\varepsilon_F\propto\rho^{\frac{4}{3}}$ となる ----③

P_F が状態方程式で求められる圧力：$P_T=\rho kT/m_N\mu$

μ は平均分子量

と比べた時、

$P_F\gg P_T$ ならば、電子の縮退が主要になる。

非相対論的：$\frac{\rho}{m_N\mu_e}\times\frac{2}{3}\varepsilon_F\gg\rho kT/m_N\mu$

$\propto\rho^{\frac{5}{3}}$

$\Rightarrow\ \rho^{\frac{2}{3}}\gg \text{factor}\times T$

相対論的：　同様にして　$\rho^{\frac{1}{3}}\gg\text{factor}\times T$

$M_{Ch} \simeq \frac{3.1}{\mu_e^2}\frac{m_{pe}}{m_p^2} = 1.47\left(\frac{2}{\mu_e}\right)^2 M_\odot$

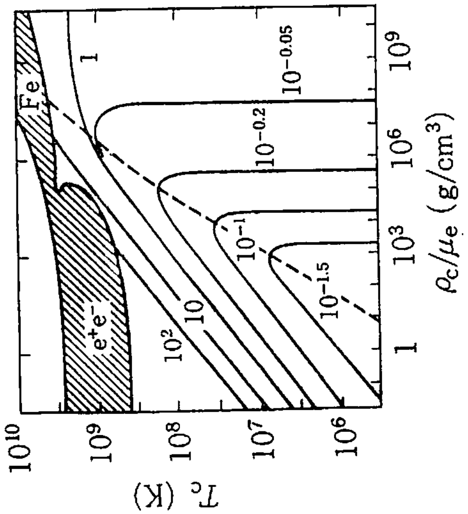

図 1-5　質量 M の星の中心温度 T_c と中心密度．各曲線の数値は M/M_{Ch} ($\mu_e=2$) で表わした星の質量値．斜線部分は電子対生成(e^+e^-)および鉄核分解(Fe)で星が不定になる領域．破線は電子 Fermi 気体で $\psi=$[化学ポテンシャル]$/kT=3$ の線（付録[C]参照）．この線より右下が縮退域，左上が非縮退域である．

$p_F > m_e c$ の相対論的な場合まで含めれば **Fermi** エネルギーは

$$\varepsilon_F = \sqrt{m_e{}^2c^4+p_F{}^2c^2}-m_ec^2 \qquad (1.38)$$

となり，超相対論 $p_F \gg m_e c$ では

$$P_F = \frac{\rho}{m_N\mu_e}\frac{1}{3}\varepsilon_F \propto \rho^{4/3} \qquad (1.39)$$

した臨界密度は，Compton 波長を λ_c と書けば

$p_F = m_e c$ となる臨界密度は,

①より, $\rho_{ec} = \mu_e m_N \frac{8\pi}{3}\left(\frac{m_e c}{h}\right)^3$

$\simeq 10^6 \mu_e \cdot g/cm^{-3}$

このような密度は, どのような質量の星で実現されるか。

星の中の力学平衡は,

$$\left.\begin{aligned}\frac{dP}{dR} &= -\rho\frac{GM}{R^2}\\ M &= \int_0^R \rho\times 4\pi r^2 dr\end{aligned}\right] \text{より} \quad \text{概略は} \left[\begin{aligned}\frac{P}{R} &\simeq \frac{GM\rho}{R^2}\\ M &= \rho R^3\end{aligned}\right.$$

$$\Downarrow$$

$P \simeq G M^{\frac{2}{3}} \rho^{\frac{4}{3}}$ — ④

あるいは, $M \simeq \left(\frac{G^{-3}P^3}{\rho^4}\right)^{\frac{1}{2}}$

Fermi 圧力でささえられている星の質量、

②をこの式に入れる。

$\boxed{M \simeq M_{Ch} \times \left(\frac{\rho}{\rho_{ec}}\right)^2}$ ---- ⑤

$M_{Ch} = \frac{1}{\mu_e^2}\frac{m_{pe}^3}{m_p^2} \sim \frac{10^{33}}{\mu_e^2} g \sim 1\times M_\odot$

ちなみに $m_{pe} \equiv \sqrt{\frac{hc}{G}} \sim 10^{-5} g \sim \frac{10^{19} GeV}{c^2}$

$M < M_{Ch}$ では, ⑤式で ρ が決まる。

星の中の 温度, 密度の 関係式は,

$P = \rho k T / m_N \mu$ 状態方程式

④の力学平衡より

$P = G M^{\frac{2}{3}} \rho^{\frac{4}{3}}$ なので

$$G M^{\frac{2}{3}} \rho^{\frac{4}{3}} = \rho k T / m_N \mu$$

$$\Rightarrow \rho = \left(\frac{kT}{m_N \mu}\right)^3 \times \frac{1}{G^3 M^2}$$

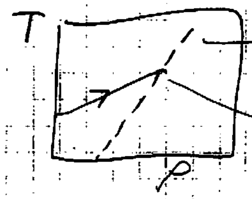

→ 右側が縮退域

→ ここで縮退密度に達して、温度に無関係な密度でつりあう。

また、$\rho \gg \rho_{ec}$ の場合は,

③式を ④式へ入れると

$$P_F \propto \rho^{\frac{4}{3}} \qquad M = \left[\frac{G^{-3} P^3}{\rho^4}\right]^{\frac{1}{2}}$$

Mは一定値となる。その値が Mch

すなわち、電子の縮退圧力によって支えられている星の質量には上限値がある。

Chandrasekhar 質量：

正確には、$M_{ch} = \frac{3.1}{\mu_e^2} \times \frac{m_{pl}^3}{m_p^2} = 1.47 \times \left(\frac{2}{\mu_e}\right) M_\odot$

☆H 燃焼

太陽と同じように

PP-cycle

$p(p,e^+\nu)\alpha(p,\gamma)^3He$

- $^3He(^3He,2p)^4He$
- $^3He(\alpha,\gamma)^7Be$
  - $^7Be(e^-,\nu)^7Li(p,\alpha)^4He$
  - $^7Be(p,\gamma)^8B(e^+,\nu)$
    $^8Be(\alpha)^4He$

CNO-cycle

$^{15}N(p,\gamma)^{16}O(p,\gamma)^{17}F(e^+,\nu)^{16}O(p,\alpha)^{14}N$

どちらも反応としては $4p \to {}^4He + 2e^+ + 2\nu_e$

太陽では CNOの寄与が1.5%位だが、太陽より重い星では CNO cycleが主となる。

☆ He燃焼

Aが5と8には安定な原子核はない。

また、^4Heと^{12}Cの間の核はすべて核子あたりの結合エネルギーが小さいので

$$\alpha(\alpha,\gamma)^8Be^*(\alpha,\gamma)^{12}C$$

☆ 重イオン燃焼

$^{12}C + {}^{12}C \to {}^{24}Mg$ の高励起レベル

$\hookrightarrow {}^{20}Ne + \alpha$

${}^{23}Na + p$

${}^{23}Mg + n$

さらに高温

$^{20}Ne(\gamma,\alpha)^{16}O$, $^{20}Ne(\alpha,\gamma)^{24}Mg$; Ne燃焼

$^{16}O + {}^{16}O \to {}^{24}Mg, {}^{28}Si, {}^{32}S, {}^{36}Ar, {}^{40}Ca$ ---

ことになる. このため(1.28)のΩとUが一定のままでEが減少することができるのである.

図1-6は原子核の質量数Aと核子当りの結合エネルギーの関係である. この特性は核力の性質と原子核全体のCoulombエネルギーの関係で決まっているものである. この関係から導かれる1つの重要な性質は^{56}Fe核のあたりで

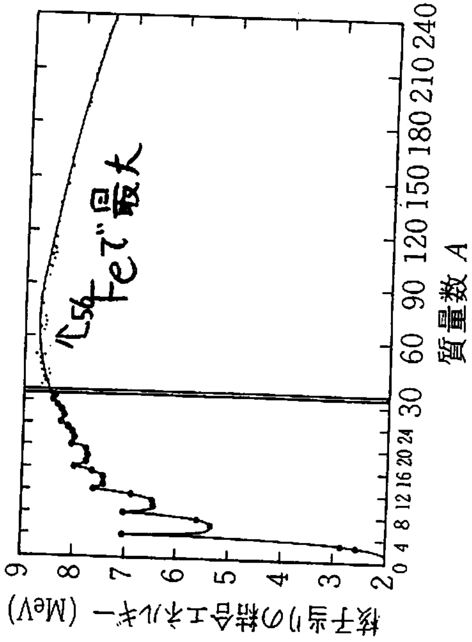

図1-6 原子核の質量数Aと核子当りの結合エネルギー. $A=1\sim30$の部分は横軸を拡大して示してある. 鉄($A=56$)付近で結合エネルギーが最大となる.（巻末文献[32].）

SN-10

197

SN-11

最終燃焼は、Si燃焼

$Si+Si \rightarrow Cr, Fe, Ni$ ………

Si燃焼の温度は、$\sim 10^{9.6}$Kであり、そこまで縮退せずに到達できる十分に重い星でなければならない。

例25M⊙の星：

H 燃焼	：	$10^{6.8}$年	6×10^{7}K
He 〃	：	$10^{5.7}$年	2.3×10^{8}K
C 〃	：	$10^{3.8}$年	9.3×10^{8}K
Ne 〃	：	1年	1.7×10^{9}K
O 〃	：	0.5年	2.3×10^{9}K
Si 〃	：	1day	4.1×10^{9}K

密度は $\sim10^{7}$g/cm^{3}に達する。

最終的にFeのコアができる。

Feが最も結合エネルギーが大きいため。

超新星爆発直前の星の姿

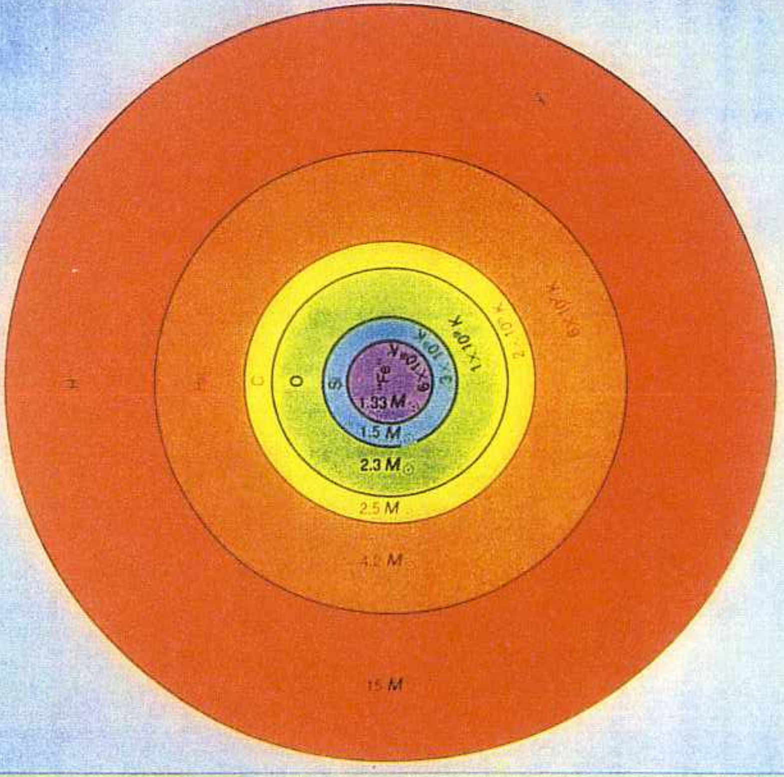

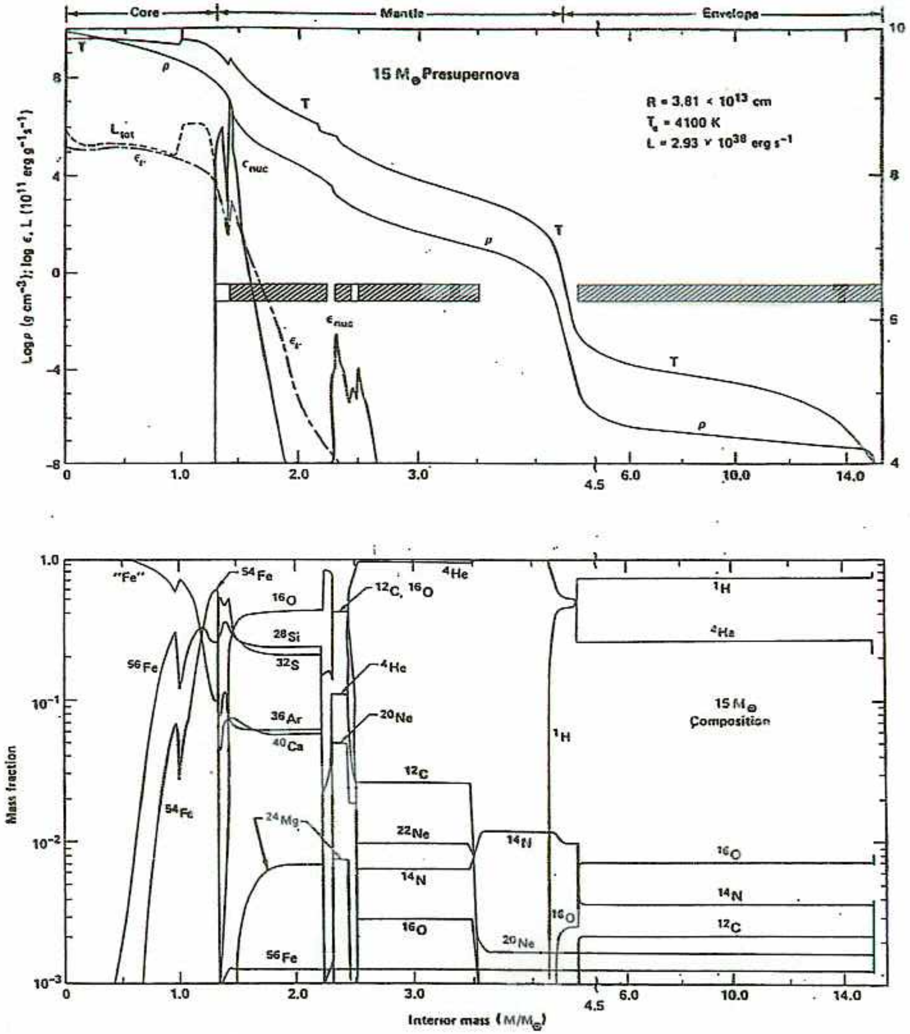

Figure 1 Structure and composition of a 15-$M_\odot$ presupernova star at a time when the edge of its iron core begins collapsing at 1000 km s^{-1}. Neutrino emission from electron capture (ε_ν) dominates photodisintegration in the total energy losses (L_{tot}) throughout most of the iron core. Central temperature here is 7.62×10^9 K and density is 9.95×10^9 g cm^{-3}. Spikes in the nuclear-energy generation rate (ε_{nuc}) show the location of active burning shells, while cross-hatched, blank, and open bars indicate regions that are convective, semiconvective, and radiative respectively. The species "Fe" includes all isotopes from $48 \lesssim A \lesssim 65$ having a neutron excess greater than ^{56}Fe. Note a scale break at 4.5 $M_\odot$. Figure adapted from Woosley & Weaver (1985).

図 3.2.1 Pre collapse structure (15M⊙)
Woosley & Weaver (1986)[1] より

超新星爆発

十分に重い星（$\gtrsim 12 M_\odot$）は、非縮退のままで Fe のコアが形成される。核燃焼はこの段階で終了するので、エネルギーの流出によってコアは収縮し温度が上がる。

すると $^{56}Fe + \gamma \rightarrow 13\,^{4}He + 4n - 124.4\,MeV$

$^{4}He + \gamma \rightarrow 2P + 2n - 28.3\,MeV$

という吸熱反応がはじまる。

星の構造不安定性について

星内部の物質の運動方程式

$$\frac{\partial^2 r}{\partial t^2} = -4\pi r^2 \frac{\partial P}{\partial M_r} - \frac{GM_r}{r^2} \quad \text{------ (ア)}$$

M_r：球殻 r 内の質量

$$\left.\begin{aligned} r(M_r) &\rightarrow \underline{r(M_r)} + \delta r(M_r, t) \\ P(M_r) &\rightarrow \underline{P(M_r)} + \delta P(M_r, t) \end{aligned}\right\} \text{のように摂動を加える。}$$

$$\frac{\partial^2 \delta r}{\partial t^2} = -8\pi r \delta r \frac{dP}{dM_r} - 4\pi r^2 \frac{d\delta P}{dM_r} + 2\frac{GM_r}{r^3}\delta r \quad \text{--- (イ)}$$

となる。

$$\frac{\partial r}{\partial M_r} = \frac{1}{4\pi r^2 \rho}$$

［質量分布の連続性］に摂動を入れて

$$\frac{\partial \delta r}{\partial M_r} = \frac{1}{4\pi r^2 \rho}\left(-2\frac{\delta r}{r} - \frac{\delta \rho}{\rho}\right) \quad \text{------ (ウ)}$$

$\delta r = \alpha r$ という摂動として考えれば、(ウ)は $\frac{\delta \rho}{\rho} = -3\frac{\delta r}{r}$ となる。断熱則：$P \propto \rho^\gamma$ なので

$$\frac{\delta P}{P} = -3\gamma \times \frac{\delta r}{r}$$

となる。

これを(イ)に入れて

$$\frac{\partial^2 \delta r}{\partial t^2} = -8\pi r \delta r \frac{dP}{dM_r} - 4\pi r^2 \times \frac{d\left[-3\times\gamma\times\frac{\delta r}{r}P\right]}{dM_r} + 2\frac{GM_r}{r^3}\delta r$$

$$= 4\pi r \times \delta r \times \frac{dP}{dM_r} \times [-2 + 3\gamma] + 2\frac{GM_r}{r^3}\delta r$$

(ア)を使って

$$= \frac{\delta r}{r}\left(-\frac{\partial^2 r}{\partial t^2} - \frac{GM_r}{r^2}\right)[-2+3\gamma] + 2\frac{GM_r}{r^3}\delta r$$

$$= \frac{\partial^2 r}{\partial t^2} \times \frac{\delta r}{r}[2-3\gamma] + \frac{GM_r}{r^3}[4-3\gamma] \times \delta r$$

平衡状態で $\frac{\partial^2 r}{\partial t^2} = 0$ とすると

$$\boxed{\frac{\partial^2 \delta r}{\partial t^2} = [4-3\gamma]\frac{GM_r}{r^3}\delta r}$$

したがって $\gamma < \frac{4}{3}$ では、δr の変化に対してそれが大きくなる方向に変化し、不安定になる。

$^{56}Fe + \gamma \rightarrow 13\,^{4}He + 4n - 124.4\,MeV$ の吸熱反応では $\gamma < \frac{4}{3}$ となり、熱圧力と重力のバランスが崩れる。

Saha の式：

$$\frac{n_{He}^{13}\, n_n^{4}}{n_{Fe}} = \frac{g_{He}^{13}\, g_n^{4}}{g_{Fe}} \times \left(\frac{kT}{2\pi\hbar^2}\right)^{24} \left(\frac{m_{He}^{13}\, m_n^{4}}{m_{Fe}}\right)^{\frac{3}{2}} e^{-\frac{Q}{kT}}$$

$\uparrow$ 統計重度

$g_{He} = 1,\ g_n = 2,\ g_{Fe} \simeq 1.4$

低温で100% Fe であったとすると X_{He} を He fraction として

$$\frac{X_{He}^{17}}{1 - \frac{14}{13}X_{He}} = 2.47\times 10^{62} \times \frac{1}{g_{Fe}}\left(\frac{\rho}{10^9\,g/cm^3}\right)^{-16}\left(\frac{T}{1\,MeV}\right)^{24} \exp\left(-\frac{Q}{T}\right.$$

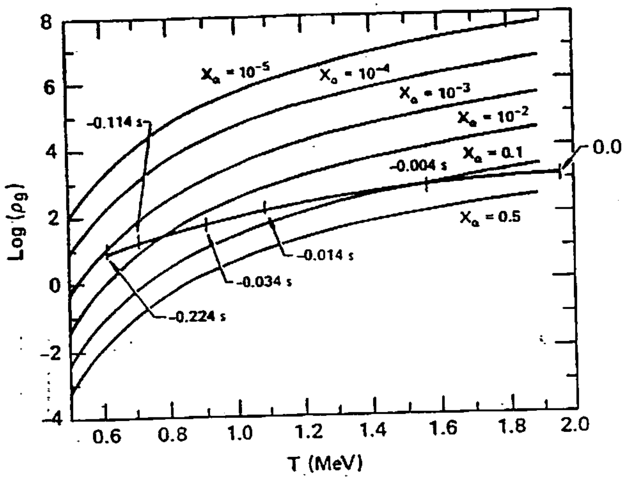

図 3.3.1. 鉄の光分解と collapsing core の軌跡 Mayle (1985)[2] より

密度の増加に伴う内部エネルギーの増加が、鉄の分解に使われてしまい、圧力の増加が小さくなってしまうために収縮をおさえることができず、反応が爆発的に進行する。

爆発のタイムスケール

- 星の dynamical な構造変化の尺度となる time scale は自由落下時間 (free-fall collapse time) は、

$$\tau_{ff} = \left(\frac{R^3}{GM}\right)^{\frac{1}{2}} \sim \frac{1}{\sqrt{G\bar{\rho}}} \sim 4\times10^{3}\sec\times\left(\frac{\bar{\rho}}{1\,g/cm^3}\right)^{-\frac{1}{2}}$$

$\bar{\rho} \sim 10^{10} g/cm^3$ を入れると

$\tau_{ff} = \sim 4\times10^{-2}$ sec 位になる。

これは、Fe のコアについてであり、外層のマントル $\rho \cong 10^2 g/cm^3$ では、$\tau_{ff} = \sim 400$sec

- また、ニュートリノ放出に対しては、星がニュートリノに対して opaque になった時のニュートリノの拡散時間：

$$\tau_{diff} = \frac{3R^2}{c\lambda_\nu}$$

λ_ν はニュートリノの mean free path

$\rho = 10^{15} g/cm^3$, $R = 10km$, $\sigma = 10^{-44}\left(\frac{E_\nu}{MeV}\right) cm^2$

$m_u = 10^{-24} g$, $\Rightarrow \lambda_\nu = m_u/\rho/\sigma \Rightarrow E_\nu = 30MeV$ で

$\lambda_\nu \cong 100m$

$$\tau_{diff} = \sim 1\sec\times\left(\frac{R}{10km}\right)^2\left(\frac{\lambda_\nu}{100m}\right)^{-1}$$

- 星からの光の放出は、コアの重力崩壊の後に重い外層をふき飛ばす必要があり、通常、数時間かかる。

ニュートリノ放出過程

- 重力崩壊時には

$$\left[\begin{array}{l} e^- p \to \nu_e n \\ e^-(A,Z) \to \nu_e (A,Z-1) \end{array}\right] \text{電子捕獲反応}$$

の反応により ν_e が生まれる。
これにより、コアは より中性子化して行き、中性子星の形成へ進む。

- コアの収縮のはじめ頃は、このニュートリノは自由に外へ出て行くが、コアの収縮が進んで密度が高くなると、ニュートリノに対しても不透明になる。ニュートリノはコアにトラップされ、ニュートリノも縮退をはじめる。これによって上記の電子捕獲反応は抑制される。([illegible])
結局、電子捕獲反応によって放出されるニュートリノは全体の$\frac{1}{100}$程度。

- コアの中心密度が核子密度 ($\rho_{nuc} \sim 2.7 \times 10^{14} g/cm^3$) を超えると核力の影響によって γ が急に大きくなり、収縮が止まる。 崩壊開始から、数10 msec たった頃である。
コアの大きさは 10 km 程度。

- このコアのバウンスによって生まれた衝撃波は外へ伝ぱんし、まわりの物質をあたためる。それによって

$$\left.\begin{array}{l} e^+e^- \to \nu\bar{\nu} \\ NN \to NN\nu\bar{\nu} \end{array}\right\} \text{のプロセスによってすべてのタイプの}$$

ニュートリノが初期中性子星の表面近く (neutrino sphere) で生まれる。

熱源となる。

$1M_\odot$ のコアは、10 MeV オーダーの ν に対して $\rho > 10^{11}$ g/cm^3 では不透明で

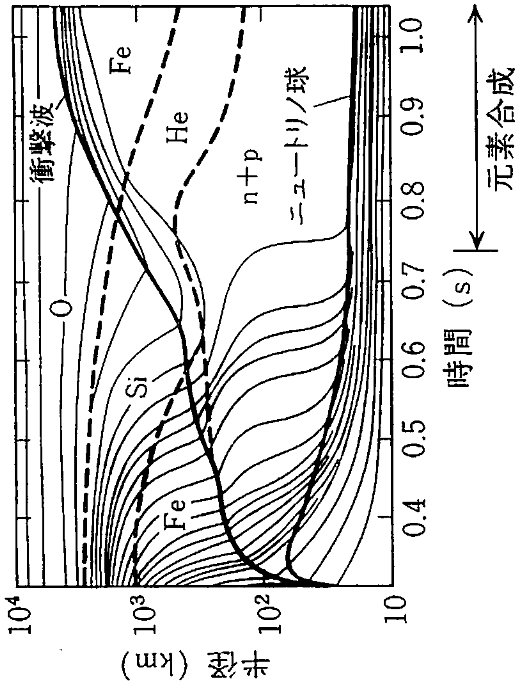

図 2-9 Ⅱ型超新星爆発の数値シミュレーションの例. ある質量シェルの半径 $r(M_r, t)$ の時間変化をいろいろの M_r について描いてある. (原図は, J.R. Wilson *et al.*: Ann. N.Y. Academy Sci. 470 (1986) 267.)

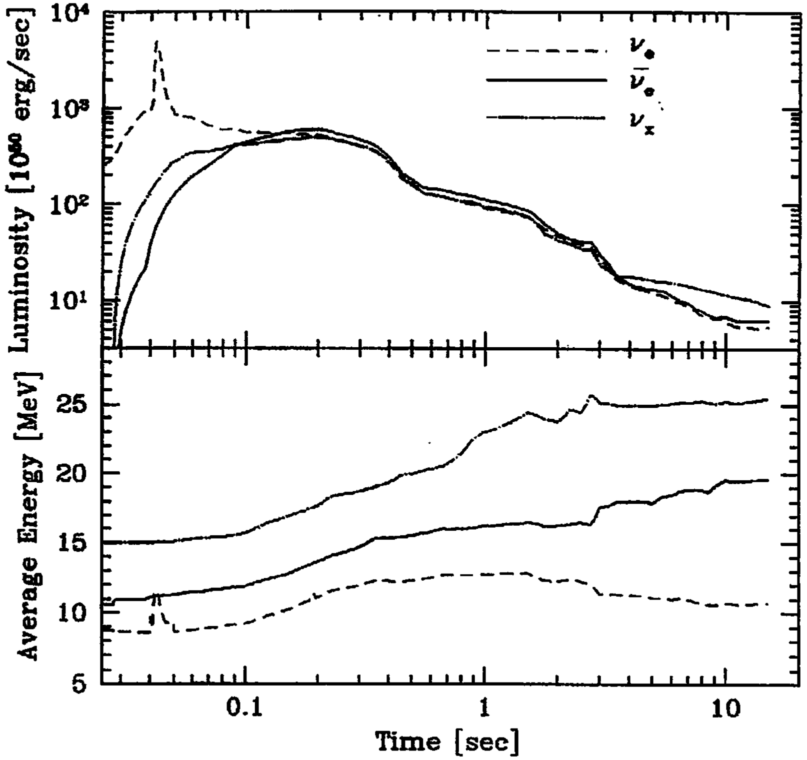

FIG. 1.—Time evolution of neutrino luminosity and average energy of the numerical supernova model used in this paper. The dashed line is for ν_e, solid line for $\bar{\nu}_e$, and dot-dashed line for ν_x (=each of ν_μ, ν_τ, $\bar{\nu}_\mu$, and $\bar{\nu}_\tau$). The core bounce time is 3–4 ms before the neutronization burst of ν_e's.

resent any expected spectral shape. For generic features of supernova neutrino emission see, e.g., Burrows et al. (1992).

Figure 3 shows the radius of selected mass points as a function of time for the present model. This model explodes by the delayed explosion mechanism, and its features are

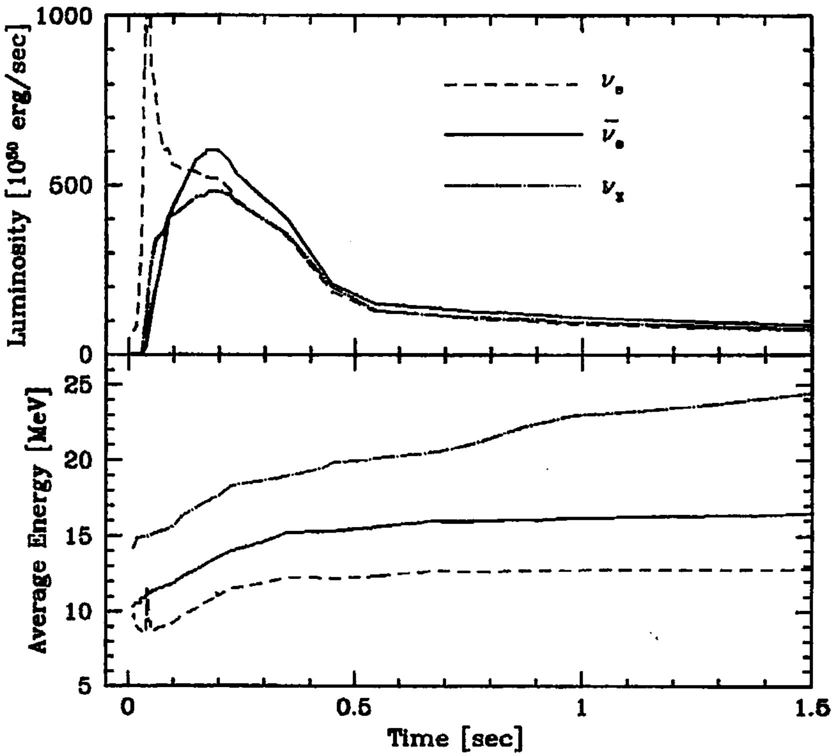

FIG. 4.—Same as Fig. 1, but for the early phase in linear coordinates

SN1987a

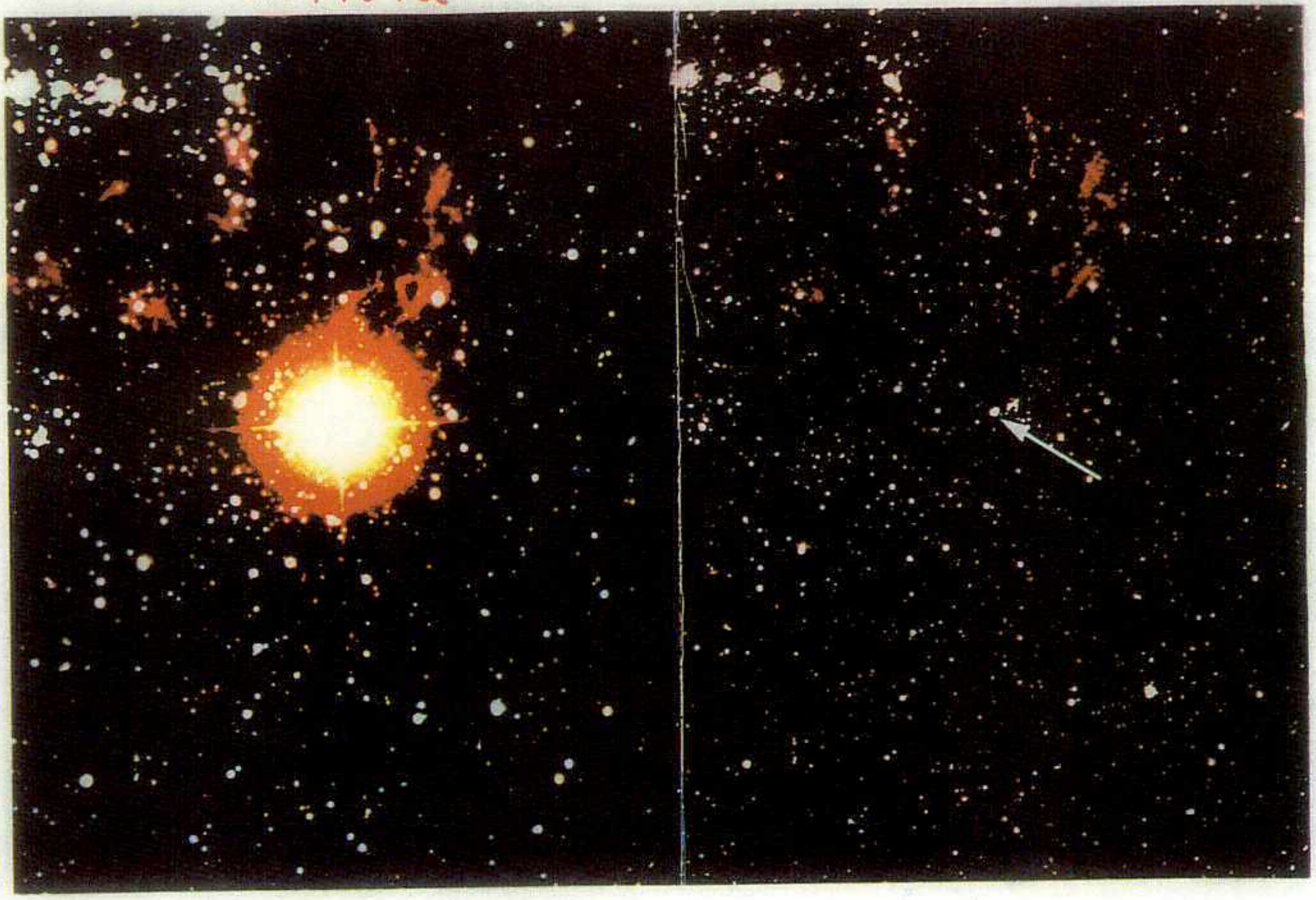

SN1987A MARCH 1987

1984

LARGE MAGELLANIC CLOUD

Photo by David Malin and Ray Sharples with the Anglo-Australian Telescope

SN-22

大マゼラン雲の位置

超新星のSN1987Aは、地球からの距離約17万光年の大マゼラン雲の中にある。大マゼラン雲は銀河系に最も近い銀河であるが、銀緯−30度以上にあるため、北半球にある日本からは観測できない。

SN-24

SN1987A signal by Kamiokande-II

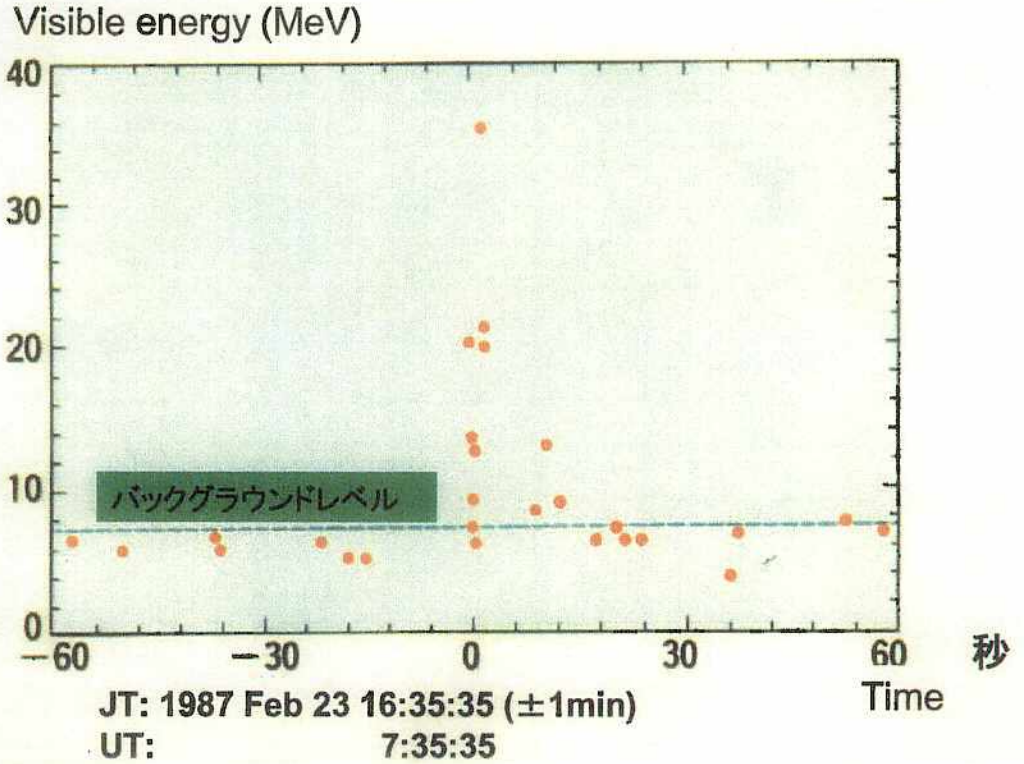

SN1987A signal by Kam-II and IMB

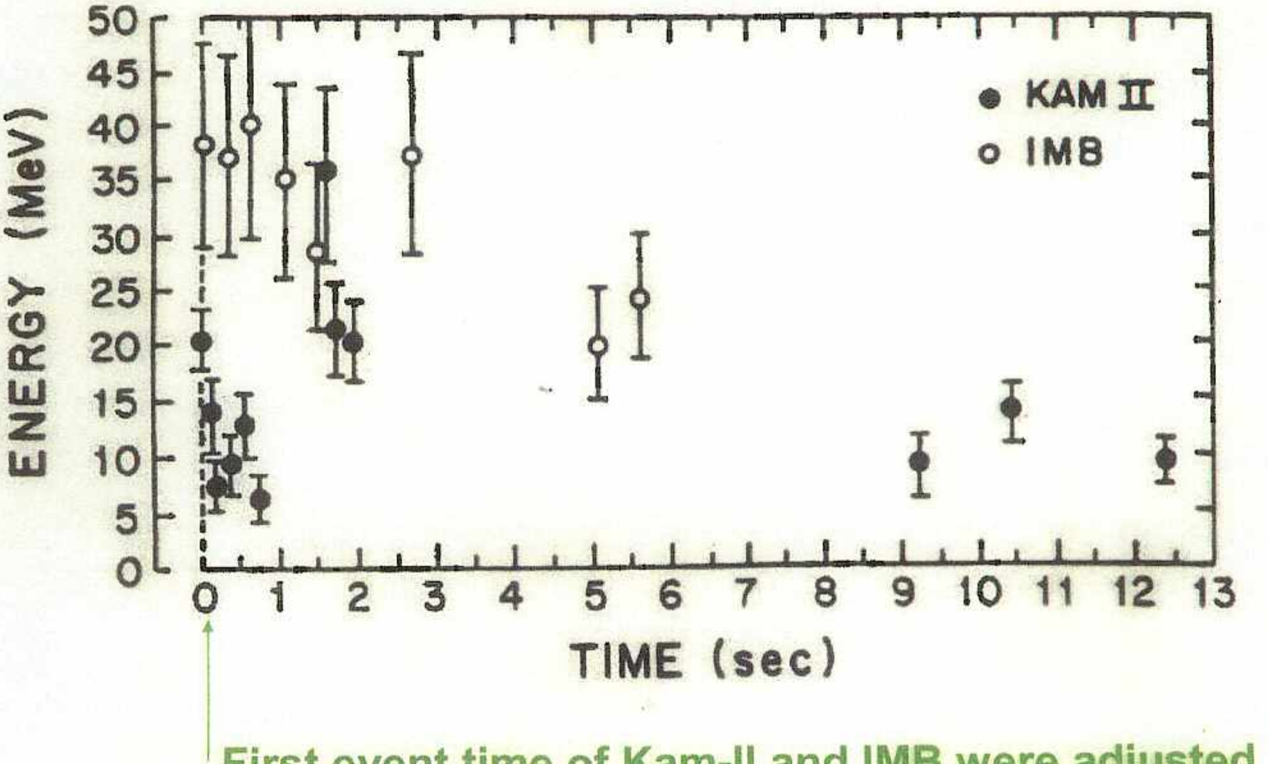

First event time of Kam-II and IMB were adjusted

SN-25

Typical event of SN1987A neutrino signal

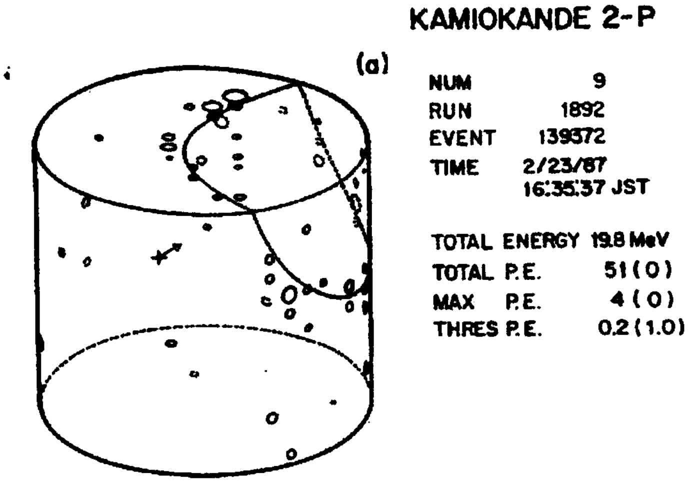

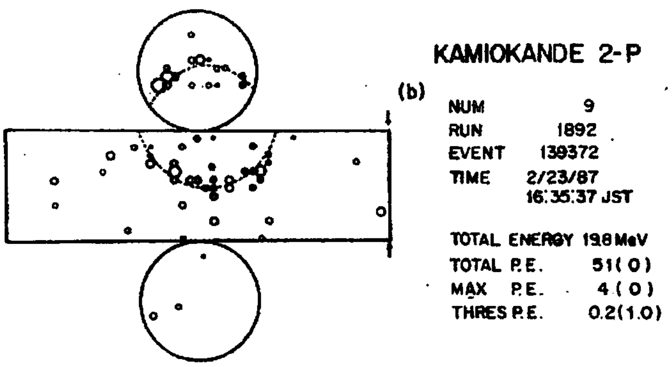

SN-20

SN1987A data (angle and energy)

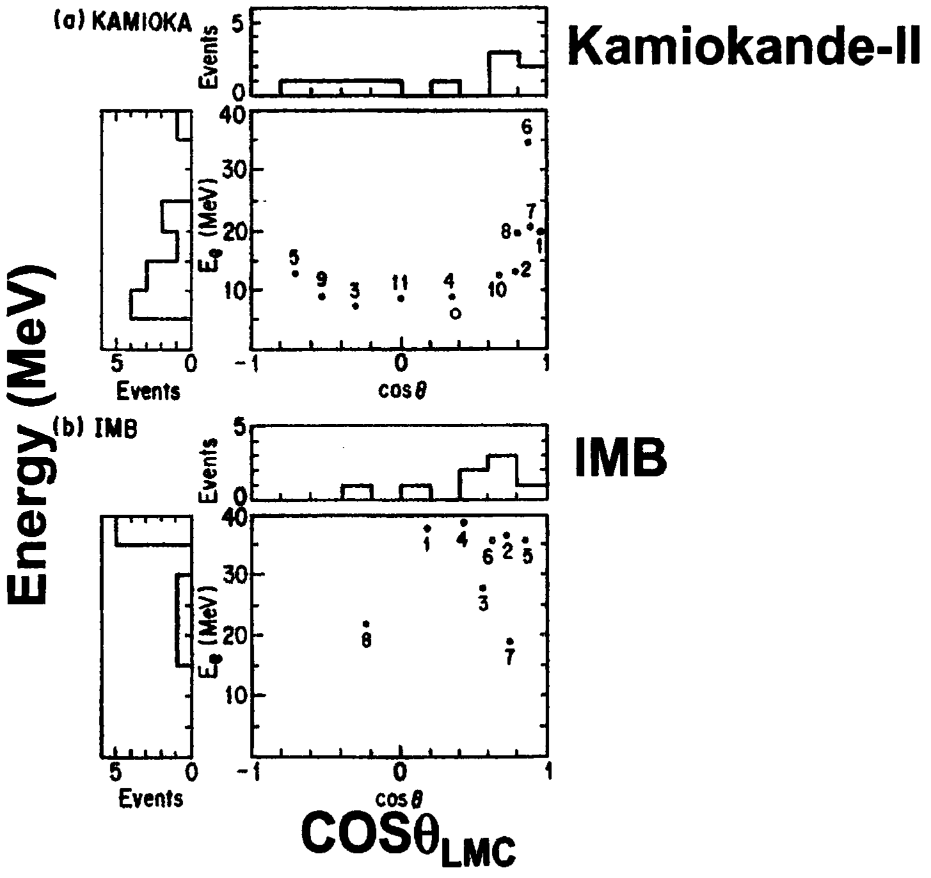

SN-27

SN-27

sec with $N_{\mathrm{hit}} \le 20$ in the 10-h period surrounding the time 7:35:35 UT.

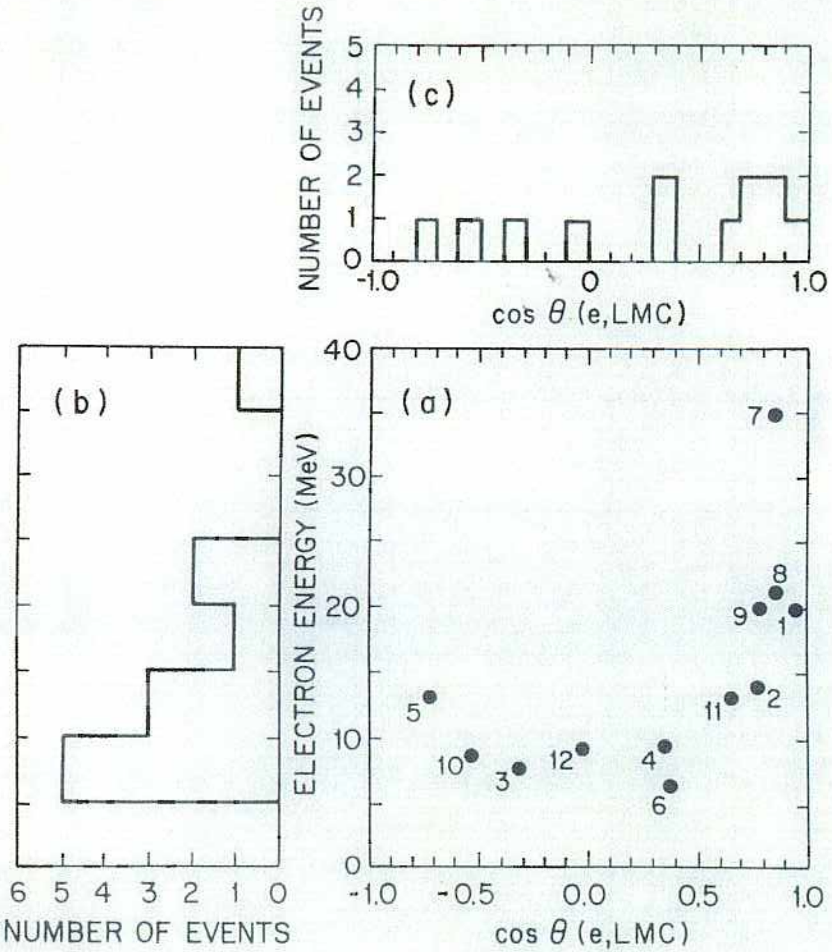

FIG. 13. (a) Scatter plot of the detected electron energy (in MeV) and the cosine of the angle between the measured electron direction and the direction of the Large Magellanic Cloud. The number to the left of each entry is the time-sequential event number from Tables I and II. The two projections of the scatter plot are displayed in (b) and (c).

206

Neutrino cross section for water target

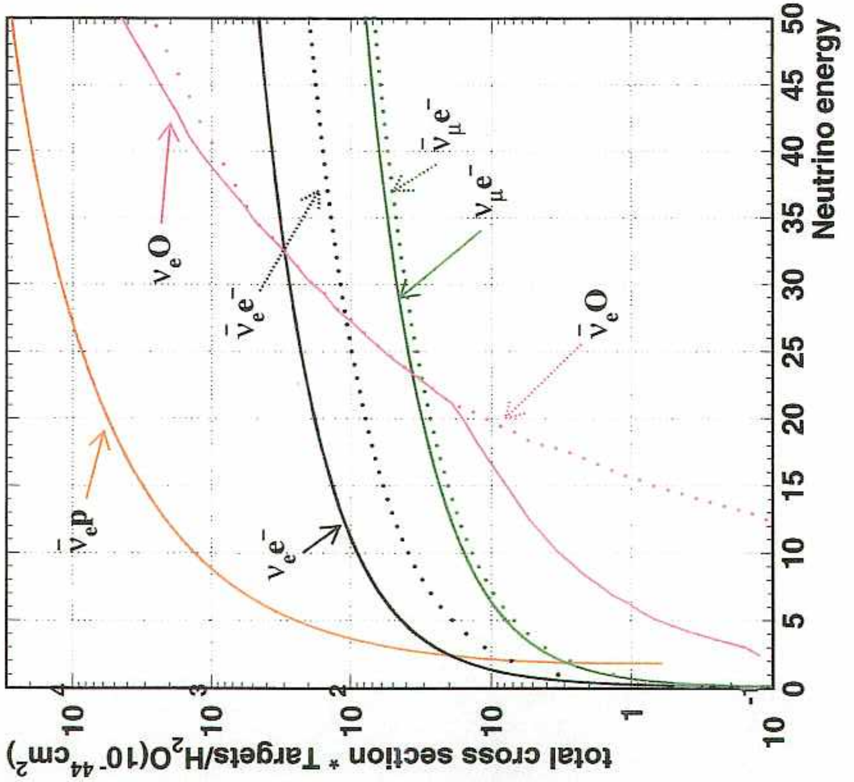

- $\bar{\nu}_e + p \rightarrow e^+ + n$
  $\sigma = 8.9 \times 10^{-42}$
  $\times (E\nu/10\mathrm{MeV})^2\ \mathrm{cm}^2$
- $\nu_e + e^- \rightarrow \nu_e + e^-$
  $\sigma = 9.3 \times 10^{-44}$
  $\times (E\nu/10\mathrm{MeV})\ \mathrm{cm}^2$
- $\bar{\nu}_x + e^- \rightarrow \bar{\nu}_x + e^-$
  $\sigma = 3.9 \times 10^{-44}$
  $\times (E\nu/10\mathrm{MeV})\ \mathrm{cm}^2$ (e)
  $\sigma = 1.3 \times 10^{-44}$
  $\times (E\nu/10\mathrm{MeV})\ \mathrm{cm}^2$ (μ, τ)
- $\nu_{\mu,\tau} + e^- \rightarrow \nu_{\mu,\tau} + e^-$
  $\sigma = 1.5 \times 10^{-44}$
  $\times (E\nu/10\mathrm{MeV})\ \mathrm{cm}^2$
- $\nu_e + {}^{16}O \rightarrow e^- + {}^{16}F$
  $\sigma = {\sim}1 \times 10^{-44}$
  $\times (E\nu\,(\mathrm{MeV}) - {\sim}13)^2\ \mathrm{cm}^2$

SN-30

Angular distribution of each reaction

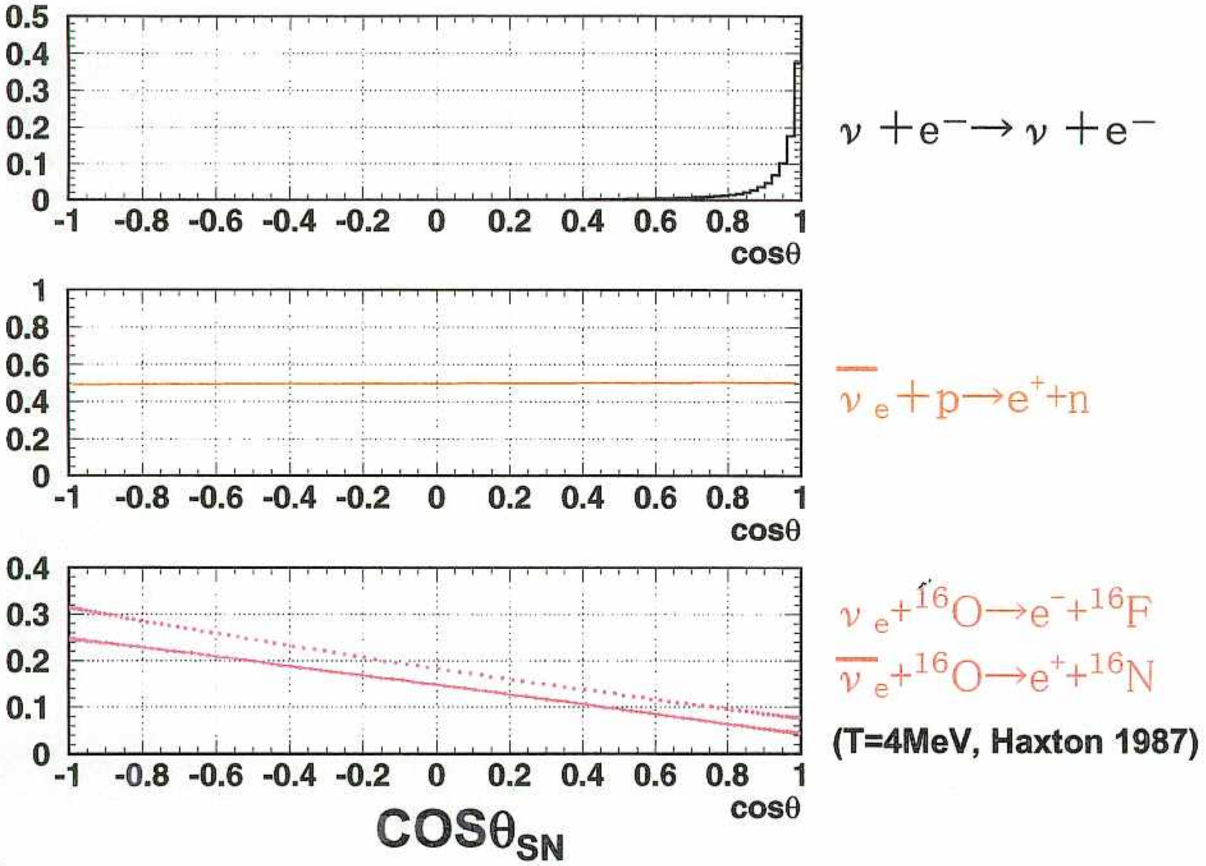

SN-31

Angular distribution of $\bar{\nu}_e + p \rightarrow e^+ + n$

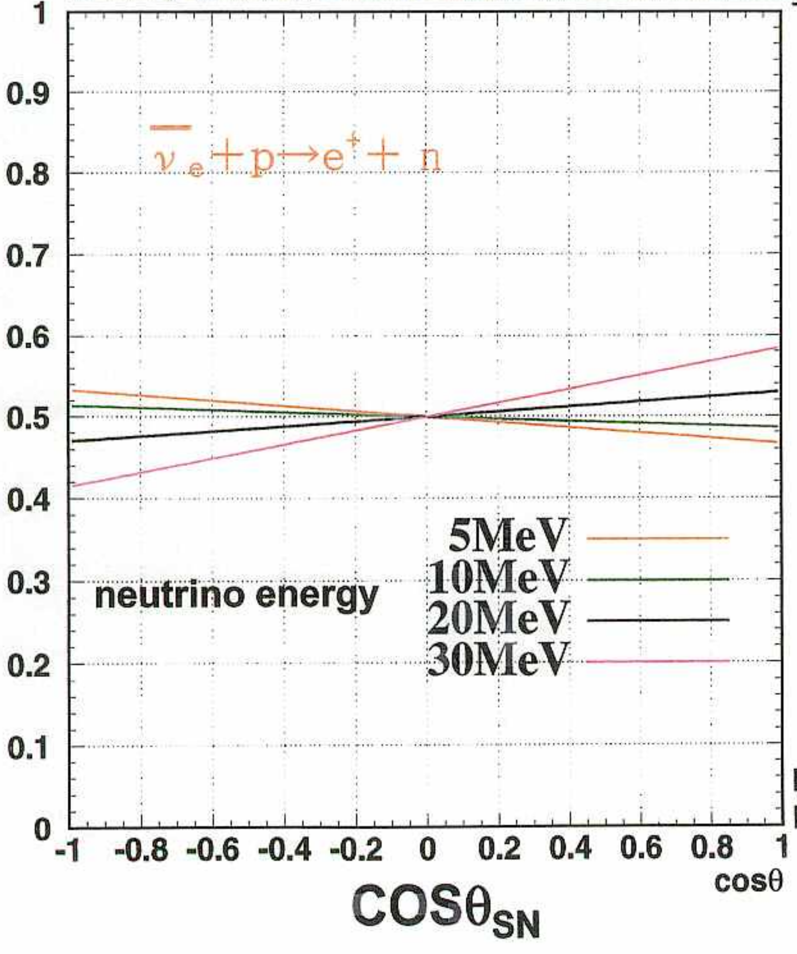

P.Vogel and J.F.Beacom,
Phys.Rev.D60(1999)053002.

Released energy by neutrinos(1)

Mean neutrino energy

$$\frac{\int_{\mathrm{thr.}}^{\infty} E_\nu \phi(E_\nu)\sigma(E_\nu)\varepsilon(E_\nu)\, dE_\nu}{\int_{\mathrm{thr.}}^{\infty} \phi(E_\nu)\sigma(E_\nu)\varepsilon(E_\nu)\, dE_\nu} = \sim 16.7 \text{ MeV by Kam-II data}$$

thr.=8.9MeV

$\phi(E_\nu)$: *spectrum* σ:*cross section* ε: *effciency*

$$F \times \frac{\alpha E_\nu^{2}}{\exp(E_\nu/kT)+1}$$

$$\int \frac{E_\nu^{2}}{\exp(E_\nu/kT)+1} = 1/\alpha$$

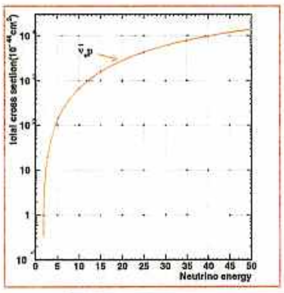

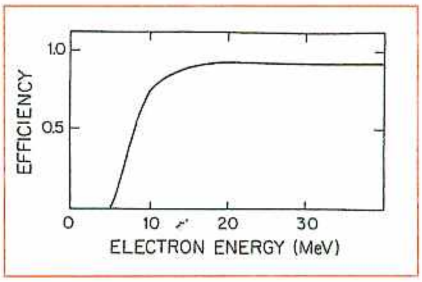

kT = ~2.7 MeV

$$\frac{\int_0^{\infty} E_\nu \phi(E_\nu)dE_\nu}{\int_0^{\infty} \phi(E_\nu)dE_\nu} = \sim 8.6\text{MeV}$$

SN-32

Released energy by neutrinos(2)

Number of events

$$\int_{\mathrm{thr.}}^{\infty} \phi(E_\nu)\sigma(E_\nu)N_p\varepsilon(E_\nu)\, dE_\nu = 11 \text{ events by Kam-II data}$$

thr.=8.9MeV

$\phi(E_\nu)$: $F \times \frac{\alpha E_\nu^{2}}{\exp(E_\nu/kT)+1}$ $\left(\int \frac{E_\nu^{2}}{\exp(E_\nu/kT)+1} = 1/\alpha \right)$

N_p : *number of free protons*

Total flux of $\overline{\nu_e}$ = ~1.8 x 10^{10} /cm^2/burst

Number of $\overline{\nu_e}$ produced = ~6 x 10^{57}

Energy release by $\overline{\nu_e}$ = ~8 x 10^{52} erg

x ~6 for all neutrinos

Total release energy neutrinos = ~5 x 10^{53} erg

SN-33

重力エネルギーの解放

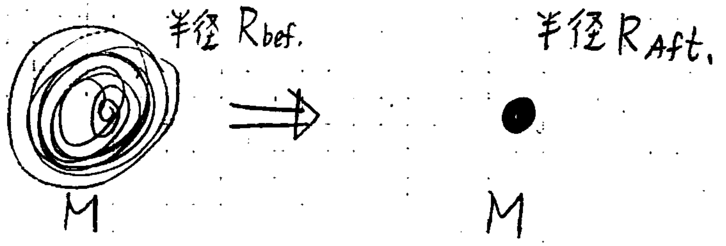

解放される energy は、

$$\left(-\frac{GM^2}{R_{bef}}\right)-\left(-\frac{GM^2}{R_{aft.}}\right)$$

$R_{bef.} \gg R_{Aft}$ とすると

$$\simeq +\frac{GM^2}{R_{Aft.}}$$

G : 6.7×10^{-11} $(m^3 kg^{-1} s^{-2})$

M : $\sim M_\odot$ とすると 1.99×10^{30} kg

これが $\sim 5\times10^{53}$ erg とすると

$\Rightarrow$ $R_{Aft.} \approx 5$ km と求まる。

1.99×10^{30} kg 中の核子は $1.99\times10^{30}\times10^{3}\times6\times10^{23}$
$= 1.2\times10^{57}$ コ

5km の半径とすると

$\frac{4}{3}\pi\times(5\,\mathrm{km})^3 = 5.2\times10^{56}\ \mathrm{fm}^3$

したがって 密度は $\boxed{\sim 2コ/\mathrm{fm}^3}$

nuclear density に達したことがわかった。

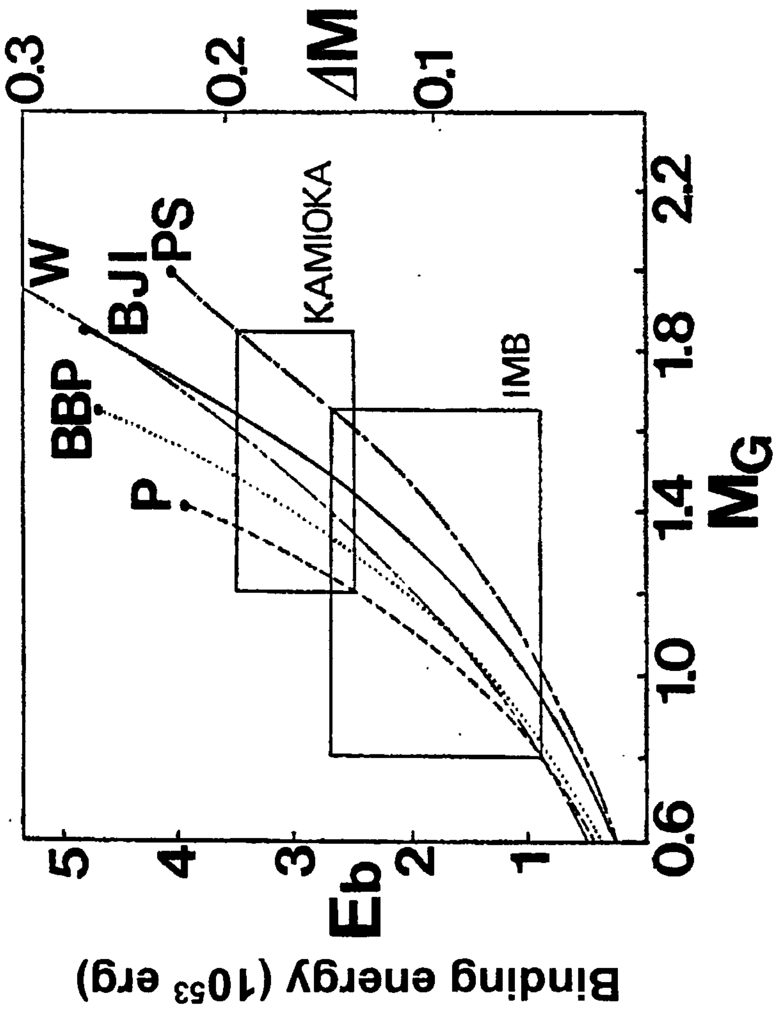

Released energy and neutron star mass

K.Sato and H.Suzuki, Phys.Lett.B196(1987)267

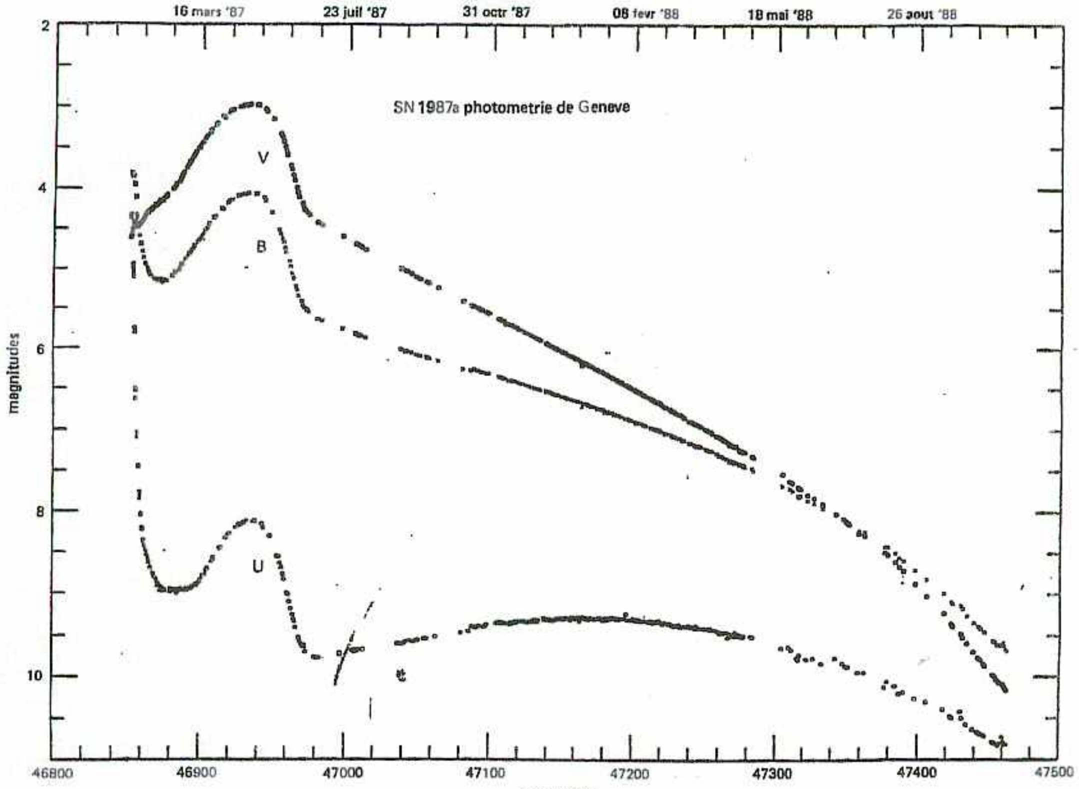

Fig. 4. Visual light curve of Supernova 1987A.

210

超新星1987Aの爆発後の星の周り

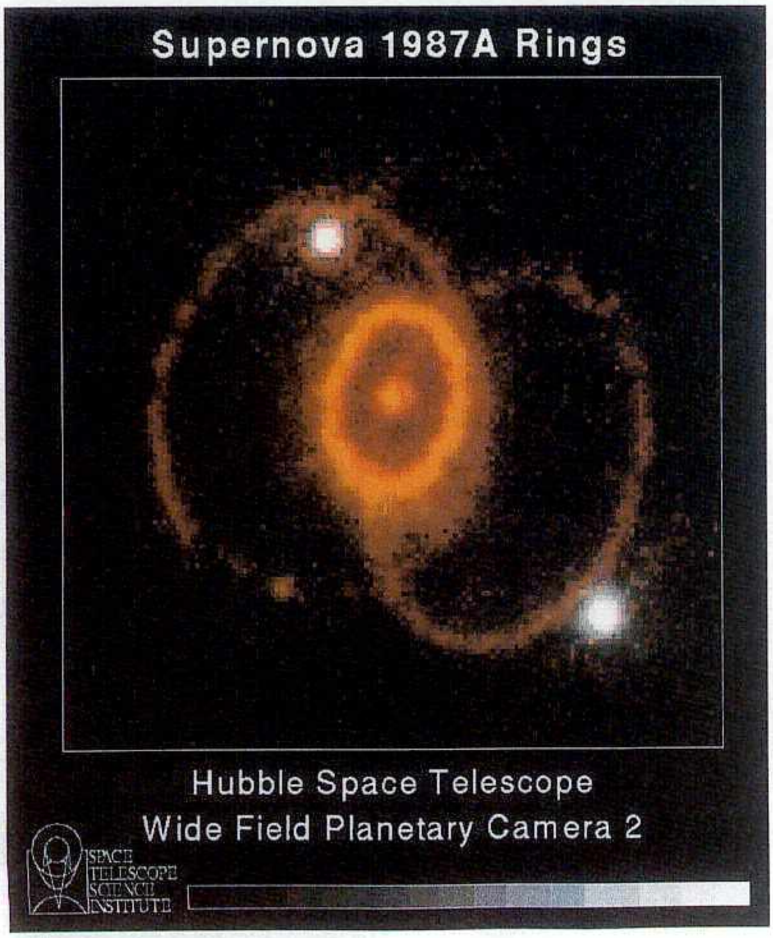

ハッブル宇宙望遠鏡
（1994年撮影）

SN-37

超新星1987Aの最近の姿

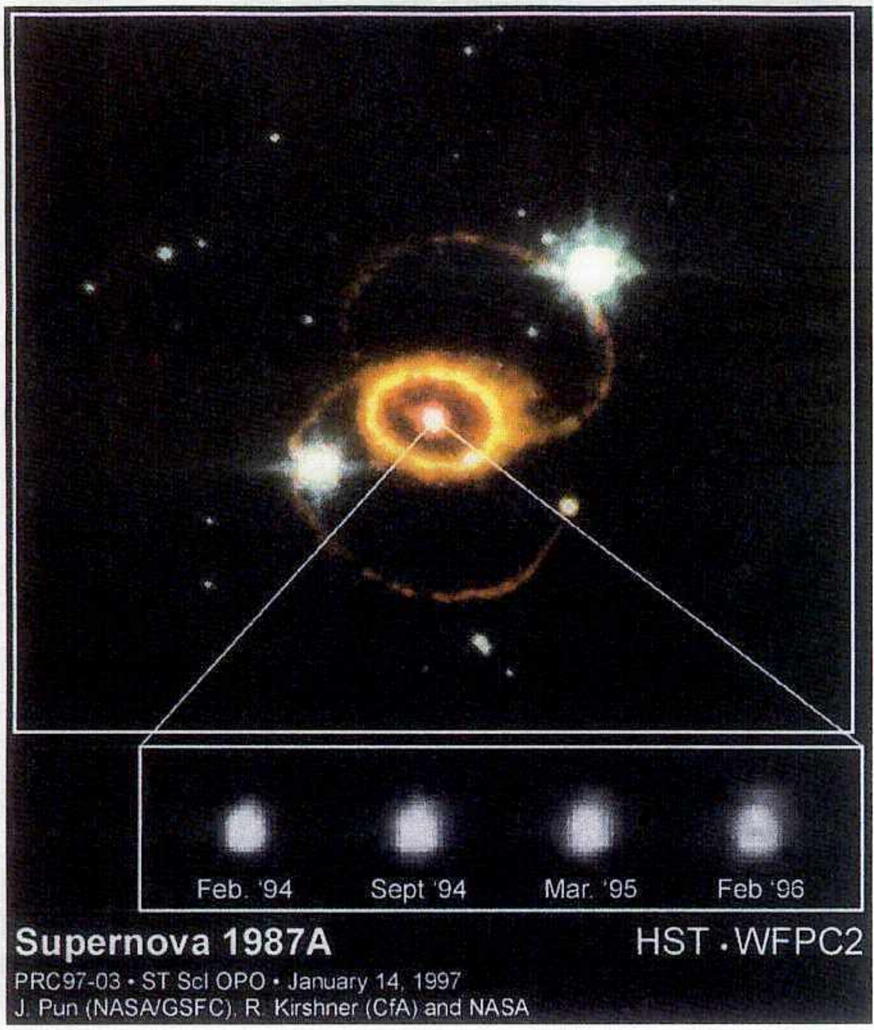

Supernova 1987A HST・WFPC2
PRC97-03・ST ScI OPO・January 14, 1997
J. Pun (NASA/GSFC), R. Kirshner (CfA) and NASA

1996年2月には、星の中心部が拡がりつつあることが観測された。

SN-38

SN1987Aの最近の姿

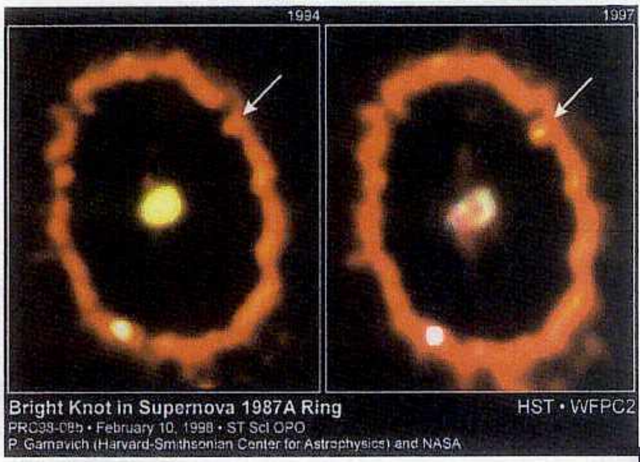

Bright Knot in Supernova 1987A Ring HST・WFPC2
PRC98-08b・February 10, 1998・ST ScI OPO
P. Garnavich (Harvard-Smithsonian Center for Astrophysics) and NASA

右上にホットスポットが現れる。
（1998年2月）

更に4カ所ホットスポットが増える。
（2000年2月）

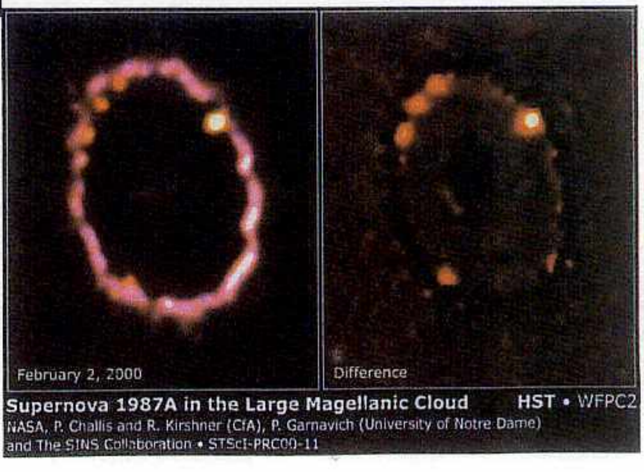

Supernova 1987A in the Large Magellanic Cloud HST • WFPC2
NASA, P. Challis and R. Kirshner (CfA), P. Garnavich (University of Notre Dame) and The SINS Collaboration • STScI-PRC00-11

SN-37

Neutrino oscillations in supernova

(ref.: A.S.Dighe and A.Yu.Smirnov, hep-ph/9907423)

Unknown parameters

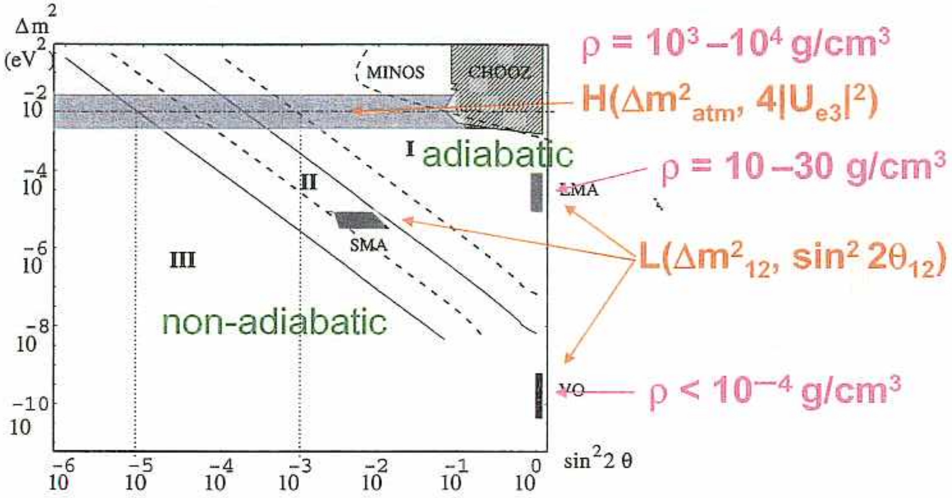

Neutrino transition diagram (for $m_3 > m_2 > m_1$)

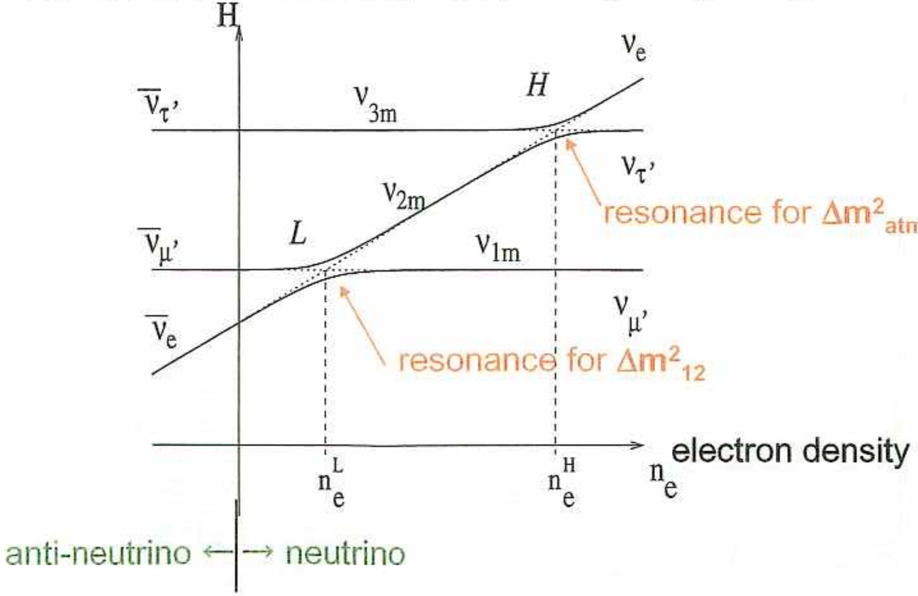

2.6 The level crossing schemes and initial conditions

In the basis of flavor eigenstates $(\nu_e, \nu_\mu, \nu_\tau)$, the evolution of neutrinos at densities $\rho < 10^6$ g/cc relevant for neutrino conversion (see below) is described by a Schrödinger-like equation with the effective Hamiltonian

$$\begin{aligned} H &= \frac{\mathcal{M}^2}{2E} + \mathcal{V} \\ &= \frac{1}{2E}\begin{pmatrix} m^2_{ee} + 2EV & m^2_{e\mu} & m^2_{e\tau} \\ m^2_{e\mu} & m^2_{\mu\mu} & m^2_{\mu\tau} \\ m^2_{e\tau} & m^2_{\mu\tau} & m^2_{\tau\tau} \end{pmatrix} \quad , \end{aligned} \tag{42}$$

where $\mathcal{V} \approx Diag(V, 0, 0)$, and $V = \sqrt{2}G_F n_e$ is the effective potential for the electron neutrinos due to their charged current interactions with electrons.

Since any rotation in the $(\nu_\mu - \nu_\tau)$ subspace does not affect the physics, it is convenient to perform a rotation of the neutrino states $(\nu_e, \nu_\mu, \nu_\tau) \to (\nu_e, \nu_{\mu'}, \nu_{\tau'})$, which diagonalizes the (ν_μ, ν_τ) submatrix of (42) [47]. (The potential V appears only in the element H_{ee}, and hence is not affected by this rotation.) The effective Hamiltonian in the new basis becomes

$$H = \frac{1}{2E}\begin{pmatrix} m^2_{ee} + 2EV & m^2_{e\mu'} & m^2_{e\tau'} \\ m^2_{e\mu'} & m^2_{\mu'\mu'} & 0 \\ m^2_{e\tau'} & 0 & m^2_{\tau'\tau'} \end{pmatrix} \quad . \tag{43}$$

At $V \gg m^2_{ij}/(2E)$, the off-diagonal terms can be neglected and the Hamiltonian (43) becomes diagonal:

$$H \approx \mathrm{Diag}(V, m^2_{\mu'\mu'}, m^2_{\tau'\tau'}) \quad . \tag{44}$$

That is, the basis states $(\nu_e, \nu_{\mu'}, \nu_{\tau'})$ are the matter eigenstates. These are the states that arrive at the conversion regions as independent (incoherent) states and transform in this region independently.

normal mass hierarchy

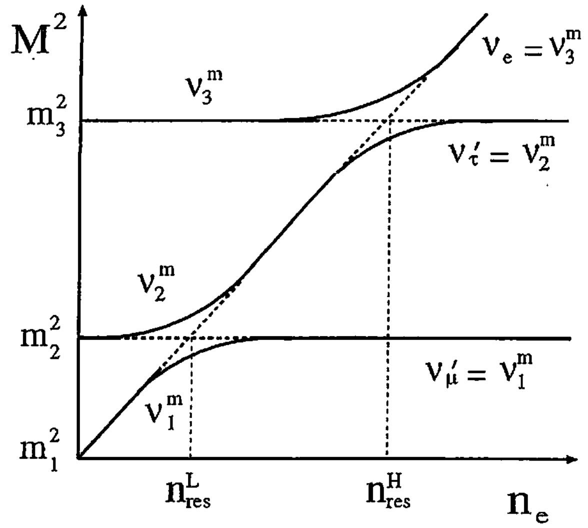

Figure 3.7: Crossing diagram for three-flavor neutrinos in the case of normal mass hierarchy.

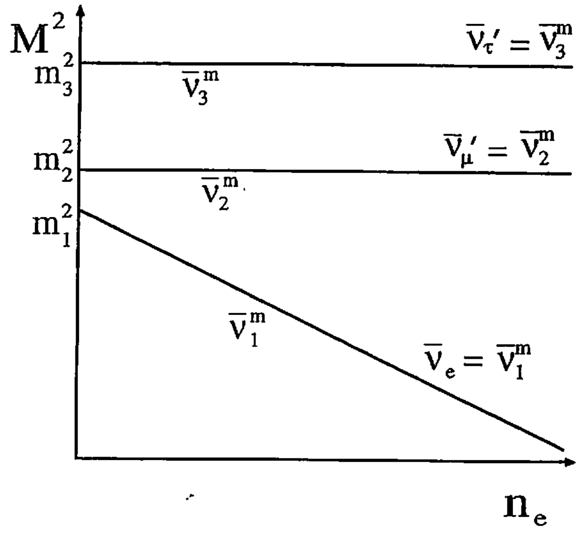

Figure 3.8: Crossing diagram for three-flavor antineutrinos in the case of normal mass hierarchy.

obtain the transformed mass matrix

$$\tilde{M}^2 = e^{-i\theta_{13}\lambda_5} e^{-i\theta_{23}\lambda_7} M^2 e^{i\theta_{23}\lambda_7} e^{i\theta_{13}\lambda_5}$$

Inverted mass hierarcy

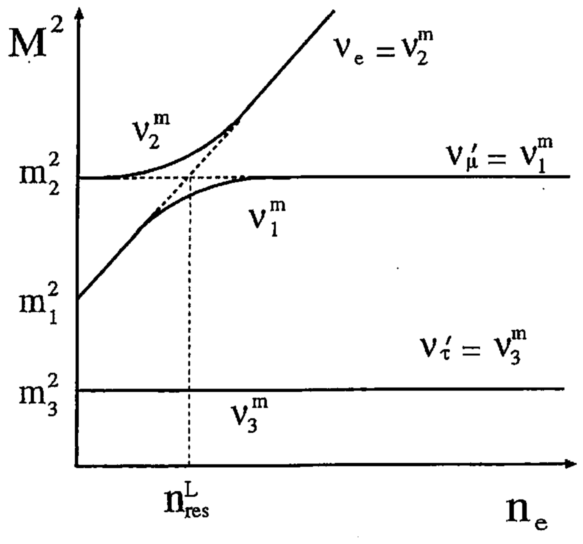

Figure 3.9: Crossing diagram for three-flavor neutrinos in the case of inverted mass hierarchy.

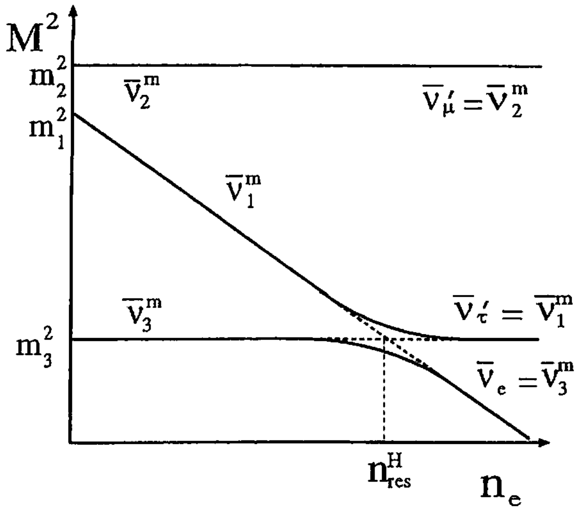

Figure 3.10: Crossing diagram for three-flavor antineutrinos in the case of inverted mass hierarchy.

traveling distance of neutrinos. In spite of these suggestions, interest in atmospheric neutrinos was not very strong until Kamiokande published a study of the atmospheric neutrino

Effect of the neutrino oscillations to the supernova spectrum

Normal hierarcy

H(Δm^2_{atm}, 4|U_{e3}|^2) resonance in adiabatic region

- $\nu_e \to \nu_3$, $\nu_{\mu'} \to \nu_1$, $\nu_{\tau'} \to \nu_2$ at H resonance
- neutronization ν_e peak $\to \nu_X(\nu_\mu,\nu_\tau)$.
- anti-neutrinos have no resonances.

$\overline{\nu_e}$ spectrum is a mixture of original $\overline{\nu_e}$ and ν_X for LMA solution.

- ν_e has harder spectrum (($E\nu_e$) > ($E\bar{\nu}_e$))

H(Δm^2_{atm}, 4|U_{e3}|^2) in non-adiabatic region

- $\nu_e \to \nu_2$, $\nu_{\mu'} \to \nu_1$, $\nu_{\tau'} \to \nu_3$ at H.
- neutronization ν_e peak $\to$ ν_e and ν_X.
- anti-neutrinos have no resonances.

$\overline{\nu_e}$ spectrum is a mixture of original $\overline{\nu_e}$ and ν_X for LMA solution.

- ν_e is a mixture of original ν_e and ν_X.

Inverted mass hierarcy

H(Δm^2_{atm}, 4|U_{e3}|^2) resonance in adiabatic region

- $\nu_e \to \nu_2$, $\nu_{\mu'} \to \nu_1$, $\nu_{\tau'} \to \nu_3$ at L resonance
- neutronization ν_e peak $\to \nu_e$ and ν_x.
- $\overline{\nu_e} \to \overline{\nu_3}$, $\overline{\nu_{\mu'}} \to \overline{\nu_2}$, $\overline{\nu_{\tau'}} \to \overline{\nu_1}$ at H resonance.

$\overline{\nu_e}$ spectrum is a mixture of original $\overline{\nu_e}$ and ν_X for LMA solution.

H(Δm^2_{atm}, 4|U_{e3}|^2) in non-adiabatic region

- $\nu_e \to \nu_2$, $\nu_{\mu'} \to \nu_1$, $\nu_{\tau'} \to \nu_3$ at L resonance
- neutronization ν_e peak $\to \nu_e$ and ν_x.
- $\overline{\nu_e} \to \overline{\nu_1}, \overline{\nu_3}$, $\overline{\nu_{\mu'}} \to \overline{\nu_2}$, $\overline{\nu_{\tau'}} \to \overline{\nu_3}, \overline{\nu_1}$ at H.

$\overline{\nu_e}$ spectrum is a mixture of original $\overline{\nu_e}$ and ν_X for LMA solution.

If neutrinos have mass,

higher energy neutrinos come earlier.

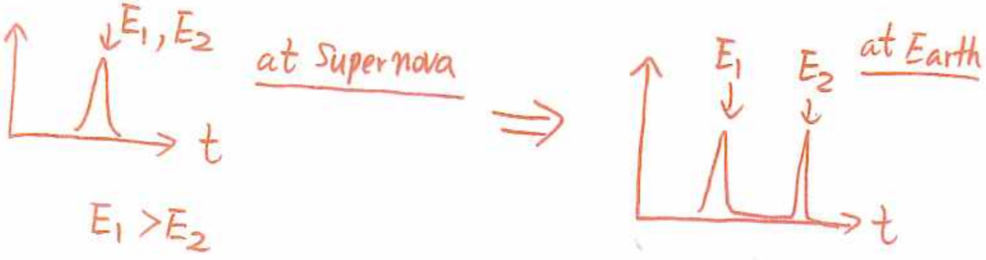

$E_1 > E_2$

Time delay (ΔT)

$$\Delta T = 2.6 \times 10^{-2}\,\mathrm{sec.} \left(\frac{m}{1\mathrm{ev}}\right)^2 \times \left(\frac{E}{10\mathrm{MeV}}\right)^{-2} \left(\frac{\ell}{50\mathrm{kpc}}\right)$$

m: ν mass (eV)

E: ν energy (MeV)

ℓ: distance to supernova (kpc)

Simulation of neutrino burst from Supernova

expected number from neutrino interactions in SuperKamiokande

- $\bar{\nu}e + p \rightarrow e^+ + n$:
  ~ 3500
- $\nu e + e^- \rightarrow \nu e + e^-$:
  ~ 160
- $\overset{(-)}{\nu}x + e^- \rightarrow \overset{(-)}{\nu}x + e^-$:
  ~ 90
- $\bar{\nu}e + e^- \rightarrow \bar{\nu}e + e^-$:
  ~ 60
- $\nu N \rightarrow \nu N + \gamma$:
  ~ 300

cf. R=10kpc ,mass=12$M_{\odot}$, and E_{ν} > 5.5 MeV

Energy spectrum

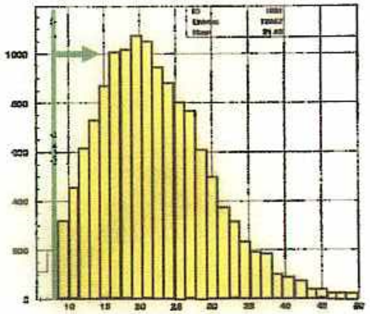

$\bar{\nu}e + p \rightarrow e^+ + n$

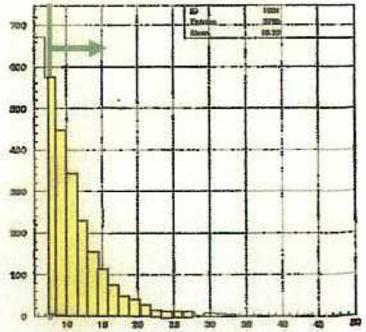

$\nu e + e^- \rightarrow \nu e + e^-$

Directionality of Supernova neutrinos

- Positrons from $\bar{\nu} e + p \rightarrow e^+ + n$ does not have directionality of incident anti-neutrinos

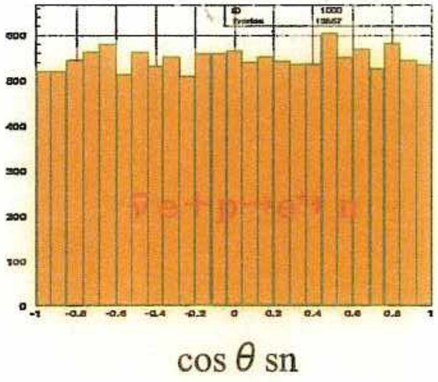

- Electrons from electron scattering have directionality of neutrinos

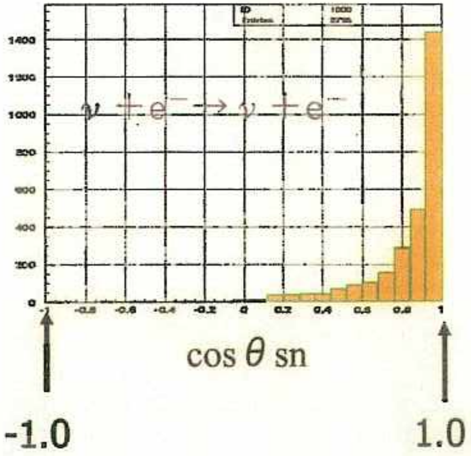

Expected time profile of supernova events in SuperK

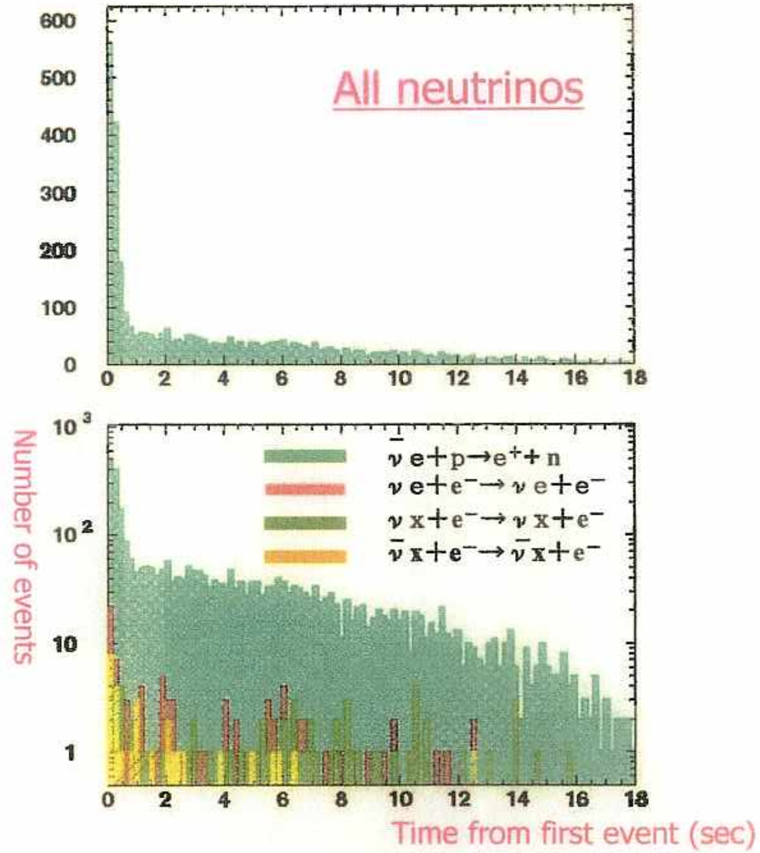

Model calculation

Supernova burst (the first 1 second)

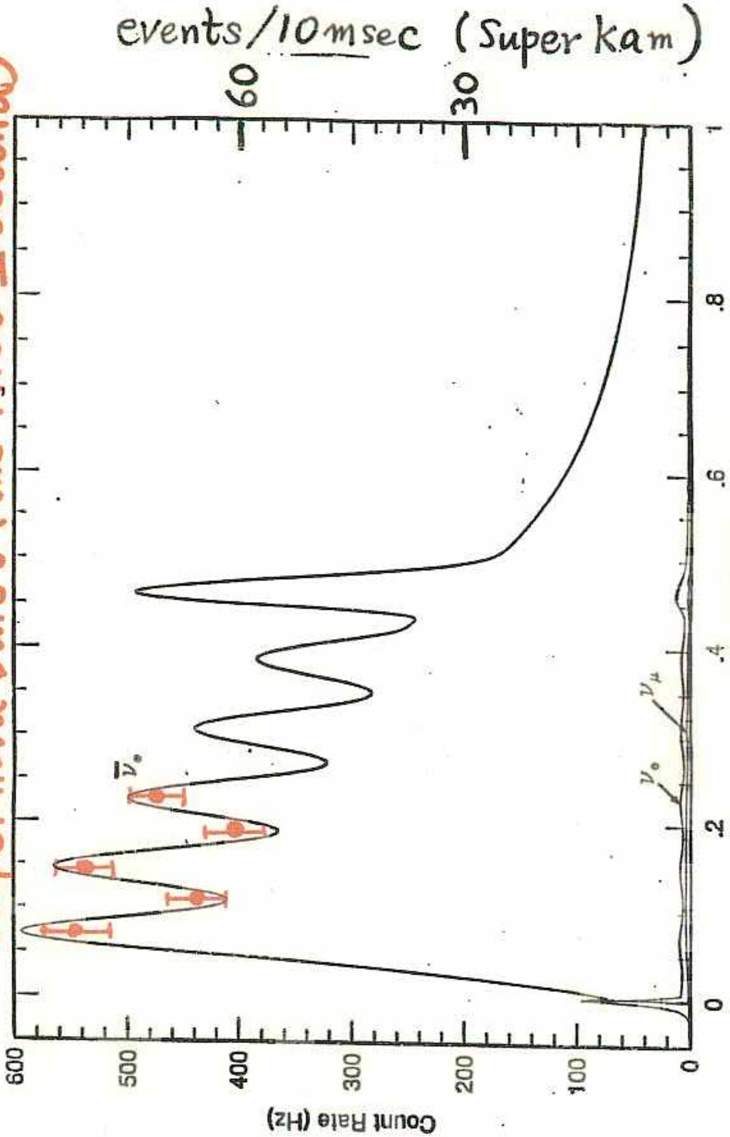

A. Burrows et al. Phys. Rev. D 45 (1992) 3361.

Direction of Supernova events on the celestial coordinate

(SN@ center of our Galaxy)

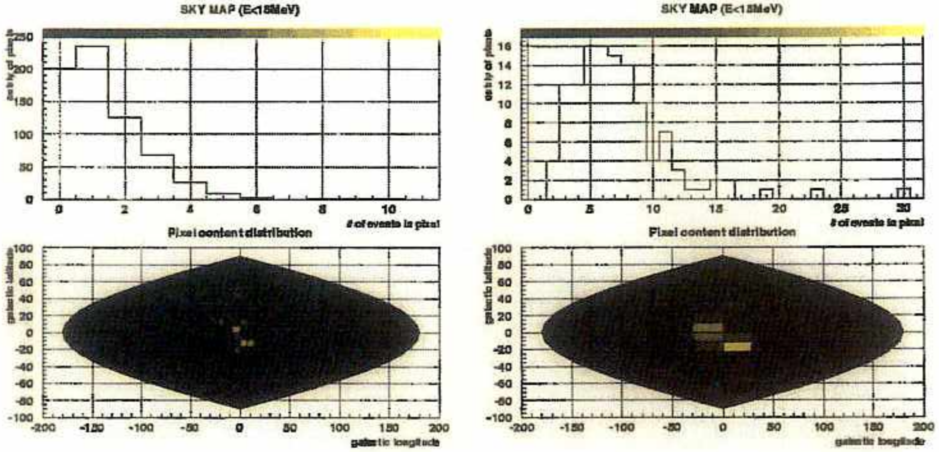

SuperKamiokande can detect the direction of supernova using neutrino-electron scattering events

Search for relic supernova neutrinos

Neutrinos from past supernovae could be observed as diffuse neutrinos.

Expected neutrino energy spectrum

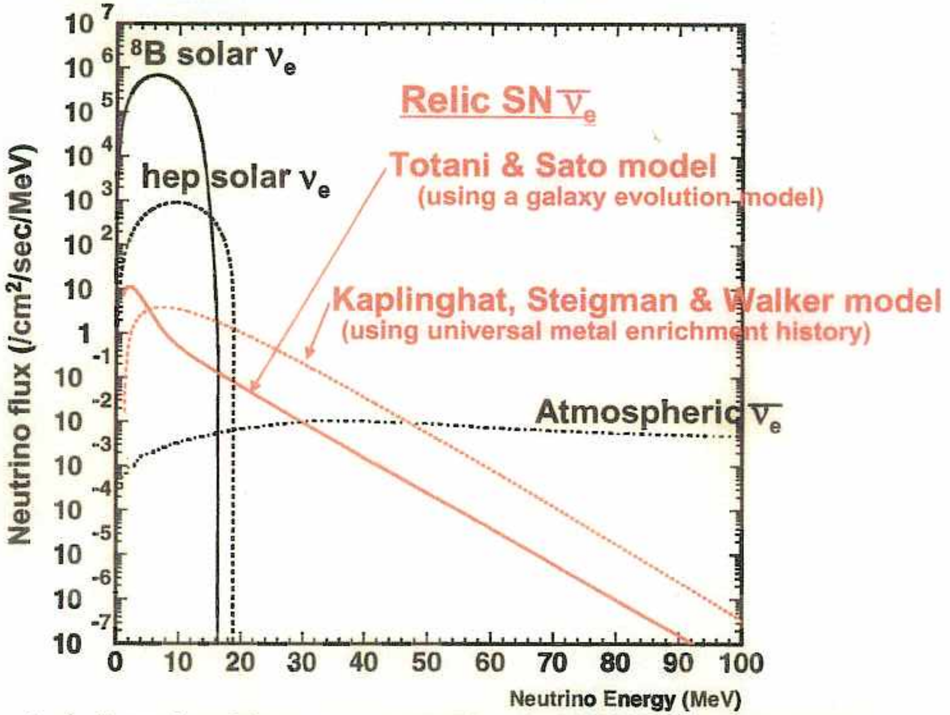

(ref. Totani and Sato, Astropart.Phys.3, 367(1995);ApJ.460,303(1996). Kaplinghat, Steigman & Walker, Phys.ReV.D62,043001(2000).)

Expected event rate: ~1.2 ev./yr for 15-40 MeV (Totani & Sato model)

Spallation background dominates < ~18 MeV

➡ Events >18 MeV is discussed.

TABLE II: The SRN search results are presented for six theoretical models. The first column describes the method used to calculate the SRN flux. The second column shows the efficiency-corrected limit on the SRN event rate at SK. The third column is the flux limit set by SK, which can be compared with the theoretical predictions that are shown in the fourth column. The fifth column shows the flux predictions above a threshold of $E_\nu > 19.3$ MeV . Note that the heavy metal abundance calculation only sets a theoretical upper bound on the SRN flux [7].

Theoretical model	Event rate limit (90% C.L.)	SRN flux limit (90% C.L.)	Predicted flux	Predicted flux ($E_\nu > 19.3$ MeV)
Galaxy evolution [4]	< 3.2 events / year	$< 130\ \bar{\nu}_e\ \mathrm{cm}^{-2}\ \mathrm{s}^{-1}$	$44\ \bar{\nu}_e\ \mathrm{cm}^{-2}\ \mathrm{s}^{-1}$	$0.41\ \bar{\nu}_e\ \mathrm{cm}^{-2}\ \mathrm{s}^{-1}$
Cosmic gas infall [5]	< 2.8 events / year	$< 32\ \bar{\nu}_e\ \mathrm{cm}^{-2}\ \mathrm{s}^{-1}$	$5.4\ \bar{\nu}_e\ \mathrm{cm}^{-2}\ \mathrm{s}^{-1}$	$0.20\ \bar{\nu}_e\ \mathrm{cm}^{-2}\ \mathrm{s}^{-1}$
Cosmic chemical evolution [6]	< 3.3 events / year	$< 25\ \bar{\nu}_e\ \mathrm{cm}^{-2}\ \mathrm{s}^{-1}$	$8.3\ \bar{\nu}_e\ \mathrm{cm}^{-2}\ \mathrm{s}^{-1}$	$0.39\ \bar{\nu}_e\ \mathrm{cm}^{-2}\ \mathrm{s}^{-1}$
Heavy metal abundance [7]	< 3.0 events / year	$< 29\ \bar{\nu}_e\ \mathrm{cm}^{-2}\ \mathrm{s}^{-1}$	$< 54\ \bar{\nu}_e\ \mathrm{cm}^{-2}\ \mathrm{s}^{-1}$	$< 2.2\ \bar{\nu}_e\ \mathrm{cm}^{-2}\ \mathrm{s}^{-1}$
Constant supernova rate [4]	< 3.4 events / year	$< 20\ \bar{\nu}_e\ \mathrm{cm}^{-2}\ \mathrm{s}^{-1}$	$52\ \bar{\nu}_e\ \mathrm{cm}^{-2}\ \mathrm{s}^{-1}$	$3.1\ \bar{\nu}_e\ \mathrm{cm}^{-2}\ \mathrm{s}^{-1}$
Large mixing angle osc. [8]	< 3.5 events / year	$< 31\ \bar{\nu}_e\ \mathrm{cm}^{-2}\ \mathrm{s}^{-1}$	$11\ \bar{\nu}_e\ \mathrm{cm}^{-2}\ \mathrm{s}^{-1}$	$0.43\ \bar{\nu}_e\ \mathrm{cm}^{-2}\ \mathrm{s}^{-1}$

is the total flux of SRNs integrated over the entire spectrum, this equation can be inverted into the following:

$$F = \frac{\alpha}{N_p \times \tau \int_{19.3\,\mathrm{MeV}}^{\infty} f(E_\nu)\sigma(E_\nu)\epsilon(E_\nu)dE_\nu} \quad (3)$$

Using the above values, the 90% C.L. SRN flux limit was calculated for each model. The results are in the third column of Table II, and can be compared with the predictions, which are in the fourth column. For the galaxy evolution model [4], the cosmic gas infall model [5], and the cosmic chemical evolution model [6], the SK limits are larger than the predictions by a factor of three to six. In these models, the dominant contribute supernovae. At Kamiokande-II, a flux limit of 780 $\bar{\nu}_e$ cm^{-2} s^{-1} was set with the assumption of a constant supernova model [9]; the SK limit on this model is 39 times more stringent.

The SRN limits vary greatly, based on the shape of the theoretical SRN spectrum at energies that are below SK's SRN analysis threshold. To remove this strong model dependence, a limit was set for $E_\nu > 19.3$ MeV. In this region, all six models have similar energy spectrum shapes, and so an experimental limit that is insensitive to the choice of model can be obtained as follows:

$$\int^{\infty} \ldots f(E_\nu)dE_\nu$$

Data reduction

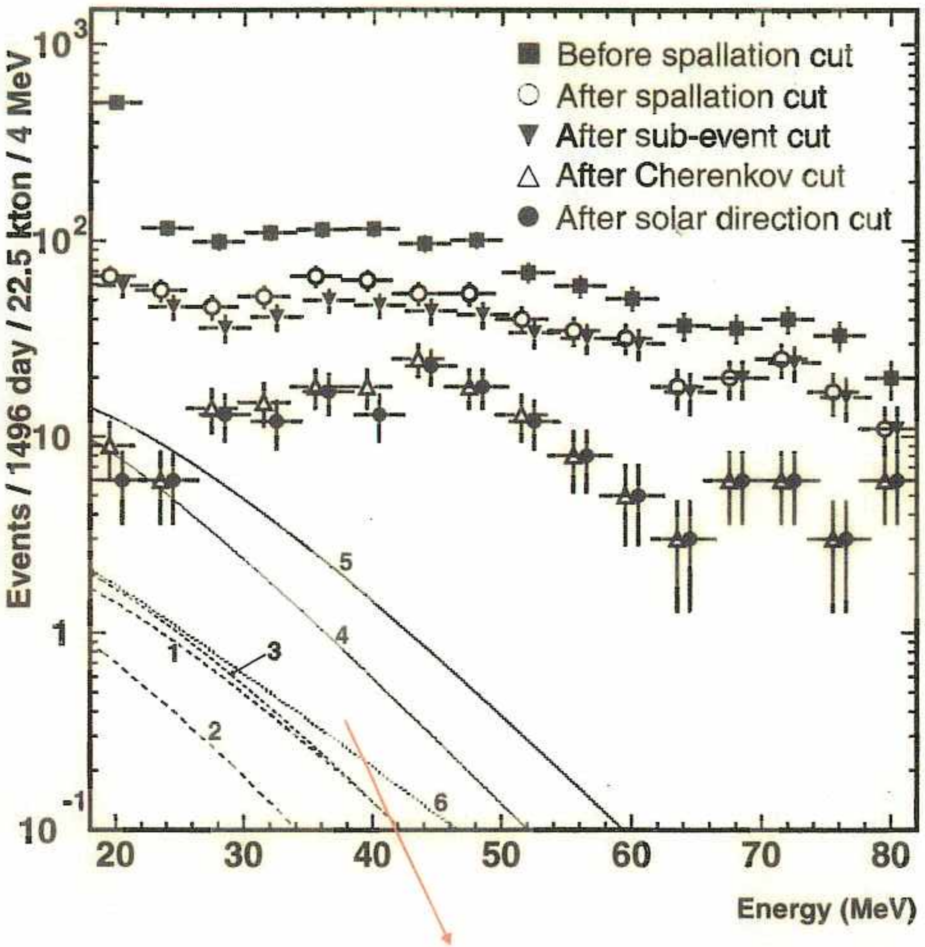

Model predictions

Energy spectrum above 18MeV and background sources

Energy spectrum above 18 MeV

Preliminary

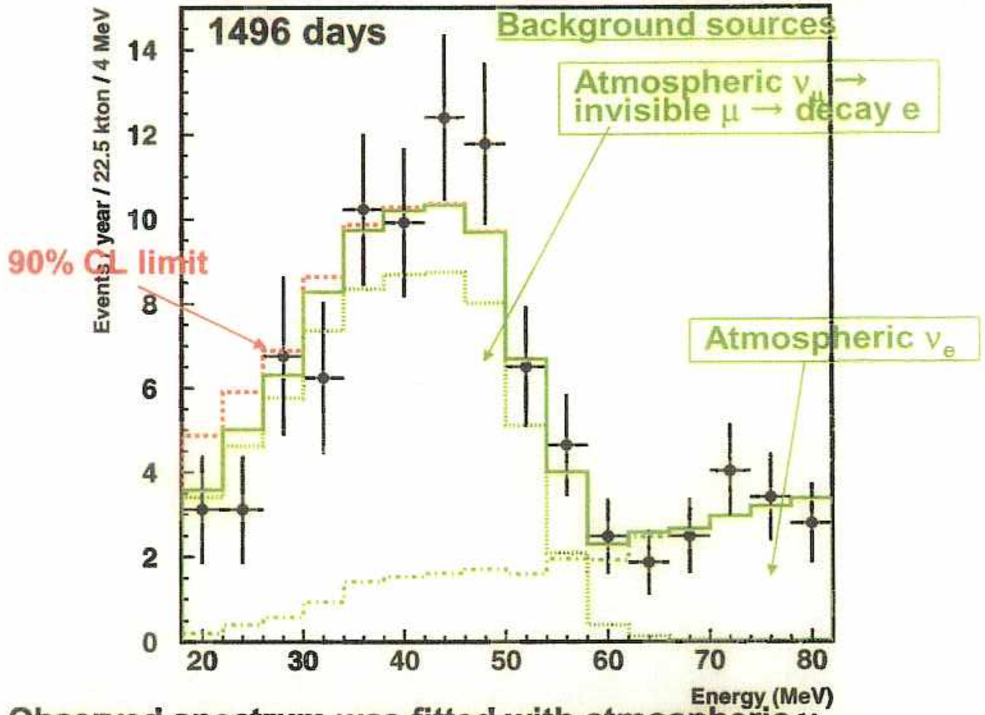

Observed spectrum was fitted with atmospheric ν backgrounds (normalization free) and possible relic SN signals.

Upper limit of relic SN events: < 3.2 events/year (>18 MeV, 90% C.L.)

Relic SN ν_e flux limit: < 130 /cm²/sec (90% C.L.)

(whole energy range, using Totani & Sato spectrum shape)

cf. Flux expectations:

Totani & Sato model : 44 /cm²/sec

Kaplinghat et al. model: < 54 /cm²/sec

⑮

Proton Decay

strong interaction

weak interaction

electromagnetic interaction

) Unified by Weiberg-Salam theory

Why not including strong interaction?

Coupling constant U(1), SU(2), SU(3) が 10^{15} GeV位でおちあう。

Atmospheric $\nu \rightarrow \Delta m^2 \cong 3\times10^{-3}\,\mathrm{eV}^2$ $\rightarrow = m_3^2 - m_2^2$

Solar $\nu \rightarrow \Delta m^2 \simeq \sim 7\times10^{-5}\,\mathrm{eV}^2$ $\rightarrow m_2^2 - m_1^2$

$$\boxed{m_3 \gg m_2 \gg 1 \text{ とすると}}$$

$$m_3^2 \approx 3\times10^{-3}\,\mathrm{eV}^2$$

$$m_3 \approx 0.05\,\mathrm{eV}$$

$$m_2 \simeq \sqrt{\sim 7\times10^{-5}} = \sim 0.008\,\mathrm{eV}$$

$$m_1 : m_2 : m_3 \simeq m_e : m_\mu : m_\tau$$

$$\frac{m_\tau}{m_3} = \frac{1.78\,\mathrm{GeV}}{0.05\,\mathrm{eV}} \cong 4\times10^{10} \text{倍}$$

$$\frac{m_\mu}{m_2} = \frac{105.7\,\mathrm{MeV}}{\sim 0.008\,\mathrm{eV}} = \sim 1.3\times10^{10} \text{倍}$$

PD -2

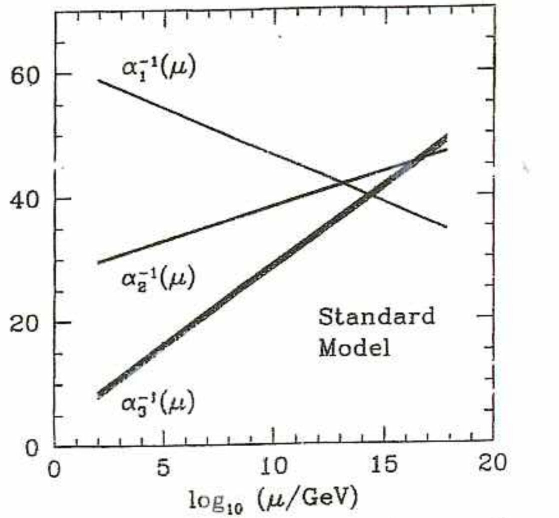

Figure 3. The failure of the running couplings, normalized according to SU(5) and extrapolated taking into account only the virtual exchange of the "known" particles of the standard model (including the top quark and Higgs boson) to meet. Note that only with fairly recent experiments [5], which greatly improved the precision of the determination of low-energy couplings, has the discrepancy become significant.

medium, since virtual particle-anti-particle pairs can screen charge. For charged gauge bosons, as arise in non-abelian theories, the paramagnetic (antiscreening) effect of their spin-spin interaction dominates, which leads to asymptotic freedom. As Georgi, Quinn, and Weinberg pointed out [4], if a gauge symmetry such as SU(5) is spontaneously broken at some very short distance then we should not expect that the effective couplings probed at much larger distances, such as

quantitative handle o
To specify the relevant
basically needs only t
scale at which the cou
sentially the scale at
try breaks), and their
unite. Given these, on
the three *a priori* ind
gauge groups in SU(3
framework is eminentl
ing thing is, how close i
3).

The GQW calculati
in explaining the obser
of couplings and the a
proton. In performin
known and confidentl
standard model exha
unification scale, and
field theory could be
ation up to this mas
magnitude beyond the
to describe. It is a tri
existential and conce

On closer inspecti
good enough. Accura
the couplings show a
ancy between the co
3. And heroic dedica
proton decay did not
clude the minimal SU
by about two orders

If we just add part
things will only get
works, so a generic
ous. Even if some
made to work, that
come from what ap
precious, elegantly

221

PD-3

基本構成粒子（クォーク・レプトン）の 3世代構造と質量の階層性

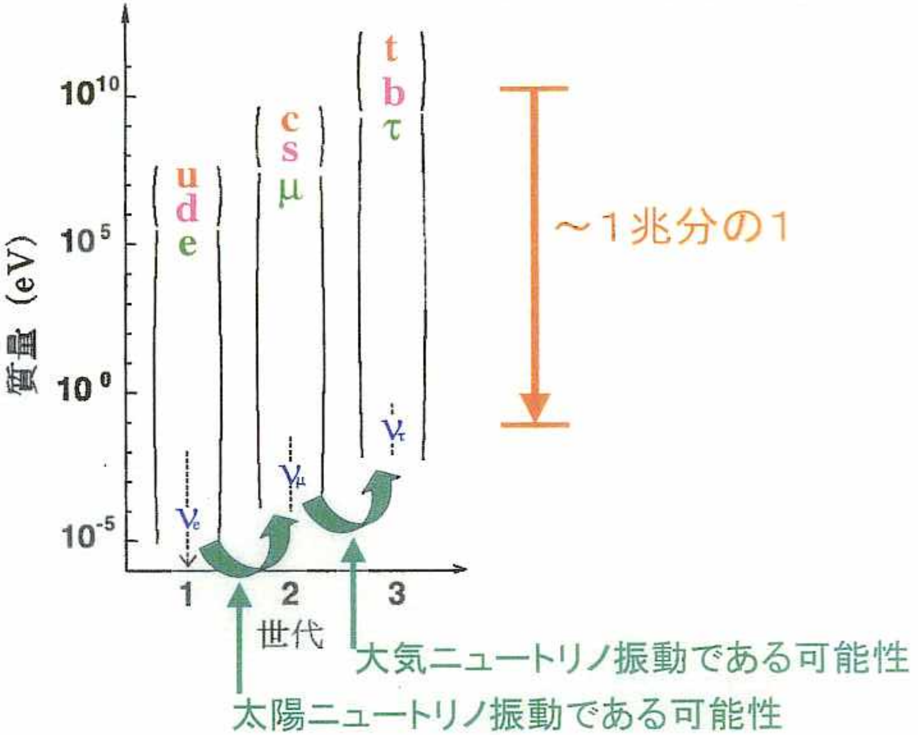

大気 / 太陽ニュートリノ観測により

ニュートリノ質量及びこのみごとな階層
に関する情報が得られ始めた

謎 クォーク・荷電レプトン質量の～１兆分の１

$$m_\nu = \frac{m_{q/l}^2}{M}$$

（シーソー機構）

背後に超高エネ
ルギーの世界
の存在を示唆

See-Saw メカニズム

$$(\overline{N_1}, \overline{N_2})\begin{pmatrix} m_L & m_D \\ m_D & m_R \end{pmatrix}\begin{pmatrix} N_1 \\ N_2 \end{pmatrix}$$

$m_L = 0$. m_D ; Quark-lepton 位。

m_R ;

固有値： $m_\nu \doteqdot \frac{m_D{}^2}{m_R}$, $m_N \doteqdot m_R$

ν_3 の mass を与えて $m_{\nu_3} \approx 0.05\,eV$

$m_D \approx m_\tau = 1.78\,GeV$

$m_R \approx 6 \times 10^{10}\,GeV$

大きな Energy scale に 10^{10} GeV 位に何かがある。

いったん ν mass をわすれて、

大統一理論の必要性

- 電子 e^-、陽子の電荷の絶対値はなぜ同じか。
- 宇宙の反粒子/粒子の非対称を説明するためには
  $\cancel{CP}$ と $\cancel{B}$ の両方が必要。

SU(5) GUTs

ν に mass はない。

$$\psi_5 = \begin{bmatrix} d_R{}^1 \\ d_R{}^2 \\ d_R{}^3 \\ e_L{}^c \\ -\nu_L{}^c \end{bmatrix}$$

1, 2, 3 は カラーの指標 R, G, B

$$\overline{\psi_5} = (\overline{d_R^1}, \overline{d_R^2}, \overline{d_R^3}, \overline{e_L^c}, -\overline{\nu_L^c})$$

$$\psi_{10} = \frac{1}{\sqrt{2}}\begin{pmatrix} 0 & u^3, & -u^2, & -u^1, & -d^1 \\ -u^3 & 0 & u^1 & -u^2 & -d^2 \\ u^2 & -u^1 & 0 & -u^3 & -d^3 \\ u^1 & u^2 & u^3 & 0 & -e^c \\ d^1, & d^2, & d^3 & e^c & 0 \end{pmatrix}_L$$

既知のフェルミオンが 5 と 10 にきっちりと入った。

ゲージ粒子

$$\left[\begin{array}{ccc|cc} & 3 & & & \\ 3 & \text{グルーオン} & & \overline{X}_1 & \overline{Y}_1 \\ & & & \overline{X}_2 & \overline{Y}_2 \\ & & & \overline{X}_3 & \overline{Y}_3 \\ \hline X^1 & X^2 & X^3 & W^0/\sqrt{2} + \frac{3B}{\sqrt{30}} & W^+ \\ Y^1 & Y^2 & Y^3 & W^- & -W^0/\sqrt{2} + \frac{3B}{\sqrt{30}} \end{array}\right]$$

X.Y 粒子が クォークと レプトンを むすびつける。

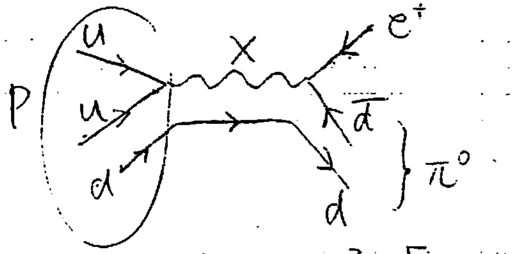

$p \to e^+\pi^0$

$\Gamma_p \propto \frac{\alpha_5^2 M_p^5}{M_X^4}$ $\tau_p \sim 4\times10^{29\pm0.7}$年になる。

しかし SKの結果は、あとで話ますが $>5.7\times10^{33}$yrs (1489days)

SU(5)はだめ

Super symmetry SU(5) は coupling constant の一致がよい。 ただし Unification の scaleは、10^{16} GeV 位まで上がってしまう。

Susy SU(5) では、 $p \to \bar{\nu}K^+$ mode が大きい。

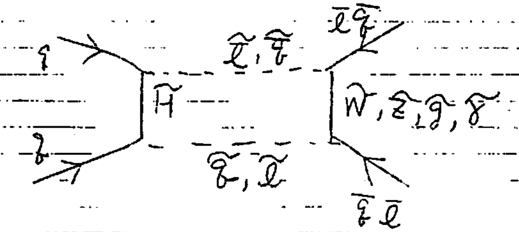

$\tilde{H}_0$は フェルミオン 振幅は $\propto \frac{1}{M(\tilde{H}_0)}$

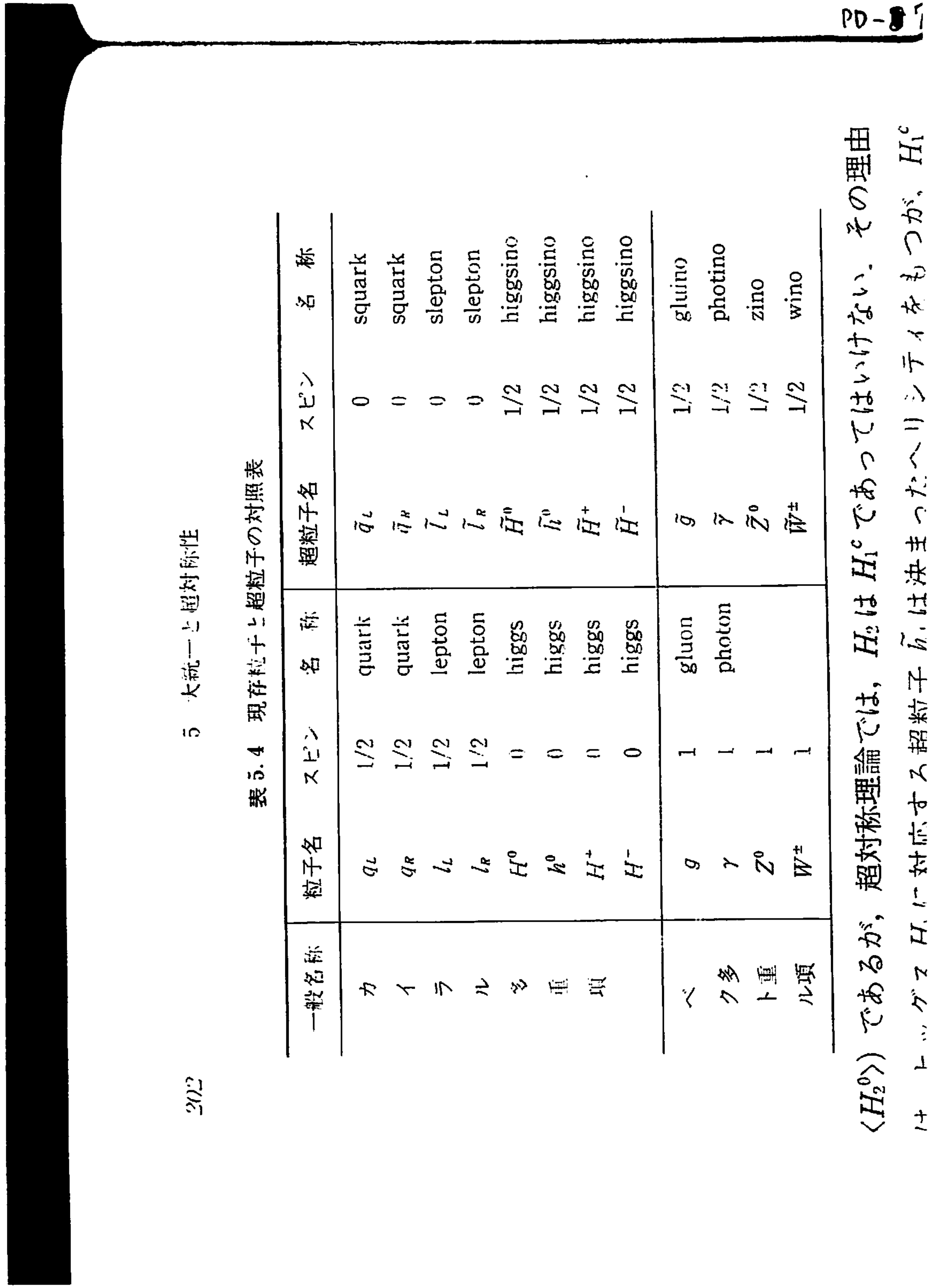

表 5.4 現在粒子と超粒子の対照表

一般名称	粒子名	スピン	名　称	超粒子名	スピン	名　称
カイラル多重項	q_L	1/2	quark	$\tilde{q}_L$	0	squark
	q_R	1/2	quark	$\tilde{q}_R$	0	squark
	l_L	1/2	lepton	$\tilde{l}_L$	0	slepton
	l_R	1/2	lepton	$\tilde{l}_R$	0	slepton
	H^0	0	higgs	$\tilde{H}^0$	1/2	higgsino
	h^0	0	higgs	$\tilde{h}^0$	1/2	higgsino
	H^+	0	higgs	$\tilde{H}^+$	1/2	higgsino
	H^-	0	higgs	$\tilde{H}^-$	1/2	higgsino
ベクトル多重項	g	1	gluon	$\tilde{g}$	1/2	gluino
	γ	1	photon	$\tilde{\gamma}$	1/2	photino
	Z^0	1		$\tilde{Z}^0$	1/2	zino
	$W^\pm$	1		$\tilde{W}^\pm$	1/2	wino

$\langle H_2^0\rangle$）であるが，超対称理論では，H_2 は H_1^c であってはいけない．その理由

はヒッグス H_1 に対応する超粒子 $\tilde{h}_1$ は決まったヘリシティをもつが，H_1^c

超対称性を含まない場合

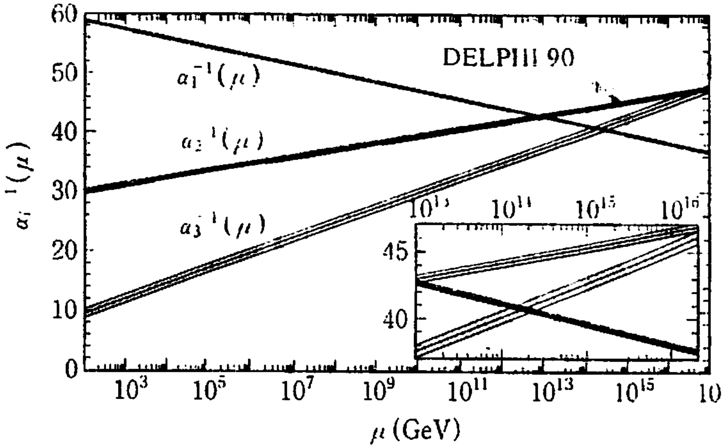

(a)

超対称性を入れた2次の計算

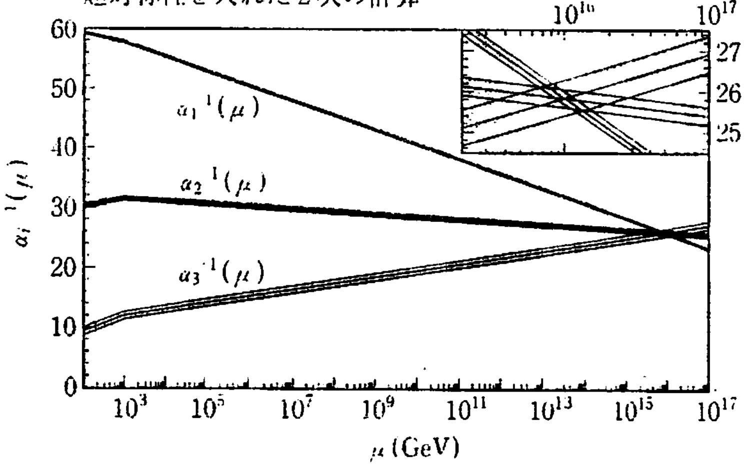

(b)

図 5.8 $SU(i)$ 群結合定数の繰り込みスケール μ による発展図
出発点に LEP の DELPHI データ$^{16,20)}$を使用した．
(a) $SU(5)$ のみ
(b) $SU(5)$+SUSY，$M_{SUSY}=1$ TeV

$SU(5)$ 理論と SUSY を入れた $SU(5)$ 理論の $\alpha_s(m_Z{}^2)$ と $\sin^2\hat{\theta}_W(m_Z{}^2)$ の予想値を示したものである$^{16,20)}$．また，SUSY-GUT によれば，$\alpha_s(M$

224

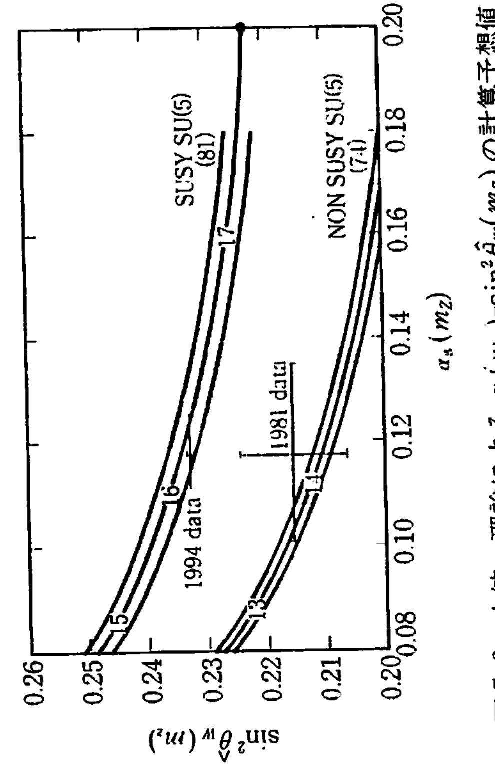

図 5.9 大統一理論による $\alpha_s(m_Z)$-$\sin^2\hat{\theta}_W(m_Z)$ の計算予想値
通常の $SU(5)$ と SUSY-$SU(5)$ の理論値を示す．3 本の線による帯は理論の不定性を表し，帯の中の数値は，エネルギースケール 10^n GeV の n を表す．古い 1981 年のデータでは通常の $SU(5)$ と合致したが，最近のデータは SUSY-$SU(5)$ に合う$^{16)}$．

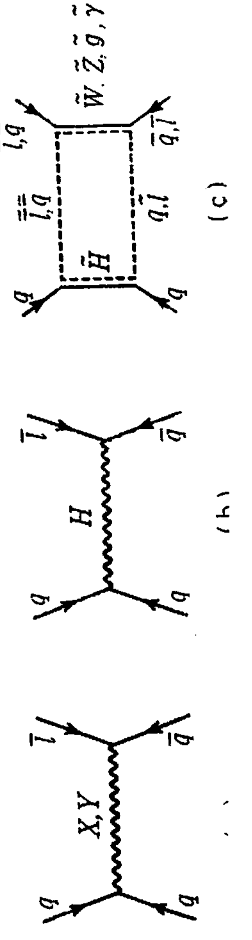

$p \to e^+\pi^0$ ($\mu^+\pi^0$)

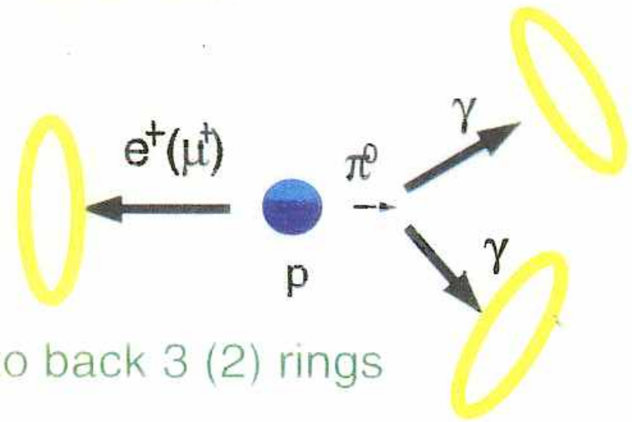

Back to back 3 (2) rings

$p \to \bar{\nu} K^+$

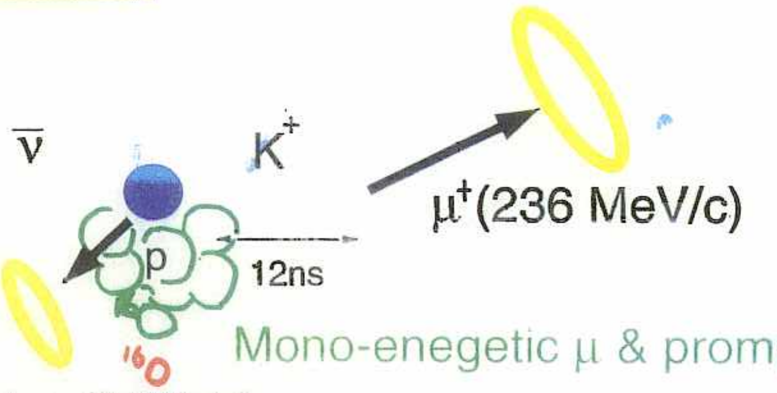

Mono-enegetic μ & prompt γ

prompt - γ (6.3MeV)

(41% probability, H.Ejiri, Phys. Rev. C. 48 (1993)1442)

Another way: $p \to \bar{\nu} K^+$
$\quad \hookrightarrow \pi^+\pi^0$

$P \to e^+\pi^0$ at Superkamiokande (Monte Carlo simulation)

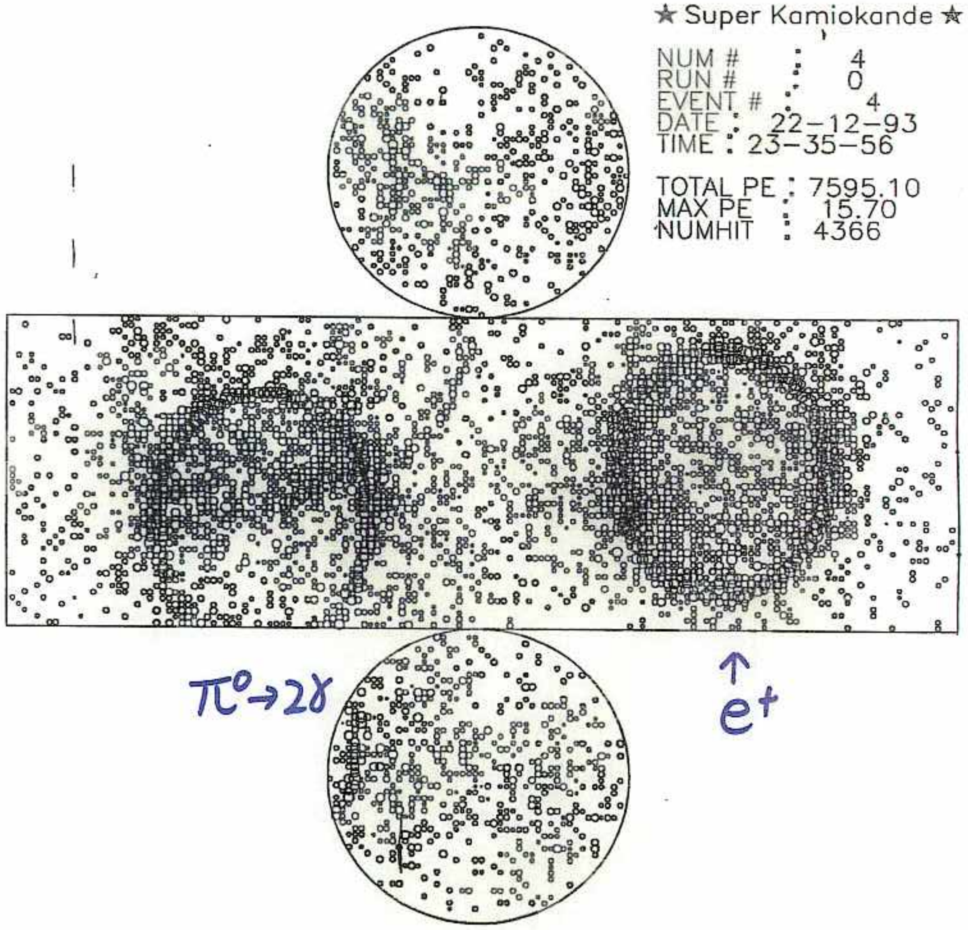

p → e⁺ π⁰: Present status

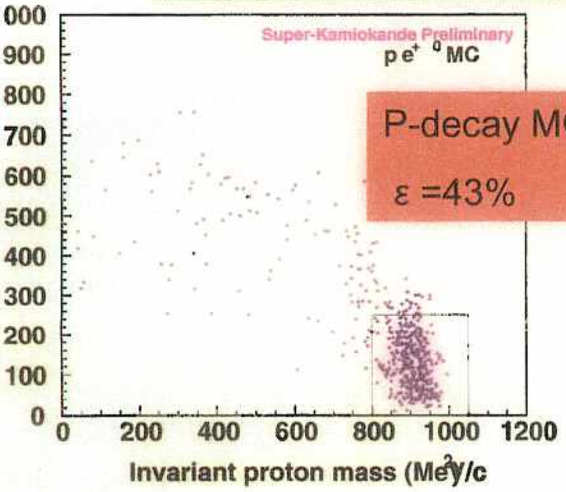

P-decay MC

ε =43%

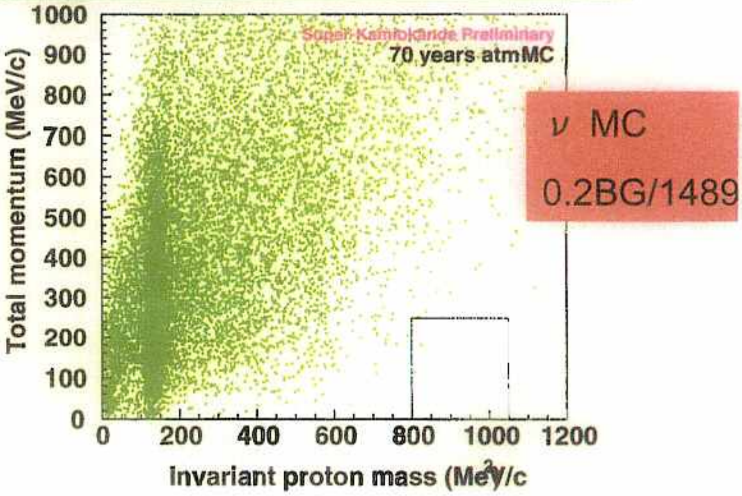

ν MC

0.2BG/1489

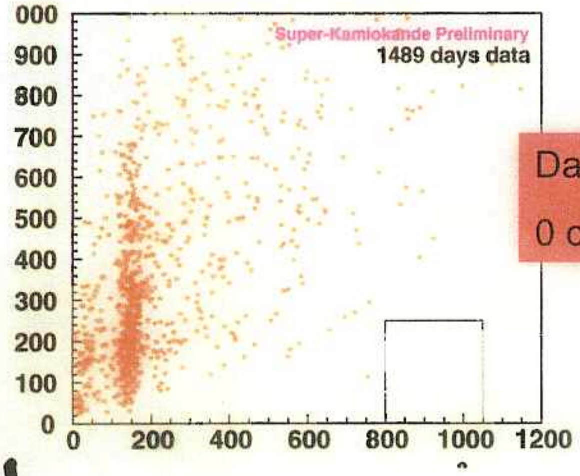

Data

0 candidate

τ/B > 5.7×10^{33}yr

(Super-K, 90%C.L)

PD-12

p → ν K+: Present status (1)

1) P → ν K$^+$, K$^+$→μ^+ ν

236 MeV/c

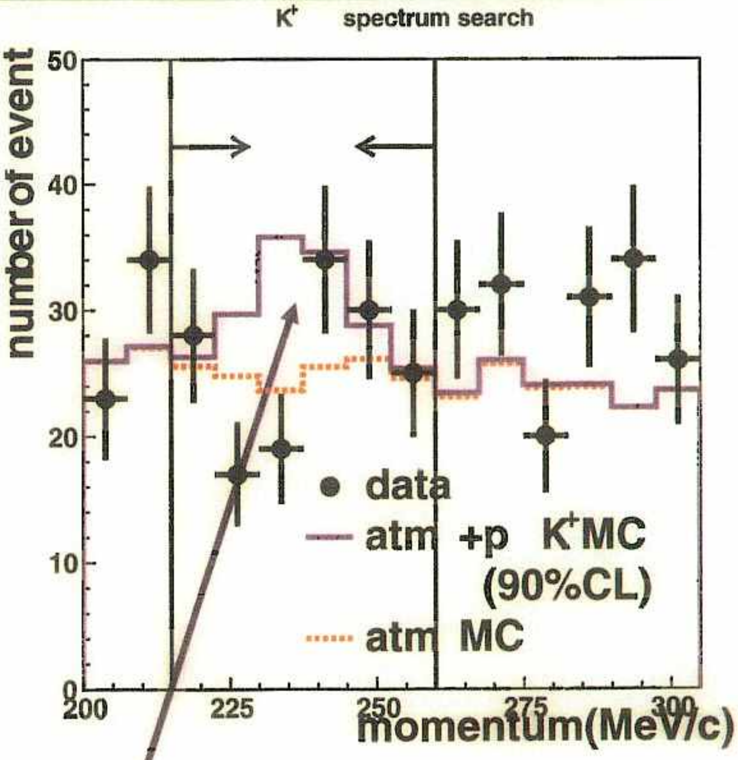

No significant excess near 236MeV/c.
(ε =33%)

PD-13

$p \rightarrow \nu K^+$: Present status (2)

2) $^{16}O \rightarrow \nu K^{+} {}^{15}N \gamma$, $K^+ \rightarrow \mu^+ \nu$, $\mu^+ \rightarrow e^+ \nu \nu$

6 – 10 MeV 236MeV/c

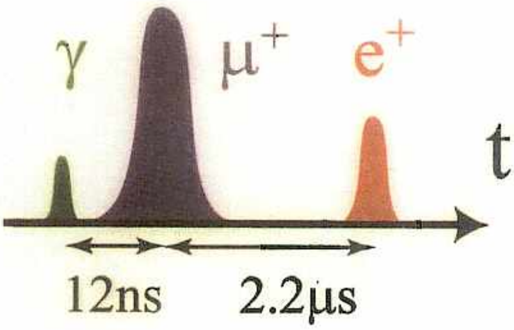

Nhit distribution for the prompt gamma search

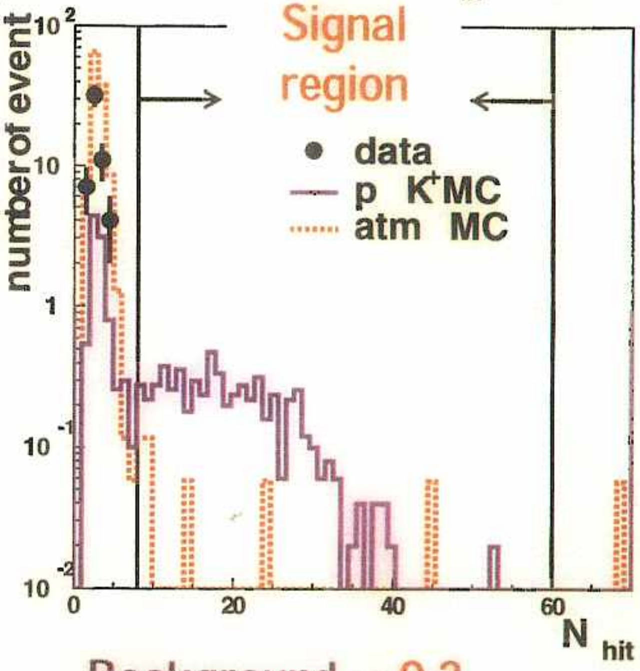

Background = 0.3

ε = 8.7%

Candidate = 0

$p \rightarrow \nu K^+$: Present status (3)

3) $P \rightarrow \nu K^+$, $K^+ \rightarrow \pi^+ \pi^0$ ...... Back to back 205MeV/c each

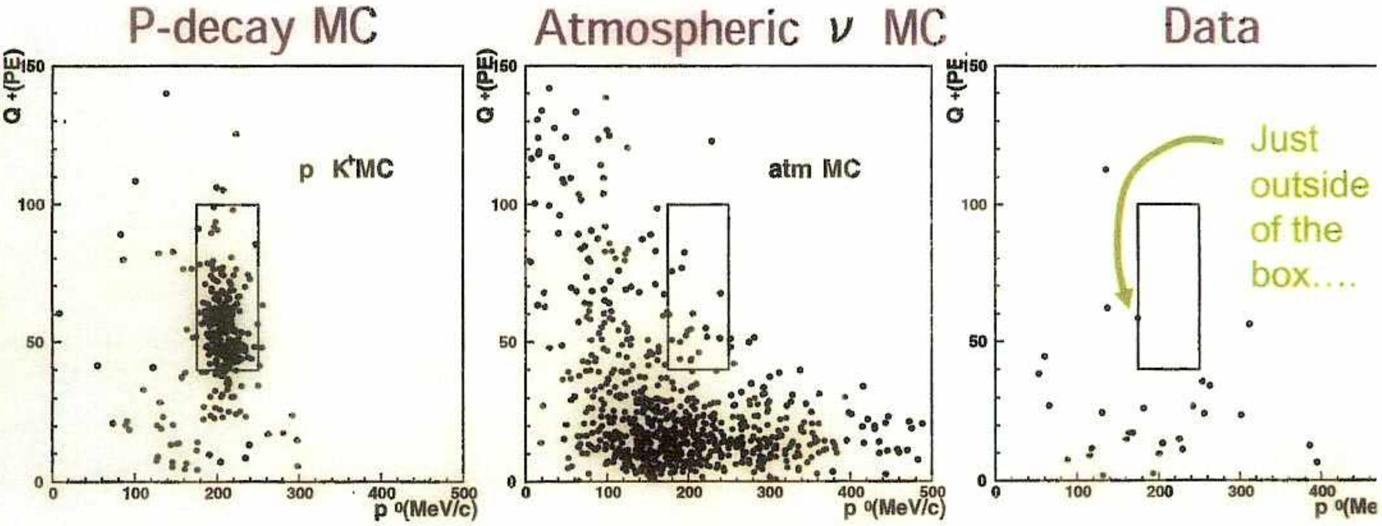

π^0 momentum

ε = 6.5 %

BG=0.9 ev/92ktonyr

Data=0 ev.

(1),(2) and (3) ⟹ $\tau/B > 2.0 \times 10^{33}$yr (90%CL, Super-K)

⑯

Future neutrino and non-accelerator experiments

ニュートリノ・非加速器物理学の将来

ニュートリノ振動に対する近未来の発展

(1) 大気 ν --- 確立 ➡ 加速器を使った精密測定

(2) Solar ν --- 証拠 ➡ SK/ SNO / KamLANDによる精密測定

残された問題

(1) ニュートリノ: 絶対質量、0νββ
(2) ダークマター
(3) 陽子崩壊

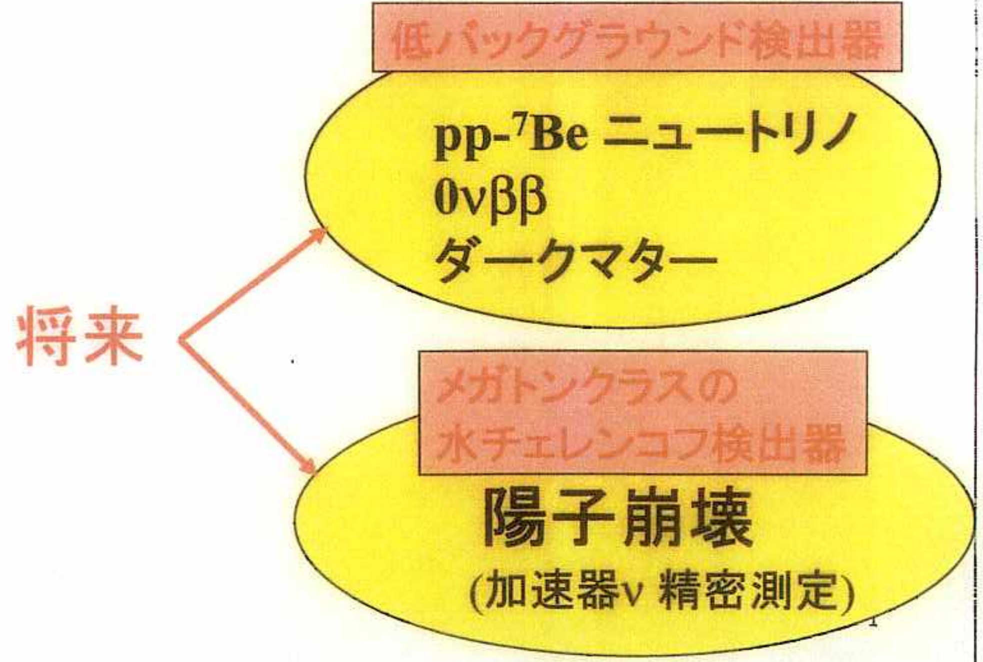

低バックグラウンド検出器

pp-^{7}Be ニュートリノ
0νββ
ダークマター

将来

メガトンクラスの水チェレンコフ検出器

陽子崩壊
(加速器ν 精密測定)

XMASS

Solar ν : Xenon MASsive detector for Solar neutrinos
Dark M: Xenon detector for weakly interacting MASSive Particles
ββ : Xenon neutrino MASS detector

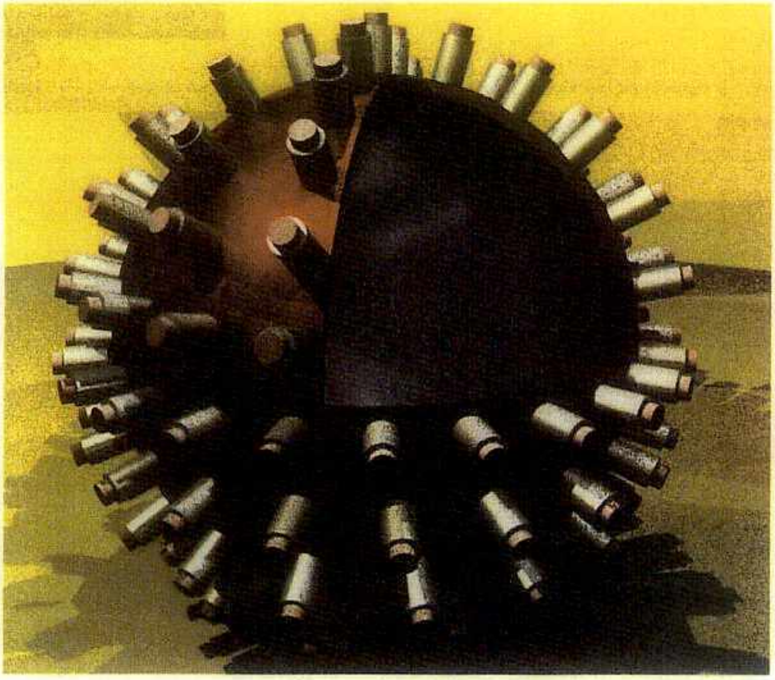

- 10 ton liquid Xe
- Viewed by many PMTs
- solar neutrinos by $\nu + e \rightarrow \nu + e$
- $0\nu\ \beta\beta \sim 5\text{x}10^{27}$ yr (5yr) ($<m_\nu> < 0.01\text{-}0.02$ eV)
- 2000 DM ev/day for 100 GeV 10^{-6} pb SI for proton

Expected rate and spectrum

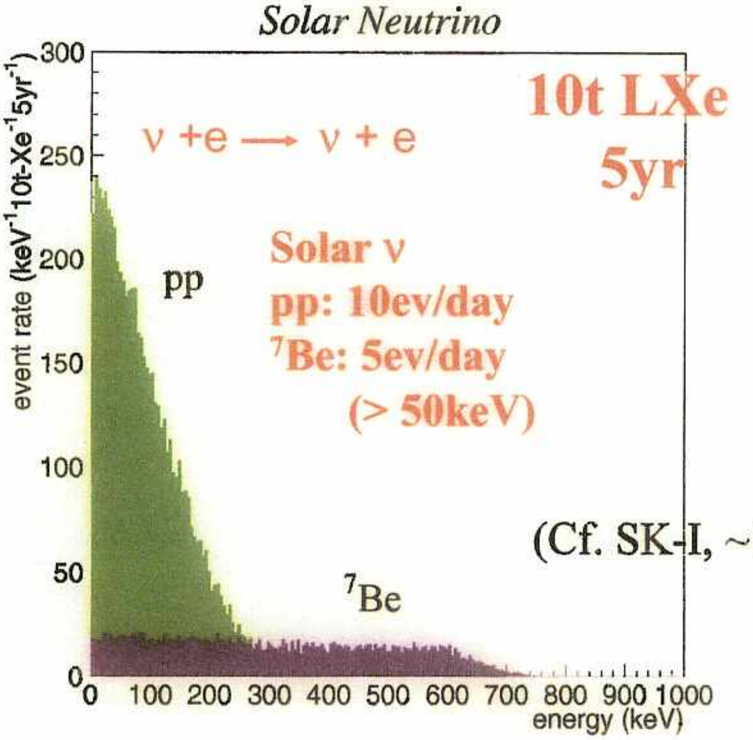

(Cf. SK-I, ~13 events/day)

QUITE HIGH STATISTICS!!

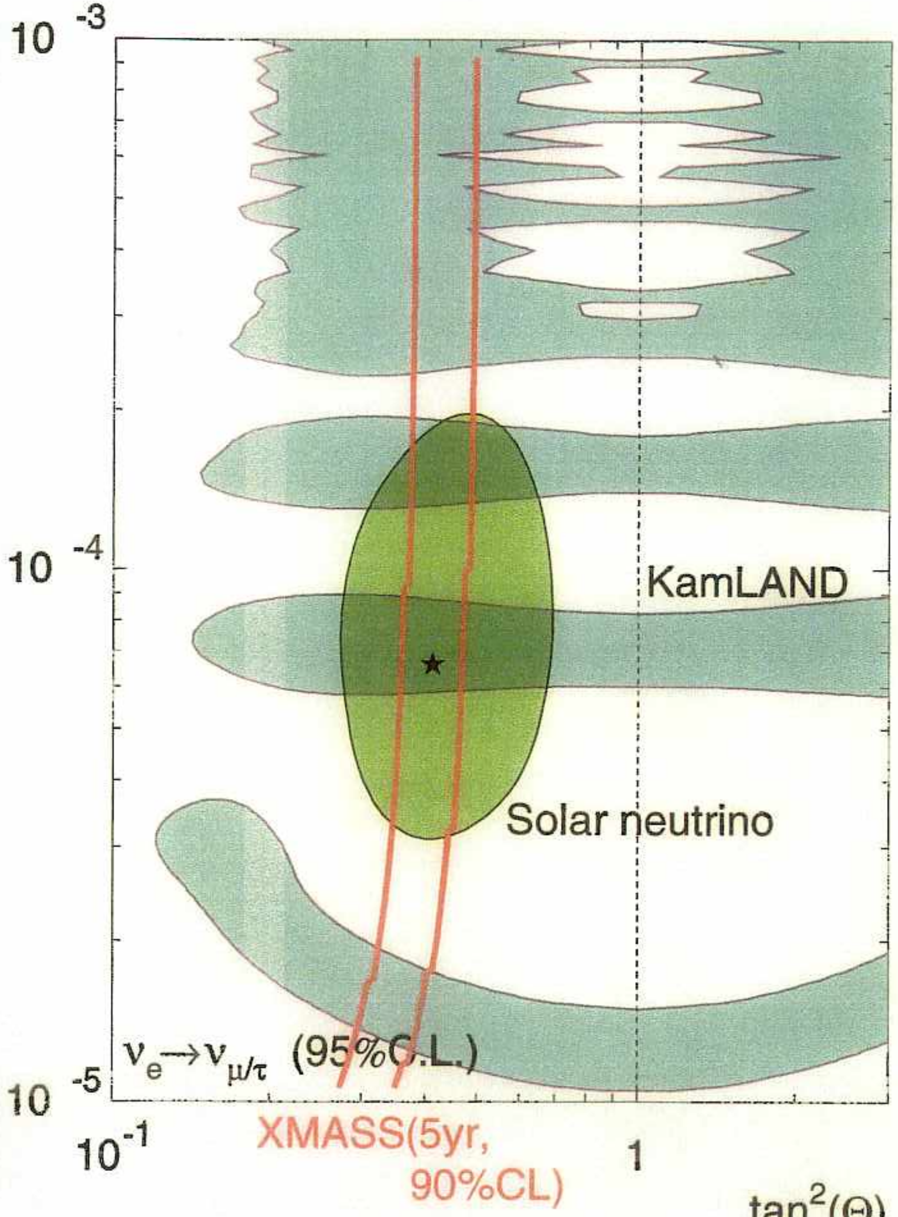

Dark matter detection

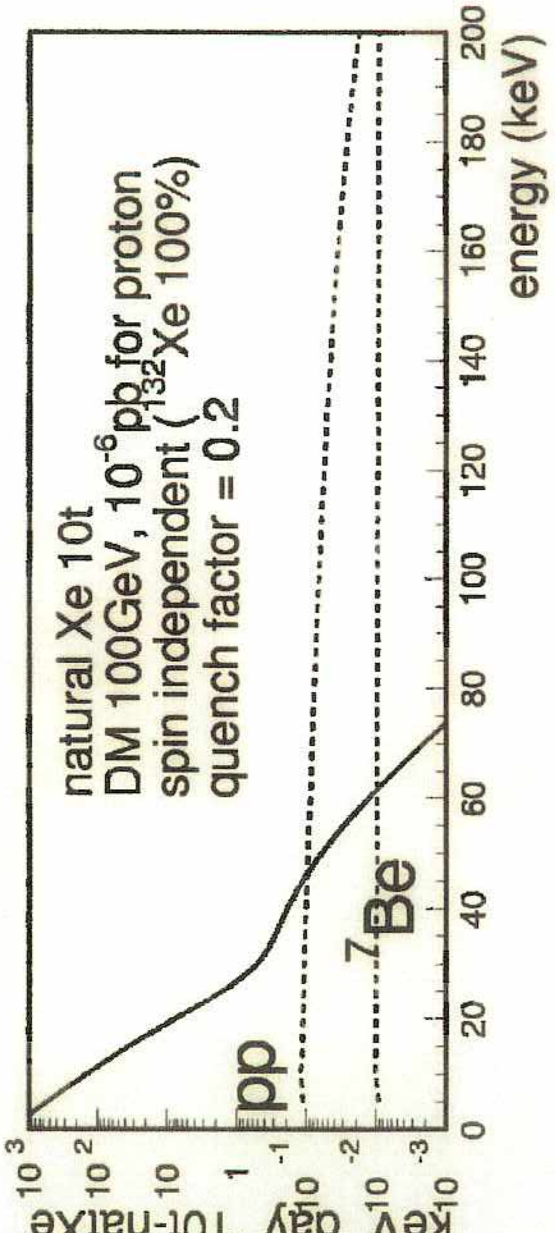

E_{th} = 20keV; 30 events/day

E_{th} = 5keV; 2000 events/day

Sensitivity

10 ton detector

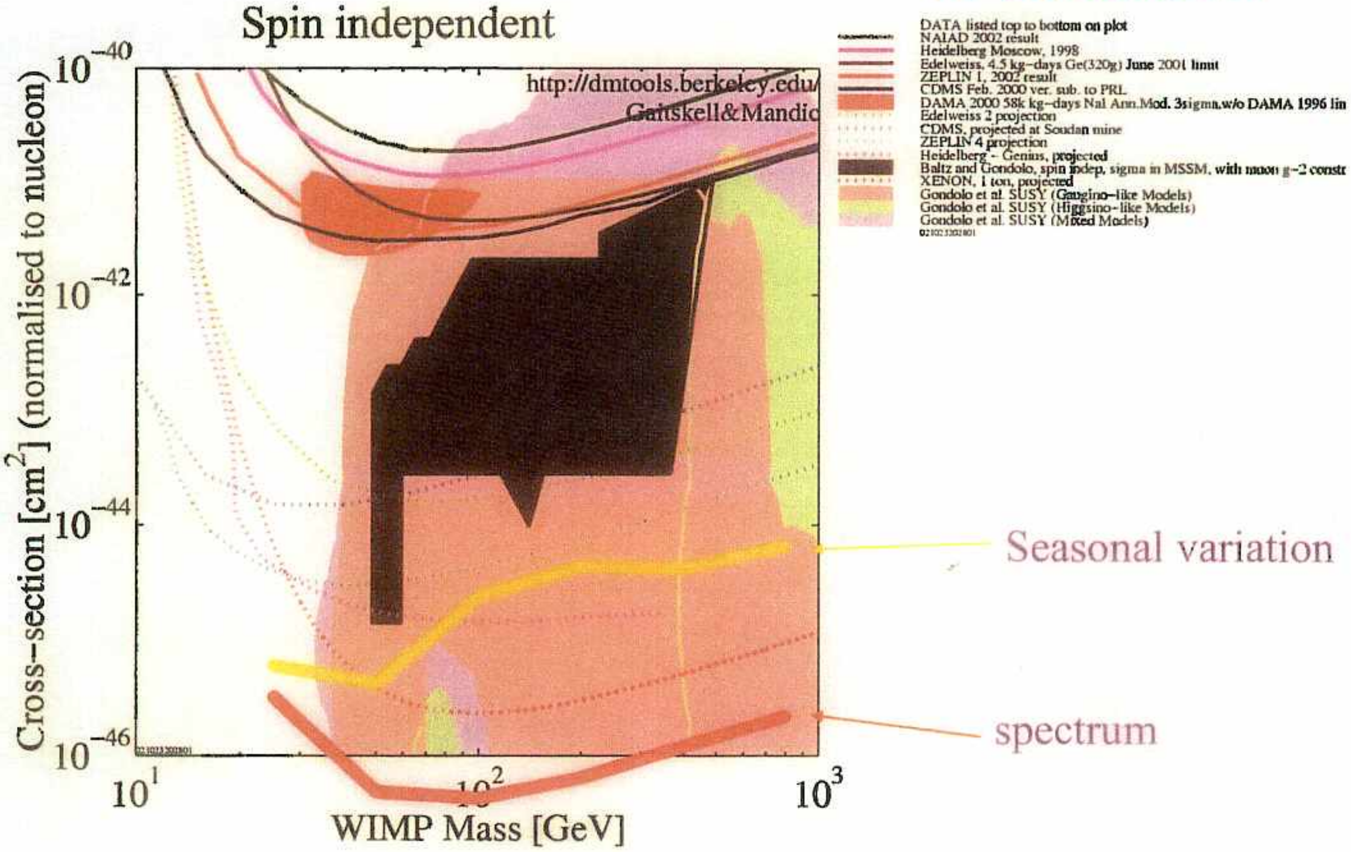

Double beta decay

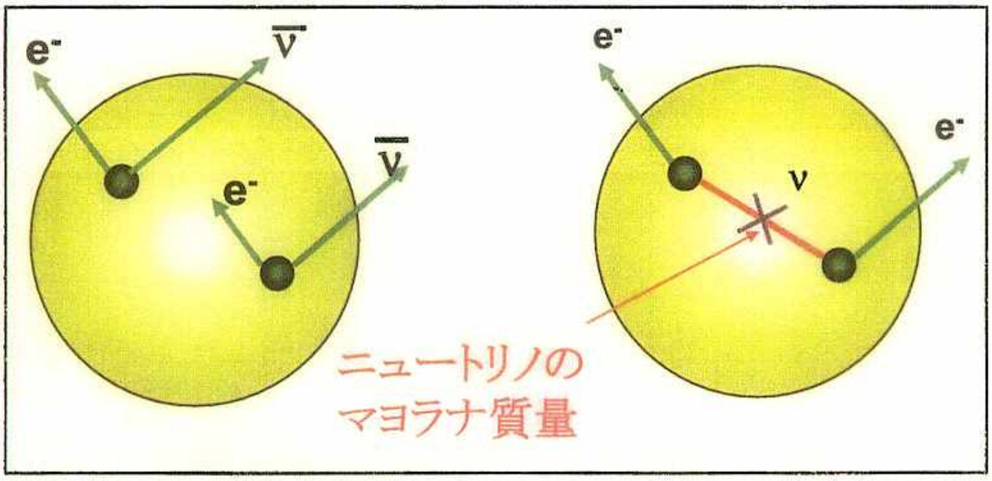

ニュートリノ質量がマヨラナ質量であるかということは、極めて重要。
シーソー機構が正しいかどうか。

0ν2β 崩壊探索の感度

10ton natural, 5 year

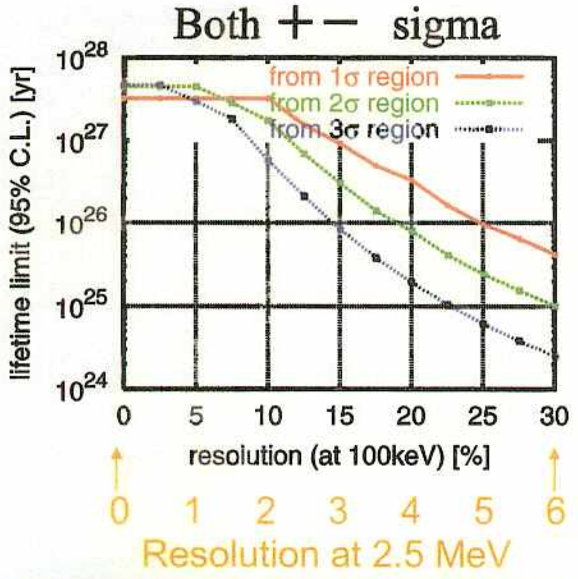

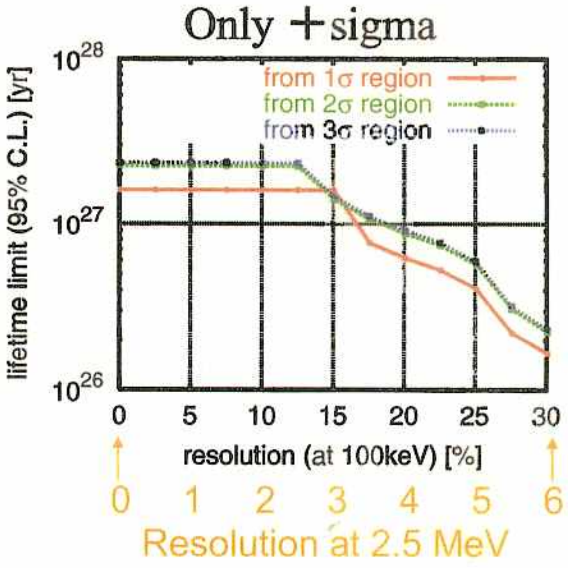

光量の統計から決まる分解能

42000p.e./MeV x 2.48MeV x 30%Q.E.

→ 31000 p.e. → 0.6 % rms

m_{Majorana} の感度として、0.01 − 0.02 eV

Hyper-Kamiokande detector

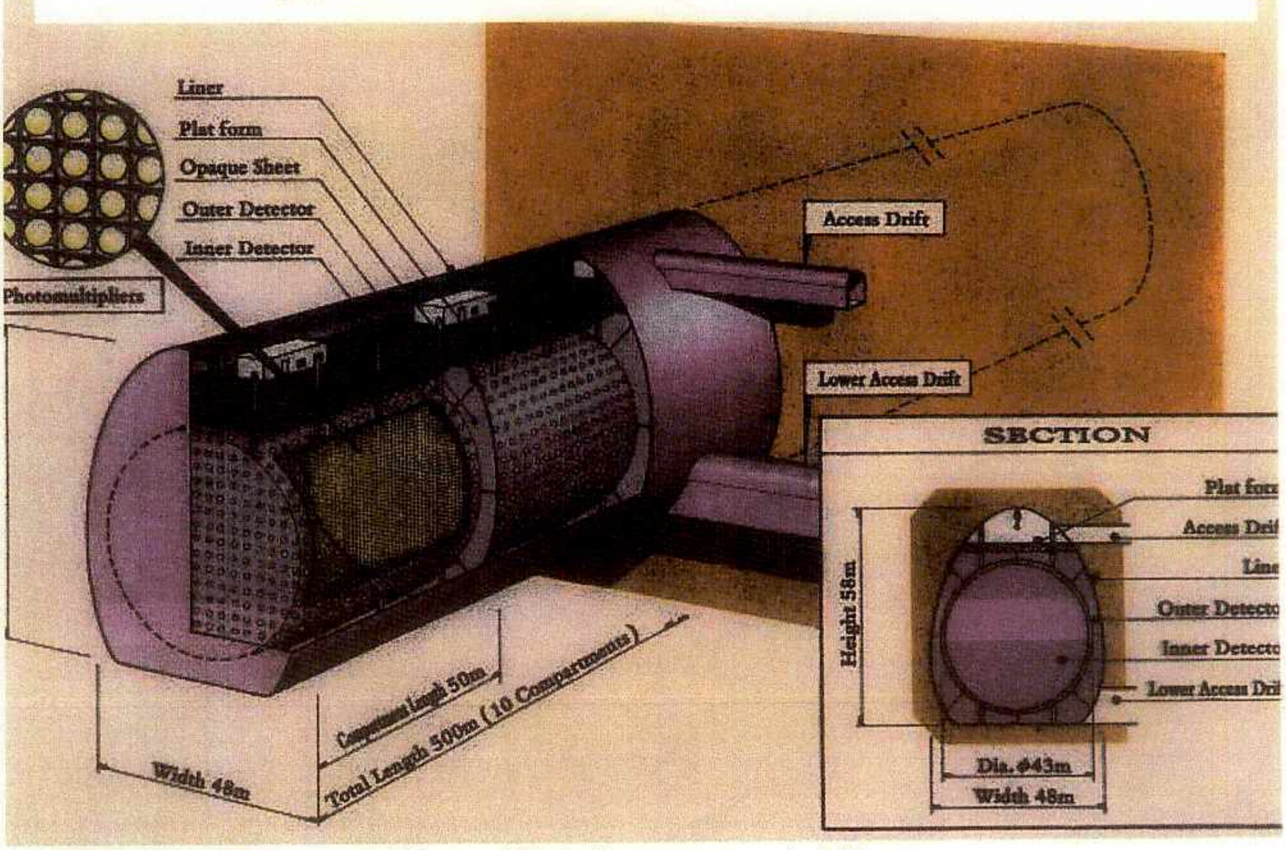

48m × 50m ×500m, Total mass = 1 Mton

Proton decay in Hyper-K

20 Mton ·yr atm ν BG MC

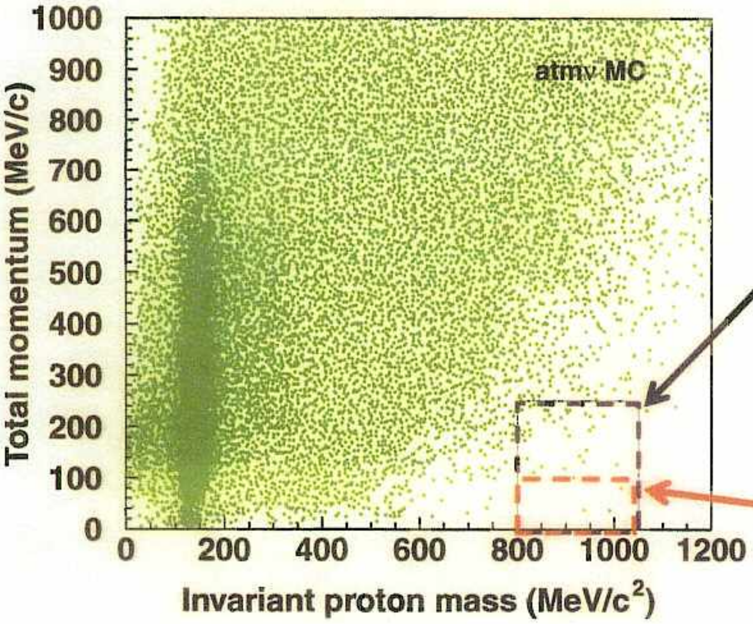

$p \rightarrow e^+ \ \pi^0$

"SK cut"

~2.3 events/Mton ·yr
ε = 43 %

"tight cut"

~0.15 events/Mton ·y
ε = 17 %

Tight momentum cut and free proton

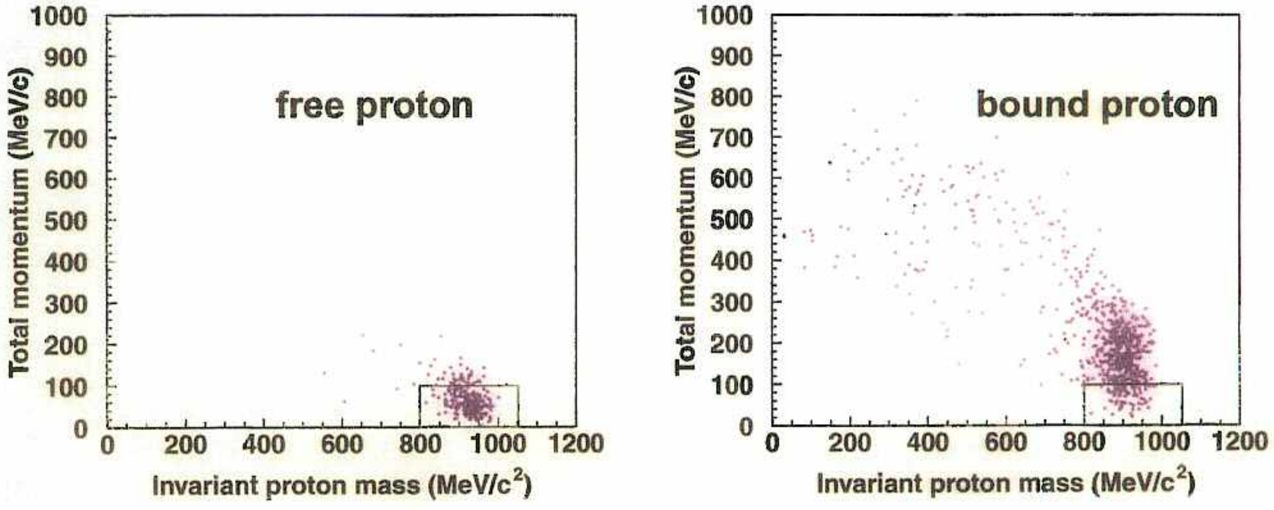

Tight momentum cut
⇒ target is mainly free protons
efficiency=17.4%

lo Fermi momentum
lo binding energy
lo nuclear effect

⇨ Small systematic uncertainty in efficiency

e π^0 sensitivity

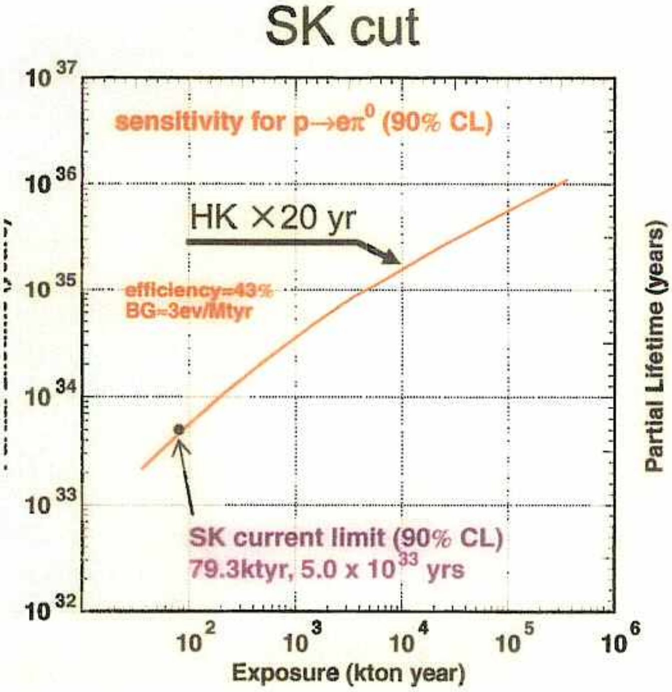

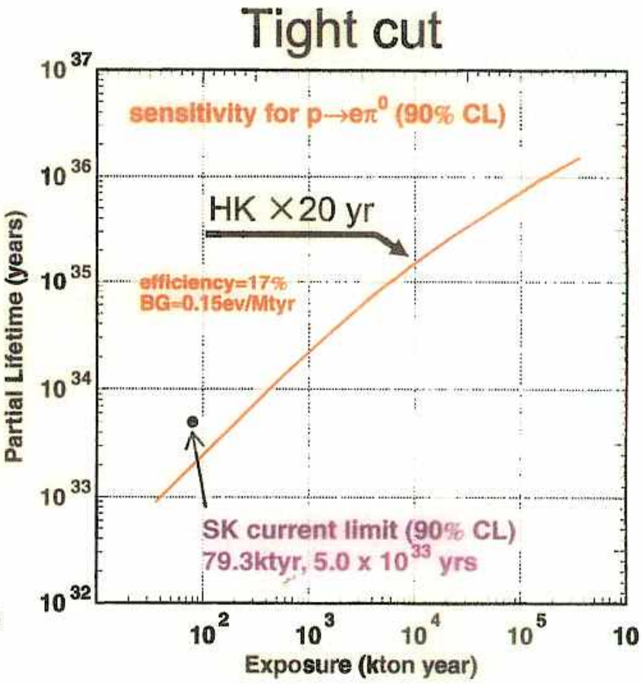

$\tau/B > 2 \times 10^{35}$ yr (Hyper-K 20yrs, 90%CL)

Reconstruction of m_p

$\tau/B(p \to e^+ \pi^0) = 1 \times 10^{35}$ yr

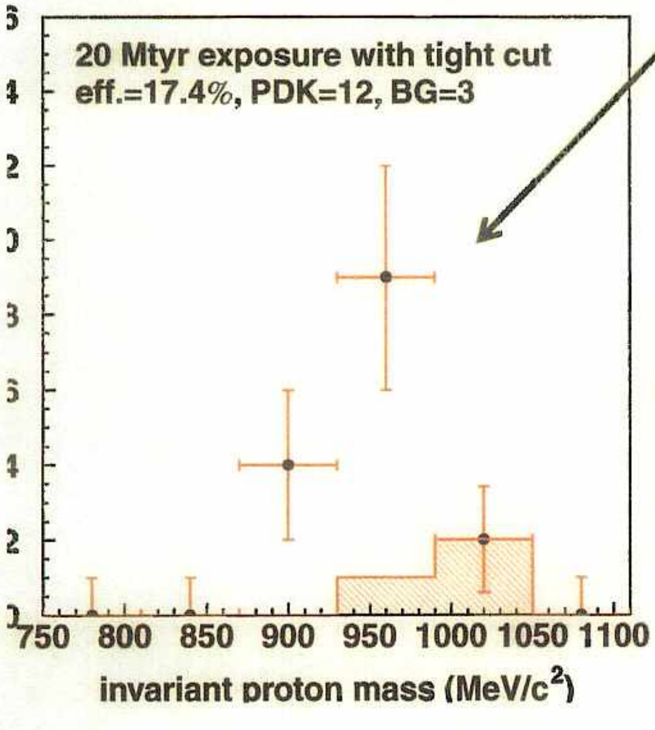

Proton mass peak
can be observed !

S/N = 4 for 1×10^{35} yr

Evidence for proton decay can b
found if $\tau/B(p \to e^+ \pi^0)$ =
1×10^{35}yr by a large water
Cherenkov detector.

νK^+ sensitivity

Slightly old cut

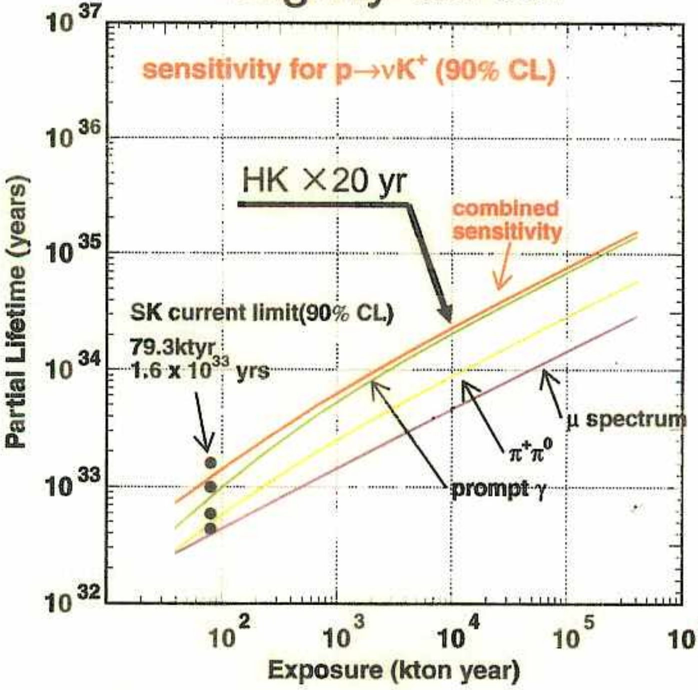

$\tau/B > 3 \times 10^{34}$ yr (Hyper-K 20yrs, 90%CL)